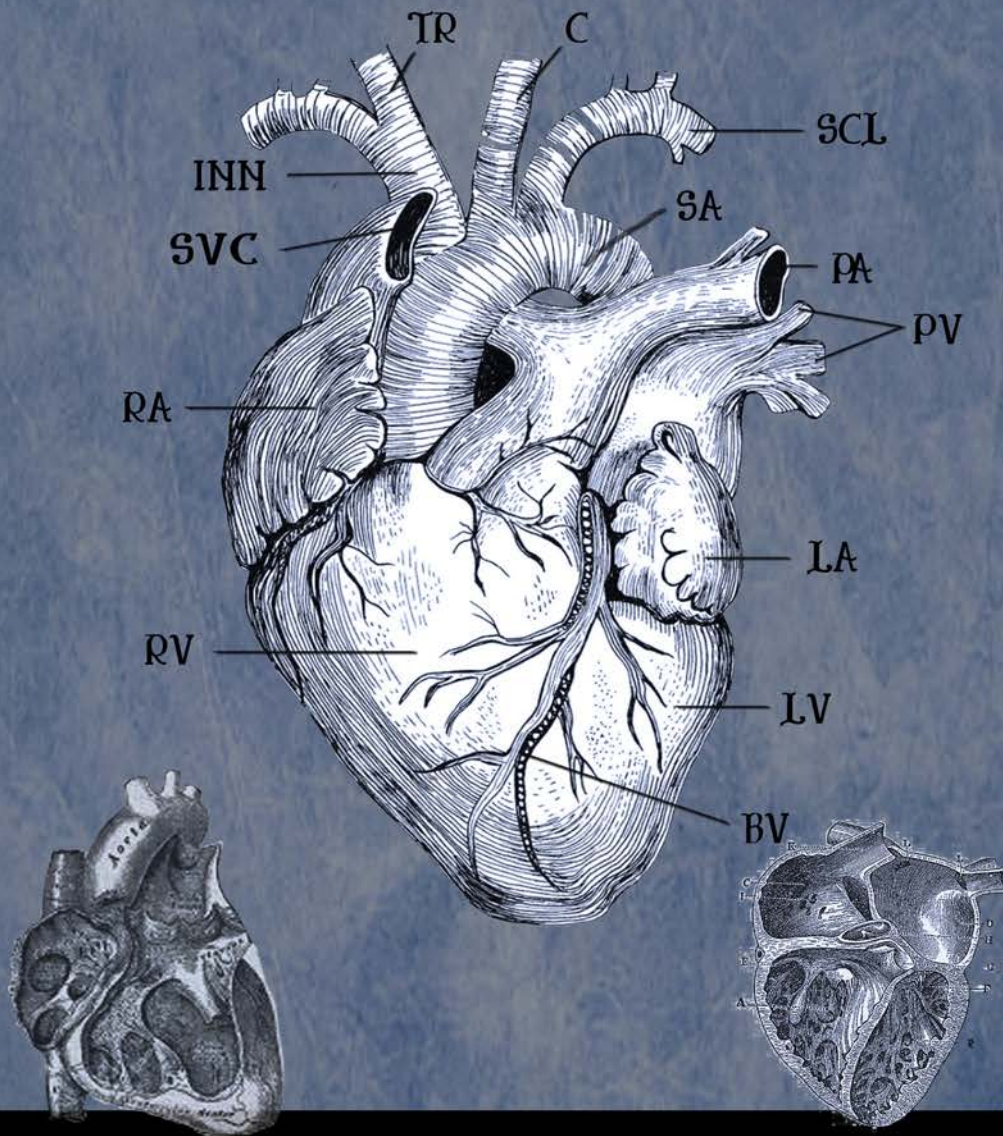


# NAVIGATING NEW FRONTIERS



neuroKINESIS

VOL 1  
2022

CORPORATION Collected Patents

Josh Shachar et al.



*“The journey to finding a solution to a problem often involves the discovery of questions you never thought to ask.”*

**JOHN TERBORG**

### ***Notes on the First Edition***

*Creating a book, even a book of this nature, is not a small undertaking. Indeed this publication took many months to write, gather the material, organize, and put it together in what we hope is a meaningful presentation. More than that time though is the realization of the years of research and development that stand behind the information and patents presented herein. Indeed, contained behind these pages are the countless hours of blood, sweat and yes, even tears from the army of engineers, team members, collaborative strategic partners and their families who all contributed pieces to each puzzle we sought to solve along the way. The depth of that dedication is not lost on us as we come to the publication of this work.*

*As of the printing of this book, the first edition of the collected patents for Neuro-Kinesis, Corp., we feel the achievements we have made in each of the technologies we have developed, has been well worth the sacrifice it took to get here. Specifically with the development of our Huygens™ Catheter – Proteus™ Robotic Arm Operating Suite, we feel that we are poised to bring a fundamental change in providing the EP surgeon a better tool that will affect their ability to bring better outcomes to their patients. If we are successful in just a small part of that change, we will have proven our journey’s worth.*





# NEUROKINESIS

CORPORATION  
Collected Patents  
FIRST EDITION

© Copyright 2022 Josh Shachar Publishing • All rights reserved.

No part of this book may be resold, reproduced or used in any other publication or media display without the express written consent of the publisher. Violators will be punished to the fullest extent of the law.

# TABLE of CONTENTS

## PREFACE

- 01 *Forward*
- 07 *Charting The Course*
- 29 *Creating A New Paradigm In EP Mapping*
- 58 *PROTEUS™ – A New Vision For Catheter Guidance*

## PATENTS

# 01

*Apparatus for Magnetically Deployable Catheter with MOSFET Sensor and Method for Mapping and Ablation*

### U.S. PATENTS

- 77 *Apparatus for Magnetically Deployable Catheter with MOSFET Sensor and Method for Mapping and Ablation* US 2007/0197891 A1
- 120 *Apparatus for Magnetically Deployable Catheter with MOSFET Sensor and Method for Mapping and Ablation* US 2009/0248014 A1
- 121 *Apparatus for Magnetically Deployable Catheter with MOSFET Sensor and Method for Mapping and Ablation* US 7,869,854 B2I
- 122 *Method And Apparatus For Magnetically Guided Catheter For Renal Denervation Employing Mosfet Sensor Array* US 2014/0018792 A1
- 126 *Method And Apparatus For Magnetically Guided Catheter For Renal Denervation Employing Mosfet Sensor Array* US 9,381,063 B2
- 127 *Method And Apparatus For Measuring Biopotential And Mapping Ephaptic Coupling Employing A Catheter With Mosfet Sensor Array* US 2014/0081114 A1
- 169 *Method And Apparatus For Measuring Biopotential And Mapping Ephaptic Coupling Employing A Catheter With Mosfet Sensor Array* US 9,220,425 B2

### INTERNATIONAL PATENTS

- 171 *Apparatus for Magnetically Deployable Catheter with MOSFET Sensor and Method for Mapping and Ablation – WIPO* WO 2007/100559A2



- 172 *Apparatus for Magnetically Deployable Catheter with MOSFET Sensor and Method for Mapping and Ablation – EUROPE/EPO* EP 1 986 560 A0
- 173 *Apparatus for Magnetically Deployable Catheter with MOSFET Sensor and Method for Mapping and Ablation – CANADA* CA2637622
- 175 *Apparatus for Magnetically Deployable Catheter with MOSFET Sensor and Method for Mapping and Ablation – CHINA* HK1123959

## 02 *Apparatus and Method for Lorentz-Active Sheath Display and Control of Surgical Tools*

### U.S. PATENTS

- 179 *Apparatus and Method for Lorentz-Active Sheath Display and Control of Surgical Tools* US 2009/0253985 A1
- 192 *Apparatus and Method for Lorentz-Active Sheath Display and Control of Surgical Tools* US 2012/0289822 A1

### INTERNATIONAL PATENTS

- 195 *Apparatus and Method for Lorentz-Active Sheath Display and Control of Surgical Tools – WIPO* WO 2009/126575 A1
- 196 *Apparatus and Method for Lorentz-Active Sheath Display and Control of Surgical Tools – EUROPE/EPO* 9730100.6
- 197 *Apparatus and Method for Lorentz-Active Sheath Display and Control of Surgical Tools – CHINA* 200980110899.X

## 03 *Method and Apparatus for Creating a High Resolution Map of the Electrical and Mechanical Properties of the Heart*

### U.S. PATENTS

- 199 *Method and Apparatus for Creating a High Resolution Map of the Electrical and Mechanical Properties of the Heart* US 2009/0275828
- 220 *Method and Apparatus for Creating a High Resolution Map of the Electrical and Mechanical Properties of the Heart* US 2012/031066 A1

**INTERNATIONAL PATENTS**

- 223 *Method and Apparatus for Creating a High Resolution Map of the Electrical and Mechanical Properties of the Heart – WIPO* WO 2009/134605
- 224 *Apparatus and Method for Lorentz-Active Sheath Display and Control of Surgical Tools – EUROPE/EPO* 97394076
- 225 *Apparatus and Method for Lorentz-Active Sheath Display and Control of Surgical Tools – CHINA* CN102065746 A

04

*System and Method for a Catheter Impedance Seeking Device*

**U.S. PATENTS**

- 227 *System and Method for a Catheter Impedance Seeking Device* US 2010/0130854 A1
- 259 *System and Method for a Catheter Impedance Seeking Device* US 8,457,714 B2
- 260 *System and Method for a Catheter Impedance Seeking Device* PCT/US2010/052696

**INTERNATIONAL PATENTS**

- 263 *System and Method for a Catheter Impedance Seeking Device – WIPO* WO 2010/065267 A1

05

*Optically Coupled Catheter And Method Of Using The Same*

**U.S. PATENTS**

- 265 *Optically Coupled Catheter And Method Of Using The Same* US 2020/0375541 A1

**INTERNATIONAL PATENTS**

- 287 *An Optically Coupled Catheter And Method Of Using The Same – WIPO* WO 2020/242753 A1

06

*Catheter for Cardiac and Renal Nerve Sensing and Mediation*

**U.S. PATENTS**

- 319 *Catheter for Cardiac and Renal Nerve Sensing and Mediation* US 2022/0047202 A1



# 07

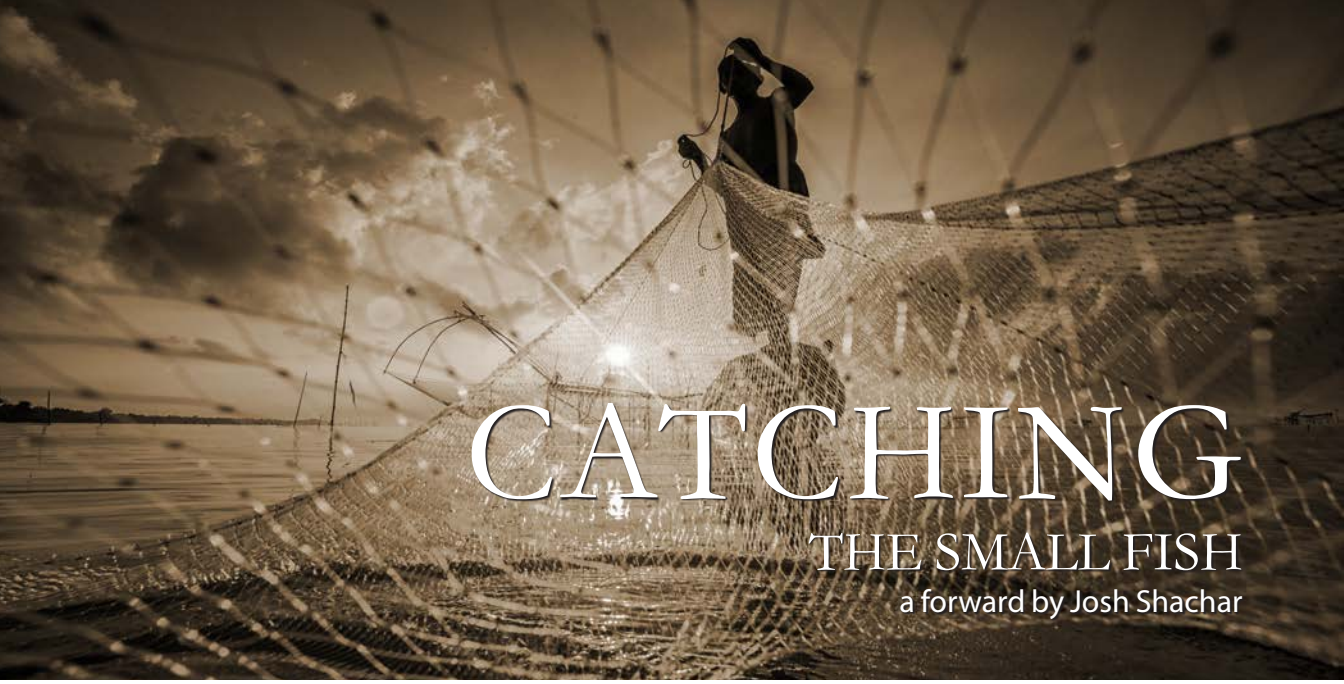
*The Use of Local Amplifiers and Huygens™ Sensor Array in Measuring Bioelectric Signals and Clinical Applications Thereof*

## **U.S. PATENTS**

**385**

*The Use of Local Amplifiers and Huygens™ Sensor Array in Measuring Bioelectric Signals and Clinical Applications Thereof*

PHA3PAU63PCT



# CATCHING

## THE SMALL FISH

a forward by Josh Shachar

One of the aims in creating the NKC's platform was the establishment of a technology which will enable a measuring apparatus to collect its input data and provides a definitive causal relationship between the electrical activity gathered by the EP catheter's set of sensing electrodes to probe the endocardial substrate and the surface electrograms.

One of the aims of creating the NKC's platform was the establishment of a technology that will enable a measuring apparatus to collect its input data and provides a definitive causal relationship between the electrical activity gathered by the EP catheter's set of sensing electrodes to probe the endocardial substrate and the surface electrograms.

This process currently performed by the existing art lacks the ability to obtain such results due to the limitations in which the physician can ascertain the geometric foci and their electrical characteristics to form an

electro-anatomical map with specificity representing the fidelity of the endocardial surfaces, thereby creating an EP map that mimics the dynamics of the electrical waveforms with a resolution which are commensurable with signals typically encountered when measuring scar-tissues which exhibits a low voltage signature.

It is not clear with the current art that we are able to pick up these casual relationships in areas where the signal value of the scar tissue, which is as low as 5-100 microvolts ( $\mu\text{V}$ ), can be measured because of the geometrically larger



orders of magnitudes the environmental electrical noise creates which mask these low-voltage signals. Indeed, in most cases what we observe is only a statistical correlation between certain behavioral features of the electrical activity over the endocardial map and what is believed to be the cause of the arrhythmia. This phenomenon of signal-to-noise ratio (SNR) is dealt with in the current art by the introduction of multiple filtering techniques which attempts to remove the artifacts created by the noise that is riding on top of the signal. As we observe, such artificial “cleaning” of the raw signal emanating from the surface of the heart chamber is most times “clearing the weeds with the daisies” in that we are eliminating valuable signal information as well as the noise.

As a result, there is a lot of information that has to be interpolated by the physician in an effort to achieve a clear path that links the electro-anatomical data to its intended therapeutic solution.

Although there are multiple therapeutic treatments for many different known pacing diseases, these solutions only cover the categories for the disease model, such as paroxysmal Afib and others, where the treatment modality follows a “cookie-cutter” approach in support of such simpler cases.

The simple pacing cases noted above provide for a clear relationship

between the diagnostic and the therapeutic for which the EP physician can apply a standard protocol for using various methods of RF ablation techniques. However, this model breaks when you start dealing with a complex arrhythmia where the causes for the pacing disturbance are multi-focal as they emanate from complicated behaviors of the endocardial surface and where a collection of scar tissue on the surface of the heart chamber results in a complex set of the causal induced phenomenon. These are not as simple to trace as the causal links require an understanding of



*Inventor of the technology Josh Shachar with one of the first prototypes for the CGCI catheter guidance technology which was the progenitor for NKC's current achievements.*

the electrical activities resulting from the deeper substrate dynamics.

When you think about the endocardial tissue, there isn't only a surface electrical event but there are also deeper substrate events that are only uncovered when you perform a substrate mapping coupled with surface electrograms while synchronously

defining the position and orientation of the wavefront direction and magnitudes. Treatment of these complex arrhythmias requires a much different and customized therapeutic approach.

Only about 60% of cardio ablation procedures are represented in these simple “cookie-cutter” approaches, such as Paroxysmal AFib where the surgeon isolates the pulmonary vein by ablating a roofline and an Isthmus line to restore the orderly pacing of the heart. When

you are exposed to a complex arrhythmia where the causal relationships are a set of electrical activities, such as those identified

«The current state of EP art is only able to effectively capture and diagnose 60% of the patient population that have arrhythmia conditions that fit the profile consistent with high-voltage scar tissue that can be addressed by a ‘cookie-cutter’ therapeutic approach.»

for example by phenomena such as “Rotors” with atrial fibrillation, you are faced with the fact that the information gathered with the existing catheter technology, falls far short because of its low resolution and poor dynamic range in being able to capture these low voltage scare tissues area and provide the EP specialist with the necessary data needed to make better therapeutic decisions. This is due to the fact that such events necessitate the uncovering of simultaneous knowledge of position, orientation, DC potential, and impedance measurement and such data must be captured at a dynamic rate of substrate electrical activities.

Scar tissues combined with a low voltage cannot be picked up by the current catheters. It is like a fisherman that goes to the ocean to catch fish where the spacing of the net openings is only 10” apart. Surely, he will catch the large fish like a tuna, but he will completely miss the smaller fish because the net simply cannot capture them. This was the main motivation of the MOSFET local amplifier module as an adjunct element to the electrodes located on the sensing catheter, which evolved

into a smart miniaturized sensing platform we now designate as the Huygens™ Catheter technology.

In addition to the low resolution of the existing catheter’s technology and its inability to properly perform at electrical potential ranges of 25-100  $\mu\text{V}$  and where such measurement needed additional circuitry to measure the conductivity of the substrate mapping with the existing art, we set a goal to solve the problem of eliminating polluting noise within the measurements we wanted to capture.

We understood from our long history of developing our MOSFET™ Catheter that there are multiple sources that can corrupt the catheter’s ability to measure bioelectrical events without massive filtering at the low range of



the spectral density of the endocardial surface. One of these problems is the distinction between far-field and near-field electrical signals coupling. When you put the catheter electrode on the endocardial surface, you are measuring not just the signals that are local, those in contact with the electrode, but the surrounding wavefront signal in such a dynamic as well. Additionally, the DC threshold stable reference cannot be maintained within the existing art. The signal-to-noise ratio issue inherent with any analog signal measurement practically obliterates signal fidelity at the relevant regime of interest to the EP physician. The question for us was, how do we go about improving such impedance microscopy within the current standard and without altering the great advances made in the art of electrophysiology, thereby incorporating with a seamless integration the solution noted by the Huygens™ Catheter's advanced digital apparatus?

To understand the order of magnitudes of the NKC's solution we should consider an optical analogy that will explain what we are hoping to achieve. Imagine a microscope that has a magnification power of 50x. If you want to see something an order below this, say 500x or 1000x, in order to achieve such optical resolution, the optical aperture will necessitate a different set of lenses to "see" the desired objects at this magnification. In electrical measurement terms, existing catheters

have no problem measuring signals of 500 $\mu$ V and up. The problem we are facing is in trying to "see" these signals on the substrate where small scar tissue signals are in the range of 25 $\mu$ V to 50 $\mu$ V. Back to our fisherman analogy, the existing nets are just not able to "capture" objects as small due to the net's dimension. In our electro anatomical domain, we are faced with massive parasitic noise coupled with the 500 $\mu$ V signal. Noise that is not only inherently part of the signal capture but also noise that is associated with the transmission of the signal to the mapping computer, which is interspaced in an operating room and where every element of the room is emitting electrical RF radiation that which contaminate the signal. This includes the 60Hz that is constantly being emitted by the operating room's lights. In addition, there are many other sources of high frequency such as the EKG and X-Ray equipment. Add to this the life support system operating at frequencies as low as 5Hz, and the cumulation of all of these sources of electromagnetic noise corrupting the native signal obtained from the patient's heart.

The low-level voltage map of the scare tissue is now mixed into the bioelectric signal from the catheter. At this point, you then have to start filtering the signal to remove this noise. But doing this also eliminates all the elements of the signal that the physician requires in order to form a consistent

causal chain that relates the disease to the formed electroanatomical map, hence the requirement for an apparatus to improve the diagnostic parameters in resolving complex arrhythmias.

The aim of NKC was to provide the physician with a new Impedance Microscopy commensurate with the disease-level electrical activity and the dynamics of the electrical wavefront so as to enable a clear understanding of the actual state of the patient heart and not just an idealized model that does not resemble the specificity of the patient.

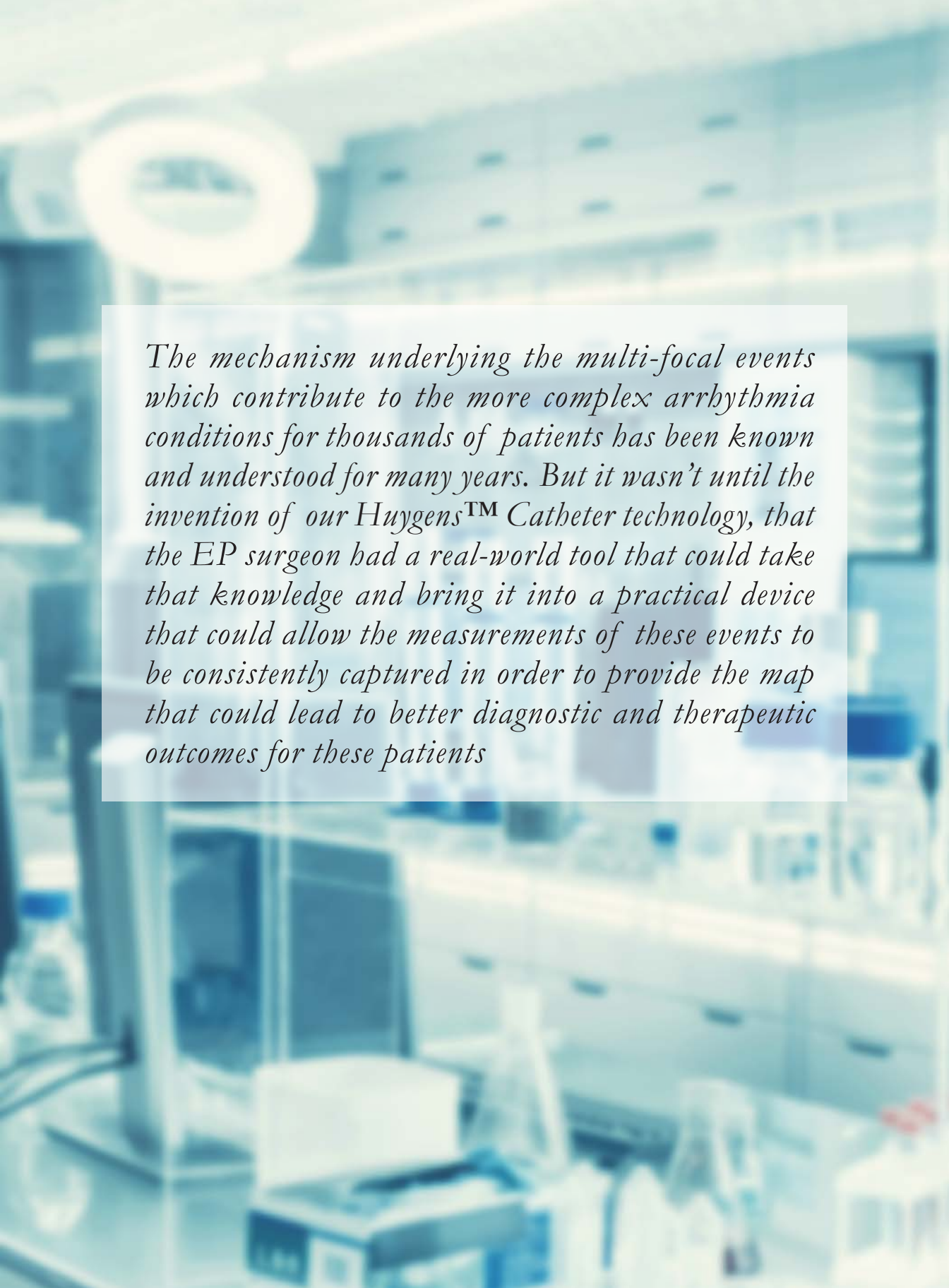
With the Huygens™ Catheter, we are able to capture the three critical parameters in order to affect the outcome of the patient disease. The ability to capture the signal locally, amplify the low-level electrical signal, identify the conductivity of the substrate at that position and obtain the coordinate of that event in a simultaneous sequence while digitizing the measurement, hence creating immunity from any other analog interference of the surrounding environment. Such signal can then be transmitted via a fiber-optic channel and its integrity is preserved.

*«The Huygens™ Catheter is able to simultaneously capture knowledge of position, orientation, DC potential, and impedance measurement within a few milliseconds of endocardial surface contact and with a resolution that is able to close the net to grab the low-voltage substrate information critical to addressing the other 40% of patients who suffer from complex arrhythmia issues.»*

These advances will position the Huygens™ Catheter to revolutionize the EP Catheter Mapping world and when coupled with the Proteus™ Robotic Arm, the EP operator will have a turnkey breakthrough in catheter-based diagnostic and therapeutic solutions that are not only far superior in results but one that offers a lower cost, plug-and-play portable answer that can be implemented anywhere. The introduction of the Huygens™ Catheter will be a game-changer for the EP physician.

In addition, our advanced catheter tip-centered technology has the potential to be implemented into any EP catheter design being manufactured

now which implies that the Huygens™ technology may be a game-changer for the strategic players which serve this global market. NKC brings the ability to change any EP catheter into a 21st Century SMART device that provides a win-win-win-win advantage to the surgeon, the patient, the healthcare facility, and the insurance provider. Huygens™ is opening the door to a whole new day in advancing EP medicine.



*The mechanism underlying the multi-focal events which contribute to the more complex arrhythmia conditions for thousands of patients has been known and understood for many years. But it wasn't until the invention of our Huygens™ Catheter technology, that the EP surgeon had a real-world tool that could take that knowledge and bring it into a practical device that could allow the measurements of these events to be consistently captured in order to provide the map that could lead to better diagnostic and therapeutic outcomes for these patients*

# Charting the Course

Neuro-Kinesis Corporation (NKC) is an advanced medical device technology company created to consolidate and commercialize its leading-edge breakthroughs in surgical tools that integrate state-of-the-art biosensor technologies, advanced micro-miniaturization design and artificial intelligence to further the ability of a physician to treat their patients.





The company was formed in 2015 when Pharmaco-Kinesis Corporation (PKC) made the decision to separate its IP into four different entities that could each focus on the area of expertise the individuals technologies addressed. Neuro-Kinesis was created to manage and develop PKC's SMART surgical tools, Cognos-Therapeutic Inc was established to handle the company's SMART Implantable drug-delivery pump systems, Sensor-Kinesis to further the biosensor technology related to biomarker detection, and Nano-Kinesis Corporation was tasked with the development of nano-particle and combinatorial drugs technologies that the company had acquired.

and development into engineering a new approach to biosensor technologies that could provide real-time, clinically-relevant measurements and analytics of targeted biometrics measurements such as biomarkers, disease pathogens, and tissue bioelectric conductivity, and then converting those measurements into digital data to be processed according to the specific application required. In addition to these proprietary biosensor technologies, PKC had also achieved evolutions in applying artificial intelligence and micro miniaturization to the embodied processing of this captured data to provide a SMART technology form to a surgical tool. In doing this, the tools that these technologies employed provided a radically new advance to both diagnostic and operative patient care.

## THE VISION

The formation of NKC from PKC represented over fifteen years of research



*Neuro-Kinesis Corp. was part of the division of technologies initiated by Pharmaco-Kinesis Corp. in 2015*



## JOSH SHACHAR

Co-founder of the PKC Group of Companies  
and Inventor of the Technologies

For more than 20 years Josh Shachar has led the innovative work behind each of the PKC Group of Companies. His bold vision casting has resulted in fundamental shifts in how diagnostic medicine, pharma-therapy and surgical device technology can improve patient outcomes.

### THE VISIONARY

The inventive steps that form the core technology of the various PKC entities is the result of a combined effort between NKC Chief Technology Officer Josh Shachar and the expertise of collaborators such as Dr. Gang on the clinical side, and our capable engineering team in the fields of robotics, magnetics, microelectronics, microfluidics, biology, virology and electrophysiology. All of the above disciplines form the core technologies nested in the various companies under the former umbrella of PKC.

Josh is an American scientist, inventor, and entrepreneur who has pioneered the discovery of ground-breaking innovations in magnetic guidance, advanced microelectronics, biological sensors, and medical device technologies. His work has continued to push the envelope of discovery in a variety of fields including national defense, aerospace communication, and medical diagnostics. Indeed, Josh's work for the U.S. Department of Defense (DoD) resulted in several

breakthroughs in the areas of vehicle delivery efficiencies, radar imaging, and advanced guidance systems. Two of the companies Josh founded in this arena, EDEL Engineering Development Corp. and Engineered Magnetecs, Inc., are still thriving today and continue to set the standard for their respective industries. Indeed, there is not a free world missile program that does not operate without EMI equipment abroad.

Josh might have remained in the DoD arena if it were not for witnessing his mother undergo a catheter stent procedure as the result of a heart attack. In watching the dance between the patient and the physician as he manually guided the catheter through her living body and into her beating heart, Josh knew that there had to be a more effective way to accomplish the task.

### **MAGNETECS – THE BEGINNINGS OF A NEW ERA IN EP CATHETER GUIDANCE**

In 2002, Josh, along with Dr. Eli Gang, MD, FACC, FACP, Clinical Professor of Medicine at the David

# Dr. ELI GANG

Co-founder of the PKC Group of Companies  
and NKC Chief Medical Officer

Dr. Gang Clinical is a Professor of Medicine at the David Geffen School of Medicine at UCLA. He is board-certified in Internal Medicine, Cardiology, and Clinical Electrophysiology. His research has included development of advanced ECG technologies as well as robotic approaches to ablation in the heart.



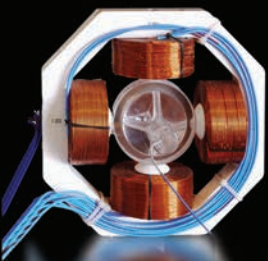
Geffen School of Medicine at UCLA, and Frank Adell, a successful entrepreneur and business leader with over 30 years of experience in strategic planning, formed Magnetecs Corporation to take Josh's insights into magnetic guidance for missile systems to see what could be done in improving the art of catheter guidance in the electrophysiology world. Josh formed his engineering team and set a vision to create a platform that would use an array of magnetic lobes that could generate high-energy magnetic fields whose strength could be individually controlled by a remote operator in order "pull" a specially

designed catheter tip through a living heart chamber with exacting location tolerances in any axis of direction. This was a bold vision but within the first four months of formation, Josh and his engineering team had constructed the first prototype for what they called the Catheter Guidance Control & Imaging (CGCI) System. This new guidance technology was described in Magnetecs first patent titled "System And Method For Radar-Assisted Catheter Guidance And Control" (US 2005/0096589 A1) which was published in May of 2005.

## CGCI Evolution

CGCI represented a major leap forward in EP catheter guidance by delivering controlled magnetic lensing to navigate the movement of a catheter in three-dimensional space. The images below show four pivotal development stages of the system from the first 4" design prototype in 2002 to the full-scale CGCI-II used in the initial human trial studies in 2010.

CGCI P1



CGCI P2



CGCI I



CGCI II



## MOSFET™

The MOSFET™ Catheter was the predecessor to NKC's Huygens™ Catheter technology. With MOSFET™ the concept of bringing signal amplification, signal capture and signal processing onto a flexible circuit board located

in the catheter tip, opened the door to the unprecedented fidelity capabilities that Huygens™ brings to the EP art.

← To the left is a first schematic concept for electrode tip signal processing used in the MOSFET™ Catheter

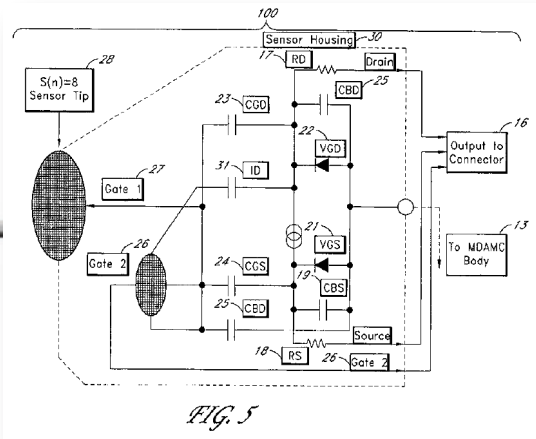


FIG. 5

During this developmental period of the catheter guidance system, Josh and the engineering team became acutely aware of the failings of the current mapping catheters to deliver detailed maps of the cardiac tissue due to the inability of the electrodes to differentiate electrical “noise” from the bioelectric signals of the heart tissue that needed to be captured to create a working map. In addition, the technology at the time was only able to capture signals of a high amplitude which meant the granular detail that would help an EP surgeon in choosing their ablation paths was not being captured as well as it could.

While moving forward with CGCI™, Josh quickly realized that the guidance of the catheter was only one side of the coin that was required for improving the existing cardio-mapping processes. In order to bring real innovation, the EP surgeon needed a better camera; i.e., a better catheter. As a result of the realization, Josh organized

a separate development team to look at creating a better mapping catheter that could overcome the two major obstacles to generating a more meaningful cardio-map; the ability to separate desired signals from extraneous noise, and the ability to measure bioelectric signals at voltage levels as low as 25 microvolts.

## REINVENTING THE EP MAPPING CATHETER

Achieving this goal required rethinking how signal capture was made inside the heart and then transmitted to the mapping computer outside the patient. Traditionally, the EP surgeon has to manually push a standard catheter into the patient’s body and navigate it into a chamber of the heart, the atrium, for example in treating AFib. The surgeon would then need to move the tip of the catheter, which contained an array of small electrodes, to make contact with the heart tissue to “capture” the bioconductivity of the tissue at that point. Data points being measured



are calculated based on RF signals being synchronistically generated by patches placed on the patient's chest. When the catheter electrode tip is pressed against the endocardial wall, these signals are captured and the time differential between the origination and the acquisition of the RF allows the mapping software to triangulate and determine a point in 3D space. This is

conductivity, the impedance will be very high. Since this voltage is so small, many variables can affect the results that the electrode produces. First is the ability to ensure the voltage being sent to the electrode remains constant. Since current EP electrode catheters use a pre-line amplifier that is located at the physician's side of the catheter outside the body to generate the voltage to the electrode

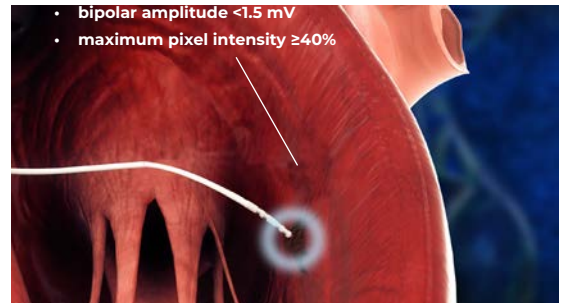
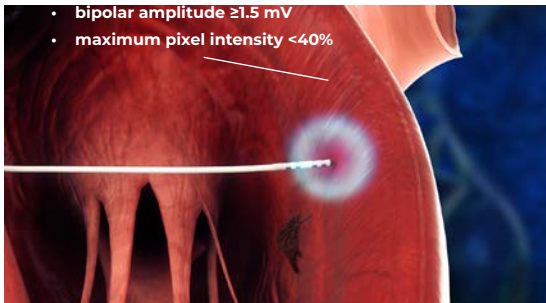


*Fig. 1 To create an accurate heart map for treating AFib, the mapping catheter must be able to detect the small electro-impedance differentials between healthy tissue that can efficiently carry electrical signals for proper heart pacing and scar tissue that cannot. With current technologies, the lower fidelity electrode sensors can often miss small scars or not be able to detect the gradation of impedance differentials to properly define the edges of the non-conductive tissue.*

then repeated over and over again until a sufficient map of the heart's geometry is constructed allowing the EP surgeon to understand the shape of the space they are working in. In addition to this anatomical mapping, an EP surgeon can also perform a substrate map whereby a very small millivolt electrical signal emitted by the catheter tip electrode is sent through the heart wall. This allows an impedance difference to be taken which informs the surgeon of the viability of the heart tissue. If the heart tissue is good, the impedance will be very low but if scar tissues exist, basically forming a barrier to electrical

tip, many factors can decrease or alter the fidelity of the signal. These include:

- Inconsistent power regulation within the amplifier.
- Degradation of the signal as it travels down the length of the catheter to the electrode due to faulty material, the actual distance being covered, and the ability to control and measure the signal being output by the electrode tip.
- Pollution of the signal due to the ambient electrical "noise" of all the surrounding tissue the catheter is moving through.

# THE NOISE PROBLEM

Current cardio mapping technology requires an analog RF signal to travel the entire circuit of the catheter's length in order to capture the bioelectric signals needed to plot both location and bio-tissue viability. As a result, the signal is subject to degradation due to the length of travel and the pollution from other RF sources in the operating room.

Fig. 2. Shows the traditional signal path for EP cardiac mapping and the various sources that create pollution in the signal making it hard to discern noise from needed tissue measurement.

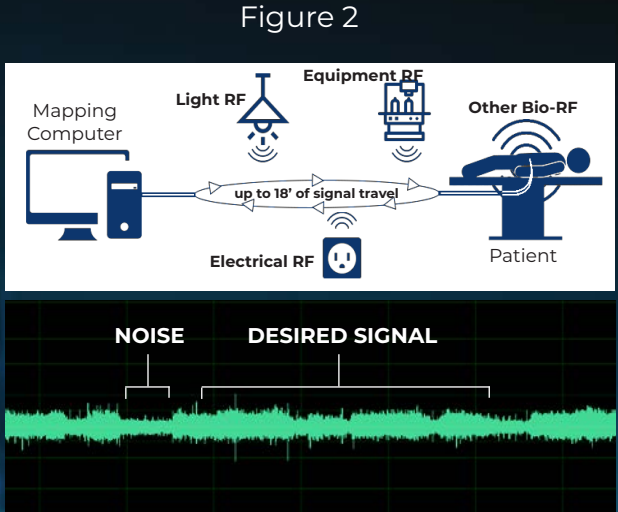


Figure 3

Fig. 3 shows the attempt to add signal amplification at the mapping station source in order to boost signal fidelity. Though this helps, the wave spectrum shows that noise is equally amplified along with the bioelectric tissue measurement.

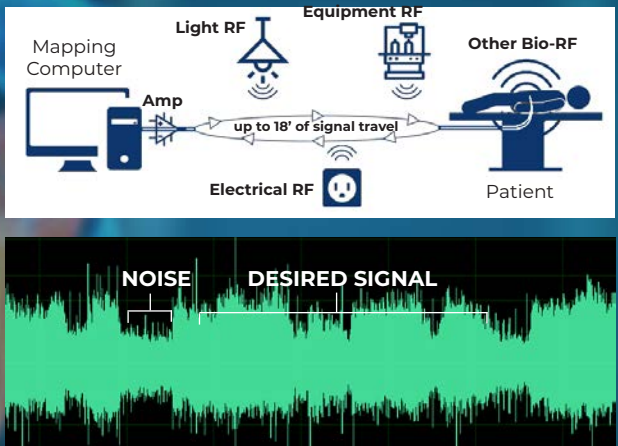
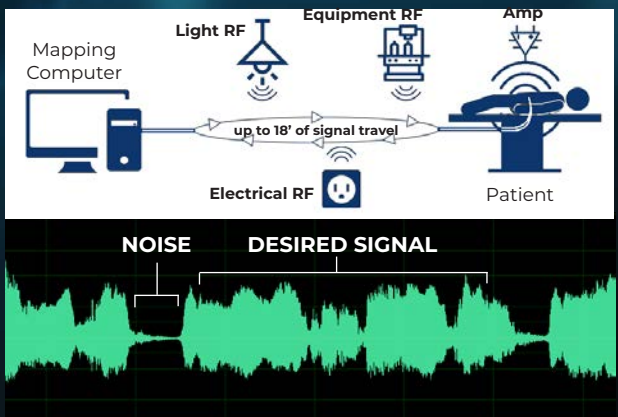


Figure 4

Fig. 4 shows the vast improvement in signal fidelity that the HuygensE Catheter brings to bio-tissue impedance capture when the signal amplification, filtering and processing occurs at the catheter tip. Further that this method then allows the analog signal to be converted to a digital format before having to travel back to the mapping computer, thereby preserving an accurate and much higher resolution signal.

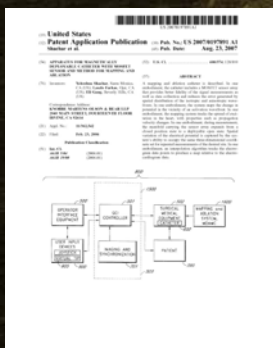


- Quality of the sensing electrode to isolate targeted tissue impedance versus all the other extraneous and ambient noise.

These issues also point to the second major limitation that needed to be overcome with the electrode mapping technology available at the time; the ability to ensure the message received is the same as the message sent. The signal path for heart mapping is not a one-way road. Not only must an electrical signal travel cleanly to the electrode tip, but it must also then be discharged against the tissue being examined, measure the resulting reading, and send it back down the catheter to the diagnostic equipment for decoding into a language the physician can understand. Since the signal is at the millivolt level in a radio frequency analog spectrum, it is easy to see how difficult it is to maintain a consistent, quality reading. It is very much akin to trying to maintain an AM radio station

on your car as you travel further and further from the originating tower. We have all experienced this phenomenon: as we get further from the transmitting source, that great song we were listening to first begins to get distorted and then fades away as more and more interfering RF waves contaminate the signal and the originating signal grows weaker and weaker. We can always try a bigger antenna but at some point, distance and signal strength will be compromised and finally lost. Add to that what happens when you travel under a bridge or through a tunnel, now the signal is not just getting worse, it gets completely cut off.

The solution to these problems was easily realized. Instead of having the signal travel to the mapping computer before processing, it would be better to create a catheter that could do all the processing at the catheter tip, convert that already processed signal to a digital format that could not be



**System And Method For Radar-Assisted Catheter Guidance And Control**

US 2005/0096589 A1)  
05/2005

## Expanding Innovation

Over the past twenty years, the engineering teams under the leadership of Josh Shachar have pushed many of the boundaries of what is possible in advanced medical device technology. As a result the companies have generated hundreds of new innovations which have been identified and protected through a vigorous patent application and procurement process. To date, more than 240 patents have been filed covering a wide array of invention which have all been focused on improving the healing arts.



**Apparatus For Magnetically Deployable Catheter With MOSFET™ Sensor And Method For Mapping And Ablation**

US 2007/0197891  
10/2009



compromised through transmission, and send that digital signal to the mapping station. This was a perfect solution in theory but realizing it had never been attempted or done.

This is where the advanced biosensor technologies and micro-miniaturization capabilities that had been underway at PKC since 2004 were integrated into helping to create a next-generation mapping catheter. Josh envisioned a technology where the bioelectrical signal being taken by the electrode could be amplified and recorded on a miniaturized micro-processing strip located inside the distal end of the catheter tip. In August of 2007, Magnetecs filed its first patent for this catheter technology titled “Apparatus For Magnetically Deployable Catheter With MOSFET™ Sensor And Method For Mapping And Ablation” (US 2007 /0197891 A1). The MOSFET™ Catheter, which stands for Metal-Oxide-Semiconductor Field-Effect Transistor, sought to solve both issues and provide a quantum leap forward in catheter-based EP electrode technology by providing:

- A source-point signal amplifier in the catheter tip to eliminate signal degradation.
- A sensor array that is much more efficient at distinguishing relevant data from extraneous noise.
- A method for interpreting the resulting data at the sensor

point instead of the post-signal processing being done at the time.

- Conversion of the analog information to true digital information after processing to transmit the signal readings in a high-definition, uncompromisable language back to the physician

With the basic concept, engineering, and math issues laid out, the engineering team began a dedicated program of system development, prototype testing, and proof-of-concept validation to bring this idea into reality.

## MOVING CGCI FORWARD

On the CGCI™ front, in 2007 after solving scalability issues and making major advancements in the needed supporting technologies for user interface, power control, and safety, as well as integrating artificial intelligence and robotic-assisted guidance to provide autonomous guidance for the ability to return a catheter automatically to a pre-mapped and targeted position, the team created a 2/3rds scale version of the CGCI™ and began its initial animal study to show guidance and targeting efficacy.

The study, which was performed at Cedars Sinai Hospital in Los Angeles, CA, consisted of 15 subjects undergoing a simulated AFib procedure to show the ability of CGCI™ to



Introducing the future of Robotic Cardiac Mapping and Ablation:

# MAGNETECS | CGCI

CATHETER GUIDANCE CONTROL AND IMAGING

CGCI is a precise and highly efficient robotic catheter control system developed by Magnetecs Corporation for minimally invasive procedures. The system represents a quantum-leap forward in the advancement of magnetically controlled catheter guidance technology.

The system's magnetic array consists of eight electromagnets in a unique configuration for intelligent guidance of a magnetically-tipped catheter, enabling a physician to precisely and consistently control surgical tools in highly dynamic or previously inaccessible environments while enhancing catheter stability, the physician's dexterity and the patient's safety.

The first application of the CGCI System is Electrophysiology for cardiac mapping and ablation procedures to correct arrhythmia. Magnetecs expects patients to benefit from improved safety and efficacy provided by the CGCI system and also expects a significant reduction in repeat AFib procedures currently needed to control arrhythmia. Hospitals are expected to benefit from the increased efficiency and patient throughput provided by this new robotic electrophysiology technology.

## CGCI BENEFITS

- Precise control
- Consistent and accurate target acquisition
- Increased catheter stability
- Transmurality of ablations
- Shorter procedure time
- Increased safety and efficacy

### MAGNETIC LOBE TECHNOLOGY

Eight dynamically regulated electromagnets create a magnetic lobe to provide 3-dimensional control with 5 degrees of freedom of movement.

### MINIMAL RADIATION EXPOSURE

CGCI's contained magnetic field allows the operating room to function as a standard non-magnetic EP lab.

### INTEGRATED CONTROLS

The CGCI Symphony™ Interface integrates advanced guidance and diagnostics systems.

### ADVANCED CATHETER DESIGN

CGCI catheter design provides greater flexibility and decreased tissue distortion compared with existing remote navigation catheters.

move a catheter to an identified target site, remember the location and then return automatically to the site on a repeated basis. The study also tested the ability of the CGCI™ to perform a simple Atrial Ablation procedure.

The success of the initial study opened the door for the company to begin the path to achieving the regulatory compliance certifications that would be required as they moved to commercialization. The first of these was USDA authorization which was quickly followed by UL Certification and ISO-13485 approval. With these in place, Magnetecs constructed a full-scale version of the CGCI™ in a dedicated operating suite at the University Hospital of La Paz in Madrid, Spain, to undergo its first human clinical trials.

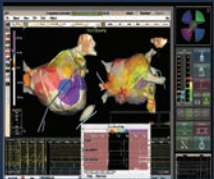
Phase One trials began in 2010 under the direction of Dr. Gang and Dr. Jose Merino. The first study consisted of 20 patients in which a highly detailed map of the heart was created along with several key target points within the various chambers being identified using a standard EP mapping catheter which had been modified with a magnetic tip. Once the mapping was completed, the catheter was moved back to its starting point and then guided robotically by CGCI™ back to the heart chambers and each identified target location. Phase One testing was successfully completed in January of 2011 and Magnetecs immediately moved into Phase Two trials of the human study which were completed in July

## CONTROL CONSOLE INTERFACE



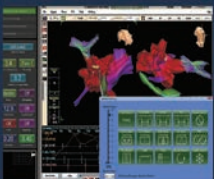
### INTUITIVE NAVIGATION CONTROL

Intelligent user interface gives the physician complete navigation control of the entire platform for true automaticity both in mapping and ablation procedures.



### ATRIAL ACTIVATION MAPPING

Atrial activation mapping technology allows the physician to accurately view the procedure environment.



### ADVANCED SYSTEM MONITORING

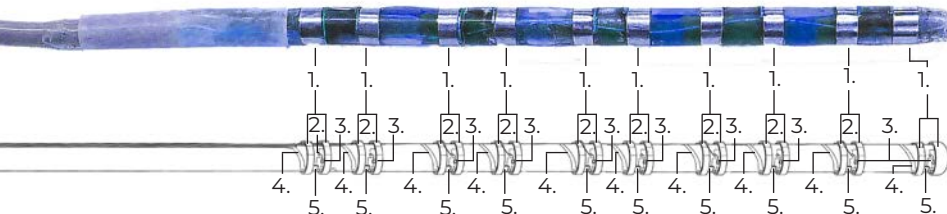
Continuous system monitoring provides real-time feedback on the operational status for every component of the CGCI platform.

of that same year. A Phase Three study consisting of 56 patients with diagnosed AFib was then constructed. The study aimed to perform a series of atrial ablation procedures of which 18 were paroxysmal atrial ablations. The study showed a dramatic 80% efficacy rate. The trial was completed successfully in December of 2011 allowing Magnetecs

EP electrode catheter. Simulated cardiac QRS signals (heartbeat rhythms as you would see on an EKG) were created by a programmable generator and measured along two different signal paths. One employed a post-amplified, current electrode technology, and the second channel utilized the locally amplified MOSFET™ sensor technology. The

## MOSFET™ ADVANTAGES

*In developing the MOSFET™ Catheter the engineering team was able to advance many new approaches in micro-miniaturization that allowed them to bring proximal end signal processing into a reality. These breakthroughs have been expanded and built upon into the creation of NKC's new Huygens™ Catheter technology*



1. Electrode Tip and Rings
2. Catheter Capacitor
3. Catheter Resistor
4. Power Leads and Output Connections
5. MOSFET Amplifiers

to apply for and be granted its CE Mark certification, which gave the company permission to begin commercial sales of CGCI™ in the European Union.

## THE MOSFET™ CATHETER

In September of 2012, Magnetecs successfully completed an initial, or pathfinder, MOSFET™ Catheter prototype that validated the concept of utilizing the localized amplification characteristics of MOSFET™ technology to increase the sensitivity and accuracy of bioelectric potential measurement.

The study showed a comparison of a local amplifier employing MOSFET™ versus a remote amplifier with a standard

first signal that was tested was tuned to just under 50 millivolts by adding a series of attenuators to the input signal of a standard electrode catheter which resulted in a total signal gain of 128. This post-amplified signal was sent through the catheter and the return signal was then measured to determine if any signal loss occurred. Not surprisingly, the measured signal was nearly imperceptible at this level due to noise degradation that had occurred along the signal path. In other words, the signal was virtually useless.

In contrast, when the same signal was run through the pre-amplified MOSFET™ path, it was shown to be well-formed and the cardiac properties



of the heartbeat were clear. The total signal gain was only 100 simply by moving the location of the gain block from one end of the catheter to another.

When the QRS-simulated signal is captured by the local amplifier in the MOSFET™ Catheter, the result was substantially identical to the “pure” standard.

### MAGNETECS COMES TO A TURNING POINT

By 2014 Magnetecs had expanded its CGCI placements to continue its global regulatory and commercialization efforts. In addition to the installations at Magnetecs headquarters, Cedars-Sinai Hospital in Los Angeles, and the University Hospital of La Paz in Madrid, two more installations were completed at the Yonsei Severance Hospital in Seoul, South Korea, and the Na Holmoche Hospital in Prague in the Czech Republic.

By 2015 Magnetecs had filed more than 90 patents on its CGCI™ system, its MOSFET™ Catheter, and a SMART catheter guidance sheath called the Lorenz™ Active Sheath. The system had been proven a success in re-imagining what catheter guidance and cardio-mapping could do and the company was entertaining many options for pursuing its commercialization path forward.

Unfortunately, a global economic downturn effectively dragged to a standstill the ability of most growing

## CGCI INSTALLATIONS

*By 2014, Magnetecs had expanded its CGCI installations to five operating suites around the globe.*

### **CGCI - Inglewood, Ca USA**

*Magnetecs Headquarters Director: Josh Shachar*



### **CGCI - Los Angeles, Ca USA**

*Cedars-Sinai Hospital Director: Dr. Eli Gang*



### **CGCI - Madrid, Spain**

*La Paz University Hospital Director: Dr. Jose Merino*



### **CGCI - Prague, Czech Rep.**

*Na Holmoche Hospital Director: Dr. Petr Neužil*



### **CGCI - Seoul, South Korea**

*Yonsei Severance Hospital Director: Dr. Hui-Nam Pak*





advanced medical device companies to achieve any ground in market share as hospitals, research universities, and the entire medical field was faced with the need to dramatically cut costs and budgets for not only new development but for core programs as well. Magnetecs was not immune to this new fiscal

reality. Rather than abandon its efforts, the management team believed that the temporary reverse in economics could be used to the company's advantage.

Magnetecs underwent a thorough re-organization of the entire company to make it leaner and more agile for the new economic reality. It re-evaluated

## The BIOSENSOR

*One of the cornerstone innovations developed by Josh Shachar was the creation of a new biosensor technology. In its simplest form, a biosensor is a device capable of identifying and or measuring a biological target of interest and converting that measurement into a digital signal which is then able to be processed by computational algorithms for whatever application is being applied. The biosensors developed by PKC Group of Companies ranged from being able to measure the biometrics of a patient, pathogenic biomarkers for diagnostic disease mitigation, environmental contaminants in food, air and water, the concentration and uptake of therapeutics being delivered to a tumor site, and the bio-conductive potential of tissue as it applied to NKC's technology. The images here show some of the biosensor types invented and the subsequent technologies the flowed from them*



First generation biosensor



SAW Biosensor for Optikus™ pathogen detection



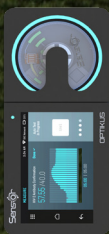
Lab-On-Chip biosensor for the Primus™ detection system



Biofet biosensor



PRIMUS™



OPTIKUS™



SMART Brain Retractor



MBP



SINNAISS™



CMMD



RPPD



PathSMART™



OvaSMART™



Tumor Fighter™



all existing relationships and contracts with strategics and vendors as well as re-negotiated relationships with its partners that would be favorable to not only staying viable during this period but poised for dramatic growth once the economy turned around.

## **PHARMACO-KINESIS - BUILDING THE BRIDGE BETWEEN THE BIOLOGIC WORLD and the DIGITAL DOMAIN**

Jumping back in time to 2004, in addition to the work being done at Magnetecs, Josh Shachar along with Dr. Gang, Frank Adell, and noted neurosurgeon Dr. Thoma Chen, Ph.D., Director of Surgical Neuro-oncology at USC, had begun work on developing a new implantable drug-delivery pump for solid tumor treatment that would incorporate some of the advanced biosensor technology Josh had been developing, along with a capability of controlled metronomic micro-dosing and wireless AI-enhanced communication. The technology, known as the Magnetic Breather Pump (MBP) at the time, had developed from the drawing board to a proof-of-concept bench-top model and by 2008 was ready for prototyping and testing. Pharmacokinetics Corp. (PKC) was formed and the company began to raise capital to pursue its regulatory and commercialization efforts. Over the next seven years, the advancements in PKC's biosensor and pump technology had generated

many breakthrough improvements in the ability to capture and measure very small biological signals of interest, whether electrical or organic in nature.

In addition, the biosensor technology was able to provide real-time feedback to the operator on the measurements being made which allowed either diagnostic or therapeutic action to be taken immediately. In the case of the MBP, this meant a treating oncologist could monitor the effectiveness of a chemotherapeutic the pump was delivering into a tumor bed and have the ability to adjust dosages up or down accordingly.

In developing this technology for the MBP, PKC began the development of a separate medical device that could measure a biomarker of interest in the fluid sample to identify not only the presence of but the amount of the biomarker that was present. This application opened the door to a whole new way of dealing with diagnostic medicine, in that a biomarker could be analyzed in the field with clinically relevant diagnostic confirmation data being given in a matter of minutes instead of waiting days or weeks for a lab analysis to be made. In the case of an infectious pathogen, such as Ebola, this could mean the difference in response from a small quarantine versus dealing with a widespread epidemic or pandemic. In the case of a biomarker such as Troponin which is the leading indicator for a heart attack, diagnostic data could be done at

the scene of a patient episode or in transit to the hospital so that proper treatment could be immediately determined and taken.

Of equal importance during this time was PKC's efforts in miniaturizing all the components needed for the pump and the pathogen detection technology down to systems that could be implantable, in the case of the pump, or portable, in the case of the pathogen detection system. In this effort, PKC's engineering team was able to make significant breakthroughs in developing lab-on-a-chip and lab-on-a-disk technologies, that could take what normally required a large dedicated laboratory space, very expensive equipment, and trained technicians, and reduce this down to a microchip-based system that would automatically handle diagnostic measurement, data processing, and data communication between the patient and the treating physician.

In addition to these technologies, PKC had also developed patents on a variety of ancillary devices including a SMART Brain Retractor, that could provide a neuro-surgeon with instant feedback on cerebral tissue biometrics during a brain surgery that would mitigate additional tissue trauma, a Vertebral Body Motion Sensor, SMART device that would allow physicians to monitor a patient's spinal alignment after spinal fusion surgery, and an implantable tooth medicated dispenser that would provide an easy method by which certain therapeutics,

such as pain medication, could be delivered to a patient's bloodstream in a metronomically controlled fashion. Other devices such as a skull-mounted optical sensor, a post-surgical pain abatement device, and even a SMART Shoe that detected changes in the acceleration and pressure of a user's foot, were technologies that came from this period. In total PKC filed more than ninety patents for these innovations.

## **THE FORMATION OF NEURO-KINESIS**

It was at this juncture in 2015 that a decision was made in light of the divergent technologies and the economic turn-down, to separate PKC into the four separate companies mentioned earlier so that efforts could be consolidated to focus on furthering each technology stream. In creating NKC, a decision was made to also roll the Magnetecs IP into NKC as part of the mission for developing SMART surgical tools.

Since that time, NKC's efforts have been solely on taking all the components and technologies developed in its creation of CGCI, MOSFET, the SMART biosensor development, and its micro miniaturization and AI enhancement breakthroughs and revision them for the new economic reality as well as the changes that had occurred in the EP field since 2002.

# PROTEUS™ ROBOTIC ARM

The first portable plug-and-play robotic-assisted AI Catheter Guidance System



## RE-VISIONING CATHETER MAPPING and GUIDANCE

Two unique problems were identified that needed to be addressed to meet these new goals. One was to find a way to take robotic catheter guidance from the 9-ton CGCI, with its need for a dedicated operating suite and specially trained technicians and reduce this down to a portable plug-and-play system that could be installed in any standard EP operating room. The second was to find a way to further refine the catheter mapping technology that could reduce the signal-to-noise ratio in the bioelectrical measurements beyond what MOSFET had been able to accomplish, while significantly increasing the sensitivity of the electrodes to measure even smaller electrical voltages in order to provide higher resolution 3D maps for the EP surgeon.

## THE PROTEUS™ ROBOTIC ARM

In the case of the robotic catheter guidance system, a whole new approach was taken that involved creating a shoe box-sized mechanical device that could provide an EP surgeon complete and fine-grain control of catheter translation (forward and backward movement), rotation, and tip deflection using a simple joy-stick Haptic controller. The result is the Proteus™ Robotic Arm which in essence reduced the CGCI system from a 9-ton structure to a 9kg device that could be held in one hand. The Proteus™ utilizes three independent drive systems to control catheter movement for rapid intravascular navigation or small precise movement inside the heart. All movement is recorded by the system's navigational software which enables user-designated fine movements of the catheter tip as macro-commands that can be user-

activated via a control interface. Further, the Proteus™ addresses the current drawback that requires a lengthy training period measured in years, to permit the clinician sufficient dexterity and muscle memory in performing the very small multi-plane changes in the position of the catheter within a beating heart. With Proteus'™ ability to command these fine movements without manually needing to rotate and steer the entire catheter, the stage was set to provide a large improvement in the success rate and safety of these procedures. By reducing the margin of human error, robotic assistance can flatten the otherwise relatively steep learning curve of present and future clinicians. The computer-aided return of a catheter tip to a designated site, or multiple sites stored on a mapping system, is very useful in clinical settings such as:

- Sites previously ablated which had resulted in a temporary cessation of a rhythm or achieved a specific EP end-point.
- Sites previously designated as “areas of interest” during a baseline mapping of a cardiac chamber.
- Multiple sites which comprise a specific designated “lesion set”, such as a line connecting two anatomic structures in the heart.

The Proteus™ Robotic Arm also utilizes a specially designed catheter handle which can be used manually as any traditional catheter steering

device currently being used, but also seamlessly slips into the Proteus™ Robotic Arm for robotic assisted computer guidance. Although designed specifically to work with NKC's catheter technology, the handle can be adapted to accommodate most standard EP catheters on the market today.

## THE HUYGENS™ CATHETER

In addressing the catheter mapping goals, NKC made several breakthrough advances to develop a cutting-edge device that advanced their previous achievements to whole new levels of success. Named the Huygens™ Catheter, after Dutch mathematician, physicist, astronomer, and inventor, Christiaan Huygens, who is widely regarded as one of the greatest scientists of all time, the catheter incorporates several key technology improvements that set it apart from all other mapping catheters. These include:

- The ability to provide a correlation of substrate and anatomical mapping.
- Improved amplification and signal pre-processing.
- Orientation-independent electrode configuration.
- Lossless optical data transfer.
- Photo-voltaic power supply.
- Contact sensing, force control, and haptics.



- Integration with Proteus™ automation and robotic-assisted guidance.
- AI and machine learning capabilities.
- An open architecture platform.

Details of this are addressed in the next section of this book, but the summation is that the Huygens™ Catheter provides the capacity to address many of the current issues in EP mapping such as balancing the need for both substrate and anatomical mapping in one procedure as well as delivering a 3D cardiac map that is 200x higher in resolution than current mapping technologies provide.

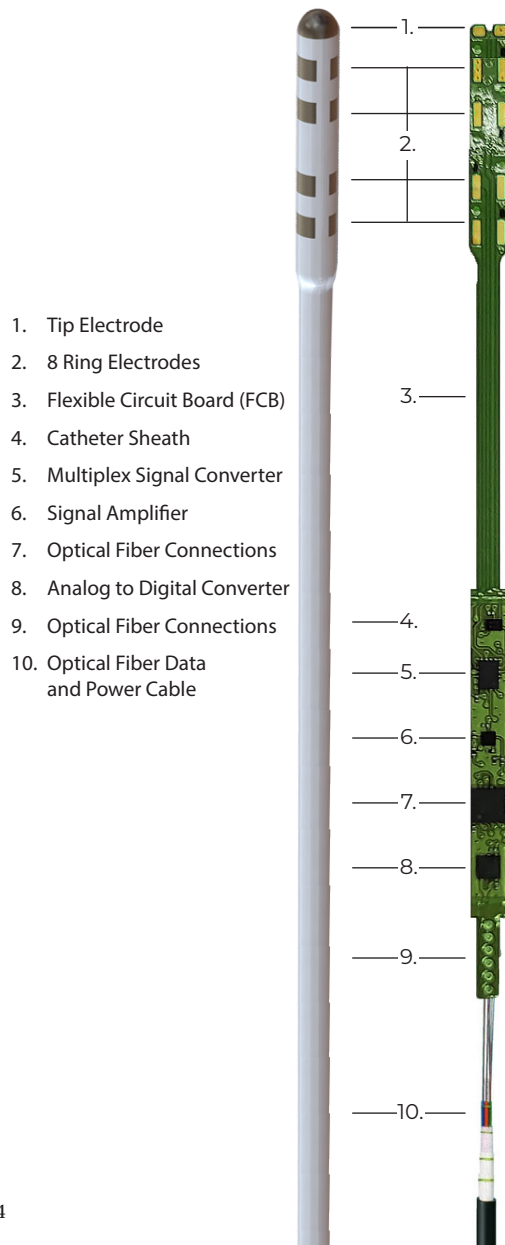
## THE HUYGENS™ – PROTEUS™ ROBOTIC SURGICAL PLATFORM

Together the Huygens™ Catheter and the Proteus™ Robotic Arm form the basis for the Huygens™ – Proteus™ Robotic Surgical Platform which combines the next-generation mapping catheter and the plug-and-play robotic guidance system with NKC’s guidance control operating station, and the NKC mapping station. The complete system can be installed in any standard EP operating room and the learning curve takes a fraction of the time to learn.

The Huygens™ – Proteus™ Robotic Surgical Platform is poised to provide the EP physician with pioneering new abilities to perform

# HUYGENS™ CATHETER

*The Huygens™ Catheter represents a major advance in EP Catheter mapping technology. With Huygens™ NKC has exponentially expanded on its innovation with the MOSFET™ Catheter technology by bringing complete AI-enhanced algorithmic signal processing of bioelectrical tissue sampling into a system completely contained within the catheter sensor tip. This advance provides a resolution increase of 200x over current technology. In addition the Huygens™ Catheter is able to convert the analog signal capture into an incorruptible digital format for processing and transmission to the NKC Mapping Station.*



1. Tip Electrode
2. 8 Ring Electrodes
3. Flexible Circuit Board (FCB)
4. Catheter Sheath
5. Multiplex Signal Converter
6. Signal Amplifier
7. Optical Fiber Connections
8. Analog to Digital Converter
9. Optical Fiber Connections
10. Optical Fiber Data and Power Cable

their art with greater precision and greater patient success by providing an exponential leap in mapping resolution and catheter guidance.

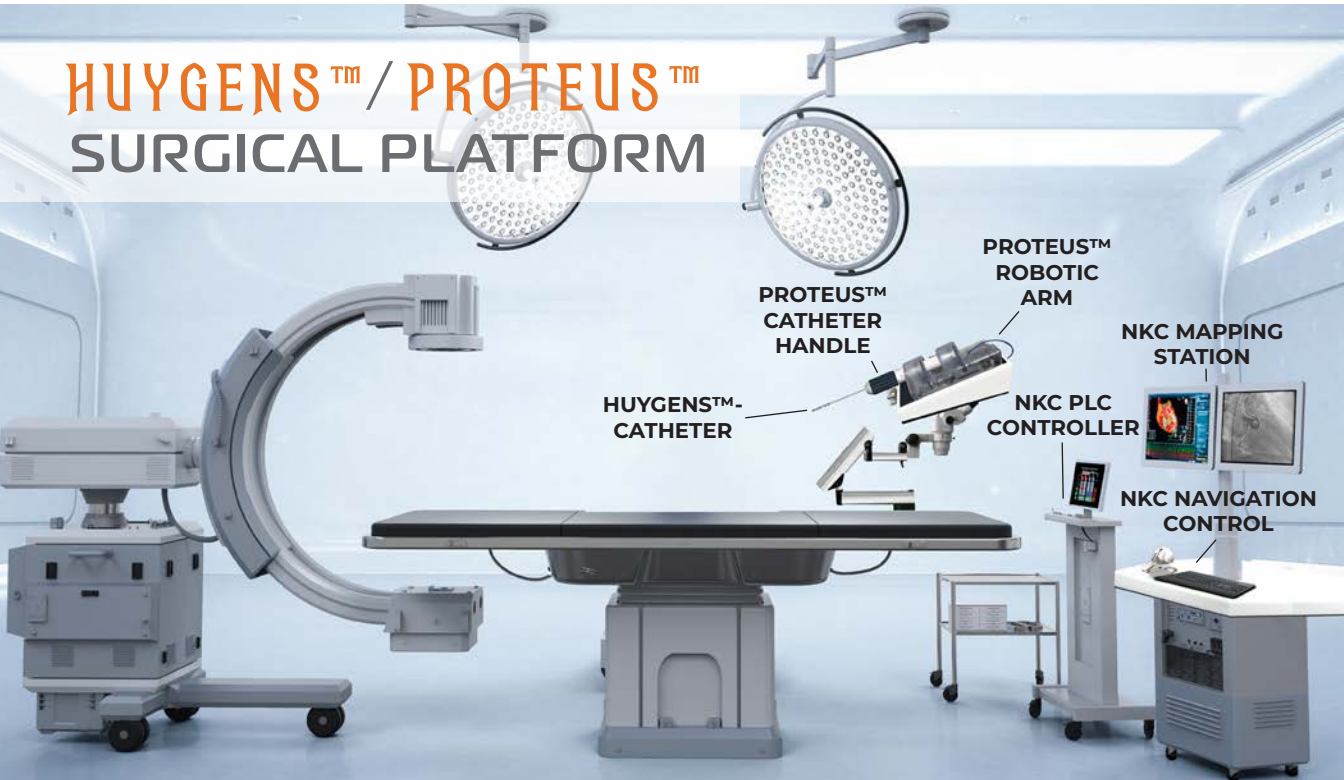
## RENAL DENERVATION - A NEW APPLICATION

With this advancement, NKC has also opened the door to new areas of potential cure in the EP world. The rapid growth in illness and death related to hypertension has put tremendous pressure on the medical field to develop better cures for those whose high blood pressure cannot be remedied with medication and lifestyle changes. One of the potential cures that have been of great interest is in Renal Denervation (RD). RD seeks to minimize or eliminate persistent hypertension through the

ablation of the renal nerves in the kidney that regulate the release of renin, a protein produced by the kidneys that regulate the body's mean arterial blood pressure. The basic proposition and understanding of how RD can impact hypertension have been well researched and extrapolated, but effectively being able to perform the procedure with consistent degrees of success has fallen far short of expectations. The issue is twofold and lies in the inability of current EP mapping and detection tools to be able to overcome certain challenges.

The first is that unlike the nerves in the heart, which are well known and fixed in their location, the sympathetic renal nerve formation and locations are individualized to each person. Much like a tree, the renal nerve plexus consists of a

# HUYGENS™ / PROTEUS™ SURGICAL PLATFORM



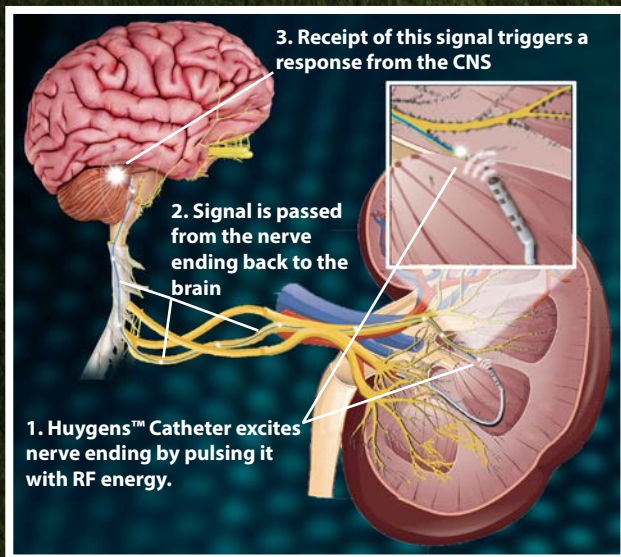
branching network of nerves that grow out from one another and attach to the renal artery in completely random locations. This makes locating them much harder to do. The second issue is that the electrical signals that the nerves produce are not a consistent regular pattern as can be measured in the beating of the heart, even an irregular beating one. Instead, electrical impulses only occur when a biological event occurs that triggers the nerve to signal the brain, which then signals back to the kidney to release renin. It is much like trying to find a road that can only be seen when the streetlight comes on except that you have no way of knowing when that will happen. In addition, the signals that are produced are of a very high frequency and extremely short duration which makes capturing them for mapping purposes extremely difficult with the resolution of current EP mapping systems.

The Huygens™ Catheter has the potential to change this paradigm and open the RD procedure to the success that has eluded efforts to date. First, the Huygens™ Catheter has the ability to generate a nerve signal to occur by “pulsing” spots in the renal artery with a small electric current. When the current is applied it excites the nerve end creating the impulse signal that causes the brain to return the triggering signal back to the nerve end. This ability to, in essence, turn the lights on for each renal nerve pathway,

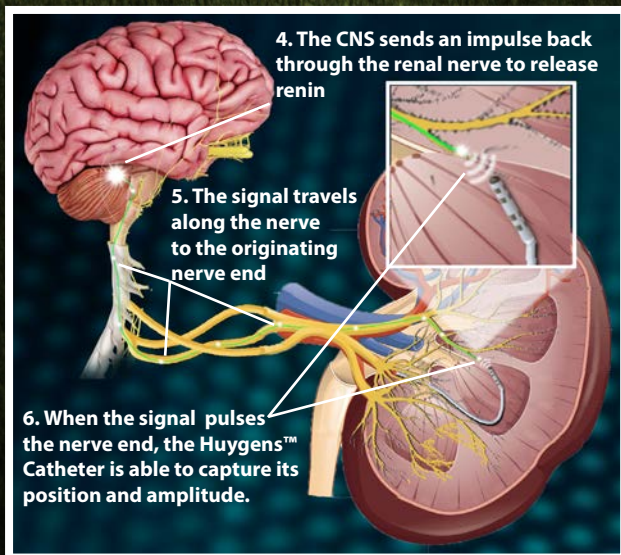
## RENAL DENERVATION

*Unlike endocardial tissue mapping where electric signal pulses are rhythmic and source points are known, in mapping the bioconductivity of renal tissue, the measurable electric impulse only occurs when a significant event is registered in the brain causing the nerve pathway to be excited in order to trigger the release of renin. The difficulty in mapping this intermittent signal is further complicated as the nerve bundles in each person's kidney is like the root system of a tree in its uniqueness of branches and pathways. With the Huygens™ Catheter, NKC is positing an approach that could make renal denervation a viable and effective treatment protocol.*

*The image below shows how the Huygens™ Catheter is positioned into the kidney to where the EP surgeon suspects the renal nerve plexus is located. The catheter tip is then moved across the tissue while it is emitting a RF signal which when it comes in contact with a nerve ending, will excite that nerve pathway causing the signal to be relayed to the CNS, in essence telling the brain that a significant renal event has occurred.*



*In response the brain then sends an impulse back down the nerve pathway telling it to release renin into the kidney. This impulse “lights-up” the termination point of the nerve allowing the Huygens™ Catheter to capture its position and bioconductivity. By repeating this process, much as in cardio-mapping, the EP surgeon is able to construct a renal map and determine where ablation should be done to correct the issue being treated.*





allows for accurate and rapid mapping of the patient's specific renal nerve plexus to provide the EP physician with the data points needed to perform an effective RD ablation. Secondly, by giving the EP physician a working technology that can actually "see" and "hear" these very short high amplitude signals, the current guesswork associated with attempts at ablation for RD can be greatly reduced. When this ability to map is coupled with Proteus™ Robotic Arm's ability to provide robotic guidance of the ablating catheter back to each identified nerve ending, NKC has indeed shifted the paradigm for Renal Denervation success.

## **MOVING FORWARD**

At the time of this publication, NKC has already filed eight patents related to the Huygens™ IP and has assembled a solid regulatory team to manage the company's trajectory to achieving both FDA and CE Mark certification to allow the platform to be commercialized in the U.S. and EU. Initial animal study protocols have been established to this end and these studies are set to be conducted in the third quarter of 2022.

Application for an Institutional Animal Care and Use Committee Approval (IACUC) has been filed for the study to be done at the Technion Institute in Haifa, Israel. The study will be conducted by both Dr. Eli Gang and Principal Investigator Dr. Rona Shofty, DVM, Ph.D., DALAM.

The study will demonstrate the ability of the Huygens™ Catheter to generate clinical data that is superior to the existing art. Specifically, the study is designed to demonstrate the ability of the Huygens™ Catheter to perform detailed mapping and target acquisition procedures in all four chambers of the test subject's heart. Success in this study will constitute proof-of-design adequacy and equipment safety in reaching the efficacy and safety goals established in the study protocols.

A separate agreement is also being finalized with Sandia National Laboratories to perform real-time simulation studies of the system under the guidance of Dr. Darren W. Branch, PhD., and is anticipated to proceed concurrently to demonstrate the embodiments that differentiate the Huygens™ Catheter from any other catheter in the marketplace today.

In addition, NKC is undertaking the installation of a full lab facility for the Huygens™ – Proteus Robotic™ Arm Surgical Platform at its headquarters in Los Angeles, California by the end of October 2022. Once completed, NKC will begin its internal validation studies in preparation for the above trials.

The lab installation will allow the NKC engineering team the ability to test prototype designs, perform quality control checks, and establish operational and test protocols while gathering the important analytical and



comparative clinical data needed to further its regulatory approval strategy.

With two decades of innovative research and development, and a track record of realizing breakthroughs that push the envelope of what is possible, NKC continues to strive to be the leader in advancing the ability of the physician to bring healing to their patients everywhere.





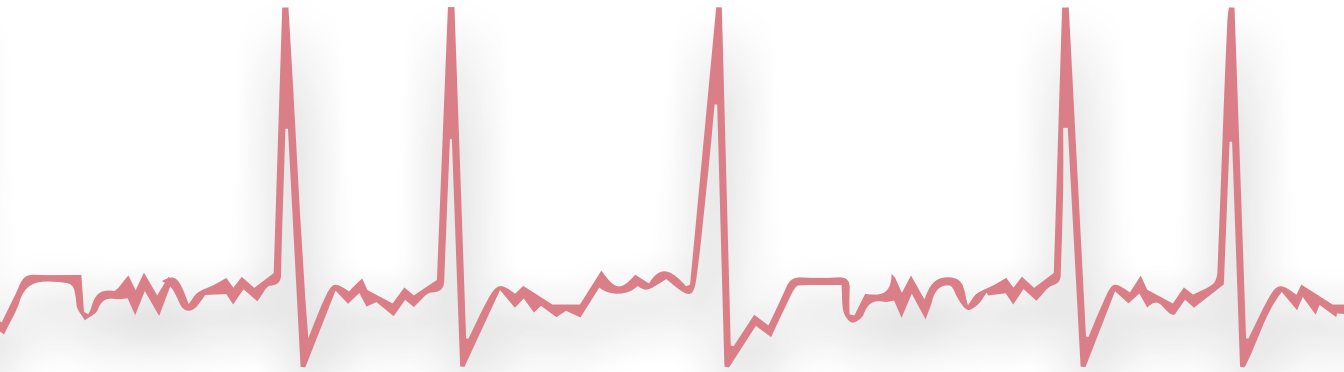
CREATING



A NEW  
PARADIGM

FOR  
EPMAPPING

In Cardiac Electrophysiology (EP), one of the most challenging problems remains in finding a definitive cure for atrial fibrillation (Afib).



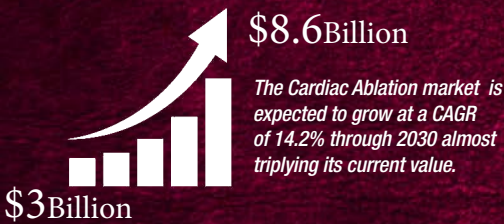
Afib is a type of arrhythmia, or abnormal heartbeat presented when a patient exhibits an extremely fast and irregular heartbeat from the upper chambers of the heart; generally exceeding 100 beats per minute.

In a normal, healthy heart, the heart contracts about once per second at rest and increases with exercise. Each contraction pushes blood from the atria (the two upper chambers) to the ventricles (the two lower chambers). The ventricles then contract and push the blood to the lungs or the rest of the body. In a person with Afib, faulty electrical signals irregularly make the atrial contractions, and with much faster pacing. The atria then gets out of sync with the ventricles. Blood can pool in the atrium, which can lead to blood clots and strokes. Afib can cause many issues for a patient including extreme fatigue, heart palpitations, dizziness or lightheadedness, shortness of breath, fainting, and chest pains. Severe Afib is also a major contributor to heart disease, stroke, and heart failure.

Afib remains one of the most common cardiovascular diseases in our society today, affecting 2.7 to 6.1 million people in the U.S., with increased morbidity rates due to thromboembolic stroke, congestive heart failure, cognitive dysfunction, and increased mortality. The curve of the increase has the potential to overwhelm our healthcare system. Current treatment modalities lie in two strategies; pharmacotherapeutic and surgical. Pharmacotherapeutic treatment of AF has been frustrating and frequently ineffective because of the significant risk of potentially intolerable or life-threatening side effects including bradycardia, palpitations, fatigue, nausea and vomiting, vision problems, and urinary retention. For some proarrhythmia is a risk. Proarrhythmia is when a therapeutic

# Mending a broken heart

*Electrophysiology continues to be one of the fastest growing sectors in healthcare; especially in the area of treating heart-related disease issues such as AFib. Due to the nexus of an aging population, increased disease issues such as hypertension and diabetes, and a more sedentary lifestyle, AFib, and other heart pacing issues, continue to be on a dramatic rise. When lifestyle and pharma therapy is not successful, the primary approach to treating these issues is Cardio Ablation. As can be seen by the statistics below, the need for qualified surgeons and effective technology are only going to continue to rise over the coming years.*

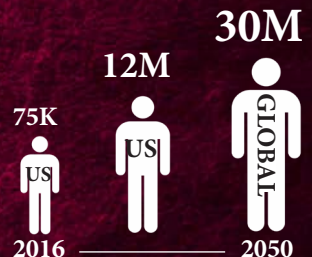


The global ablation device market is anticipated to reach \$16 billion by 2028

A recent study showed that AF ablation procedures had an increase of more than 450% over the 10-year period examined.



The global growth in the number of patients needing AF treatments continues to be of utmost concern.





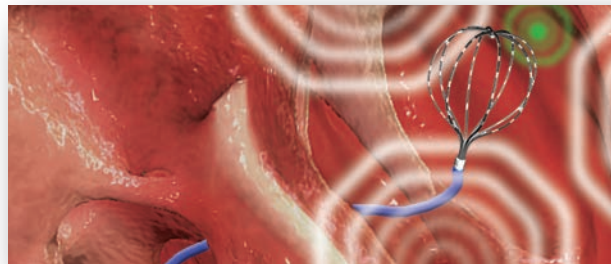
drug used in controlling Afib provokes a new arrhythmia or the aggravation of a pre-existing one. In addition to primary drug therapy, patients generally also must be on anticoagulation therapy. Both anticoagulants and antiplatelet drugs can increase a patient's risk for severe bleeding issues.

On the surgical front, the use of RF catheter ablation (CA) has become the growing choice for EP physicians for treating severe issues of Afib and other arrhythmic cardiac disorders. Although there are many approaches in using CA, such as wide circumferential anatomic pulmonary vein (PV) electrical isolation,

linear lesions (mitral isthmus, roof), PV antrum isolation, PV ostia isolation, continuous complex fractionated electrograms (EGMs) ablation, and autonomic ganglionated plexi ablation, the end goal is generally the same, find where the electrical signal is being disrupted in the atrium's endocardial wall and create a new path to restore the electrical pathway by ablating or creating scar tissue, that forces the signal path to reroute around the damaged tissue.

As currently practiced, all these approaches remain challenging because of the inherent state-of-the-art in the procedure. Some of these issues include:

- 1** The manual nature of the procedure requires a skilled EP surgeon with years of training to move and guide the catheter into the heart and then to successfully navigate the interior for mapping, followed by the ablation process
- 2** The inadequacies of existing catheter electrode technology to capture meaningful signals that are not polluted by ambient noise, signal path degradation, and an inability to measure lower voltage potentials that could provide a more accurate heart map.
- 3** The length of the procedure increases the patient's and the physician's exposure to radiation from the use of fluoroscopy or other imaging devices used by the EP surgeon to see their position in the heart.



Most of these were covered in the “Navigating the Future of Electrophysiology” section of this book, but further explanation is warranted here.

## CREATING THE MAP

To review, CA requires the EP surgeon to first make a 3D map of the interior of the heart chamber(s) to both understand the geometry of the space and to measure the bio-conductivity of the tissue to determine where the electrical current is being interrupted so that ablation points can be established to restore proper sinus rhythm to the heart.

The problem to be solved is how to identify the arrhythmogenic causes of these fibrillations by measuring the impedance value of the tissue, to create an actual measure of the anisotropic wave propagation.

The current state of the art with electrophysiology mapping techniques and its applications is detailed and described in a review paper by Li et al titled “Standardizing Single-Frame Phase Singularity Identification Algorithms and Parameters in Phase Mapping During Human Atrial Fibrillation”<sup>1</sup>, stating that “Recent investigations failed to reproduce the positive rotor-guided ablation outcomes shown by initial studies for treating persistent atrial fibrillation (persAF). Phase singularity (PS) is an important feature

for AF driver detection, but algorithms for automated PS identification differ.”

The authors conclude that “In the present study, we demonstrate that automated Phase Singularity detection – and consequently persAF ablation target identification – vary significantly for the same individual, depending on the method being used and parameters being applied. The present study represents a step toward a unified definition/algorithm of phase-derived PS detection with standardized gradient and spatial thresholds, which is essential to allow objective comparisons of outcomes of rotor ablation for persAF therapy among different research/clinical centers.”

$$H(u)(t) = \frac{1}{\pi} \text{p. v.} \int_{-\infty}^{+\infty} \frac{u(\tau)}{t - \tau} d\tau$$

*Fig 1: The Hilbert Transform is an equation used in mathematics and signal processing that defines a the transform in which phase angle of all components of the signal is shifted by  $\pm 90^\circ$*

As noted by Li et al in a comprehensive monograph noted above, in which the authors’ process of obtaining the spatial coordinates of the PS is based on mathematical-statistical methods where a computational algorithm is capable of sorting the locus of the rotor generator focal position of the electrical activity by employing a “2048-channel virtual electrogram (VEGM) and electrocardiogram signals were collected for 30 s from 10 patients

1 Front. Physiol., 21 July 2020 – <https://www.frontiersin.org/articles/10.3389/fphys.2020.00869/full>

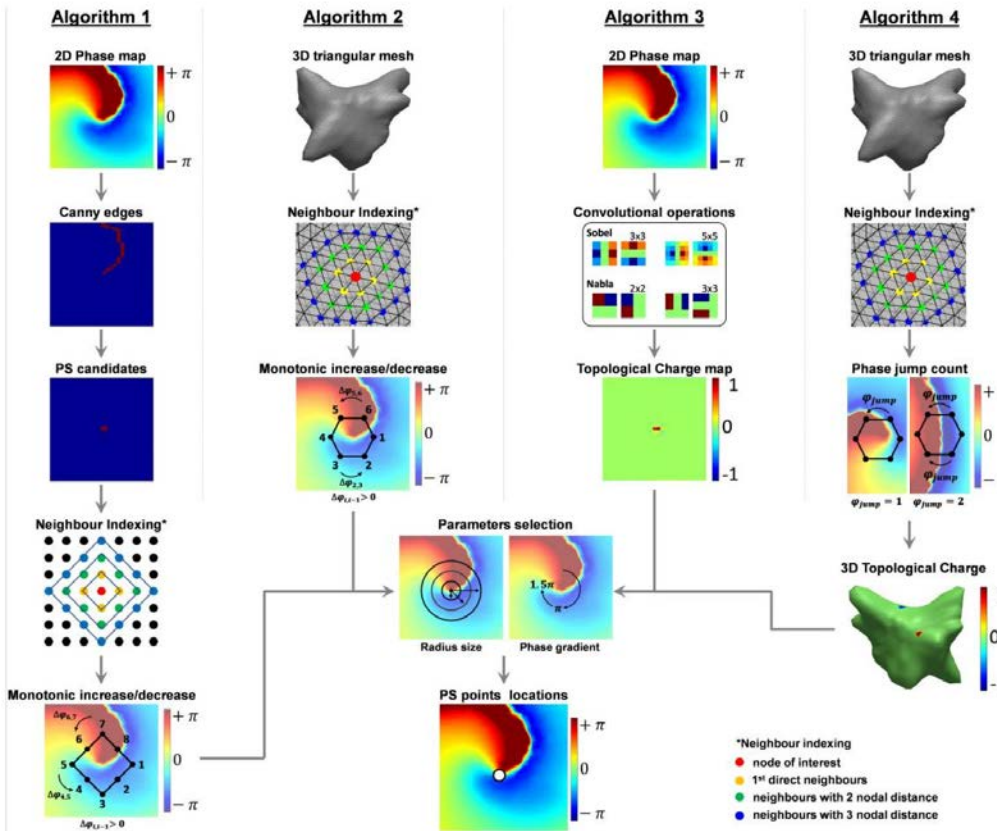


Fig 2: The illustration above shows a representation of the four algorithms used by Li et al. in the research paper titled “Standardizing Single-Frame Phase Singularity Identification Algorithms and Parameters in Phase Mapping During Human Atrial Fibrillation” which looked at ways of creating a unified definition for phase singularity detection as it applied to EP endocardial mapping

undergoing persAF ablation. QRST-subtraction was performed and virtual electrogram EGMs were processed using sinusoidal wavelet reconstruction. The phase was obtained using the Hilbert transform (Fig 1). PSs were detected using four algorithms (Fig 2): (1) two-dimensional image processing based and neighbor-indexing algorithm; (2) three-dimensional neighbor-indexing algorithm; (3) two-dimensional kernel convolutional algorithm estimating topological charge; and (4) topological charge estimation on a three-

dimensional mesh. PS annotations were compared using a structural similarity index (SSIM) and Pearson’s correlation coefficient (CORR). Optimized parameters to improve detection accuracy were found for all four algorithms using F score and 10-fold cross-validation compared with manual annotation. Local clustering with density-based spatial clustering of applications with noise was proposed to improve algorithms 3 and 4.”

It is clear from the four methods proposed and the data acquisition

modes by which the identification of the Phase Singularity is obtained are highly dependent on the complex and subjective selections of parameters which in turn are subjected to the “F score” analysis, due to assignments of non-symmetric preferences of some of the parameters relative value in assessing the locus of the Phase Singularity.

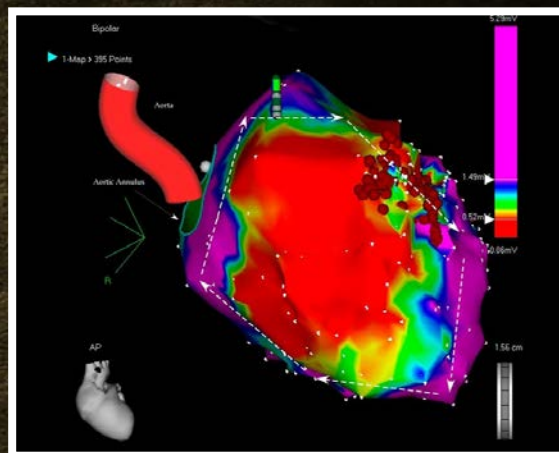
The differentiation between atrial flutter and atrial fibrillation in a location where such phenomenon occurs is another source of error that add

## Reading the map

*The heart map is foundational to the Electrophysiologist’s ability to affect cure. The map provides the EP surgeon all the information regarding the topography of the heart chamber they are working in as well as the health of the tissue strata in its ability to conduct the electrical impulses that keep a heart in proper rhythm.*

*This map shows the anterior-posterior projection of an enlarged left ventricle with a large scar on almost all the anterior wall. Any voltage bellow 0.5 mV (red color) is considered scar tissue and any voltage above 1.5 mV is considered normal myocardium (purple color). In between are three transitional tissues collared in yellow, green and blue. In this case, no tissue penetrated the scar and no central pathways could be mapped. The arrows show the large reentry cycle around the scar and dark red dots show the ablation points the surgeon has chosen to block the isthmus between the two scars.*

Modeling Biopotential Activity with the Poynting Energy Vector (PEV)” described below. This technique is not available anywhere in the leading theories of the underlying mechanisms which defines the difference between a phenomenon called “atrial flutter” and one called “atrial fibrillation”. While flutter is marked by the gap associated with scar and fibrotic tissue, which inhibits the transport of the ionic charge of the wave propagation along the conduction path, fibrillation is a phenomenon



to the identification of Phase Singularity.

The challenge is to develop an apparatus and method for the identification of the locus associated with atrial fibrillation by the use of a mapping catheter that has an ability to measure with near real-time the impedance as well as the tissue potential and thereby solving the variables in the algorithm we employ titled “Signal Anisotropy,

physically correlated with a physical phenomenon described as “rotors”.

In summary, the differentiation between flutter and fibrillation due to the anisotropic behavior of the wavefront dynamics, is the regeneration of the fibrillating foci, where the front of the wave and the tail of the wave are spiraling, while flutter is a simple fractionated electrogram, where the tail is just an



end represented by a capacitance delay. In fibrillation the focus of the energy is a generator where its equivalent circuit representation is a variable resistor. The main difference between fibrillation and flutter is the gap or the nature of the encroachment of the front into the tail: the gap is fully excitable and quite large in flutter, whereas it is smaller and partially excitable in AF, because of the intermingled front and tail. A detailed study of the physics as well as the physiology of cardiac cell

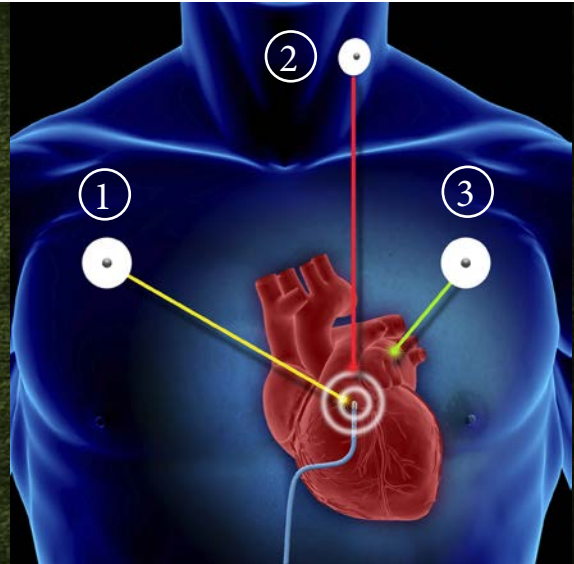
the operation and the related risks. In brief the two types of mapping consist of:

**Anatomical Mapping** – Four RF generating electrode patches are placed along the three orthogonal axes of the patient. One on both sides of the patient’s chest (x-axis), one on the back of the neck (z-axis), and one on the inner left thigh (ground). The three orthogonal electrodes are used to send three independent, alternating, low-power currents of 350 mA at a frequency of 5.7 kHz through the patient’s chest

# M Mapping the surface

*In order to map the topographical surface of a heart chamber, the EP surgeon utilizes an anatomical mapping technique where three electrode are placed on strategic points on the patient’s body; the left chest, the right chest and the back of the neck. RF signals are sent sequentially from each of the three electrodes into the patient’s body.*

*Once the EP catheter tip is in place inside a heart chamber, the EP surgeon moves the tip to a point of contact on the endocardial tissue. The catheter electrode is able to detect the “Time of Arrival” of the electrode signals. By calculating the time difference between signal sent and signal received by the catheter sensor, the mapping software is able to triangulate a position in 3D space of where the catheter is located. By repeating this process, the EP surgeon is able to build up a topographic map showing him the shape of the heart chamber walls as well as the location points of valves, veins and arteries.*



mechanism is articulated by Sandeep V. Pandit and José Jalife “Rotors and the Dynamics of Cardiac Fibrillation”.

Currently, there are two types of CA-based heart-mapping techniques, anatomical and substrate. The EP surgeon generally uses one of the two, and in rare instances may use both, but doing so dramatically increases the length of

with slightly different frequencies of approximately 30 kHz used for each direction. The catheter electrodes in the heart pick up these signals which are sent back to a mapping computer. The mapping computer is then able to calculate the time between an electrode signal’s time of origination and the catheter’s reception of the signal. By calculating these three time differentials,

a geographic point can be triangulated to create a point inside the heart in 3Dspace. This is repeated by advancing the catheter around the interior of the heart until the EP surgeon determines a sufficient map has been generated for him to create a road map for ablation.

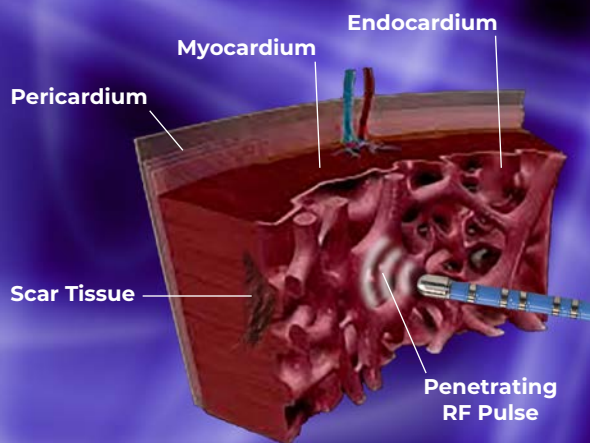
Obviously, the more points gathered the more detailed the map will be. But doing this manually is extremely time-consuming and all the issues related to dexterity, signal degradation, and length of procedure come into play.

## Below the surface

*In substrate mapping, the EP surgeon is looking to determine both the depth of the cardiac tissue as well as the tissue's electrical bioconductivity. In RF Catheter ablation the surgeon is diagnosing where the electrical energy flow needed for proper sinus rhythm of the heart is being disrupted by damaged or scarred tissue. Such tissue will generally have a denser mass than healthy tissue and therefore create a barrier to the flow of the heart's electrical currents.*

*To determine what is happening below the surface, the EP surgeon makes contact with the outer endocardial tissue and sends an electrical impulse into the surface. This allows an impedance resistance measurement to be taken to determine the status of the tissue. Again by repeating this process over and over, the surgeon is able to generate a map of the endocardial, myocardial and pericardial tissue in the patient's heart.*

Substrate mapping essentially looks at the density of the tissue by measuring the impedance differential of a small microvolt signal that is passed through a contact point by the catheter electrode into the endocardial wall. The electrode measures the impedance differential between the signal generated and the signal returned in order to determine the viability of the tissue. Heart tissue that has become ridged or developed scar tissue will have a high impedance differential and indicate tissue that will not easily allow or may not allow any of



**Substrate Mapping** – substrate mapping, unlike anatomical mapping, is designed not to gather a surface level topographic view of the heart's geometry, but rather to look through the endocardial tissue to determine the bio-conductive health of the tissue to carry the electrical signals being generated in order to keep the heart in normal rhythm.

the electrical signals being generated for heart pacing to pass through this tissue. By determining these areas of limited or zero bio-conductivity potential, the EP surgeon can determine where ablation needs to be performed to create a pathway around these areas.

It is important to stress that all the associated issues with EP mapping

must be weighed and balanced when performing this type of mapping.

In either mapping case the desired outcome is the same as for a traveler in a car; to be able to see a detailed approximation of the geography where they will be traveling and to determine all the potential routes and hazards to calculate the best way to get where they are going. The heart-map is the key to a successful journey for the EP surgeon. The better the detail of the landscape and understanding of the topography and substrate, the better the surgeon's choices will be in determining their course of action in the ablation process in order to effect a cure.

With the increase in acceptance of CA for treating cardio-disease issues such as Afib, there has been tremendous growth in companies developing mapping hardware and software for the creation of the needed heart map. Some of the biggest and most widely used technologies include the Abbott/St. Jude EnSite NavX System, the Medtronic CardioInsight™ System, the Acutus Medical AcQ Heart Mapping System, and the Boston Scientific Rhythmia HDx™ Mapping System. Though there are many differences in the features and prices of these machines, each of them performs the essential function of creating a high-resolution interactive 3D map of a heart chamber. These maps are designed to show the tissue shape and electrical viability through a topographic



**ABBOTT/ST. JUDE ENSITE NAVX**



**MEDTRONIC CARDIOINSIGHT™**



**ACUTUS MEDICAL ACQ**



**BOSTON SCIENTIFIC RHYTHMIA HDx™**



color scheme. The machines will also display other patient vitals such as heart rate, pulse rate, and a running EKG. The systems will also allow the EP surgeon the ability to plot their ablation points onto the heart map to be used as guide points for the ablation

catheter. Additional features such as catheter type suggestions, analysis tool-sets that provide deeper insights into tissue substrate, tissue resistivity, and lesion formation, and grid interpolation which uses algorithmic prediction software to help fill in detail between

# the HUYGENS™ difference

*With the HUYGENS™ Catheter the NKC engineering team has taken all the advancements made with its MOSFET™ Catheter technology and moved it into an entirely new level of sophistication in advancing the art of RF Catheter Mapping into a tip-based signal capture and processing lab which manages all the functions that used to take large machines outside the patient's body receiving corrupted and degraded analog signals from a mapping catheter over 6' to 9' away in order to create some type of heart map for the EP surgeon to work with.*

*The HUYGENS™ Catheter removes these barriers and for the first time provides an EP surgeon an ability to do both anatomical and substrate mapping with a fidelity that over 200x greater than current mapping software systems provide.*

1

*The sensor electrodes on the catheter capture a bioconductivity reading of the endocardial tissue. This reading can be as small as .5mv. In addition to the bioelectric signal desired, the electrode can still pick up extraneous electrical noise which pollute the signal the surgeon is looking for.*

2

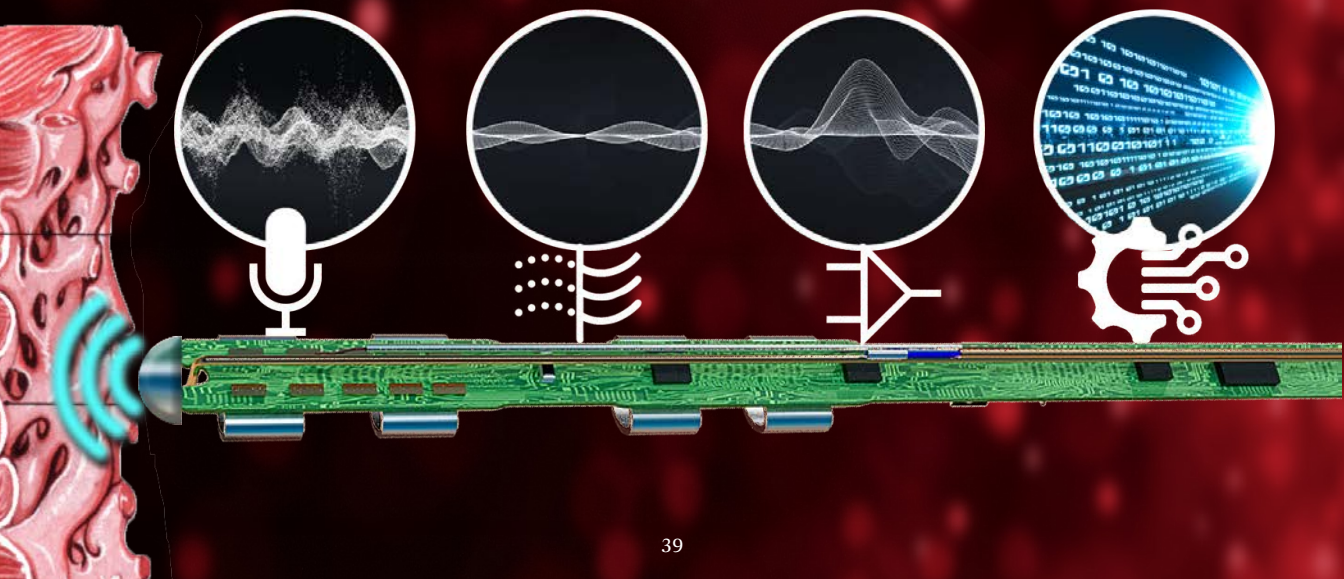
*The captured signal is then run through a sophisticated filtering algorithm which is able to make a distinction between the bio-current tissue signal and all the rest of the noise. The noise is filtered out and the clean bioelectric signal is passed onto the next stage.*

3

*The clean bioelectric signal is then passed through a proprietary amplification algorithm which boosts the millivolt signal into easy to read microvolt level while still preserving all the signal's information.*

4

*Finally the cleaned and amplified analog signal is converted into a digital data stream before it is sent by fiberoptic cable to the mapping station. This process completely eliminates any potential for signal degradation to occur during its travel .*





detection points using predictive analysis are incorporated to provide a better tool-set for the EP surgeon.

No matter the system, all of these technologies are entirely dependent upon the information they receive via the signals from the mapping catheter the surgeon is using. The mapping catheter, thus is the linchpin upon which successful mapping succeeds or fails.

## LOSING THE SIGNAL

Of the three areas mentioned previously that determine the success of a CA procedure, the mapping catheter's signal fidelity still remains the largest barrier to progress in advancing the art. At its core, a heart-mapping catheter is simply a very long wire, usually 6'-9' in length, connected on one end to a mapping computer and the other end to an electrode that both passes electrical energy to the heart tissue it is contact with and captures and send electrical information back to the computer. The sheathing of the wire may vary, as well as the shape and number of electrodes, but in the end, the standard EP heart mapping catheter is just a very thin flexible wire that must be pushed and moved into place by the physician inside a beating human heart in order to get the tip in a position to where it can capture information to send back to the other end of the wire where it is translated into the data needed to create an effective heart-map.

Due to the length of this conductive wire from the catheter tip to the mapping station, and the analog nature of the signal, the catheter is subject to picking up non-essential electrical noise that can distort the actual measurement that the EP surgeon is trying to obtain. Though we think of an operating room as being a very quiet place, from an electrical RF and electromagnetic interference (EMI) standpoint, the space is incredibly noisy. RF and EMI noise from the electrical power for the equipment, lights, cell phones and other wireless devices and even the other bioelectric signals in the patient's body, work to create a wall of noise that the EP surgeon and the catheter must navigate through to discern what is desired from what is not.

Through time, EP catheter designers have tried many methods to try and clean and filter out the noise from the desired signal. Most of these methods have either involved a "raising the bridge" approach, where amplifiers are used to increase the amplitude of the captured signals to make the distinction between noise and needed bio-current signal easier to see, or a "lowering the bridge" approach where different types of filters are used to try and separate the noise from the bio-current signal that is being sought.

To greater and lesser degrees, these methods have helped, but the bio-potential signals are so very small relative to the noise, ranging as low as 25 $\mu$ V, even

A portrait of Christiaan Huygens, a Dutch astronomer, physicist, and engineer. He is shown from the chest up, wearing a dark coat and a white collar. The background is dark.

## Christiaan Huygens

1629 – 1695

Christiaan Huygens is regarded as one of the greatest scientists of all time and a major figure in the scientific revolution. Born in the Hague, Christiaan attended the University of Leiden where his father's hope was that he would become a diplomat. But the sciences and mathematics were what captured Christiaan's attention and he devoted himself to the fields of physics, astronomy, engineering and math.

His work in physics and engineering led to many foundational discoveries in advancing the principles of telescope.

In 1655, using a 50 power refracting telescope he designed himself, he became the first astronomer to identify Saturn's Rings and was the first astronomer to observe the largest of Saturn's moons – Titan.

This melding of the curious astronomer and the exacting engineer also led him to the discovery of the pendulum as a regulator for clocks. His invention of the pendulum clock, which he prototyped by the end of 1656, was a breakthrough in timekeeping, allowing for more accurate clocks than were available at the time.

Huygens' legacy in bringing to light new horizons in so many fields has earned him a pivotal position in the pantheon of scientific discovery. It is no wonder that the brightest interior of the Orion Nebula bears his name; the Huygens Region.

when noise is removed using a complex filtering system at the distal end mapping station, there remains a potentially high risk of throwing the baby out with the bathwater because of the finite ability of filtering to discern a bio-potential signal from unwanted background noise. As a result, today's electro-physiologic mapping suffers from the shortcomings of existing recording equipment as well as limitations of the physician's ability to interpret the acquired intra-cardiac electrograms (EGM) due to lack of signal clarity and an inability to fully discern the nature of the propagated signal in complex tissues.

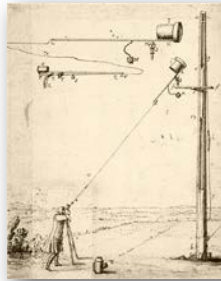
In 2015, with this in mind and with all the advancements that the NKC engineering team had made in advancing proximal-end signal capture with its MOSFET catheter, a new vision was set by NKC Co-founder Josh Shachar to see if the remaining hurdles of micro-volt signal capture, signal to noise separation, and preservation of signal fidelity back to the mapping station could be overcome to be able to deliver an EP surgeon a 3D heart-map with far greater resolution, as well as one that took far less time to capture.

The hypothesis that Josh and the engineering team came up with was to see if the inherent improvement of catheter-based data acquisition could be improved by employing a methodology whereby the signal fidelity at the endocardial site would

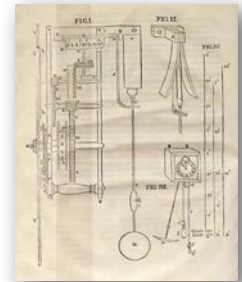
be preserved by the use of a novel electronic scheme where the catheter tip electrodes were connected to a local amplifier, which then ran the signal through advanced algorithmic signal/noise filtering to separate bio-tissue signal from local noise. At that point the signal would be digitized and transmitted via an optical serialized data line, thereby preserving the native signal. By preserving the native electro-anatomical site potential, without continuous filtering, this catheter would allow the EP surgeon to observe a realistic representation of the electrical activity of the endocardial surfaces and uncover the arrhythmogenic cause of any pacing disturbance.

The proposed catheter platform was named the Huygens™ Catheter after Christiaan Huygens, who was a 17th century Dutch mathematician, physicist, astronomer and inventor, and who is widely regarded as one of the major figures in the scientific revolution.

This approach of employing an active sensor electrode array with a local amplifier to enable an accurate “one-to-one” correlation for forming an electrophysiological map establishes a key foundational base for advancing the measurement of bio-tissue electrical potential. A bio-potential measurement using such technology substantially improves the representation of the energy contents on the spatial and time domains of the complex waveform,



1.



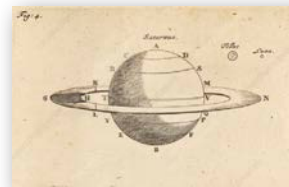
21..



3.



4.



5

*The insights proposed by Christiaan Huygens at the time caused fundamental shifts in thinking in each of the areas of inquiry he worked in. Above are some examples including: 1. an illustration of a tubeless telescope, 2. initial drawings describing the mechanics of the pendulum clock, 3. his concept for an early internal combustion engine powered by gunpowder, 4. an illustration from his general treatise on the dynamics of bodies in motion, and 5. a drawing describing the rings of Saturn and their position around the planet.*

which leads to a recursive relationship between the graphical representation and the underlying bio-potential substrate which causes such electrical activity. The ability of such a catheter to capture the QRS complex from the heart and locate scar tissue based on the electrical potential reading of that tissue is many factors higher than existing technology. A typical QRS complex has a

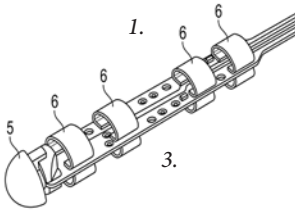
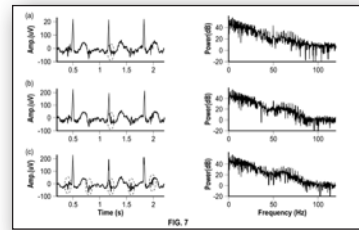
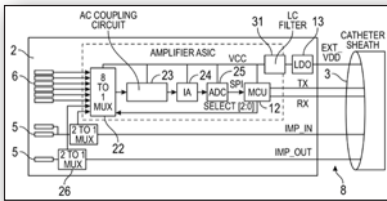


FIG. 11

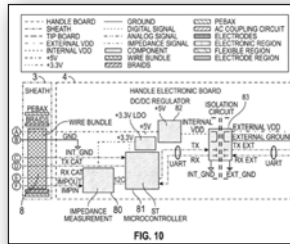
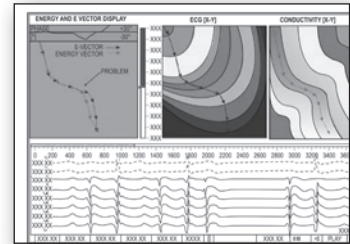


FIG. 10



2.

4.

5.

Much as the innovation by Christiaan Huygens were ground-shaking in their impact in the ways contemporaries thought about solutions to the problems being addressed, the concepts and ideas behind the NKC Huygens™ Catheter are causing the manner in which EP catheter mapping is done, to be reconsidered. Now from the drawing board to the real world, NKC is hoping the Huygens™ Catheter will have the same impact on electrophysiology as Huygens discoveries had on the areas of physics and engineering he opened up.

Above are some of the drawings from the Huygens™ Catheter patent showing: 1. a circuit block diagram of the Huygens™ Catheter, 2. three traces of the cardiac amplitude and corresponding power spectrographs, 3. a perspective view of a non-encapsulated Huygens™ Catheter, 4. a circuit block diagram of the impedance measurement circuitry used in the Huygens™ Catheter, 5. ECG and conductivity map over a time graph of an EP signal showing how the location of a rotor or other endocardial blockage is determined.

duration of 120ms at a frequency of 1Hz. The amplitude of the QRS is around 7mV, but the scar tissue can have an amplitude as low as 50uV. Therefore, the catheter is required to read a dynamic range of 0 – 10mV with 10uV resolution to precisely define the location of a scar tissue.

As indicated by the current status of clinical results, there are presently two approaches to determining the underlying mechanism for modeling disease: the reductionist approach, which advocates for “substrate mapping” correlations with ECG, and the anatomical approach, which supports “anatomical mapping.” However, in

contrast, Josh Shachar argued that the true discussion should be centered on the nature of the measuring apparatus’s fidelity and the establishment of a model in electrophysiology which could employ both methodologies to form a uniform mapping standard. This model would provide for a common method of assessing the data and its elementary building blocks, which would improve not only the diagnostic and mapping procedures but also the therapeutic outcome.

One of the foremost goals of the EP community is to develop a comprehensive mapping technique that



would be able to characterize the global dynamics of wavefront activation. This must first be anchored in a bottom-up consensus where these building blocks are accepted and agreed upon metrically, and whereby the cellular etiology and its electrical counterparts, that is, its dielectric and conductivity are defined. The complexity and inter-relationships of these “avalanche” dynamics which are translated through the myocardial space, due to ionic potential on the spatial as well as time domains, can be resolved by the use of heuristic top-down causal theory, when employing a local amplifier, active sensor array.

In understanding this, the relationship between the quality of the measuring apparatus and its ability to resolve the signal accuracy and its signal-to-noise ratio (SNR), as well as the fidelity and repeatability of the data generated becomes very apparent. Current attempts to resolve the myriad of above mentioned issues utilize the method of post-production processing which employs algorithmic tools such as the Fast Fourier Transform (FFT) technique or recursive methods, subsequent to the native measurement. As a result, the EP community is currently faced with the myriad of issues as described and exemplified in many published clinical journals.

The NKC Huygens™ Catheter addresses these issues with its open architecture design, digital processing

and recording features, make it ideal for acquisition and indexing of complex data for machine learning set-training, research analysis and machine-assisted diagnosis, among other applications.

The active sensor technology that is incorporated into the Huygens™ Catheter tip utilizes impedance spectroscopy at the event site of the bio-potential signal. Just as microscopy provided for magnification which produced a novel view of matter at orders of magnitude which were then imperceptible, impedance spectroscopy provides an additional tool in the armamentum of the electrophysiologist that can resolve the distortions caused by the noise of the current art and as well as helping to further understanding the inherent relationship between the substrate and its electrical activity counterpart.

By employing a local amplifier in the form of an active sensor array as a solution to such shortcomings, NKC aims to achieve the following outcomes with the Huygens™ Catheter:

- Native bioelectrical signal in the form of ionic electrochemical avalanche dynamics can be addressed by locating the preamplifier (Active Sensor) element adjacent to the measurement site; and
- Measurements using such technology are capable of “mining”

the “energetic event” by relating its inherent characteristics of time, magnitude and direction, without post-processing of the native signal, as is customary in the current art.

The shortcoming of the current electrode technology is emphasized by comparison with the substantive improvements provided by the Huygens™ Catheter technology. Simply stated, a local amplifier which acts as variable resistor, and its on-site electrical ground, that is, a ground not subject to the 5-ft. antenna/conductor, formed out of the catheter shaft, acting as a receiver/ carrier for equipment located at the operating room with frequencies ranging from 50-60 Hz to

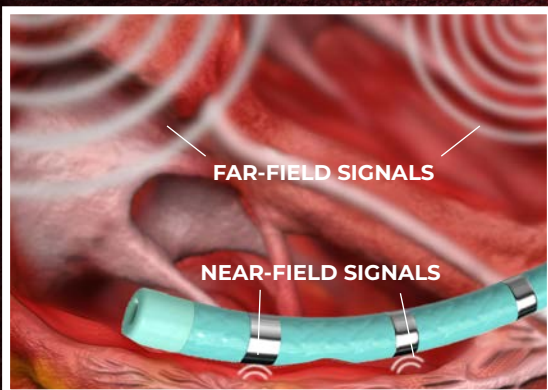
5-10 kHz, and where such an antenna is the origin for some of these noise-generating sources, all but eliminates the SNR issue. The Huygens™ Catheter employs pre-amplification technology which substantially improves SNR, Spurious-Free Dynamic Range (SFDR), signal fidelity, sampling rate, bandwidth, differentiation of far-field from near-field components, further outlined in this introduction and the accompanying patents provided.

Those familiar with the art of measuring small bioelectrical signals understand that this active sensor technology provides a new foundation for a wide variety of medical applications. For example, electrophysiological maps

## NEAR- and FAR-FIELD SIGNALS

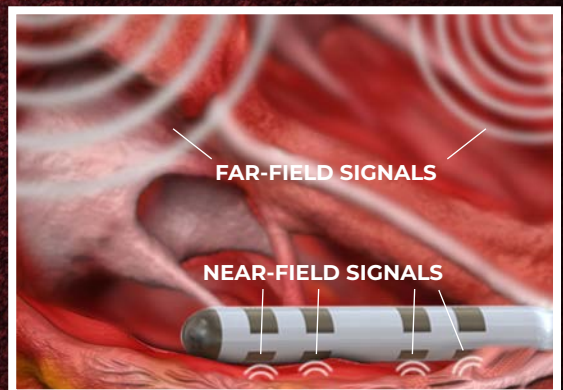
*The goal of an effective EP mapping catheter is to accurately capture the small millivolt bio-electrical impedance signals from the endocardial tissue while ignoring any other signals that may pollute the reading. One of the issues with current EP catheters is in the full-ring electrode design used on the catheter shaft. The design though was to maximize potential surface contact with the heart tissue no matter the catheter angle, however once the electrode ring is in contact with the tissue, the entire ring is energized and the majority of its surface is now open to “hearing” noise from the surrounding blood-pool. The HUYGENS™ Catheter drastically reduces this contamination potential by incorporating a unique half-ring electrode design on each side of the catheter shaft. When an electrode surface is in contact with the endocardial tissue, its paired opposite on the other side is not activated and will not pick up any unwanted signals.*

### Standard Full Ring Electrodes



*Once in contact with tissue, the entire electrode ring is energized and subject to picking up blood pool noise.*

### HUYGENS™ Half-Ring Electrodes



*The HUYGENS™ half-ring electrode design mitigates blood pool noise contamination by ensuring only the electrode surface in contact with the tissue is energized.*

can be formed to establish accurate diagnostic maps which improve the subsequent therapeutic outcome. In addition, new platforms can be opened for the detection of axonal nerve endings for applications such as renal denervation and the measurement of ganglionic plexus activities and neuronal cellular matrices. The electrical characteristics of the active sensor can resolve many of the existing problems emanating from the electrode technology interface, where the ratio of signal magnitude compared to the noise impairs the ability of the clinician to form an adequate and reliable diagnosis. The active sensor array can supplement existing technologies used in Implantable Cardioverter Defibrillator and other implantable devices, neuromodulation, and pacemaker leads, where the fidelity of the signal is essential for its optimal performance.

Electrode technology is limited in providing uniform diagnostic metrics, and therefore the clinical observations provided are oftentimes merely anecdotal indications due to the current state of the technology. The active sensor array, as a model for local pre-amplification in supplement to the current electrode technology, provides many benefits by complementing the existing technology when incorporated into a single platform. The current architecture of leading mapping apparatuses such as CARTO™ or EnSite®, as well as their tool sets, need

not be modified as to their generic metrics (e.g., bipolar, quadripolar, decapolar, balloon, basket), and are not altered as the local amplifier and its associated circuitry is adopted within the existing catheter shaft, rather, this novel sensor technology can be seamlessly incorporated into the existing hardware, and, to the operator, the change would be essentially invisible.

## REDESIGNING THE ELECTRODE

A typical feature of electrophysiology (EP) mapping catheters in common use is the placement of a plurality of electrode rings along the length of the distal tip of the mapping catheter. These electrodes take a series of impedance measurements when placed in contact with the myocardial tissue while navigating along the interior surface of the heart and various specific points of interest therein.

For mapping, it is desirable to have relatively small mapping electrodes. It has been found that smaller electrodes record more accurate and discrete electrograms whereas larger electrodes are susceptible to detecting both desirable near-field signals and undesirable far-field signals. When a portion of an electrode is not in contact with tissue, it is exposed to blood which can propagate far-field electrical signals from other regions of the heart. The far-field signals interfere with the near-field

signals, making accurate measurement of the near-field signals difficult.

In addition, ring electrodes are susceptible to detecting far-field signals when the catheter is laid sideways against tissue because as half of each ring electrode may be out of contact with tissue and thus exposed to blood. Current full ring electrodes increase the surface area of the impedance electrode to a disadvantageous extent, such that even while a tangential portion of its surface may be in contact with the myocardial tissue of interest (116 – 130  $\Omega$ ), a significant area is also in contact with the lower-impedance blood pool (65 – 90  $\Omega$ ) constantly flowing through the heart. Interference from far-field sources through this electrolytic medium introduces noise which obscures finer levels of detail within the reading of the actual tissue being probed.

In developing the Huygens™ Catheter, Josh saw that a need existed for an electrophysiology catheter with electrodes having relatively small surface areas and an electrode configuration that maximizes tissue contact for more accurate measurement of near-field activity even when the catheter is laid sideways against the myocardial tissue.

To take full advantage of the local amplification capability of the Huygens™ Catheter, it was desirable to reduce the introduction of these far-field signals, both at the catheter

tip, as well as along the length of the transmission cable in the catheter itself.

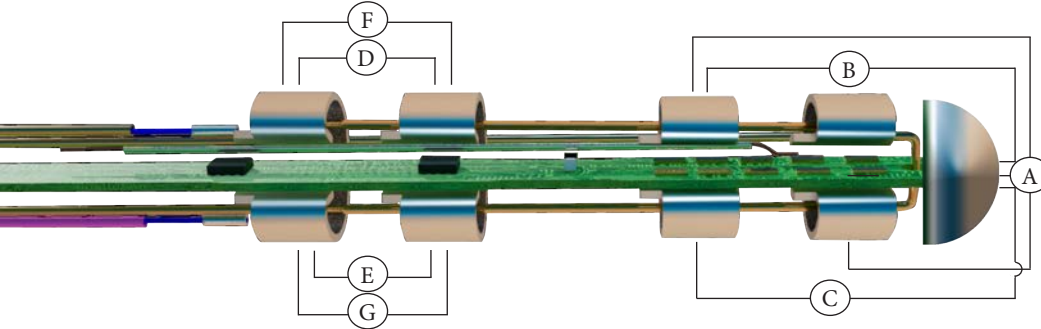
By directionally limiting the contour of a single electrode to a segment of the full catheter diameter, and thereby reducing its surface to a facing area, when placed in contact with myocardial tissue the effective contact surface area of a single split electrode is maximized, while its paired opposite electrode may still be in full contact with the blood pool. The impedance data collected by the contact electrode therefore comprises a greater degree of direct signal from the tissue being studied, while any far-field signals being received by the complementing split electrode being exposed to the blood can be discriminated. The sampling from the exposed electrode can be discerned apart from the fine-resolution transient myocardial signals of interest in the 10 $\mu$ V range, and further attenuated from the locally amplified output by noise cancellation filtering capabilities of the digital signal processor (DSP) if desired.

A further improvement of the Huygens™ Catheter over the existing art was the incorporation of semi-circular electrodes formed with a flange for bonding onto a central spine of a flexible printed circuit board (FPC) substrate by solder or laser weld, which connected them to the local amplification circuitry mounted on the FPC. A single pair of such split-ring electrodes are positioned on opposite sides of the FCP



## BIPOLAR ELECTRODE PAIRING

The HUYGENS™ Catheter can not only act as a traditional unipolar mapping catheter, but can also operate as a bipolar mapping catheter where the quad pair ring electrodes work in conjunction with the tip sensor to provide tissue differential mapping data. The pairing protocols are described below.



to form a complete circumference of the catheter outer diameter, flush with the adjacent surface. The Huygens™ Catheter consists of a tip electrode and a quadripolar (4 electrode rings), with two electrode plates per ring, totaling nine electrodes reading biopotentials.

The tip electrode is connected directly to the FPC, where the two plates of the tip slides are directly soldered onto the pads of the FPC. The tip electrode is connected to the first input of a multiplexer (MUX) which serializes the input signals from all the electrodes. When the catheter is in bipolar mode, the signal from the tip electrode is subtracted by either the top or bottom of the first ring electrodes.

The pairs of the quadripolar rings are distributed evenly just behind the tip electrode. The reason each ring is divided into top and bottom portion is to precisely differentiate the tissue wall from the blood. Each electrode can perform a unipolar reading, or it

can combine with adjacent electrode to perform bipolar reading. Each ring is designed to capture a bioelectrical impulse which can then be compared to the impulse captured by the other electrode rings to provide a precise measure of conductivity and position.

- (A) 1st Ring Electrode Bottom – When the catheter is in bipolar mode, the reading from this electrode pairs with the reading from the Tip Electrode or the 2nd Ring Electrode Top, and the difference of them is sent to the MUX.
- (B) 2nd Ring Electrode Top – When the catheter is in bipolar mode, the reading from this electrode pairs with the reading from Tip Electrode, and the difference of the two is outputted.
- (C) 2nd Ring Electrode Bottom – When the catheter is in bipolar mode, the reading from this electrode pairs with the reading

from Tip Electrode, and the difference of the two is outputted.

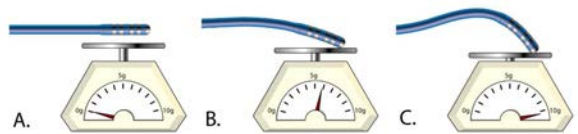
- (D) 3rd Ring Electrode Top – When the catheter is in bipolar mode, the reading from this electrode pairs with the reading from 4th Ring Electrode Top, and the difference of the two is outputted.
- (E) 3rd Ring Electrode Bottom – When the catheter is in bipolar mode, the reading from this electrode pairs with the reading from 4th Ring Electrode Bottom, and the difference of the two is outputted.
- (F) 4th Ring Electrode Top – When the catheter is in bipolar mode, the reading from this electrode pairs with the reading from 3rd Ring Electrode Top, and the difference of the two is outputted.
- (G) 4th Ring Electrode Bottom – When the catheter is in bipolar mode, the reading from this electrode pairs with the reading from 3rd Ring Electrode Bottom, and the difference of the two is outputted.

The stacked height of tip electronic components and FPC is 2mm and the width is 2.5mm. The MCU is connected to an analog-to-digital converter (ADC), which translates the analog signal from the instrumentation amplifier (IA). The IA is connected to the MUX which serializes the input signals

from the electrodes. The MUX is coupled to the plurality of active electrodes on catheter and to the tip electrode.

### CATHETER CONTACT FORCE IN FORMING AN ELECTROANATOMICAL MAP

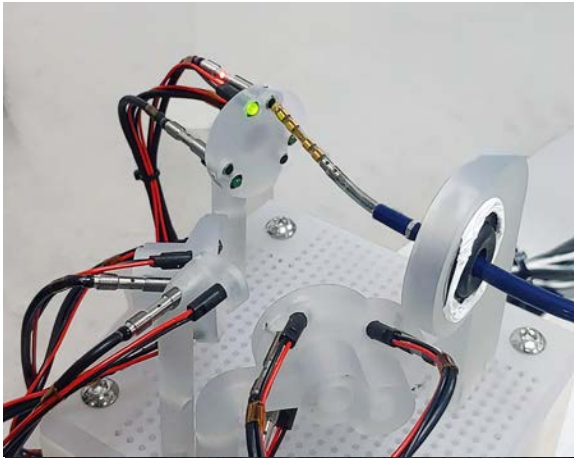
The degree of force applied to myocardial tissues by the catheter tip is an existing concern in various EP catheterization procedures, most commonly in RF ablation where firm



*The illustration above shows how regulating Contact Force at the catheter tip, up to 10g of applied force is optimal for tissue interface.*

contact with the ablation site of interest is required to create a lesion with the depth needed for full isolation. From a patient safety standpoint, force control and measurement at the catheter tip is also a desirable precautionary feature to regulate the application of mechanical pressure which can be potentially damaging to endocardial structures. Similarly, contact force (CF) has significance in EP mapping procedures, where there is a direct correlation of the degree of electrode-tissue contact with the quality of the bioelectrical signal detected.

While visualization methods are of primary importance during such procedures, intuitive navigation assistance methods which can improve

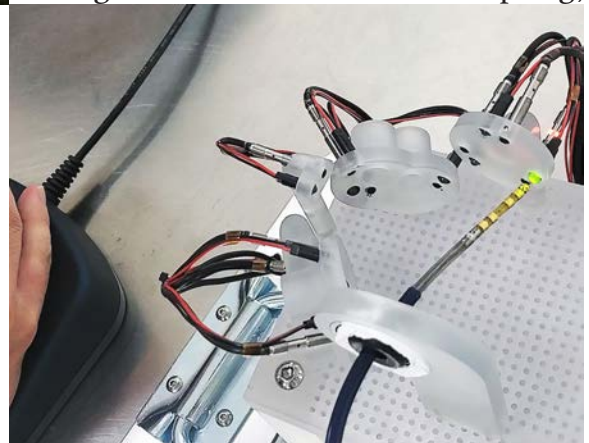


*The NKC engineering team has been able to show that precision control of the HUYGENS™ Catheter can be accomplished by a remote operator utilizing a simple haptic joystick control device that allows force-feedback response to the catheter operator to assist them in being able to remotely “feel” the quality of the tissue being contacted to ensure proper force is applied for consistent bioelectric signal capture while assuring the excessive tissue damaging force is not being applied.*

Ostensibly, the design of a “smart” catheter should incorporate feedback from a number of digital sensory components with the goal of reducing the abstractions of the remotely-guided tool, and thereby enhancing the ability of the physician to better perceive the tool as an extension of their own body in performing the most delicate of manual tasks. The scalpel, the needle and the saw are all tactile, intuitive implements compared to a catheter, a remote-controlled camera or a marionette. To bridge the gap between the virtual and the intuitive, the Huygens™ Catheter is designed with such intention.

The Huygens™ Catheter features a potentiometer-actuated deflection control situated in the handle, whereby the user can precisely adjust the angle of the catheter via a motorized drive governing the guide wire. This control system is calibrated to the full functional range of adjustable deflection. In ideal conditions the degree of force on the catheter tip might be determined by deflection angle. In practice this information by itself is an insufficient force measurement due to variables in catheter position and orientation, and site morphology which affect the tension of the catheter length supporting the distal tip.

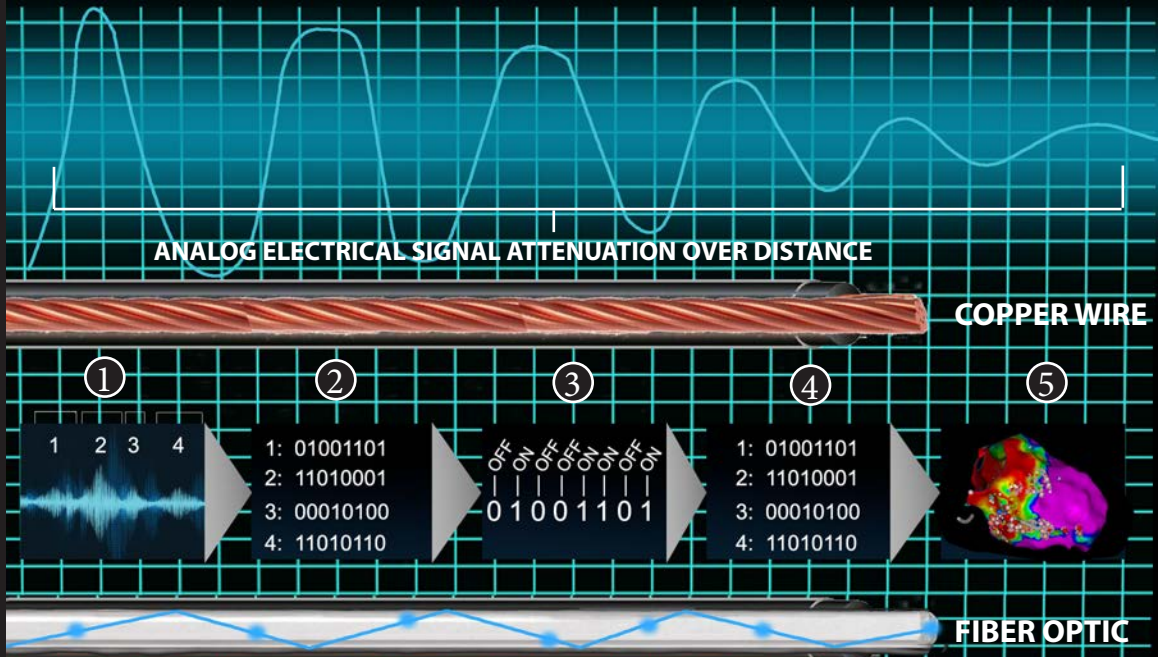
However, the measurement of local impedance provides greater insight into catheter-tissue coupling,



*In its lab, the NKC engineering team has constructed this open-air simulation of a heart chamber with strategically placed sensor plates containing target sites that would reflect the space and positioning an EP surgeon would be dealing with in an actual heart mapping procedure. Under manual joystick control, the catheter is performing perfectly. The next step will be to run these tests with the catheter under the control of the Proteus™ Robotic Arm.*



# MOVING AT THE SPEED OF **LIGHT**



*One of the main issues with traditional EP mapping is the degradation that occurs to the measured signal at the catheter tip inside the heart when it is transmitted anywhere from 9' to 20' to the receiving computer in the operating room. Not only is there signal contamination from other RF sources, but analog electrical signals quickly attenuate, that is they degrade in voltage and quality, very quickly over even a distance as short as this. With fiber optic data transmission though, as signal can be sent up to 40 miles before signal quality needs to be amplified to maintain integrity; and that signal can be sent at the speed of light. With the Huygens™ Catheter, NKC uses fiber-optic data communication to both send and receive between the catheter and the mapping station which all but eliminate the issues associated with typical analog signal attenuation. But just how is data sent by light from one end to the other?*

1. The small millivolt signal is captured by the catheter electrode and through the amplifier/filter which removes any locally captured noise so that the desired signal(s) can be isolated to distinguishable waveforms.
2. The waveforms are converted into a digital data format which are simply packets of bits and bytes consisting of unique combinations of ones and zeros.
3. These packets are then synchronistically converted to pulses of light in a Morse code fashion through the fiber optic cable where the ones are represented by a pulse of light and the zeros are represented by no light.
4. At the receiving end of the fibreoptic cable, the pulses of light and darkness are converted back to the digital packets of ones and zeros.
5. The mapping software can then read these signal and convert them to spatial point and display them on the monitor.

and this information is already at our disposal directly. Because of the material difference between the impedance of myocardial tissue and that of the blood pool medium (approx. 130  $\Omega$  vs. 90  $\Omega$ ), any recorded signal can be evaluated by a corresponding resistance measurement. Signals below a desired threshold can

be selectively squelched, providing a complementary data masking channel for discriminate signal filtering between “hot” localized measurements and “cool” proximal measurements which are much more susceptible to the influence of far-field signals. This extra layer of surrogate information can be



feasibly extrapolated for use in visual displays, audio enhancements, device feedback and control, including those of approximate force determination, haptic response, and conceivably extensible to pseudo-robotic automated functions to one familiar with the related arts.

As the Huygens™ Catheter gathers, digitizes and records all signals received in addition to parametric data about the state of the device itself such as degree of deflection and orientation to a fiducial reference, this data is indexed to a lookup table, permitting various forms of detailed analysis including but not limited to a correlation of the deflection extent from the control potentiometer in the handle to the clarity and position of the measured impedance from the distal electrodes. Real-time comparative operations on this matrix yield a qualitative assessment of the electrode-tissue interface at the time of recording to provide further indication of optimal contact with the target structure.

## **OPTICAL FIBER COMMUNICATION**

In a conventional diagnostic catheter, the weak biopotential signals picked up by the electrodes in the distal tip are amplified in external equipment that is separated from the electrodes by several feet of wiring. This wiring is vulnerable to noise contamination from 60 Hz power mains and higher frequency interference from operating room

equipment. As a result, signals such as complex fractionated atrial electrograms with amplitudes in the 10's of  $\mu\text{Vpp}$  are often buried in this tidal wave of noise.

Existing intra-cardiac recording techniques, while they have served the clinician and basic scientists reasonably well over the past three to four decades, suffer from several inherent limitations. By the very nature of utilizing electrodes connected by long cables to a distant differential amplifier, these systems are subject to line noise, ambient EMI, cable motion artifacts, and faulty connections.

Desirable local signals are subject to recording of undesirable far-field signals, which at times render the interpretation of complex, rapid arrhythmias very difficult, if not impossible.

The conflation of far-field and signals of real interest, such as pulmonary vein fiber potentials, accessory pathway signals, and slow pathway potentials, can sometimes be the cause of failed ablations. The ability to record local electric activity with great precision and to the exclusion of far-field signals has always been seen as a game-changer for EP.

Current recording systems frequently cannot differentiate low-amplitude, high-frequency signals from background noise. Extremely low-amplitude signals, such as those

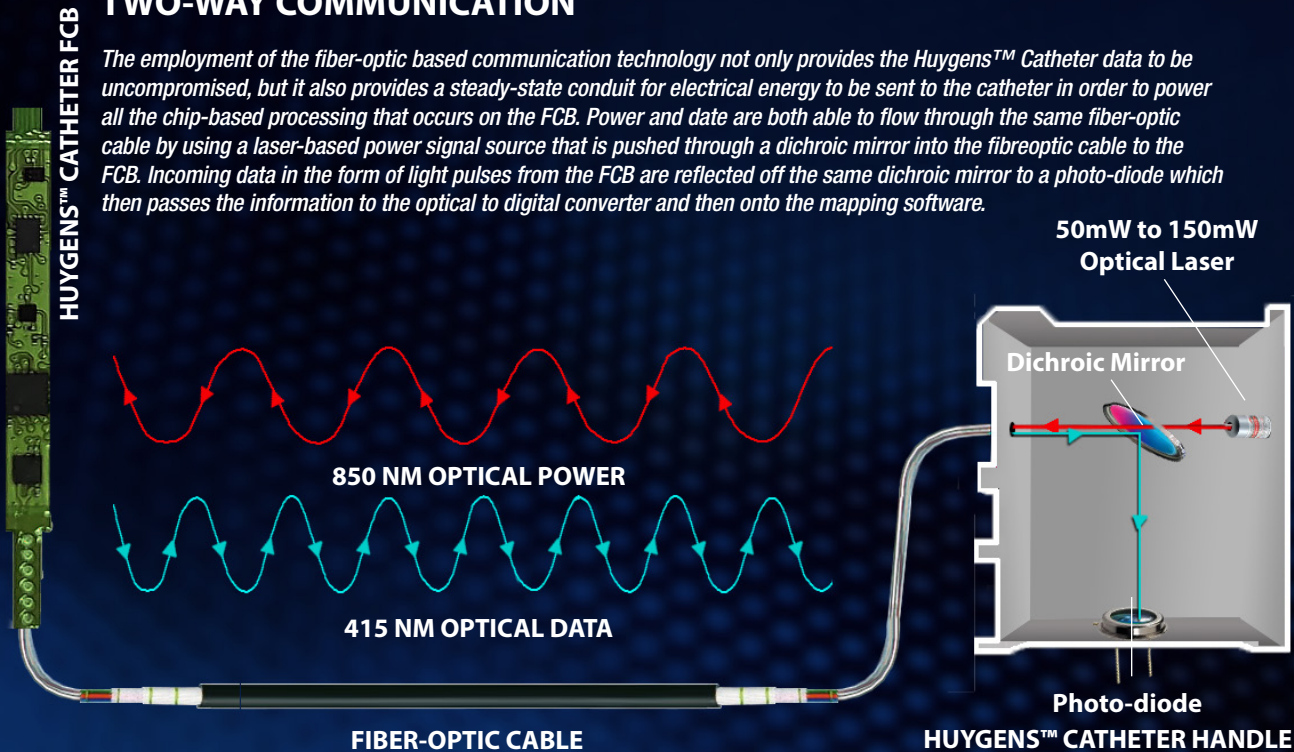
generated during slow conduction within a myocardial scar, are frequently missed or lost in the background noise when amplifier gain is made sufficiently high to attempt to record such signals. This is exemplified in the axiom that a rising tide lifts all boats. The more you amplify the signal you want, the more you raise the noise you do not.

and electro-physiologic information. For example, these signals may represent important areas of scarring that are responsible for formation of rotors. Alternatively, they may be manifesting discharges from contiguous epicardial parasympathetic ganglionated plexi.

Barbara Hubbard, in the text “The World According to Wavelets”,

## TWO-WAY COMMUNICATION

*The employment of the fiber-optic based communication technology not only provides the Huygens™ Catheter data to be uncompromised, but it also provides a steady-state conduit for electrical energy to be sent to the catheter in order to power all the chip-based processing that occurs on the FCB. Power and data are both able to flow through the same fiber-optic cable by using a laser-based power signal source that is pushed through a dichroic mirror into the fibreoptic cable to the FCB. Incoming data in the form of light pulses from the FCB are reflected off the same dichroic mirror to a photo-diode which then passes the information to the optical to digital converter and then onto the mapping software.*



Continuous, low amplitude, fractionated high-frequency signals such as those frequently seen in the atria of patients with chronic atrial fibrillation, cannot be further characterized using existing recording technologies. These signals may contain important biologic

expresses the fundamental problem of filtering as a method for smoothing the wave characteristics employing low-pass and high pass filtering, and the obvious problem of separating the noise component from the native signal, which is the inability of the system to identify

which is which. If we know that a signal is smooth, that is, changing slowly, and that the noise is fluctuating rapidly, we can filter out noise by averaging adjacent data to eliminate fluctuations while preserving the trend. Noise can also be reduced by filtering out high frequencies. For smooth signals, which change relatively slowly and therefore are mostly lower frequency, this will not blur the signal too much. However, many signals of interest are not smooth; they contain high-frequency peaks. Eliminating all high frequencies mutilates the message, “cutting the daisies along with the weeds,” in the words of Victor Wickerhauser of Washington University in St. Louis, which adequately expresses the main drawback of post-processing such signals.

In light of these considerations, Josh and the engineering team proposed that a further improvement to the existing technology could be made with the use of optical fiber in place of electrical wiring, permitting the signals detected by the active sensor array in the catheter tip to be converted into an inconvertible “digital message” which could then be sent as an optical data stream. This data could then be transmitted to the user, immune to any RF or EMF noise or interference, through an optical interface device in the bi-directional control handle of the device.

The optical interface used in the Huygens™ Catheter provides power to the active sensor array in the catheter tip and serves to handle data flow to and

from the catheter. A laser or laser diode with about 50mW to 150MW optical output is included in the optical interface which is then controlled by the DSP.

Any electrical control signals from the computer are communicated through the DSP to the laser, where they are output as optical or photonic signals, and are coupled into the optical fiber. Similarly, photonic data on the optical fiber then inputs into the optical interface and is received by a photo-diode and converted into an electrical data signal communicated to the DSP, and further to the mapping computer. A dichroic mirror diverts a portion of the output of the laser to the photo-diode for feedback control of the laser level. The dichroic filter acts as a beam-splitter that transmits 415nm and reflects 850nm wavelengths, permitting power, control, and data to be transmitted simultaneously and bi-directionally.

The transmitted photonic signals from the optical interface are communicated through the catheter cable to the emitting end of the optical fiber which is then directed into a GaN LED, such as a Philips Lumileds Luxeon Z or an InGaN/GaN light emitting diode (LED), and a photo-detector (PD). According to the direction of bias applied to the LED/PD, it will operate either to receive a photonic signal and convert it into an electrical replica, when biased as a photo-diode or to generate a photonic signal in response to an electrical input, when biased



as an LED. A semiconductor such as InGaN/GaN with multiple quantum well (QW) structure commonly used for light emitting diodes, is employed for dual functions of optoelectronic devices exhibiting photo-detector properties under variable load conditions (bias).

The principle of such a device is noted by the fact that optical emission resulting from 405 nm selective photo-excitation of carriers in the InGaN/GaN QW active region of the light-emitting diode, reveals two recombination channels. The first recombination channel is the recombination of photo-excited carriers in the InGaN QWs. The second recombination channel is formed by carriers that leak out of the InGaN QW active region, which in turn self-bias the device in forward direction, thereby inducing a forward current, and

subsequently, recombine in the InGaN active region in a spatially distributed manner. The results indicate dynamic carrier transport involving active, confinement, and contact regions of the device. Thus, one can easily integrate photo-detectors with LEDs using the same epi-structure to realize a GaN-based optoelectronic integrated circuit (OEIC).

## HAPTIC FEEDBACK

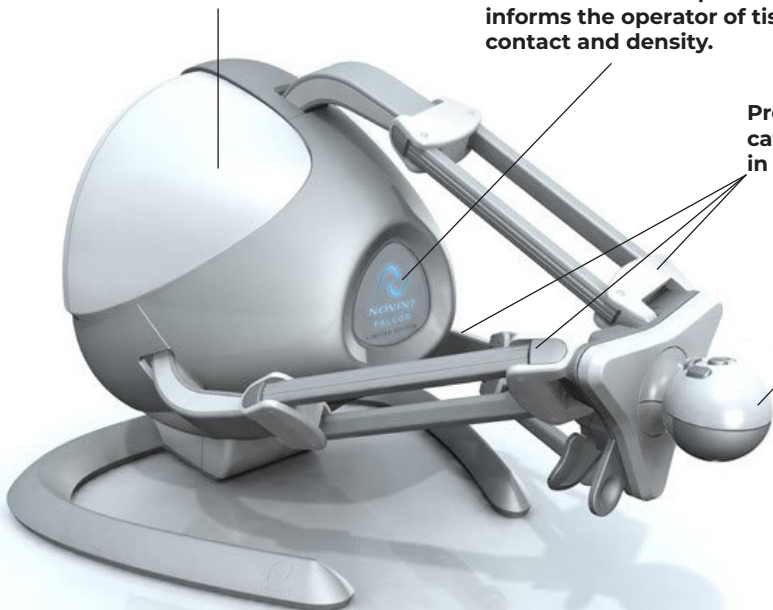
Tactile-responsive input devices offer a distinct advantage in a demanding environment dominated by visual data, enabling the user to immediately sense feedback by touch without additional clutter in their field of vision. Distinguishing elastic tissues from more rigid structures, the amount of force applied, such as that employed

**Almost zero-latency between operator movement and catheter response when used with the Proteus™ Robotic Arm.**

**Force feedback response informs the operator of tissue contact and density.**

**Precision control of catheter X, Y, Z position in 3D space.**

**Full rotational control of catheter tip deflection.**



## HAPTIC CONTROL

during percutaneous procedures, as well as the defined acquisition of tissue interface at the distal tip are all concerns within the tactile domain that can be communicated to the physician with a haptic system. Due to the pliable nature of the catheter itself, other haptic solutions frequently suffer from common limitations, as noted by the existing art:

The long, flexible nature of cardiac catheters that makes them easy to maneuver into the body also makes them poor at transferring force feedback information to the operator. As a catheter tool connects with the tissue, the contact force is balanced by the catheter compliance and frictional losses from seals and viscous fluids. By removing these limitations and giving the clinicians tactile information about the forces at the tip of the catheter, a range of new diagnostic and interventional procedures becomes possible. Haptic feedback also increases the information available to the clinician beyond what is currently provided by x-ray or ultrasound imaging.

The Huygens™ Catheter, when used in conjunction with the Huygens™ – Proteus™ Robotic Arm Surgical Platform, system provides haptic feedback to the user in the form of various mild vibration patterns produced by a motor-driven asymmetrical weight in the handle which generates a distinct range of tactile “textures” ranging from finer to coarser vibrations, conceivably inclusive of pattern-like impulses indicative of

additional channels of tactile data. This haptic response system is driven by a real-time function of the recorded impedance, force and parametric device data arrays.

## CONCLUSION

With the Huygens™ Catheter, NKC has definitively pushed the envelope of the current EP mapping art. With its advanced sensor-electrode technology, its proprietary distal-end signal processing and optically transmitted data communication, the Huygens™ Catheter is poised to provide solutions and advances to the EP surgeon, that will have a meaningful impact on patient treatment.

The Huygens™ Catheter is the only tool in existence today that can measure both the DC potential as well as the tissue contact impedance (conductivity) for the same tissue area. This enables the Huygens™ Catheter to employ the

$$\mathbf{E} = \frac{1}{\mu} (\mathbf{E} \times \mathbf{B}) + \mathbf{s} \text{ where } \nabla \cdot \mathbf{s} = 0$$

$$(\nabla \cdot \sigma) \nabla V_m = 0 \text{ and } \mathbf{E} = -\nabla \cdot V_m$$

$$\mathbf{E} = \frac{1}{\mu} \left( (\mathbf{E} \cdot \mathbf{E}) \frac{1}{Z} \right) + c$$

$$90^\circ - \alpha = \beta$$

*The equations above show the adaptations Josh Shachar made to Maxwell's second set of time-varying equations by substituting the magnetic energy vector (MEV) with the Poynting Energy Vector (P) where we substitute the B terms with the impedance measured value Z thereby allowing DC potential as well as the tissue contact impedance (conductivity) to be measured at the same time for the same tissue area.*

second set of time-varying equations, by substituting the magnetic energy vector (MEV) with the Poynting Energy Vector (P) where the B terms are substituted with the impedance measured value Z. The impedance Z is measured nearly simultaneously with the measurement of the electric potential E of the heart wave using separately sensing electrodes on the Huygens™ catheter and sensing and signal processing circuitry. Since the E and B fields are in temporal quadrature, their strengths cannot be simultaneously measured, but they can be measured in near simultaneity since the sample rate of the Huygens™ Catheter is of the order of 1 kHz compared to the 1Hz beat rate of the heart and the heart wave. Thus, an approximate value of the Poynting vector,  $E \times B$ , can be measured at any given time, substituting the measured impedance Z for a computed value for B. This is a derivation that was never described in the literature of the causal relationship between conduction path

and fibrillation. The mechanism used to describe fibrillation is associated with the theory defined under the heading “phase singularity” whereby the computer on the back-end of the Huygens™ Catheter performs a phase study separating normal tissue from fibrotic/scar tissue. The disclosed technique using the Huygens catheter with the algorithm provided using Maxwell’s equations distinguishes the invention from the existing art.

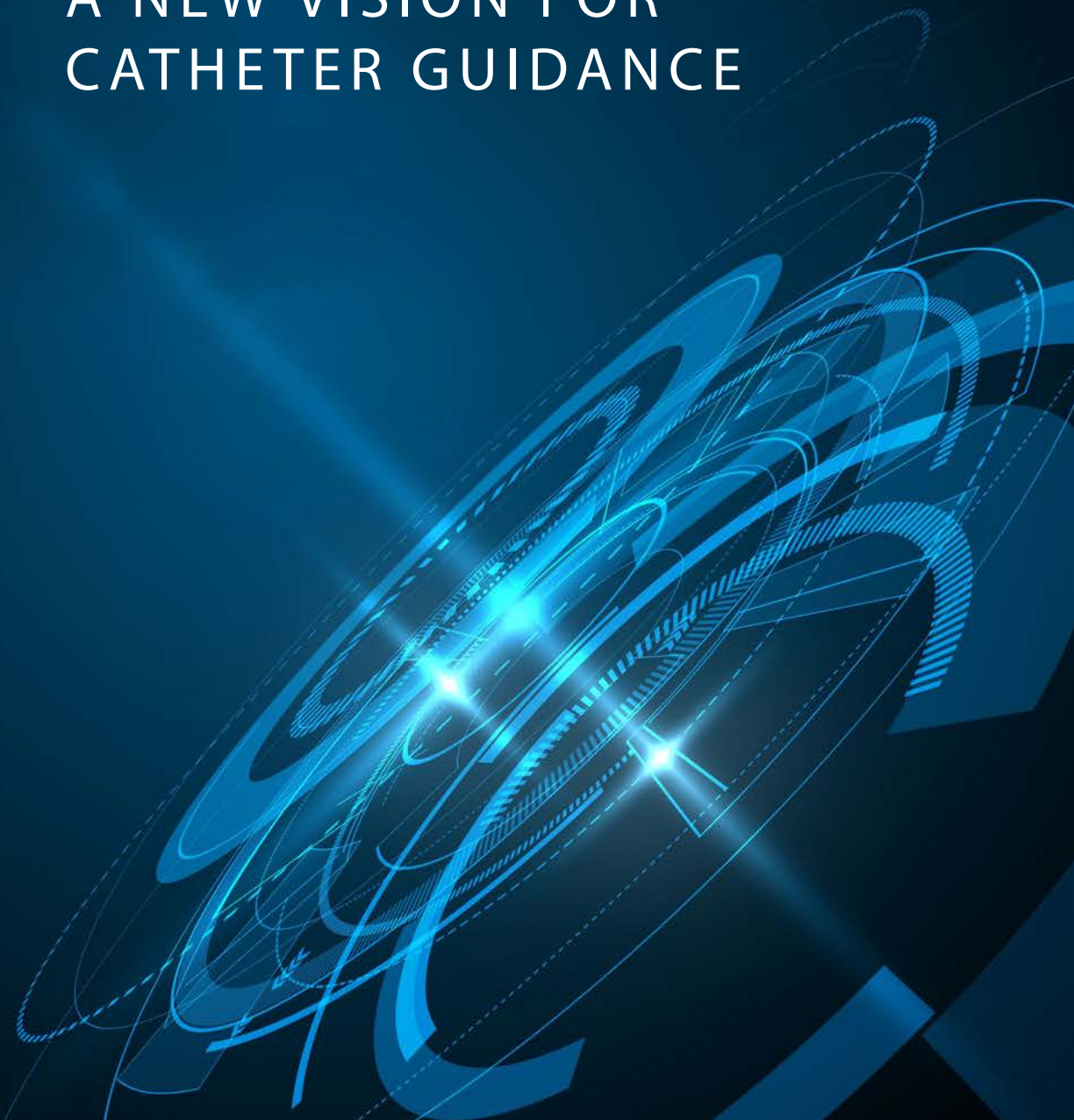
When coupled with the Proteus™ Robotic Arm and the NKC mapping and guidance systems as part of the Huygens™ – Proteus™ Robotic Arm Surgical Platform, the Huygens™ Catheter becomes the central key in finally providing a potential comprehensive standard in EP mapping technology for capturing the global dynamics of wavefront activation in the human heart and other tissues. In doing this, NKC is hoping to advance both the diagnostic and therapeutic care the physician can provide.





# PROTEUS™

A NEW VISION FOR  
CATHETER GUIDANCE



As discussed in the previous “Navigating the Future of Electrophysiology” section of this book, one of the mandates in creating Neuro-Kinesis (NKC) was to forward its previous technology developments into new systems that would meet the challenges of present-day surgical medicine.

*“And the winds and the waves are always  
on the side of the ablest navigators.”*

– Edward Gibbon

Chief amongst those platforms was the pioneering work that had been done in robotic-assisted catheter guidance under the Magnetecs banner. Magnetecs, under the leadership of Josh Shachar, created the first computer-based robotic navigation system for EP catheters using magnetic fields to advance a catheter effectively inside the living human heart for cardiac-mapping and ablation procedures. The system called the Catheter Guidance Control and Imaging (CGCI) platform had broken new ground on several fronts for robotic-assisted catheter guidance including the ability to:

- Demonstrate that a catheter could be guided using a software-based computer system to control a remote robotic-assisted mechanical guidance platform instead of the traditional manual technique of pushing and pulling a catheter by a surgeon's hand.
- Show that this system could produce a viable and oftentimes superior cardiac map upon which the EP surgeon could effectively diagnose their ablation protocols.
- Provide a fully autonomous methodology that once the cardiac map was created, and targets identified, the system could repeatably return a catheter to that targeted spot on its own.

Through several iterations in technology and engineering

advancements, and three separate human trials, the CGCI platform had demonstrated a reliable and viable advancement for the EP art. Though this advancement was groundbreaking on many fronts, the downturn in the economy in 2015 showed that hospitals were reticent to invest the millions of dollars the installation and



*Josh Shachar inspects the MOSFET™ Catheter's ability to be controlled by the CGCI guidance system.*

maintenance of a dedicated CGCI suite required, even though the need for better solutions to the growing rate of cardiac disease issues like AFib were becoming an ever-growing concern.

With the creation of NKC and the assignment of the CGCI IP to the company, the challenge became how to take the innovations from CGCI and revision them for the needs of this new era in EP medicine. The needs were very plain, how to revision robotic-assisted catheter guidance to be:

- Lower cost.
- Plug and play installation anywhere.



- Portable.
- Able to interface with both existing catheter technology, as well as the Huygens™ Catheter.
- Have the ability to integrate with current major heart mapping technologies.

And to achieve all the above without sacrificing any of the advances that CGCI brought to catheter guidance, and where, if possible, to advance and enhance those capabilities.

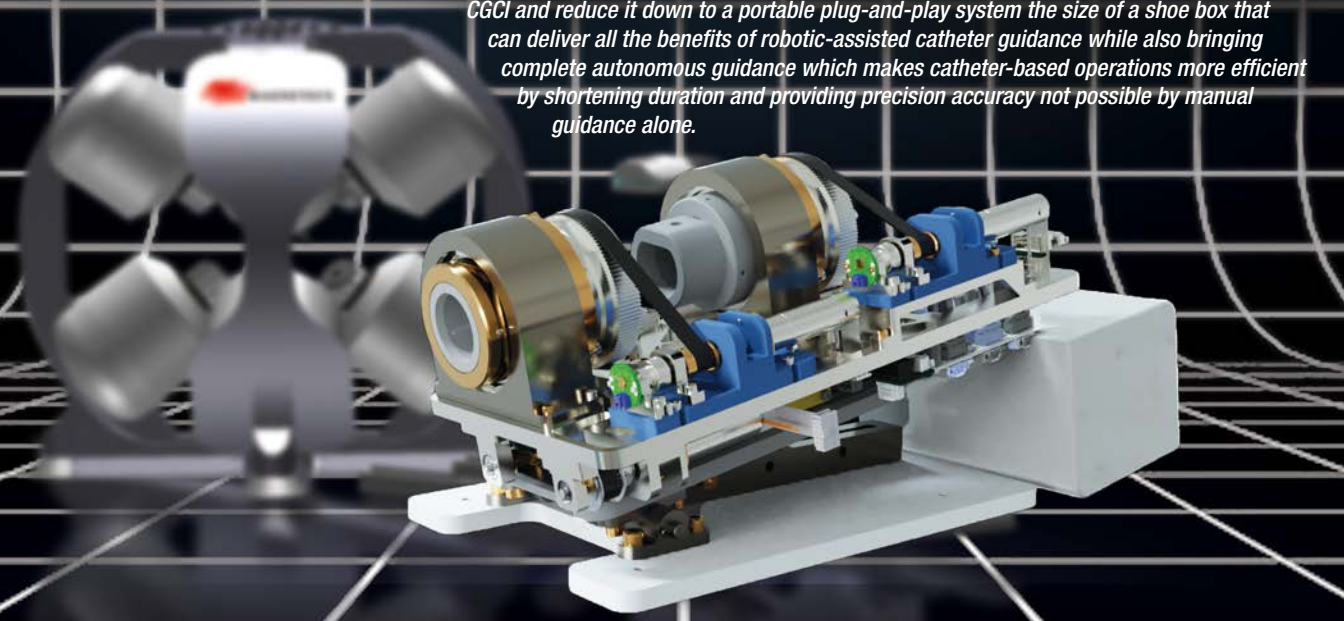
## THE INCREDIBLE SHRINKING MACHINE

Since it became clear that the new system had to be portable as well as plug-and-play, the system would not only have to be very small compared to

CGCI, but that control of the catheter tip would have to move from using large magnetic fields surrounding a patient that could pull a catheter inside the body to one that could augment and automate the existing manual process of an EP surgeon pushing a catheter into place from outside the body. CGCI offered the distinct advantage that navigational force was being applied at the tip to move it with fine-grain efficiency. By moving the guidance back to the proximal end of the catheter, the problem was how could precision movement translate from a mechanical system at the end of a 6' foot long wire to the other end of that wire in all degrees of movement needed to circumnavigate the area of interest, in this case, the heart. Anyone who has ever tried to thread a needle understands

# PROTEUS™ ROBOTIC ARM

*The PROTEUS Robotic Arm represents over two decades of innovation in robotic-assisted catheter guidance for the EP marketplace. Beginning with the achievements made with the CGCI platform, which proved the feasibility and reliability for an advanced catheter guidance technology, the NKC engineering team have been able to take the capabilities of the 9-ton CGCI and reduce it down to a portable plug-and-play system the size of a shoe box that can deliver all the benefits of robotic-assisted catheter guidance while also bringing complete autonomous guidance which makes catheter-based operations more efficient by shortening duration and providing precision accuracy not possible by manual guidance alone.*



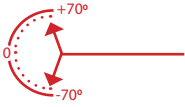


# PRECISION STEERING

The PROTEUS™ Robotic Arm incorporates three independent drive systems that provide precise control of the catheter tip inside the heart chamber. Whether in robotic-assisted manual operation or full autonomous mode, the PROTEUS™ is able to maneuver the catheter with a level of accuracy far superior to current technologies.

### DEFLECTION DRIVE

Control of the deflection of the catheter tip up to 70° from center.



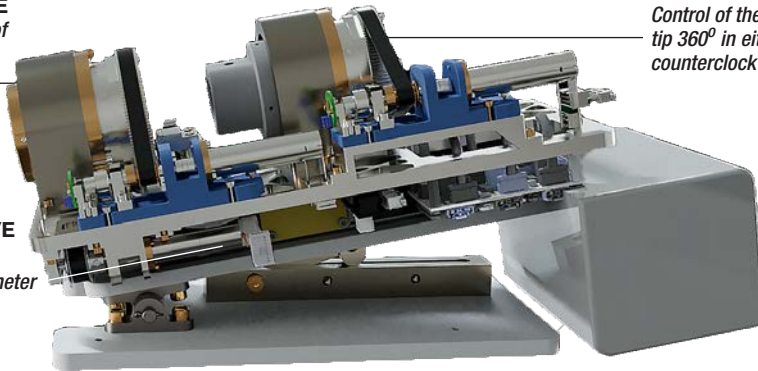
### TRANSLATION DRIVE

Control of the forward and reverse position of the catheter in a 50 mm range.



### ROTATION DRIVE

Control of the rotation of the catheter tip 360° in either a clockwise or counterclockwise direction.



the difficulty in getting such precision targeting and movement accomplished.

For Josh and the team, the answer became clear that to overcome this barrier there would have to be innovation in not just the creation of an electromechanical device capable of manipulating a catheter, but one that could interpret and execute an interplay between the information coming from the catheter, the imaging systems, the mapping software and the real-time decisions for movement coming from the EP surgeon. This new system would have to in essence be able to “dance” with all these partners to move and position the catheter exactly where it needed to go.

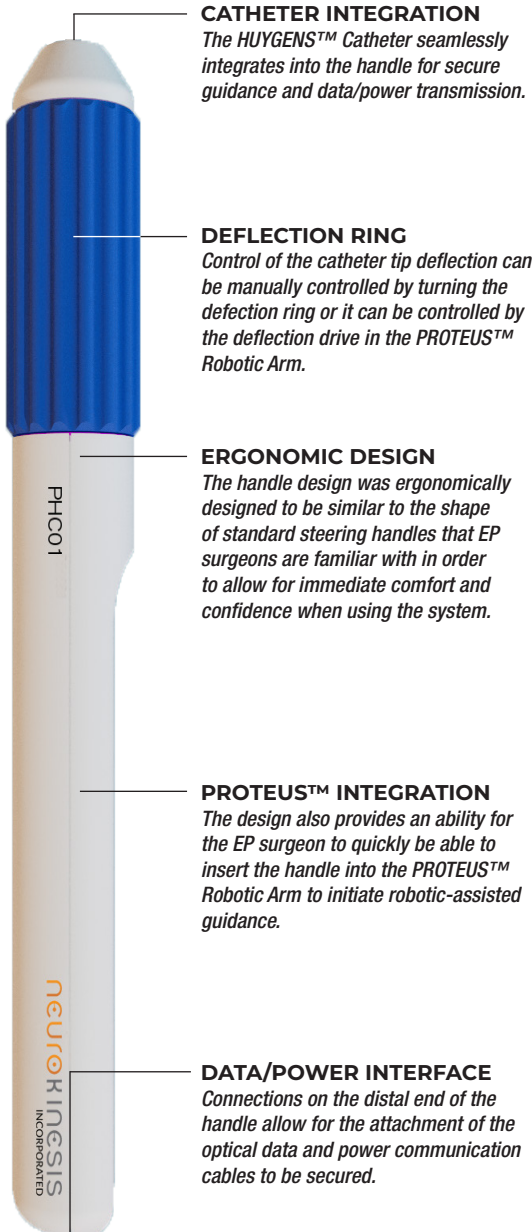
The result was the Proteus™ Robotic Arm which in essence reduced CGCI from a 9-ton structure to a 9kg device that could be held in one hand.

The electro-mechanical aspect of the Proteus™ Robotic Arm proved

challenging only in that servo motors that could provide catheter movement had to be miniaturized to be able to fit the footprint of the planned platform as well as to be medically durable and safe to meet the regulatory standards for such a device in an operating theater. To meet this need, the engineers integrated three separate drive mechanisms to move a catheter inside the patient’s body. The first was a rotation drive, which would be able to rotate the catheter in either a clockwise or counterclockwise direction through 180 degrees. The second was a translation drive that would move the catheter forward or backward up to 50mm in either direction and finally a deflection drive that would allow the tip of the catheter to be bent at an angle. Each of these motors allowed for a variable speed proportional response based on the input from the steering device, either the haptic joystick in the surgeon’s hand or the computer-controlled navigation software, in as fine

# HUYGENS™ CATHETER HANDLE

The HUYGENS™ Catheter Handle was designed to work specifically with the HUYGENS™ Catheter and the PROTEUS™ Robotic Arm to provide the interface between the catheter's FCB data and processing systems and the NKC Mapping Station. In addition all power transfer is handed through the handle. The handle can operate as a typical manual catheter steering device but can then be easily locked into the PROTEUS™ Robotic Arm for robotic control.



grain an advancement as small as 1.5mm at a speed of up to 10mm per second.

## DESIGNING A STEERING WHEEL FOR EP CATHETERS

With the mechanical movement issue solved, the next step was to provide the mechanical interface that would translate these motions to the Huygens™ Catheter. In current EP procedures, the EP mapping catheters are connected to a steering device to allow them to execute these movements. The steering devices are basically a handle that fits in a surgeon's hand. To advance a catheter forward or backward, the surgeon either pushes or pulls the handle into or out of the patient's body. To rotate the catheter, he twists their hand in the direction they want to rotate. To deflect the tip, the handle will have either a movable ring or a slider that when manipulated will pull on guide wires in the catheter, causing the tip to bend to whatever degree of deflection the surgeon wants.

Josh and the engineering team set out to devise its version of the catheter steering device for its Huygens™ Catheter. In creating this, the team had three goals in mind:

1. To make a handle that could serve the EP surgeon as any traditional manual handle could.
2. To make the handle easily fit into and be maneuverable by the

Proteus™ Robotic Arm.

3. To allow the Huygens™ Catheter's electronic and optical communications to be relayed between the electrode tip and the mapping computer.

After several paths were considered, the team settled on the core design and begin prototype building and testing a working model. Called the Huygens™ Catheter Handle, the device was ergonomically designed to fit comfortably into a surgeon's hand for manual control of both rotation and translation movements. A circular ring at the end of the handle allows for standard tip deflection to be easily performed by twisting it either clockwise or counterclockwise. Grooves in the deflection ring interlock with the deflection drive mechanism on the Proteus™ for robotic control, and the entire handle slips easily into and out of the robotic arm to facilitate simple switching between manual and robotic guidance. Serialized data ports at the backside of the handle allow for the Huygens™ Catheter's power and communication cable to be attached.

## **THE HUYGENS™ / PROTEUS™ ROBOTIC ARM SURGICAL PLATFORM**

The next part of development for the team was to visualize and build the operator station where navigation control could be carried out, mapping data processed and

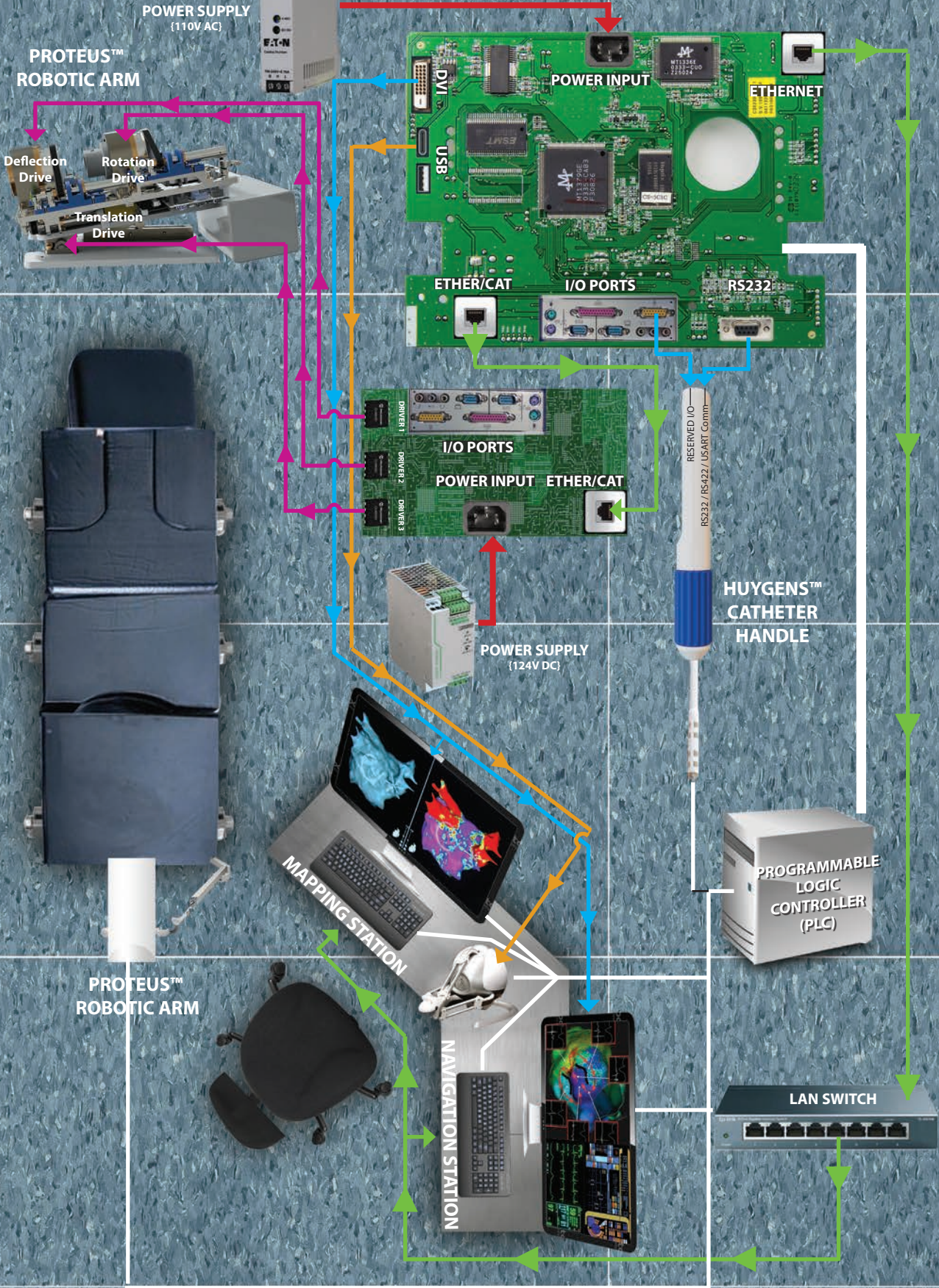
displayed, and patient biometrics from ancillary equipment such as X-ray, EKG, and fluoroscopy could be monitored. This suite of systems had to work together to provide the EP surgeon with the tools needed for the successful diagnostic mapping, the ablation point strategy development, and then the actual ablation procedure.

For the Huygens™ / Proteus™ Robotic Arm Surgical Platform, the NKC Control Suite is command central for the entire system. The Control Suite consists of three separate stations that are all networked together to work together for gathering information, correlating data, and effecting catheter guidance for both the diagnostic mapping and the RF ablation.

### **Station One – Navigation**

Robotic-assisted and autonomous navigation is carried out at this location. The operating physician can see real-time high-resolution displays of the 3D heart map as it is being created by the mapping station, as well as to see live fluoroscopy images, and monitor patient biometrics such as EKG, pulse rate, O2 saturation, and other vitals. The surgeon can control the movement of the Huygens™ Catheter via an advanced haptic controller, which translates any of the surgeon's commands into immediate movement with virtually no latency between command and action.







The surgeon can see in real-time an animation of the catheter tip as it moves inside the heart and the catheter tip's sensors provide sensory feedback to the haptic control allowing the surgeon to "feel" the endocardial tissue as the catheter is moved about.

## Station Two – Mapping

The NKC Mapping Station consists of a dedicated mapping system specifically designed for creating electro-cardio maps of the heart. For the Huygens™ / Proteus™ Robotic Arm Surgical Platform, NKC partnered with Abbott Laboratories and St. Jude Medical to license the use of their EnSite NavX EP mapping system. The EnSite NavX EP mapping system is considered to be one of the highest performing systems on the market today and is recognized as an industry standard for its ability to deliver high-resolution 3D anatomical and substrate maps with precision and rapidity that rivals other available technologies.

The mapping system takes the data being generated by the Huygens™ Catheter and converts it into a visual

representation of both the internal topography of the heart chamber as well as the impedance bioconductivity of the tissue of each point measured. The biopotential of the tissue is color coded on the map to represent the electrical viability of the tissue. Tissue that is healthy and conductive will generally appear in the blue and green spectrum whereas tissue that is less viable or non-conductive, such as scar tissue, will appear in the orange to the red color spectrum. Colors between these extremes indicate tissue in varying states of healthy electrical bio-conductive states. This is much like a topographic map one might see to determine elevations on a terrain, where red and orange would indicate high elevations that would be difficult to transverse in a car but blue and green would indicate an easily drivable valley floor.

As each data point is measured and displayed, the corresponding information on its physical position in 3D space, and its position in relation to major components of the chamber, such as the aorta, the pulmonary vein, and the mitral valve, in the case of the right atrium, as well

---

*The illustration on the previous page shows how communication, power and data is managed in the NKC Huygens™ – Proteus™ Robotic Arm Surgical Platform. The ability to connect the various independent systems and have them talk to each other with zero latency between EP surgeon or controller input and device input/output is a herculean task that is managed by the NKC Programmable Logic Controller (PLC). The PLC acts a virtual traffic cop, air-traffic controller and judge in determining what signals go where and to which outputs and if a command request, data packet, output value is accurate and can be acted upon or should be dismissed. The PLC conducts this millions of times over and over again to ensure the orchestra that is the NKC Huygens™ – Proteus™ Robotic Arm Surgical Platform performs its symphony perfectly, every time.*

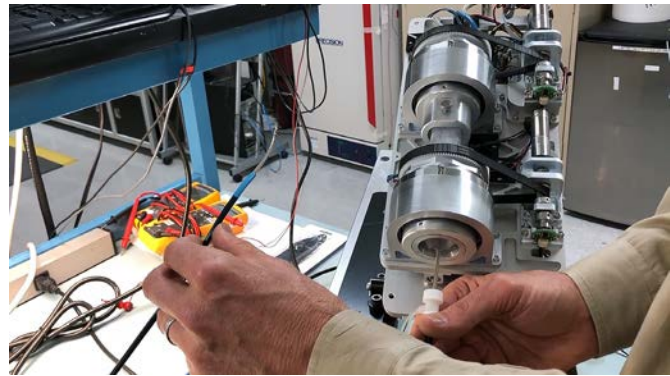
as the bioconductivity of the tissue, are all stored and are accessible to the surgeon at the Navigation Station.

### Station Three – Programmable Logic Controller

The Programmable Logic Controller (PLC) is the central hub for the entire Huygens™ / Proteus™ Robotic Arm Surgical Platform. The PLC is an industrialized computer that can receive data through its inputs and send operating instructions through its outputs. Fundamentally, a PLC's job is to control a system's functions using the internal logic programmed into it. The PLC takes in information, whether from automated data capture points or human input points such as switches or buttons and then, based on its programming, the PLC then decides whether or not to change the output. A PLC's outputs can control a huge variety of equipment, including motors, solenoid valves, lights, switchgear, safety shut-offs, and many others.

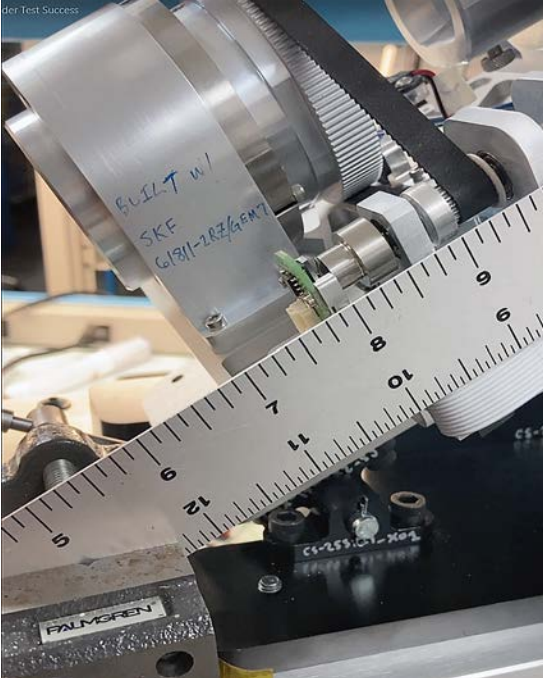
For the Huygens™ / Proteus™ Robotic Arm Surgical Platform, the PLC takes the sensory input information being sent from the Huygens™ Catheter through the optical data stream and converts it into a machine code that is readable by the EnSite Mapping station, and outputs that digital data to the mapping processor. Once processed by the EnSite mapping computer, that information is fed back to the PLC

and sent to the navigation display at the Navigation Station. Navigation movements by the EP surgeon are then sent to the PLC where they are translated into a separate machine code and then relayed to the computer control on the Proteus™ Robotic Arm, which in turn, executes the movement. That movement is registered by both the catheter and the telemetry electrodes on the patient and the new position coordinates and tissue measurements are returned back to the PLC. This cycle happens in a fraction of a second and it is all controlled by the PLC.

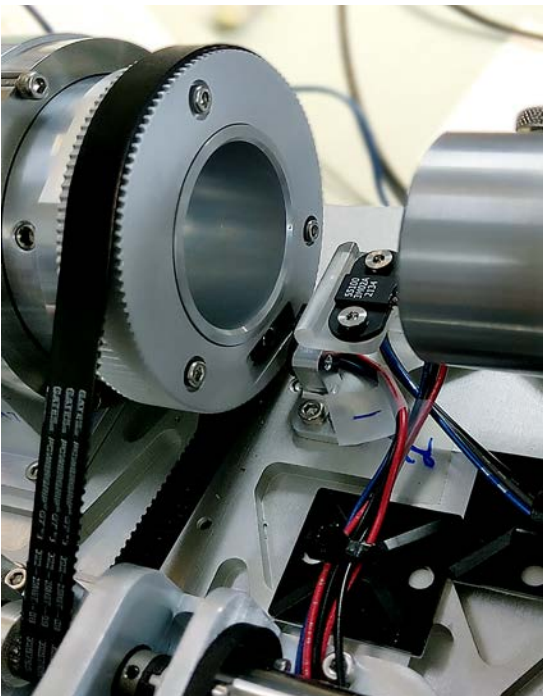


*Engineers perform bench test of the Proteus™ Robotic Arm's ability to control the deflection of the Huygens™ Catheter tip.*

Thus, the PLC acts as a Universal Translator, which as one might recall from the Star Trek series, enables the communication between all the separate machines and systems, each of whom speak a different language, to be able to communicate and work together. In this case, the PLC acts as the traffic controller for the Huygens™ / Proteus™ Robotic Arm Surgical Platform functions to move communication between the Huygens™ Catheter, the Proteus™ Robotic Arm,



*The Proteus™ Robotic Arm provides precision control of catheter positioning for any axis of direction in 3D space. In the photo above, engineers test the accuracy of the Translation drive and in the photo below, the Rotation drive is measured for accuracy in performing 360° rotations.*



the EnSite Mapping system, and the navigation controls. But as the PLC can handle most any type of input and output and provide data syncing and control, future hopes for the NKC PLC are to integrate every portion of the EP Operating room into a single unified control hub to include imaging system control, respiratory systems, and even patient bed operation and room lighting control.

With the entire system in place, Josh and the engineering team began integrating all the separate components into a working platform and began its initial base testing and protocol standardization development. The team was successful in its vision of taking the multi-million dollar 9-ton CGCI system and its early pioneering in the MOSFET catheter technology to create a shoe-box sized 9 kg robotic navigation controller that could effectively steer and control the movement of its next-gen Huygens™ Catheter inside the living dynamic of the human body to provide the EP surgeon a tool-set that could take their healing art to new levels of care.

The last component of the technology platform that remained to be integrated was the advances the early Magnetecs team had made in robotic-assisted AI control of the catheter for autonomous control for maneuvering the catheter.



## ARTIFICIAL INTELLIGENCE AND MACHINE LEARNING FOR ELECTROPHYSIOLOGY

Artificial intelligence (AI) refers to the machine-based data processing to achieve objectives that typically require human cognitive function. In the modern era, AI has mined dense data and provided the potential to classify complex patterns and novel representations of data beyond direct human interpretation. Machine learning (ML) is a sub-discipline of AI and employs algorithms to learn patterns empirically from data. ML extends the range of traditional statistics because it can identify nonlinear relationships and high-order interactions between multiple variables that may be challenging for traditional statistics. Deep learning (DL) has emerged as a powerful ML approach that leverages large datasets and recent increases in computational power to make efficient decisions on complex data. The successes of ML and DL in diverse disciplines, ranging from language processing, gaming, computer vision, engineering, industrial, and scientific arenas, have led to increasing public awareness of the promise of AI across multiple facets of life.

AI is not a new concept in cardiac electrophysiology, with automated ECG interpretation existing since the 1970s. However, with the relatively recent development of large electronic databases

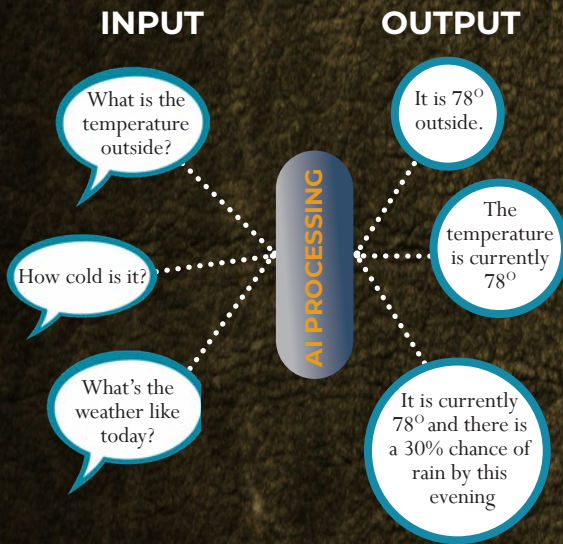
where data has been generated and can be shared, innovations in algorithms, software tools, and hardware capabilities are rapidly transforming the role of AI in cardiovascular imaging and cardiac electrophysiology. AI tools have shown promise in automating and assisting disease diagnosis, and tools are now being developed to enhance the prediction of disease prognosis and response to therapeutics and provide a novel characterization of health and disease.

### AI DATA INTERPRETATION

AI interpretation of data requires input data to be structured as feature vectors. A feature refers to a quantifiable property of the input data. Features are assembled into feature vectors to mathematically represent the input data and are subsequently computationally processed by ML algorithms. Features are inclusive of a wide variety of data. In their simplest form, features are minimally processed from the original data, such as clinical variables stored in the electronic medical record (EMR). In traditional ML studies that do not use Deep Learning (DL), handcrafted features are engineered by humans to measure specific, relevant attributes of the data. For example, in early attempts to automate ECG interpretation, typical features consisted of coefficients of mathematical representations of ECG waveform morphology. Meanwhile, modern DL approaches are capable of

# UNDERSTANDING *AI, ML, NN and DL*

Understanding Artificial Intelligence (AI) and its subsets of Machine Learning (ML), Neural Networks (NN) and Deep Learning (DL), can take a lifetime of dedicated study, and yet we work with and use each of these on a daily basis in our interactions with almost any electronic device. In short, AI can be described as the field of bringing intelligent data-processing to a problem in order to get a correct solution. At its most simple level AI takes an input, processes it through a defined algorithmic set of rules which is then able to produce a desired correct output. As the illustration below shows, here an input about the state of the weather is being made from a variety of sources. Note the input is not presented exactly the same. The AI algorithm though is able to filter out the similar key words, weigh the meaning and intent and determine that is being asked to output information on the weather. Also note that the output, though supplying the correct information, is not restricted to just a single type of response but can vary it depending on other criteria. Hence the data processing is exhibiting a human-type response exhibiting AI.



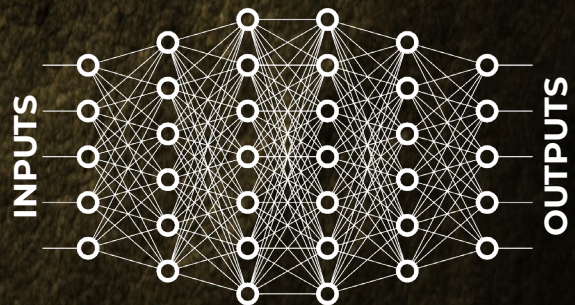
Machine Learning is a subset of AI which describes the tools and processes of building more complex algorithms that are able to take input and process it through several filter nodes. These nodes comprise a Neural Network (NN) which allows the input data to be analyzed, weighed as to its various levels of importance and then make decisions on an output response. In combining these more complex algorithms with NN filtering, the system is actually able to learn on its own how to respond and act.

## ML IN FACIAL RECOGNITION



Deep Learning is a further subset of AI and ML in which the complexity of the inputs, neural networks and potential outputs are multiplied and layered in a way in which far greater interaction and processing can be done in order to produce solutions or actions which require a much higher level of deductive and inductive reasoning to be performed. Deep learning systems also have a higher degree of self-learning and adaptability as more data and repartition of actions are performed. Examples of practical Deep Learning systems can be found in translation software, service chat-bots, autonomous vehicles, and fraud detection.

## NEURAL NETWORK



automatically computing and selecting relevant features from raw input data.

## DEEP LEARNING

DL is a powerful subtype of ML and has shown state-of-the-art performance

in speech recognition, computer vision, and image/video processing, game-playing, and medical diagnosis. When compared with traditional supervised ML, the ultimate strength of DL is that it is a powerful, flexible way of representing complex raw input data that does not



require manual feature engineering. For example, in the problem of automated ECG interpretation, early traditional supervised ML studies relied on human-defined ECG features. Meanwhile, a modern DL model learned patterns within raw ECGs to diagnose sinus rhythm and multiple other arrhythmias, with performance similar to cardiologists.

## **COMPUTATIONAL MODELING AND ML TO STUDY AF**

The explosion of mapping and imaging in AF patients provides increasingly detailed data that could be used by AI to classify AF and personalize therapy for patients. In studies of computer models derived from magnetic resonance images (MRI) of left atrial geometry in AF patients, ML of spatial atrial fibrosis patterns predicted sites of AF drivers that were unaffected by ablation. In separate work, ML has been shown to potentially clarify the controversial field of AF mapping.

A major unmet need in EP is to reduce ambiguity in mapped AF patterns because current AF mapping systems require operator interpretation by automatically identifying ablation targets. Deep convolutional neural networks were recently trained on 175 000 AF maps from 35 patients to identify potential sites for ablation, including termination sites of persistent AF, and provided an accuracy of 95%.

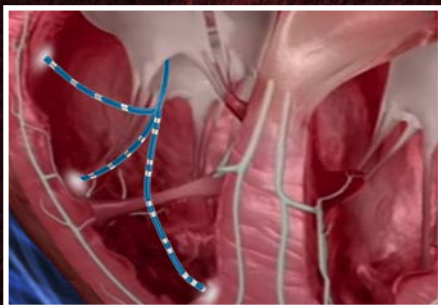
Computer modeling of AF is becoming more complex with the advancement of cell-level, tissue-level, and organ-level models. These models have provided crucial insights into the relationships driving AF including the nature of automatic and rotational foci, the role of fibrosis, and the effect of channel types. ML may prove a useful tool in integrating the significant high-dimensional data produced by computer modeling. Possibilities include the definition of phenotypes using UL or the prediction of AF rotors based on patient-specific attributes, thus guiding ablation strategy using SL.

## **AI AND THE HUYGENS™ / PROTEUS™ ROBOTIC ARM SURGICAL PLATFORM**

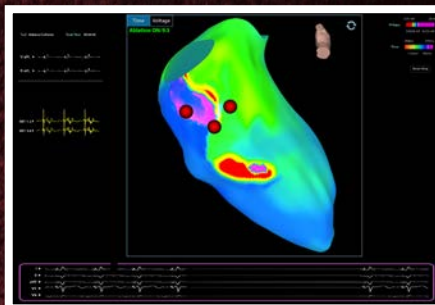
As has been mentioned, current mapping is dependent upon the EP surgeon advancing a catheter manually along as many points of contact inside the tissue of interest, in this case, the chamber of a heart, to create the “map”. Manually doing this is much like taking a snapshot of a landscape in front of you, turning 90 degrees, and taking another, and another until you have captured four images of the landscape in front of you. When placed side by side, you would now have a pretty good idea of what the terrain looked like around you but you would not be sure what the terrain actually was between those 90-degree shots. You could extrapolate out what you think would be there to



# BRINGING **BRAINS** TO THE **HEART**

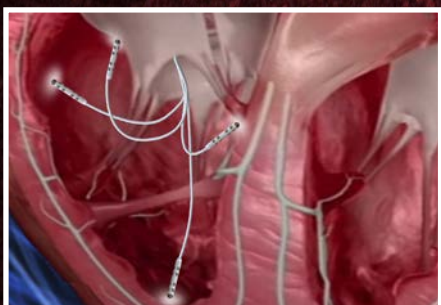


TRADITIONAL  
MAPPING



*Bioelectric measurements are made by manually moving a catheter around the chamber. This process is subject to many points being missed.*

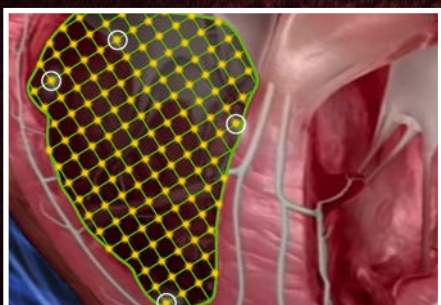
*The mapping software must interpolate any missing spaces resulting in that can be more interpretive than actual.*



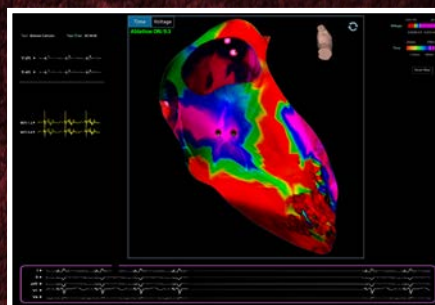
Currently an EP surgeon must manually maneuver a catheter inside a patient's heart chamber to take a measurement which generates a point on the mapping software. As a result of the manual nature of this process, the software must interpolate the points "between" the actual measurements resulting in a map that requires more interpretation and experiential guesswork on the part of the surgeon to determine where ablation needs to occur.

With the Huygens™ / Proteus™ system, only major cardinal points inside the heart chamber need to be captured. After that the computer's AI is able to build a grid map of the interior surface and the Proteus™ can then autonomously navigate the catheter to measure all the "in between points to generate a more accurate data-driven map of the chamber for the EP surgeon to work with.

*The Huygens™/Proteus™ system only needs to manually capture the major surface points in the heart chamber.*



Huygens™ /  
Proteus™  
MAPPING



*The software can then build an intelligent grid of the heart chamber and autonomously navigate the catheter to capture all the data-points in between.*

*The result is much higher resolution heart map based on actual bioelectric information upon which the EP surgeon can build an ablation plan.*

fill in the gaps and this would help in getting a clearer picture, but you would just be guessing what was there based on what you knew surrounded the missing space. This is exactly what current heart

mapping systems do, they take the data points the EP surgeon can provide via manual manipulation of the catheter and record those points as a visual representation, Where the EP surgeon

is not able to capture data, the machine uses its AI to “fill-in” the missing data.

Now, what if you took your same camera and put it on a robotic-controlled tripod. You then took those same four pictures at 90 degree increments to establish a 360-degree panoramic field of interest. You then returned the camera to its starting point and told the robotic control to now take a snapshot at every degree point not captured yet in the circle. The camera then advances to the 10 mark, takes a picture and advances to the 20 mark, takes a picture and so on until you now have shot 360 images of the terrain of interest you wanted to map. How much more accurate would that map be?

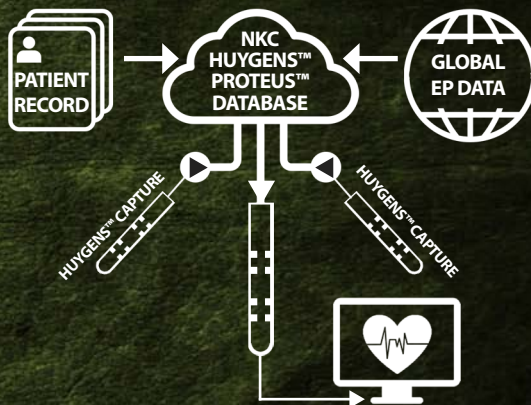
This intelligent “grid-mapping” ability is part of what sets the Huygens™ / Proteus™ Robotic Arm Surgical Platform apart from any other system on the market today. With the Huygens™ / Proteus™ Robotic Arm Surgical Platform, the EP surgeon can set all their cardinal mapping points into the system via the initial manual mapping of the heart chamber. Once the points

are established, the Huygens™ Catheter Handle is placed inside the Proteus™ Robotic Arm, where the surgeon is then able to define the mapping quadrants they want to be captured at the Navigation Station. This program is then initiated and the Proteus™ uses its proprietary AI programming to robotically move the catheter along the coordinates defined in 1.5mm advances of rotation, translation, and deflection to create a comprehensive grid map of the entire heart chamber, thereby giving the EP surgeon not just an approximation of the geography, but a detailed and complete map of the area. Because of the Huygens™ ability to capture bio-tissue measurements with much greater fidelity, not only is the resulting map more complete, but the detail is 200 better in resolution and information than any mapping system can currently provide.

In addition to this autonomous grid-mapping capability, the Huygens™ / Proteus™ Robotic Arm Surgical Platform robotic-assisted AI can also be used to execute exacting ablation

## THE FUTURE OF EP AND AI

*The vision of NKC is to expand the potential of AI and Deep Learning in its Huygens™/Proteus™ systems to encompass an ability for the system to incorporate cloud-driven Big Data generated by its systems to help in developing better predictive interpretation of the bio-measurements being made so that the EP surgeon can better determine course of action. By being able to have a database that can compare historical bioelectric measurements, to ablation procedures, to effectiveness results, and analyze this against a specific patient's records, the Huygens™/Proteus™ system will be able to better interpret the signals it captures and to make recommendations based on a customized heart map for each patient.*





procedures. Once the detailed heart map is complete, the EP surgeon can draw their ablation points directly onto the navigation map. Ablation points generally consist of straight lines, small arcs, or circles. Once defined, an ablation catheter is inserted into the heart chamber where it uses RF energy to essentially burn the tissue along the ablation point to create a scar. These scars allow an EP surgeon to create new paths for the bioelectric energy used to control the pacing of the heart rhythm to be restored to normal function.

In traditional EP ablation procedures, the surgeon has to manually re-advance the ablation catheter back into the heart chamber. Then using their ablation map overlay on the heart map, along with monitoring the fluoroscopy imaging, they must manually move the ablation catheter to a start point, engage the RF energy, and carefully transverse their ablation path by hand.

With the Huygens™ / Proteus™ Robotic Arm Surgical Platform, the surgeon simply inserts the ablation catheter into the heart chamber and moves the tip to known navigation coordinate to sync the catheter position to the navigation system. At that point, the surgeon can engage the ablation routine and the system will autonomously advance the catheter to the first ablation point, perform the ablation, and then automatically advance to each additional ablation point, thereby shortening the

procedure time while delivering a higher accuracy positioning of the ablations.

If desired, the robotic-assisted AI of the Huygens™ / Proteus™ Robotic Arm Surgical Platform also allows the EP surgeon to quickly remap the heart chamber after an ablation procedure to see how the ablation worked in restoring bio-tissue conductivity for proper pacing. If any abnormalities remain, the EP surgeon can simply refine the ablation points to fine-tune their corrective procedure.

## MOVING FORWARD

At the time of this publication, NKC has completed all of its proof-of-concept-engineering, and prototype development and is now in production of the Proteus™ Robotic Arm and the Huygens™ / Proteus™ Robotic Arm Surgical Platform in preparation for its initial animal trials of the Huygens™ Catheter. This will be followed by clinical testing of the entire system as it pursues FDA clearance and then CE mark certification for its catheter mapping and guidance technology.

With the entry of the Huygens™ / Proteus™ Robotic Arm Surgical Platform, NKC is opening the world of EP cure to new vistas of possibilities. The Proteus™ Robotic Arm and the Huygens™ / Proteus™ Robotic Arm Surgical Platform prove that dreams do come true. Sometimes, one just needs to dream smaller.







U.S. PATENT OFFICE FILINGS FOR:  
***Apparatus for Magnetically Deployable Catheter  
with MOSFET Sensor and Method for  
Mapping and Ablation***

***INVENTOR: Yehoshua Shachar  
Lazlo Farkas  
Dr. Eli Gang***

DIVISIONAL PATENTS:  
***Method And Apparatus For Magnetically Guided Catheter  
For Renal Denervation Employing MOSFET Sensor Array***  
***Method And Apparatus For Measuring Biopotential And Mapping  
Ephaptic Coupling Employing A Catheter With MOSFET Sensor Array***



(19) **United States**  
 (12) **Patent Application Publication** (10) **Pub. No.: US 2007/0197891 A1**  
**Shachar et al.** (43) **Pub. Date: Aug. 23, 2007**

(54) **APPARATUS FOR MAGNETICALLY DEPLOYABLE CATHETER WITH MOSFET SENSOR AND METHOD FOR MAPPING AND ABLATION**

(52) **U.S. Cl.** ..... **600/374; 128/899**

(76) **Inventors:** **Yehoshua Shachar**, Santa Monica, CA (US); **Laszlo Farkas**, Ojai, CA (US); **Eli Gang**, Beverly Hills, CA (US)

(57) **ABSTRACT**

**Correspondence Address:**  
**KNOBBE MARTENS OLSON & BEAR LLP**  
**2040 MAIN STREET, FOURTEENTH FLOOR**  
**IRVINE, CA 92614**

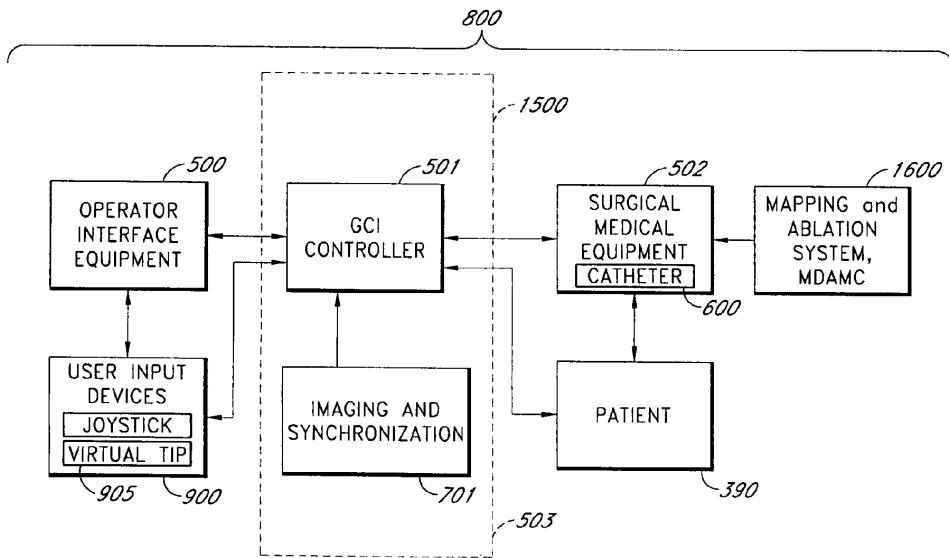
A mapping and ablation catheter is described. In one embodiment, the catheter includes a MOSFET sensor array that provides better fidelity of the signal measurements as well as data collection and reduces the error generated by spatial distribution of the isotropic and anisotropic wavefronts. In one embodiment, the system maps the change in potential in the vicinity of an activation wavefront. In one embodiment, the mapping system tracks the spread of excitation in the heart, with properties such as propagation velocity changes. In one embodiment, during measurement, the manifold carrying the sensor array expands from a closed position state to a deployable open state. Spatial variation of the electrical potential is captured by the system's ability to occupy the same three-dimensional coordinate set for repeated measurements of the desired site. In one embodiment, an interpolation algorithm tracks the electrogram data points to produce a map relative to the electrocardiogram data.

(21) **Appl. No.:** **11/362,542**

(22) **Filed:** **Feb. 23, 2006**

**Publication Classification**

(51) **Int. Cl.**  
**A61B 5/04** (2006.01)  
**A61B 19/00** (2006.01)





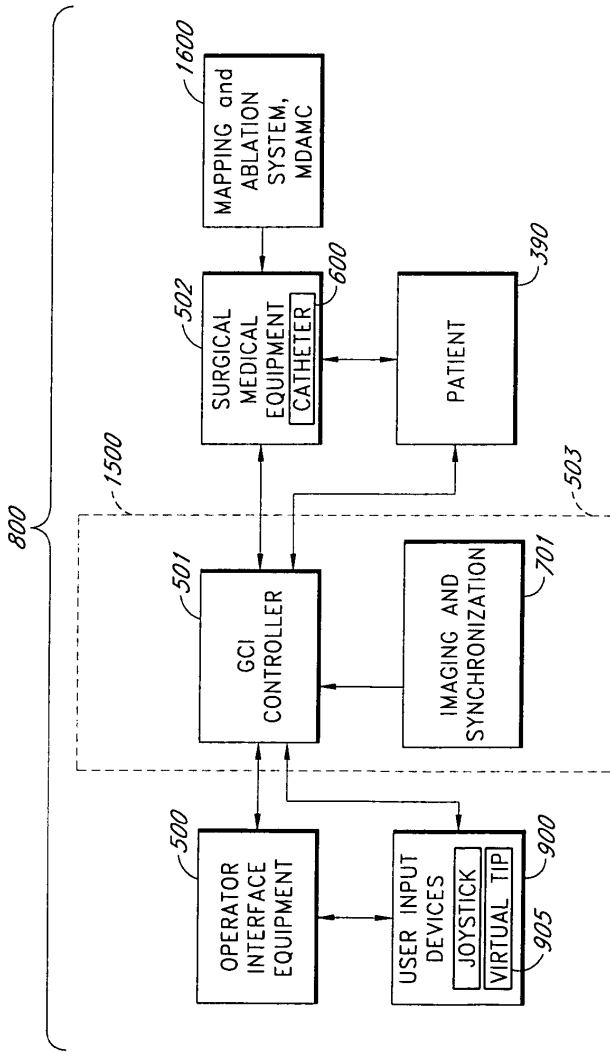


FIG. 1

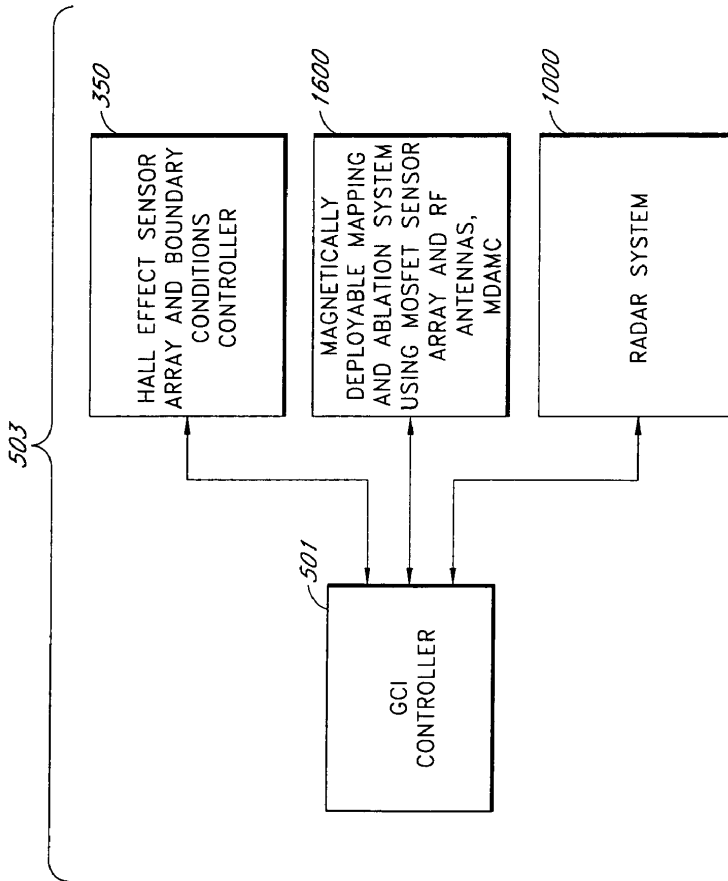


FIG. 1A

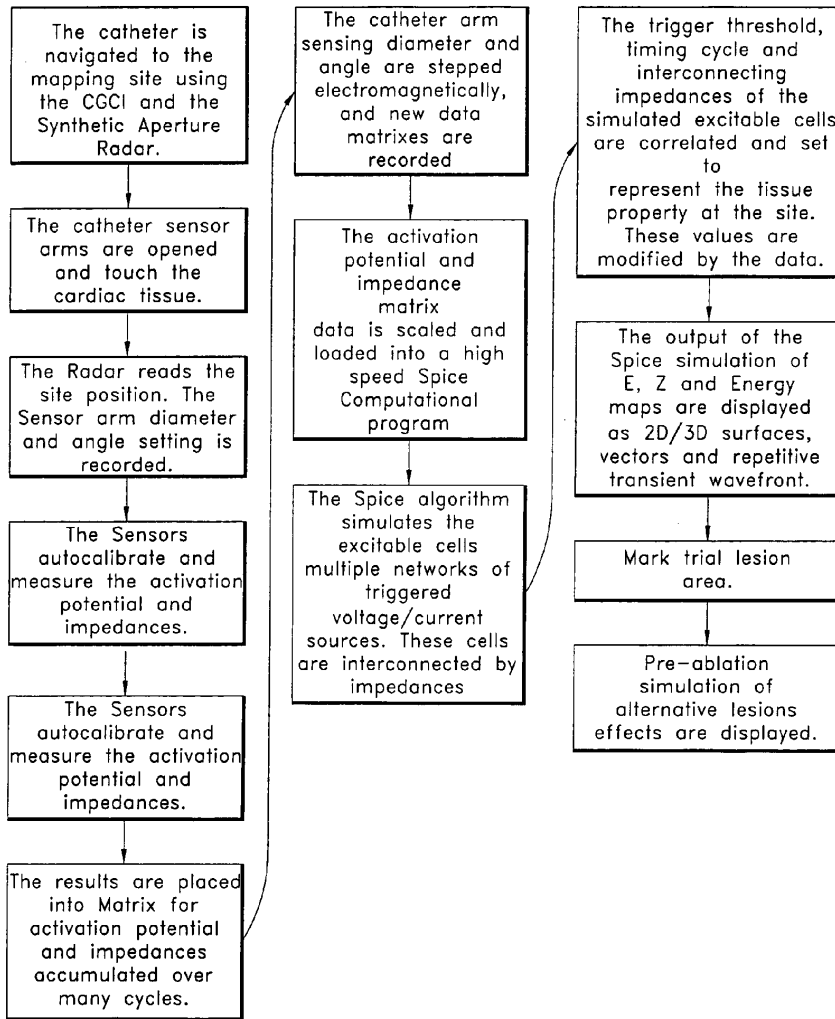


FIG 1B



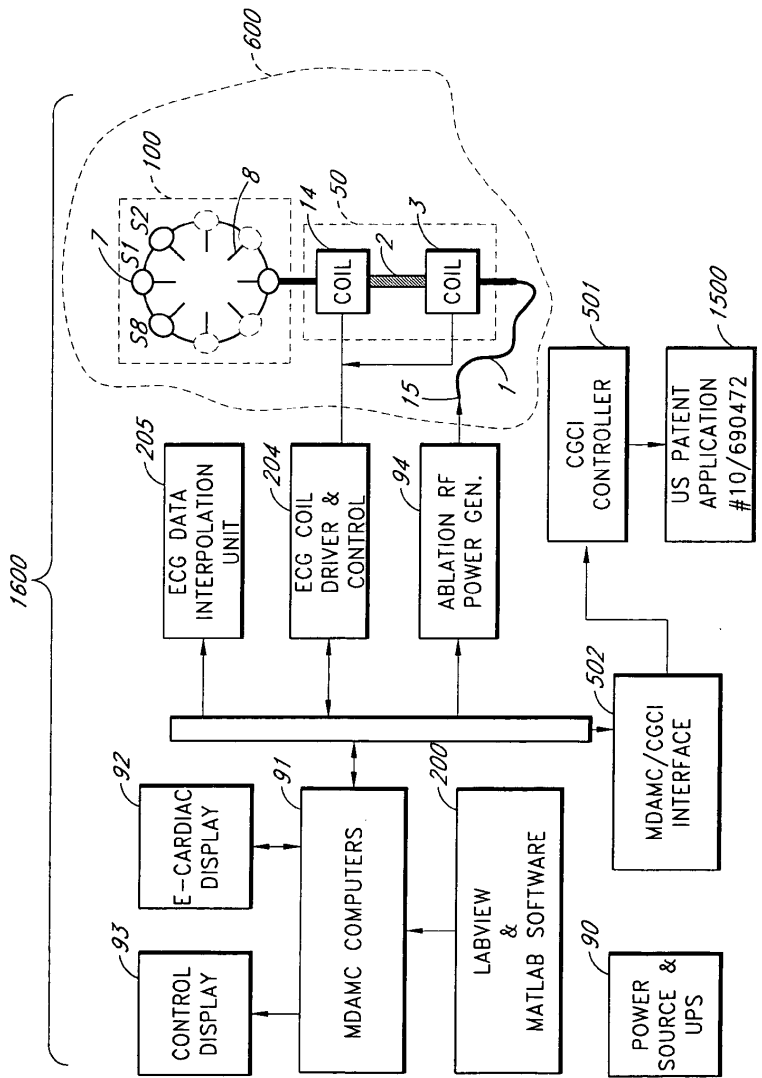


FIG. 2

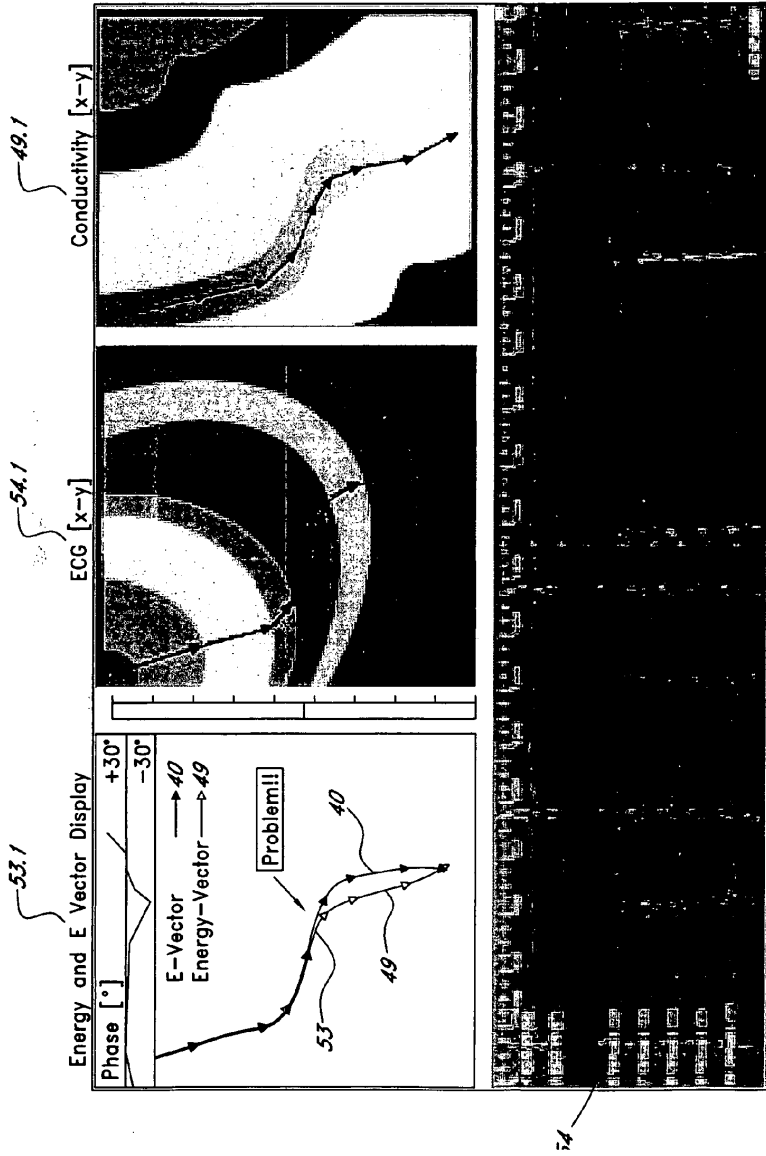
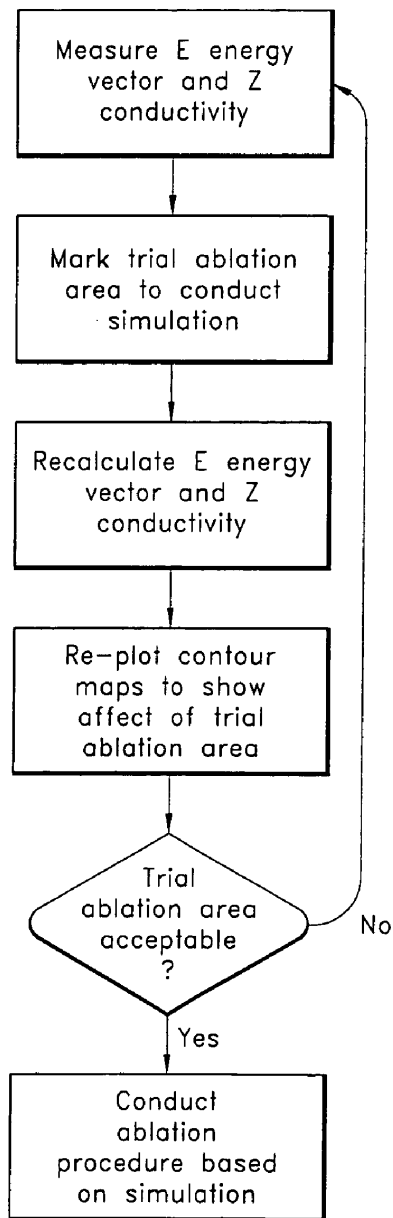


FIG. 3

*FIG 2A*



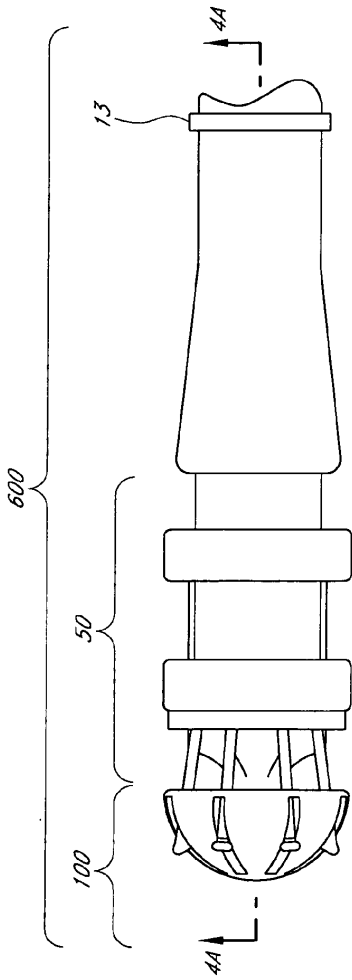


FIG. 4

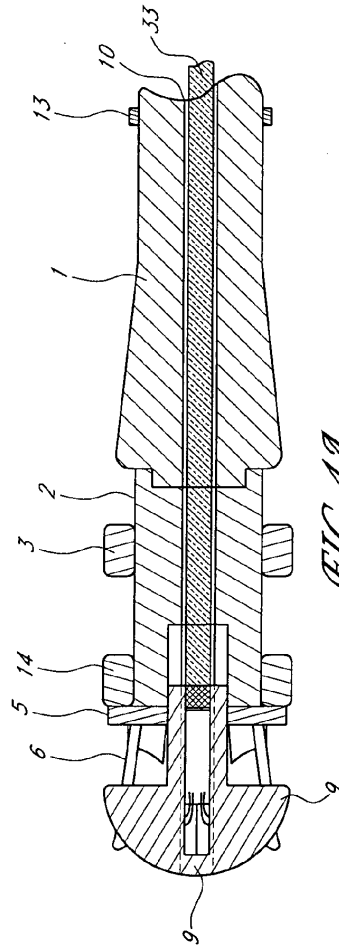


FIG. 4A

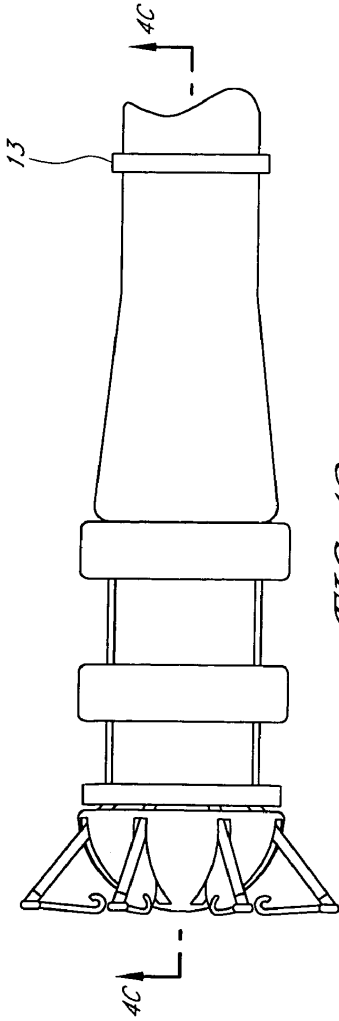


FIG. 4B

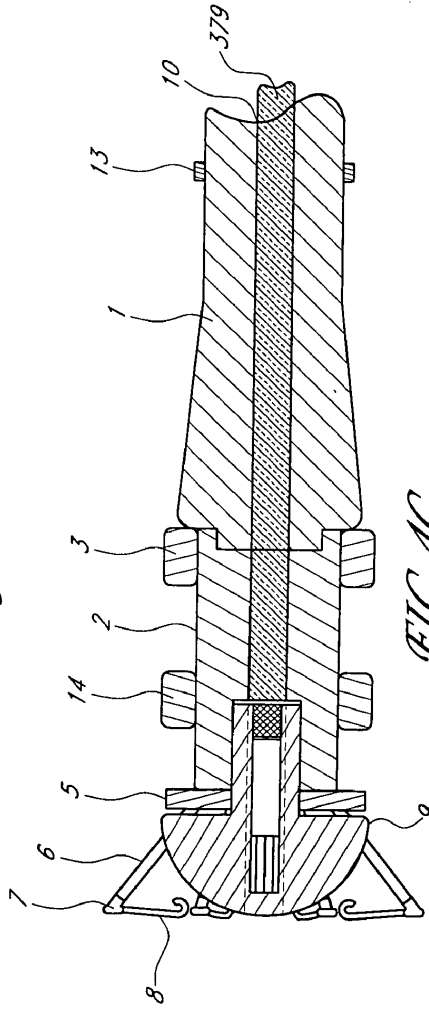
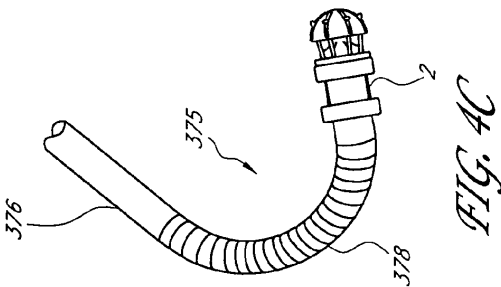
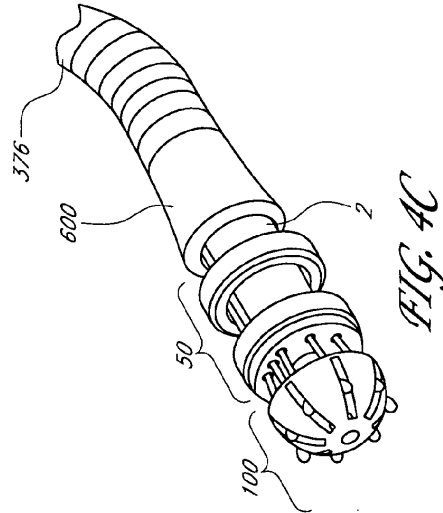
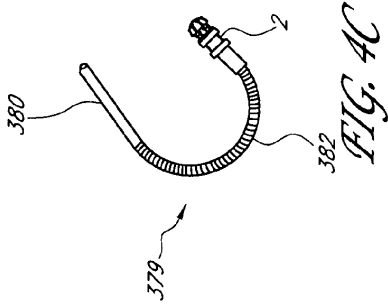
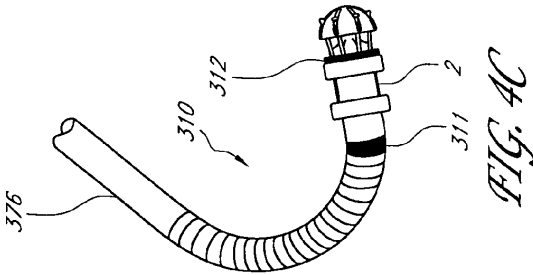
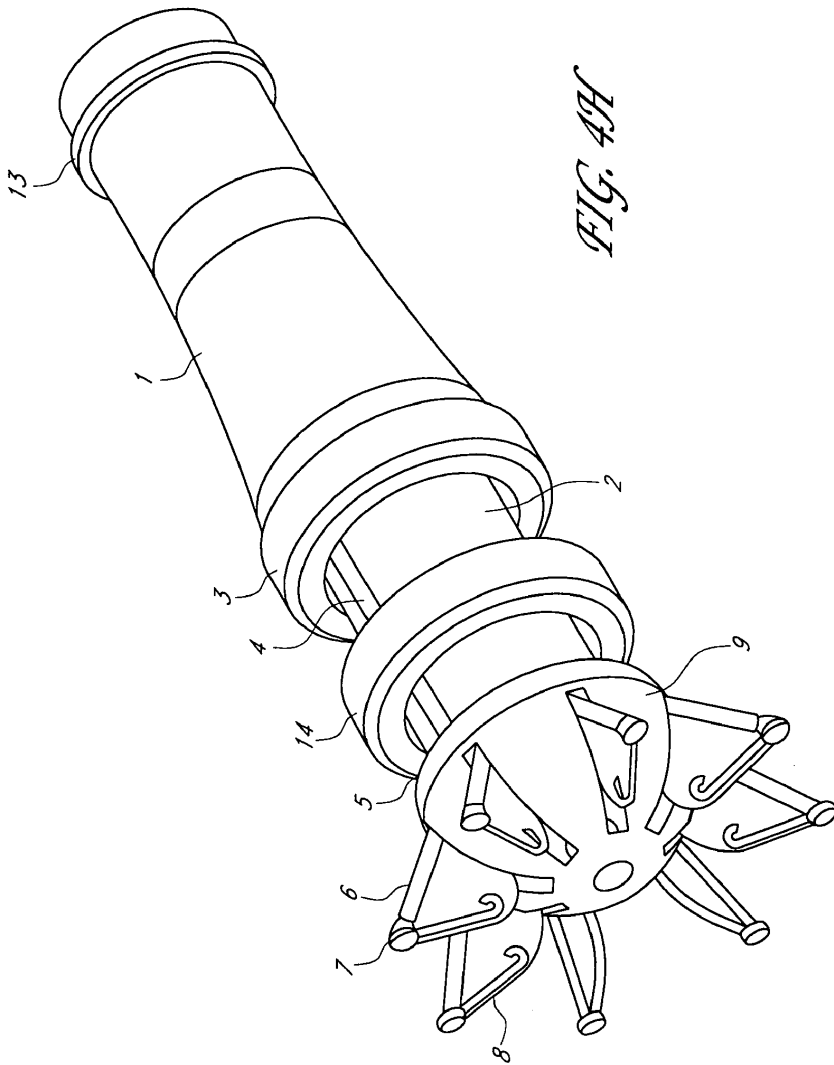
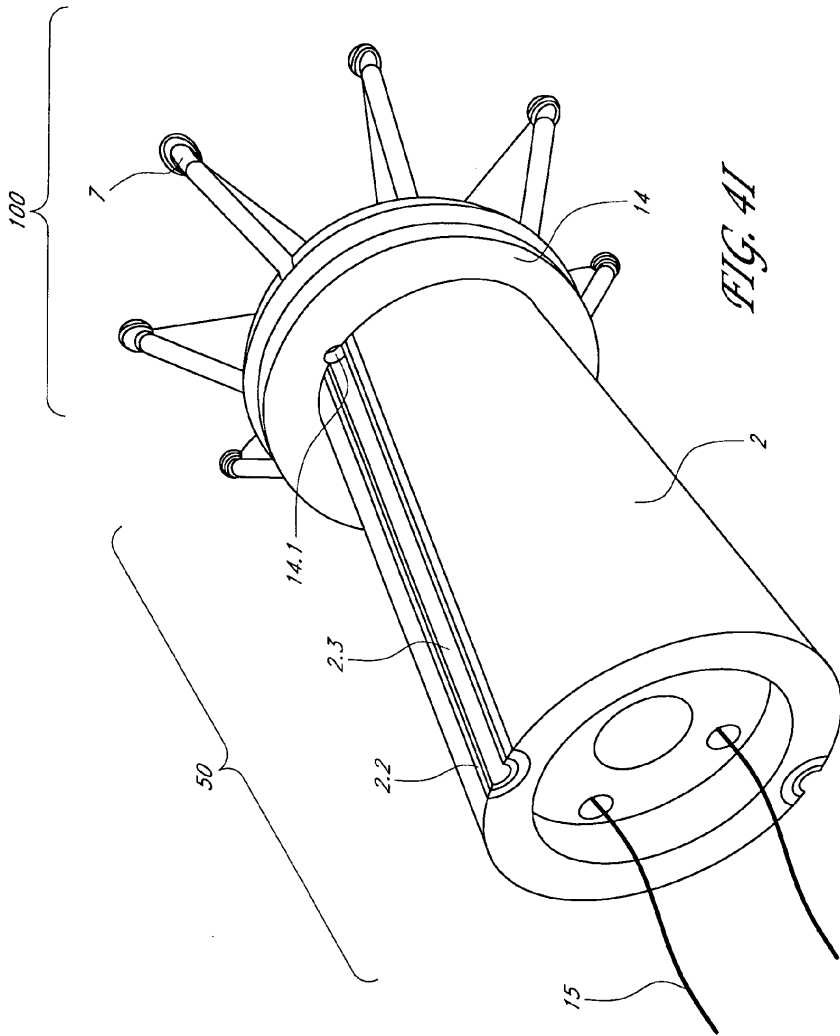


FIG. 4C









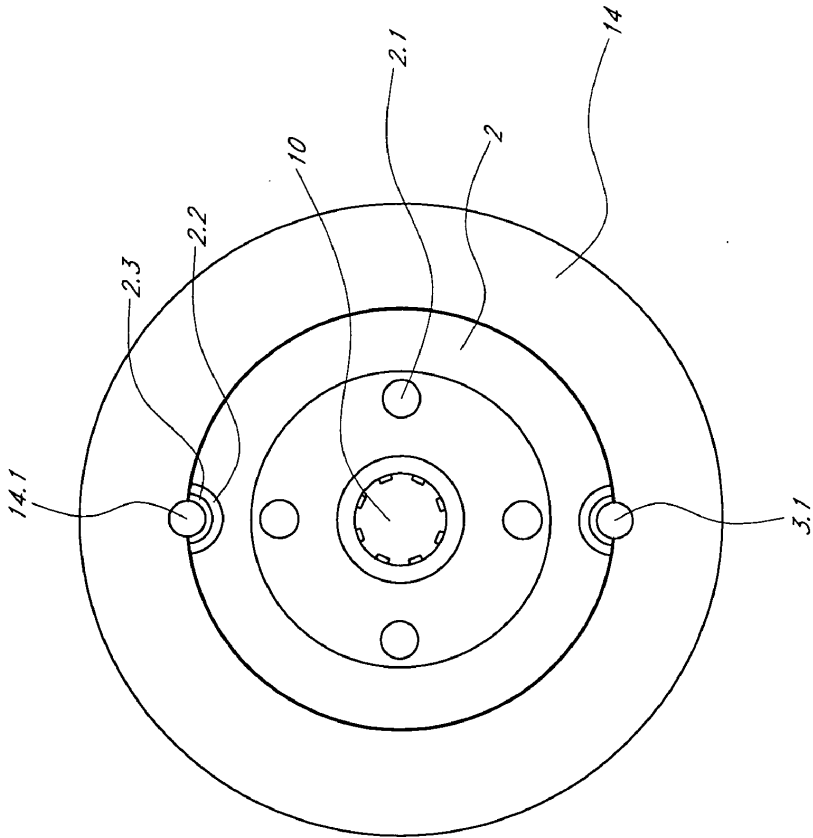
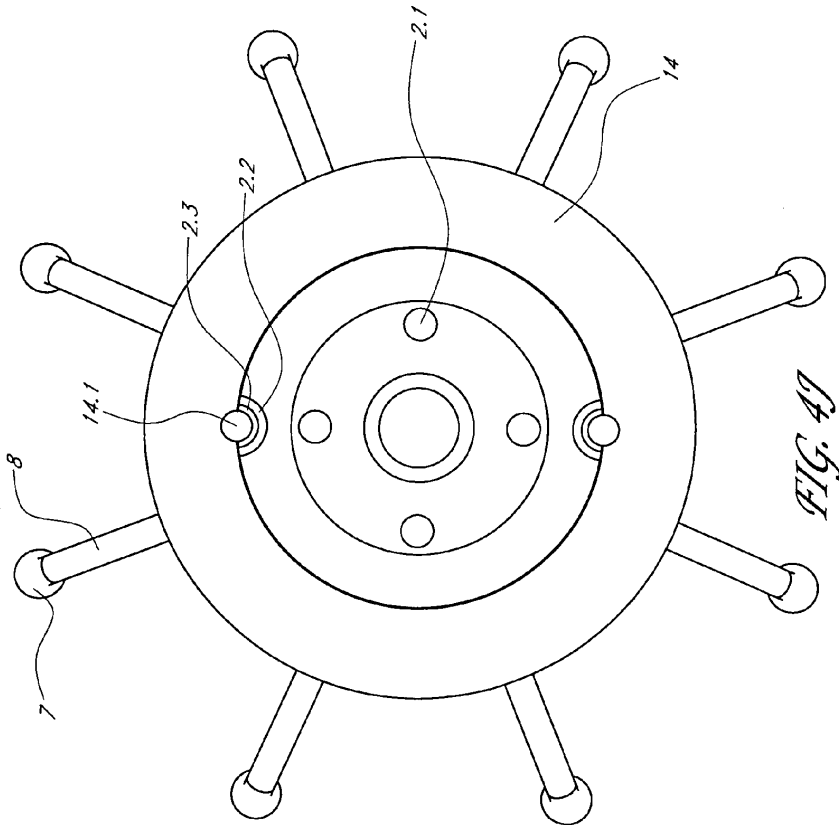


FIG. 4J



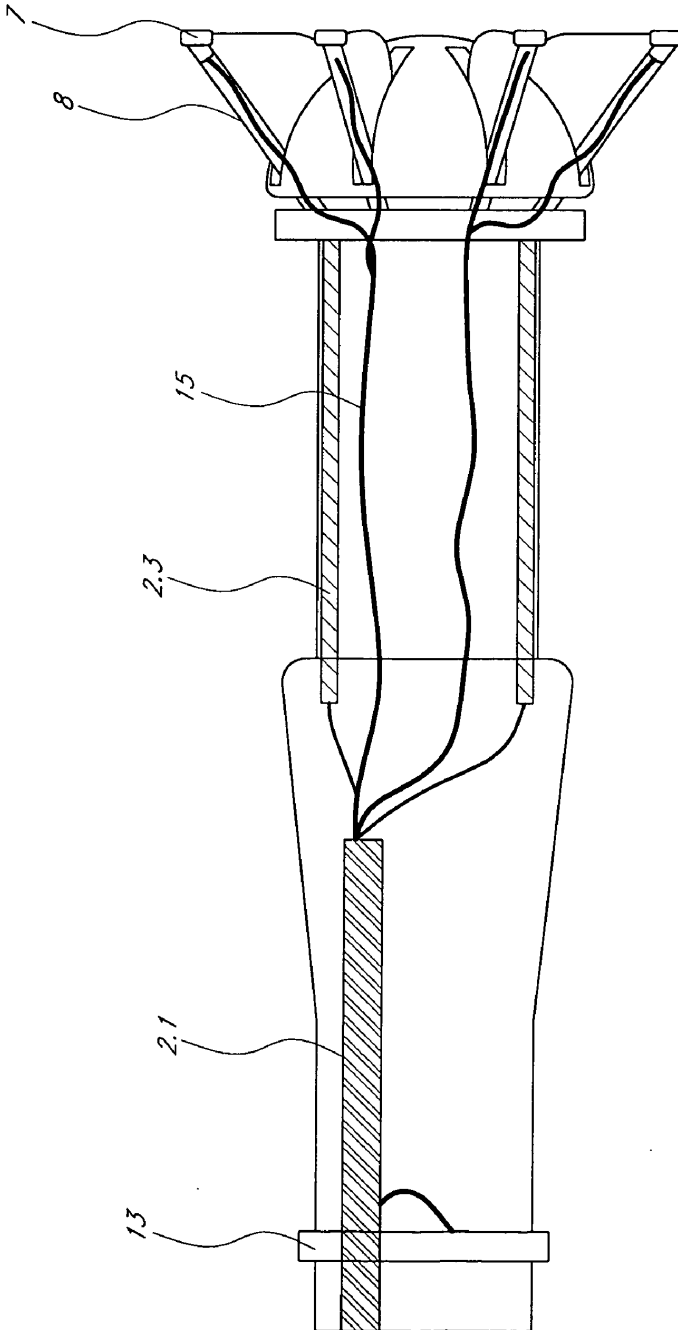
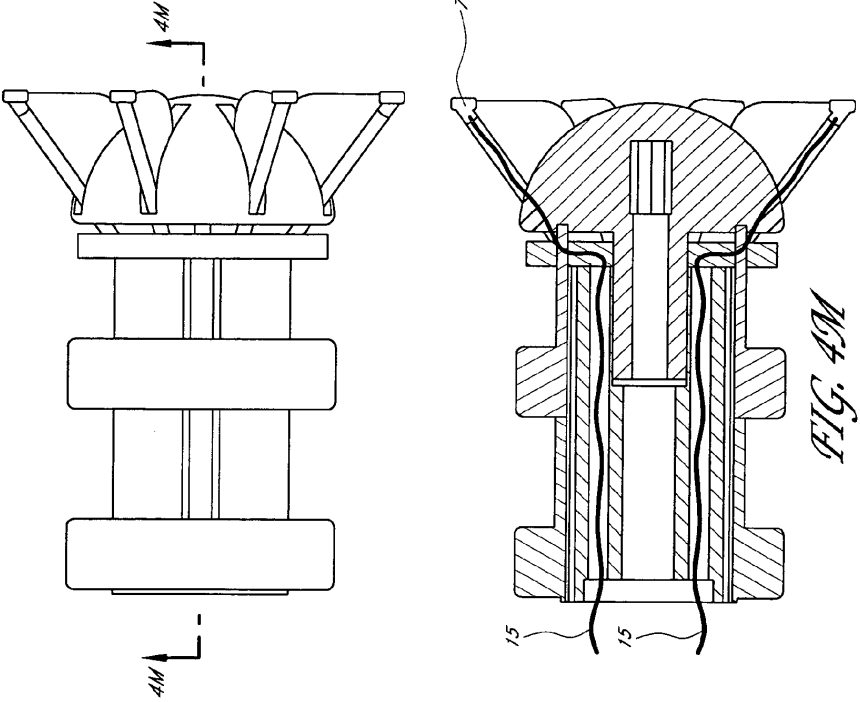


FIG. 4L





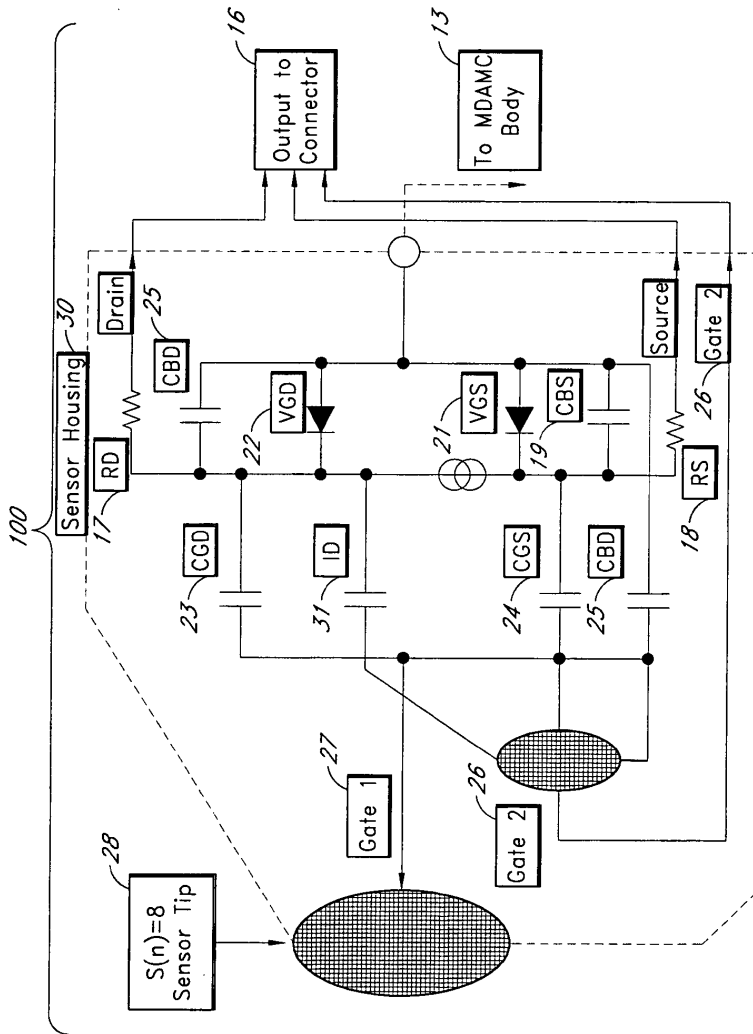


FIG. 5

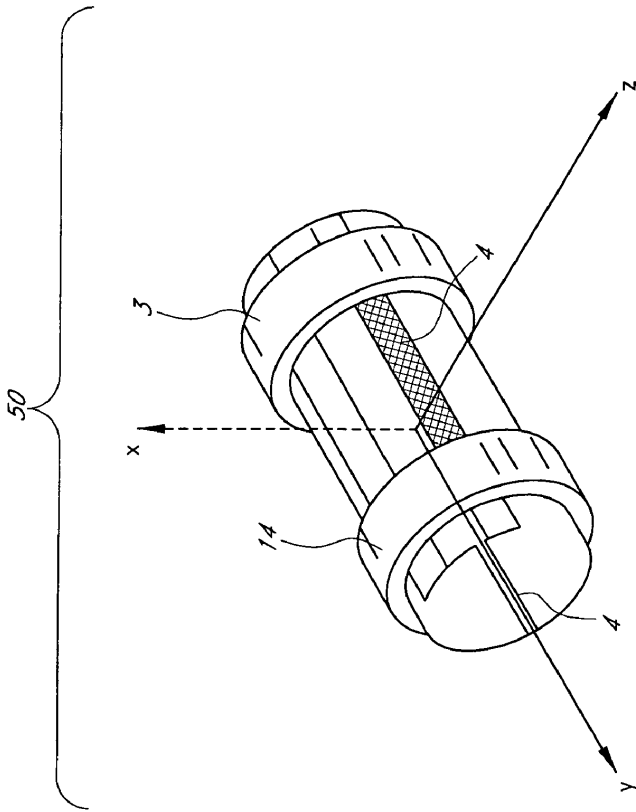
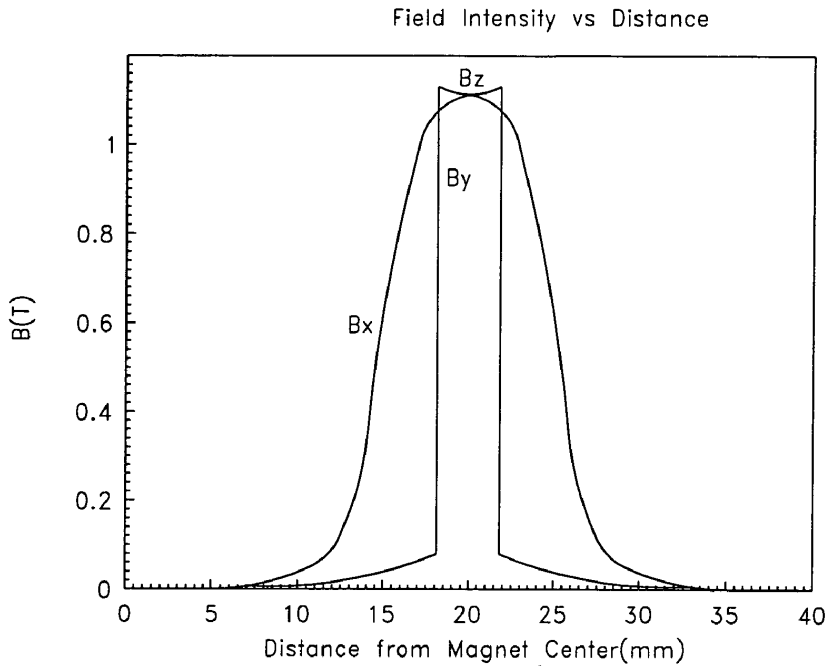
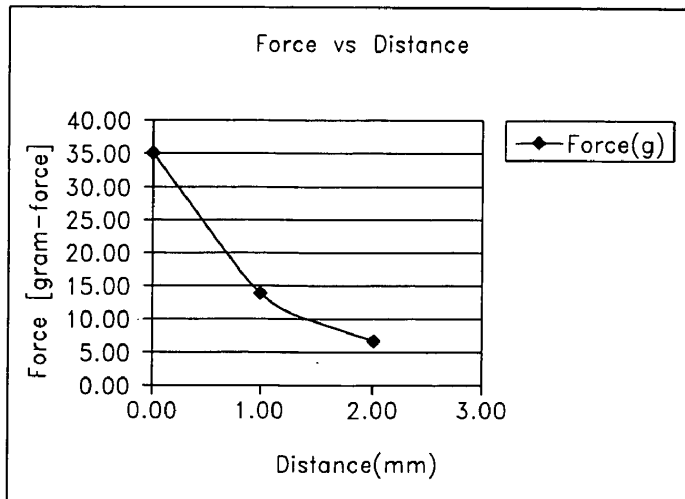


FIG. 6

*FIG. 6A**FIG. 6B*



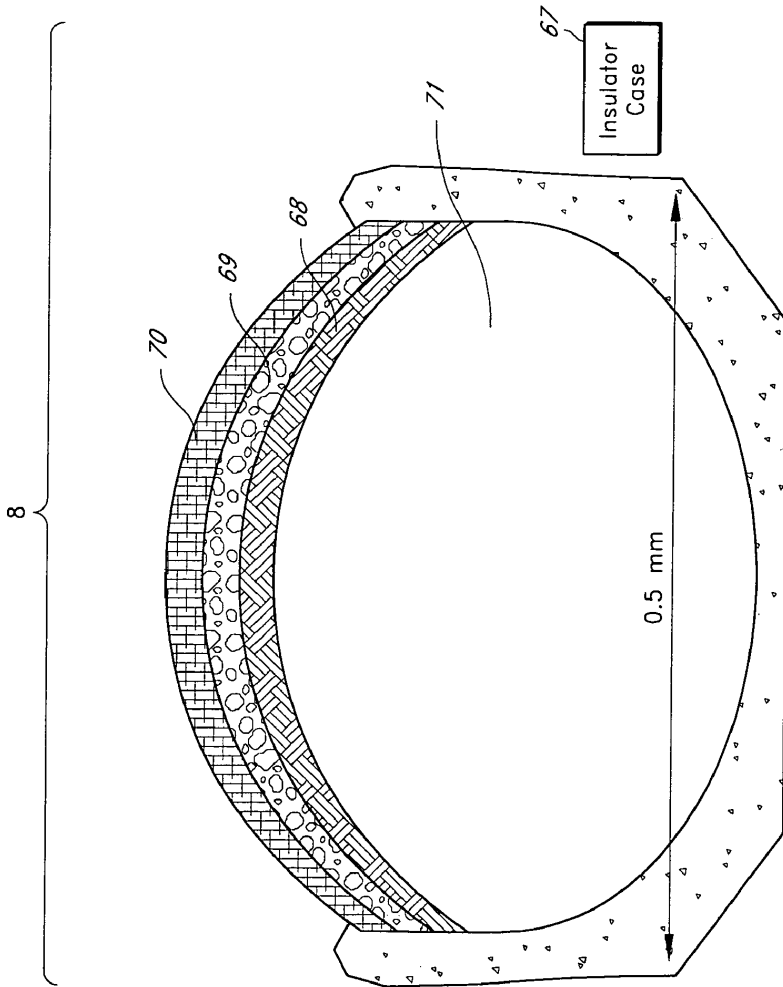


FIG. 7

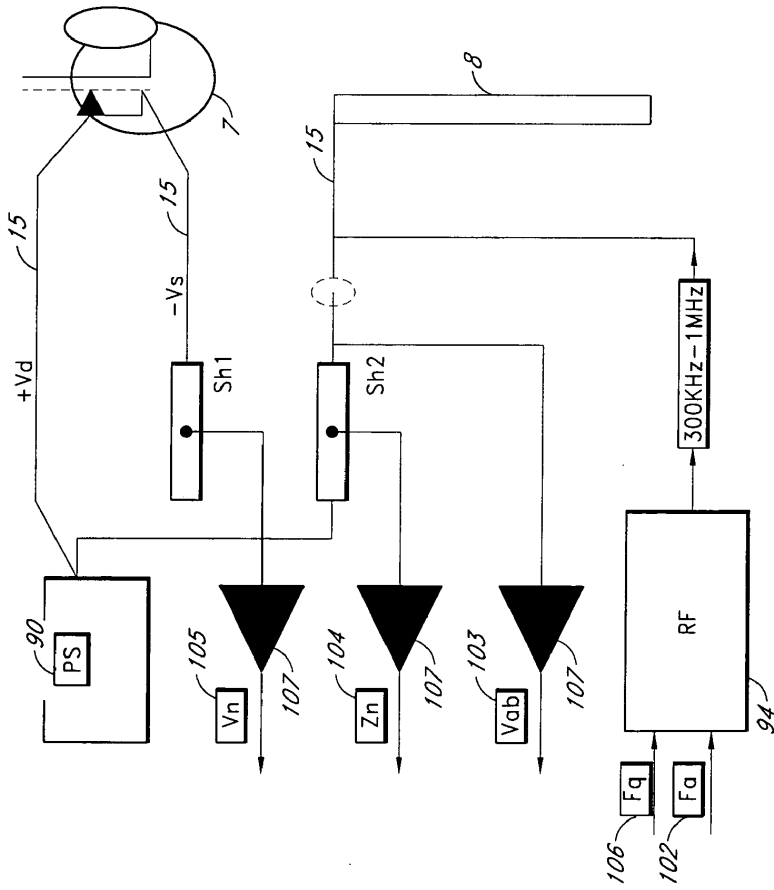
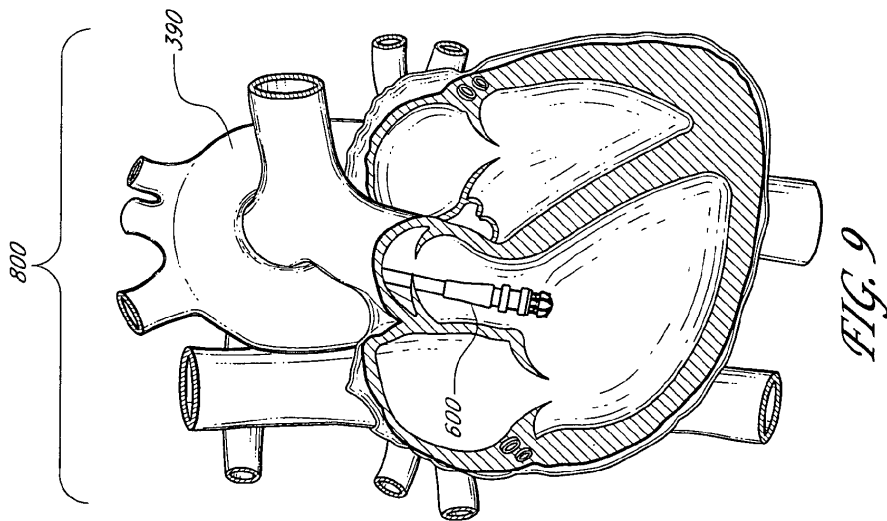
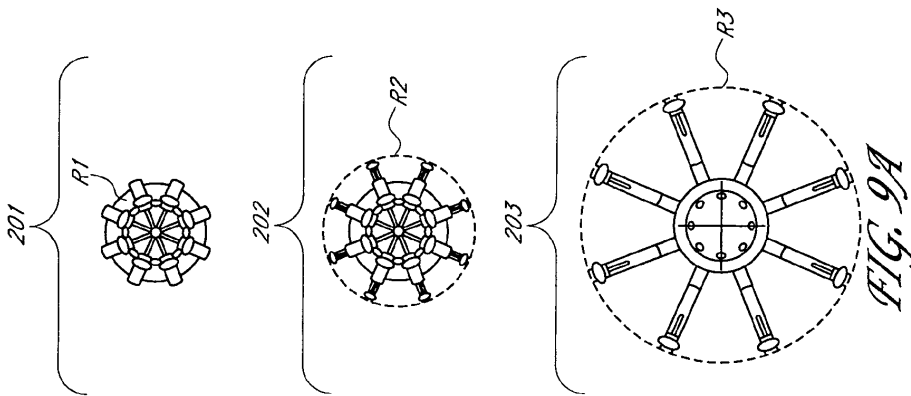


FIG. 8



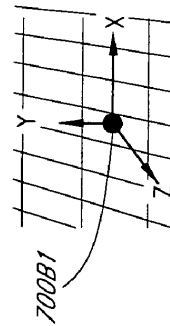
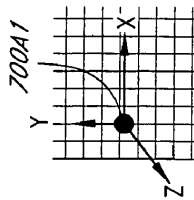
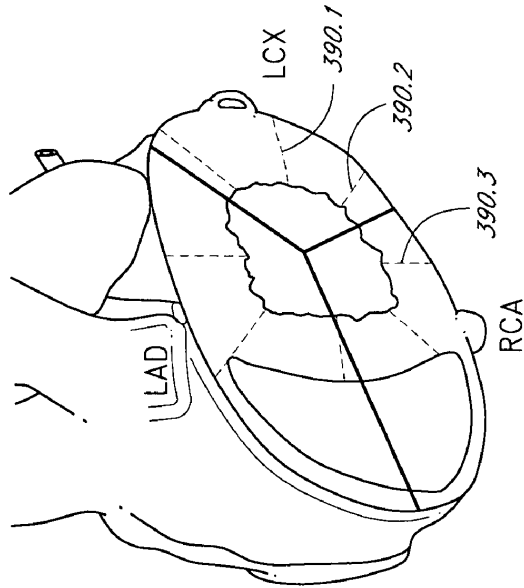
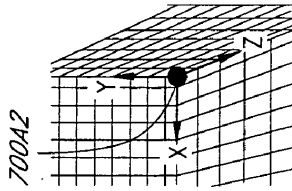
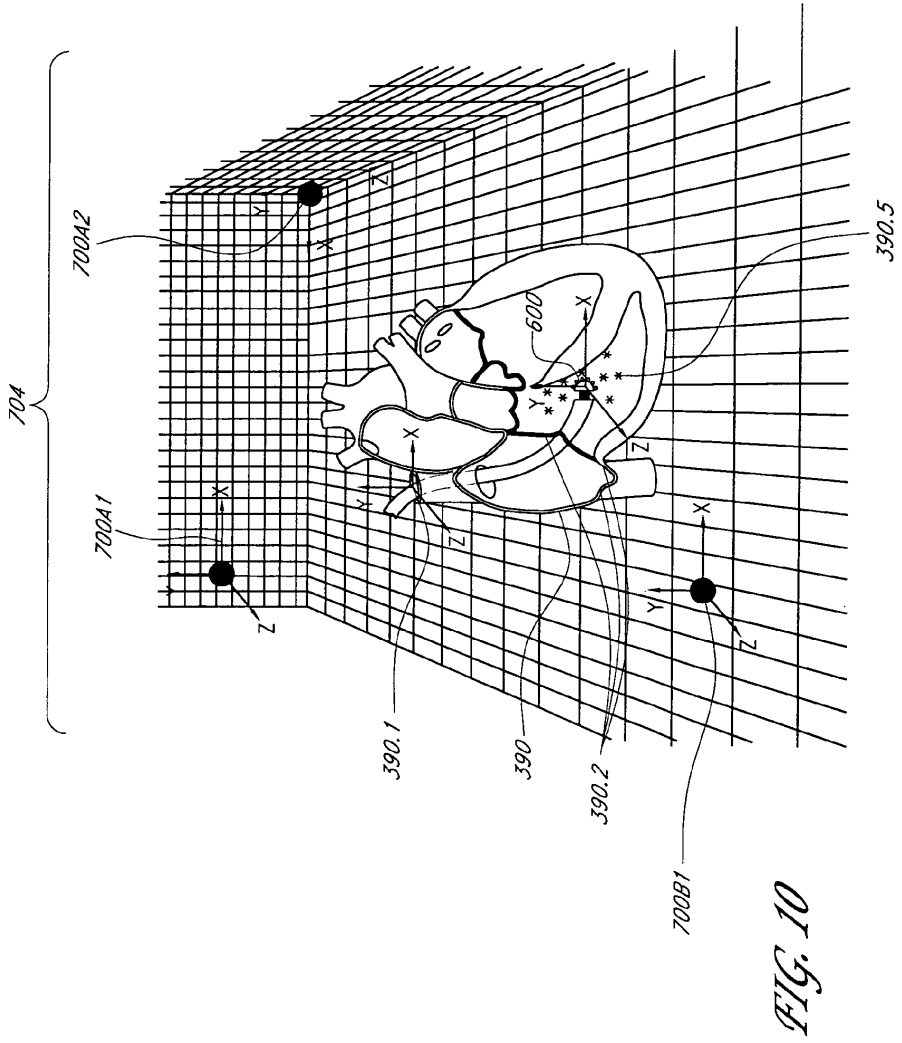


FIG. 9B





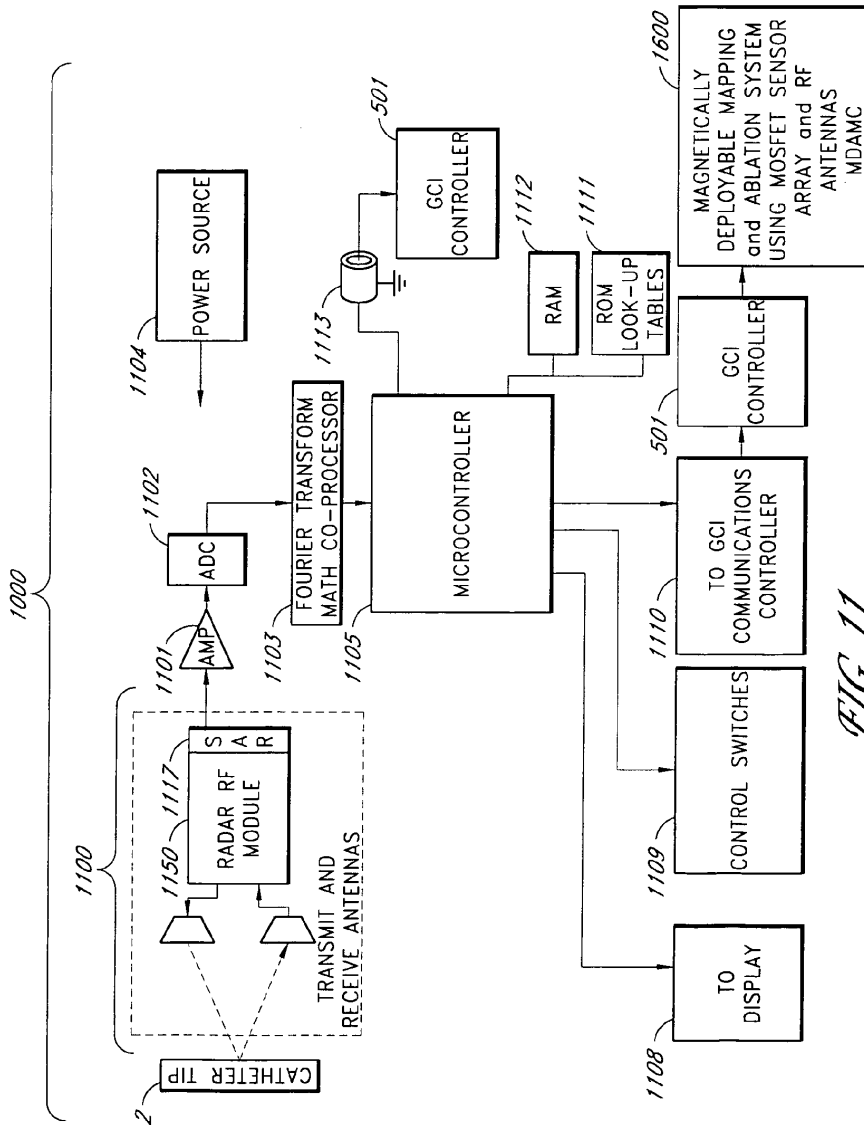
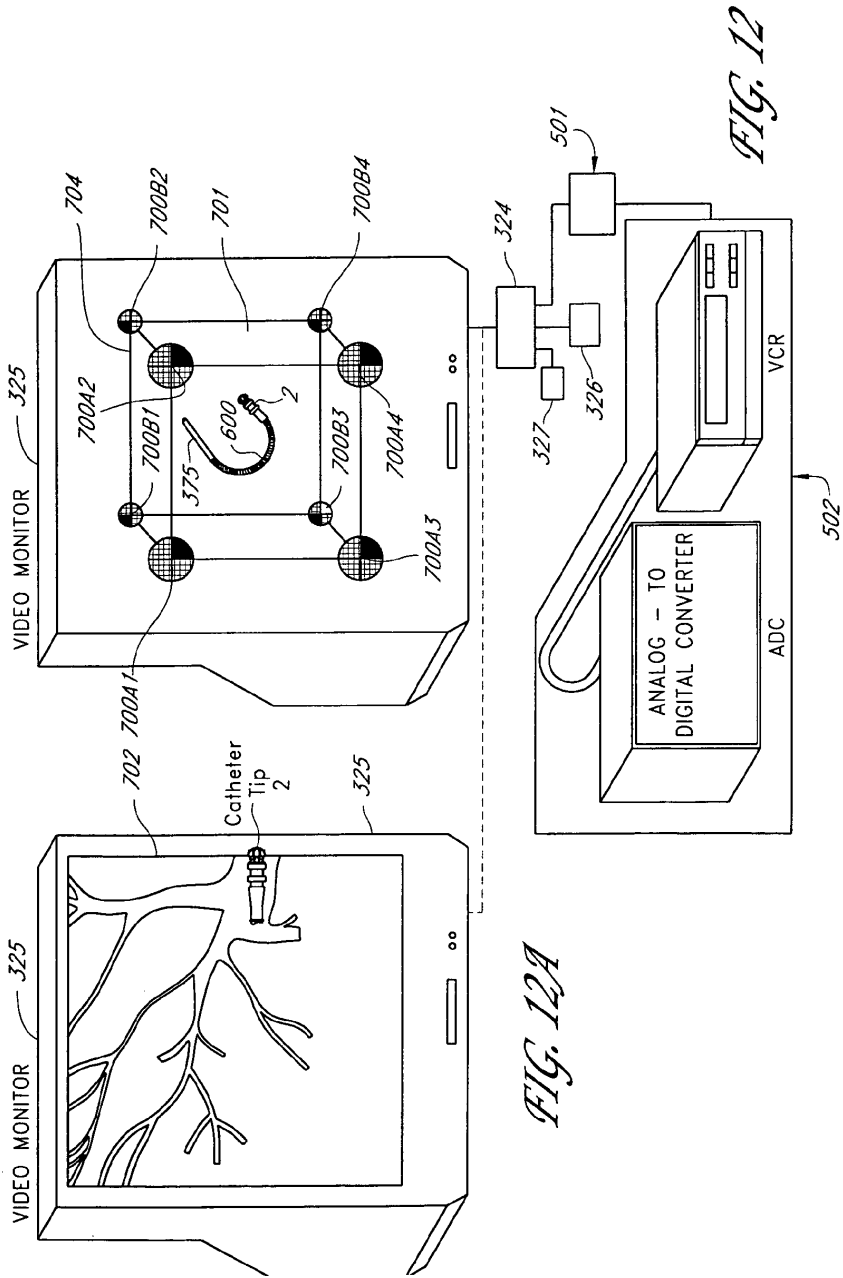


FIG. 11







**APPARATUS FOR MAGNETICALLY  
DEPLOYABLE CATHETER WITH MOSFET  
SENSOR AND METHOD FOR MAPPING AND  
ABLATION**

FIELD OF THE INVENTION

**[0001]** A method and apparatus for navigating and recording electrical characteristics of the heart using a MOSFET sensor guided by a magnetically-deployable mechanism is described.

BACKGROUND

**[0002]** Cardiac mapping using catheters introduced precutaneously into the heart chambers while recording the electrical potential and subsequently correlating the endocardial electrograms to specific anatomy of the heart suffers from multiple drawbacks. The use of fluoroscopy for correlating geometry and metrics is limited by the two-dimensional imagery of the fluoroscopy. The geometrical interpolation of the data and error reduction technique used in order to “best fit” the electrode and the site is at best an approximation. Another drawback of the existing art is the inability of existing methods to determine the measurement position in order to collect additional data points.

**[0003]** Therefore, there is a substantial and unsatisfied need for an apparatus and method for guiding, steering, advancing, and locating the position of the mapping electrode for measurement of electrical potential and for providing a three-dimensional image data.

SUMMARY

**[0004]** These and other problems are solved by providing a magnetically-deployable catheter control and system using a MOSFET sensor array. In one embodiment, the sensor provides better fidelity of the signal measurements as well as data collection and reduces the error generated by spatial distribution of the isotropic and anisotropic wavefronts. In one embodiment, the system maps the change in potential in the vicinity of the activation wavefront, which provides data on the thickness of the activation wavefront. In one embodiment, the mapping system tracks the spread of excitation in the heart, with properties such as propagation velocity changes. In one embodiment, during measurement, the manifold carrying the sensor array expands from a closed position state to a deployable open state [umbrella], which can sample and hold a set of data points for each QRS cycle. Spatial variation of the electrical potential is captured by the system’s ability to occupy the same three-dimensional coordinate set for repeated measurements of the desired site. In one embodiment, an interpolation algorithm tracks the electrogram data points so as to produce a map relative to the electrocardiogram data.

**[0005]** In one embodiment, a magnetically-deployable catheter uses a MOSFET sensor matrix for mapping and ablation. In one embodiment, a MOSFET sensor array and RF radiating antennas are configured to provide multiple states of deployable sensor configurations (radial). In one embodiment, radial umbrella-like arrays are used. The arrays sense activation spread as an energetic event. The dynamic variations of electric potential during de-polarization and re-polarization of the excitable cells of the heart can be measured as the activation avalanches.

**[0006]** In one embodiment, the electrical and magnetic fields during cell activation, are measured. In one embodiment, an algorithm describes these fields and calculates the dynamic spread of the energy contained in the electric and magnetic fields, and in the multi-source excitable cell of the hearts myocardium region.

**[0007]** The energy event as a methodology of representing the cardiac activation spread can be used for diagnostic and pathological assessment as well as for forming maps of the superimposed electric and energy wave upon the anatomical detail generated by x-ray imagery or other imaging methods (e.g., MRI, CAT scans, etc.).

**[0008]** In one embodiment, a magnetically-deployable catheter with MOSFET sensor controlled by a magnetic catheter guidance, control, and imaging apparatus as described in U.S. patent application Ser. No. 10/690,472 titled, “System and Method for Radar Assisted catheter Guidance and Control” and US Patent 2004/0019447 and provisional application No. 60/396,302, the entire contents of which are hereby incorporated by reference.

**[0009]** In one embodiment, the system provides ablation and mapping while navigating and controlling the movements of the sensors and antennas manually.

**[0010]** In one embodiment, the system provides electrocardiographic maps of the myocardium region.

**[0011]** In one embodiment, the ablation and mapping apparatus is magnetically-deployable using mechanism which provides the measurement of surface potential and activation time matrix by the use of a plurality of sensing points. This measurement is further refined (Error Reduction Technique) along one or more measurement radii change in desired increments, and further enhanced by measurement steps along the circumference for each radius.

**[0012]** The electric potential data table provides for at least 24 element pairs ( $E_n$  and  $t_n$ ) for each catheter position along the myocardium.

**[0013]** In one embodiment, the sensor head measures the conductivity matrix between the sensing points during activation. The measurement can be refined (Error Reduction Technique) along radii changed in desired increments. In one embodiment, the measurements fidelity is improved by rotating the measurements as a sequence of measurements around the circumference for each radius. The conductivity data table has multiple elements for each new catheter position along the myocardium.

**[0014]** In one embodiment, the mapping capabilities of electric potential and conductivity activation spread measurements is supplemented with a display of the magnitude and direction of the activation energy wave along the myocardium. This energy wave contains complimentary information to the electric field measurements about the anisotropy of the myocardium related to its conductivity during the activation excitation spread.

**[0015]** In one embodiment, the apparatus displays the directional anisotropy between the electric field and the conductivity vector for cardiac disorder or pathology correlation.

**[0016]** In one embodiment, the system includes an RF ablation tool. The RF ablation antennas can be selected and activated independently by configuring the driving RF (300 kHz to 1 MHz) voltage phase-angle to obtain the required lesion geometry, such as, for example, elongated linear cuts with desired ablation depth.

[0017] In one embodiment, the ablation and mapping catheter uses the radar imaging and fiducial marker technique identified by U.S. application Ser. No. 10/690,472, hereby incorporated by reference, for use by catheter fitted with magnetically coupled devices.

[0018] In one embodiment, the collected potential, timing, conductivity and energy wave data is interpolated between the sensors and extrapolated into the muscle tissues of the heart. The results are then overlaid and displayed together with the apparatus noted by application Ser. No. 10/690,472 or other imaging systems.

[0019] In one embodiment, the catheter guidance system includes a closed-loop servo feedback system. In one embodiment, a radar system is used to determine the location of the distal end of the catheter inside the body, thus, minimizing or eliminating the use of ionizing radiation such as X-rays. The catheter guidance system can also be used in combination with an X-ray system (or other imaging systems) to provide additional imagery to the operator. The magnetic system used in the magnetic catheter guidance system can also be used to locate the catheter tip to provide location feedback to the operator and the control system. In one embodiment, a magnetic field source is used to create a magnetic field of sufficient strength and orientation to move a magnetically-responsive catheter tip in a desired direction by a desired amount.

[0020] In one embodiment, a multi-coil cluster is configured to move and/or shape the location of a magnetic field in 3D space relative to the patient. This magnetic shape control function provides efficient field shaping to produce desired magnetic fields for catheter manipulations in the operating region (effective space).

[0021] One embodiment includes a catheter and a guidance and control apparatus that allows the surgeon/operator to position the catheter tip inside a patient's body. The catheter guidance and control apparatus can maintain the catheter tip in the correct position.

[0022] One embodiment includes a catheter and a guidance and control apparatus that can steer the distal end of the catheter through arteries and forcefully advance it through plaque or other obstructions.

[0023] One embodiment includes a catheter guidance and control apparatus that is more intuitive and simpler to use, that displays the catheter tip location in three dimensions, that applies force at the catheter tip to pull, push, turn, or hold the tip as desired, and that is configured to producing a vibratory or pulsating motion of the tip with adjustable frequency and amplitude to aid in advancing the tip through plaque or other obstructions. One embodiment provides tactile feedback at the operator control to indicate an obstruction encountered by the tip.

[0024] In one embodiment, the Catheter Guidance Control and Imaging (CGCI) system allows a surgeon to advance, position a catheter, and to view the catheter's position in three dimensions by using a radar system to locate the distal end of the catheter. In one embodiment, the radar data can be combined with X-ray or other imagery to produce a composite display that includes radar and image data. In one embodiment, the radar system includes a Synthetic Aperture Radar (SAR). In one embodiment, the radar system includes a wideband radar. In one embodiment, the radar system includes an impulse radar.

[0025] One embodiment includes a user input device called a "virtual tip." The virtual tip includes a physical

assembly, similar to a joystick, which is manipulated by the surgeon/operator and delivers tactile feedback to the surgeon in the appropriate axis or axes if the actual tip encounters an obstacle. The Virtual tip includes a joystick type device that allows the surgeon to guide the actual catheter tip through the patient's body. When the actual catheter tip encounters an obstacle, the virtual tip provides tactile force feedback to the surgeon to indicate the presence of the obstacle. In one embodiment, the joystick includes a PHANTOM® Desktop™ haptic device manufactured by Sensable Technologies, Inc. In one embodiment, the virtual tip includes rotary control systems such as those manufactured by Hitachi Medical Systems America, Inc.

[0026] In one embodiment, the physical catheter tip (the distal end of the catheter) includes a permanent magnet that responds to the magnetic field generated externally to the patient's body. The external magnetic field pulls, pushes, turns, and holds the tip in the desired position. One of ordinary skill in the art will recognize that the permanent magnet can be replaced or augmented by an electromagnet.

[0027] In one embodiment, the physical catheter tip (the distal end of the catheter) includes a permanent magnet and two or more piezoelectric rings, or semiconductor polymer rings to allow the radar system to detect the second harmonics of the resonating signal emanating from the rings.

[0028] In one embodiment, the CGCI apparatus provides synchronization by using a radar and one or more fiducial markers to provide a stereotactic frame of reference.

[0029] In one embodiment, the CGCI apparatus uses numerical transformations to compute currents to be provided to various electromagnets and position of one or more of the electromagnet to control the magnetic field used to push/pull and rotate the catheter tip in an efficient manner.

[0030] In one embodiment, the CGCI apparatus includes a motorized and/or hydraulic mechanism to allow the electromagnet poles to be moved to a position and orientation that reduces the power requirements desired to push, pull, and rotate the catheter tip.

[0031] In one embodiment, the CGCI apparatus is used to perform an implantation of a pacemaker during an electrophysiological (EP) procedure.

[0032] In one embodiment, the CGCI apparatus uses radar or other sensors to measure, report and identify the location of a moving organ within the body (e.g., the heart, lungs, etc.) with respect to the catheter tip and one or more fiducial markers, so as to provide guidance, control, and imaging to compensate for movement of the organ, thereby, simplifying the surgeon's task of manipulating the catheter through the body.

[0033] In one embodiment, a servo system has a correction input that compensates for the dynamic position of a body part, or organ, such as the heart, thereby, offsetting the response such that the actual tip moves substantially in unison with the dynamic position (e.g., with the beating heart).

[0034] In one embodiment of the catheter guidance system: i) the operator adjusts the physical position of the virtual tip, ii) a change in the virtual tip position is encoded and provided along with data from a radar system, iii) the control system generates servo system commands that are sent to a servo system control apparatus, iv) the servo system control apparatus operates the servo mechanisms to adjust the position of one or more electromagnet clusters by varying the distance and/or angle of the electromagnet

clusters and energizing the electromagnets to control the magnetic catheter tip within the patient's body, v) the new position of the actual catheter tip is then sensed by the radar, thereby, allowing synchronization and superimposing of the catheter position on an image produced by fluoroscopy and/or other imaging modality, vi) providing feedback to the servo system control apparatus and to the operator interface, and vii) updating the displayed image of the catheter tip position in relation to the patient's internal body structures.

#### BRIEF DESCRIPTION OF THE FIGURES

**[0035]** FIG. 1 is a system block diagram for a surgery system that includes an operator interface, a catheter guidance system (CGCI) and surgical equipment including a system for mapping and ablation apparatus.

**[0036]** FIG. 1A is a block diagram of the imaging module for use in the CGCI surgery procedure that includes the catheter guidance system, a radar system, Hall Effect sensors and the mapping and ablation apparatus.

**[0037]** FIG. 1B is a flow chart of the process for conducting an ablation procedure using the CGCI system that includes a radar system, Hall Effect sensors and the mapping and ablation apparatus.

**[0038]** FIG. 2 is a block diagram of the mapping and ablation control and mapping system.

**[0039]** FIG. 3 shows computer-generated and E-cardiac images including: an ECG graph with its corresponding ECG plot on an x-y plane; a conductivity map represented on the x-y plane; and a composite energy and E-vector display.

**[0040]** FIG. 3A is a flow chart of the pre-ablation simulation used to predict the ablation results prior to performing the actual ablation procedure.

**[0041]** FIGS. 4, 4A, 4B and 4C shows an orthographic representation of the mapping and ablation catheter with its physical attributes.

**[0042]** FIGS. 4D, 4E, 4F, and 4G are orthographic depictions of a magnetically-deployable guidewire and ablation tool and catheter.

**[0043]** FIG. 4H shows an orthographic representation of the mapping and ablation catheter in a deployed state.

**[0044]** FIGS. 4I, 4J, 4K, 4L, and 4M are orthographic depictions of the wiring and electrical connections of the antennas, MOSFETs, and coils forming the circuit layout of the ablation and mapping assembly.

**[0045]** FIG. 5 is a schematic diagram of the MOSFET sensor used in measuring the electric potential.

**[0046]** FIGS. 6, 6A, and 6B show the magnetically-deployable mechanism used to reduce the measurement error and increase the surface area of the measured event.

**[0047]** FIG. 7 is a cross-sectional view of the RF antenna.

**[0048]** FIG. 8 is a schematic representation of the ablation tool and its attributes.

**[0049]** FIGS. 9 and 9A show the catheter with closed, intermediary and fully open geometry states.

**[0050]** FIG. 9B shows the endocardial electrogram map resulting from sequential measurements of electrical potential detected by the catheter at various open geometry states.

**[0051]** FIG. 10 is an isometric drawing of the image capture and maps formation.

**[0052]** FIG. 11 is a block diagram of the radar used in forming the dimensional manifold of the electrogram.

**[0053]** FIGS. 11A and 11B illustrate identification of the catheter position and the anatomical features.

**[0054]** FIGS. 12 and 12A show the manifold with its fiducial markers used in forming the stereotactic frame.

#### DETAILED DESCRIPTION

**[0055]** FIG. 1 is a system block diagram for a surgery system 800 that includes an operator interface 500, a CGCI system 1500, the surgical equipment 502 (e.g., a catheter tip 2, etc.), one or more user input devices 900, and a patient 390. The user input devices 900 can include one or more of a joystick, a mouse, a keyboard, a virtual tip 905, and other devices to allow the surgeon to provide command inputs to control the motion and orientation of the catheter tip 2.

**[0056]** In one embodiment, the CGCI system 800 includes a controller 501 and an imaging synchronization module 701. FIG. 1 shows the overall relationship between the various functional units and the operator interface 500, auxiliary equipment 502, and the patient 390. In one embodiment, the CGCI system controller 501 calculates the Actual Tip (AT) position of the distal end of a catheter. Using data from the Virtual Tip (VT) 905 and the imaging and synchronization module 701, the CGCI system controller 501 determines the position error, which is the difference between the actual tip position (AP) and the desired tip position (DP). In one embodiment, the controller 501 controls electromagnets to move the catheter tip in a direction selected to minimize the position error (PE). In one embodiment, the CGCI system controller 501, provides tactile feedback to the operator by providing force-feedback to the VT 905.

**[0057]** FIG. 1A is a block diagram of a surgery system 503 that represents one embodiment of the CGCI system 1500. The system 503 includes the controller 501, a radar system 1000, a Hall effect sensor array 350 and a hydraulically-actuated system 1600. In one embodiment, the sensor 350 includes one or more Hall effect magnetic sensors. The radar system 1000 can be configured as an ultra-wideband radar, an impulse radar, a Continuous-Wave (CW) radar, a Frequency-Modulated CW (FM-CW) radar, a pulse-Doppler radar, etc. In one embodiment, the radar system 1000 uses Synthetic Aperture Radar (SAR) processing to produce a radar image.

**[0058]** In one embodiment, the radar system 1000 includes an ultra-wideband radar such as described, for example, in U.S. Pat. No. 5,774,091, hereby incorporated by reference in its entirety. In one embodiment, the radar 1000 is configured as a radar range finder to identify the location of the catheter tip 2. The radar 1000 is configured to locate reference markers (fiducial markers) placed on or in the patient 390. Data regarding location of the reference markers can be used, for example, for image capture synchronization 701. The motorized hydraulically and actuated motion control system 1600 allows the electromagnets of the cylindrical coils 51AT and 51DT to be moved relative to the patient 390.

**[0059]** In one embodiment, the use of the radar system 1000 for identifying the position of the catheter tip 2 has advantages over the use of Fluoroscopy, Ultrasound, Magnetostrictive sensors, or SQUID. Radar can provide accurate dynamic position information, which provides for real-time, relatively high resolution, relatively high fidelity compatibility in the presence of strong magnetic fields. Self-calibration of the range measurement can be based on time-of-flight and/or Doppler processing. Radar further provides for measurement of catheter position while ignoring "Hard" surfaces such as a rib cage, bone structure, etc., as

these do not substantially interfere with measurement or hamper accuracy of the measurement. In addition, movement and displacement of organs (e.g., pulmonary expansion and rib cage displacement as well as cardio output during diastole or systole) do not require an adjustment or correction of the radar signal. Radar can be used in the presence of movement since radar burst emission above 1 GHz can be used with sampling rates of 50 Hz or more, while heart movement and catheter dynamics typically occur at 0.1 Hz to 2 Hz.

[0060] In one embodiment, the use of the radar system 1000 reduces the need for complex image capture techniques normally associated with expensive modalities such as fluoroscopy, ultrasound, Magnetostrictive technology, or SQUID which require computationally-intensive processing in order to translate the pictorial view and reduce it to a coordinate data set. Position data synchronization of the catheter tip 2 and the organ in motion is available through the use of the radar system 1000. The radar system 1000 can be used with phased-array or Synthetic Aperture processing to develop detailed images of the catheter location in the body and the structures of the body. In one embodiment, the radar system 1000 includes an Ultra Wide Band (UWB) radar with a relatively high resolution swept range gate. In one embodiment, a differential sampling receiver is used to effectively reduce ringing and other aberrations included in the receiver by the near proximity of the transmit antenna. As with X-ray systems, the radar system 1000 can detect the presence of obstacles or objects located behind barriers such as bone structures. The presence of different substances with different dielectric constants such as fat tissue, muscle tissue, water, etc., can be detected and discerned. The outputs from the radar can be correlated with similar units such as multiple catheters used in Electro-Physiology (EP) studies while detecting spatial location of other catheters present in the heart lumen. The radar system 1000 can use a phased array antenna and/or SAR to produce 3D synthetic radar images of the body structures, catheter tip 2, organs, etc.

[0061] In one embodiment, the location of the patient relative to the CGCI system (including the radar system 1000) can be determined by using the radar 1000 to locate one or more fiducial markers. In one embodiment, the data from the radar 1000 is used to locate the body with respect to an imaging system. The catheter position data from the radar 1000 can be superimposed (synchronized) with the images produced by the imaging system. The ability of the radar and the optional Hall effect sensors 350 to accurately measure the position of the catheter tip 2 relative to the stereotactic frame allows the controller 501 to control movement of the catheter tip.

[0062] FIG. 2 is a functional block diagram of the magnetically-deployable electrocardiographic (ECG) and RF ablation catheter (MDAMC) and its associated supporting equipments. The system 1600 includes a catheter assembly, having an electrocardiographic and ablation tool. An ECG sensor head 100 includes eight MOSFET sensors 7 ( $S_1, S_2, S_3, S_4, S_5, S_6, S_7, S_8$ ) and eight RF antennas 8, a coil 3, and its counterpart coil 14 (forming the magnetic mechanism), an elongated catheter body having a proximal end and an internal longitudinal lumen 1, and a bus wire harness 15. The tool is connected via the bus wire 15 to the ECG coils 3 and 14 driver and control 204. The electrocardiographic mapping and ablation catheter is provided to an ECG data

interpolation unit 205. Data analyzed by the ECG interpolation unit 205 is used by the ablation RF power generator 94 which activates the RF antennas 8. The information generated by the ECG probe is provided to the application specific computer 91 with its software 200 made by National Instrument and MathLab processing software used to control the probe to display its findings on the control display 93, as well as the electrocardiac display 92. The system is powered by a UPS 90.

[0063] In one embodiment, a diagnostic method employed by the magnetically deployable mapping and ablation catheter (MDAMC) is statistically based on correlating electrical activity with anatomical features which further allows the practitioner to evaluate certain patterns. In one embodiment, a biophysical model is used with the electrophysiological outputs to cardiac function as well as to the waveform obtained to form a map or maps of the cardiac wave. The data points measured by the sensor 100 with its MOSFET devices 7 coupled with the wavefront characterization as defined by the Poynting Energy Vector (PEV) 49, are analyzed and graphically represented using the control display 93 and the e-cardiac display 92. Correlating the electric generator during the depolarization phase in the cardiac model is related to the fact that surface-carrying elementary current dipoles (from the cellular ion kinetics across membranes) imply the subsequent avalanche (wavefronts) as it progresses through the myocardium (see e.g., A. Van Oosterom "Source Modeling of Bioelectric Signals", Proc. 3-ed, Rayner Granit Symposium (J. Malmivno ed.) Vol. 8-6, pp 27-32 1994).

[0064] FIG. 1B is a flow chart of the process for conducting an ablation procedure using the CGCI system that includes a radar system, Hall Effect sensors and the mapping and ablation apparatus. In one embodiment, the catheter is navigated to the mapping site using the CGCI and the Synthetic Aperture Radar. The catheter sensor arms are opened and touch the cardiac tissue. The radar reads the site position, and the sensor arm diameter and angle setting is recorded. The sensors then autocalibrate and measure the activation potential and impedances. The results are placed into the matrix created for activation potential and the matrix created for impedances; the results are accumulated over many cycles. The diameter and angle of the catheter is detected and then both are increased electromagnetically, and new data matrixes are recorded at the new diameter and angle. The activation potential and impedance matrix data is scaled and loaded into a high speed Spice computational program. The trigger threshold, timing cycle and interconnecting impedances of the simulated excitable cells are correlated and set to represent the tissue property at the site. These values are modified by the data. The output of the Spice simulation of the E vector map, the impedance map, and the Energy map are displayed as 2D/3D surfaces, vectors and repetitive transient wavefronts. Then the user marks a trial lesion area. Then the system displays the effects of the pre-ablation simulation of the trial lesion.

[0065] FIG. 2 is a functional diagram of the main attributes which will become clear for those familiar with the art as will reading the descriptions and ensuing objects noted by the drawings which accompany them.

[0066] FIG. 3 shows the wavefront showing the Poynting Energy Vector (PEV) 49 measuring the electrical potential and interpretation of the electrical activity as well as mapping of such wavefront propagation. In one embodiment, a



mathematical algorithm is used for interpolation so as to achieve a relatively coherent view of the activation path while deriving a set of secondary measurable values such as Electric Heart Vector (EHV), Magnetic Dipole (MHV) as well as impedance measure of the myocardium wall.

**[0067]** The first assumption this method used is that cardiac activation spread is a relatively energetic event. It is further assumed in this model that in addition to the dynamic variations of electrical potentials during de-polarization and re-polarization of the excitable cell of the heart, a spread of electro magnetic energy is observed as the activation avalanches.

**[0068]** In one embodiment, the system measures both the electric and magnetic fields during cell activation. (model relationship of normal activation sequences and degree of inter individual variability is detailed, for example, in K. Simelius et al, "Electromagnetic Extra cardiac fields simulated with bidomain propagation model," Lab of Biomedical Engineering, Fin-02015, Hut, Finland, hereby incorporated by reference).

**[0069]** The dynamic spread of the energy contained in the electric and magnetic fields are then described by the use of Maxwell equations as applied to the conduction system of the individual rather than reproducing the anatomical variation that leads to anisotropic myocardium. This "energy model" approach provides for calculation of the dynamic spread of energy contained in the electric and magnetic fields and respectively in the multisource excitable cells of the heart's myocardium region to be represented and hence mapped without the assumptions of idealized models.

**[0070]** The data analysis and extraction of diagnostic as well as pathological information can be mapped as a super-imposed electric and energy wave.

**[0071]** To overcome the measurement limitations of myocardial anisotropy, and due to production of slam magnetic fields during an activation sequence, the algorithm and apparatus is able to regain the detection capability of a magnetic dipole (MHV) by the use of another vector derived from Maxwell's equations, the Poynting Energy Vector (PEV) **49**.

**[0072]** Clinical observations reported that measuring the angle between vectors of equivalent electric dipole (electric heart vector, EHV) and magnetic dipole (Magnetic Heart Vector) provides significant corollary information about the myocardium conductivity. The overall anisotropic case of the myocardium conductivity is represented by a tensor. The degree of anisotropic conductivity manifestation is characterized by an angle along the transversal and axial conductivity paths.

**[0073]** The solution for measuring and deriving the relationship between the Electric Heart Vector (EHV) and its respective magnetic dipole vector (MHV), (hence, supplementing the analytical mapping with additional information about the myocardium conductivity and anisotropy), is derived from Maxwell's equation as the Poynting Energy Vector (PEV) **49**. The PEV is constructed from the multiple potential and impedance vectors of the measurements. In one embodiment, a magnetically-deployable mapping and ablation catheter using MOSFET is used for potential sensing. A matrix arrangement for phase rotation for RF generation and the angle  $\beta$  between the PEV and EHV is used to infer the features of anisotropy in the myocardium. The anisotropy of the conductivity is uniform, hence activation energy change generated and consumed by the ionic diffu-

sion process is within the activation region of the measurement. Thus, the volume integrations is accurate, with a margin of error reduction based on two independent techniques, one statistical (monte carlo) and Tikhonov regularization filtering.

**[0074]** In one embodiment, the law of energy conservation is used for the time period of the two QRS cycle (e.g., 1152 data measurements) to acquire the initial baseline data foundation to form the map.

**[0075]** The validity of the Poynting Energy Vector (PEV) **49** derivation is corroborated by the fact that the activation spread obeys the mathematical identity that the Poynting Energy Vector (PEV) **49** is directly exhibiting the E and B fields phase angle relationship. The integral form of Maxwell's equations leads to the Poynting Energy Vector (PEV) **49**, and to the substitution of E and Z derivations of this vector.

**[0076]** Maxwell's second set of time varying equations can be written as:

$$\nabla \times E = -\frac{dB}{dt} \quad (1)$$

**[0077]** and

$$\nabla \times B = \zeta\mu\frac{dB}{dt} + \mu J \quad (2)$$

**[0078]** By multiplying B and E respectively and subtracting Equation (2) from Equation (1) and using vector identities yields

$$B \cdot (\nabla \times E) = -B \cdot \frac{dB}{dt} \quad (3)$$

**[0079]** and

$$E \cdot (\nabla \times B) = \zeta\mu\left(E \cdot \frac{dB}{dt}\right) + \mu(E \cdot J) \quad (4)$$

**[0080]** Subtracting, rearranging and using vector identities yields.

$$\nabla \cdot (E \times B) = B \cdot (\nabla \times E) - E \cdot (\nabla \times B) \quad (5)$$

$$\nabla \cdot (E \times B) = -\frac{d}{dx}\left(\frac{1}{2}B \cdot B\right) - \frac{d}{dx}(\zeta\mu E \cdot E) - \mu JE \quad (6)$$

$$\nabla \cdot \left[ \left( \frac{1}{\mu} E \times B \right) \right] + \frac{d}{dx} \left[ \frac{\zeta}{2} E^2 + \frac{1}{2\mu} B^2 \right] + J \cdot E = 0 \quad (7)$$

[0081] Integrating both sides of Equation (7) over the volume V and within the boundary Y gives:

$$\int_{\mu}^1 (E \times B) \cdot dS + \frac{d}{dx} \int \left( \frac{\sigma}{2} E^2 + \frac{1}{2\mu} B^2 \right) d\tau + \int (J \cdot E - \sigma E^2) d\tau = 0 \tag{8}$$

[0082] Equation (8) is a representation of the energy equation in which the first term (8.1) is the energy flux out of Y boundary of V. The second term (8.2) is the rate of change of the sum of the electric and magnetic fields. The third term (8.3) is the rate of work within V done by the fields on the ionic charges.

[0083] The last term in Equation (8) assumes the inclusion of the energy of the multiple sources of cell, ionic charge exchanges, thus:

$$\int_{\mu}^1 (E \times B) \cdot dS + \frac{d}{dx} \int \left( \frac{\sigma}{2} E^2 + \frac{1}{2\mu} B^2 \right) d\tau + \int (J \cdot E - \sigma E^2) d\tau = 0 \tag{9}$$

[0084] Equation (9) leads to the Poynting Energy Vector (PEV) 49 of

$$E = \frac{1}{\mu} (E \times B) + s \text{ where } \nabla \cdot s = 0 \text{ (Poynting Energy Vector)} \tag{10}$$

[0085] The parameter of interest is the angle between the electric field and energy field. The vector E is obtained from energy vector from E field measurements by calculating the Z impedance vector.

[0086] By using the measured potentials  $V_m$  and by employing Poisson equation, the E electric field is obtained:

$$\nabla \cdot \sigma \cdot \nabla V_m = 0 \text{ and } E = -\nabla V_m \tag{11}$$

[0087] Then, the Poynting Energy Vector (PEV) 49 can be written:

$$E = \frac{1}{\mu} \left( (E \cdot E) \cdot \frac{1}{Z} + c \right) \bar{n} \tag{12}$$

[0088] Where the E vector and impedance Z can be calculated from the measured data points.

[0089] One can further calculate the angle  $\beta$  between the E field and E energy vector, where the difference is such that:

$$90^\circ - \alpha = \beta. \tag{13}$$

[0090] A display of the E energy vector is useful for cardiac disorder identification. The E potential display serves a similar purpose as with other ECG systems, and the Z conductivity display is used to calculate the RF ablation power setting prior to the ablation procedure. FIG. 3A is a flow chart showing use of the pre-ablation simulation to verify the ablation results prior to performing the ablation

procedure. In one embodiment, measurements 3000 of E energy data and Z conductivity data are collected from the electrocardiographic mapping and ablation catheter 600. This data is processed and displayed on a control display 93 and/or e-cardiac display 92. The user can mark a trial ablation area 3001 to conduct a simulation to verify the ablation results prior to performing the lesion. After the user marks the trial ablation area 3001, the system recalculates the E energy vector and Z conductivity to account for the hypothetical lesion, and determines the amount of RF energy that is necessary to create the lesion such that the desired conduction path is severed. Then the system displays the information 3002 on control display 93 and e-cardiac display 92. After analyzing the information, the user makes a decision 3003 as whether the user desires to repeat the process or conduct the ablation procedure based on the simulation.

[0091] The Poynting Energy Vector (PEV) 49 indicates that there is a flux of energy where E and B are simultaneously present. The spread of the energy flux in the case of Maxwell's derivation is further defined by the wave equation:

$$\nabla \times E = -\frac{dB}{dt} \tag{14}$$

[0092] taking the curl of each side

$$\nabla \times \nabla \times E = -\frac{d}{dx} (\nabla \times B) \tag{15}$$

[0093] then

$$\nabla (\nabla \cdot E) - \nabla^2 E = -\frac{d}{dx} \left( \zeta \mu \frac{dE}{dt} \right) \tag{16}$$

[0094] Hence

$$\nabla^2 E - \zeta \mu \frac{\partial^2 E}{\partial t^2} = 0 \tag{17}$$

[0095] which is the wave equation.

[0096] In one embodiment, a simplified FEA program is used to extrapolate the energy wave for display.

[0097] The conditions for defining the actual material constants  $\zeta \mu$  and the measured Z are related to Hadamard observation for a well posed problem so as to yield a solution for each data set.

[0098] FIG. 3 is a computer generated 91 and E-cardiac displayed 92 image comprising of 4 basic visual; an ECG graph 54 with its corresponding ECG plot and an x-y plane; a conductivity map represented on the x-y plane and a composite energy and E-vector display 53.1. The visual shown in FIG. 3 is the result of the observation that cardiac activation spread is an energetic event as defined by the formalism presented. The apparatus 1600 measure the cardiac activation spreads as an energetic event (using the MOSFET Sensor Head 100). The dynamic variations of

electric potentials during de-polarization and re polarization of the excitable cells is measured, computed, and displayed as a spread of electromagnetic energy (as an activation avalanches). This energy is generated by the myriads of excitable cells and expands within the heart by propagating as an energy wavefront described by the formalism in Equation (17).

**[0099]** This wavefront propagation provides the clinician additional diagnostic information in addition to the prior art ECG measurements.

**[0100]** Deducing the magnetic heart vector (MHV) by using, at least in part, the energy heart vector PEV 49 is facilitated by the fact that the CGCI navigating and combining apparatus 501. By using the measured conductivity value and the corresponding ECG data, it is possible to derive the PEV 49 value which represent the energy heart vector (EHV), were E and Z is substituted for B. The apparatus 1600 measures and constructs the energy vector from the multiple potential and impedance vectors of the measurements and the algorithm for computing the PEV 49 and the EHV. The computer 91 and its software 200 such as, for example, Labview and MathLab, can calculate and display the composite image of the energy vector 49 and the E-vector 40 shown as an image 53.1. From the angle between the PEV 49 and the EHV 40, the physician can infer the features of anisotropy in the myocardium. In summary, FIG. 3 shows the electrocardiographic maps of the myocardium region with details of directly measured potentials on the endocardial surface. It further measures the surface potential and activation time matrix. The apparatus 1600 measures the conductivity-time matrix between the sensing points during activation. The composite display indicates the directional anisotropy between the sensing points during activation. The composite display shows the directional anisotropy between the electric potential vector and the energy vector for the cardiac disorder.

**[0101]** FIGS. 4, 4A, 4B, 4C and 4H are orthographic representations of the magnetically-deployable ablation and mapping catheter 600. An elongated catheter 1 body having a proximal end and an internal longitudinal distal end lumen. The catheter 1 is coupled to permanent magnet 2, forming part of the dynamic mechanism of the deployable sensor head assembly 50. The magnetically-deployable sensor head 50, includes a flange holder 5, which supports the semi-spherical dome 9, protecting the eight sensors 7, and their associated RF antennas 8, in a cluster as shown. The sensor head 50 extends towards catheter 1 body to form cylinder 9A which is received into a cavity 3 that is within the permanent magnet 2. The interior of cylinder 9A contains one or more spiral ridges 9B for engaging a screw, bolt or other device with corresponding spiral ridges. In one embodiment, arms 6 connect to a plurality of springs which connect to the deployable sensor head 50 such that the deployable sensor head 50 is in the closed state when the springs are relaxed. When the axial movement of coils 3 and 14 displaces the arm 6 (which holds the sensors 7 and the RF antenna 8) so as to form an "umbrella" with multiple deployment states (201, 202, and 203), the plurality of springs provide resistance to bias the arms 6 towards the closed position. In one embodiment, arms 6 connect to a cable that allows the user to mechanically open and close the deployable sensor head 50 without the use of axial movement of coils 3 and 14.

**[0102]** Two coils 3 and 14 are shown as traveling on a guide rail 4. The assembly is further fitted with an irrigation

tunnel 10, and a cooling manifold (not shown for clarity). The catheter 600 is further embedded with a conductive ring 13, forming the ground of the electrical circuit of the ablation and potential measurements (a feature which becomes clearer in the ensuing Figures).

**[0103]** FIG. 4A depicts the sensor head assembly 50, in its closed state where the antennas 8, are nested in the semi-spherical dome 9 and its function is explained in detail while comparing the intermediary state 202 and fully deployable state (the umbrella) shown in FIG. 4C. The relationships between the three deployable states; 201 closed, 202 intermediary and fully deployable state 203 in connection with the MOSFET sensor 7 measurements and the RF antenna 8 radiating mode are described.

**[0104]** The configuration shown in FIG. 4 where the irrigation tunnel is leading to the irrigation manifold 10, is used to provide a saline water solution so as to cool the radiating antennas 8, while improving the conductivity measurements 62 (impedance (Z)) during the ablation procedure.

**[0105]** FIG. 4B further shows the use of a guidewire 379, inserted through the tunnel cavity 10 (used for irrigation) so as to afford a safety measure to allow the catheter head 50 to be retrieved back to its closed state 201. In one embodiment, guidewire 379 screws into region 9B to connect to cylinder 9A. The safety procedure is such that when a power failure or debris collecting on the catheter (such as fat tissue, plaque, or a combination thereof) surfaces prevents retrieval of the antennas 8 to its closed state 201. The operator then inserts a guidewire 379 through the irrigation tunnel, engages cylinder 9A, and mechanically pulls the flange 5 back to its closed state.

**[0106]** FIGS. 4D and 4E show an improved catheter assembly 375 and guidewire assembly 379 to be used with the CGCI apparatus 1500. The catheter assembly 375 is a tubular tool that includes a catheter body 376 which extends into a flexible section 378 that possesses increased flexibility for allowing a more rigid responsive tip 2 to be accurately steered through a torturous path.

**[0107]** The magnetic catheter assembly 375 in combination with the CGCI apparatus 1500 reduces or eliminates the need for the plethora of shapes normally needed to perform diagnostic and therapeutic procedures. This is due to the fact that during a conventional catheterization procedure, the surgeon often encounters difficulty in guiding the conventional catheter to the desired position, since the process is manual and relies on manual dexterity to maneuver the catheter through a tortuous path of, for example, the cardiovascular system. Thus, a plethora of catheters in varying sizes and shapes are to be made available to the surgeon in order to assist him/her in the task, since such tasks require different bends in different situations due to natural anatomical variations within and between patients.

**[0108]** By using the CGCI apparatus 1500, only a single catheter is needed for most, if not all patients, because the catheterization procedure can be achieved with the help of an electromechanical system that guides the magnetic catheter and guidewire assembly 379 to the desired position within the patient's body 390 as dictated by the surgeon's manipulation of the virtual tip 905, without relying on the surgeon pushing the catheter, quasi-blindly, into the patient's body. The magnetic catheter and guidewire assembly 379 (e.g., the magnetic tip can be attracted or repelled by the electromagnets of the CGCI apparatus 1500) provides the

flexibility needed to overcome tortuous paths, since the CGCI apparatus 1500 overcomes most, if not all the physical limitations faced by the surgeon while attempting to manually advance the catheter tip 2 through the patient's body.

[0109] The guidewire assembly 379 is a tool with a guidewire body 380 and a responsive tip 2 to be steered around relatively sharp bends so as to navigate a relatively tortuous path through the patient. The responsive tips 2 of both the catheter assembly 375 and the guidewire assembly 379, respectively, include magnetic elements such as permanent magnets. The tip 2 includes permanent magnets that respond to the external flux generated by the electromagnets as detailed by patent application Ser. No. 10/690,472.

[0110] In one embodiment, the responsive tip 2 of the catheter assembly 375 is tubular, and the responsive tip 2 of the guidewire assembly 379 is a solid cylinder. The responsive tip 2 of the catheter assembly 375 is a dipole with longitudinal polar orientation created by the two ends of the magnetic element positioned longitudinally within it. The responsive tip 2 of the guidewire assembly 379 is a dipole with longitudinal polar orientation created by two ends of the magnetic element 2 positioned longitudinally within it. These longitudinal dipoles allow the manipulation of both responsive tip 2 with the CGCI apparatus 1500, as the electromagnet assemblies act on the tips 2 and "drag" it in unison to a desired position as dictated by the operator.

[0111] FIG. 4F illustrates a further embodiment of the catheter assembly 375 and guidewire assembly 379 to be used with the CGCI apparatus 1500. In FIG. 4F, a catheter assembly 310 is fitted with an additional two (or more) piezoelectric rings 311, and 312, located as shown. An ultrasonic detector in combination with the apparatus 1500 provides an additional detection modality of the catheter tip whereby an ultrasonic signal is emitted as to excite the two piezoelectric rings and provide a measure of rotation of the catheter tip relative to the North Pole axis of the magnet 2. With the aid of the computer, the CGCI apparatus 1500 is capable of defining the angle of rotation of the tip 2 and in the piezoelectric rings 311, 312 can provide additional position information to define the position, orientation, and rotation of the catheter tip 2 relative to the stereotactic framing available from the fiducial markers 700AX and 700BX.

[0112] FIG. 4G is an orthographic representation of the catheter assembly 600 used for mapping and ablation. The catheter 600, in combination with the CGCI apparatus 1500, allowing the guidance, control, and imaging of the catheter 600 as it is push/pulled, rotated, or fixed in position. The catheter 600 includes an elongated catheter body 376 having a proximal end and an internal longitudinal distal end lumen, where a permanent magnet 2 (e.g., a magnet formed out of NbFe35 is used as the coupling elements for the CGCI apparatus 1500 in navigating the catheter 600 to its desired designation. The catheter is also fitted with assembly 50 (magnetically deployable mechanism) and sensor/antenna head assembly 100.

[0113] FIG. 4I shows the sensor head assembly 100 and the deployable magnetic mechanism 50. FIG. 4I also shows wiring and conduction elements forming the electrical circuit. A conductor 15 is threaded through a conductor 2.1 formed out of suitable polymer and is nested inside permanent magnet 2. The permanent magnet 2 is further modified to accommodate an electrical insulator 2.2 and an electrical ribbon 2.3. The coil electrical contact 14.1 travels over the

ribbon 2.3 to form the "hot" lead (+) of the electrical circuit, while the return path (-) is the permanent magnet 2. Coil 14 and coil 3 (not shown for clarity) travels over the electrical ribbon 2.3 and similarly coil 3 travels over electrical ribbon 2.3 located 180° and electrical contact occurs when coil contact 3.1 is activated.

[0114] FIG. 4J is a cross sectional view of the catheter magnetic device 50 whereby, coil 14 is shown with its coil contact 14.1 and electrical ribbon 2.3 provide electrical connection between coil 14 and Power Supply 90 (shown in FIG. 8). The electrical isolation between the permanent magnet 2 and the electrical ribbon 2.3 is achieved with insulator 2.2. Further depicted are the conductor carriers (4 each) 2.1 and the irrigation tunnel 10.

[0115] FIG. 4K shows a top view cross section of the MOSFET sensor head 100 (shown in FIG. 2) where the electrical wiring schematic is defined relative to the antenna 8 and the MOSFET sensor 7.

[0116] FIG. 4L is an orthographic depiction of the wiring and electrical circuit wherein conductor 15 pairs are connected to the antenna 8 and the MOSFET sensor 7. Electrical ribbon 2.3 with its conductors are threaded through conductor carrier 2.1. A ground path is provided to ground ring 13 to close the electrical circuit.

[0117] FIG. 4M provides a view and its cross section of the wiring layout for the sensor 1600.

[0118] FIG. 5 is an orthographic depiction of the internal equivalent circuit of the sensor array. In one embodiment, there are eight MOSFET sensors on the ablation and mapping apparatus 600.

[0119] The MOSFET potential sensing device is a junction field effect transistor that allows a current to flow which is proportional to an electric field, basically emulating a voltage-controlled resistor. The module 100 includes a resistor. The resistor RD 17, is a linear resistor that models the ohmic resistance of source. The charge storage is modeled by two non-linear depletion layer capacitors, CGD 23 and CGS 24, and junction capacitors CBD 25, CGD 23, and CBS 19. The P-N junctions between the gate and source and gate and drain terminals are modeled by two parasitic diodes, VGD 22, and VGS 21. Gate 1 of the MOSFET sensor tip 28 is item 27 and gate 2 of the MOSFET sensor assembly 100 is item 26. Gate 1 with reference designator 27 at the sensor tip S(n) (n=1, 2, 3, . . . 8) is a relatively high impedance, insulated semiconductor structure. The device 100 behaves as voltage-controlled resistor. The potential between the gate structure 26, 27 and the drain-source structure (RS 18, RD 17) semiconductor substrate defines the transconductance of the output connections 16.

[0120] By connecting the drain-source 17, 18 structure to the sensor body 100, the potential reference for measurement is established. This reference is configured as a ring 13 along with the catheter body as shown. The measurement process of probe 100 is set to a zero voltage as the drain-source 17, 18 structure, the sensor's gate junction 27 assumes the tissue potential with a relatively small charging current flowing into the net parallel sum of the junction capacitors, CBD 25, CGD 23, and CGS 19. The drain-source 17, 18 voltages is then applied gradually to the device charging these capacitors from the outside power source, thereby "nulling" the current needed to form the gate so as to obtain the operating potential (about 6 VDC). The sensing procedure is relatively noninvasive to the cell as well as to the potential level and current drain of the probe 100 upon



the cardiac tissue. Gate 2, item 27 provides a biasing input so as to provide a continuous active mode for the probe 100. This input is also used for self-calibration of the probe 100.

[0121] FIGS. 6, 6A, and 6B are isometric representations of the actuating mechanism of the magnetically-deployable ablation catheter 50 including the coil 3 and its counterpart coil 14 traveling axially on the permanent magnet 2 (NbFe35). In one embodiment, coil 3 and its counterpart coil 14 travel axially inside the permanent magnet 2. By applying a current, the coil moves toward or opposite to the N-S tips of the magnet Z. The magnitude of the coil currents define the position of the sensing head 100.

[0122] The ablation magnetic assembly 50 includes a 10 mm long and 3.8 mm diameter NbFe permanent magnet (item 2) and the coils 3 and 14. In one embodiment, the coils 3 and 14 carry an equivalent current of 200 ampere-turns maximum. The coils experience force along the "x" axis. The magnetic field strength is about 1.2 tesla at the tips. The forces on the coils range from approximately 0 to  $\pm 35$  gram-force at approximately 100 mA current. Controlling the coil current magnitude and polarity sets the desired tool positions (states 201, 202, and 203). The field intensity along the axis in the permanent magnet 2, is charted by FIG. 6A. The travel and force (gram-force) of the assembly 50, along the axis "x" is shown by FIG. 6B.

[0123] The ablation sensor head 100 (including the MOSFET sensors 7 and RF antennas 8) travels along the "x" axis to form the measurements path, by providing an axial travel and opening the manifold to provide: activation state measurement and calibration 200, deployable state sensor head at intermediary state 202, and fully open state 203. The mechanical opening of the sensor head 100, to form various spatial positions (201, 202, and 203) allowing the apparatus to acquire the desired measurements on the same region during at least one or more QRS complex activation sequences and record the data points for relatively high fidelity measurements and error analysis techniques. The use of a magnetically-deployable mechanism to form the position during one or more QRS complex cycles further allows the apparatus to locate the electrical wavefront characteristics, so as to determine the geometry of the wavefront spreading through the myocardium.

[0124] A three-state measurement in the same region while detecting the electrical activity of the heart improves the measurements where signal quality is poor and provides more data points for construction of the isopotential lines. The error generated due to the abrupt change in potential is further reduced by the use of the deployable states. The deployable state positions allow the apparatus to acquire local features of the wavefront such as conduction velocity, potential gradient and/or breakthrough. A neighborhood of a relatively larger area during the activation sequence further provides for stability of the acquired measurement and the establishing of statistical significance of the wavefront event recording.

[0125] FIG. 7 is a cross section view of the RF antenna 8 used in the ablation mapping apparatus. In one embodiment, there are eight antennas spaced around the sensor semi-spherical head 9. The antenna 8, serves two functions: it is an electrode that measures the tissue impedance (Z) between the antennas, and it is also serving as the RF ablation tool (the radiator).

[0126] The antennas 8 typically should not interfere with the measurements by injecting or draining the surface poten-

tials 46. The functional requirements of the ablation and mapping probe is first to be conductive during the impedance tests (Z) 62, and the RF ablation, while the antennas 8 should in a relatively high-impedance state during the ECG mapping 60. In one embodiment, the antennas 8 are formed using, from N junction 68, and P junction 69, semiconductor (N-P junction).

[0127] The operational characteristics of the RF antennas 8 is such that during the relatively sensitive ECG potential tests where the controller 1600 activates the S<sub>1</sub> MOSFET through S<sub>s</sub> sensor (MOSFETS) the silver coating 70 of the antenna 8 is set in a reverse-biased mode. In the reverse biased mode (acting as a diode) leakage current is small (e.g., <1  $\mu$ A). During the test mode, the tissue is interfaced with the antenna as an electrode where the junction is set in a forward-biased mode, to conduct the measuring current.

[0128] During the RF ablation mode 65, the antennas are set in dual modes of conduction 62 and radiation 63. There is a conductive path to the tissue through the forward biased P-N junction while applying the RF voltage, while the antenna also radiates 63. The arrangement of the antennas 8 are set in pairs so that the antennas receive P-N and N-P semiconductor layers, thus conduction symmetry is maintained. In one embodiment, the P-N layers are shaped around the edges where the conductive part of the antenna 8 meets the insulating case 67, to reduce uneven spot-heating. (The flow effects lesion formation during RF cardiac catheter ablation as the lesion dimensions and tissue heating are dependent not only on temperature but on other secondary conditions such as heat sinking of blood flow and impedance value of the tissues).

[0129] The antennas 8, radiate 63, about 6 W of RF power each and total radiating power 63 is approximately 48 W maximum.

[0130] The Figure includes the ion flow of measurements performed by the cardiac potential sensors 7 using an isolated MOSFET gate and wiring bus nested by the arm 6 which carries the conductors 15 feeds by the power supply 89.

[0131] FIG. 8 is an orthographic depiction of the mapping and ablation catheter 600 whereby power supply 94 is provided to the sensor 7 for measuring the electric potential on the interior cardiac surface, V<sub>n</sub> 105 which is a data set electric potential value V<sub>i</sub> at time T<sub>i</sub> forming a spatio-temporal manifold 704 (V<sub>i</sub>, T<sub>i</sub>, X<sub>i</sub>, Y<sub>i</sub>, Z<sub>i</sub>) and calibration points 700AX and 700BX forming an electric map over the 704 grid (manifold). Amplifier 107 transmits a signal measured by the Sensor 7 to the data interpolation unit 205 which correlates the space temporal electric value anatomy on the map (s) which is generated and updated by the wavefront algorithm (e.g., using the Poynting Energy Vector PEV 49). In one embodiment, there are eight antenna arms 8 spaced around the central magnetic head 100, which are controlled so as to form at least three spatial states 201, 202, and 203 forming different aperture sizes. The antennas items 8 work during RF ablation in dual modes of conduction and radiation. The conductive path to the tissue through the forward biased P-N junction 68 and 69 during RF (300 kHz-1 MHz) voltage application 103 (performed by Amp 107 and RF generator 94). Antenna 8 also radiates in pairs (4 sets) where the antenna receive P-N and N-P semiconductor layers, thus conduction symmetry is maintained. Conductivity measurements and impedance values (Z<sub>n</sub>) 104 are displayed so as to control the ablative energy. In one

embodiment, the value of radiative energy is 6 W of RF power for each antenna with a total energy of approx. 48 W maximum.

[0132] During ablation the system 1600 generates RF energy which produces relatively small, homogeneous, necrotic lesions approximately 5-7 mm in diameter and 3-5 mm in depth. The system 1600 with its mapping and ablation catheter 600 is fitted with an irrigation tunnel 10 which sprays a saline water over the antennas to allow the ablation system to control the energy delivery and rapidly curtail energy delivery for impedance  $Z_n$  (104) rise. The saline cools the antennas 8 which minimizes impedance rises and provides for creation of larger and deeper lesions. In one embodiment, the apparatus 1600 and its MDAMC computer 91 is provided with look-up-tables so as to afford a predetermined ablation geometry formation as a function of multiple parameters affecting the lesion geometry.

[0133] In one embodiment, the system 1600 is configured to target the slower pathway in AVNRT (the inferior atrionodal input to the atrioventricular (AV) node serves as the anterograde limb (the slow pathway). In the case of WPW (Wolff-Parkinson White Syndrome), the system 1600 is configured to ablate the accessory pathway which carries the WPW syndrome. In cases such as atrial flutter due to a large reentrant circuit in the right atrium a linear lesion of this isthmus cures this form of atrial flutter.

[0134] The ability of the ablation system 1600 to form a predefined lesion geometry is provided by the antenna 8 construction P-N, N-P doping and the ability of the generator 204 to vary the frequency (Fq) 106 and phase (F $\alpha$ ) 102 so as to afford a precision delivery of energy which forms the lesion.

[0135] In one embodiment, the system 1600 maps the breakthrough and potential while maintaining contact with the myocardium ( $Z_n$ ), tissue desiccation created by the RF energy (500 kHz) which causes a thermal injury such as desiccation necrosis. RF energy delivered by the antennas 8 located on the ablation head assembly 100 causes the resistive heating of the predefined geometry (linear, section circumference zig zag, etc.) of the tissue in contact with the antenna 8. Cooling the radiating antennas 8 is performed by the irrigation tunnel 10. In one embodiment, temperature is maintained at approx. 50° C.

[0136] FIGS. 9 and 9A show the ablation and mapping catheter 600 as it is introduced precutaneously into the heart chambers and sequentially record the endocardial electrograms for correlating local electrograms to cardiac anatomy. In one embodiment, the catheter is advanced by the use of magnetic circuits which are capable of generating a magnetic field strength and gradient field to push/pull and bend/rotate the distal end of the catheter 600 and as detailed by Shachar U.S. patent application Ser. No. 10/690,472 titled "System and Method for Radar Assisted Catheter Guidance and Control" hereby incorporated by reference. The catheter 600 is navigated and controlled locally with the aid of fluoroscopy and by the radar as it is detailed by the ensuing drawings and its accompanying descriptions.

[0137] In one embodiment, the catheter 600 is manually advanced into the heart chambers and sequentially recorded the endocardial electrograms, again using the radar and fiducial markers for local definition of the site, while advancing the performing the mapping and ablation procedure.

[0138] FIG. 9 shows the catheter 600 as it is advanced through the heart chambers 390. FIG. 9A shows the catheter 600 in various deployable states. In one embodiment, during measurement, the manifold holding the sensor array 8 in the catheter 600, expands from a closed position state 201 to a deployable open state [umbrella]. At various open geometry states, sensor array 8 samples electrical potentials to create a set of data points. In one embodiment, the catheter in the deployable state forms a circular shape as the manifold expands to form various open geometry states. The intermediary open state 202 indicates an enlarged circumference and the fully deployable open state 203 represents the sensor array 8 in its maximum spatial coverage.

[0139] The intracardiac mapping is performed by measuring the electrical potential as it moves from state 201 through the state 202 and finally through the open state 203. The data is provided to the computer and processing functional unit 1600 which controls the procedures.

[0140] FIG. 9B shows the endocardial electrogram map 54 resulting from sequential measurements of electrical potential detected by the sensor array 100 (including the MOSFET sensor 7 and antenna array 8) in the catheter 600 at various open geometry states 201, 202, 203. The conductivity data collected sensor array 8 is processed and graphically represented using the control display 93 and the E-cardiac display 92. In one embodiment, the conductivity data collected by sensor array 8 is displayed in a contour map 49.1 as depicted in FIG. 3, which also displays a contour map 54.1 of the ECG data, and a vector map 53.1 of the Energy and E Vector data. In one embodiment, contour map 49.1 of the conductivity data also graphically displays a previous ablation site 9004 from created from stored data generated from a previous ablation procedure. Previous ablation site 9004 represents an area of high impedance. In one embodiment, the location of previous ablation site 9004 is verified using the new data collected from sensor array 8 before previous ablation site 9004 is displayed in contour map 49.1.

[0141] FIG. 9B further depicts the fiducial marker 700A1, 700A2, and 700B1 as shown on the dimensional grid providing the numerical x-y-z coordinate set for the catheter electrical, impedance, measurement performed using the catheter 600. Anatomical markers 390.1, 390.2, and 390.3 are noted on the grid and recorded as to their dimensional as well as clinical significance during the travel log of the ablation and mapping catheter 600. Further detail of the procedure by which catheter 600 acquires the electrical and conductivity data relative to dimensional as well as anatomical marker are described in FIG. 10.

[0142] The system 1600 with its mapping and ablation catheter 600 performs the tasks of mapping using the sensor array 100 as follows: calibration and position definition using radar 1000, cardiac morphology and geometry synchronization with images generated by x-ray fluoroscopy or MRI etc is established. (Synchronization methodology is provided by radar 1000 and fiducial markers 700AX and as it is detailed by FIGS. 11 and 11A).

[0143] Data obtained from sensor array of catheter 600 is processed and its geometry and dimensional attributes are defined as to its physiological reference. Data of maps are stored relative to its fiducial markers, so it can be retrieved and used during the ablation sequence.

[0144] The ablation catheter is then directed to its desired site. The wavefront characteristics are established using the Poynting Energy Vector (PEV) 49 and the reconstruction of

the potentials and maps of the wavefront is established as detailed as shown in FIG. 10 and its mathematical algorithm in connection with FIG. 3.

[0145] The computer-generated maps and model analysis of the endocardium is periodically updated as the catheter head assembly 100 with its sensor array 7 is moved along the cardiac chamber.

[0146] The electrogram is synthetically constructed upon the x-ray fluoroscopy image which is pixelized and voxelized so as to allow the mapping of the wavefront characteristics as it is dimensionally, as well as, graphically layered over the heart morphology. The geometrization of the electrical potential and its maps is further detailed by FIGS. 8 and 9.

[0147] FIG. 10 is an isometric representation of the image capture technique used by the system 1600 in identifying the position and coordinate of the catheter 600 as it moves through the heart chambers. The electric potential measurements taken by the catheter 600 are tracked and gated by the radar 1000 to allow determination of the 3D position coordinates of the catheter tip in real time. The radar and its fiduciary markers provide for the detail dimensional travel map of the catheter as it is sampling (S/H) the electric potential. The system 1600 reconstructs the maps on a grid formed as a 2D pixelized layout superimposed over the reconstructed myocardium chambers or as a voxel 3D vector position. The details of such scheme are outlined by FIGS. 11, 11A, 12, and 12A.

[0148] The catheter 600 position is determined by the radar 1000, which maintains a position and orientation above the patient. In one embodiment, the radar 1000 is set approx. 1 meter from the fiduciary markers placed on or in the patient's body so that phase and range data is defined and beam compensation can be determined. To obtain the calibration points so as to track the moving catheter (range of movements is between 0.2-2 Hz band). The volume integrated, i.e., the cardio chamber (s) is denoted by voxels. Temporal filter such as an FFT denoted by FIG. 11, item 1103, allows the rendering of the signal received from the catheter 600 to be position bound to the original calibrating points.

[0149] In one embodiment, the ablation and mapping catheter 600 electromechanical characteristics are; the catheter in closed state 201 is 5.12 mm in diameter. The sensor tip movement is between 1-10 mm diameter (fully opened state 203), the axial movement is 2 mm and the sensor head 100 tool force is 0 to  $\pm 35$  gram, total radial movement along 360° is 24 position (15° along the circumference), the ablation power is 50 WRF with ablation cut size of 1-2.5 mm. The ablation tool force is 0-35 grams. Eight antennas 8 are spaced along the protective dome 9 which carry eight MOSFET sensors 7.

[0150] When the catheter 600 is used while employing the CGCI apparatus, as noted by U.S. patent application Ser. No. 10/690,472, the catheter 600 exerts a force control of 0 to  $\pm 37$  grams with torque control of 0 to  $\pm 35$  grams.

[0151] The catheter 600 is detected by the radar 1000 and it is placed over the manifold 704 which is placed over the imaging x-ray fluoroscopy 702 while gated by the fiduciary markers 700AX, the normalization procedure performed by the system computer 91 (orthogonal basis) allows the calibration of the catheter tip 2 relative to the fiduciary markers 700AX located on the patient 390 body forming the stereotactic frame used in forming the manifold 704. Navigating

the catheter 600 is tracked by denoting the radar initial position as  $600 \times \text{radar}(t)$ , the time-varying position of the catheter tip 2, while the fiduciary markers 700AX is denoted by  $X_o(t)$  and is determined as voxel o. The other fixed targets are for example the fiduciary markers mounted on the operating table 700BX (fixed targets).

[0152] The ranges of the fiduciary markers 700AX and 700BX are denoted by  $X_i(t)$ ;  $i=1, 2, \dots, n$ . The fiduciary markers are passive devices emitting a radar cross section (RCS) suitable for formation of the manifold 704, while traveling for example through the coronary sinus, the system 1600 record each sign post which facilitates the formation of anatomical sign posts while forming the map (cardio chamber geometry). The sign posts are anatomical in nature and assist in realistic rendering of the synthetically-generated virtual heart surface. Electric potential data sets of ordered pairs  $\langle E_i, T_i \rangle$  are recorded and are placed on the dimensional grid (manifold 704) generated by the radar 1000. The mapping process is data set of  $\langle E_i, T_i \rangle$  60, a corresponding  $\langle M_i, T_i \rangle$  61 and an impedance value  $\langle Z_i, T_i \rangle$  62, data points are gated to the dimensional grid 704 (the manifold with its fiduciary markers 700AX and permanent reference markers 700BX). The radar 1000 generates a dimensional 3D travel map which is kept for further use. Cardiac motion and pulmonary outputs are gated by the fiduciary marker calibration and body electrogram (ECG). QRS complex cycle is employed in correcting algorithms. The data points  $\langle E_i, M_i, Z_i, \text{ and } T_i \rangle$  are correlated to the grid 704 while correction of position as well as calibration is performed in background mod.

[0153] The sensor array 100 with its measuring devices (as detailed by FIGS. 2 and 5) used by the mapping and ablation catheter is designed to enhance the acquisition of temporal/electric potential measurements within the cardiac chambers while correlating space temporal data reconstructed from 3D fields. The system 1600 further provides data sets from and around the ablation area tissue surface. In one embodiment, data of the spread of excitation and the magnitude of the time-varying electric potential in 3D is obtained by the use of the sensors 7, which are galvanically isolated from the tissue to be measured.

[0154] The sensor 7 further provides for substantial increase of signal to noise ratio due to an device-signal-amplification. The catheter assembly 600 is introduced percutaneously into the heart chambers, by the CGCI apparatus (see U.S. patent application Ser. No. 10/690,472 incorporated herein its entirety).

[0155] The catheter tip 2 and the sensor head 100 is initially set at closed position (state 201). The catheter 600 is then activated so as to energize coil 3 and coil 14, deploying the sensor 7 array 100 to its fully open position (state 203).

[0156] The sensor array 7 is used to provide readings at two or three positions (201, 202, 203) with incremental radii sensor 7 ( $S_1-S_8$ ). The electric potential (with its temporal as well as dimensional elements) is provided to the ECG data interpolation unit 205, based on the data fidelity the system controller 91 instructs the sensor head assembly 100 to move by deploying the magnetic apparatus 50 so as to form measurements along the different states 201, 202, and 203. The axial movement of magnetic assembly 50 with its two electromagnetic coils travels along the guide rail 4.

[0157] The axial movement of coils 3 and 14 displaces the arm 6 (which holds the sensors 7 and the RF antenna 8) so

as to form an “umbrella” with multiple states (**201**, **202**, and **203**). The action of the magnetic assembly **50** is the result of the solenoid action generated by polarity and magnitude of the coils **3** and **14** relative to the permanent magnet **2**.

**[0158]** In one embodiment, the CGCI apparatus **1500** is used to generate a magnetic field parallel to the axis of the catheter **600** permanent magnet **2**, holding the catheter tip in position (desired position) and the CGCI apparatus produces a gradient in this aligned field without changing its holding direction (the precision of fixing the catheter **600** in its location allows repeated measurements).

**[0159]** The catheter **600** and its associated controller as shown in FIG. **2** can be used to measure the activation time ( $t_a$ ) by sampling the location (site) repeatedly, generating multiple elements of ( $E_r$ - $T_r$ ) pairs to characterize the geometrical layout of electric potential on 2D (pixels) or 3D (voxels) maps. Such maps are generated using the electric heart vector (EHV), the correlated magnetic dipole (MHV) as well as impedance values ( $Z$ ) and superimposition of such maps over the synthetically generated endocardium.

**[0160]** In one embodiment, the endocardium chamber geometry is modeled by an algorithm such as a simplified FEA, which models the wavefront Poynting Energy Vector **49**, hence identifying sites of ectopic activation. Automatic activation geometry is further located by the radar signals forming the grid **704** to locate the path of anisotropy due to transmural fiber rotation, that were reconstructed with spatial resultant of  $>0.5$  mm. The data points received from the catheter **600** with its sensors **7**, electronically interact with the cardiac cells and such interactions are collected as measured data. The energy wavefront Poynting Energy Vector (PEV) **49** is used in solving the non-linear parabolic partial differential equation. The transmembranes potential typically behaves similar to a cellular automation. Hence, the use of the Hausdorff Neighborhood theorem is an appropriate description of the electrophysiological avalanche. The maps generated by the algorithm described as the Poynting Energy Vector (PEV) **49** can be reconstructed as images using color for differentiating regions based on density distribution or a mash technique of geodesic line representing the electric potential (on a grid with time domain) as an elevation above the ground potential (zero), and/or as abnormal low voltage represents scar tissue which might express the underlying arrhythmia.

**[0161]** FIG. **11** is a block diagram of a radar system **1000** used in one embodiment of the CGCI apparatus **1500**. The radar **1000** shown in FIG. **11** includes a phased-array radar module **1100** having transmit/receive antenna elements and a Radio Frequency (RF) module **1150**. The radar system **1000** includes an amplifier **1101**, an A/D converter **1102**, a Fast Fourier Transform module **1103**, and a microcontroller **1105**. The apparatus further includes a memory module in the form of RAM **1112**, and a look-up table in the form of a ROM **1111**.

**[0162]** One embodiment includes a voice messaging and alarm module **1110**, a set of control switches **1109**, and a display **1108**. The data generated by the radar system **1000** is provided to the GCI apparatus **501** via communications port **1113**.

**[0163]** The radar system **1000** includes a phased-array and uses Microwave Imaging via Space-Time (MIST) beam-forming for detecting the catheter tip **2**. An antenna, or an array of antennas, is brought relatively near the body of the patient and an ultra wideband (UWB) signal is transmitted

sequentially from each antenna. The reflected backscattered signals that are received as radar echoes are passed through a space-time beam-former of the radar unit which is designed to image the energy of the backscattered signal as a function of location. The beam-former focuses spatially on the backscattered signals so as to discriminate from the background clutter and noise while compensating for frequency-dependent propagation effects. The contrast between the dielectric properties of normal tissue and the catheter tip **2** in the regions of interest provides sufficient backscatter energy levels in the image to distinguish normal tissue from the catheter tip **2**, affording detection and discern ability. In one embodiment, a data-adaptive algorithm is used in removing artifacts in the received signal due to backscatter from the body tissue interface (e.g., the skin layer). One or more look-up tables containing the known dielectric constants of the catheter tip contrasted against the background dielectric information relative to the biological tissue can be used to identify features in the radar image.

**[0164]** The physical basis for microwave detection of the catheter tip **2** in the biological tissue is based on the contrast in the dielectric properties of body tissue versus the signature of the catheter tip **2**. The contrast of the dielectric values of biological tissue versus that of the catheter tip **2** is amplified, filtered and measured.

**[0165]** A typical summary of dielectric properties in living tissues for medical imaging in the range of 10 Hz to 20 GHz and parametric models for the dielectric spectrum of tissues are configured to an ( $\epsilon'$ ) of 5-60 and electrical conductivity ( $\sigma$ ) of 0.065-1.6 Siemens/m (S/m) the relative complex permittivity,  $\epsilon_c$ , of a material is expressed as:

$$\epsilon_c = \epsilon' - j\epsilon''$$

$$\epsilon' = \epsilon'/\epsilon_0$$

$$\epsilon'' = \sigma/\epsilon_0\omega$$

**[0166]** Where  $\epsilon$  is the permittivity,  $\epsilon_0$  is the permittivity of free space=8.854e-12 Farads/m,  $\epsilon''$  is the relative dielectric loss factor, and  $\omega$  is the angular frequency.

**[0167]** The return waveform from the radar **1000** is provided to a computer using a software such as MATLAB. A target such as the catheter tip **2** is sampled with a transmitted pulse of approx. 100 ps in duration containing frequency from 400 Hz to 5 GHz with a range of approx. 1 meter in air (the range of the electromagnetic coil location). The radar emits a pulse every 250 ms (4 MHz). The return signals are sampled and integrated together to form the return waveform as measured on circuit **1000**. A specific window of data of the radar interaction with the target **2** is obtained and a Fast Fourier Transform (FFT) of the window of data is taken to produce the frequency response of the target **958**:

$$X(k) = \sum_{j=1}^N x(j)W_N^{j(k-1)}$$

**[0168]** and by taking a Fast Fourier Transform (FFT) **1103** it is possible to identify the differences between metal **2**, or human tissues, etc. The synthetic aperture radar **1117** (SAR) aids in the signal processing by making the antenna seem like it is bigger than it really is, hence, allowing more data to be collected from the area to be imaged.



[0169] The radar can use time-domain focusing techniques, wherein the propagation distance is given:

$$d=2\sqrt{(x)^2+(z)^2}$$

[0170] and alternatively a propagation time computed given by:

$$t = \frac{2\sqrt{(x)^2+(z)^2}}{v}$$

[0171] In one embodiment, target identification and matching is performed by characterizing the target waveform of the catheter tip 2 into a single vector. The dot product is taken from the identification vector and the data whereby, perfectly aligned data and ID results in a dot product of 1, and data perpendicular to the ID (2) is resulting in dot product equal to zero. The radar controller 1105 converts the results to a percent match (dielectric value, conductivity measure) of the data of the identification vector.

[0172] The catheter tip 2 has a microwave scattering cross-section that is different relative to biological tissue of comparable size. The difference in scattering cross-section is indicated by the different back-scatter energy registered by the receiver, and processed so as to afford a pictorial representation on a monitor 325 with a contrast between the two mediums. The pictorial view of the catheter tip 2 generated by the radar system 1000 can be superimposed over the X-ray fluoroscopy image 702 and its coordinate data set linked to the GCI controller 501 for use as a position coordinate by the servo feedback loop. In one embodiment, microwave imaging via space-time (MIST) beam-forming is used for detecting backscattered energy from the catheter tip 2 while the background is biological tissue.

[0173] In one embodiment, a data set  $\langle E_i, T_i \rangle$  and  $\langle x; y; z \rangle$  position coordinates are used with the ablation and mapping apparatus 1600 in forming the maps as shown in FIG. 10.

[0174] The radar system 1000 detects the presence and location of various microwave scatters, such as the catheter tip 2, embedded in biological tissue 390. The space-time beam-former assumes that each antenna in an array transmits a low-power ultra-wideband (UWB) signal into the biological tissue. The UWB signal can be generated physically as a time-domain impulse 960 or synthetically 1117 by using a swept frequency input. In one embodiment, the radar system 1000 uses a beam-former that focuses the backscattered signals of the catheter tip 2 so as to discriminate against clutter used by the heterogeneity of normal tissue and noise while compensating for frequency-dependent propagation effects. The space-time beam-former achieves this spatial focus by time-shifting the received signals to align the returns from the targeted location. One embodiment of the phased-array radar 1000 forms a band of finite-impulse response (FIR) filters such as high dielectric doping in the antenna cavity, forming the reference signal, where the doping is relative to the device of interest (e.g., catheter tip 2). The signals from the antenna channels are summed to produce the beam-former output. A technique such as weights in the FIR filters can be used with a "least-squares fitting" technique, such as Savitzky-Golay Smoothing Filter to provide enhancement of the received signal and to compute its energy as a function of the

dielectric properties versus the scattered background noise of body tissue, thereby providing a synthetic representation of such a signal. The system can distinguish differences in energy reflected by biological tissues 390 and the catheter tip 2 and display such energy differences as a function of location and co-ordinates relative to the fiduciary markers 700Ax through 700Bx. In one embodiment, the radar module 1000 uses an FFT algorithm 1103 which uses a filtering technique to allow the radar 1000 sensor to discern varieties of dielectric properties of specific objects known to be used in a medical procedure, such as a guidewire 379 and/or a catheter 310 with piezoelectric ring 311 and 312 so as to afford differentiation of various types of instruments like catheters, guide-wires, electrodes, etc.

[0175] FIG. 11A is a graphical representation of the catheter tip 2 embedded with one, two or more piezoelectric rings 311 and 312 such as Lead-Zirconate-Titanate (PZT) and/or molecularly conjugated polymers such as switchable diodes (polyacetylene). The second harmonics generated by the rings 311 and 312 provide an identifiable return signature in the second harmonic due to the non-linearity of the material. While the fundamental harmonic (e.g., 5 MHz) is transmitted by the radar, the second harmonic (e.g., 10 MHz) is readily distinguishable by the radar system 1000. This allows the radar system 1000 to discern between the catheter tip 2 (which typically has a ferrite such as samarium-cobalt SmCo5, or neodymium-iron-boron, NdFeB) and the PZT rings 311 and 312. The ability to distinguish between the signal return from catheter tip 2 and the PZT rings 311 and 312, allows the radar system 1000 to filter out the background clutter received from the body tissue and to recognize the position and orientation of the rings 311 and 312 and the position co-ordinates of the catheter tip 2. The technique of using two different dielectric properties and electrical characteristics of the tip 2 versus the PZT 311 and 312 provides the catheter tip 2 with a radar signature that can be recognized by the radar system 1000.

[0176] FIG. 11B further illustrates how the radar system 1000 with its transmit and receive antennas is used to detect the position co-ordinates and orientation of catheter tip 2 relative to its two PZT rings 311 and 312. A geometrical manipulation is employed by the radar system 1000 and its associated FFT filter 1103 by the resident microcontroller 1105. As shown in FIGS. 4D, 4E, 4F; a catheter-like device is provided with a magnetically-responsive tip 2. In one embodiment, the tip 2 includes a permanent magnet. The polarity of the permanent magnet is marked by two PZT rings where the north pole is indicated by a PZT ring 312 and the distal end of the ferrite where the semi-flexible section 310 of the catheter 376 is marked with the additional PZT ring 311, also marking the south pole of the ferrite.

[0177] In one embodiment, the ferrite 2 in the catheter tip is used by the ablation and mapping catheter 600 as described by FIG. 4 and its accompanying descriptions.

[0178] The radar system 1000 transmits a burst of energy that illuminates the ferrite catheter tip 2. The return signal from the catheter tip 2 is received by the radar and its position is registered by observing the time of flight of the energy, thereby determining the location of the catheter tip 2 as position co-ordinates in a three-dimensional space. By employing the two PZT rings 311 and 312, the radar detector 1000 is also capable of discerning the location of the tip 2 relative to the two PZT rings so as to afford a measurement of PZT ring 312 relative to the second piezoelectric ring 311

with reference to the position co-ordinates of catheter tip 2. The radar detector 1000 can discern the return signal from PZT rings 311 and 312 due to the non-linear characteristic of PZT material that generates a second harmonic relative to the incident wave. By comparing the strength of the fundamental frequency and the second harmonic, the radar system 1000 is able to discern the position and orientation of the two PZT rings relative to the ferrite 2, thereby providing position and orientation of the catheter tip 2.

[0179] FIG. 11B illustrates the technique of measuring the position and orientation of the catheter tip 2 by the use of the radar detector 1000 and using the fiduciary markers 700AX and 700BX to form a frame of reference for the catheter dynamics such as movement relative to the frame of reference. As shown in FIGS. 11A and 11B the fiduciary markers 700AX and 700BX form a manifold 701. The locations of the markers 700AX and 700BX are measured by the radar system 1000.

[0180] In one embodiment, the markers are electrically passive and can be made from a polymer or PZT material to allow the radar antenna to receive a signal return which is discernable. Criteria such as the conductivity of a substance such as catheter tip 2 relates at least in part to how much the radar signal is attenuated for a given depth (e.g., the higher the conductivity the higher the loss for a constant depth). An average conductivity of 1 S/m at 1 GHz signal would penetrate the human body 390 approximately 1.8 cm.

[0181] The dielectric constant of all targets is typically less than 5 (e.g., cotton(1.35), Nylon 5, etc.). The conductivity of metals is relatively large, and relatively small for most dielectrics (with Nylon on the order  $1e-3$  and that of cotton and rayon being saturated by that of water, blood and tissue). The relative permittivity of the targets will be in the order of 2-3 orders of magnitude lower than that of the surrounding tissue, and the conductivity of the metals will be 6-7 orders of magnitude greater than that of the surrounding tissue.

[0182] The dielectric properties as well as the conductivity measure of the target catheter tip 2 and/or its directional markers PZT rings 311 and 312 allow the radar 1000 to discern the target out of the surrounding clutter (body tissue 390) and perform the task of position definition 2 within the referential frame of fiduciary markers 700AX and 700BX.

[0183] In one embodiment, the return waveform is recorded for a static (clutter) environment, and then a target is inserted into the environment and once the clutter is subtracted from the return waveform the radar 1000 processes a target response (clutter is a general term referring to anything the radar will interact with that is not a desired target). In one embodiment, the data is processed and defined in terms of a machine language as model for the CGCI controller 501 and is used by the controller to close the servo loop. In one embodiment, the data generated by the radar 1000 is used for mapping and ablation system 1600 and its computer 91 to form the grid/manifold 704 so as to enable the dimensional placement of the  $\langle E_i, T_i \rangle$  pairs  $\langle M_i, T_i \rangle$  pairs. The data 60 and 61 are then used by the imaging graphic generator 200 to form the vectoral electrocardiograph maps.

[0184] FIGS. 12 and 12A show an image displayed on the monitor 325. The cineangiographic image 702 of an arterial tree is shown with a reconstructed radar signature of the catheter tip 2. The image 702 contains a numerical grid defined and calculated by the radar 1000 and a data set of

coordinate or vector representation of catheter position where the Actual Position (AP) is displayed. A similar data set of catheter position 2 is fed to the CGCI controller 501 or to the ablation computer 91 for the purpose of closing the loop of the servo control system of the CGCI apparatus 1500 and for definition of the dimensional grid for ablation. A graphic depiction of the catheter tip 2 is shown in FIG. 12 where the monitor 325 displays the stereotactic frame formed by the fiduciary markers 700AX and 700BX obtained from the radar signature 1000. The catheter tip 2 is shown in the approximate cube formed by the fiduciary markers 700AX and 700BX. The ensemble of position data relative to coordinates, is formed as dynamic manifold 704. The manifold 704 is used for a processing synchronization of the catheter tip position (AP) relative to the stereotactic frame 701. The process of synchronization is gated in the time domain with the aid of an EKG electrocardiogram 502, whereby the controller 501, internal clock is synchronized with the EKG QRS complex so as to provide a Wiggers' diagram. Synchronization allows the CGCI controller 501 to gate the dimensional data and coordinate set of fiduciary markers so as to move in unison with the beating heart. The technique noted by Image Synchronization 701 allows the ablation catheter 600 and its computer 91 to update the electrocardiograph maps on a real time basis hence enabling the system 1600 to form an accurate view of the mapping and ablation and therefore reduce the use of x-radiation.

[0185] Synchronization of the image of the catheter tip 2 or guidewire 379, captured by the radar system 1000, is superimposed onto the fiduciary markers which are represented digitally and are linked dynamically with the image 702. This is done so as to create a combined manifold 704, which is superimposed onto the fluoroscopic image 702, and moves in unison with the area of interest relative to the anatomy in question. For example, the beating heart and its cardio-output; the pulmonary expansion and contraction, or spasm of the patient 390, all these are dynamically captured and linked together so as to achieve a substantial motion in unison between the catheter's tip and the body organ in question.

[0186] Synchronization 701 of the catheter tip 2 with its referential markers 700AX and 700BX allows for dynamically calibrating the relative position and accurately gating the cineographic image (or ultrasonic) with the beating heart. Further, the CGCI 1500 and the ablation/mapping catheter 1600 can be used to capture the data set-manifold 704 in the time domain of the patient 390 EKG signal. The CGCI controller 501 and/or the ablation system 1600 can display and control the movement of the catheter tip 2 in unison with the beating heart. Synchronization by the use of fiduciary markers 700AX and 700BX captured by the catheter tip 2, using the data set 704, and superimposing it over the cineographic image 702 and gating it based on EKG signal from the patient's body 390, allows the position data to be linked to the controller 501/91 to close the servo loop and to provide the dimensional grid for forming the electrical maps.

[0187] The CGCI controller 501/91 can perform the data synchronization without the active use of x-ray imagery since data of catheter position is provided independently by the radar signal 1000.

[0188] The invention is not limited only to the examples described above. Other embodiments and variations will be

apparent to one of ordinary skill in that art upon reading the above disclosure. Thus, the invention is limited only by the claims.

What is claimed is:

1. A catheterization system, comprising:
  - a catheter having a catheter distal end for insertion into a patient, said distal end configured with a first deployable member and a second deployable member;
  - a first MOSFET sensor provided to a distal end of said first deployable member;
  - a second MOSFET sensor provided to a distal end of said second deployable member;
  - a first electrical contact provided to said first deployable member, said first electrical contact configured to make electrical contact with tissue;
  - a second electrical contact provided to said second deployable member, said second electrical contact configured to make electrical contact with tissue; and
  - a deployment mechanism configured to increase a separation between said distal end of said first deployable member and said distal end of said second deployable member.
2. The catheterization system of claim 1, said catheter distal end further comprising a magnet.
3. The catheterization system of claim 2, wherein said deployment mechanism comprises a coil provided to said first deployable member and to said second deployable member.
4. The catheterization system of claim 2, wherein said coil is configured to increase a separation between said distal end of said first deployable member and said distal end of said second deployable member when current is provided to said coil.
5. The catheterization system of claim 1, wherein said first electrical contact comprises a PN junction.
6. The catheterization system of claim 1, wherein said first electrical contact comprises a first PN junction oriented such that P material of said first PN junction is provided to said tissue and said second electrical contact comprises a second PN junction oriented such that N material of said second PN junction is provided to said tissue.
7. The catheterization system of claim 1, wherein said first electrical contact comprises a first and said second electrical contact comprises a second PN junction, wherein an said first and second PN junctions are configured with opposite polarity.
8. The catheterization system of claim 1, wherein said first electrical contact comprises an antenna.
9. The catheterization system of claim 1, wherein said catheter comprises a lumen.
10. The catheter system of claim 1, further comprising:
  - a magnetic field source for generating a magnetic field, said magnetic field source comprising a first coil corresponding to a first magnetic pole and a second coil corresponding to a second magnetic pole, wherein said first magnetic pole is moveable with respect to said second magnetic pole; and
  - a system controller for controlling said magnetic field source to control a movement of said catheter distal end, said distal end responsive to said magnetic field, said controller configured to control a current in said first coil, a current in said second coil, and a position of said first pole with respect to said second pole.
11. The catheterization system of claim 10, said system controller comprises a closed-loop feedback servo system.
12. The catheterization system of claim 10, wherein one or more magnetic field sensors are used to measure said magnetic field.
13. The catheterization system of claim 10, said distal end comprising one or more magnetic field sensors.
14. The catheterization system of claim 10, said distal end comprising one or more magnetic field sensors for providing sensor data to said system controller.
15. The catheterization system of claim 1, further comprising an operator interface unit.
16. The catheterization system of claim 10, wherein said servo system comprises a correction factor that compensates for a dynamic position of an organ, thereby offsetting a response of said catheter distal end to said magnetic field such that said distal end moves in substantial unison with said organ.
17. The catheterization system of claim 16, wherein said correction factor is generated from an auxiliary device that provides correction data concerning said dynamic position of said organ, and wherein when said correction data are combined with measurement data derived from said sensory catheterization system to offset a response of said servo system so that said distal end moves substantially in unison with said organ.
18. The catheterization system of claim 17, wherein said auxiliary device is at least one of an X-ray device, an ultrasound device, and a radar device.
19. The catheterization system of claim 10, wherein said system controller includes a Virtual Tip control device to allow user control inputs.
20. The catheterization system of claim 10, wherein said first magnetic pole is extended and retracted by a hydraulic piston.
21. The catheterization system of claim 10, further comprising:
  - first controller to control said first coil; and
  - a second controller to control said second coil.
22. The catheterization system of claim 21, wherein said first controller receives feedback from a magnetic field sensor.
23. The catheterization system of claim 22, wherein said magnetic field sensor comprises a Hall effect sensor.
24. The catheterization system of claim 10, wherein said system controller coordinates flow of current through said first and second coils according to inputs from a Virtual tip.
25. The catheterization system of claim 24, wherein said Virtual Tip provides tactile feedback to an operator.
26. The catheterization system of claim 24, wherein said Virtual Tip provides tactile feedback to an operator according to a position error between an actual position of said distal end and a desired position of said distal end.
27. The catheterization system of claim 24, wherein said system controller causes said distal end to follow movements of said Virtual Tip.
28. The catheterization system of claim 24, further comprising:
  - a mode switch to allow a user to select a force mode and a torque mode.
29. The catheterization system of claim 10, further comprising:
  - a controllable magnetic field source having a first cluster of poles and a second cluster of poles;

wherein at least one pole in said first cluster of poles is extendable;  
 a radar system configured to produce a radar image of organs of said body; and  
 one or more magnetic sensors to sense a magnetic field.

**30.** The catheterization system of claim **29**, said distal end comprising one or more magnetic field sensors.

**31.** The catheterization system of claim **29**, said distal end comprising one or more magnetic field sensors for providing sensor data to a system controller.

**32.** The catheterization system of claim **29**, further comprising an operator interface unit.

**33.** The catheterization system of claim **29**, wherein said first cluster of poles is coupled to said second cluster of poles by a magnetic material.

**34.** A catheterization method, comprising:

guiding a distal end of a catheter to a desired region of tissue;

spreading sensor arms of said catheter;

establishing contact between said sensor arms and the region of tissue;

sensing a position of said sensor arms;

measuring activation potential data using sensors provided to said sensor arms;

measuring impedance data of tissue between said sensor arms using contacts provided to said sensor arms; and  
 displaying a map of activation potential and impedance of said region of tissue.

**35.** The method of claim **34**, further comprising using said activation potential data and said impedance data in a calculation to predict an RF ablation lesion.

**36.** The method of claim **35**, further comprising creating an RF ablation lesion.

**37.** The method of claim **34**, wherein said sensors comprise MOSFET sensors.

**38.** The method of claim **34**, wherein said contacts comprise PN junctions.

**39.** The method of claim **34**, wherein said contacts comprise alternating PN junctions.

**40.** The method of claim **34**, further comprising calculating an angle between an E vector and an energy vector in said region of tissue.

**41.** The method of claim **40**, further comprising identifying anomalies in activation vector spreads where an angle between said E vector and said energy vector exceeds a threshold.

**42.** The method of claim **34**, wherein said position of said sensor arms is measured using radar.

**43.** The method of claim **34**, wherein said position of said sensor arms is measured using X-rays.

**44.** The method of claim **34**, further comprising:

calculating a desired direction of movement for said distal end;

computing a magnetic field needed to produce said movement;

controlling a plurality of electric currents and pole positions to produce said magnetic field; and

measuring a location of said distal end.

**45.** The method of claim **34**, further comprising controlling one or more electromagnets to produce said magnetic field.

**46.** The method of claim **34**, further comprising simulating a magnetic field before creating said magnetic field.

\* \* \* \* \*





US 20090248014A1

(19) **United States**

(12) **Patent Application Publication**  
**Shachar et al.**

(10) **Pub. No.: US 2009/0248014 A1**

(43) **Pub. Date: Oct. 1, 2009**

(54) **APPARATUS FOR MAGNETICALLY DEPLOYABLE CATHETER WITH MOSFET SENSOR AND METHOD FOR MAPPING AND ABLATION**

**Publication Classification**

(51) **Int. Cl.**  
*A61B 18/14* (2006.01)  
*A61B 5/053* (2006.01)  
(52) **U.S. Cl.** ..... **606/41; 600/547**

(75) **Inventors:** **Yehoshua Shachar**, Santa Monica, CA (US); **Laszlo Farkas**, Ojai, CA (US); **Eli Gang**, Beverly Hills, CA (US)

(57) **ABSTRACT**

A mapping and ablation catheter is described. In one embodiment, the catheter includes a MOSFET sensor array that provides better fidelity of the signal measurements as well as data collection and reduces the error generated by spatial distribution of the isotropic and anisotropic wavefronts. In one embodiment, the system maps the change in potential in the vicinity of an activation wavefront. In one embodiment, the mapping system tracks the spread of excitation in the heart, with properties such as propagation velocity changes. In one embodiment, during measurement, the manifold carrying the sensor array expands from a closed position state to a deployable open state. Spatial variation of the electrical potential is captured by the system's ability to occupy the same three-dimensional coordinate set for repeated measurements of the desired site. In one embodiment, an interpolation algorithm tracks the electrogram data points to produce a map relative to the electrocardiogram data.

**Correspondence Address:**

**KNOBBE MARTENS OLSON & BEAR LLP**  
**2040 MAIN STREET, FOURTEENTH FLOOR**  
**IRVINE, CA 92614 (US)**

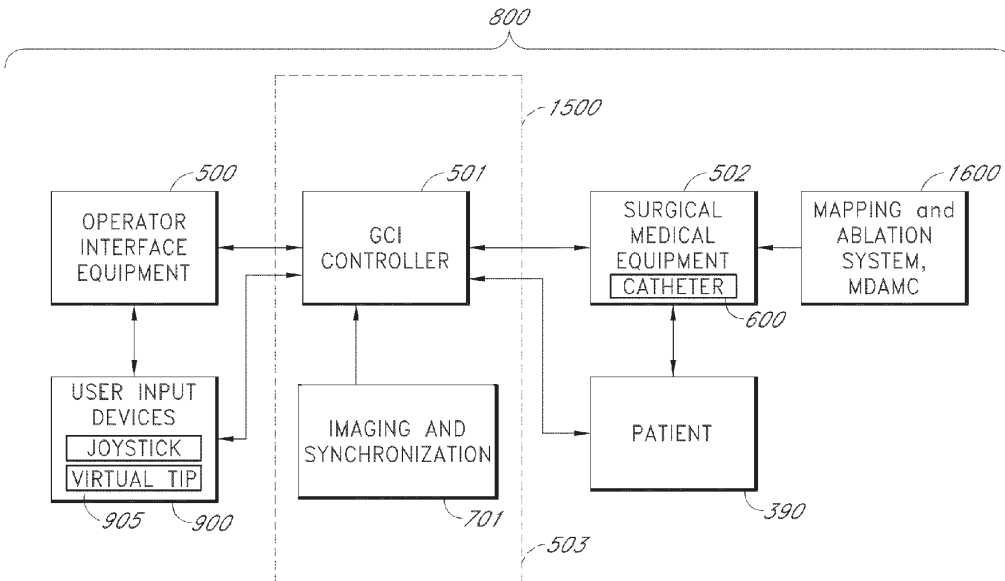
(73) **Assignee:** **Magnetecs, Inc.**, Inglewood, CA (US)

(21) **Appl. No.:** **12/480,566**

(22) **Filed:** **Jun. 8, 2009**

**Related U.S. Application Data**

(62) Division of application No. 11/362,542, filed on Feb. 23, 2006.





(12) **United States Patent**  
**Shachar et al.**

(10) **Patent No.:** **US 7,869,854 B2**  
(45) **Date of Patent:** **Jan. 11, 2011**

(54) **APPARATUS FOR MAGNETICALLY DEPLOYABLE CATHETER WITH MOSFET SENSOR AND METHOD FOR MAPPING AND ABLATION**

FOREIGN PATENT DOCUMENTS

DE 102005045073 A1 3/2007

(75) Inventors: **Yehoshua Shachar**, Santa Monica, CA (US); **Laszlo Farkas**, Ojai, CA (US); **Eli Gang**, Beverly Hills, CA (US)

(Continued)

(73) Assignee: **Magnetecs, Inc.**, Inglewood, CA (US)

OTHER PUBLICATIONS

(\* ) Notice: Subject to any disclaimer, the term of this patent is extended or adjusted under 35 U.S.C. 154(b) by 1013 days.

Faddis, Mitchell, et al. Novel, Magnetically Guided Catheter for Endocardial Mapping and Radiofrequency Catheter Ablation. Journal of the American Heart Association. [retrieved online: Jun. 22, 2009]. Nov. 11, 2022.\*

(21) Appl. No.: **11/362,542**

(Continued)

(22) Filed: **Feb. 23, 2006**

Primary Examiner—George Manuel

(65) **Prior Publication Data**

(74) Attorney, Agent, or Firm—Knobbe, Martens, Olson & Bear, LLP

US 2007/0197891 A1 Aug. 23, 2007

(57) **ABSTRACT**

(51) **Int. Cl.**

**A61B 5/04** (2006.01)

(52) **U.S. Cl.** ..... **600/374**

(58) **Field of Classification Search** ..... 606/34, 606/32; 600/393, 374, 508, 509

See application file for complete search history.

A mapping and ablation catheter is described. In one embodiment, the catheter includes a MOSFET sensor array that provides better fidelity of the signal measurements as well as data collection and reduces the error generated by spatial distribution of the isotropic and anisotropic wavefronts. In one embodiment, the system maps the change in potential in the vicinity of an activation wavefront. In one embodiment, the mapping system tracks the spread of excitation in the heart, with properties such as propagation velocity changes. In one embodiment, during measurement, the manifold carrying the sensor array expands from a closed position state to a deployable open state. Spatial variation of the electrical potential is captured by the system's ability to occupy the same three-dimensional coordinate set for repeated measurements of the desired site. In one embodiment, an interpolation algorithm tracks the electrogram data points to produce a map relative to the electrocardiogram data.

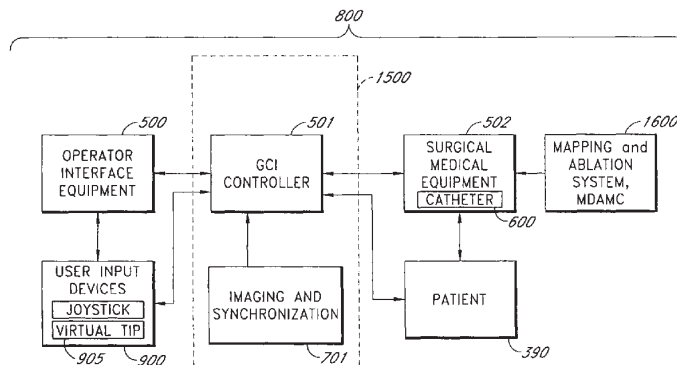
(56) **References Cited**

U.S. PATENT DOCUMENTS

3,043,309 A	7/1962	McCarthy
3,358,676 A	12/1967	Frei et al.
3,622,869 A	11/1971	Golay
3,628,527 A	12/1971	West
3,746,937 A	7/1973	Koike
3,961,632 A	6/1976	Moossun
4,063,561 A	12/1977	McKenna
4,096,862 A	6/1978	DeLuca
4,162,679 A	7/1979	Reenstierna
4,173,228 A	11/1979	Van Steenwyk et al.

(Continued)

**33 Claims, 26 Drawing Sheets**





(19) **United States**  
(12) **Patent Application Publication**  
**Gang et al.**

(10) **Pub. No.:** US 2014/0018792 A1  
(43) **Pub. Date:** Jan. 16, 2014

(54) **METHOD AND APPARATUS FOR MAGNETICALLY GUIDED CATHETER FOR RENAL DENERVATION EMPLOYING MOSFET SENSOR ARRAY**

(52) **U.S. Cl.**  
CPC ..... *A61B 18/1492* (2013.01)  
USPC ..... *606/41*

(75) Inventors: **Eli Gang**, Los Angeles, CA (US);  
**Yehoshua Josh Shachar**, Santa Monica, CA (US)

(57) **ABSTRACT**

(73) Assignee: **MAGNETECS INC.**, Inglewood, CA (US)

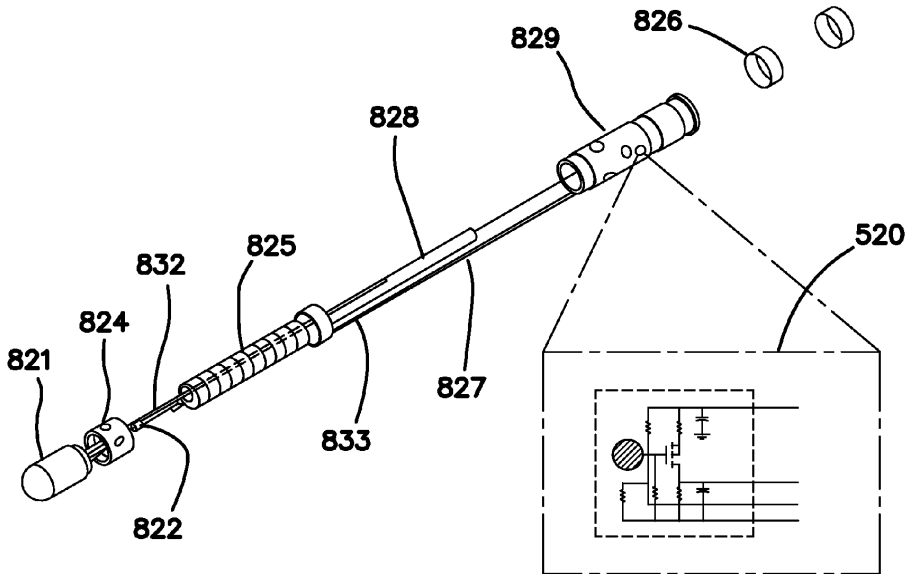
A system for a mapping and ablation catheter. The catheter includes a MOSFET sensor array that provides better fidelity of the signal measurements as well as data collection and reduces the error generated by spatial distribution of the isotropic and anisotropic wave fronts and error associated with near and far field's signal averages. The system maps the change in bioelectric potential in the vicinity of an activation wave front. During measurement, the manifold carrying the sensor array translates and rotates so as to achieve a measure of high potential employing an impedance value. The system of guiding and controlling the movement of the catheter distal end is able to deliver energy for ablating the renal artery nerve and thereby providing a safe and efficient method and apparatus for neuromodulation.

(21) Appl. No.: **13/549,341**

(22) Filed: **Jul. 13, 2012**

**Publication Classification**

(51) **Int. Cl.**  
*A61B 18/14* (2006.01)



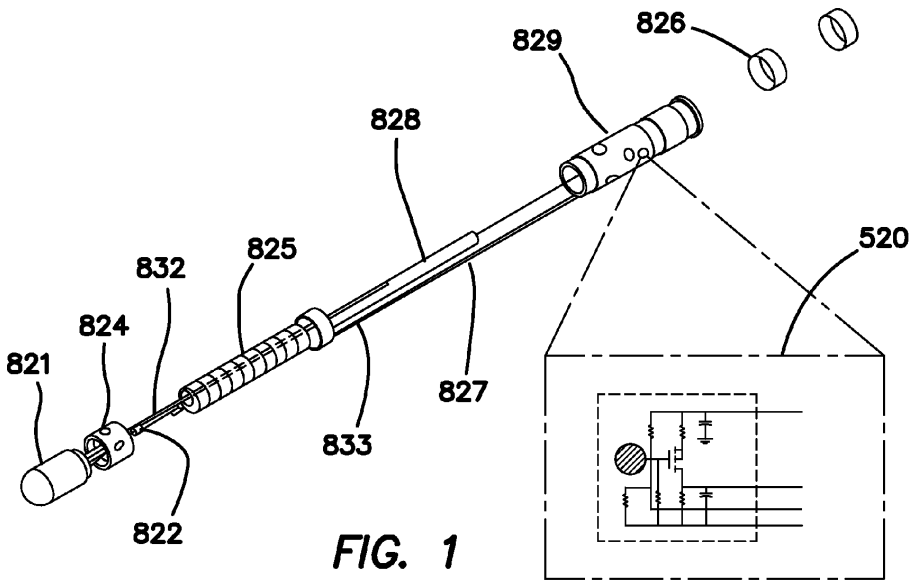


FIG. 1

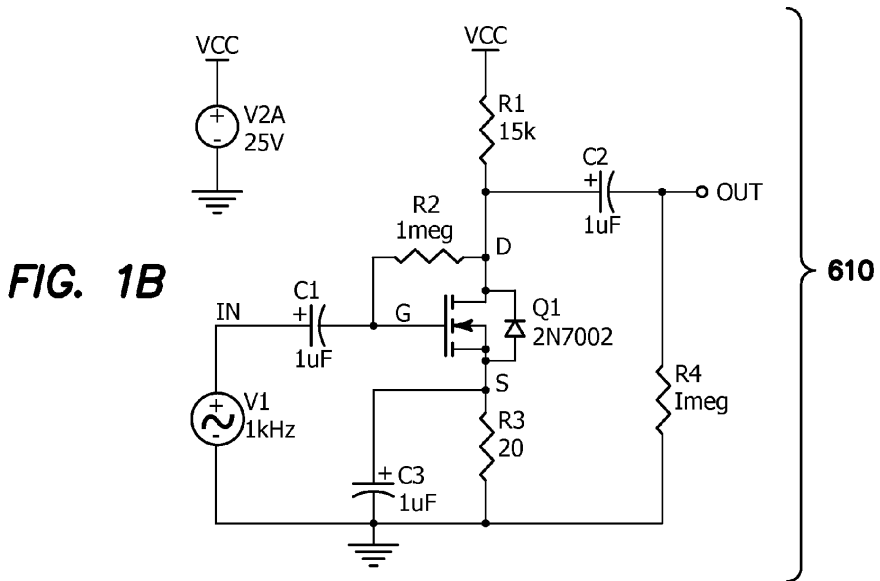


FIG. 1B



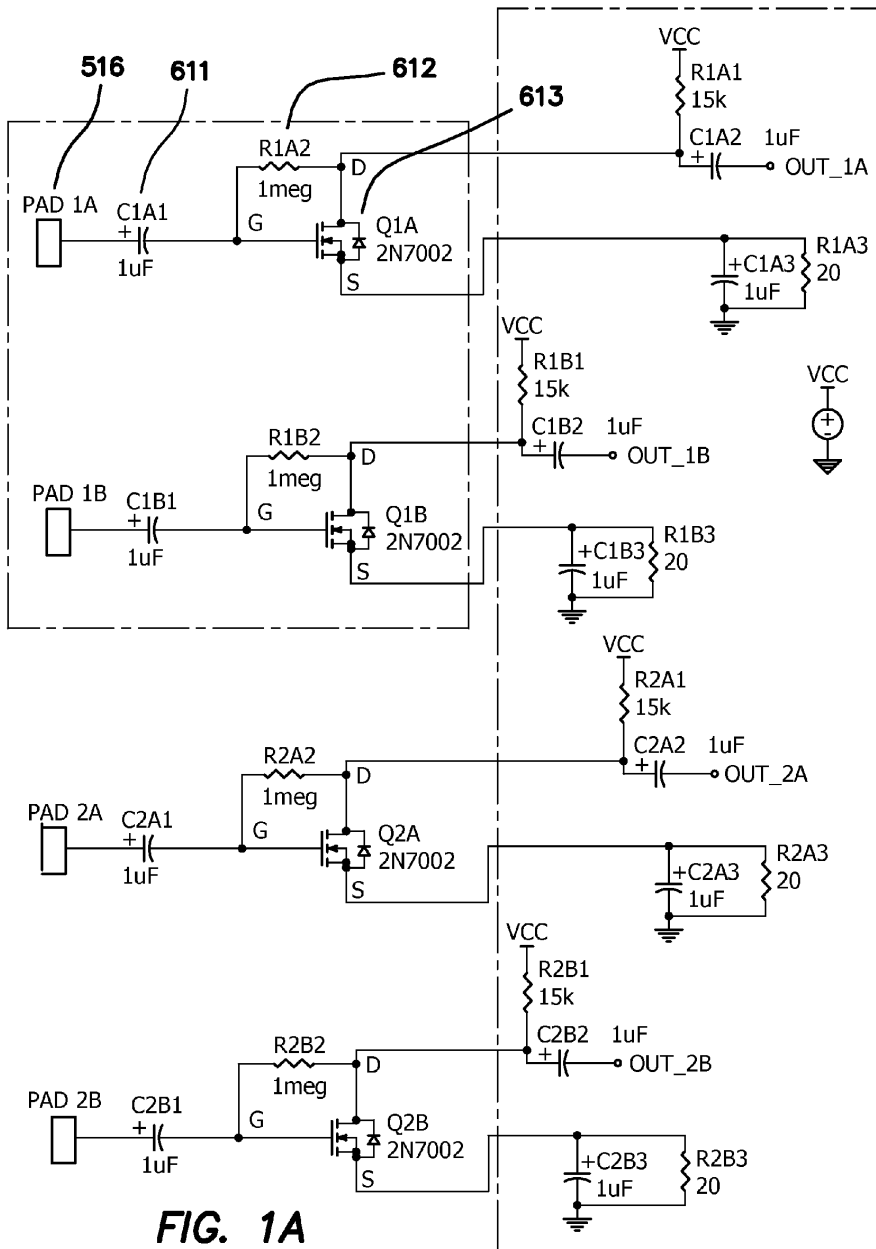
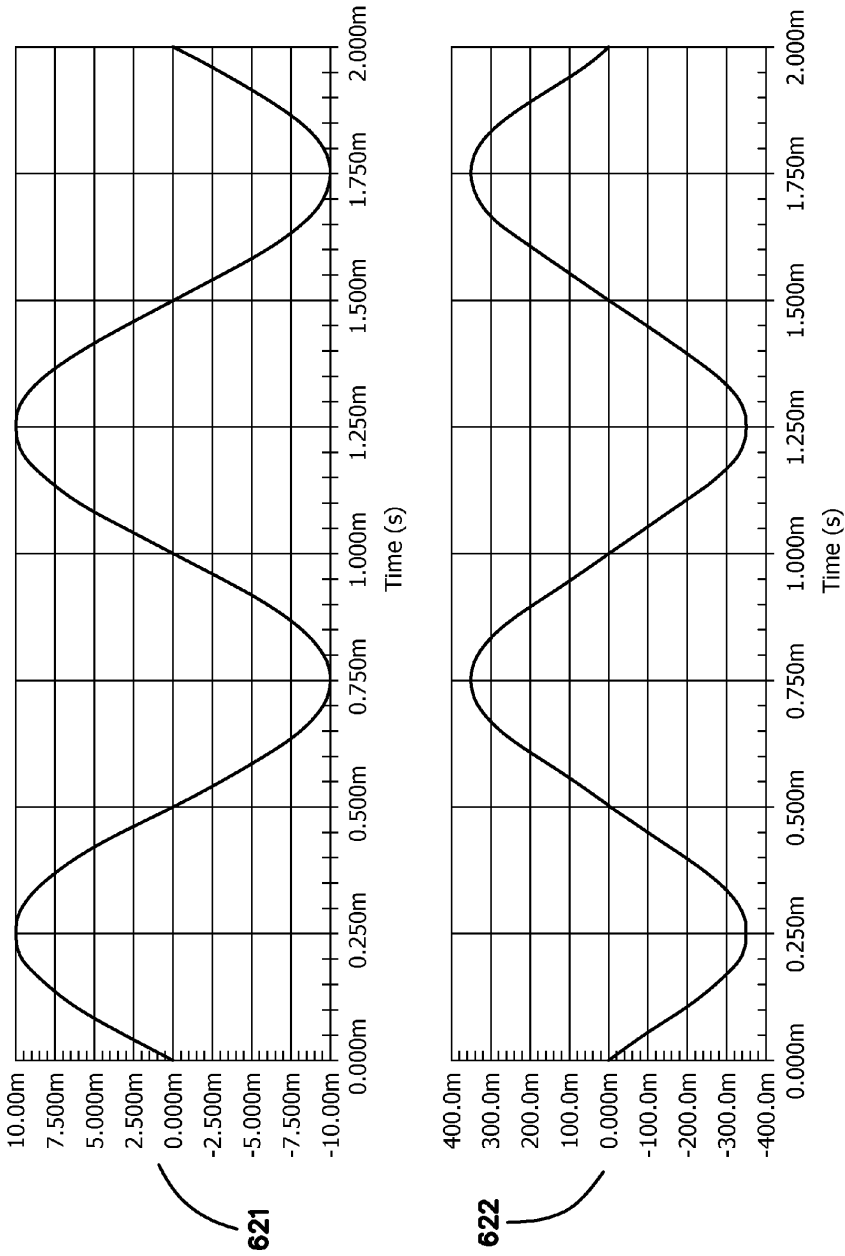


FIG. 1A





US009381063B2



(12) **United States Patent**  
**Gang et al.**

(10) **Patent No.:** **US 9,381,063 B2**  
(45) **Date of Patent:** **Jul. 5, 2016**

(54) **METHOD AND APPARATUS FOR MAGNETICALLY GUIDED CATHETER FOR RENAL DENERVATION EMPLOYING MOSFET SENSOR ARRAY**

(75) Inventors: **Eli Gang**, Los Angeles, CA (US);  
**Yehoshua Josh Shachar**, Santa Monica, CA (US)

(73) Assignee: **Magnetecs Inc.**, Inglewood, CA (US)

(\* ) Notice: Subject to any disclaimer, the term of this patent is extended or adjusted under 35 U.S.C. 154(b) by 818 days.

(21) Appl. No.: **13/549,341**

(22) Filed: **Jul. 13, 2012**

(65) **Prior Publication Data**

US 2014/0018792 A1 Jan. 16, 2014

(51) **Int. Cl.**

**A61B 18/04** (2006.01)  
**A61B 18/14** (2006.01)  
**A61B 5/05** (2006.01)  
**A61B 18/00** (2006.01)

(52) **U.S. Cl.**

CPC ..... **A61B 18/1492** (2013.01); **A61B 34/73** (2016.02); **A61B 5/05** (2013.01); **A61B 18/04** (2013.01); **A61B 2018/00404** (2013.01); **A61B 2018/00434** (2013.01); **A61B 2018/00511** (2013.01); **A61B 2018/00577** (2013.01); **A61B 2018/00839** (2013.01)

(58) **Field of Classification Search**

CPC ..... A61N 1/00; A61N 1/18; A61N 1/375; A61N 2/00; A61N 5/00; A61B 5/00; A61B 6/00; A61M 25/0133

See application file for complete search history.

(56) **References Cited**

U.S. PATENT DOCUMENTS

7,280,863 B2	10/2007	Shachar
7,617,005 B2	11/2009	Demarais
7,620,451 B2	11/2009	Demarais
7,647,115 B2	1/2010	Levin
7,653,438 B2	1/2010	Deem
7,769,427 B2	8/2010	Shachar
7,869,854 B2	1/2011	Shachar
7,937,143 B2	5/2011	Demarais
2006/0114088 A1	6/2006	Shachar
2006/0116633 A1	6/2006	Shachar
2006/0116634 A1	6/2006	Shachar
2006/0142801 A1	6/2006	Demarais
2006/0206150 A1	9/2006	Demarais
2006/0212078 A1	9/2006	Demarais
2006/0265014 A1	11/2006	Demarais
2006/0276852 A1	12/2006	Demarais
2007/0016006 A1	1/2007	Shachar
2007/0129720 A1	6/2007	Demarais
2007/0197891 A1	8/2007	Shachar
2007/0265687 A1	11/2007	Deem

(Continued)

*Primary Examiner* — Christopher D Koharski

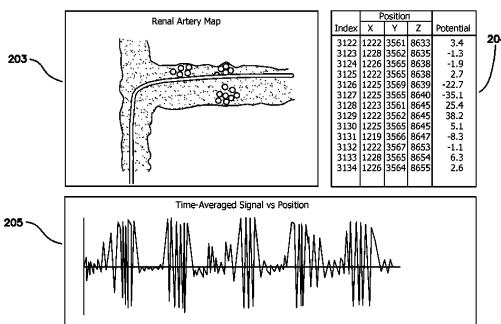
*Assistant Examiner* — Elizabeth K So

(74) *Attorney, Agent, or Firm* — Marcus C. Dawes; Daniel L. Dawes

(57) **ABSTRACT**

A system for a mapping and ablation catheter. The catheter includes a MOSFET sensor array that provides better fidelity of the signal measurements as well as data collection and reduces the error generated by spatial distribution of the isotropic and anisotropic wave fronts and error associated with near and far field's signal averages. The system maps the change in bioelectric potential in the vicinity of an activation wave front. During measurement, the manifold carrying the sensor array translates and rotates so as to achieve a measure of high potential employing an impedance value. The system of guiding and controlling the movement of the catheter distal end is able to deliver energy for ablating the renal artery nerve and thereby providing a safe and efficient method and apparatus for neuromodulation.

**20 Claims, 25 Drawing Sheets**





(19) **United States**

(12) **Patent Application Publication**  
**Shachar et al.**

(10) **Pub. No.: US 2014/0081114 A1**

(43) **Pub. Date: Mar. 20, 2014**

(54) **METHOD AND APPARATUS FOR MEASURING BIOPOTENTIAL AND MAPPING EPICARDIC COUPLING EMPLOYING A CATHETER WITH MOSFET SENSOR ARRAY**

(52) **U.S. Cl.**  
CPC ..... *A61B 5/04001* (2013.01); *A61B 5/0478* (2013.01)  
USPC ..... **600/378; 600/373; 600/547**

(71) Applicants: **Yehoshua Shachar**, Santa Monica, CA (US); **Eli Gang**, Los Angeles, CA (US)

(57) **ABSTRACT**

(72) Inventors: **Yehoshua Shachar**, Santa Monica, CA (US); **Eli Gang**, Los Angeles, CA (US)

(73) Assignee: **MAGNETECS INC.**, Inglewood, CA (US)

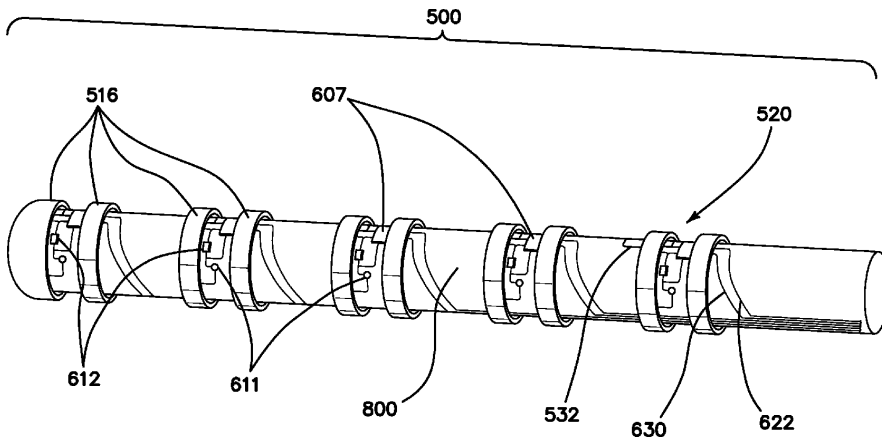
(21) Appl. No.: **13/621,727**

(22) Filed: **Sep. 17, 2012**

**Publication Classification**

(51) **Int. Cl.**  
*A61B 5/04* (2006.01)  
*A61B 5/0478* (2006.01)

This invention relates generally to electro-anatomical mapping method and an apparatus using a catheter and more particularly to a mapping catheter having an embedded MOSFET sensor array for detecting local electrophysiological parameters such as biopotential signals within an excitable cellular matrix geometry, for determining physiological as well as electrical characteristics of conduction path and its underlying substrate within the endocardial and epicardial spaces, the arterial structure and in ganglionic plexus. The apparatus with its MOSFET sensor is geometrically configured as a decapolar linear array and optionally with an 8x8 sensor matrix placed on a balloon-like structure.





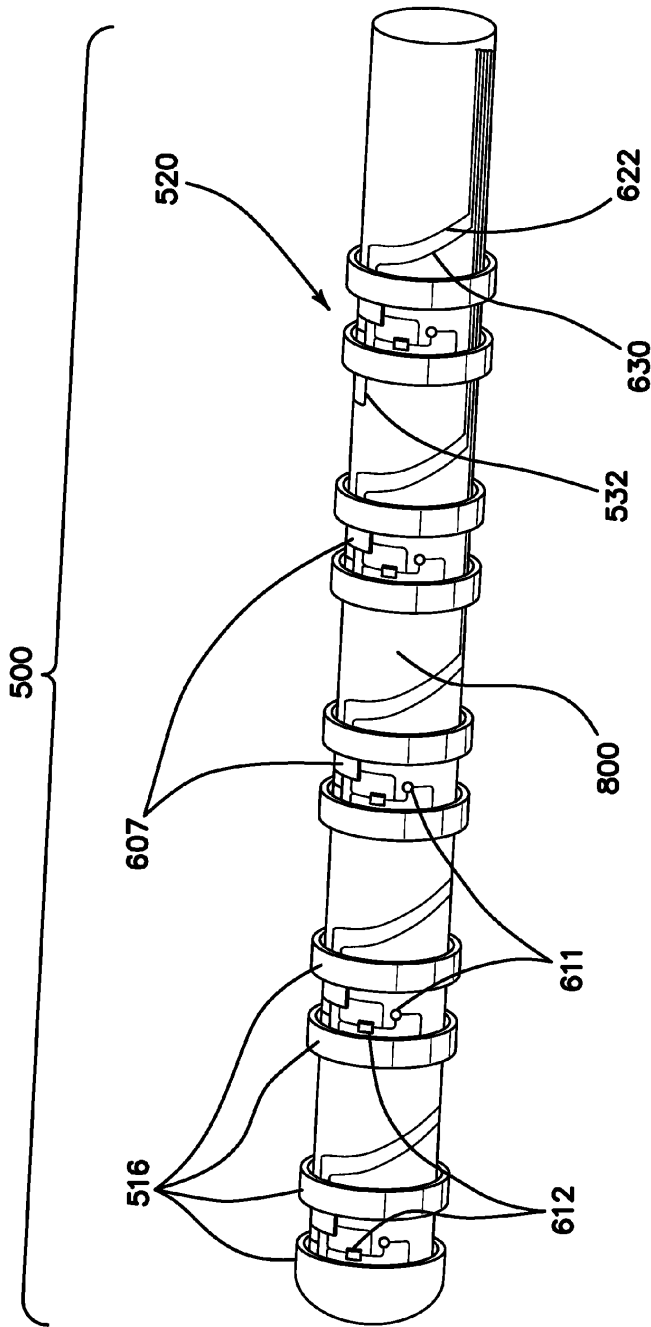


FIG. 1

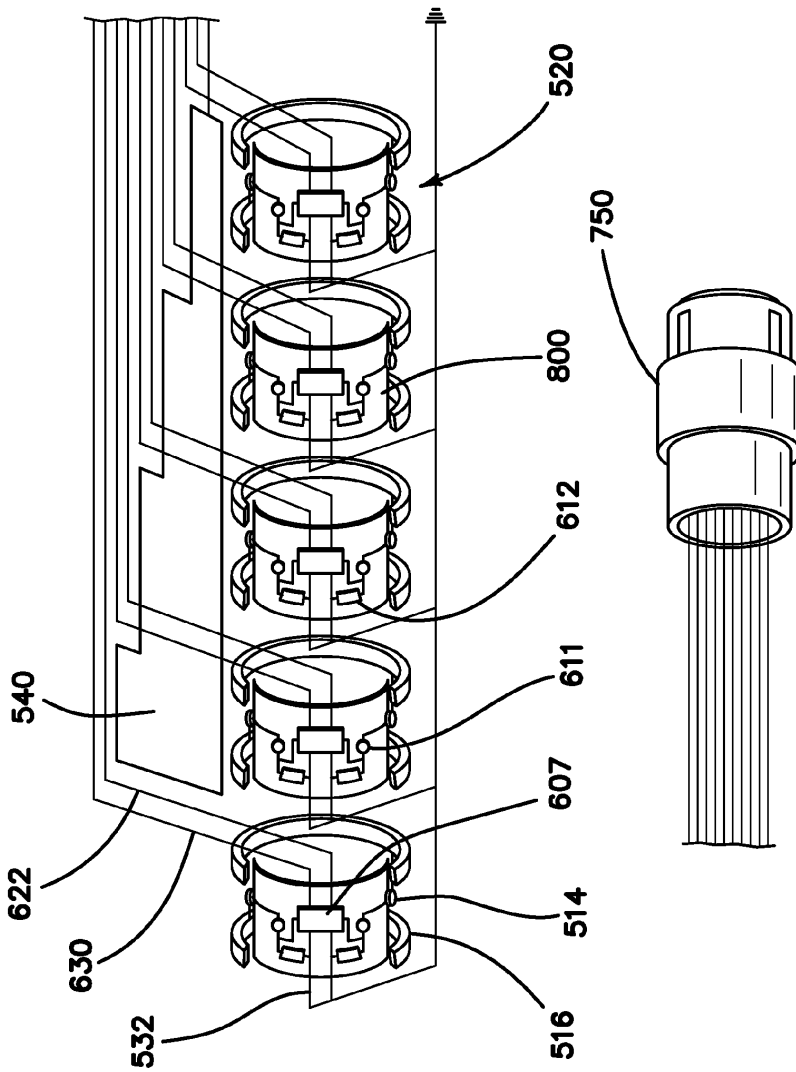


FIG. 1A

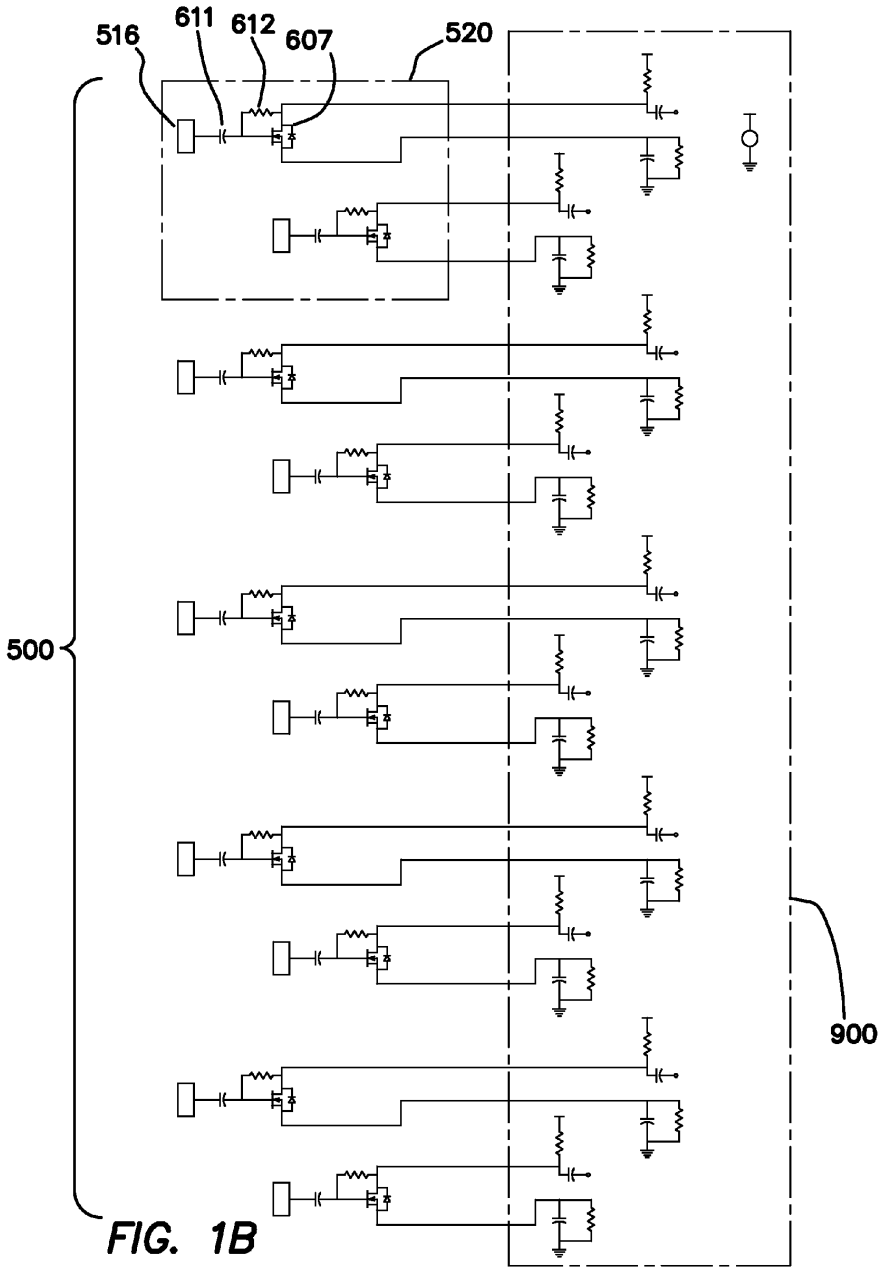


FIG. 1B

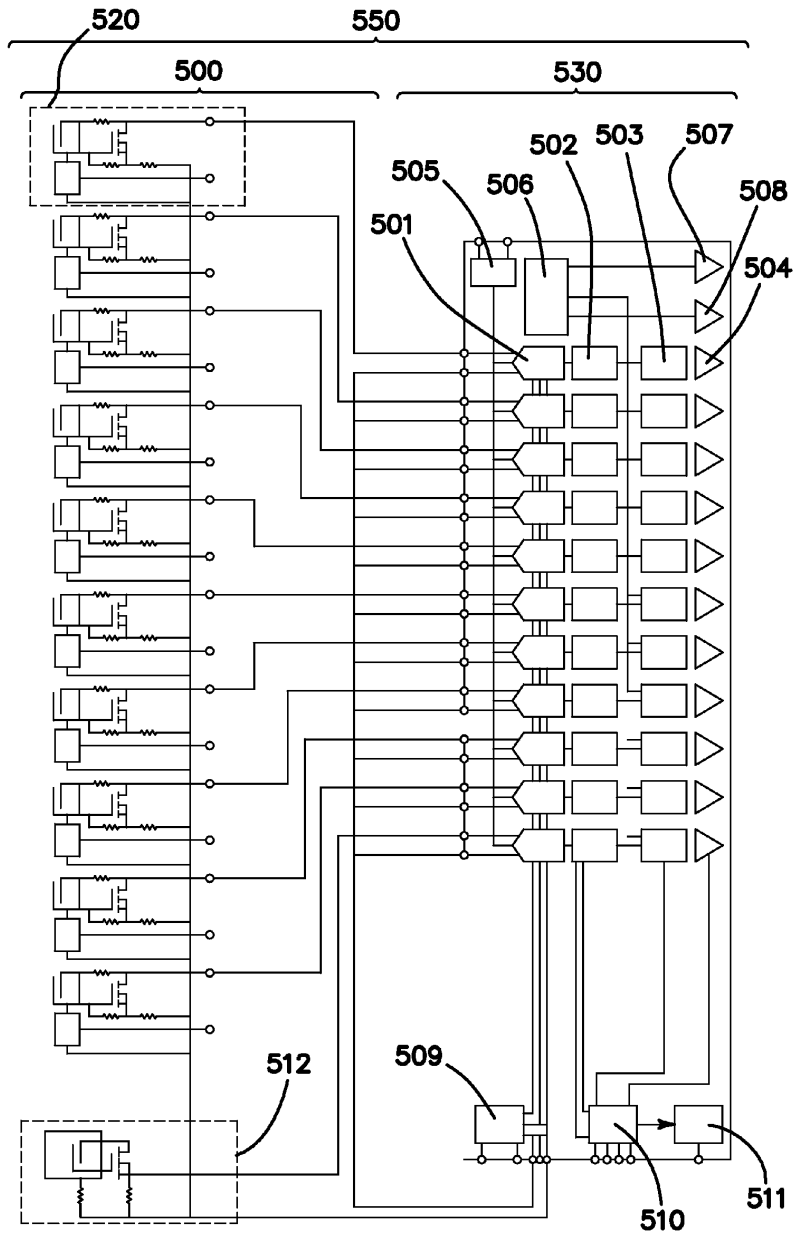


FIG. 1C

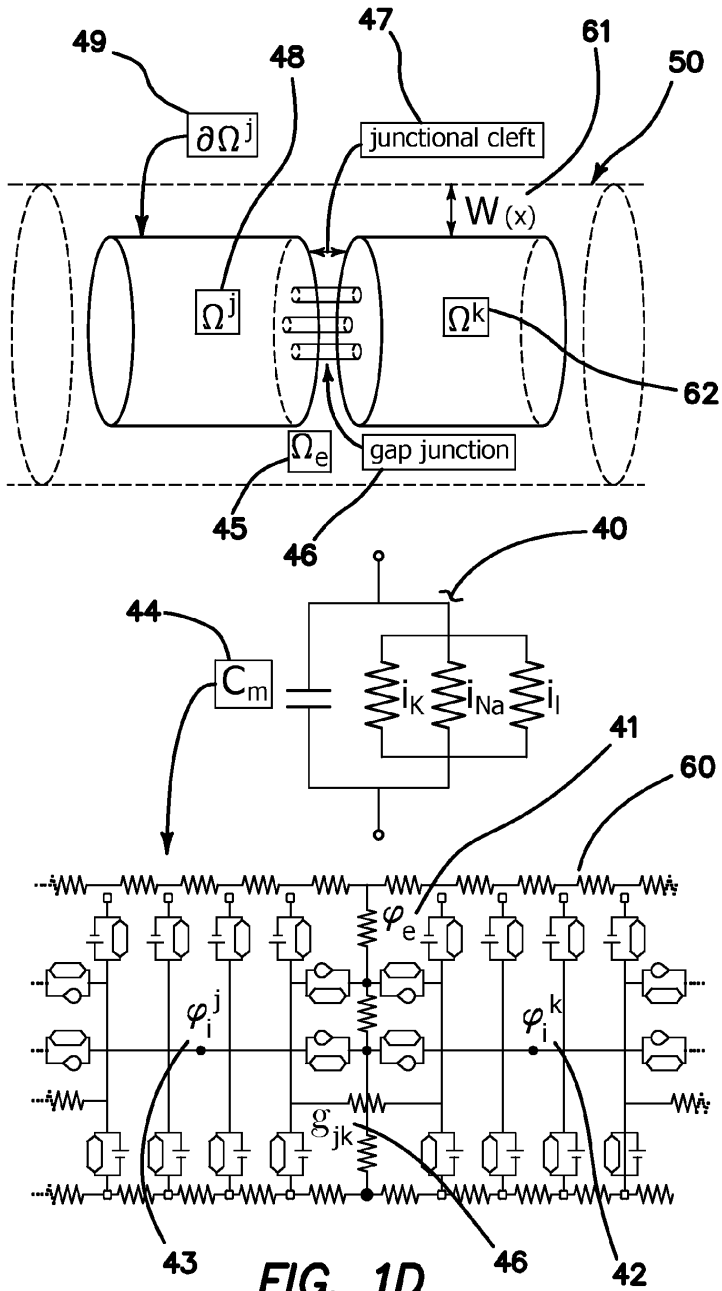


FIG. 1D



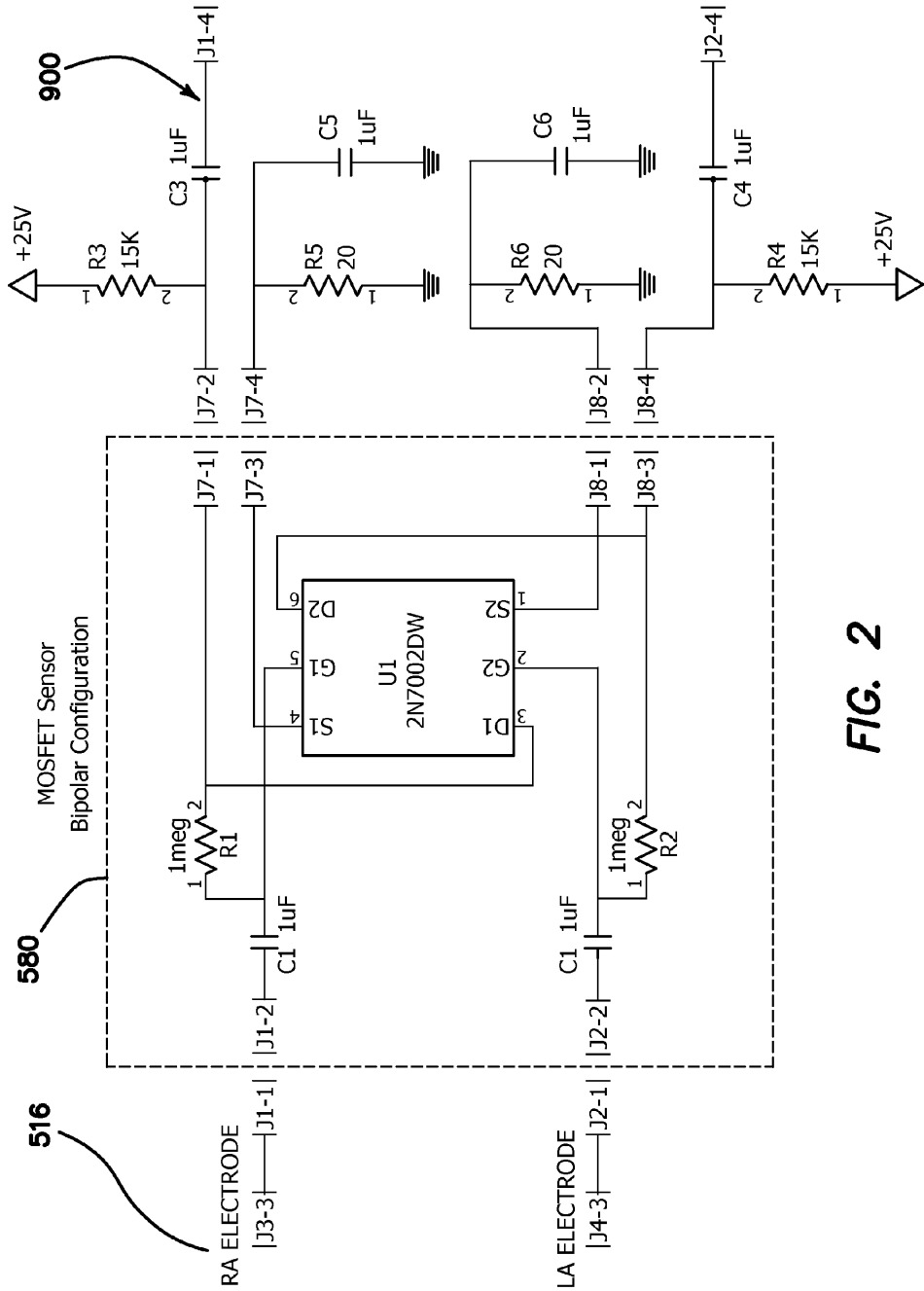


FIG. 2

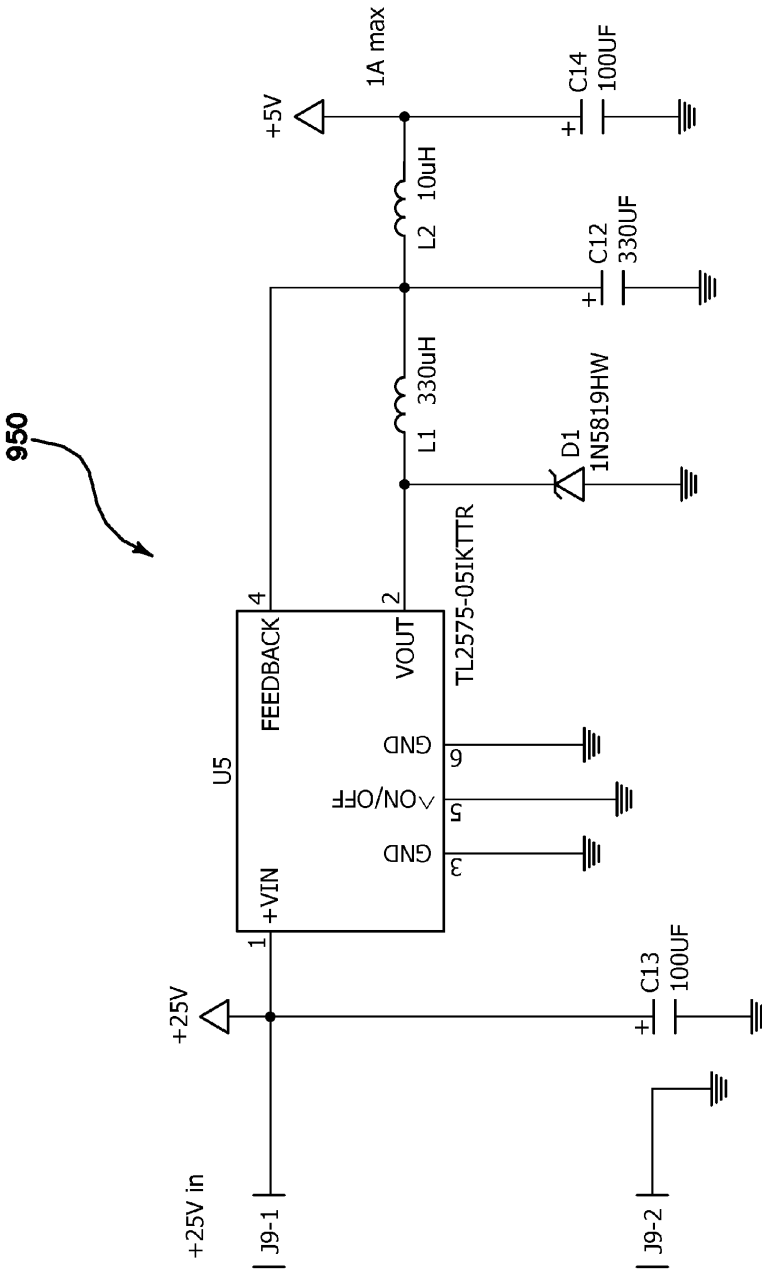


FIG. 2A

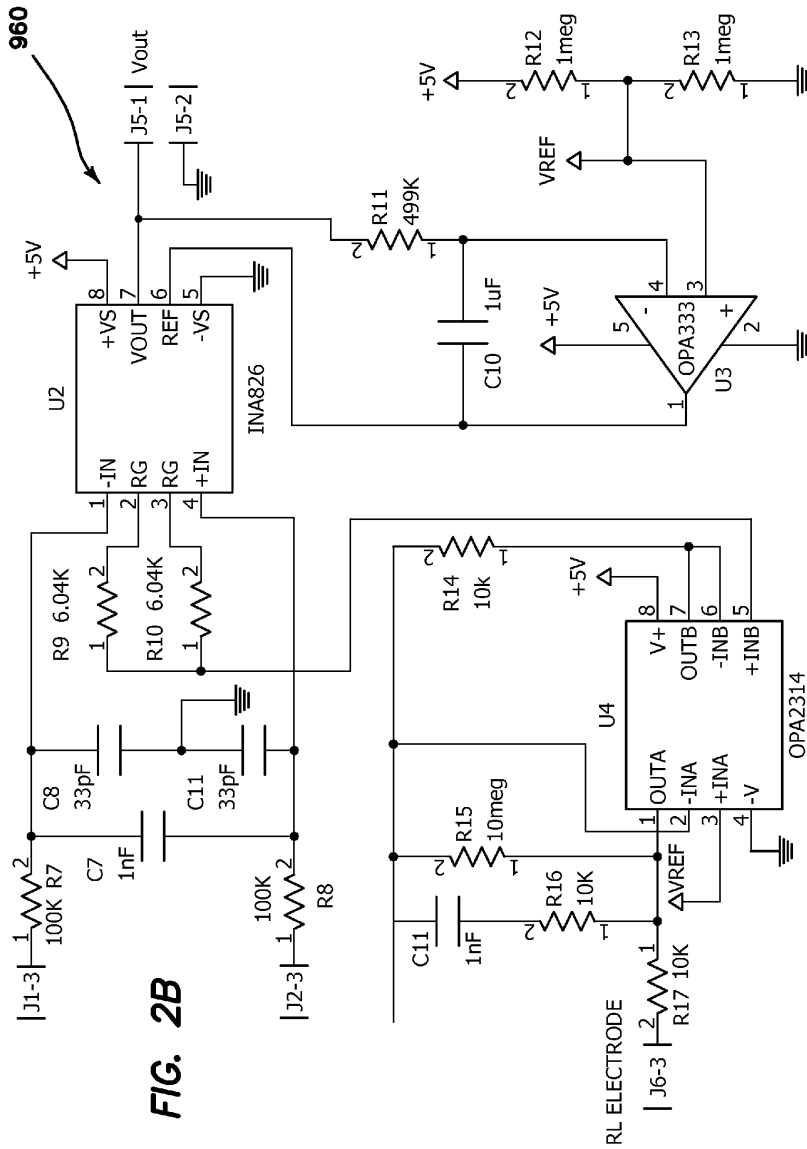


FIG. 2B

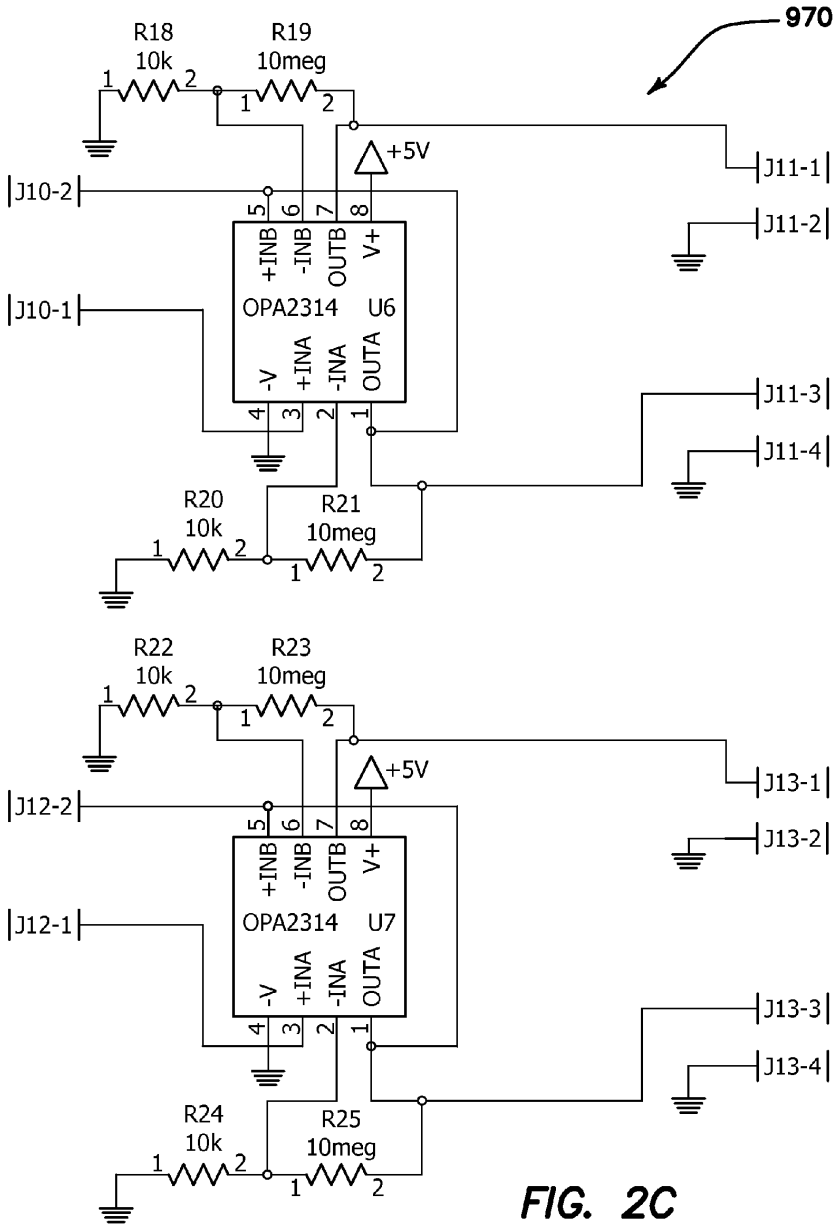


FIG. 2C

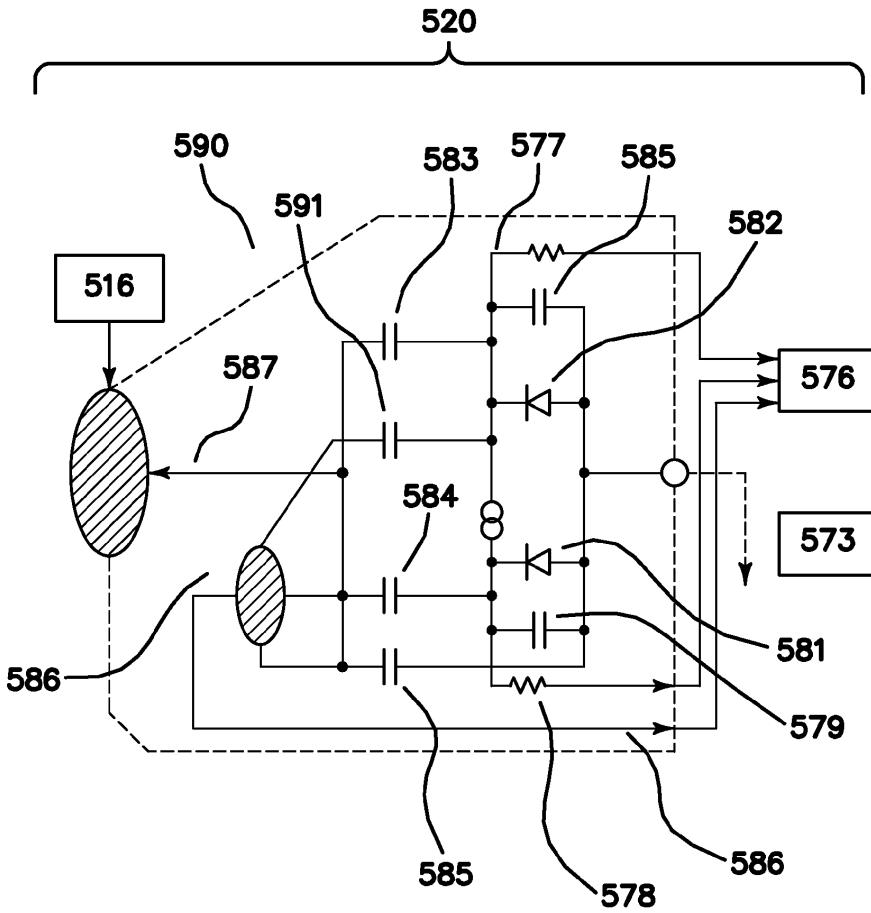


FIG. 2D



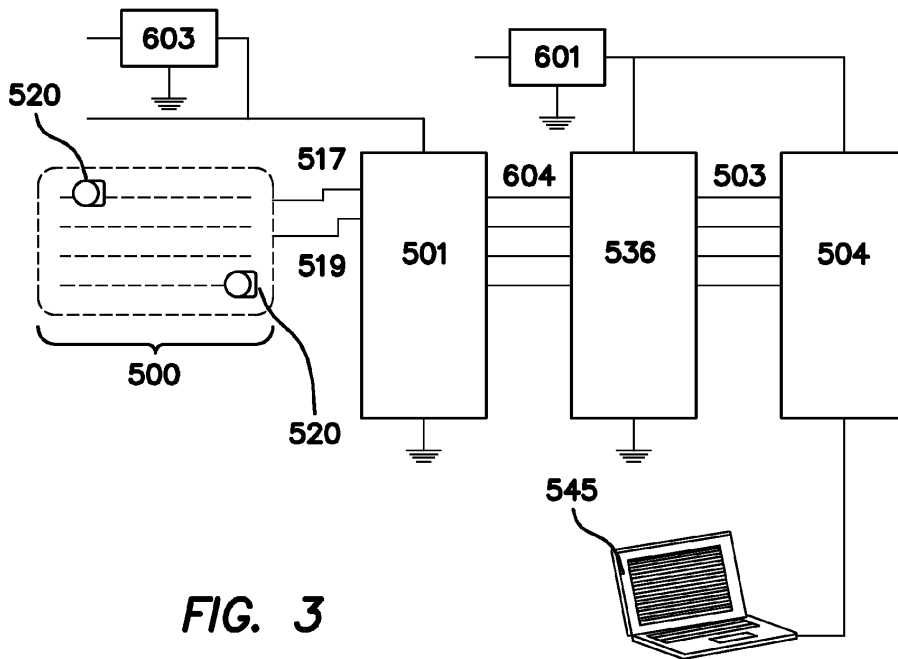


FIG. 3

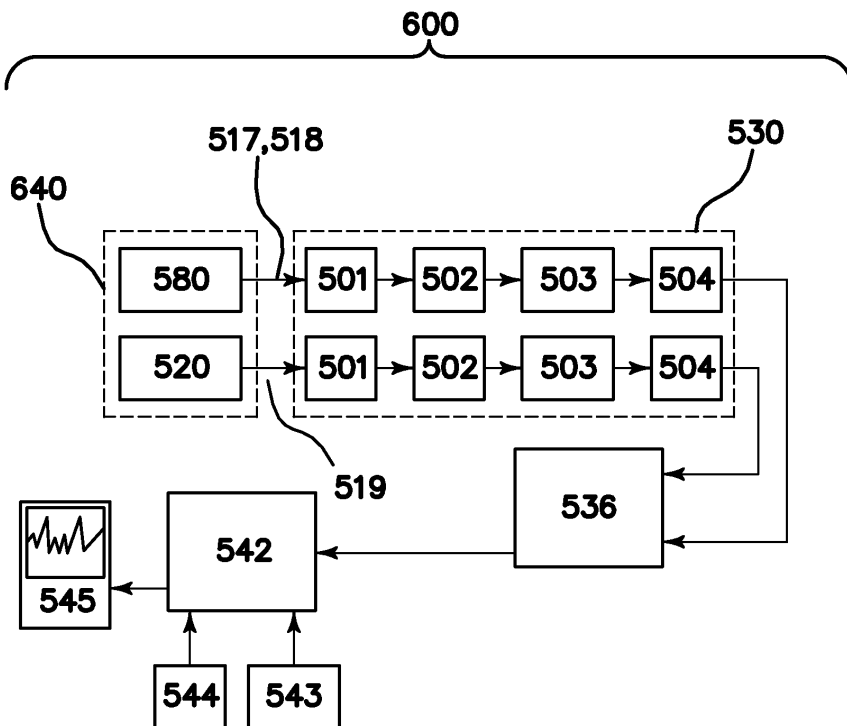
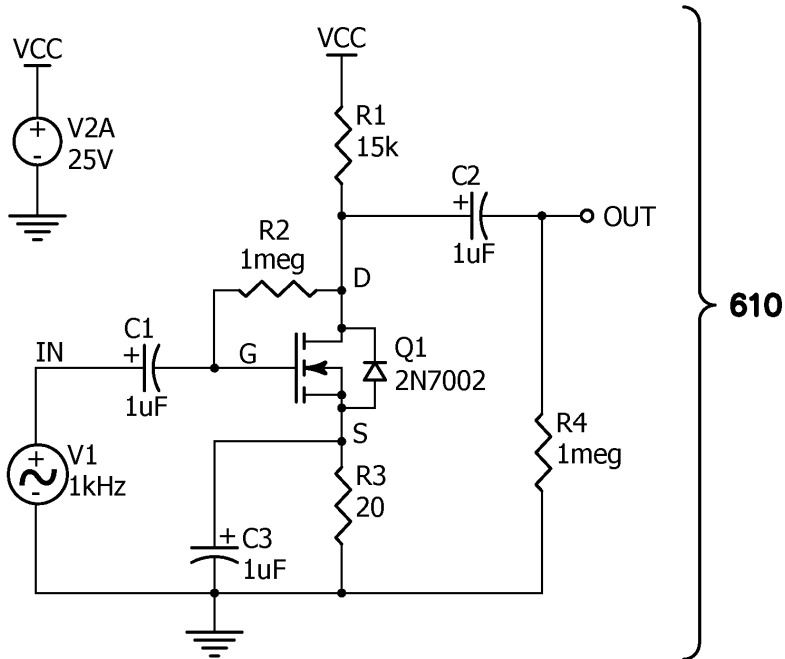


FIG. 3A



**FIG. 4**

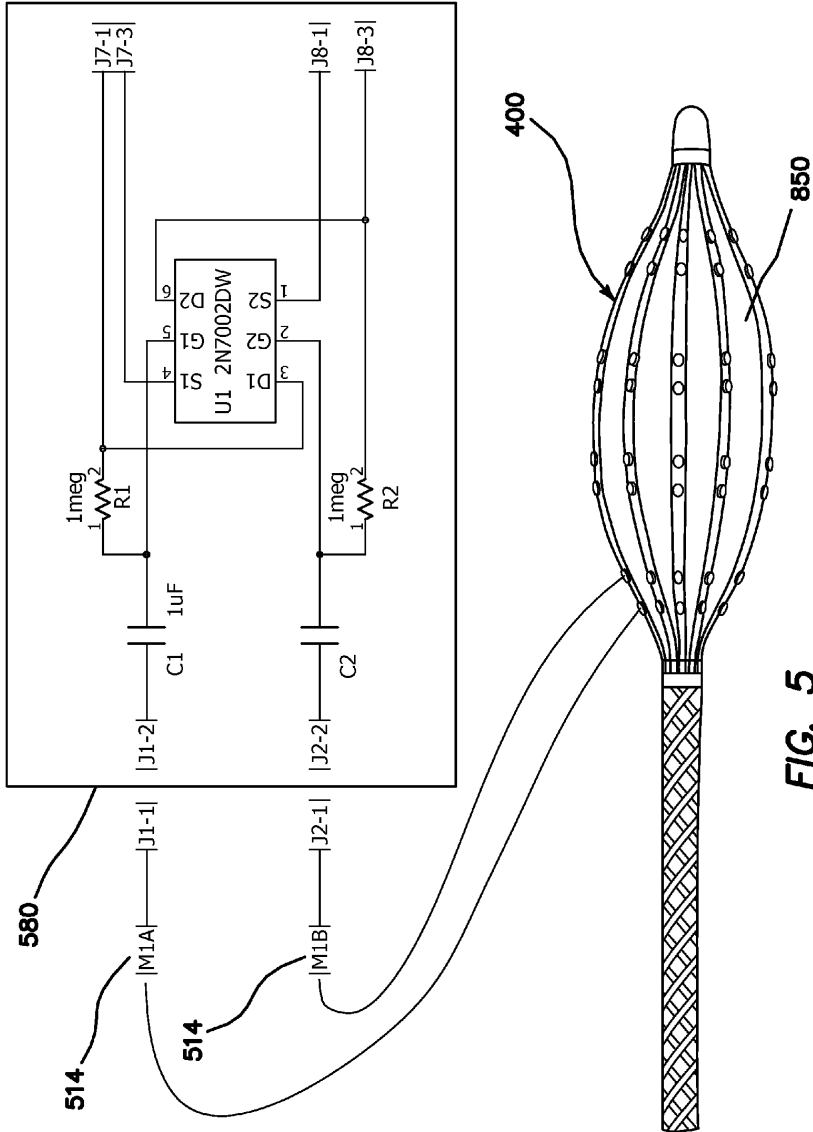
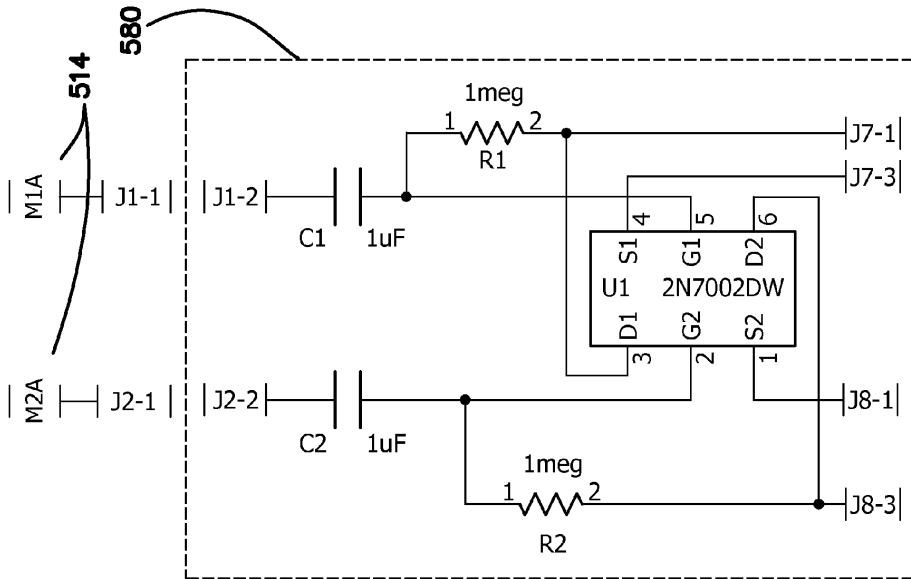
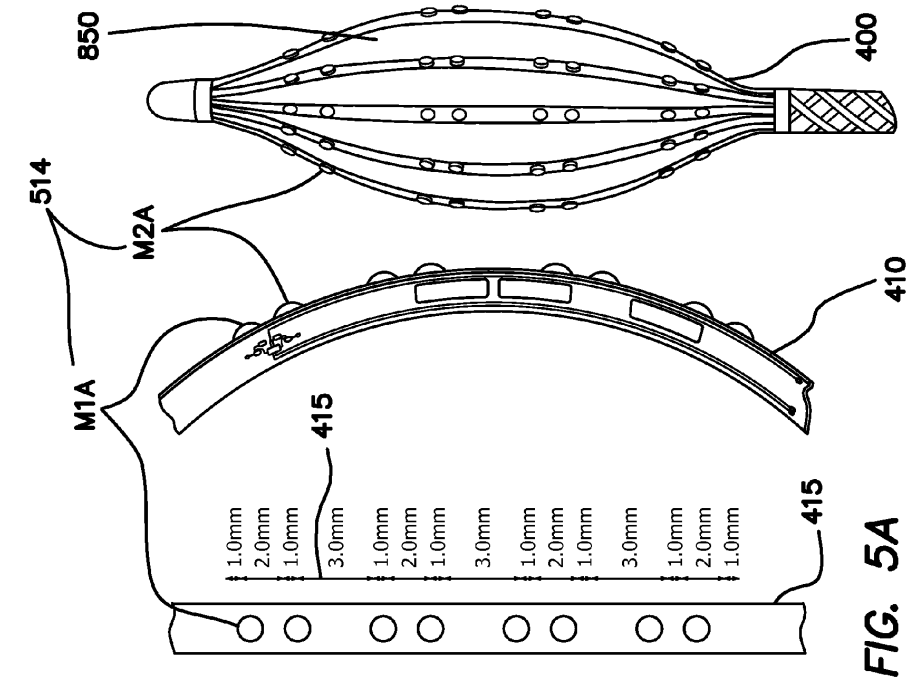


FIG. 5





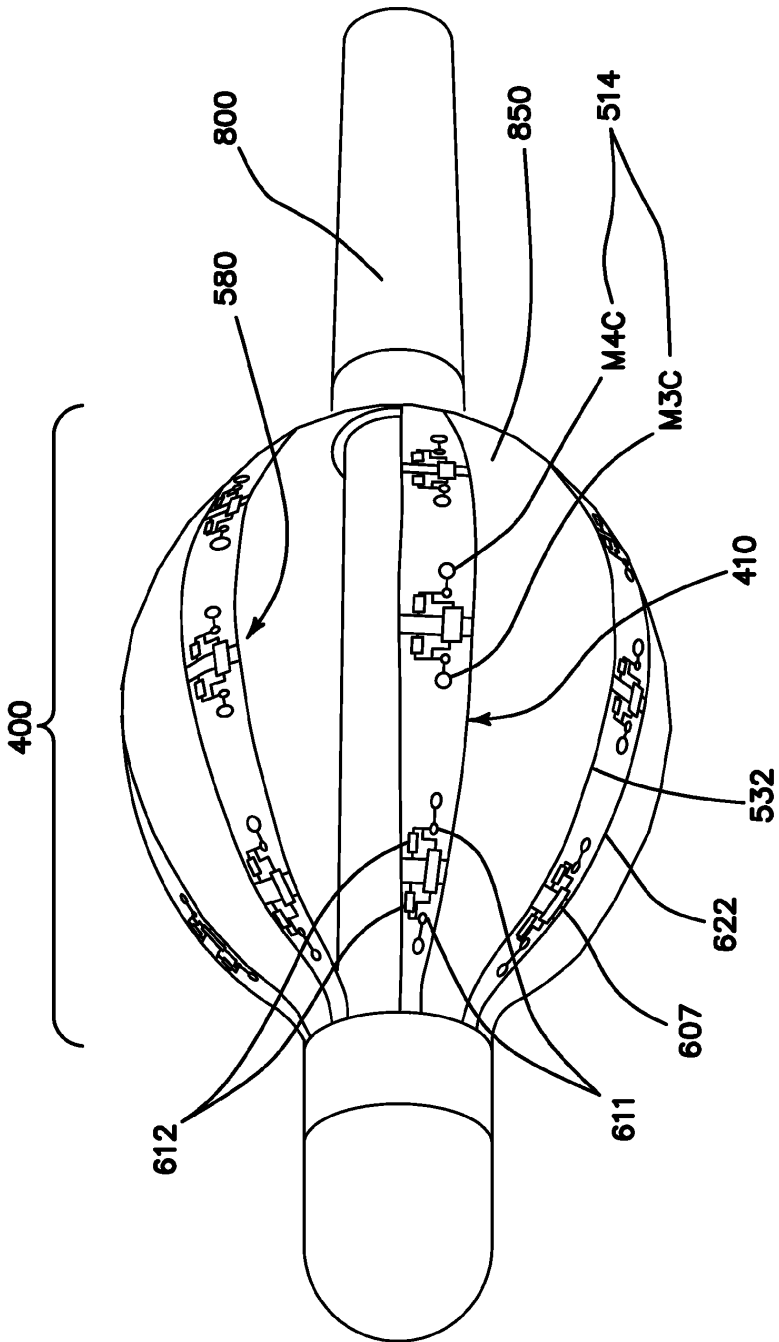


FIG. 5B

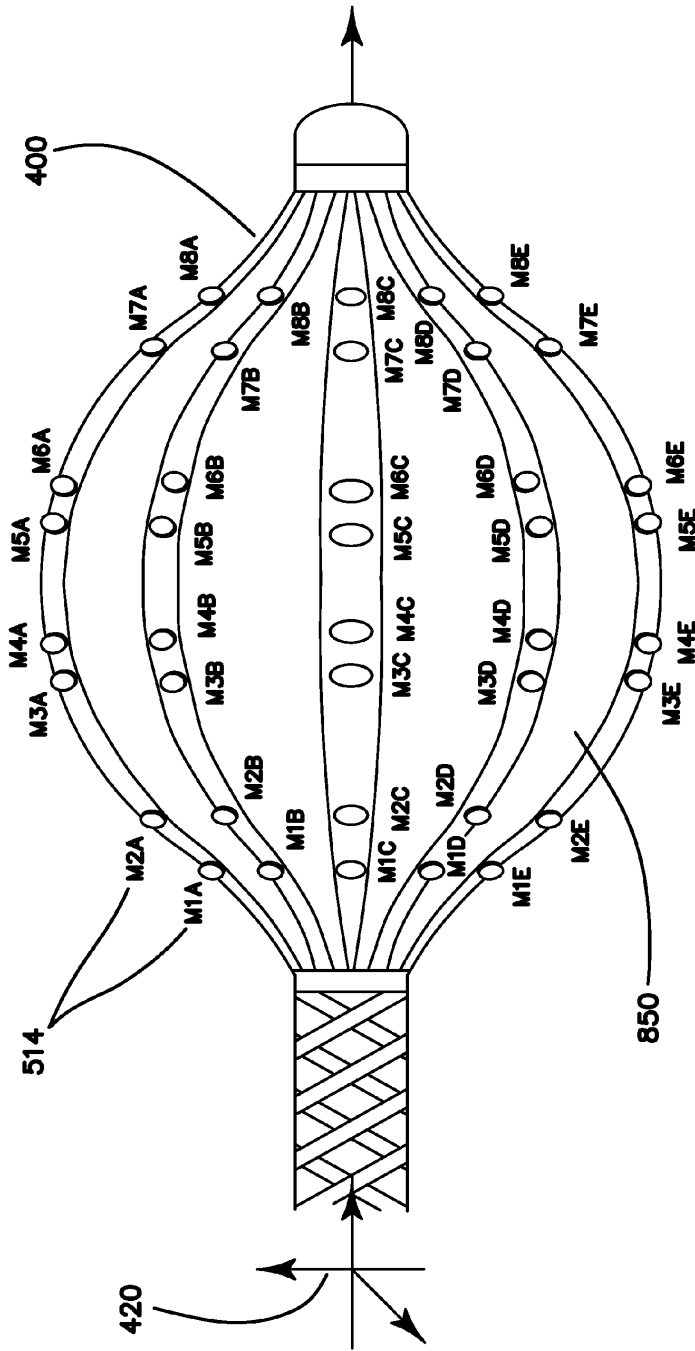


FIG. 5C

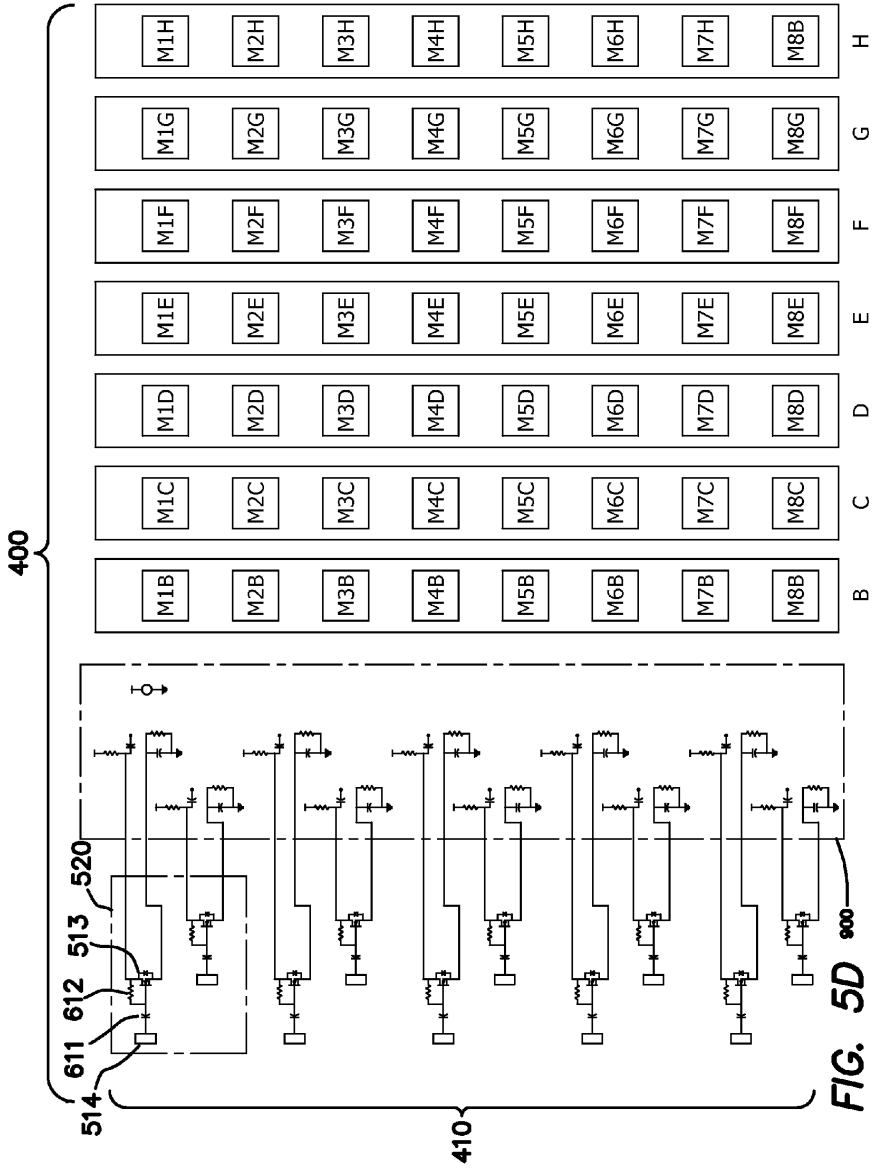


FIG. 5D

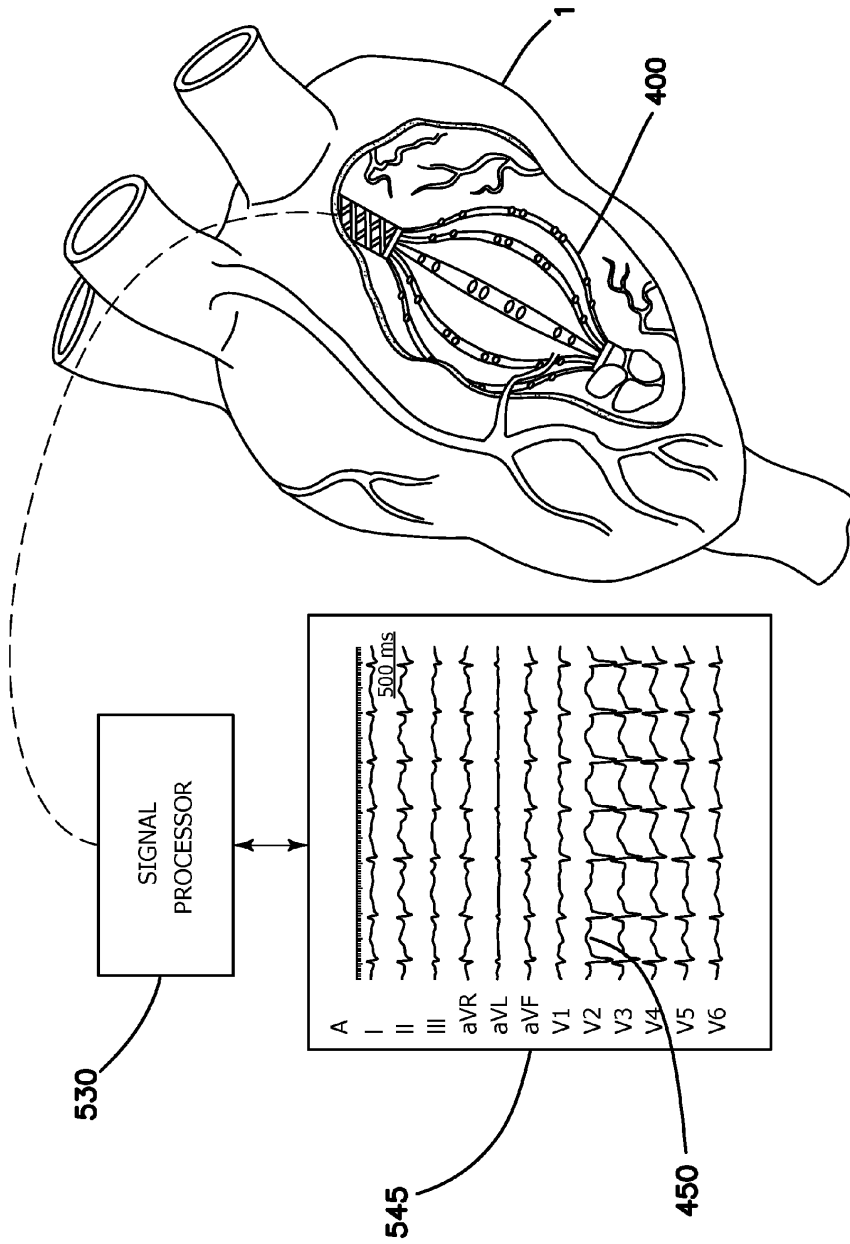


FIG. 5E

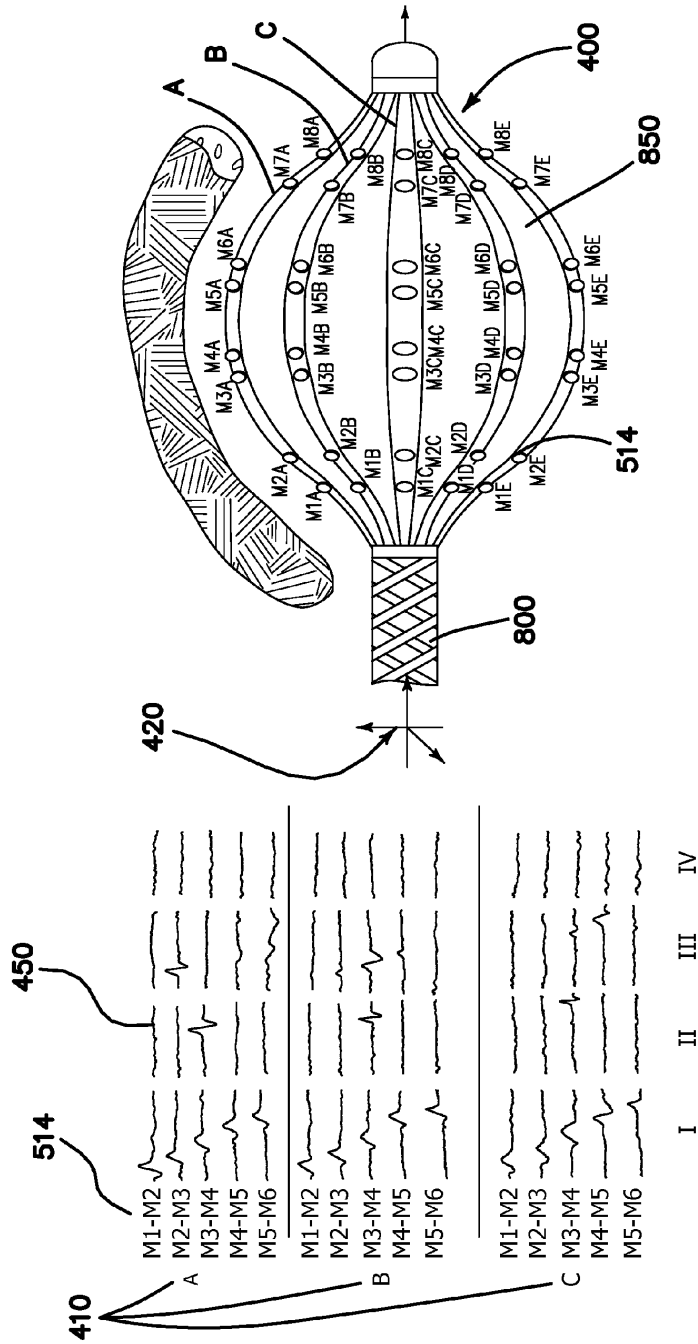
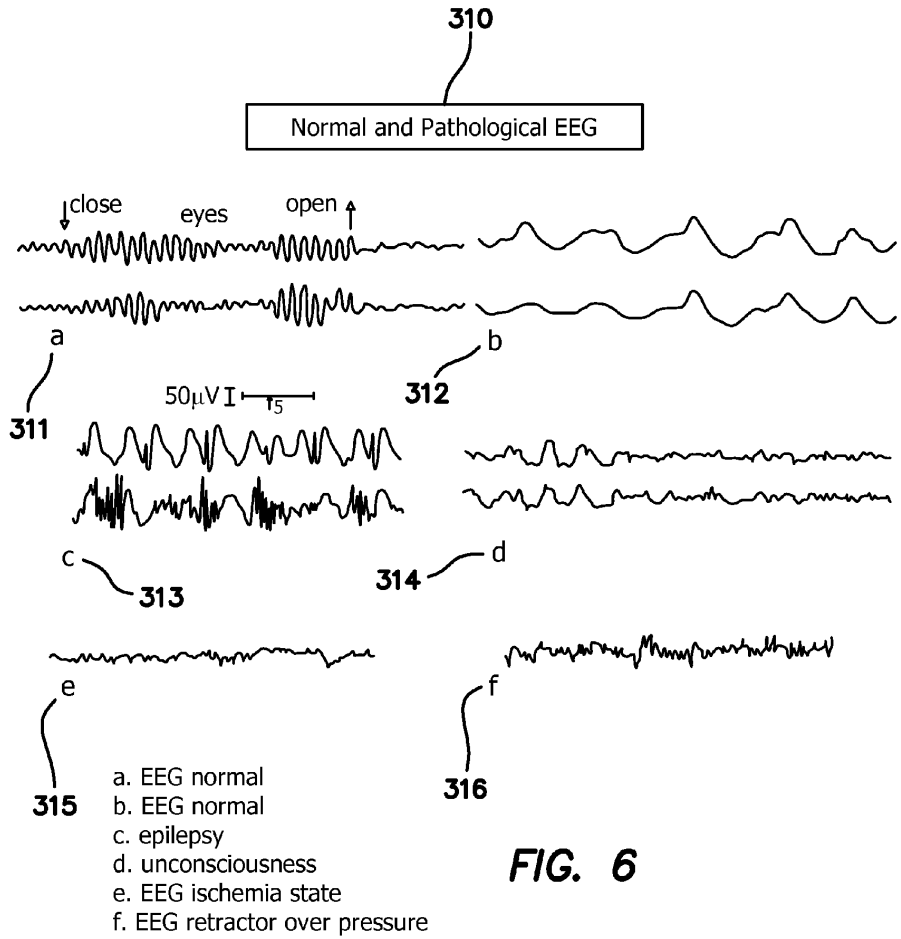


FIG. 5F





**FIG. 6**

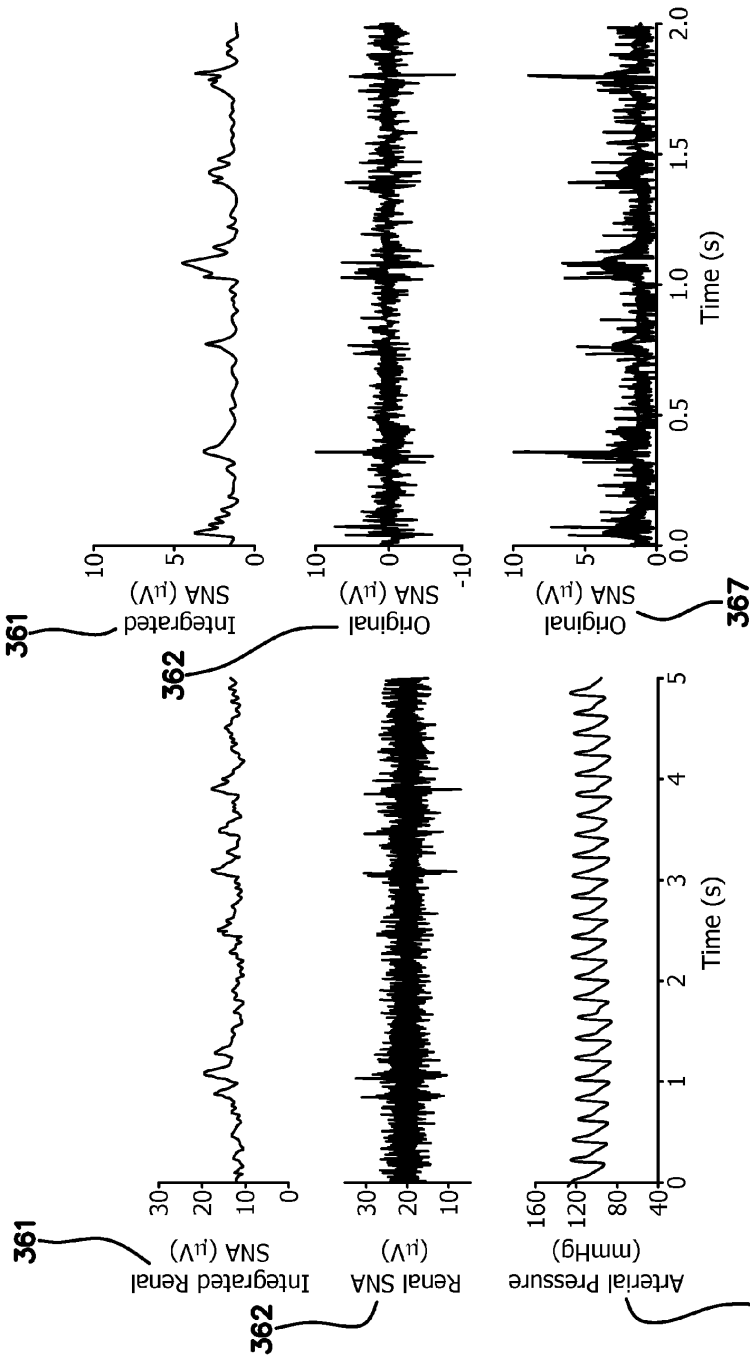


FIG. 6B

FIG. 6A

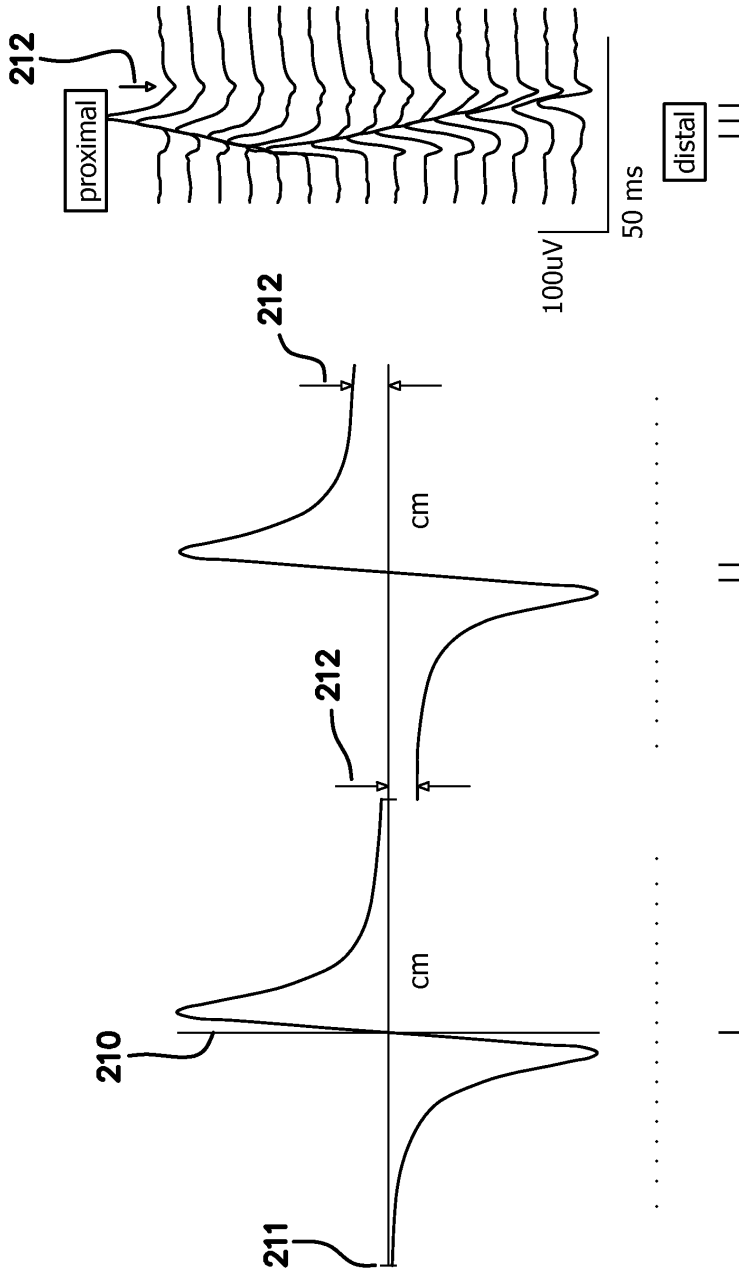
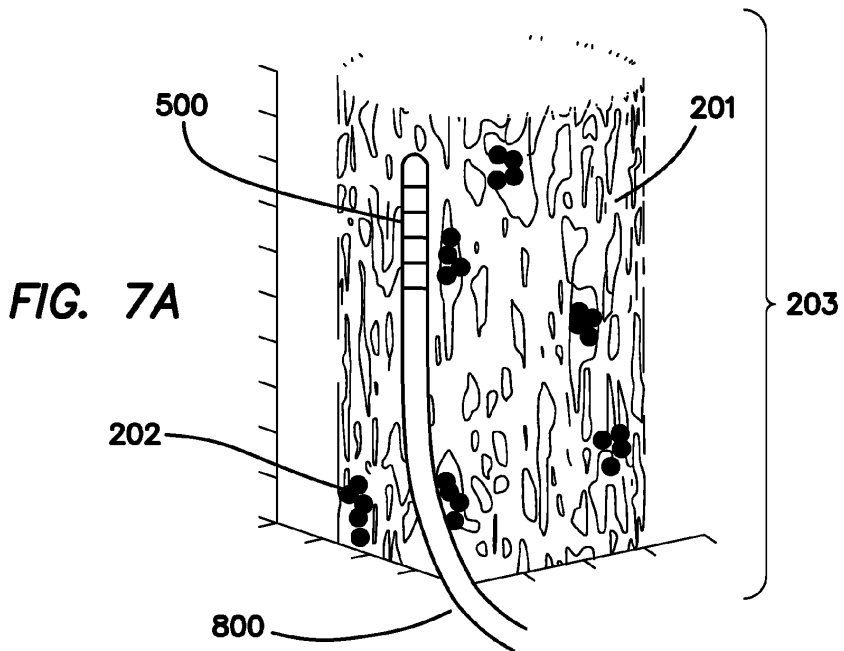
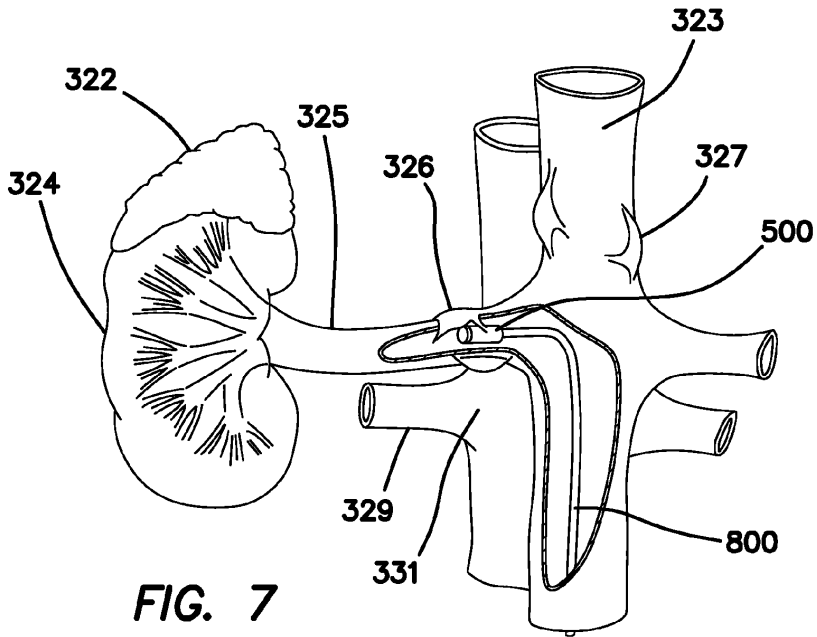


FIG. 6C



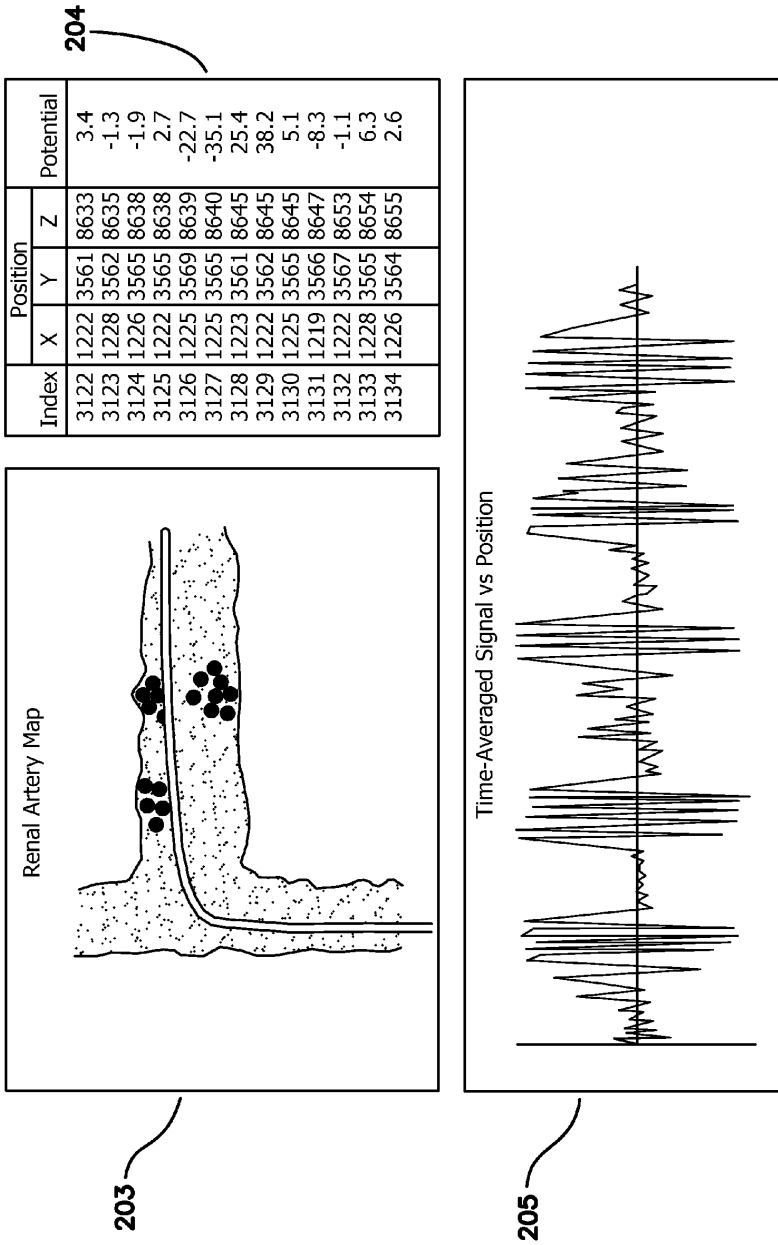


FIG. 7B



**METHOD AND APPARATUS FOR  
MEASURING BIOPOTENTIAL AND  
MAPPING EPHAPTIC COUPLING  
EMPLOYING A CATHETER WITH MOSFET  
SENSOR ARRAY**

FIELD OF THE INVENTION

**[0001]** The invention relates to the a method and apparatus for navigating and recording electrical characteristics of electrophysiological signals using a MOSFET sensor guided by a magnetically-deployable mechanism.

BACKGROUND

**[0002]** Apparatus for magnetically deployable catheter with MOSFET sensor and method for mapping and ablation,” U.S. Pat. No. 7,869,854, filed on Feb. 23, 2006, published as U.S. Pat. Application No. 2007/0197891, assigned to Magnetec Corporation, which discloses a MOSFET sensor guided by a magnetically-deployable mechanism, is incorporated herein by reference. Corresponding applications include EPO Patent No. 07751190.5; Canadian Patent No. 2637622; and Hong Kong Patent No. 09104053.7.

**[0003]** Nevertheless, there is a great and still unsatisfied need for an apparatus and method for measuring biopotential activity with the use of a MOSFET sensor. This application further improves the efficacy and safety of the procedure by enabling an accurate disclosed method and apparatus which provides for high fidelity sensing of the nerve bundle electrical activity which has a direct measure to the outcome of the procedure efficacy and safety.

**[0004]** The art of electrophysiology studies employs variety of devices, specifically catheters with different electrical configurations of electrodes using magnetic as well as electrical impedance technique to form an electro-anatomical map. Because of its high success rate and low morbidity, radiofrequency (RF) catheter ablation has become a first line treatment for many arrhythmias. In this procedure, one or more electrode catheters are advanced percutaneously through the vasculature to contact cardiac tissues. Radiofrequency energy of up to 50 W for 60 seconds is delivered so as to remodel the electrical path or circuit within the heart chamber.

**[0005]** However, ablation of more complex arrhythmias, including some atrial tachycardias, many forms of intra-atrial re-entry, most ventricular tachycardias, and atrial fibrillation, continues to pose a major challenge. (Paul A Friedman Heart. 2002 June; 87(6): 575-582). This challenge stems in part from the limitations of fluoroscopy and current mapping catheter construction and sensory apparatus to locate accurately both the geometry and time domain of the wavefront activity generated by the “avalanche” of the cellular excitable matrix. The inability of the current electrode technology to account for the cellular biopotential transfer with the resolution and the ionic transfer time depicting the actual energetic event is insufficient in the measurement as well as representing the “avalanche” dynamics of this bioenergetic event. This is the main drawback of the existing and prior art relating to “electrode technology”.

**[0006]** The drawback noted above, whereby the existing art does not account for the dynamics of the ionic potential with the necessary fidelity which mimics the actual energetic event, is further supported by the use of the “conductor geometry” theory, which represents the cellular path as a cable i.e.:

“the cable theory”, or the mathematical modeling of bioelectrical current along passive neuronal fibers. Existing hardware employing electrode technology, coupled with the general algorithmic representation of the biopotential dynamics under such theory (both hardware and cable theory) suffer from the limitations which the invention disclosed below solves by the use of the MOSFET sensor array and its method of map reconstruction, as shall be annotated by the figures and their associated description.

**[0007]** In summary, the problem of reconstruction of the electrophysiological activity in the prior art is two-fold: At the one hand it is the results of the use of electrodes and its associated electrical circuit design, and on the other hand it is further handicapped by modeling the biopotential activity as a physical phenomenon whereby excitable cells are modeled by employing the “cable theory” with isotropic behavior. The use of electrodes and cable theory is a good approximation of idealized conditions of such energetic events, but suffers from the inability to associate accurately the intracardiac electrogram with a specific endocardial site which also limits the reliability with which the roving catheter tip can be placed at a site that was previously mapped. This results in limitations when the creation of long linear lesions is required to modify the substrate, and when multiple isthmuses or “channels” are present. Additionally, since in conventional endocardial mapping a single localization is made over several cardiac cycles, the influence of beat-to-beat variability on overall cardiac activation cannot be known.

**[0008]** The need to improve modeling of cellular electrical activity is central to physiology and electrophysiological studies. Biopotential recording and mapping of such electrical activity enables the physician or researcher to form and fashion his or her understanding of the fundamental data gathering and analysis of such diverse biological activities as sensory perception, communication between neurons, initiation and coordination of skeletal-muscle contraction, synchronization of the heart beat, and the secretion of hormones.

**[0009]** Most mathematical models of cellular electrical activity are based on the cable model, which can be derived from a current continuity relation on a one-dimensional ohmic cable. As such, its derivation rests on several assumptions: ionic concentrations are assumed not to change appreciably over the time of interest, and a one-dimensional picture of cell geometry is assumed to be adequate for purposes of describing cellular electrical activity. These assumptions, however, may not hold in many systems of biological significance, especially in the central nervous system and cardiac tissue, where micro-histological features may play an essential role in shaping physiological responses.

**[0010]** The invention and its embodiments, as featured by the use of an integrated MOSFET Sensor Array, solves this and other problems of local definition of reporting on essential electro-physiological parameters, without the compromise noted the prior art, some of which are described by Bin Yin et al US Pat. Pub. 2011/0137200, which describes a system and a method in which an electrophysiological signal is sensed capacitively with at least two closely spaced electrodes such that the electrodes experience strongly correlated skin-electrode distance variations.

**[0011]** Chii-Wann Lin et al in US Pat. Pub. 2010/0145179, describes a high-density micro-electrode array connected to the same conducting wire. Serial switches enable sequential electrical connection of the micro-electrode array.

**[0012]** Paul Haefner in US Pat. Pub. 2007/0293896 describes an arrhythmia discrimination device and method which involves receiving electrocardiogram signals and non-electrophysiological signals at subcutaneous locations. Both the electrocardiogram signals and non-electro physiologic signals are used to discriminate between normal sinus rhythm and an arrhythmia.

**[0013]** These methods have limited success in reaching and reporting on an electro-anatomical site and reduces the ability of the operator to provide a clinically optimal resolution to the problem of identifying accurately the source and its location and further, the prior methods and their exemplified apparatus cannot achieve such precision, and hence results in suboptimal successes of remodeling the heart electrical signal propagation, as well as neuromodulation and their intended clinical outcomes.

#### BRIEF SUMMARY OF THE INVENTION

**[0014]** The disclosure provides a method and an exemplary apparatus which enables the creation of an electro-anatomical map with fidelity and accuracy depicting a local electrogram with their native dynamics, and their geometrical as well as its time domain specificity, and further providing for reconstruction of the anatomical and etiological characteristics of the cellular matrix which the apparatus surveying. In some embodiments of the technology, a diagnostic study is performed to define the arrhythmia mechanism, and subsequently, an ablation catheter is optionally positioned adjacent to the arrhythmogenic substrate to perform a curative procedure (e.g.: ablation).

**[0015]** The sensory apparatus and method we disclose in this application captures the complexity, as well the time domain of such energetic events, synchronously. The MOSFET sensor array with its fidelity further mimics the underlying dynamics, and will improve conventional catheter based mapping techniques by localizing and identifying precisely the arrhythmogenic substrates that are removed from fluoroscopic landmarks and lack characteristic electrogram patterns.

**[0016]** The disclosed embodiments employ a MOSFET sensor array for the detection and recording of bioelectric potential, as the use of the MOSFET sensor array embedded within a decapolar catheter and/or a balloon catheter. Generally the method includes the steps of first the mapping of the site so as to diagnose and define the relevant optimal location for remodeling of electrical pathways, using methods such as RF, laser and cryo-ablation modalities, and further by applying such methods to provide for neuromodulation of nerve or ganglionic plexus.

**[0017]** The main tenets of the use of transistorized electrodes employing a MOSFET sensor array embedded in a catheter distal end, is to provide a method and an exemplary apparatus for generating an electro-anatomical map that its specificity with reference to the local tissue substrate (within the cardiac chambers) which will reveal the relationship between anatomical characteristics and the corresponding substrate map underlying the muscle tissue. Specifically, we refer to the fact that electrical activity and its vectorial trends are the results of the electrical properties of the underlying substrate, i.e. conductivity ( $\rho$  or  $S\text{-m}^{-1}$ ) and with excitable cells and/or fibrotic formations which, if mapped, will enable a physician to diagnose the underlying arrhythmogenic cause of a disease model. This hypothesis is corroborated with the use of the disclosed MOSFET sensor array, as it enables the

local mapping of the underlying substrate with its electrical and magnetic components, as shall be demonstrated by the ensuing paragraphs and their accompanying figures.

**[0018]** It is clear to those familiar with the art of electrophysiology mapping, that methods using electrode technologies of all different combinations as noted by the prior art, suffer from the inability to differentiate between signals emanating from "near" and "far fields" as the electrodes in the prior art are typically made of a metal-electrolyte interface. The interface impedance in this relation is represented as a capacitor, and in a non-polarized electrode, the impedance is represented as a resistor. But in practice both capacitive and resistive components are present in the existing art, while the disclosed method and the accompanying apparatus of this invention employ the MOSFET isolated junction, which measures the action potentials without the parasitic capacitive or resistive loads characteristic of the prior art.

**[0019]** In one embodiment of this invention, the apparatus is not dependent on the phenomenological representation of resultant summations of multiple path conduction venues or, alternatively, as a set of complex averages, but provides a true representation of the local conduction path which mirrors the underlying substrate and its fibrotic as well as its excitable path. The aim of the transistorized arrangement is to reveal the true causal relationship between electrical activity and its underlying biological substrate.

**[0020]** In one embodiment, we disclose that cellular etiology does provide us with electrophysiological indications in support of the use of the MOSFET sensor array in assessing and evaluating the signal generated by bioelectric potential as well as direct measurements of nerve and ganglionic activities.

**[0021]** The invention and its embodiments, as featured by the use of an integrated MOSFET Sensor Array, solve this and other problems of local definition of reporting on essential electro-physiological parameters, without the compromises noted in the prior art.

**[0022]** In spite of these many obstacles, the disclosed embodiments have the potential to overcome these anatomic and technical difficulties and further improve the indices of success by reducing unnecessary injury by the use of local monitoring of nerve impulse activity. In one embodiment, the bioelectric signal measurements and the construction of cell and organ electromagnetic field activity maps based on these measurements improves the bioelectric signal measurement, and has a wide range of biomedical application in modeling and diagnostic procedures. The difficulty in the prior art of measurement and mapping procedures mainly relates to the degree with which the measuring tools interfere with the measured bioelectric fields and signals, thus affecting the fidelity of the boundary conditions from which the modeling and diagnostic maps are generated.

**[0023]** In one embodiment, a minimally invasive biosensor technique advantageously applies high impedance and low capacitance semiconductor sensing technology combined with techniques of eliminating the traditional double-layer ionic transfer and conductive charge injection effects. The double-layer ionic transfer and conductive charge injection effects distort the regular electromagnetic fields and activation potentials of the measured tissue. The system can also be used to diagnose conditions of cardiac arrhythmias providing ECG signals for electrocardiographic mapping, and provide EEG signals for the localization and analysis of spontaneous

brain activities including the ability of measuring ganglionic bioelectrical activity for pre- or post-operational monitoring.

**[0024]** In one embodiment, the use of high impedance and low capacitance semiconductor sensing technology has the advantages when using the MOSFET sensor array, which is described in the present disclosure and is based on the ability of the apparatus to measure the bioelectric potentials with a substantially improved sympathetic nerve activity (SNA) ratio.

**[0025]** In one embodiment, the measurement is achieved by using isolated FETs based on an integrated MOSFET sensor technology with its differential output, coupled with its high noise immunity and low static power consumption, and provides additional advantages with the static CMOS gates which are very power efficient because they dissipate nearly zero power when idle, hence do not inject additional noise to the tissue.

**[0026]** In other embodiment, the system uses a non-invasive boundary condition sensor technique in which a plurality of measuring devices is embedded on the distal end of a catheter. The measuring devices collect simultaneous signal data sets from the surface of an area covered by the catheter adjacent, for example, to the cardiac tissue or renal artery. The usefulness of the collected data is evident by: (i) the location of the data points and the measured signals (such as, for example, biopotential, pressure and temperature), which provide direct and local values of critical parameters at particular places within the investigated region, and (ii) the data location and signal value-matrices provide the boundary conditions of the patient's tissue so as to compute and map the field and signal propagation and distribution within the volume of the investigated region. In the situation where the arterial structure (e.g. the renal artery) is being monitored, this system advantageously pinpoints the main sources and high intensity loci of spontaneous nerve activity. From the specific data (iii) the physician can monitor particular areas and symptoms, for example, using data from the plurality of the MOSFET measuring devices and (iv) a nerve impulse signal(s) map can be generated by the ensuing description associated with solution to electro-anatomical map formation.

**[0027]** The accuracy of the measurement for both the monitoring and mapping procedures depends on the Minimally-invasive qualities of the MOSFET sensor measuring device. The interface of the present innovation with the active biopotential region is capacitive. The dielectric between the device sense-plate and, for example, the renal artery plexus is an insulating material in the electrolyte of the blood.

**[0028]** In one embodiment, the electrostatic field conditions can be computed for this interface and if the inverse-problem mapping method is used, the system can employ Poisson's and Laplace's formalise, where the measured data serves as the boundary condition for all computations. In cases where brain activity is measured, the system proposed by the invention can change the baseline constants of the dielectric coefficients of the brain tissue, for example: gray matter dielectric constant is about 56  $\kappa$ ; brain's white matter is about 43  $\kappa$ , while brain's meninges are about 58  $\kappa$ . Further details of the boundary condition modeling will improve the accuracy of the predictable algorithm when using the apparatus for measuring brain activity. Further specificity of the charge density coefficient of e.g. the cerebro-spinal fluid can be estimated or continuously when measuring for these computations, similarly blood vessel are modeled and set as parameters for comparison when actual measurements are

conducted employing the MOSFET sensor array. A practitioner familiar with the art will understand the use of such sensors in measuring the myocardial biopotential activity.

**[0029]** In cases where modeling of the bioelectric activity of nerve impulse and/or excitable cellular matrix in the endocardium we employ the Poisson's Equation, which teaches that the electrostatic field in a material with dielectric and charge properties is:

$$\frac{\partial^2 V}{\partial x^2} + \frac{\partial^2 V}{\partial y^2} + \frac{\partial^2 V}{\partial z^2} = \frac{\rho_v}{\epsilon} \quad (1)$$

**[0030]** Where  $\rho_v$  is the measured volume charge density, and

i. Is the average dielectric constant

**[0031]** Known solutions of partial differential equations fitting the Poisson's Equation is performed to obtain the electrostatic field distribution along the surface area of the measurement site and/or the field map within the tissue.

**[0032]** Laplace's Equation describes for the charge-free insulation layer of the sensing array:

$$\frac{\partial^2 V}{\partial x^2} + \frac{\partial^2 V}{\partial y^2} + \frac{\partial^2 V}{\partial z^2} = 0 \quad (2)$$

**[0033]** The solution methods, using the boundary condition locations and measured signal values are similar to the Poisson's Equation. Other numerical solutions may employ a known differential equation which results in a minimum error for the boundary conditions.

**[0034]** In one embodiment, the MOSFET sensing by the electrode surface has an insulated silver (or platinum) plate to sense the facing tissue electrostatic field. The electric field intensity between this plate and the tissue is optionally calculated from the Poisson's Equation and is further simplified for the case of two parallel plates representing the capacitor formed by the insulated sensing plate, and the tissue, at distance d.

$$E_d = \frac{\rho_v \cdot d^3}{3 \cdot \epsilon} - \frac{\rho_v \cdot d^2 \cdot d_0}{2 \cdot \epsilon} + \frac{\rho_v \cdot d_0^3}{12 \cdot \epsilon} \quad [\text{V/m}] \quad d \geq d_0 \quad (3)$$

i. Where  $d_0$  is the minimum distance defined by the insulation layer.

**[0035]** In one embodiment, however, using any of these methods requires accurate boundary condition measurements which produce minimum error due to the measurement itself. The present disclosure describes measuring techniques which enable such measurements.

**[0036]** In one embodiment, a MOSFET having a matrix formed of sensors embedded therein is described which directly measures the local biopotential with its fractionated and continuous signals, analyzes such bioelectrical potentials and displays a measurement.

**[0037]** In other embodiment, a MOSFET array sensor system is fitted with an analyzing module for processing bioelectric signals so as to render a predictive value relative to the viability of the local tissue sampled by the apparatus is disclosed.

**[0038]** In an embodiment a monitoring system for displaying measured parameters such as bioelectric potential, pressure as a measure of impedance, temperature, and impedance of the tissue underlying the MOSFET sensor array is disclosed. The sensor embedded in the catheter can take the form of any of several sensing devices which directly measures a parameter indicative of cellular metabolism, tissue blood flow, or tissue oxygenation as it is reflected by its electrical equivalent values through capacitive, conductive, and or resistive processes.

**[0039]** In an embodiment, a plurality of sensors is strategically mounted in a matrix like arrangement so as to monitor various parameters, such as, for example, surface tension, blood flow, tissue metabolism, bioelectric potential, EEG, or the like.

**[0040]** In an embodiment, the signal processing unit can be a multi-channel processor combined with a matrix array sensor. The signal processor is configured to convert the signals from the sensors from an analog signal to a digital signal using an ADC, digitizer, serializer and/or a buffer.

**[0041]** In an embodiment, the signal is amplified and fed to a display unit which may be a strip chart recorder, CRT or LCD display.

**[0042]** Other objects, features and advantages of the present invention will become apparent from a reading of the following detailed description and appended claims when taken in conjunction with the accompanying drawing.

#### BRIEF DESCRIPTION OF THE DRAWINGS

**[0043]** FIG. 1 is side perspective view of a decapolar catheter fitted with a MOSFET sensor module in an array format.

**[0044]** FIG. 1A is perspective diagrammatic exploded view of a decapolar catheter configured as a 5-bipolar node with its wiring end connector.

**[0045]** FIG. 1B is a circuit schematic of the decapolar catheter with its electrodes and power circuitry.

**[0046]** FIG. 1C is a circuit block diagram of the MOSFET sensor array matrix with its associated circuitry for digital signal processing.

**[0047]** FIG. 1D are diagrams of the cellular conductance modeling of electrical activity in myocardial tissue capturing the effects of ephaptic coupling.

**[0048]** FIG. 2 is a circuit diagram of the embodiment of the MOSFET catheter with its associated circuitry.

**[0049]** FIG. 2A is a circuit diagram of the embodiment of the power supply.

**[0050]** FIG. 2B is a circuit diagram of the embodiment of EKG amplifier employed by the MOSFET sensor.

**[0051]** FIG. 2C is a circuit diagram of the MOSFET sensor in a bipolar scheme.

**[0052]** FIG. 2D is a circuit diagram of the internal equivalent circuit of the MOSFET module.

**[0053]** FIG. 3 is a system block diagram or a circuit for measuring and recording of the signals from the MOSFET sensor array.

**[0054]** FIG. 3A is a system block diagram with multiple data collection channels.

**[0055]** FIG. 4 is a circuit schematic of a simulation layout circuit describing the basic electrical characteristics of the MOSFET sensor module.

**[0056]** FIG. 5 is perspective diagram of the decapolar MOSFET catheter with an inflatable balloon and a corresponding circuit that can be employed to generate an electro-anatomical map in a body tissue.

**[0057]** FIG. 5A are diagrams of the embodiment of the MOSFET sensor elements formed over a balloon with a corresponding circuit.

**[0058]** FIG. 5B is perspective view of the embodiment of the 8x8-Polar MOSFET sensor array formed over an inflated balloon catheter.

**[0059]** FIG. 5C is perspective view of the MOSFET sensor nodes and their relative position.

**[0060]** FIG. 5D is a schematic diagram of the 8x8-Polar MOSFET array catheter with its electrodes and power circuitry.

**[0061]** FIG. 5E is a perspective diagram of the catheter employed in a heart while being used to characterize the body tissue and in the left portion of the figure a graphical representation of the detected cardio signals.

**[0062]** FIG. 5F is a perspective diagram of the MOSFET array catheter of FIG. 5 and in the left portion of the figure a graph of the electrical signal which can be obtained from the array.

**[0063]** FIG. 6 is a graph of detected brain waves using an embodiment of the invention.

**[0064]** FIGS. 6A & 6B are graphs of the electro-anatomical signals of the renal plexus using an embodiment of the invention.

**[0065]** FIG. 6C are graphs of the difference between "far field" and "near field" waveform characteristics.

**[0066]** FIG. 7 is an illustration of the right renal anatomy which depicts a catheter fitted with a MOSFET sensor array being magnetically guided therein.

**[0067]** FIG. 7A is a perspective view of the renal artery detail and catheter tip.

**[0068]** FIG. 7B is a diagram of a catheter with its MOSFET sensor array guided to the target site with a table of sensed signals and position and a graph of a time-averaged signal verses position.

**[0069]** The following summary of the invention is provided to facilitate an understanding of some of the innovative features unique to the present invention and is not intended to be a full description. A full appreciation of the various aspects of the invention can be gained by taking the entire specification, claims, drawings, and abstract as a whole. Additional objects and advantages of the current invention will become apparent to one of ordinary skill in the art upon reading the specification.

**[0070]** The accompanying figures, in which like reference numerals refer to identical or functionally-similar elements throughout the separate views and which are incorporated in and form part of the specification, further illustrate the present invention and together with the detailed description of the invention, serve to explain the principles of the present invention.

#### DETAILED DESCRIPTION OF THE PREFERRED EMBODIMENTS

**[0071]** FIG. 1 is an autographic representation of a decapolar catheter formed with the disclosed MOSFET Sensor Array 500 for measuring bioelectric potential for example, while performing electrophysiological studies within the endocardial tissue. The assembly is comprised of a series of typical electrode rings 516 shown in a decapolar configuration. This layout can be configurable in any combination suitable to those familiar with the art while employing the device while measuring bioelectric potential in a biological media or environment. Electrodes 1A 516 are coupled to a sensor module



**520** including a capacitor **C1A1 611** and resistor **R1A2 612** which form an electrical unit coupled to a MOSFET **607**. The discrete electronic components are mounted on a flexible substrate such as anisotropic conductive film (ACF), mechanically reinforced by the catheter structure **800** formed of polyurethane or silicone, etc. materials commonly used in such construction. The electrical circuit is formed with ground leads **532**, power leads **630** and its output **622** connections.

**[0072]** In one embodiment, we cite the electrophysiological studies conducted by Dipen Shah, et al (“Electrophysiological evaluation of pulmonary vein isolation”, *Europace*, 2009, 11-11), as a justification for the use of the disclosed technology in improving the shortcomings and sub-optimal results generated by existing mapping catheters as described in that article. The observations provided by this and many nth papers, points to the fact that identifying complex arrhythmogenic causes requires an electro-anatomical mapping with a resolution and accuracy not currently attainable by previous electrode technology. This application teaches that using transistorized electrode pads (e.g. using MOSFETs) with a local amplifier will substantially advance the art of electrophysiological studies, and provide for better resolution in a temporal domain of the waveform characteristics while distinguishing far-field” from “near-field” sources, resulting in improved identification of local arrhythmogenic causes. The abstract of the above article notes that “. . . Additional unnecessary ablation and possibly complications can be avoided by the recognition of non-pulmonary vein (non-PV) myocardial contributions to pulmonary vein (PV) electrograms, . . . .” And the authors explain that “. . . The posterior wall of the left atrial (LA) appendage contributes far-field electrograms to recordings from all left superior PVs (LSPV), the low lateral LA to 80% of left inferior PV (LIPV) recordings and the superior vena cava to 23% of right superior PV (RSPV) recordings. Each of these far-field components can be recognized in sinus rhythm as well as during ongoing atrial fibrillation by the disclosed apparatus and methods. Finally, the creation of temporally stable and definitive PV isolation remains a currently unsolved problem”. The study further states that “. . . “A precise understanding of the electrical activation of the PVs and of the neighboring atrial structures forms the basis of the electrophysiological evaluation of PV isolation. Rigorously verified PV isolation is a cornerstone of catheter ablation for atrial fibrillation (AF). Prompt recognition of non-PV electrogram components can prevent unnecessary radio frequency (RF) ablation and may even reduce complications such as PV stenosis and phrenic nerve palsy. The use of the disclosed MOSFET sensor array **500** solves these and other problems noted by the study.

**[0073]** FIG. 1A depicts an exploded isometric view of a decapolar catheter configured as five bipolar differential signals **580** (not shown in FIG. 1A), and ten unipolar signals **570** (not shown in FIG. 1A) formed at the sensor module **520** nodes. The entire electronic node array is mounted on the underlying polymer catheter structure **800**, the sensor electronics includes a resistor **612**, capacitor **611**, and MOSFET **607** connected to electrode rings **516** for the signal capture. The sensor module **520** is shielded with a ground plane **540**, and includes ground leads **532**, the power leads **630** and output leads **622** connected to an external molded multi-pin male connector **750**. This geometry and layout of the electrode pad **514** and its associated electrode ring **516** on a

catheter shaft is optional and can be variously configured based on application according to the teachings of this disclosure.

**[0074]** FIG. 1B is a schematic representation of a diagnostic catheter with its preferred embodiments comprising of its MOSFET sensor array **500** which acts as a transistorized electrode. The figure describes an array of electrode pads **514** connected to MOSFET common-source amplifiers **607**. A high impedance resistor **612** between the gate (G) and drain (D) terminals of the MOSFET biases the transistor in active mode. A resistor **612** and capacitor **611** between the source (S) and ground improve and stabilize small-signal gain of the circuit. Capacitors **611** between the gate (G) and the pad, and the drain and load isolate the DC signal and ensure the small-signal (AC) amplification of the sensor module **520**.

**[0075]** The figure further depicts the basic configuration of a platinum electrode pad **1A 616** connected to a capacitor **C1A1 (1 μF) 611** which provides the variable gain (G) on MOSFET **Q1A** (such as noted by the exemplary use of **2N7002) 607** with its resistor **R1A2, (1 meg) 612**.

**[0076]** The sensor module **520**, forms an element in a matrix to enable an architecture of the MOSFET sensor array **500** comprising of n-tuple arrangements of <8, 12, 16, 32, 64, 128> members) of the basic sensory inputs from a biological tissue or nerve ending firing or a summation of ganglionic plexus electrical activity.

**[0077]** The details of operation and the principles that govern the disclosed circuit are illustrated by the figures and their accompanying descriptions which demonstrate the improvements of signal fidelity of the proposed arrangements over the existing art which employs electrode technology to capture the unipolar **570** or bipolar **580** characteristics of the bioelectric potential, and where the ability of the existing electrode art to record electrical values of 1-2 microvolts of biopotential are limited by the physical inability to differentiate the integrated SNA signals of the systolic wave onslaught as well as the “far field” propagation of multiple signals originating from the various ganglionic sources. The difference in resolution provided by the proposed technology of the MOSFET sensor array **500** is the difference between a single static image generated by the current electrode technology verses an impedance spectroscopy, revealing the entire dynamic of the wavefront characteristics in the time domain.

**[0078]** In other embodiments of the use of transistorized MOSFET pads gives rise to the ability to measure local potential of a spatio-temporal event without the compromise associated with the averaging of a signal and where near field response verses far field response are registered. It should be recalled that when biopotentials in a beating heart are measured, the near field signals for any given sensor will fluctuate significantly more than the far field signals for that given sensor. Hence, the temporal fluctuation of the signals can be processed to differentiate between near and far field signals at any given sensor provided that the sensitivity is high enough so that the small near field signals are not swamped by the far field signals. According to the illustrated embodiments a sensor sensitivity of 0.1 μV or better is sufficient to allow this type of differentiation to occur without signal loss, although typical signal magnitudes are of the order of 4 μV. Further, movement of the catheter, and hence sensors, relative to the measured tissues, provides for another means of differentiating between near and far field signals even in applications here the measured tissue itself is substantially stationary. A further use of transistorized MOSFET pads is to employ the



device in recording transmembrane ionic current flow, a bioelectric event which necessitates a fast, local and dynamic registration of the “electrical avalanche” characteristic of such biological phenomenon and further to enable the recordings of current flow distribution in extracellular space.

**[0079]** In another embodiment of this application, the use of the MOSFET sensor array **500** is to solve many diagnostic dilemmas associated with existing methods for the mapping of electro-anatomical signal as well the temporal origin of bioelectrical activities, to be deciphered without the contributions of far field events which contemporaneously mask the true nature of the wave front, leading to erroneous diagnoses. The proposed transistorized electrode technology with its spatiotemporal local and precise differentiation of the origin, time, intensity, frequency and multiple other matrices, is a marked advantage of the invention.

**[0080]** FIG. 1C is a schematic outline of the MOSFET sensor array **500** residing on the distal end of the catheter shaft **800** depicting an architecture which enhances the sensor module **520** by demonstrating the ability of the circuit to capture, record, and analyze the bioelectric-potential data generated from a local site and transmitted to a signal processor **530** without the degradation associated with the prior technology.

**[0081]** The system architecture is comprised of three blocks. One of the blocks is a multi-channel integrated MOSFET sensor array **500**. The MOSFET sensor array **500** includes sensor modules **520**. Sensor modules **520** include an optional pressure transducer with its extended MOSFET gate, a biopotential detector employing a MOSFET gate, and with an optional temperature sensor. The circuit of the combined three sensors and its configuration are identified by reference designator **520**. The MOSFET sensor array **500**, is linked to a calibration element **512**. The calibration element **512** has another MOSFET gate with a fixed value at a nominal potential. The difference between the sensor module **520** and the reference element **512** provides the output. The integrated sensor array outputs are fed to the signal processor **530** of the system. The signal processor **530** includes an analog-to-digital converter (ADC) **501**, a digitizer **502**, a serializer **503**, an output driver **504**, a clock buffer **505**, a phase lock loop **506**, a clock buffer #1 and #2 **507**, **508** respectively, a reference **509**, set registers **510**, and ADC controls **511**. In summary the integrated sensor array **500** is connected to an ADC through a signal processor **530**. The advantage of such an embedded MOSFET sensor array is clear to those familiar with the art, as is described by the detail description of its intended operation and specifically its use in identifying the precise site of a biopotential activity and the sensor ability to discern “near field” from “far field” signals.

**[0082]** FIG. 1D is a schematic representation of the cellular conductance modeling of electrical activity in myocardial tissue capturing the effects of ephaptic coupling. The need to assess the prior method(s) and apparatus of electrode technology is two-fold. At the one hand is the accuracy and resolution improvements associated with the MOSFET technology, which is the aim of any theory and or scientific observation, but as such the disclosed MOSFET sensor array technology would be recognized as an improvement on the art of electrophysiological studies, we rather contend that the use of the MOSFET sensor array is important, if not necessary for uncovering the arrhythmic cause in a complex arrhythmia, where the conduction path and signal velocity represented by the prior method of electrode technology cannot

account for the secondary effect of the ephaptic coupling as well as the magneto-electrogram propagation within the cellular matrix. “Ephaptic coupling” refers to the coupling of adjacent (touching) nerve fibers caused by the exchange of ions between the cells, or it may refer to coupling of nerve fibers as a result of local electric fields. In either case, ephaptic coupling can influence the synchronization and timing of action potential firing in neurons and excitable cellular paths. The argument on the nature and effect of magneto-electrogram propagation is extensively reviewed and modeled by Shachar, et al, U.S. Pat. No. 7,869,854, where a mapping catheter is described which includes a MOSFET sensor array providing better fidelity of the signal measurements as well as data collection and reduces the error generated by spatial distribution of the isotropic and anisotropic wavefronts.

**[0083]** In one of its embodiment the above patent further describes a system for forming maps depicting the change in potential in the vicinity of an activation wavefront. In other embodiments, the mapping system tracks the spread of excitation in the heart, with properties such as propagation velocity changes. In one embodiment, an interpolation algorithm tracks the electrogram data points to produce a map relative to the electrocardiogram data. As we review the data generated by the prior method(s) and its proliferated electrode variations of catheters, be it bipolar, quadripolar, decapolar, or multi-electrode basket-type geometry, we observe that the need to provide higher-resolution and sampling rate supplementing the pre-existing electrode technology is essential as in the cases of complex arrhythmic causes mapped by the prior art electrode technology, where we are unable to accurately capture the dynamics and complexity of the wave front propagation. Our aim in proposing the disclosed MOSFET sensor in an array form(s) is to address a more fundamental problem in the art of electrophysiology-measurement, where cases with complex dynamics of bioelectrical events are present. To illustrate these facts, this application cites a paper describing the effects of ephaptic coupling with its formalism. The paper describes two observational phenomena relating to the needs to capture energetic events which the prior technology cannot fully account for, and further supporting the needs to employ the proposed MOSFET sensor technology in conducting electroanatomical studies.

**[0084]** The inability of the prior electrode technology to address the dynamics and resolution of such energetic events (forming the electrical circuit of the heart cycle), suffers from the inability of the prior art to account for ephaptic coupling and the physical influence of the magneto-electrogram propagation. The energetic event represented by the electrical circuit of the heart (the cable theory) is described by an ionic potential, as it is traveling through its conduction path of the excitable cells. The figures and the accompanying descriptions will provide an additional support for the use of the MOSFET sensor array as the preferred modality for capturing and identifying the cause(s) in a complex arrhythmic disturbance. The inherent circuit formation of the prior art, suffers from the limitation where the ground potential and its amplifier are located at distance from the biopotential activation site (origin) resulting in poor SNA effects, coupled with the signal fidelity which synchronously is compromised by the “averaging” of mixed signals, emanating from “far” and “near field” sources. These and other limitations described by the prior art, including the growing body of clinical observations cited by the medical literature, are the cause, why the prior electrode technology cannot account for the cellular

biopotential transfer or dynamics of the wave front accurately. These factors coupled with limited resolution of the prior art, are the main drawback of electrode technology in accounting for the “ionic transfer time domain” (represented by a conditions defined as “avalanche” dynamics of this bioenergetics event.

**[0085]** Using electrode technologies with its different combinations of electrodes, noted by the prior art, users suffer from the inability to differentiate between signals emanating from “near” and “far fields” since the electrodes in the prior art are typically made of metal-electrolyte interface. The interface impedance in this relation is represented as a capacitor, and in a non-polarized electrode, the impedance is represented as a resistor. But in practice both capacitive and resistive components are present in the existing art. Existing models of electrical activity in myocardial tissue are unable to easily capture the effects generally defined as “ephaptic coupling” (PNAS Dec. 7, 2010 vol. 107 no. 49 20935-20940).

**[0086]** Homogenized models do not account for cellular geometry, while detailed spatial models are too complicated to simulate in three dimensions. Here we propose a unique model and disclose apparatus that accurately captures the geometric effects of the cellular ionic dynamics of the biopotential transfer, including a data capture of such activity, and with computationally efficient methodology, which the MOSFET sensor array can solve.

**[0087]** We use this apparatus to enable modeling of such effects by capturing the changes in extracellular geometry, gap junctional coupling, and sodium ion channel distribution on propagation velocity by using a MOSFET sensor array. In support of previous studies, we teach in this application that the use of local amplifier in the form of a MOSFET sensor module, the disclosed apparatus and its algorithmic approach enable the capture of ephaptic coupling by further defining the propagation velocity at low gap junctional conductivity and report on propagation velocity.

**[0088]** This application also finds that conduction velocity is relatively insensitive to gap junctional coupling when sodium ion channels are located entirely on the cell ends and cleft space is small. The numerical efficiency of this model, verified by comparison with more detailed simulations, allows a thorough study in parameter variation and shows that cellular structure and geometry has a nontrivial impact on propagation velocity. This model can be relatively easily extended to higher dimensions while maintaining numerical efficiency and incorporating ephaptic effects through modeling of complex, irregular cellular geometry. Existing homogenized models, while computationally accessible, are not able to deal with the effects of micro-domains as the data generated by the existing electrode technology is insufficient in capturing the dynamics of such bioelectric events. The bioelectric potential is a time domain-dependent event whereby the ionic flux transfer cannot be captured by the prior technology, as it cannot distinguish between far and near field attenuations due to limited bandwidth.

**[0089]** These limitations are solved by the use of the system **600** with its MOSFET sensor array **500** which provides for the physical signal distinction between “near field” and “far field” due to the ability of the system to distinguish the emanation of biopotential from localized anatomy, and from the surrounding corporal structures. Whereas a near-field potential waveform has clear changes in amplitude, polarity, wave shape and/or latency when the position of the active electrode is changed over a small distance, conversely, in the far-field

the signal characteristics are not changed by moving the electrode position, hence the far-field signal component is a non-moving potential, further elaborated in FIG. 6C. The MOSFET sensor solves such and other limitations and hence captures the effects of ephaptic coupling “far field” and “near field” crosstalk.

**[0090]** Here we present a model that captures the effects of the intricate cellular geometry with simplifications that will allow the model to be extended more readily to three dimensions while maintaining computational efficiency. With this model we expect to be able to study the effects of changes in geometry (for example, due to hydration or dehydration, medication induced cellular impedance variation etc.) and pathology (such as ischemia) on propagation velocity.

**[0091]** The classical derivation of the equations for action potential propagation makes use of Cable Theory, in which the extracellular resistance is assumed to be isopotentially zero and the intracellular space conductivity is taken to be proportional to the cross-sectional area of the cell. We cite the research article published by Joyce Lin and James P. Keener (published in PNAS Dec. 7, 2010 vol. 107 no. 49 20935-20940), describing a revision to the existing models of electrical activity in myocardial tissue which is unable to capture the effects of ephaptic coupling. The proposal of employing a unique model that accurately captures the geometric effects is due to the fact that with the use of the MOSFET sensor array the simplification of the computational and efficient modeling of the ionic avalanche dynamics is attainable without the use of a complex three dimensional rendering. The native data generated by the MOSFET sensor module need not be manipulated from the information gap extrapolation required in generating a mapping of electro-potential dynamics, as well as isochronal representation, where a three dimensional map of electro-potential in the endocardium is shown on a bit-by-bit basis, and where localized sites of origin of premature beats are reconstructed with their activation sequence.

**[0092]** This application employs the modeling of the effects of changes in extracellular geometry, gap junctional coupling, and sodium ion channel distribution on propagation velocity in a single one-dimensional strand of cells in order to exemplify the limitations of the prior art of electrode technology. In one embodiment while studying the primary as well as secondary effects, be it magnetic wave propagation and/or the ephaptic coupling, this model, verified by comparison with more detailed simulations, shows that cellular structure and geometry has a nontrivial impact on propagation velocity.

**[0093]** In this application we follow the authors and the clinical observations in setting the formal representation and the assumptions which form such modeling. Referring to FIG. 1D the  $j$ th cell **49** occupies the space  $\Omega_j$  **48**. The extracellular space **50** the complement of intracellular space; however because this generally quite thin, we view extracellular space as the two dimensional surface of three dimensional cells, hence the extracellular space **50** is defined by  $\Omega_e = \cup_j \partial \Omega_j$ . The junctional clefts **47** are part of extracellular space. For each point  $x$  in the extracellular space there are  $\kappa(x)$  adjoining cells specified by the index set  $E(x)$ . For  $x$  on the boundary of the tissue,  $\kappa(x)=1$ , and otherwise  $\kappa(x)=2$ . Similarly, each cell has neighbors to which it is coupled by gap junctions **46**, denoted by the indices  $lj$ . The gap junctional coupling strength between cell  $j$  and its neighbors **62** by  $g_{jk}(x)$  for  $k \in lj$  and  $g_{jk}$  can be nonzero only for  $x$  such that cells  $j$  and  $k$  are adjoining (this assumption is well within the cable theory approach to cellular conduction). The membrane

capacitance **44** is denoted by  $C_m$ , extracellular conductivity by  $C_e$ , extracellular width **61** by  $W(x)$ , ionic currents by  $I_{ion}^j$ , intracellular potential **43** by  $\phi_i^j$  and extracellular **41** potential  $\phi_e$ . The right portion of the figure represents an equivalent circuit diagram of the model in the left portion of the figure with the electrical components of resistors and capacitors modeling the energetic event with an idealized geometrical and discretized electrical notation as shown in the right portion of the figure.

**[0094]** Current conservation in the extracellular space represented by the extracellular potential  $\phi_e$  **41** is

$$-\nabla \cdot (W(x)C_e \nabla \phi_e) = \sum_{j \in E(x)} \left( C_m \frac{\partial}{\partial t} (\phi_i^j - \phi_e) + I_{ion}^j (\phi_i^j - \phi_e, x) \right). \quad [1]$$

**[0095]** The current conservation in the intracellular potential **43** and **42** respectively is

$$\chi^j C_m \frac{\partial \phi_i^j}{\partial t} - C_m \frac{\partial}{\partial t} \int_{\partial \Omega^j} \phi_e dx + \int_{\partial \Omega^j} I_{ion}^j (\phi_i^j - \phi_e, x) dx = \sum_{k \in I^j} \int_{\partial \Omega^j} g_{jk}(x) (\phi_i^k - \phi_i^j) dx, \quad [2]$$

**[0096]** Where  $\chi^j = \int_{\partial \Omega^j} dx$  is the total surface area of the  $j$ th cell. Rearranging and simplifying the expression,

$$\kappa(x) C_m \frac{\partial \phi_e}{\partial t} - C_m \frac{\partial}{\partial t} \sum_{j \in E(x)} \phi_i^j = \nabla \cdot (W(x)C_e \nabla \phi_e) + \sum_{j \in E(x)} I_{ion}^j (\phi_i^j - \phi_e, x), \quad [3]$$

$$\chi^j C_m \frac{\partial \phi_i^j}{\partial t} - C_m \frac{\partial}{\partial t} \int_{\partial \Omega^j} \phi_e dx = \sum_{k \in I^j} \int_{\partial \Omega^j} g_{jk}(x) (\phi_i^k - \phi_i^j) dx - \int_{\partial \Omega^j} I_{ion}^j (\phi_i^j - \phi_e, x) dx. \quad [4]$$

**[0097]** we obtain the result that the author indicates. This model, verified by comparison with more detailed simulations, shows that cellular structure and geometry has a non-trivial impact on propagation velocity. The study further concludes that "... In agreement with previous studies, we find that ephaptic coupling increases propagation velocity at low gap junctional conductivity while it decreases propagation at higher conductivities. We also find that conduction velocity is relatively insensitive to gap junctional coupling when sodium ion channels are located entirely on the cell ends and cleft space is small". As concluded by this and other clinical as well as etiological studies, the extracellular pace and its extracellular potential  $\phi_e$  **41** with its varying conductivities and capacitive values  $C_m$  relative to its intracellular potential **43**  $\phi_i^j$ , demonstrate that cellular structure and geometry has a nontrivial impact on propagation velocity.

**[0098]** The use of the sensor module **520** solves these and other problems by enabling the investigator in his electrophysiological study to identify the spatial location of the bioelectric potential by further accounting for the ephaptic effect of the conduction path with the MOSFET sensor's

ability to mimic the potential via a variable resistor as well as a local amplifier and a ground potential set locally within the contact between the cell and the sensor surface. The use of the MOSFET sensor with its significant SNA ratio, greatly reduces noise and provides the signal fidelity necessary to emulate the ephaptic effects as noted by the above citation, that it has a nontrivial impact on propagation velocity. Complex arrhythmogenic causes cannot be accounted by the prior electrode technology due to the limitations as noted by the art.

**[0099]** FIG. 2 is a schematic representation of MOSFET output in its optional configuration as unipolar **570** (not shown in FIG. 2) and bipolar differential output of the sensor configuration **580** circuitry the figure depicts the connections to the electrode ring **516** and further indicates the wiring arrangement to the power conditioning circuitry **900**. The use of U1 2N7002DW, noted by the schematic can be substituted for optional configurations employing other MOSFET devices, such as MAX9638AVB single-supply CMOS input op amp, mfg by Maxim Integrated Products Inc. Sunnyvale, Calif.

**[0100]** FIG. 2A is a schematic representation of the power supply **950** for the system apparatus **600** in an exemplary configuration using Texas Instruments TL2575-051KTTR simple step-down switching voltage regulator to provide the necessary power conditioning circuitry for the EKG amplifier **960**. A practitioner familiar with the art can conceive of many variations for such architecture to achieve the same function.

**[0101]** FIG. 2B is a schematic representation of the EKG Amplifier **960** circuitry, in one embodiment where the amplifier is fitted with using a Texas Instruments OPA2314 CMOS operational amplifier, supply instrumentation amplifier, and precision zero drift CMOS operational amplifier. This architecture is an exemplary embodiment of the signal conditioning and amplification generated by the disclosed MOSFET sensor array **500**, and a practitioner familiar with the art can conceive of many alternatives of substituting such an apparatus.

**[0102]** FIG. 2C is a schematic representation of the bipolar MOSFET sensor module low-power amplifier **970** with two channels providing unipolar and differential bipolar output. In one embodiment of the system **600**, the disclosed MOSFET sensor array **500** is fitted with alternative architecture as an interface performing the signal conditioning and digital signal processing (DSP) functions.

**[0103]** FIG. 2D is an orthographic depiction of the internal equivalent circuit of the sensor module **520** (an element of the MOSFET sensor array **500**). In one embodiment a decapotor catheter with ten MOSFET sensors is fitted on the snapping catheter **800**.

**[0104]** The MOSFET potential sensing device is a junction field effect transistor that allows a current to flow which is proportional to an electric field, basically emulating a voltage-controlled resistor. The sensor module **520** includes a resistor. The resistor RD **577** is a linear resistor that models the ohmic resistance of the source. The charge storage is modeled by two non-linear depletion layer capacitors, CGD **583** and CGS **584**, and junction capacitors CBD **686**, ID **591**, and CBS **579**. The P-N junctions between the gate and source and gate and drain terminals are modeled by two parasitic diodes VGD **582**, and VGS **581**. Gate #1 of the MOSFET sensor tip is item **587** and gate #2 of the sensor module **520** is item **586**. Gate #1 with reference designator **587** at the electrode ring **516** is designated by (n)A (n=1, 2, 3, ... 10) is a relatively high impedance, insulated semiconductor struc-

ture. The sensor module 520 behaves as voltage-controlled resistor. The potential between the gate structure 587, 586 and the drain source structure (RS 578, RD 577) semiconductor substrate defines the transconductance of the output connections 576.

[0105] By connecting the drain-source 577, 578 structure to the electrode ring 516 the potential reference for measurement is established. This reference is configured as an electrode ring 516 along with the catheter body 800 as shown in FIG. 1A. The measurement process of sensor module 520 is set to a zero voltage as the drain-source 577, 578 structure, the sensor's gate junction 587 assumes the tissue potential with a relatively small charging current flowing into the net parallel sum of the junction capacitors, CBD 585, CGD 583, and CGS 584. The drain-source 577, 578 voltages is then applied gradually to the device charging these capacitors from the outside power source, thereby "nulling" the current needed to form the gate so as to obtain the operating potential (about 6 VDC). The sensing procedure is relatively noninvasive to the cell as well as to the potential level and current drain of the sensor module 520 upon contact with biopotential of the tissue. Gate #2, item 586 provides a biasing input so as to provide a continuous active mode for the sensor module 520. This input is also used for self-calibration of the sensor module 520.

[0106] FIG. 3 is an illustration of an embodiment of the apparatus 600 for measuring and predicting electrophysiological parameters associated with the use of the MOSFET sensor array 500. In one embodiment, the system apparatus 600 is employed in defining the proximity of the sensor array to the tissue surface and for measuring the bioelectric potential of the site. In another embodiment, the apparatus 600 is optionally fitted with pressure information relative to a correlated impedance values such as it is known in the art as "look-up tables", and as shall be evident from the theory and principle of operation of the sensor module 520. Data extracted by the catheter 800 on the surface of, for example, the artery inner lumen and/or endocardial surface further provides a measure of pressure generated while touching the arterial inner diameter of the artery by means of electrical properties such as dielectric and conductivity variation of arterial versus vein structure, similarly the apparatus 600 provides for a proximity impedance measure relative to the endocardial tissue. The principle articulated by this application provides for a measure of differentiation between blood pull impedance versus excitable cells or alternatively by measuring the nerve ending impulse in ganglionic plexus. In one embodiment, the conductivity ( $\sigma$ ) measured in S/m and dielectric of the tissue ( $\kappa$ ) at the site of measurements providing a measure of relative impedance which can be addressable by the look-up tables.

[0107] In one embodiment of the present invention the MOSFET sensor array 500 employ an integrated measure of contact as a measure of impedance value. The impedance measure derived from the MOSFET sensor array 500 produces analog voltage signals corresponding to biopotential, impedance measure, and temperature information by the MOSFET sensor array and its signal processor 630. The bioelectric potential signal output 518 is conveyed by the AC voltage at one of the outputs 517 of the measured biopotential due to pressure exerted between the sensor located at the distal end of the catheter 800, while the DC voltage of the third output 519 indicates if the catheter is in contact with the arterial structure or the catheter distal end is suspended within

the lumen of the vascular inner diameter and/or the endocardial chamber blood pull. This measure is a function of the varying impedance values relative to the electrical properties of the vessel's dielectric, conductivity  $\sigma$  and relative permeability  $\mu$ .

[0108] The basic relationship between the MOSFET sensor array 500 and the biological media while measuring impedance value is characterized by

$$Z = \sqrt{\frac{j\omega\mu}{\sigma + j\omega\epsilon}}$$

where  $\mu$  is the magnetic permeability,  $\epsilon$  is the electric permittivity and  $\sigma$  is the electrical conductivity of the biological substrate, the wave travelling through the media is measured in the angular frequency of the wave  $\omega$ . An example of such expression in free space is noted by [text missing or illegible when filed]<sup>7</sup> H/m and  $\epsilon = 8.854 \cdot 10^{-12}$  F/m. So, the value of wave impedance in free space is approx.  $Z = [\text{text missing or illegible when filed}] \Omega$ , the Z measure vary within the population, but it is clearly differentiated when measured while the sensor module 520 is in suspended state as compared with its Z value when the MOSFET sensor array 500 of the catheter 800 is touching alongside of the artery or cardiac tissue. The Z value vides the MOSFET sensor array 500 with a clear measure of determining the sensor proximity to the arterial structure or its contact. This measure is used by this invention to facilitate a consistent application of the sensory apparatus during the mapping phase of the procedure when defining the exact location of the site i.e. depicting the biopotential value, amplitude, frequency etc and by enabling an accurate account of the position measured, using such information, the operator is able to deliver the curative energy to effect the intended goal of neuro-modulation as well as remodeling of the electrical activity of an arrhythmogenic site within the cardiac chamber of the heart.

[0109] FIG. 3A is an illustration of the system 600, block diagram of the triple signal processing modules. Each channel 520 has three outputs. Output A 518 and output B 517 are the bioelectric potential and pressure signals respectively. The third output 519 is the temperature measurement signal. These outputs are analogue signals. Each of these signals is converted into 16 bit data packets of digitalized information via the ADC 501, which are serially transmitted to the microcontroller 536. The microcontroller coordinates the signal processing and display procedures. A computer console 542 with associated display 545, keyboard 543 and mouse 544 facilitates the monitoring and mapping procedures, as well as the alert system notification via the algorithm as well as parametric analysis. The signal analysis relay on the fidelity of the signal generated by the apparatus 600. Further analyses generated by the microcontroller 536. Or the host computer 542 is for example amplitude, mean frequency and or spectral density using a fast Fourier transform (FFT) method. In one embodiment of the system 600, the disclosed MOSFET sensor array 500 is fitted with alternative architecture as an interface performing the signal conditioning and digital signal processing functions. The device, RHA1016, mfg by Intan Technologies, LLC of Salt Lake City, Utah, is an integrated, low-power amplifier array containing 16 fully-differential amplifiers with programmable bandwidths suitable for use by system 600 while incorporating the signal generated by the sensor module 520 and by further providing bioinstrumentation monitoring and recording capabilities.



[0110] FIG. 4 is a schematic representation of a simulation layout circuit 610 describing the basic electrical characteristics of the sensor module 520, whereby the sensor module was excited with a 1 kHz using function generator (V1) and whereby the output was measured as shown in the embodiment and specification. The figure further describes a MOSFET common-source amplifier in SPICE simulation, R2 between the gate (G) and drain (D) terminals of the MOSFET biases the transistor in active mode. R3 and C3 between the source (S) and ground improves and stabilizes the small-signal gain of the circuit, C1 and C2 isolate the DC signal and ensures the small-signal (AC) amplification of the MOSFET circuit. The simulation indicates the ability of the circuit to vary the gain on the transistor (Q1 2N7002, N-channel enhancement mode field effect transistor) by varying the capacitance (C1) and its effect on the gain (G) of the transistor (Q1).

[0111] A practitioner familiar with the art can conceive of multiple other uses of similar MOSFET gates to perform the function as noted by this application. The elements disclosed by this application enhance the ability of the sensor module 520 to measure bioelectric potential at a site with fidelity and accuracy, including spatio-temporal representation of the local activity without the acquisition of "far field" and "near field" averages.

[0112] FIG. 5 is diagram of the 8x8 matrix electrode array 400 MOSFET fitted on a catheter with an inflatable balloon that can be employed to generate an electro-anatomical map in a cardiac tissue. The mapping catheter is comprised of an open lumen catheter shaft 800 with a collapsible, basket shaped distal end 850 fitted with electrode pads 514 connected to MOSFET sensor module 580. Currently basket catheters include eight equidistant metallic arms, providing a total of 64 unipolar or 32 bipolar electrodes capable of simultaneously recording electrograms from a cardiac chamber. The catheters are constructed of a superelastic material to allow passive deployment of the array catheter and optimize endocardial contact. The size of the basket catheter used depends on the dimensions of the chamber to be mapped, requiring antecedent evaluation (usually by echocardiogram) to ensure proper size selection. The collapsed catheters are introduced percutaneously into the appropriate chamber where they are expanded.

[0113] FIG. 5A illustrates an octopolar MOSFET spline array 410 with the electrode pads 514 as part of a bipolar MOSFET Sensor configuration 580, situated on the surface of a balloon catheter structure 850 in an 8x8 matrix electrode array 400 comprising of 64 MOSFET sensor nodes. The dimensional scale 415 of the array is utilized as a demonstration of the embodiment, but many optional spacing and array configurations can be formed based on the application and use.

[0114] FIG. 5B is a diagram of an inflated balloon 850 on the catheter structure 800 fitted with a typical 8x8 matrix electrode array 400 formed of eight separate octopolar MOSFET spline arrays 410 in an octopolar arrangement of four individual bipolar MOSFET Sensor configurations 580 include the MOSFET 607 with its capacitors 611 and resistors 612, connected locally to their electrode pads 514 and externally by an output 622 and ground leads 532.

[0115] FIG. 5C is an autographic representation detailing a catheter structure 800 with balloon 850 formed with an 8x8 matrix electrode array 400 with the discrete indexing of electrode pads M1A, M2A, etc. 514 correlated to the sensor array

orientation 420 extrapolated from the sensor output. The indexing of the array is logically connected to the auxiliary DSP and power units so as to enable measurement relative to orientation of the catheter spline proximal to the tissue surface as defined by the vector orientation 420.

[0116] FIG. 50 shows a schematic of an 8x8 matrix electrode array 400 for balloon catheter 850 such as described in FIG. 5 above, with a detail of a typical octopolar MOSFET spline marked as A 410 which is repeated on splines B-H, symmetrically distributed around the balloon surface and running lengthwise from the base of the balloon to the distal tip. The MOSFET spline array 410 is in further detail described by a sensor module 520 with its associated paired electrode pads M1A 514 and connecting capacitors 611, resistors 612 and MOSFET Q1A 607, governed by the external power conditioning circuitry 900.

[0117] FIG. 5E is a depiction of an atrial mapping procedure by balloon catheter fitted with an 8x8 matrix electrode array 400 inside the chamber volume of the heart 1, and the resulting output signal passed through a digital signal processor (DSP) 530 to a display 545 permitting real-time monitoring of the EKG waveform output 450.

[0118] The mapping system includes an signal processor 530 connected to a computer, which is capable of simultaneously processing: (1) 32 bipolar electrograms from the basket catheter; (2) 16 bipolar/unipolar electrograms signals; (3) a 12 lead ECG; and (4) a pressure signal. Color coded activation maps are reconstructed on-line. The electrograms and activation maps are displayed on a computer monitor 545 and the acquired signals can be stored on optical disk for off-line analysis. Activation marks are generated automatically with either a peak or slope (dV/dt) algorithm, and the activation times are then edited manually as needed.

[0119] The multi-electrode endocardial mapping system 600 shown in FIG. 3A allows simultaneous recording of electrical activation from multiple sites, and fast reconstruction of endocardial activation maps. This may limit the time endured in tachycardia compared to single point mapping techniques, without the insertion of multiple electrodes and facilitate endocardial mapping of hemodynamically unstable tachycardias.

[0120] With this system 600, a mapping catheter with tip and matrix electrode array 400 to record unipolar and bipolar signals is advanced percutaneously to the chamber of interest. The mapping procedure involves positioning the mapping catheter at sequential points along the endocardium. Catheter tip location and electrograms are simultaneously acquiring while the catheter remains in stable contact with endocardium. Local activation times are calculated relative to the body surface ECG or a fixed (reference) intracardiac electrode. The balloon catheter 850 fitted with disclosed MOSFET sensor array can be interfaced with existing mapping and processing apparatus, such as EnSite of St. Jude Medical, Minneapolis, Minn. and/or Carto Mfg by J&J BioSense Webster. A description of such data capture analysis and display are known to those familiar with the art of electrophysiology. Such a system continuously monitors the quality of catheter-tissue contact and local activation time stability to ensure validity and reproducibility of each local measurement. The acquired information is then color-coded and displayed. As each new site is acquired, the reconstruction is updated in real time to progressively create three-dimensional chamber geometry color-encoded with activation time. In addition to activation time maps, dynamic propagation maps displayed



as movies of sequential activation on the computer workstation can be created. Additionally, the collected data can be displayed as voltage maps depicting the magnitude of the local peak voltage in a three dimensional model. These can be useful to define areas of scarring and electrically diseased tissue.

[0121] Mapping's high density parallel data acquisition yields high resolution maps of the entire cardiac chamber from a single beat of tachycardia, enabling registration of transient or hypotensive arrhythmias. Other useful features include radiation-free catheter navigation, re-visitation of points of interest, and cataloging ablation points on the three dimensional model. Mapping with high density parallel data acquisition employing the disclosed matrix electrode array 400 yields high resolution maps of the entire cardiac chamber from a single beat of tachycardia, enabling registration of transient or hypotensive arrhythmias.

[0122] The figure further illustrates additional detail of the example MOSFET 607. In this particular example, the electrodes are disposed on multiple splines, four of which are visible, and the splines are shown at an example treatment site inside a body cavity (e.g., the atrium shown in a partial cut-away view inside a patient's heart).

[0123] The distal inflatable balloon portion 850 includes a number of MOSFET sensors 607 on its expandable surface that can be employed to electrically characterize tissue that is in contact with the electrode pads 514 at the treatment site. In particular, for example, the electrodes can be configured to support a detailed intracardiac electrophysiology study. Other types of electrodes or sensors can also be included on or near the surface of the balloon, such as, for example, thermal or pressure sensors.

[0124] The signal processor 530 electrically characterizes body tissue that is in contact with the sensor module 520. In particular, the signal processor 530 generates visual displays, such as isochronal or isopotential maps of the tissue, enabling a physician to identify aberrant electrical pathways at locations in the body tissue that are candidates for ablation. The visual display 545 provides the necessary graphical representations of the EKG waveform output 450 for analysis. In some implementations, the preferred embodiment may include a pressure sensor inside the balloon 850. In another embodiment, the balloon catheter 850 can carry a temperature sensor inside the balloon structure. Many variations on the theme of additional sensory output are conceivable for a practitioner familiar with the art, and can incorporate such diverse sensory output as temperature, pressure, pH, flow rate, capacitive and resistive measurements, to form additional data channels in support of the clinical needs associated with the formation of an electroanatomical map.

[0125] FIG. 5F includes a chart illustrating the spatial-temporal corroboration between EKG waveform output 450 from sequentially-ordered pairs of electrode pads 514 along the length of the octopolar MOSFET spline arrays A, B, C, . . . H 410 with their placement around the circumference of a balloon catheter 850, generating the EKG waveform output 450 (noted by the chart) used to create the bioelectrical potential and activation map. The balloon catheter 850 with its matrix electrode array 400 is shown adjacent to an orthographic cross-section of the cardiac tissue 2. The chart depicts the electrode pads 514 to detect an electrical signal designated "I" that propagates in this example parallel to the length of the pulmonary vein (and along the longitudinal axis of the splines). The chart illustrates an electrical signal is initially

detected by MOSFET sensors M1 and M2 on splines A, B and C at nearly the same time. The time domain is represented by the x-axis represented by arrow 420, the signal is detected subsequently at MOSFET sensor pair M2-M3, then pair M3-M4, then at pair M4-M5, then at pair M5-M6. Information about electrical signals, such as here shown, can be displayed in the user interface 545. In some implementations, the electrical characterization information includes static screen captures of biopotential information at different points in a particular region of body tissue. Points corresponding to electrode pads 514 on the inflatable balloon 850 provide information which includes customary description available from such systems known commercially as St. Jude Medical ENSITE or CARTO by J&J BioSense Webster, enabling a catheter to locate a target within anatomical context and by providing geometrical coordinates of specific anatomical destination. In addition, animations illustrating time-varying biopotential information includes color-coded isochronal or isopotential data; the graphic display can incorporate other information previously or contemporaneously obtained with other equipment. The figure further illustrates electrical signal designated by "II" that propagates along the circumference of the pulmonary vein and in a direction transverse to the splines, relative to the X axis 420. In this example, the electrical signal II is first detected by MOSFET sensor pair M3-M4 on spline A, then on electrode pair M3-M4 on spline B, then on electrode pair M3-M4 on spline C. Another example, designated by reference "III" indicates the EKG waveform output 450 propagating both circumferentially and longitudinally along the cardiac tissue 2. The electrical signal is first detected primarily by MOSFET sensor pair M2-M3 of spline A and secondarily by MOSFET sensor pair M2-M3 of spline B. Next, it is detected by the MOSFET sensor pair M3-M4 of spline B, followed by MOSFET sensor pair M4-M5 of spline B. Finally, the signal is detected by MOSFET sensor pair M4-M5 of spline C.

[0126] A final example, reference designator "IV", is provided in which no substantial electrical activity is detected at any MOSFET sensor pairs on any of the splines depicted. This example may correspond to a pulmonary vein that has been ablated to eliminate aberrant electrical signal sources or pathways that may be giving rise to or contributing to an adverse condition, such as atrial fibrillation.

[0127] FIG. 6 is a graphical representation which depicts various brain waves typical of rhythms, powers or amplitude corresponding to occurrences which the presently described method is capable of identifying and isolating due to the ability of the sensor module 520 performance to sense a small biopotential value within the anatomical detail of brain electrical activity and by extension, to the SNA within the arterial structure of the renal artery or any ganglionic plexus. The MOSFET sensor array 500 described by this application is capable of collecting, sampling and measuring the power and amplitude of the signal generated, for example, by the renal artery plexus while dynamically traveling through the vascular tree. An example of such biopotential measurements are noted when comparing normal brain wave activities versus abnormal behavior associated with increased pressure or due to pathological inducement; Panel (a) 311 corresponds to normal (under no specific conditions) electroencephalogram brain wave readings. The leftmost signal corresponds to typical beta band waves when the person has his eyes closed. The center wave corresponds to the change in rhythm when the eyes are open, and so forth. Panel b, 312 suggests a similar

wave pattern of a person under a different task, stereotypically of 'default mode' activity that could arise in the temporal or frontal lobes under EEG readings. Panel c, **313** corresponds to the same subject as panel b, **312** while the person is having an epileptic seizure. The rhythms become more pronounced, with rapid ripples and increased synchronicity on the envelope of the prior wave bands. In an embodiment of the presently described system employing the MOSFET sensor array **500**, the system enables the physician to discern and identify these changes in power. Panel d, **314** is suggestive of an unconscious person's EEG reading. The decreased power, yet stable rhythm, is suggestive of a loss of consciousness. Panel e, **315** indicates the EEG reading of a lesion brain region, suggestive of the immediate effect of permanent pressure on the arterial structure or tissue, reflected by the MOSFET sensor array reading and is identified by the system **600**. Panel f, **316** graphically represents the effect of over-pressure such as indicated by Mean Arterial Pressure minus the catheter surface with its MOSFET sensor array **500** pressure producing a state whereby the differential pressure is less than 70 mm Hg (<70 mm Hg) so as to further generate a typical wave reading as indicated. The use of the MOSFET sensor array in neuro surgical procedure, either for measuring synaptic firing, as well as brain or ganglionic electrical activity, is supported by the fact that any mechanical change exerted over the nerve ending will evoke a waveform characteristic that the MOSFET sensor array is capable of detecting, a further proof to the quality of measurement associated with the use of local measurement by a MOSFET sensor as we teach in this application. A patient undergoing pressure of 550 mm of water shows increased wave amplitudes in the MOSFET sensor array **500** reading, as well as short ripples suggestive of bursts of evoked potential in the area of where the catheter is exerting its pressure. Qualitative indications of the relationship between the etiological and mechanical state of the cellular structure under pressure and its electrical nerve activity are indicated by the use of the proposed disclosed technology. All of these cases are identified and isolated by the presently described system which further indicate the usefulness of employing a sensor with local amplifier and ground potential as exhibited by the use of MOSFET technology.

**[0128]** Employing the MOSFET sensor array **500** is contemplated when measuring sympathetic nervous system activity (SNA). The system **600** provides the physician (optionally using AI routines) with details of the electrical activity with a higher resolution on an order of magnitude beyond the prior electrode technology, as the MOSFET sensor module, exemplified by the apparatus described in this application, detects signal with a 0.1  $\mu\text{V}$  sensitivity or less and with a 40-microsecond or higher sampling update rate (25 kHz). Such use of the sensor module **520** at the nerve ending of any ganglionic plexus provides signal fidelity and dynamic capture of the waveform or nerve impulse unmatched by the current electrode technology.

**[0129]** FIG. 6A is a graphical representation of a signal generated by a study using animals, which demonstrates the complexity of collecting bioelectrical potential signal data from ganglionic and nerve endings associated with the sympathetic nervous system (SNA). The ensuing figures, cited from Guild et al, in the study "Quantifying sympathetic nerve activity: problems, pitfalls, and the need for standardization," published in *Experimental Physiology* (95.1, pp. 41-50), details "the common ways of describing SNA . . . [Assessments of] the quality of SNA are made, including the use of

arterial pressure wave-triggered averages and nasopharyngeal stimuli. Calculation of the zero level of the SNA signal from recordings during ganglionic blockade, the average level between bursts and the minimum of arterial pressure wave-triggered averages are compared and shown to be equivalent." The paper further recommends that the scale of measurement of neural and ganglionic activity in various plexuses must be set at the scale of microvolts and, as shown by the figures presented, the renal artery and the baroreceptor measurements represent a difference of  $\pm 10 \mu\text{V}$  with a resolution of  $\geq 1.45 \mu\text{V}$ .

**[0130]** FIG. 6B is a graphic representation further elaborating on the observation that a recording of a short (2-second) example of renal SNA reveals that the integrated SNA **361**, comprised of the original SNA **362**, whereby the integrated SNA (shown as the black graph in the bottommost graph above) overlays the rectified original SNA signal indicated as the grey graph in the bottommost graph **367**. As clearly exemplified by the figure, the use of electrode technology to identify the SNA signal and differentiate it from the ECG, electrogram, and multiple electrical noises generated by various biological centers of body control, we must find the common mode rejection to enable the collection of high-fidelity ganglionic signal.

**[0131]** In another embodiment of the invention, it is clearly identified that an electrode pad **514** lying on the surface of a biological tissue is better suited to depict signal on the order of 1-5  $\mu\text{V}$  without the distortion associated with the systolic wave emanating from the left ventricle during the cardiac cycle. The illustrated embodiment presented herein provides for local versus far-field signal, ground potential on-site (within the electrode pad **514**), and fast-acting variable resistors based on MOSFET technology.

**[0132]** FIG. 6C is a graphic representation of the difference between "far field" and "near field" waveform characteristics. "Near field" and "far field" are distinguished as regions of bioelectrical emanation from localized anatomy, and from the surrounding corporal structures. Whereas a near-field potential waveform has clear changes in amplitude, polarity, wave shape and/or latency when the position of the active electrode is changed over a small distance, conversely, in the far-field the signal characteristics are not changed by moving the electrode position, hence the far-field signal component is a non-moving potential. In the seminal study by Cracco R Q et al, titled, "Somatosensory Evoked in Man: Far-field Potentials" *Electroenceph Clin Neurophysiol* 1976; 41:460-46, this phenomenon is represented in graph II as the non-vanishing portion of the decaying signal. The obvious background of such lack of waveform changes is the location of the electrode at a large distance from the bioelectrical source.

**[0133]** A fundamental aspect of clinical electrophysiology, the discipline of diagnosing and treating cardiac arrhythmias, is the interpretation of intracardiac electrical signals (electrograms), typically referred to as EGM's. All EGM's represent a voltage difference between two electrodes, whether the electrodes are in close proximity, i.e., bipolar EGM's, or at a relatively great distance (theoretically an infinite distance), i.e., unipolar EGM's. EGM's have traditionally been obtained as differential recordings formed between an anodal input to a distant amplifier versus a cathodal input to the amplifier. The EGM is thought to record local wavefronts of depolarization and repolarization, and typically assumes the viability of 1 to 2  $\text{cm}^3$  of myocardium under the recording electrode.

**[0134]** The unipolar EGM has an important role in the diagnosis of the origin of electrical impulses within the heart. By convention, the contact (“exploring”) electrode is connected to the anodal input of the recording amplifier, hence in a uniformly conducting sheet of myocardium the approaching wavefront generates an upward deflection, which then becomes negative as the wavefront flows away from the recording electrode. An initial downward deflection is conventionally called a Q wave, whereas the upward signal is called an R wave, and the secondary negative signal (after the initial R) is labeled an S wave. For mapping purposes in the basic and clinical laboratories the maximum negative slope ( $-dV/dt$ ) of the unipolar R/S signal coincides with the arrival of the wavefront directly under the recording electrode. When complex maps are generated by recording from many simultaneous unipolar and bipolar EGM’s, this maximal negative slope of the R/S signal is calculated at each recording site and a propagation scheme is generated based on the spatial temporal differences between the different sampling sites. Possibly the single most important use of unipolar EGM’s in the clinical laboratory is thought to be the use of specific morphologies of the recorded EGM. The morphology of the unipolar EGM is thought to indicate the direction of a wavefront propagation, such that when the exploring (anodal) electrode is at the site of initial wavefront activation, such as a focal tachycardia or an accessory pathway, a QS (all negative) signal is generated, as the depolarizing wavefront spreads away from this electrode. Theoretically, application of RF energy at a site manifesting a unipolar QS signal should prove to be successful ablation when the target arrhythmia is thought to be “focal” in nature. The reasons why this is not always the case are listed below.

**[0135]** Filtering of unipolar EGM’s is typically performed using a corner frequency for the high pass filter of between 0.05 to 0.5 Hz. The high pass filter is needed to attenuate lower frequency baseline drifts caused by respiration, catheter movement and variable catheter-tissue contact. Higher corner frequencies for high pass filtering of unipolar EGM’s are occasionally used when mapping ventricular scars, but it should be noted that filtering changes the morphology of the signal and renders it not useful as an indication of the direction of wavefront propagation, i.e. a QS signal generated by a filtered unipolar EGM cannot be used to infer a site of earliest activation.

**[0136]** A major disadvantage of unipolar recordings is that they contain significant amount of “far-field” signal, i.e., signals generated by depolarization of tissue remote from the recording electrode. As noted above, in normal, homogeneous tissue, the maximal negative slope is indicative of local depolarization occurring underneath the exploring electrode. In fibrotic or scarred tissue, small amounts of healthy tissue beneath the electrode may generate relatively smaller potentials than the surrounding myocardium, hence a large far-field signal can dwarf or obscure a small local potential. In addition, the size of an area generating a diagnostic QS at times exceed a centimeter and thus may be much larger than an arrhythmia producing focus. Thus, a unipolar QS signal is necessary, but not sufficient, in guiding a successful ablation of a “local” tachycardia. It should also be remembered that a unipolar QS complex can be recorded when the exploring electrode is not in contact with the tissue, but, rather, may be floating some distance away within the cavity. Clinicians counter this problem when they recognize that the initial negative slope of the recorded QS signal is typically relatively

slow when tissue contact is lacking, suggesting that the EGM is a far-field signal. This observation is quite subjective and often overlooked.

**[0137]** Bipolar EGM’s are obtained by summing the potentials recorded from two adjacent electrodes which overlay the area of interest in the heart. The potential at the negative input is inverted, and thus subtracted from the positive input. In a homogeneous sheet of myocardium, the arrival of a depolarization wavefront coincides with the initial peak of the bipolar EGM. It is thought that bipolar EGM’s are less prone to far-field distortion, hence they are primarily used to locate a point of earliest activation relative to a stable reference recording during a tachycardia or abnormal impulse formation. The signals are typically filtered using a high pass filter of 30 Hz and a low pass filter of 250 Hz. The 30 Hz corner frequency in this setting is thought to minimize far-field distortion and to preserve accuracy and timing of local activation.

**[0138]** Despite the theoretic considerations mentioned above, far-field signals are frequently recorded using relatively close bipolar recordings, i.e., 2.5 mm interelectrode distances. For example, EGM’s from pulmonary vein ostia frequently manifest large “far field” atrial signals recorded from regions that are at the border between the atrium and pulmonary vein. Separating the signal of interest, i.e. pulmonary vein fiber potential (high frequency signal) from the “far-field” atrial signal (lower frequency, usually much larger signal) can sometimes be difficult, and requires pacing maneuvers and empiric RF energy application. In addition, differences in electrode sizes, for example large ablation distal electrode vs a smaller proximal electrode, might exaggerate the potential differences between the two electrodes and distort the resultant EGM signal amplitude, which is important for recording scar voltage. In addition, the direction of wavefront propagation influences the amplitude of the bipolar EGM (but not that of the unipolar EGM). Theoretically, a wavefront that propagates in a direction that is exactly perpendicular to the axis of the recording dipole would produce no potential difference, hence no EGM signal. The clinical significance of this scenario in mapping scarred tissue is unknown, as these maps are dependent on displaying areas of “low voltage” as areas of scarred myocardium.

**[0139]** Existing intracardiac recording techniques, while they have served the clinician and basic scientist reasonably well over the past three to four decades, suffer from several inherent limitations, which this patent application seeks to address:

**[0140]** By their very nature, i.e., electrodes connected by long cables to a distant differential amplifier, these systems are subject to line “noise”, ambient EMI, cable motion artifact, faulty connections.

**[0141]** Local signals, as described above, are subject to recording of “far field” signals, which at times render the interpretation of complex, rapid arrhythmias very difficult, if not impossible.

**[0142]** The conflation of “far field” and signals of real interest, such as pulmonary vein fiber potentials, accessory pathway signals, “slow pathway” potentials, can sometimes be the cause of failed ablations. The ability to record local electric activity with great precision and to the exclusion of “far field” signals would be of paramount importance.

**[0143]** Current recording systems frequently cannot differentiate low amplitude, high frequency signals from background noise. Extremely low amplitude signals, such as sig-

nals generated during slow conduction within a myocardial scar, are frequently missed or lost in the background noise when amplifier gain is made sufficiently high to attempt to record such signals.

**[0144]** Continuous, low amplitude, “fractionated” high frequency signals such as those frequently seen in the atria of patients with chronic atrial fibrillation, cannot be further characterized using existing recording technologies. These signals may contain important biologic and electrophysiologic information. For example, these signals may represent important areas of scarring that are responsible for formation of “rotors.” Alternatively, they may be manifesting discharges from contiguous epicardial parasympathetic ganglionated plexi.

**[0145]** Graph I represents a near-field waveform characteristic, where the horizontal axis **210** denotes distance, and the vertical axis **211**, the voltage. It is clear that the potential decreases monotonously with distance along the horizontal axis, therefore, the profile shown in graph II indicates the presence of additional far field source component **212** for the potential, as it is constant and non-vanishing, i.e.: representing the difference in potential between “far-field” and “near-field”. This difference between the waveform relative to the horizontal axis **210**, does not decrease over time, and can be subtracted by using the fast-acting local bipolar measurement available through the use of the disclosed MOSFET sensor array **500**.

**[0146]** Graph III of FIG. 6C further indicates the fact that when unipolar measurements are made along the fiber directions of a muscle, the signal can be isolated from the surface EMG whereby the waveforms are composed of two main components, the propagating negative part (upward) in two directions, and the positive, non-propagating components, indicated by the arrow **213**, which represent that the non-moving “far field” property is in the upper 9 traces, and “near field” characteristics in the lower 6 traces. This graph III represents the distinction between moving and non-moving components distribution of the far-field vs. the near-field.

**[0147]** FIGS. 7 and 7A are illustrations of the right kidney depicting anatomical details of the renal artery with its plexus, and a detail of a perspective view representing a renal artery signal map **203** containing both low level signal areas **201** and high level signal areas **202** as well as a visualization of the catheter **800**. The cutaway of the renal artery further indicates the presence of a catheter **800** fitted with a MOSFET sensor array **500**. The use of the disclosed apparatus **600** is demonstrated so as to enable an improved clinical procedure associated with the detection of the SNA emanating from the nerve ending. The common procedure for neuromodulation of the SNA on the renal artery plexus is a standard care currently employing the electrode technology to detect the location of the nerve ending within the adventitia structure.

**[0148]** In the ensuing paragraphs we highlight the fact that cellular etiology does provide us with electrophysiological indications, we further instruct in this application that the use of the apparatus proposed solves these and other problems associated with surgical ablation, and by the consistent application of the methods and embodiments of this invention a robust predictive outcome is enabled so as to dramatically reduce the incidence of morbidity associated with the use of mechanically translating and rotating catheter in the renal artery. While using a catheter to perform a neuromodulation by applying energy to block or redirect peripheral nerve impulse.

**[0149]** The figure further illustrates the incorporation of apparatus for facilitating remote magnetically guided delivery of a MOSFET mapping and ablation catheter **800** to innervated tissue and ganglia that contribute to renal sympathetic nerve activity in accordance with embodiments of the invention.

**[0150]** The standard method for neuromodulation associated with the curative approach to hypertension is to employ a mapping and ablation catheter to denervate the renal artery ganglionic plexus within the inner surface of the artery, proximal to the right or left kidney. In the standard care employed an RF ablation catheter is used cooperatively with an imaging system such as known in the art for example as St. Jude Medical ENSITE or magnetic localization system such as CARTO made by J&J BioSense Webster. This procedure of renal denervation, where a surgical intervention deactivates the ability of the sympathetic nerve or its ganglia to influence the activity of the sympathetic autonomic nervous system to further achieve a clinical outcome of reduction of hypertension is the mainstay of the existing art.

**[0151]** The disclosed MOSFET sensor array **500** will improve the clinical outcome by enabling the apparatus **600** with its catheter **800** to identify the position of high bioelectrical potential, by enabling the sensor module **520** to depict SNA emanating signal (from the renal ganglionic plexus) on the order of 1-5  $\mu\text{V}$ , further providing a specific impedance value which indicates contact with the tissue. In one embodiment, the MOSFET sensor array is capable of at once reassuring a signal on the order of 0.1  $\mu\text{V}$ , while contemporaneously measuring and indicating the proximity of the catheter **800** to the tissue, which is an additional improvement of the current invention.

**[0152]** The process described is governed by the use of the apparatus ability to first provide an indication of position and orientation of the catheter **800** with constant impedance value indicating surface contact with the vessel lumen so as to be able to deliver the necessary RF energy through the adventitia and where the ablating energy is transmitted to the renal nerve and the ganglionic plexus in an optimal and safe mode.

**[0153]** In accordance with various embodiments described herein, one or more physiologic parameters can be monitored during the ablation procedure to determine the effect of the ablation on the patient’s renal sympathetic nerve activity. For example, a matrix of MOSFET sensors is situated in contact with the inner or outer wall of the renal artery **325** near opposing sides of the renal artery.

**[0154]** In the ensuing paragraphs we highlight the fact that cellular etiology do provide us with electrophysiological indications, we further instruct in this application that the use of the apparatus proposed solve these and other problems associated with surgical ablation, and by the consistent application of the methods and embodiments of this invention a robust predictive outcome is enabled so as to significantly reduce the incidence of morbidity associated with the inability of the current electrode technology to detect nerve ending impulse in the orders of 0.1-10  $\mu\text{V}$ . The use of the disclosed mapping technology will improve neuromodulation as an additional optional use of the proposed technology we teach in this application.

**[0155]** FIG. 7B illustrates catheter **800** with its MOSFET sensor array **500** is guided to the target site, the catheter is first performing the electro anatomical mapping procedure where the arterial structure is identified and the bioelectric potentials **205** are recorded. The data set **204** is emulated so as to form



a graphic representation of the anatomy with its associated dimensional coordinates, the bioelectrical potential values measured by the sensor modules **520** are then correlated, so as to form a data set comprising of an data set **204** (X, Y, Z,  $\langle \text{IMP}\Omega \rangle T^{\circ}$ ), and where the X, Y, Z are the coordinates of sensor module **520** from the MOSFET sensor array **500**, and the value  $\langle \text{IMP}\Omega \rangle$  is the impedance of the site and where  $T^{\circ}$  is the temperature registered at the site. The operator or physician uses the map generated by the MOSFET sensor array **500** and its graphical display **206** so as to enable the operator to optimally proceed with the therapeutic phase of the neuromodulation.

**[0156]** The figure further describes graphically the renal sympathetic efferent and afferent nerves, which schematically represented adjacent to the wall of the renal artery **325**, described previously in FIG. 7. The importance of proper mapping of the axonal terminus of the nerve lying in and within the renal nerves in patients with hypertension can now be defined with the disclosed development of percutaneous minimally invasive mapping apparatus **600**, coupling such precise identification by the MOSFET sensor array **500** with the use of an RF energy generator, the operator can improve the procedure of neuromodulation (renal denervation). The use of the disclosed MOSFET sensor array **500**, enables the formation of an accurate spatio-temporal definition of the electro-anatomical characteristics of the renal artery nerve endings. The embodiments of the disclosed apparatus **600** are directly related to the nature of the sensor module **520** due to its ability to collect electrical data in the order of 0.1 microvolts.

**[0157]** The words used in this specification to describe the invention and its various embodiments are to be understood not only in the sense of their commonly defined meanings, but to include by special definition in this specification structure, material or acts beyond the scope of the commonly defined meanings. Thus if an element can be understood in the context of this specification as including more than one meaning, then its use in a claim must be understood as being generic to all possible meanings supported by the specification and by the word itself.

**[0158]** The definitions of the words or elements of the following claims are, therefore, defined in this specification to include not only the combination of elements which are literally set forth, but all equivalent structure, material or acts for performing substantially the same function in substantially the same way to obtain substantially the same result. In this sense it is therefore contemplated that an equivalent substitution of two or more elements may be made for any one of the elements in the claims below or that a single element may be substituted for two or more elements in a claim. Although elements may be described above as acting in certain combinations and even initially claimed as such, it is to be expressly understood that one or more elements from a claimed combination can in some cases be excised from the combination and that the claimed combination may be directed to a subcombination or variation of a subcombination.

We claim:

1. A method for making a temporal and spatial electro-anatomical map of bioelectrically active tissue with fidelity and accuracy depicting a local electrogram with native dynamics while simultaneously including geometric and time domain specificity comprising:

providing a catheter with a MOSFET sensor array for the detection and recording of bioelectric potential;

detecting a plurality of bioelectric potentials in the bioelectrically active tissue using the MOSFET sensor array at a plurality of selectively chosen sites in the bioelectrically active tissue at a selected time;

differentiating between signals emanating from "near" and "far fields" in the detected plurality of bioelectric potentials;

storing the detected plurality of bioelectric potentials and locations of the corresponding selectively chosen sites;

constructing the electro-anatomical map of bioelectrically active tissue from the stored plurality of bioelectric potentials and locations of the corresponding selectively chosen sites for the selected time; and

repeating the steps of detecting, differentiating, storing and constructing at a plurality of additional selected times to provide a temporal electro-anatomical map with spatial resolution.

2. The method of claim **1** where providing a catheter with a MOSFET sensor array comprises providing the MOSFET sensor array configured on a multipolar catheter and/or a balloon catheter.

3. The method of claim **1** where differentiating between signals emanating from "near" and "far fields" in the detected plurality of bioelectric potentials further comprises detecting the plurality of bioelectric potentials using at each sensor of the array a MOSFET isolated junction to measure action potentials without the parasitic capacitive or resistive loads.

4. The method of claim **1** where differentiating between signals emanating from "near" and "far fields" in the detected plurality of bioelectric potentials further comprises detecting the plurality of bioelectric potentials using at each sensor of the array a MOSFET isolated junction to apply a high impedance and low capacitance semiconductor sensor and to eliminate double-layer ionic transfer and conductive charge injection effects.

5. The method of claim **1** where differentiating between signals emanating from "near" and "far fields" in the detected plurality of bioelectric potentials further comprises detecting the plurality of bioelectric potentials using at each sensor of the array an integrated MOSFET isolated junction with a differential output with high noise immunity and low static power consumption with static CMOS gates to dissipate nearly zero power when idle and to avoid injection of noise to the bioelectrically active tissue.

6. The method of claim **1** further comprising detecting and storing nonelectrical biosignals simultaneously with the bioelectric potentials, constructing a boundary condition map of the tissue from the stored plurality of bioelectric potentials, nonelectrical biosignals and locations of the corresponding selectively chosen sites, and generating a comparative boundary condition and electro-anatomical map to allow for physician diagnosis.

7. The method of claim **6** where detecting nonelectrical biosignals and detecting bioelectric potentials is capacitive with a specific dielectric interface between each sensor of the MOSFET sensor array and the tissue depending on the tissue and where constructing the boundary condition and bioelectric signal maps are computed for the dielectric interface with selected baseline constants of a dielectric coefficient for the specific tissue.

8. An apparatus for making a temporal, spatial electro-anatomical map of bioelectrically active tissue with fidelity and accuracy depicting a local electrogram with native



dynamics while simultaneously including geometric and time domain specificity comprising:

a catheter with a MOSFET sensor array for the detection of a bioelectric potential with each sensor of the MOSFET sensor array having a MOSFET locally disposed in or on the catheter proximate to a corresponding sensor pad; where the MOSFET sensor array detects a plurality of bioelectric potentials in the bioelectrically active tissue at a plurality of selectively chosen sites in the bioelectrically active tissue at a plurality of times; a memory for storing the detected plurality of bioelectric potentials and locations of the corresponding selectively chosen sites for each of the plurality of times; and a processor coupled to the MOSFET sensor array for differentiating between "near" and "far field" signals at each of the corresponding MOSFET sensors of the MOSFET sensor array, and for constructing the temporal spatial electro-anatomical map of bioelectrically active tissue from the stored plurality of bioelectric potentials and locations of the corresponding selectively chosen sites and plurality of times.

9. The apparatus of claim 8 where each sensor of the MOSFET sensor array comprises a MOSFET isolated junction to measure action potentials without the parasitic capacitive or resistive loads with at least 0.1  $\mu\text{V}$  sensitivity.

10. The apparatus of claim 8 where each sensor of the MOSFET sensor array comprises a MOSFET isolated junction with a high impedance and low capacitance semiconductor sensing element to eliminate double-layer ionic transfer and conductive charge injection effects.

11. The apparatus of claim 8 where each sensor of the MOSFET sensor array comprises an integrated MOSFET isolated junction with a differential output with high noise immunity and low static power consumption with static CMOS gates to dissipate nearly zero power when idle and to avoid injection of noise to the bioelectrically active tissue.

12. The apparatus of claim 8 further comprising a sensor for detecting nonelectrical biosignals simultaneously with the bioelectric potentials, where both the nonelectrical biosignals and bioelectric potentials are stored in the memory, and where the processor constructs a boundary condition map of the tissue from the stored plurality of bioelectric potentials, nonelectrical biosignals and locations of the corresponding selectively chosen sites, and generates a comparative boundary condition and electro-anatomical map to allow for physician diagnosis.

13. The apparatus of claim 12 where each sensor of the MOSFET sensor array is capacitive with a specific dielectric interface between each sensor of the MOSFET sensor array and the tissue depending on the tissue and where the proces-

sor constructs the boundary condition and bioelectric signal maps for the dielectric interface with selected baseline constants of a dielectric coefficient for the specific tissue.

14. The apparatus of claim 8 where each MOSFET sensor of the MOSFET sensor array includes an amplifier with a DC to at least a 1 kHz bandwidth, with at least 95 dB common mode rejection, and at least 0.1  $\mu\text{V}$  sensitivity.

15. An apparatus for making a temporal, spatial electro-anatomical map of bioelectrically active tissue characterized by a temporal biopotential generated by a plurality of cells, the temporal, spatial electro-anatomical map depicting a local electrogram with native dynamics with fidelity and accuracy while simultaneously including geometric and time domain specificity comprising:

a catheter;

a plurality of sensing pads on or in the catheter organized with a bipolar, quadripolar, decapolar, or multi-electrode basket-type geometry;

a local MOSFET sensor circuit array in or on the catheter at or near the plurality of pads and coupled to the plurality of pads for the real time detection of bioelectric potential at each electrode of adjacent bioelectrically active tissue, the MOSFET sensor circuit array comprising a plurality of sensor circuits, each of which mimic sensed biopotential via a variable resistor, a local amplifier and a ground potential which is set locally within the contact between the cell and the corresponding pad; and

a processor for constructing the temporal, spatial electro-anatomical map of bioelectrically active tissue from the plurality of pads.

16. The apparatus of claim 15 further comprising a balloon having a surface, where the plurality of pads are organized as a collapsible basket on or in the balloon surface and/or carried by a plurality of expandable arms disposed on or in the balloon surface.

17. The apparatus of claim 16 where each MOSFET sensor circuit of the MOSFET sensor circuit array is disposed on or in one of the plurality of expandable arms and coupled to at least one adjacent electrode.

18. The apparatus of claim 15 where the local MOSFET sensor circuit array detects biopotential signals with at least 0.1  $\mu\text{V}$  sensitivity or less and with a 25 kHz or higher sampling rate.

19. The apparatus of claim 15 where the plurality of pads are configured in a geometry on the catheter adapted to sense biopotentials of bioelectrically active renal tissue.

20. The apparatus of claim 15 where the plurality of pads are configured in a geometry on the catheter adapted to sense biopotentials of bioelectrically active brain tissue.

\* \* \* \* \*



US009220425B2

(12) **United States Patent**  
**Shachar et al.**

(10) **Patent No.:** **US 9,220,425 B2**  
(45) **Date of Patent:** **Dec. 29, 2015**

(54) **METHOD AND APPARATUS FOR MEASURING BIOPOTENTIAL AND MAPPING EPICARDIAL COUPLING EMPLOYING A CATHETER WITH MOSFET SENSOR ARRAY**

USPC ..... 600/372-374, 377, 378, 381, 393, 509, 600/544-545  
See application file for complete search history.

(71) Applicants: **Yehoshua Shachar**, Santa Monica, CA (US); **Eli Gang**, Los Angeles, CA (US)

(72) Inventors: **Yehoshua Shachar**, Santa Monica, CA (US); **Eli Gang**, Los Angeles, CA (US)

(73) Assignee: **Magnetecs Corp.**, Ingelwood, CA (US)

(\*) Notice: Subject to any disclaimer, the term of this patent is extended or adjusted under 35 U.S.C. 154(b) by 580 days.

(21) Appl. No.: **13/621,727**

(22) Filed: **Sep. 17, 2012**

(65) **Prior Publication Data**

US 2014/0081114 A1 Mar. 20, 2014

(51) **Int. Cl.**

**A61B 5/04** (2006.01)  
**A61B 5/0428** (2006.01)  
**A61B 5/00** (2006.01)  
**A61B 5/042** (2006.01)  
**A61B 5/0478** (2006.01)

(52) **U.S. Cl.**

CPC ..... **A61B 5/04001** (2013.01); **A61B 5/042** (2013.01); **A61B 5/04284** (2013.01); **A61B 5/6858** (2013.01); **A61B 5/0478** (2013.01)

(58) **Field of Classification Search**

CPC ..... A61B 5/0402; A61B 5/0422; A61B 5/04284; A61B 5/0408; A61B 5/04085; A61B 5/042; A61B 5/0478; A61B 5/72-5/7296; A61B 2562/0209; A61B 2562/06; A61B 2017/00053; A61B 2017/00044; A61B 2017/00026; A61B 2017/00022

(56) **References Cited**

U.S. PATENT DOCUMENTS

3,229,686 A *	1/1966	Edmark, Jr.	600/502
5,083,562 A *	1/1992	de Coriolis et al.	607/7
5,607,433 A *	3/1997	Polla et al.	606/107
6,023,638 A *	2/2000	Swanson	600/510
2004/0015065 A1 *	1/2004	Panescu et al.	600/374
2004/0082860 A1 *	4/2004	Haissaguerre	600/466
2006/0265039 A1 *	11/2006	Bartic et al.	607/116
2007/0093801 A1 *	4/2007	Behnke	606/34
2007/0197891 A1 *	8/2007	Shachar et al.	600/374
2010/0160737 A1 *	6/2010	Shachar et al.	600/202
2014/0018792 A1 *	1/2014	Gang et al.	606/41

\* cited by examiner

*Primary Examiner* — Lee S Cohen

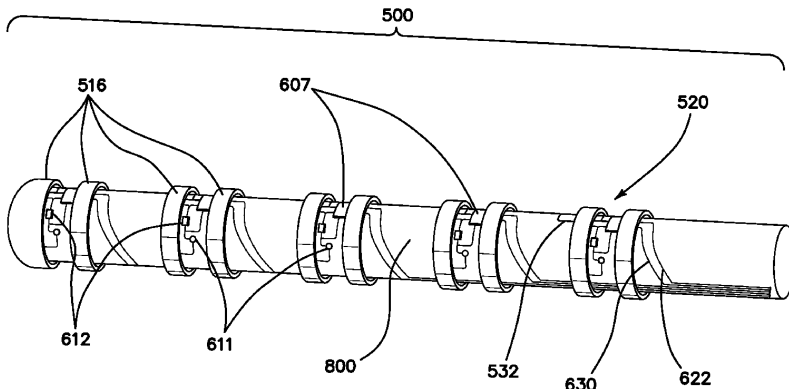
*Assistant Examiner* — Erin M Cardinal

(74) *Attorney, Agent, or Firm* — Marcus C. Dawes; Daniel L. Dawes

(57) **ABSTRACT**

This invention relates generally to electro-anatomical mapping method and an apparatus using a catheter and more particularly to a mapping catheter having an embedded MOSFET sensor array for detecting local electrophysiological parameters such as biopotential signals within an excitable cellular matrix geometry, for determining physiological as well as electrical characteristics of conduction path and its underlying substrate within the endocardial and epicardial spaces, the arterial structure and in ganglionic plexus. The apparatus with its MOSFET sensor is geometrically configured as a decapolar linear array and optionally with an 8x8 sensor matrix placed on a balloon-like structure.

**13 Claims, 25 Drawing Sheets**





INTERNATIONAL FILINGS FOR:  
*Apparatus for Magnetically Deployable Catheter  
with MOSFET Sensor and Method for  
Mapping and Ablation*

***INVENTOR: Yehoshua Shachar  
Lazlo Farkas  
Dr. Eli Gang***



(19) World Intellectual Property Organization  
International Bureau



(43) International Publication Date  
7 September 2007 (07.09.2007)

PCT

(10) International Publication Number  
WO 2007/100559 A2

- (51) International Patent Classification:  
A61B 18/14 (2006.01) A61B 5/04 (2006.01)
- (21) International Application Number:  
PCT/US2007/004416
- (22) International Filing Date:  
20 February 2007 (20.02.2007)
- (25) Filing Language: English
- (26) Publication Language: English
- (30) Priority Data:  
11/362,542 23 February 2006 (23.02.2006) US

(81) Designated States (unless otherwise indicated, for every kind of national protection available): AE, AG, AL, AM, AT, AU, AZ, BA, BB, BG, BR, BW, BY, BZ, CA, CH, CN, CO, CR, CU, CZ, DE, DK, DM, DZ, EC, EE, EG, ES, FI, GB, GD, GH, GI, GM, GT, HN, HR, HU, ID, IL, IN, IS, JP, KE, KG, KM, KN, KP, KR, KZ, LA, LC, LK, LR, LS, LT, LU, LV, LY, MA, MD, MG, MK, MN, MW, MX, MY, MZ, NA, NG, NI, NO, NZ, OM, PG, PH, PL, PT, RO, RS, RU, SC, SD, SE, SG, SK, SL, SM, SV, SY, TJ, TM, TN, TR, TT, TZ, UA, UG, US, UZ, VC, VN, ZA, ZM, ZW.

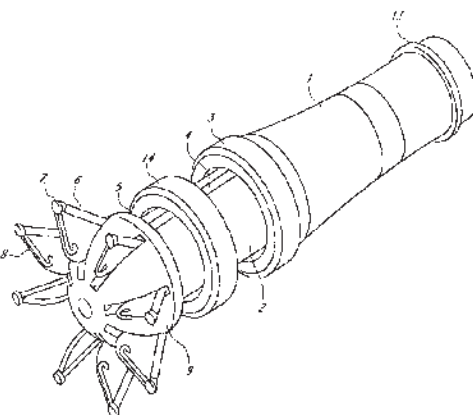
(84) Designated States (unless otherwise indicated, for every kind of regional protection available): ARIPO (BW, GH, GM, KE, LS, MW, MZ, NA, SD, SI, SZ, TZ, UG, ZM, ZW), Eurasian (AM, AZ, BY, KG, KZ, MD, RU, TJ, TM), European (AT, BE, BG, CH, CY, CZ, DE, DK, EE, ES, FI, FR, GB, GR, HU, IE, IS, IT, LT, LU, LV, MC, NL, PL, PT, RO, SI, SK, TR), OAPI (BF, BJ, CF, CG, CI, CM, GA, GN, GQ, GW, ML, MR, NI, SN, TD, TG).

- (71) Applicant (for all designated States except US): MAGNETECS, INC. [US/US]; 10524 S. La Cienega Blvd., Inglewood, California 90304 (US).
- (72) Inventors: SHACHAR, Yehoshua; 2417 22nd Street, Santa Monica, California 90405 (US); FARKAS, Kaszko; 29 Taormina Lane, Ojai, California 93023 (US); GANG, Eli; 414 North Camden Drive, Beverly Hills, California 90210 (US).
- (74) Agent: DELANEY, Karoline, A.; Knobbe, Martens, Olson & Bear, LLP; 2040 Main Street, 14th Floor, Irvine, California 92614 (US).

Published:  
without international search report and to be republished upon receipt of that report

For two letter codes and other abbreviations, refer to the "Guidance Notes on Codes and Abbreviations" appearing at the beginning of each regular issue of the PCT Gazette.

(54) Title: APPARATUS FOR MAGNETICALLY DEPLOYABLE CATHETER WITH MOSFET SENSOR AND METHOD FOR MAPPING AND ABLATION



(57) Abstract: A mapping and ablation catheter is described. In one embodiment, the catheter includes a MOSFET sensor array that provides better fidelity of the signal measurements as well as data collection and reduces the error generated by spatial distribution of the isotropic and anisotropic wavefronts. In one embodiment, the mapping system tracks the change in potential in the vicinity of an activation wavefront. In one embodiment, the mapping system tracks the spread of excitation in the heart, with properties such as propagation velocity changes. In one embodiment, during measurement, the manifold carrying the sensor array expands from a closed position state to a deployable open state. Spatial variation of the electrical potential is captured by the system's ability to occupy the same three-dimensional coordinate set for repeated measurements of the desired site. In one embodiment, an interpolation algorithm tracks the electrogram data points to produce a map relative to the electrocardiogram data.



WO 2007/100559 A2

(19)



(11) Veröffentlichungsnummer:

(11) Publication number:

**EP 1 986 560 A0**

(11) Numéro de publication:

Internationale Anmeldung veröffentlicht durch die  
Weltorganisation für geistiges Eigentum unter der Nummer:

**WO 2007/100559** (Art. 153(3) EPÜ).

International application published by the World  
Intellectual Property Organization under number:

**WO 2007/100559** (Art. 153(3) EPC).

Demande internationale publiée par l'Organisation  
Mondiale de la Propriété Intellectuelle sous le numéro:

**WO 2007/100559** (art. 153(3) CBE).





(86) Date de dépôt PCT/PCT Filing Date: 2007/02/20  
 (87) Date publication PCT/PCT Publication Date: 2007/09/07  
 (85) Entrée phase nationale/National Entry: 2008/08/20  
 (86) N° demande PCT/PCT Application No.: US 2007/004416  
 (87) N° publication PCT/PCT Publication No.: 2007/100559  
 (30) Priorité/Priority: 2006/02/23 (US11/362,542)

(51) Cl.Int./Int.Cl. *A61B 18/14* (2006.01),  
*A61B 5/04* (2006.01)

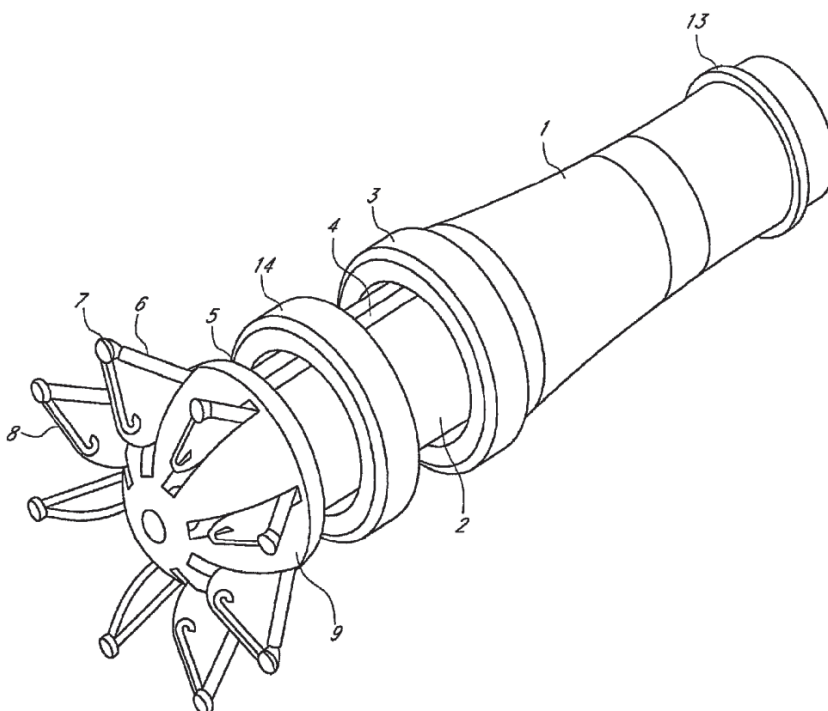
(71) Demandeur/Applicant:  
 MAGNETECS, INC., US

(72) Inventeurs/Inventors:  
 SHACHAR, YEHOSHUA, US;  
 FARKAS, KASZLO, US;  
 GANG, ELI, US

(74) Agent: SIM & MCBURNEY

(54) Titre : APPAREIL POUR CATHETER EXTENSIBLE DE FACON MAGNETIQUE AVEC CAPTEUR MOSFET ET  
 PROCEDURE DE CARTOGRAPHIE ET D'ABLATION

(54) Title: APPARATUS FOR MAGNETICALLY DEPLOYABLE CATHETER WITH MOSFET SENSOR AND METHOD  
 FOR MAPPING AND ABLATION



(57) Abrégé/Abstract:

A mapping and ablation catheter is described. In one embodiment, the catheter includes a MOSFET sensor array that provides better fidelity of the signal measurements as well as data collection and reduces the error generated by spatial distribution of the



(57) **Abrégé(suite)/Abstract(continued):**

isotropic and anisotropic wavefronts. In one embodiment, the system maps the change in potential in the vicinity of an activation wavefront. In one embodiment, the mapping system tracks the spread of excitation in the heart, with properties such as propagation velocity changes. In one embodiment, during measurement, the manifold carrying the sensor array expands from a closed position state to a deployable open state. Spatial variation of the electrical potential is captured by the system's ability to occupy the same three-dimensional coordinate set for repeated measurements of the desired site. In one embodiment, an interpolation algorithm tracks the electrogram data points to produce a map relative to the electrocardiogram data.



香港特別行政區政府知識產權署專利註冊處  
 Patents Registry, Intellectual Property Department  
 The Government of the Hong Kong Special Administrative Region

專利註冊紀錄冊 REGISTER OF PATENTS  
 註冊紀錄冊記項 REGISTER ENTRY

申請編號 **Application No.** :09104053.7

提交日期 **Filing date** :30.04.2009

法律程序所用語文 **Language of Proceedings** :En

聲稱享有的優先權 **Priority claimed** :23.02.2006 US 11/362,542

發表編號 **Publication No.** :HK1123959

專利說明書首次發表日期 **Date of first publication** :03.07.2009/A

歐洲專利發表編號 **EP Publication No.** :EP 1986560  
 歐洲專利申請發表日期 **EP Application Publication Date** :05.11.2008  
 歐洲專利申請編號 **EP Application No.** :07751190.5  
 歐洲專利申請提交日期 **EP Application Filing Date** :20.02.2007

國際發表編號 **International Publication No.** :WO2007/100559  
 國際發表日期 **International Publication Date** :07.09.2007  
 國際申請編號 **International Application No.** :PCT/US2007/004416  
 國際申請提交日期 **International Application Filing Date** :20.02.2007

**發明名稱 Title**  
 用於具有MOSFET傳感器的可用磁力展開的導管的設備以及用於標測和切除的方法  
 APPARATUS FOR MAGNETICALLY DEPLOYABLE CATHETER WITH MOSFET SENSOR AND METHOD FOR  
 MAPPING AND ABLATION

**申請人 Applicant**  
 MAGNETECS, INC  
 10524 S. La Cienega Blvd.  
 Inglewood, CA 90304  
 UNITED STATES/UNITED STATES OF AMERICA

**發明人 Inventor**  
 SHACHAR, Yehoshua

FARKAS, Kaszlo

GANG, Eli

**分類** :A61B  
**Classified to**

**送達地址**  
**Address for Service**

Rebecca Lo & Co  
1408 Dina House, Ruttonjee Centre  
11 Duddell Street, Central, HONG KONG

**代理人地址**  
**Agent's Address**

1408 Dina House, Ruttonjee Centre, 11 Duddell Street, Central, Hong Kong

<b>狀況</b> <b>Status</b>	申請有效 Application in force
----------------------------	------------------------------

註冊紀錄冊記項完結  
\*\*\*\* END OF REGISTER ENTRY \*\*\*\*

---

維持標準專利申請詳情 MAINTENANCE DETAILS OF STANDARD PATENT APPLICATION

---

**發表編號** :HK1123959  
**PUBLICATION NO.**

**申請人**  
**APPLICANT**  
MAGNETECS, INC  
10524 S. La Cienega Blvd.  
Inglewood, CA 90304  
UNITED STATES/UNITED STATES OF AMERICA

**指定專利申請提交日期** :20.02.2007  
**DATE OF FILING OF DESIGNATED PATENT APPLICATION**

**記錄請求發表日期** :03.07.2009

**DATE OF PUBLICATION OF REQUEST TO RECORD**

維持費到期繳交日期 : 20.02.2015  
**DATE OF MAINTENANCE FEE DUE**

上次維持費繳交日期 :  
**DATE OF LAST MAINTENANCE**

提交註冊及批予專利申請日期 :  
**APPLICATION FOR REGISTRATION & GRANT FILING DATE**

狀況 申請有效  
**STATUS** Application in force

報告完結  
\*\*\*\* END OF REPORT \*\*\*\*





02

U.S. PATENT OFFICE FILINGS FOR:  
*Apparatus and Method for  
Lorentz-Active Sheath Display  
and Control of Surgical Tools*

***INVENTOR: Yehoshua Shachar  
Bruce Marx  
Leslie Farkas  
David Johnson  
Lazlo Farkas***



US 20090253985A1

(19) **United States**  
(21) **Patent Application Publication**  
**Shachar et al.**

(10) **Pub. No.: US 2009/0253985 A1**  
(43) **Pub. Date: Oct. 8, 2009**

(54) **APPARATUS AND METHOD FOR  
LORENTZ-ACTIVE SHEATH DISPLAY AND  
CONTROL OF SURGICAL TOOLS**

(75) Inventors: **Yehoshua Shachar**, Santa Monica, CA (US); **Bruce Marx**, Ojai, CA (US); **Leslie Farkas**, Ojai, CA (US); **David Johnson**, West Hollywood, CA (US); **Laszlo Farkas**, Ojai, CA (US)

Correspondence Address:  
**KNOBBE MARTENS OLSON & BEAR LLP**  
2040 MAIN STREET, FOURTEENTH FLOOR  
IRVINE, CA 92614 (US)

(73) Assignee: **Magnetecs, Inc.**, Inglewood, CA (US)

(21) Appl. No.: **12/099,079**

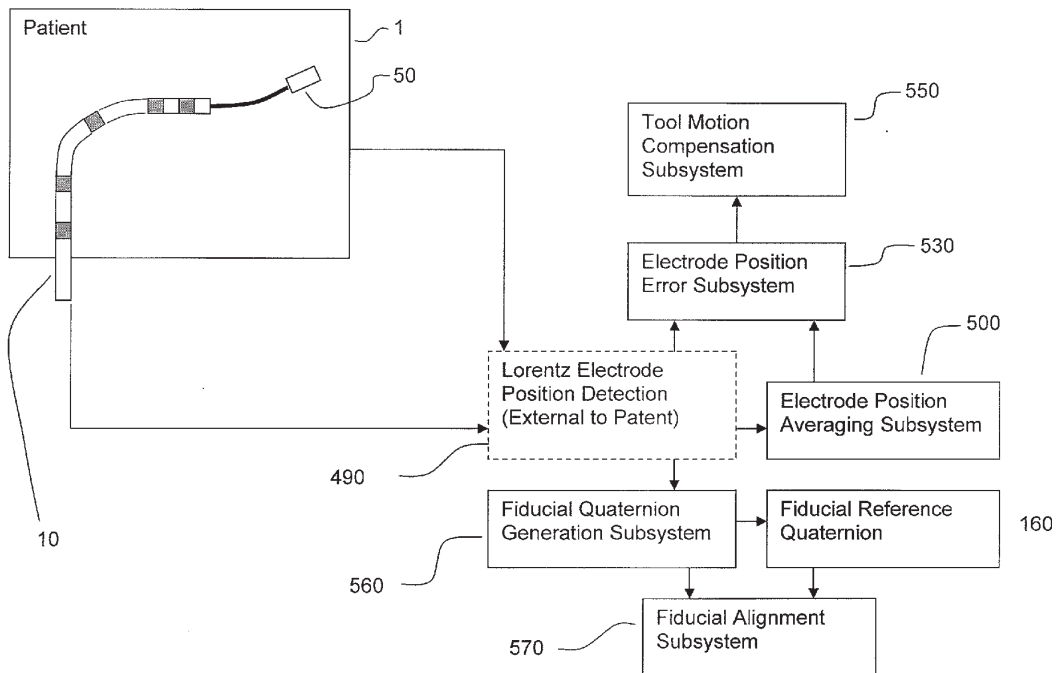
(22) Filed: **Apr. 7, 2008**

**Publication Classification**

(51) **Int. Cl.**  
**A61B 5/06** (2006.01)  
(52) **U.S. Cl.** ..... **600/424**

(57) **ABSTRACT**

The Lorentz-Active Sheath (LAS) serves as a conduit for other medical devices such as catheters, balloons, biopsy needles, etc. The sheath is inserted through a vein or other body orifice and is guided into the area of the patient where the operation is to be performed. The position and orientation of the LAS is tracked via an industry standard position detection system which senses electrical signals that are emitted from several electrodes coupled to the LAS. The signals received from the LAS are used to calculate an accurate and reliable assessment of the actual position of the LAS within the patient. The electrode signals also serve to create a reference frame which is then used to act as a motion compensation filter and fiducial alignment system for the movement of the LAS-hosted medical tool.



02

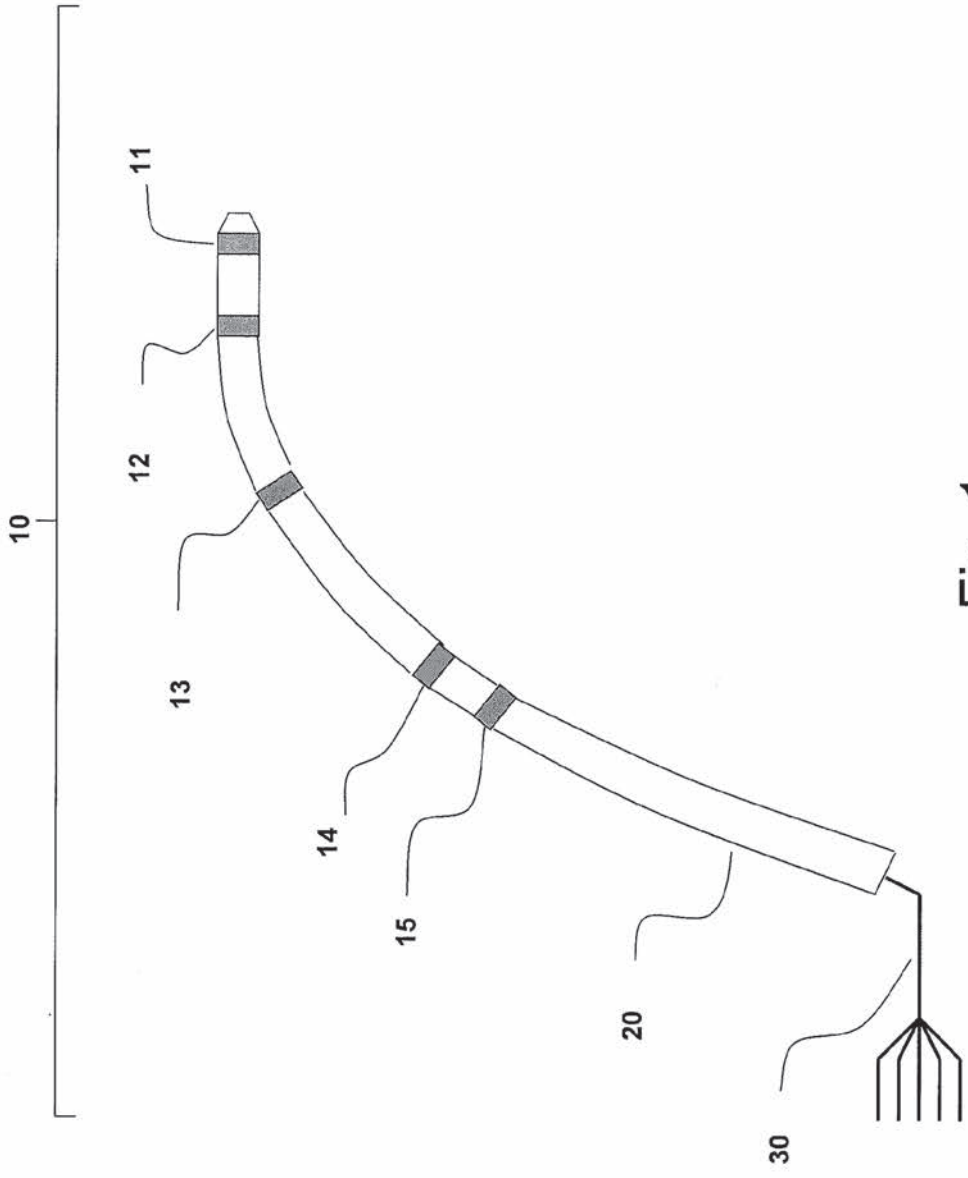


Fig. 1

02

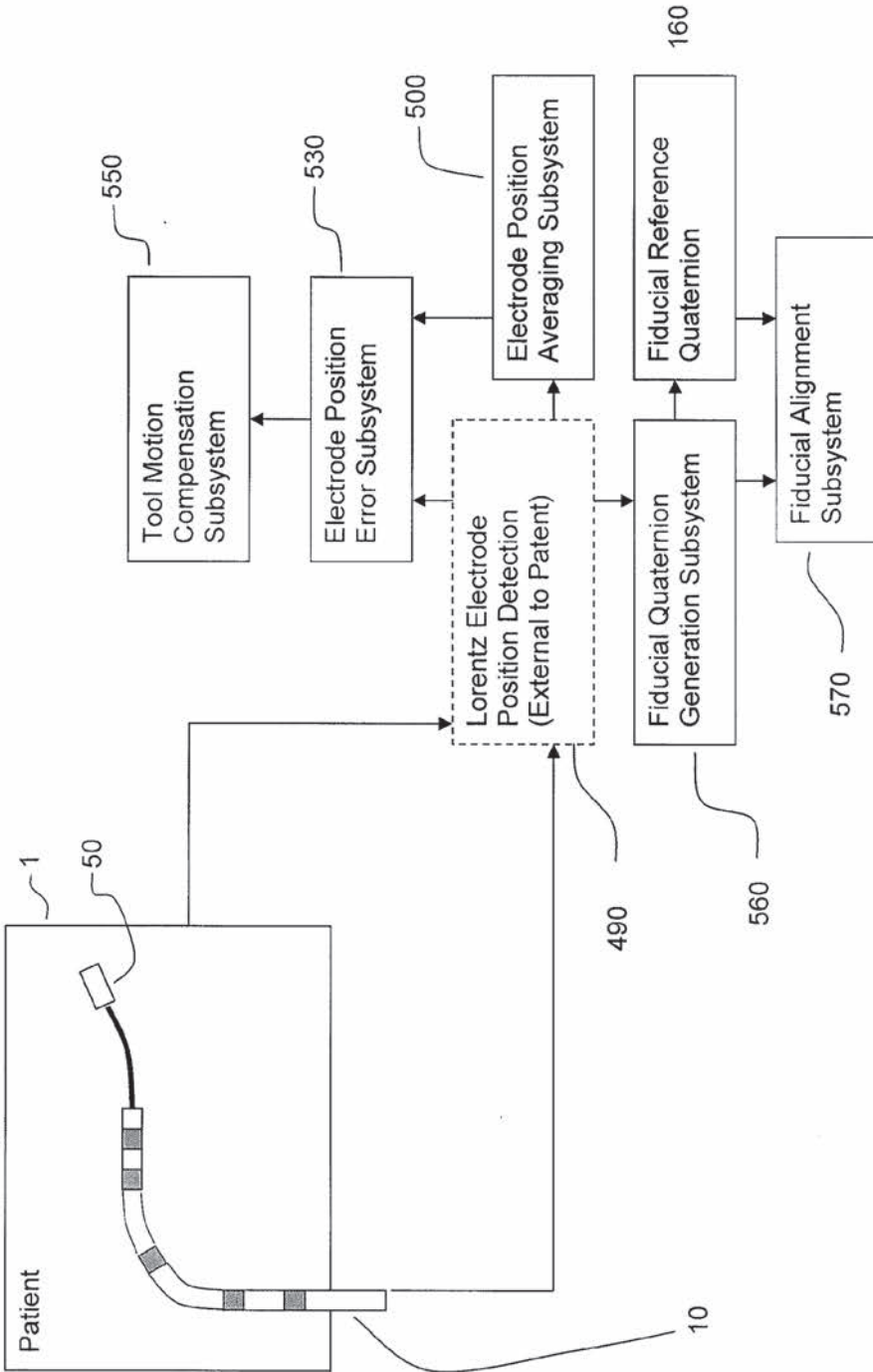


Fig. 2

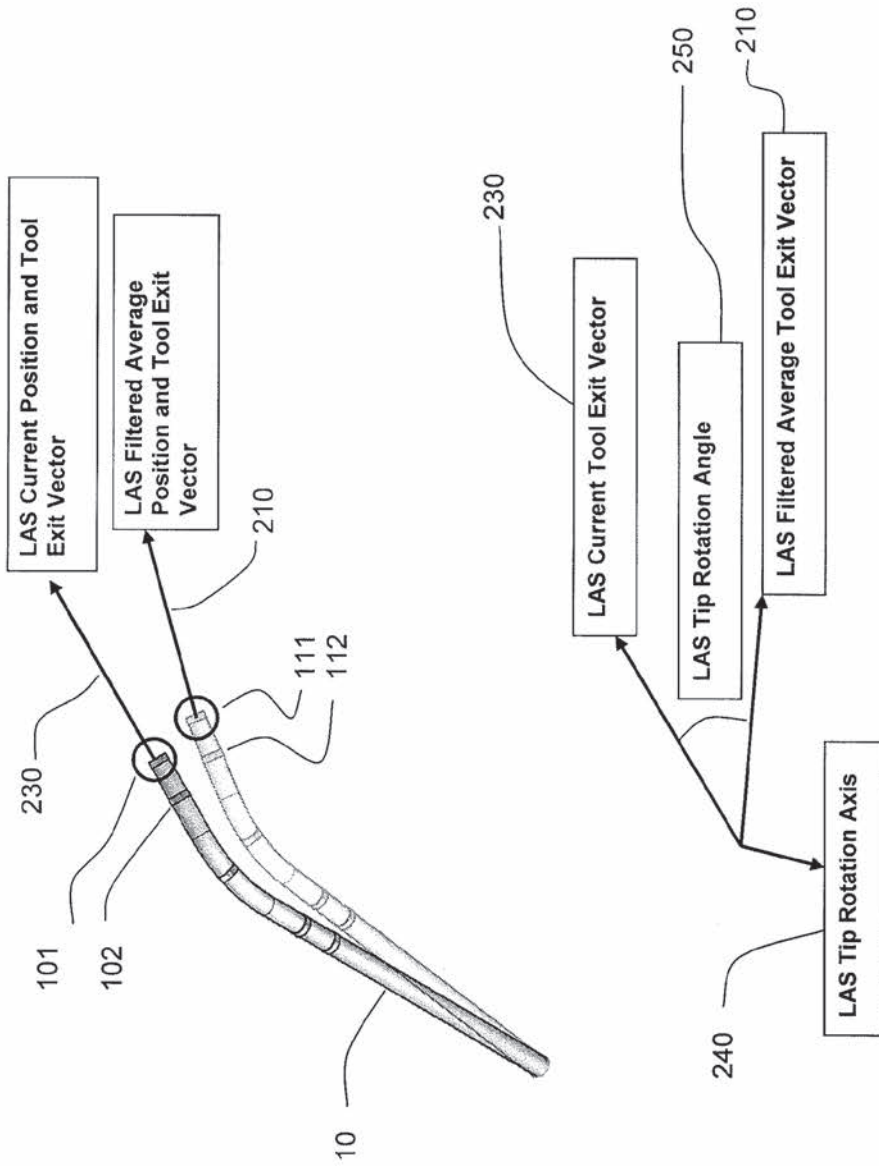


Fig. 3



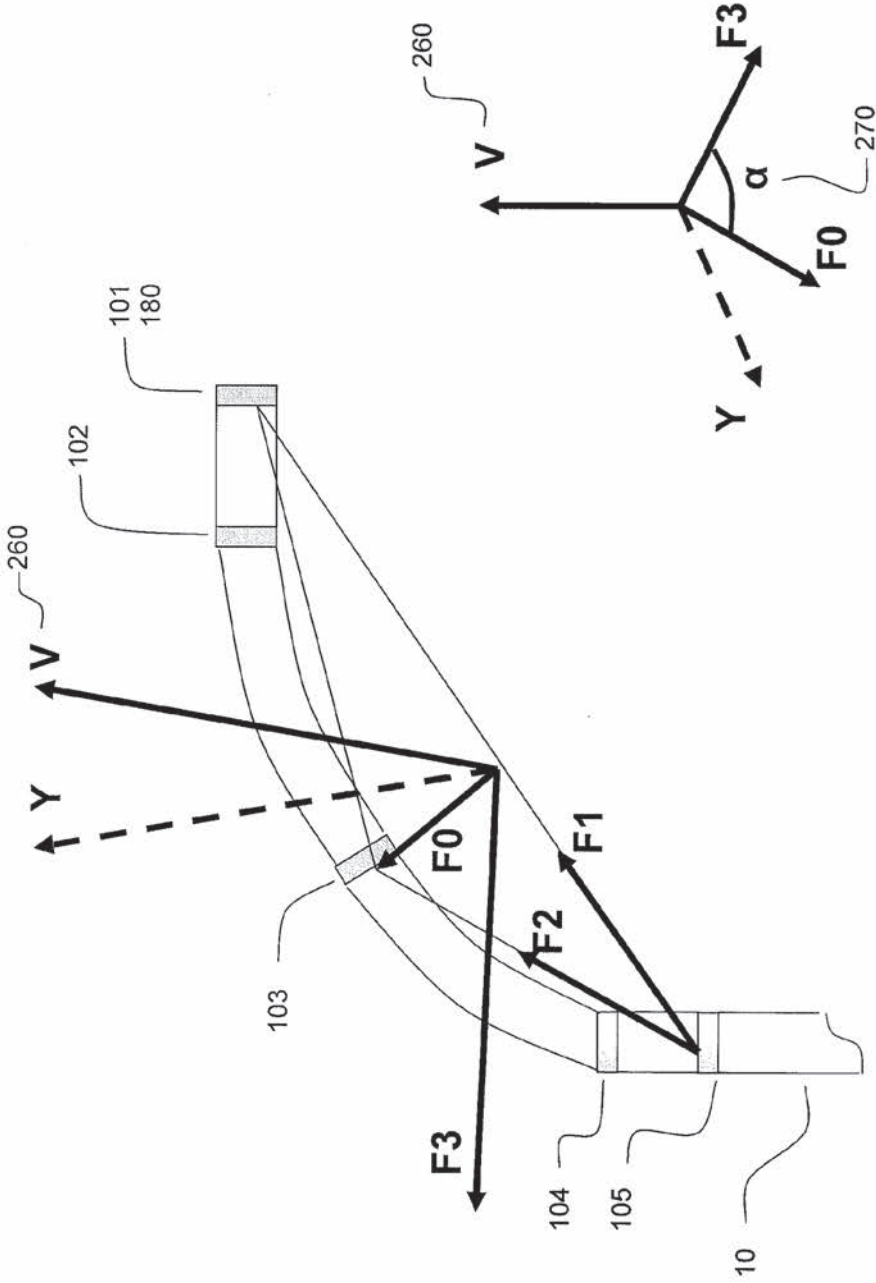


Fig. 4

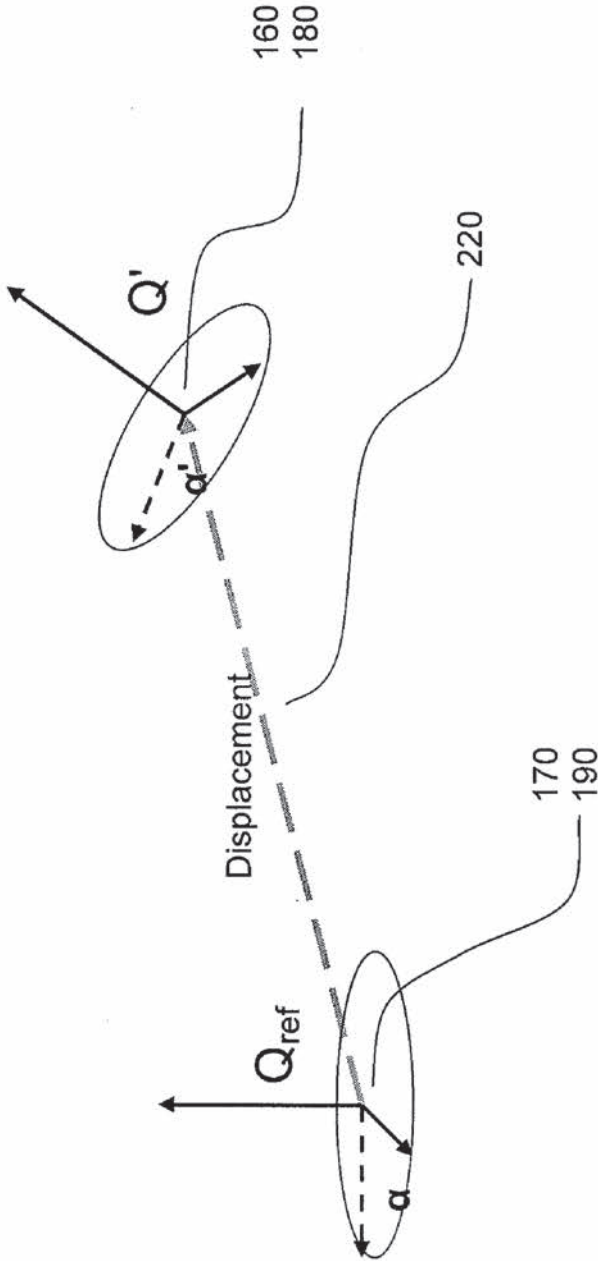


Fig. 5

02

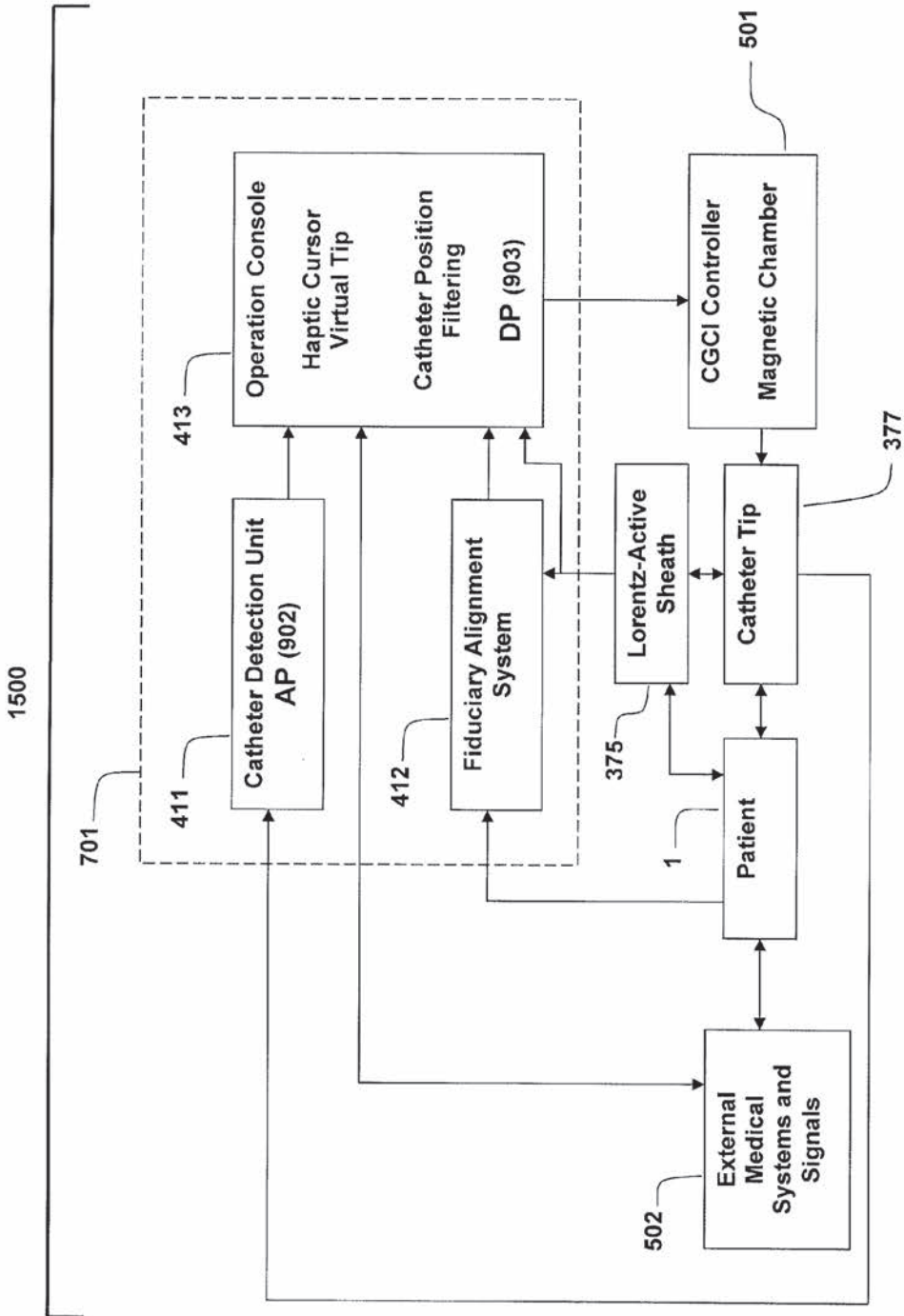


FIG. 6

## APPARATUS AND METHOD FOR LORENTZ-ACTIVE SHEATH DISPLAY AND CONTROL OF SURGICAL TOOLS

### BACKGROUND OF THE INVENTION

#### [0001] 1. Field of the Invention

[0002] The invention relates to the field of determining the location, orientation, and movement of an invasive medical device within a patient while compensating for undesired tool and patient motion.

#### [0003] 2. Description of the Related Art

[0004] Medical sheaths have long been used to introduce a variety of medical tools into a patient during an operation. Typically, the sheath is inserted into the patient via a vein or other orifice and is manipulated until it has reached its target location such as an atrium of the heart. Invasive medical tools such as catheters, balloons, and biopsy needles are then deployed through the sheath in order to work on the patient.

[0005] While the prior art has been successful in treating many patients, the techniques of the prior art are not without their drawbacks and difficulties. Fluoroscopy or x-rays can be used to image fiducial points such as the radio-opaque markers or rings that have been placed on the medical sheath and transmits them to a display. The physician is then able to view and analyze the sheath's current location and orientation of the sheath's distal tip. If the sheath is in the wrong area, needs to be adjusted, or has been dislocated, the sheath must be moved or recovered and then another medical image must be taken. This process is repeated until the sheath has reached the desired location.

[0006] The prior art does not provide a consistent, and reliable fix on the location of the sheath as well as maintaining a known orientation of the distal tip of the sheath. The prior art uses fiducial markers such as the ones presented above which can only be seen when using an ionizing field source such as an x-ray or CT scan and are useless when employed in a radar based navigation system.

[0007] Also not contemplated by the prior art is the use of a medical sheath as a motion compensation filter for the deployment of medical tools. The prior art has so far failed to employ the sheath itself for motion compensation.

### SUMMARY OF THE INVENTION

[0008] The system and methods described herein solve these and other problems by adding navigation electrodes to the medical sheaths that are used to deploy catheters, balloons, biopsy needles, and other medical tools within a patient during invasive surgery. The system is capable of continuously determining the location and position of the sheath's distal tip in up to six degrees of freedom or even more and within 1 mm of the tip's actual position within a patient. Navigational electrodes that emit an electrical signal to a nearby receiver are located at or near the tip of the sheath and along down the shaft to determine key locations of the sheath and to serve as a global fiducial reference frame. This reference frame that is created by the sheath is then used to compensate for changes in the patient's or local organ's orientation.

[0009] One embodiment includes a system that can continually determine the position and location of the distal tip of a medical sheath and track its movements in six degrees of freedom as it is manipulated through a patient while compensating for the movement of the patient or organ it is working

in without the use of fluoroscopy or other medical imaging devices that use an ionizing field source.

[0010] In one embodiment, a Lorentz-Active Sheath (LAS) is used during invasive surgery in a moving organ such as the heart where medical tools such as catheters, biopsy needles, balloons, and the like are required. The position of the LAS electrodes are tracked in the presence of dynamic variables such as the mechanical contraction and repolarization of the heart muscle. The data acquired from the tracking of the LAS electrodes is then used to produce a reference frame of the sheath as it moves in conjunction with the patient or moving tissue.

[0011] In one embodiment, the average position and orientation of the LAS distal tip is continuously determined with respect to the previously measured positions of the tip over a specific time period. This process provides a reference position and orientation that is later used for compensating the motion of the LAS-hosted medical tools.

[0012] In one embodiment, the motion of the LAS is defined with respect to the aforementioned average position. This process provides a position and orientation error value that is later incorporated into motion compensation and fiducial alignment modalities.

[0013] In one embodiment, the position and orientation error values of the LAS are used to subtract the motion of the LAS from the motion of the LAS-hosted medical tool. This in effect along with the previous three embodiments forms a motion compensation filter and provides a stable fiducial reference for tool position control systems and thus provides the operating physician with an accurate assessment of the sheath's true position within the patient.

[0014] In one embodiment, the positions of the LAS navigation electrodes are used to determine a six-degree of freedom reference frame.

[0015] In one embodiment, the reference frame (e.g., six degrees) that was created from the LAS navigation electrodes in the previous embodiment is used to track changes in the patient's or local organ's orientation.

[0016] While the apparatus and method is described for the sake of grammatical fluidity with functional explanations, it is to be expressly understood that the claims, unless expressly formulated under 35 USC 112, are not to be construed as necessarily limited in any way by the construction of "means" or "steps" limitations, but are to be accorded the full scope of the meaning and equivalents of the definition provided by the claims under the judicial doctrine of equivalents, and in the case where the claims are expressly formulated under 35 USC 112 are to be accorded full statutory equivalents under 35 USC 112. The invention can be better visualized by turning now to the following drawings.

### BRIEF DESCRIPTION OF THE DRAWINGS

[0017] FIG. 1 is an isometric diagram of the Lorentz-Active Sheath (LAS) assembly.

[0018] FIG. 2 is a block diagram of the signals and systems that determine the Lorentz-Active Sheath position, position error, position compensation, and patient fiducial alignment.

[0019] FIG. 3 is a schematic diagram of the motion compensation vectors.

[0020] FIG. 4 is a schematic diagram of the LAS electrodes used to determine the fiducial quaternions and position reference.

[0021] FIG. 5 is a schematic diagram of the patient fiducial alignment quaternions.

**[0022]** FIG. 6 is a block diagram of an embodiment of the invention which incorporates the Lorentz-Active Sheath into a Catheter Guidance Control and Imaging (CGCI) system and depicts its function of providing a reference between the catheter, the patient, the fiducial alignment system, and a console catheter data filtering system.

**[0023]** The invention and its various embodiments can now be better understood by turning to the following detailed description of the preferred embodiments which are presented as illustrated examples of the invention defined in the claims. It is expressly understood that the invention as defined by the claims may be broader than the illustrated embodiments described below.

#### DETAILED DESCRIPTION

**[0024]** In general, the Lorentz-Active Sheath (LAS) serves as a conduit for other medical devices such as catheters, balloons, biopsy needles, etc. The sheath is inserted through a vein or other body orifice and is guided into the area of the patient where the operation is to be performed. The position and orientation of the LAS is tracked via a conventional position detection system which senses electrical signals that are emitted from several electrodes coupled to the LAS. The signals received from the LAS are used to calculate an accurate and reliable assessment of the actual position of the LAS within the patient. The electrode signals also serve to create a reference frame which is then used to act as a motion compensation filter and fiducial alignment system for the movement of the LAS-hosted medical tool.

**[0025]** FIG. 1 is an isometric diagram of the LAS assembly 10. Detection system-sensitive electrodes 11-15 are integrated into the LAS shaft 20. The electrodes 11-15 are used to generate electrical signals which are sensed by a position detection system 490 shown in FIG. 2. The electrodes 11-15 can be sensors, such as, for example, impedance sensors, radar sensors, hall-effect sensors, etc. and/or sources, such as, for example, radio-frequency sources, radio-frequency coils, piezoelectric rings, etc.

**[0026]** The two most distal electrodes 11 and 12 on shaft 20 are used to determine the tool exit position and tool exit direction 230 from the LAS 10 as illustrated in FIG. 3. FIG. 1 also shows that electrodes 11-15 are connected to the position detection system 490 by embedded electrode wires 30 which are attached to a coupling connector (not shown).

**[0027]** In one embodiment, one or more electrodes 11-15 sense the electrical signals transmitted between a plurality of surface electrode patches. The system collects electrical data from the one or more electrodes 11-15 and uses this information to track or navigate their movement and construct three-dimensional (3-D) models of the tissues.

**[0028]** In one embodiment, one or more electrodes 11-15 sense the electrical signals transmitted between three pairs of EnSite NavX surface electrode patches, such as, for example the EnSite NavX surface electrode patches used in connection with the EnSite System. The system collects electrical data from the one or more electrodes 11-15 and uses this information to track or navigate movement of the one or more electrodes 11-15 and construct three-dimensional (3-D) models of the chamber.

**[0029]** FIG. 2 is a block diagram of the signals and systems used to determine the position, position error, position compensation, and patient fiducial alignment of the LAS 10.

**[0030]** The LAS 10 is inserted into a patient 1 through a medical incision or body orifice. A LAS-hosted medical

50 such as a catheter, balloon, biopsy needle, or any other medical device that may be required during an invasive operation is inserted through the LAS 10 and deployed into the patient volume in which the operation is to occur. The detection system-sensitive electrodes 11-15 that are provided to the LAS 10, the LAS-hosted tool 50, and patient 1 are provided to the position detection system 490 by standard connectors and patches (not shown).

**[0031]** In one embodiment, the LAS 10 is used to act as a motion compensation device and subtract unwanted motion of the sheath from the motion of the currently deployed LAS-hosted medical tool 50. The position detection system 490 provides the current positions of the electrodes located on the LAS 10 as well as the positions of the electrodes located on the LAS-hosted medical tool 50 through a system of network communications and standard computer software interfaces. The position data of the LAS 10 that has been collected by the position detection system 490 is then sent to the Electrode Position Averaging Subsystem 500 as depicted in FIG. 2. The Electrode Position Averaging Subsystem 500 averages the positions of the electrodes located on LAS 10 over a select time period in order to obtain a stable baseline reference of the position of the LAS. This new averaged electrode position is then subtracted from the current electrode position provided by the position detection system 490 by the Electrode Position Error Subsystem 530. The error measurement that has been created by the Electrode Position Error Subsystem 530 is then sent to the Tool Motion Compensation Subsystem 550 which is employed to subtract unwanted sheath motion from the motion of the currently deployed LAS-hosted tool 50.

**[0032]** Further understanding of the process described above can be obtained by turning to the following example. As depicted in FIG. 1, detection system-sensitive electrodes 11 and 12 are located on the shaft 20 of the LAS 10. The position detection system 490 locates electrodes 11 and 12 and thus the sheath while the LAS is in the operating volume of the patient 1. The raw data that the position detection system 490 collects produces an image of the position of electrodes 11 and 12 and displays them as current LAS electrode positions 101 and 102 respectively as shown in FIG. 3. This process is then repeated a number of times over a specified time period.

**[0033]** After the position detection system 490 has found multiple data points for current electrode positions 101 and 102, the data for each electrode is then sent to the Electrode Position Averaging Subsystem 500. The Electrode Position Averaging Subsystem 500 begins to average the last n number of current positions obtained for each electrode using equation (1). For example, current electrode position 101 that was obtained originally from electrode 11 is averaged in the following manner:

$$\text{LAS Average Electrode 101 Position} = \text{SUM}(\text{LAS Current Electrode 101 Positions})/n \quad (1)$$

**[0034]** where n is the number of measurements taken. Once current electrode positions 101 and 102 have been applied to equation (1) and filtered, the average electrode positions 111 and 112 are obtained respectively as shown in FIG. 3. It is to be expressly understood that any multitude or plurality of current electrode positions may be analyzed in this manner.

**[0035]** Current electrode positions 101 and 102 and filtered average electrode positions 111 and 112 can then be used to calculate the position and exit orientation of a medical tool that is to be deployed by the LAS 10. The exit orientation exit vector of a deployed medical tool is found by normalizing



the difference in position between the two most distal electrodes **101** and **102** using equation (2):

$$\text{LAS Tool Exit Vector} = (\text{LAS Electrode 101 Position} - \text{LAS Electrode 102 Position}) / (\text{LAS Electrode 101 Position} - \text{LAS Electrode 102 Position}) \quad (2)$$

**[0036]** This equation thus produces a current exit vector **230** for a deployed medical device as shown in FIG. 3. Equation (2) is also applied to the filtered average electrode positions **111** and **112** to produce an average exit vector **210** for a deployed medical device also shown in FIG. 3. This newly obtained exit vector gives the operating physician a clear and reliable reading on exactly where his instruments are within the patient volume and in what orientation the instruments are traveling in. As shown from the description above, if the LAS is in the wrong position or is being manipulated into the wrong direction, the physician may quickly and easily reposition the LAS in real time without the use of fluoroscopy or other medical images that use an ionizing field source.

**[0037]** After the position data has passed from the Electrode Position Averaging Subsystem **500** and through the Electrode Position Error Subsystem **530**, it is relayed to the Tool Motion Compensation Subsystem **550** where the motion of the sheath is subtracted from the motion of the LAS-hosted tool **50** to produce an extremely accurate and consistent assessment of the medical tool's location within the patient volume in six degrees of freedom. In order to accomplish this, the motion compensation due to the displacement of the LAS tip is performed by subtracting the LAS motion with respect to the average tip position of the LAS which is given by equation (3):

$$\text{Tool Position}' = \text{Tool Position} - [\text{LAS Electrode 101 Position} - \text{LAS Filtered Average Electrode 111 Position}] \quad (3)$$

**[0038]** Similarly, motion compensation due to tip rotation of the LAS is performed by un-rotating the tool-to-LAS tip position vector using equation (4).

$$\text{Tool Position Vector} = \text{Tool Position} - \text{LAS Electrode 101 Position} \quad (4)$$

**[0039]** The LAS filtered average tool exit vector **210** is crossed with the LAS current tool exit vector **230** to give the LAS tip rotation axis **240** given in equation (5) and as shown in FIG. 3.

$$\text{LAS Tip Rotation Axis} = (\text{LAS Filtered Average Tool Exit Vector}) \times (\text{LAS Current Tool Exit Vector}) \quad (5)$$

**[0040]** The dot product of the same two vectors in equation (6) gives the LAS tip rotation angle **250**.

$$\text{LAS Tip Rotation Angle} = (\text{LAS Filtered Average Tool Exit Vector}) \cdot (\text{LAS Current Tool Exit Vector}) \quad (6)$$

**[0041]** The tool position vector is then rotated about the LAS tip rotation axis **240**, the result of equation (5), by the negative of the LAS tip rotation angle **250**, the result of equation (6), to give the adjusted tool position vector using standard rotation matrices and equation (7).

$$\text{Tool Position}'(\text{angle}) = \text{Tool Position rotated about} (\text{LAS Tip Rotation Axis}) \text{ by } -(\text{LAS Tip Rotation Angle}) \quad (7)$$

**[0042]** Finally, the total compensation due to the position angle shifts of the LAS may be found by combining equations (7) and (3) into equation (8).

$$\text{Tool Position}'(\text{total}) = \text{Tool Position}'(\text{angle}) - [\text{LAS Electrode 101 Position} - \text{LAS Filtered Average Electrode 111 Position}] \quad (8)$$

**[0043]** In one embodiment, the LAS device is used to track local tissue motion and alignment. In FIG. 2, the current electrode positions **101** and **102** and any other electrodes that may be placed on the shaft **20** of the LAS that are generated by the Position detection system **490** are sent to the LAS Fiducial Quaternion Generation Subsystem **560** which in turn generates a six-degree of freedom reference set of the LAS Current Fiducial Reference Quaternion **160** and LAS Current Fiducial Position **180** (shown in FIG. 4). These two newly acquired data sets are then used by the LAS Fiducial Alignment Subsystem **570** to track the motion and alignment of local tissue.

**[0044]** FIG. 4 is a schematic diagram of the LAS electrodes used to derive the fiducial quaternion and position reference. The position of the first current electrode **101** defines the LAS Current Fiducial Position **180**. Current electrode **101** along with current electrodes **103** and **105** form a fiducial reference triangle. The LAS Current Fiducial Quaternion **160** (shown in FIG. 5) is determined by the vector normal to the triangle plane and the rotation of the triangle with respect to the patient axis Y, projected into the fiducial plane.

**[0045]** The fiducial triangle orientation FO, is calculated by using basic trigonometry in equation (9).

$$F0 = (\text{LAS Electrode 103 Position}) - (\text{LAS Electrode 101 Position}) / 2 - (\text{LAS Electrode 105 Position}) / 2 \quad (9)$$

**[0046]** Two additional fiducial reference vectors, F1 and F2, are needed to determine the fiducial triangle and are derived from equations (10) and (11).

$$F1 = (\text{LAS Electrode 101 Position}) - (\text{LAS Electrode 105 Position}) \quad (10)$$

$$F2 = (\text{LAS Electrode 103 Position}) - (\text{LAS Electrode 105 Position}) \quad (11)$$

**[0047]** The cross product of vectors F1 and F2, shown in equation (12), is then normalized by equation (13) to give the LAS Fiducial Vector **260** as shown in FIG. 4.

$$v_s = (F1 \times F2) / |F1| |F2| \quad (12)$$

$$v = v_s / |v_s| \quad (13)$$

**[0048]** The LAS Fiducial Vector **260** is then crossed in equation (14) with the patient axis Y to give a reference vector in the fiducial triangle plane, F3, which is then used in equation (15) to calculate the LAS Fiducial Rotation Angle  $\alpha$  **270**.

$$F3 = (v \times (Y\text{-Axis})) \quad (14)$$

$$\alpha = \text{arc cosine}(F3 \cdot F0 / |F0|) \quad (15)$$

**[0049]** The LAS Current Fiducial Quaternion **160** of FIG. 5 is then calculated by the standard method to give the four-element quaternion vector shown in equation (16).

$$Q = \{v \cos(\alpha/2), \sin(\alpha/2)\} = \langle v_x \cos(\alpha/2), v_y \cos(\alpha/2), v_z \cos(\alpha/2), \sin(\alpha/2) \rangle \quad (16)$$

**[0050]** FIG. 5 is a schematic diagram of the patient fiducial alignment quaternions and fiducial reference displacement used to normalize patient motion to the reference position and orientation. The LAS Reference Fiducial Quaternion **170** is set to the LAS Current Fiducial Quaternion **160** when the patient is at the reference position. Also when the patient is at the reference position, the LAS Current Fiducial Position **180** becomes the LAS Reference Fiducial Position **190**. Any



deviation from this reference position and orientation may be used to normalize the system vectors between the new patient position and orientation, and the reference position and orientation.

**[0051]** Given the LAS Reference Fiducial Quaternion **170**, LAS Reference Fiducial Position **190**, LAS Current Fiducial Quaternion **160**, and the LAS Current Fiducial Position **180**, any vector **V** may be referenced back to the reference orientation by the standard quaternion algebra.

**[0052]** Vector **V** is defined in three dimensions with respect to the fourth by appending zero to the vector in equation (17). This is done whenever multiplying a vector by a quaternion using quaternion algebra.

$$V = \langle x, y, z, 0 \rangle \tag{17}$$

**[0053]** Referencing **V** in current space to the reference orientation requires that it is rotated in the opposite direction by the current quaternion and rotated by the reference. The standard rotation equation for the rotation of a vector by a quaternion is given in equation (18),

$$v' = qvq^* \tag{18}$$

where  $q^*$  is the conjugate of the unit quaternion  $\langle -x, -y, -z, w \rangle$ . To un-rotate the vector by **Q** then re-rotate the vector by  $Q_r$ , the standard form is given in equation (19) below.

$$V_{ref} = Q_r Q^* v Q Q_r^* \tag{19}$$

**[0054]** Referencing a vector **V** in reference space to the current orientation is done similarly in equation (20).

$$V = Q Q_r^* V_{ref} Q_r Q^* \tag{20}$$

**[0055]** Converting a position in current space to reference space is done by rotating the relative position vector and then accounting for the displacement of the LAS Fiducial Position **220**. The relative position vector, **Prel**, is calculated with respect to the LAS Current Fiducial Position **180** in equation (21) below.

$$Prel = P - (\text{LAS Current Fiducial Position}) \tag{21}$$

**[0056]** **Prel** is then rotated into reference space by equation (22).

$$Prel' = Q_r Q^* Prel Q Q_r^* \tag{22}$$

**[0057]** **P'** is then calculated in equation (23) by adding the reference position and subtracting the fiducial position change from the result obtained by equation (22).

$$P' = Prel' + \text{LAS Fiducial Reference Pos} - (\text{LAS Current Fiducial Position} - \text{LAS Fiducial Reference Position}) \tag{23}$$

**[0058]** **P'** will reflect the same relative position on the un-rotated patient as **P** in the current patient orientation.

**[0059]** To reference a position in reference space to current space, the same method is applied. The relative position vector **Prel** is calculated with respect to the LAS Reference Fiducial Position **190** in equation (24) below.

$$Prel = P - (\text{LAS Reference Fiducial Position}) \tag{24}$$

**[0060]** **Prel** is then rotated into current space by equation (25).

$$Prel' = Q Q_r^* Prel Q_r Q^* \tag{25}$$

**[0061]** **P'** is then calculated much like before by adding the reference position and subtracting the fiducial position change to the resultant of equation (25) as shown in equation (26).

$$P' = Prel' + \text{LAS Current Fiducial Position} - (\text{LAS Reference Fiducial Position} - \text{LAS Current Fiducial Position}) \tag{26}$$

**[0062]** **P'** will reflect the same relative position on the rotated patient as **P** in the reference patient orientation.

**[0063]** Once all the equations above have been solved by the Fiducial Alignment Subsystem **570**, the operating physician can then track the movement of the LAS device in its relation to the surrounding patient operation volume. This feature of the device is extremely useful in circumstances where the LAS must be employed in an invasive surgery within a beating heart or other similar moving tissue. The fiducial alignment system allows the motion of the moving tissue to be tracked and anticipated and therefore, movement of the patient or the surrounding operation volume does not interfere or complicate the physician's procedure.

**[0064]** FIG. 6 is a block diagram of a CGCI unit **1500** that incorporates the Lorentz-Active Sheath into a Catheter Guidance Control and Imaging (CGCI) system. This combination provides a LAS reference coordinate set to the CGCI fiducial alignment system **412** and data filtration routines of the CGCI operation console **413** in order to stabilize the undesired motion of the catheter tip **377** and align it within the patient **1**.

**[0065]** The CGCI unit **1500** which includes a magnetic chamber along with an adaptive regulator, a joystick haptic device for operator control, and a method for detecting a magnetically-tipped catheter is described, for example in U.S. patent application Ser. No. 16/697,690 titled "Method and Apparatus for Controlling Catheter Positioning and Orientation" and is hereby incorporated by reference. A detailed description of the preferred embodiments using the Lorentz Active Sheath (LAS **375**) in combination with the magnetic chamber forming the CGCI **1500** is noted by U.S. patent application Ser. No. 10/621,196 "Apparatus for Catheter, Guidance, Control, and Imaging", U.S. patent application Ser. No. 11/331,781, "System and Method for Controlling Movement of a Surgical Tool", U.S. application Ser. No. 11/331,994, "Apparatus and Method for Generating a Magnetic Field", U.S. application Ser. No. 11/331,485, "System and Method for Magnetic Catheter tip," "System and Method for Radar Assisted Catheter Guidance and Control" U.S. application Ser. No. 10/690,472, titled, "System and Method for Radar Assisted Catheter Guidance and Control," U.S. application Ser. No. 11/140,475, "Apparatus and Method for Shaped Magnetic Field Control for Catheter, Guidance, Control and Imaging," U.S. application Ser. No. 11/362,542, "Apparatus for Magnetically Deployable Catheter with Mosfet Sensors and Method for Mapping and Ablation.", hereby incorporated by reference. The above magnetic navigation system **1500** is further augmented by the Lorentz Active Sheath **375** so as to render the error generated by the dynamic movements of the mural to be filtered using the sensory ring **11**, **12**, **13**, **14**, and **15** and the computer software algorithm forming a filtering technique such as, for example, a Kalman Filter.

**[0066]** In the present embodiment, the catheter tip **377** and Lorentz-Active Sheath **375** are being operated within the patient **1**. The CGCI imaging and synchronization unit **701** detects the actual position (AP) **902** of the catheter tip **377** and the position and orientation of the LAS **375**. The CGCI imaging and synchronization unit **701** filters and aligns the data and specifies a desired position (DP) **903** for the cathete **377** under operator input through the CGCI virtual tip **500**.

The CGCI catheter detection unit **411** remotely senses the actual position and orientation **902** of the catheter tip **377** and the LAS **375** with respect to the CGCI global coordinate system **100**. The LAS provides the CGCI fiduciary alignment system **412** with an LAS current fiducial quaternion **160** and an LAS reference fiducial quaternion **170** to normalize the AP **902** under patient rotation and translation within the CGCI global coordinate system **100**. The position and orientation of the LAS current fiducial quaternion **160** establishes the patient tissue reference position and orientation within the global coordinate system **100**. The position and orientation of the LAS reference fiducial quaternion **170** is initialized at a known tissue position and orientation to normalize LAS **375** and catheter tip **377** coordinates to medical data and models, such as those provided by the external medical systems and signals **502**. The desired position **903** is then specified in reference to such medical data and models as to allow the CGCI controller **501** to regulate between the actual position **902** and the desired position **903** within the local patient coordinate frame **200**.

**[0067]** The LAS filtered average positions **10** are used by the CGCI operation console **413** to remove any undesired catheter tip motion due to the motion of the distal end of the LAS.

**[0068]** Under dynamic variables, such as mechanical contractions and repolarization of the heart muscle, the CGCI filtering of the catheter tip motion becomes a dominant concern. The CGCI fiducial alignment system **412** acts to filter the dynamic motion of the LAS current fiducial quaternions by limiting the fiducial alignments system's response to gross patient motion while at the same time not interfering with the use of the LAS as a QRS regiments filter for the actual position **902** of the catheter tip.

**[0069]** In the absence of dynamic variables, such as surgery in the brain, the CGCI fiducial alignment system **412** will dominate the normalization of the incoming AP values so as to maintain a precise alignment between the sensed positions, tissue, and acquired data models.

**[0070]** Many alterations and modifications may be made by those having ordinary skill in the art without departing from the spirit and scope of the invention. Therefore, it must be understood that the illustrated embodiment has been set forth only for the purposes of example and that it should not be taken as limiting the invention as defined by the following invention and its various embodiments.

**[0071]** For example, one skilled in the art may choose to imbed a large plurality of detection system-sensitive electrodes, such as ten or more, along the shaft of the LAS **10** to provide an even more accurate and precise motion compensation filter and fiducial alignment system. Additionally, one skilled in the art may also choose to use alternate devices other than electrodes to signal the position of the LAS device or use alternate means of receiving the signals other than a position detection system.

**[0072]** Therefore, it must be understood that the illustrated embodiment has been set forth only for the purposes of example and that it should not be taken as limiting the invention as defined by the following claims. For example, notwithstanding the fact that the elements of a claim are set forth below in a certain combination, it must be expressly understood that the invention includes other combinations of fewer, more or different elements, which are disclosed in above even when not initially claimed in such combinations. A teaching that two elements are combined in a claimed combination is

further to be understood as also allowing for a claimed combination in which the two elements are not combined with each other, but may be used alone or combined in other combinations. The excision of any disclosed element of the invention is explicitly contemplated as within the scope of the invention.

**[0073]** The words used in this specification to describe the invention and its various embodiments are to be understood not only in the sense of their commonly defined meanings, but to include by special definition in this specification structure, material or acts beyond the scope of the commonly defined meanings. Thus if an element can be understood in the context of this specification as including more than one meaning, then its use in a claim must be understood as being generic to all possible meanings supported by the specification and by the word itself.

**[0074]** The definitions of the words or elements of the following claims are, therefore, defined in this specification to include not only the combination of elements which are literally set forth, but all equivalent structure, material or acts for performing substantially the same function in substantially the same way to obtain substantially the same result. In this sense it is therefore contemplated that an equivalent substitution of two or more elements may be made for any one of the elements in the claims below or that a single element may be substituted for two or more elements in a claim. Although elements may be described above as acting in certain combinations and even initially claimed as such, it is to be expressly understood that one or more elements from a claimed combination can in some cases be excised from the combination and that the claimed combination may be directed to a subcombination or variation of a subcombination.

**[0075]** Insubstantial changes from the claimed subject matter as viewed by a person with ordinary skill in the art, now known or later devised, are expressly contemplated as being equivalently within the scope of the claims. Therefore, obvious substitutions now or later known to one with ordinary skill in the art are defined to be within the scope of the defined elements.

**[0076]** The claims are thus to be understood to include what is specifically illustrated and described above, what is conceptually equivalent, what can be obviously substituted and also what essentially incorporates the essential idea of the invention.

What is claimed is:

1. A medical apparatus to be used during an invasive surgery comprising:

- a sheath capable of deploying a multitude of medical tools and adapted for insertion into the body of a patient;
- at least one electrode coupled to the sheath;
- a position detection system coupled to the sheath capable of sensing said electrode coupled to the sheath;
- a computer software program coupled to the position detection system capable of compensating for the unwanted motion of the sheath by subtracting said sheath motion from the motion of the sheath-hosted tool;
- and
- a computer software program coupled to the position detection system capable of tracking the sheath's progress through the surrounding tissue of a patient by means of fiducial alignment.

2. The apparatus of claim 1 further comprising a plurality of electrodes coupled to the sheath.

3. The apparatus of claim 1 wherein the computer software program capable of compensating for unwanted sheath motion further comprises a subsystem coupled to the position detection system for averaging the electrode position.

4. The apparatus of claim 3 wherein the computer software program capable of compensating for unwanted sheath motion further comprises a subsystem for calculating the electrode position error coupled to both the position detection system and the subsystem for averaging the electrode position.

5. The apparatus of claim 4 wherein the computer software program capable of compensating for unwanted sheath motion further comprises a subsystem that compensates for tool motion coupled to the subsystem for calculating the electrode position error.

6. The apparatus of claim 1 wherein the computer software program capable of tracking the sheath's progress through the surrounding tissue of a patient by means of fiducial alignment further comprises a subsystem coupled to the position detection system that generates a fiducial quaternion.

7. The apparatus of claim 6 wherein the computer software program capable of tracking the sheath's progress through the surrounding tissue of a patient by means of fiducial alignment further comprises a fiducial alignment subsystem coupled to the subsystem that generates a fiducial quaternion.

8. The apparatus of claim 1 further comprising a means for incorporating the device into a catheter guidance control and imaging system.

9. A method of tracking and compensating for medical tool motion during an invasive surgery within the body a patient comprising:

inserting a medical sheath capable of deploying a multitude of medical tools comprising at least one electrode coupled to the sheath into an incision or other body orifice of the patient;

detecting the position and orientation of the electrode using a position detection system;

sending the data collected by the position detection system through a series of computer software subsystems that produce from a series of calculations a motion compensation filter for the sheath-hosted tool; and

sending the data collected by the position detection system through a series of computer software subsystems that track the motion of the sheath and sheath-hosted tool by a means of fiducial alignment.

10. The method of claim 9 wherein detecting the position and orientation of the electrode using a position detection system further comprises incorporating the device into a catheter guidance control and imaging system.

11. The method of claim 9 further comprising inserting a medical sheath capable of deploying a multitude of medical tools comprising a plurality of electrodes coupled to the sheath.

12. The method of claim 9 wherein sending the data collected by the position detection system through a series of computer software subsystems that produce from a series of calculations a motion compensation filter for the sheath-hosted tool further comprises providing a reference position and orientation for motion compensation for sheath-hosted tools by an average position and orientation of the sheath's distal end being continuously determined with respect to several measured positions over a set time period.

13. The method of claim 9 wherein sending the data collected by the position detection system through a series of

computer software subsystems that produce from a series of calculations a motion compensation filter for the sheath-hosted tool further comprises providing a position and orientation error value by defining the sheath's motion with respect to an average position and orientation of the sheath.

14. The method of claim 9 wherein sending the data collected by the position detection system through a series of computer software subsystems that produce from a series of calculations a motion compensation filter for the sheath-hosted tool further comprises providing a stable fiducial reference for a tool position control system of the position detection system by subtracting position error values from the motion of the sheath-hosted tool.

15. The method of claim 9 wherein sending the data collected by the position detection system through a series of computer software subsystems that track the motion of the sheath and sheath-hosted tool by a means of fiducial alignment further comprises employing the electrode to determine a six-degree of freedom reference frame.

16. The method of claim 9 wherein sending the data collected by the position detection system through a series of computer software subsystems that track the motion of the sheath and sheath-hosted tool by a means of fiducial alignment further comprises employing a six-degree of freedom reference frame to track changes in a patient's or local organ's orientation.

17. The apparatus of claim 3 wherein the subsystem for averaging the electrode position further comprises a means for determining the average position of the distal electrode coupled to the sheath.

18. The apparatus of claim 3 wherein the subsystem for averaging the electrode position further comprises a means for determining the average exit vector of the deployed medical tool as it leaves the distal end of the sheath.

19. The method of claim 9 wherein sending the data collected by the position detection system through a series of computer software subsystems that track the motion of the sheath and sheath-hosted tool by a means of fiducial alignment further comprises a means for determining the average position of the distal electrode coupled to the sheath.

20. The method of claim 9 wherein sending the data collected by the position detection system through a series of computer software subsystems that track the motion of the sheath and sheath-hosted tool by a means of fiducial alignment further comprises a means for determining the average exit vector of the deployed medical tool as it leaves the distal end of the sheath.

21. A medical apparatus to be used during an invasive surgery comprising:

a sheath capable of deploying a multitude of medical tools and adapted for insertion into the body of a patient;

at least one electrode coupled to the sheath;

means for compensating for the unwanted motion of the sheath from the desired motion of the sheath-hosted tool; and

means for tracking the sheath and sheath-hosted tool through the surrounding tissue of a patient by means of fiducial alignment.

22. The apparatus of claim 21 wherein the sheath capable of deploying a multitude of medical tools and adapted for insertion into the body of a patient further comprises a plurality of electrodes coupled to the sheath.





US 20120289822A1

(19) **United States**

(12) **Patent Application Publication**  
**Shachar et al.**

(10) **Pub. No.: US 2012/0289822 A1**

(43) **Pub. Date: Nov. 15, 2012**

(54) **APPARATUS AND METHOD FOR  
LORENTZ-ACTIVE SHEATH DISPLAY AND  
CONTROL OF SURGICAL TOOLS**

(75) **Inventors:** **Yehoshua Shachar**, Santa Monica, CA (US); **Bruce Marx**, Ojai, CA (US); **Leslie Farkas**, Ojai, CA (US); **David Johnson**, West Hollywood, CA (US); **Laszlo Farkas**, Ojai, CA (US)

(73) **Assignee:** **MAGNETECS, INC.**, Inglewood, CA (US)

(21) **Appl. No.:** **13/450,148**

(22) **Filed:** **Apr. 18, 2012**

**Related U.S. Application Data**

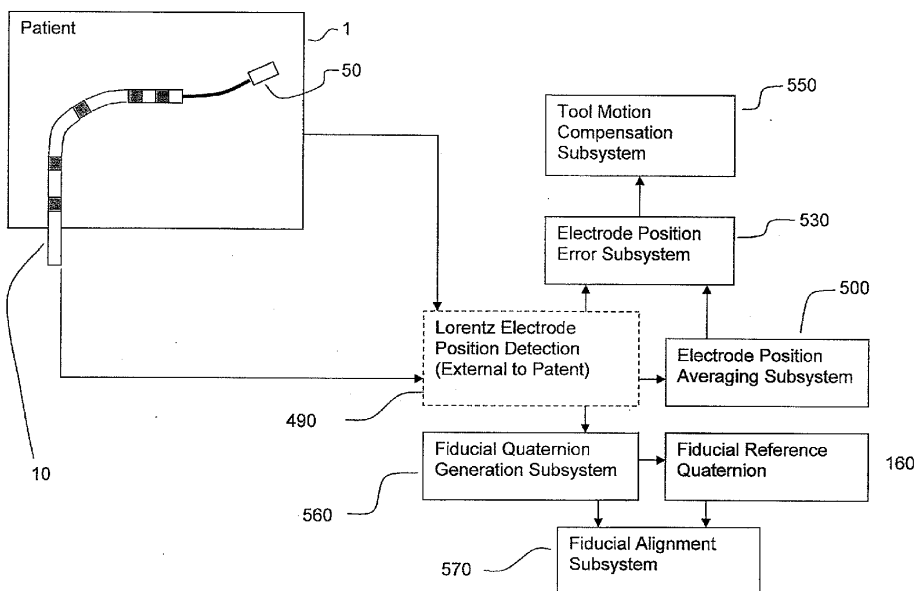
(63) Continuation of application No. 12/099,079, filed on Apr. 7, 2008, now abandoned.

**Publication Classification**

(51) **Int. Cl.**  
*A61B 1/32* (2006.01)  
*A61B 6/00* (2006.01)  
(52) **U.S. Cl.** ..... **600/424; 600/202**

(57) **ABSTRACT**

The Lorentz-Active Sheath (LAS) serves as a conduit for other medical devices such as catheters, balloons, biopsy needles, etc. The sheath is inserted through a vein or other body orifice and is guided into the area of the patient where the operation is to be performed. The position and orientation of the LAS is tracked via an industry standard position detection system which senses electrical signals that are emitted from several electrodes coupled to the LAS. The signals received from the LAS are used to calculate an accurate and reliable assessment of the actual position of the LAS within the patient. The electrode signals also serve to create a reference frame which is then used to act as a motion compensation filter and fiducial alignment system for the movement of the LAS-hosted medical tool.









INTERNATIONAL FILINGS FOR:  
*Apparatus and Method for  
Lorentz-Active Sheath Display  
and Control of Surgical Tools*

***INVENTOR: Yehoshua Shachar  
Bruce Marx  
Leslie Farkas  
David Johnson***





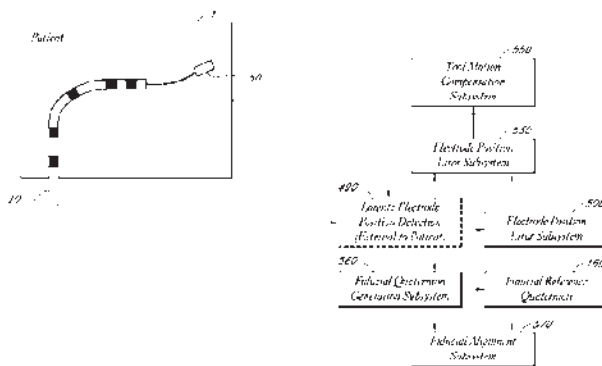
- (51) International Patent Classification:  
A61B 1/00 (2006.01)
- (21) International Application Number:  
PCT/US2009/039659
- (22) International Filing Date:  
6 April 2009 (06.04.2009)
- (25) Filing Language: English
- (26) Publication Language: English
- (30) Priority Data:  
12'099,079 7 April 2008 (07.04.2008) US
- (71) Applicant (for all designated States except US): **MAGNETECS, INC.** [US/US]: 10524 S. Ta Conega Blvd., Inglewood, CA 90304 (US).
- (72) Inventors: **SHACHAR, Yehoshua**; 2417 22nd Street, Santa Monica, California 90405 (US). **MARX, Bruce**; 1233 Avila Drive, Ojai, California 93023 (US). **FARKAS, Leslie**; 254 N. Amaz Street, Ojai, California 93023 (US). **JOHNSON, David**; 8450 Delongpre Avenue #6, West Hollywood, CA 90069 (US). **FARKAS, Laszlo**; 29 Taormina Lane, Ojai, California 93023 (US).
- (74) Agent: **DELANEY, Karoline, A.**; Knobbe, Martens, Olson & Bear, LLP, 2040 Main Street, 14th Floor, Irvine, CA 92614 (US).

- (81) Designated States (unless otherwise indicated, for every kind of national protection available): AE, AG, AL, AM, AO, AT, AU, AZ, BA, BB, BG, BH, BR, BW, BY, BZ, CA, CH, CN, CO, CR, CU, CZ, DE, DK, DM, DO, DZ, EC, EE, EG, ES, FI, GB, GD, GE, GI, GM, GT, HN, HR, HU, ID, IL, IN, IS, JP, KE, KG, KM, KN, KP, KR, KZ, LA, LC, LK, LR, LS, LT, LU, LY, MA, MD, ME, MG, MK, MN, MW, MX, MY, MZ, NA, NG, NI, NO, NZ, OM, PG, PH, PL, PT, RO, RS, RU, SC, SD, SE, SG, SK, SL, SM, ST, SV, SY, TJ, TM, TN, TR, TT, TZ, UA, UG, US, UZ, VC, VN, ZA, ZM, ZW.
- (84) Designated States (unless otherwise indicated, for every kind of regional protection available): ARIPO (BW, GH, GM, KE, LS, MW, MZ, NA, SD, SL, SZ, TZ, UG, ZM, ZW), Eurasian (AM, AZ, BY, KG, KZ, MD, RU, TJ, TM), European (AT, BE, BG, CH, CY, CZ, DE, DK, EE, ES, FI, FR, GB, GR, HR, HU, IE, IS, IT, LT, LU, LV, MC, MK, MT, NL, NO, PL, PT, RO, SE, SI, SK, TR), OAPI (BF, BJ, CF, CG, CI, CM, GA, GN, GQ, GW, ML, MR, NE, SN, TD, TG)

**Published:**  
with international search report (Art. 21(3))  
— before the expiration of the time limit for amending the claims and to be republished in the event of receipt of amendments (Rule 48.2(h))

(54) Title: APPARATUS AND METHOD FOR LORENTZ-ACTIVE SHEATH DISPLAY AND CONTROL OF SURGICAL TOOLS

FIG. 2



(57) Abstract: The Lorentz-Active Sheath (LAS) serves as a conduit for other medical devices such as catheters, balloons, biopsy needles, etc. The sheath is inserted through a vein or other body orifice and is guided into the area of the patient where the operation is to be performed. The position and orientation of the LAS is tracked via an industry standard position detection system which senses electrical signals that are emitted from several electrodes coupled to the LAS. The signals received from the LAS are used to calculate an accurate and reliable assessment of the actual position of the LAS within the patient. The electrode signals also serve to create a reference frame which is then used to act as a motion compensation filter and fiducial alignment system for the movement of the LAS-hosted medical tool.

02



WO 2009/126575 A1

(19)



Anmeldenummer:

Application Number: 9730100.6

Numéro de la demande :

02

Internationale Antrag an das  
Weltorganisation für geisties Eigentum unter der Nummer:

**PCT/US2009/039659**

International application submitted to the World Intellectual  
Property Organization under number:

**PCT/US2009/039659**

La demande internationale a présenté à l'Organisation  
mondiale de la propriété intellectuelle sous le numéro:

**PCT/US2009/039659**

02



Application Number: 200980110899.X

International application submitted to the World Intellectual  
Property Organization under number:

**PCT/US2009/039659**





03

U.S. PATENT OFFICE FILINGS FOR:  
*Method and Apparatus for Creating  
a High Resolution Map of the  
Electrical and Mechanical  
Properties of the Heart*

**INVENTOR: Yehoshua Shachar  
Bruce Marx  
Leslie Farkas  
David Johnson  
Lazlo Farkas**



(19) **United States**  
(12) **Patent Application Publication**  
**Shachar et al.**

(10) **Pub. No.: US 2009/0275828 A1**  
(43) **Pub. Date: Nov. 5, 2009**

(54) **METHOD AND APPARATUS FOR CREATING A HIGH RESOLUTION MAP OF THE ELECTRICAL AND MECHANICAL PROPERTIES OF THE HEART**

**Publication Classification**

(51) **Int. Cl.**  
*A61B 5/00* (2006.01)  
*A61B 5/053* (2006.01)  
(52) **U.S. Cl.** ..... **600/425; 600/509**  
(57) **ABSTRACT**

(75) **Inventors:** **Yehoshua Shachar**, Santa Monica, CA (US); **Bruce Marx**, Ojai, CA (US); **Laszlo Farkas**, Ojai, CA (US); **David Johnson**, West Hollywood, CA (US); **Leslie Farkas**, Ojai, CA (US)

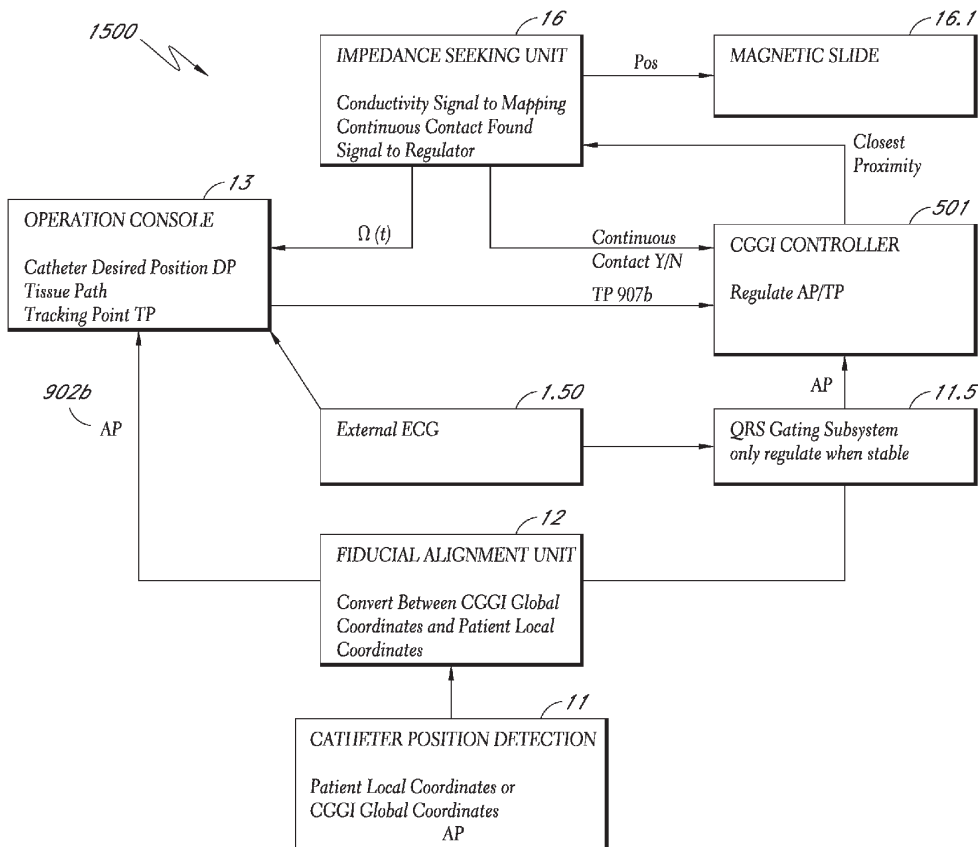
Correspondence Address:  
**KNOBBE MARTENS OLSON & BEAR LLP**  
**2040 MAIN STREET, FOURTEENTH FLOOR**  
**IRVINE, CA 92614 (US)**

(73) **Assignee:** **Magnetecs, Inc.**, Inglewood, CA (US)

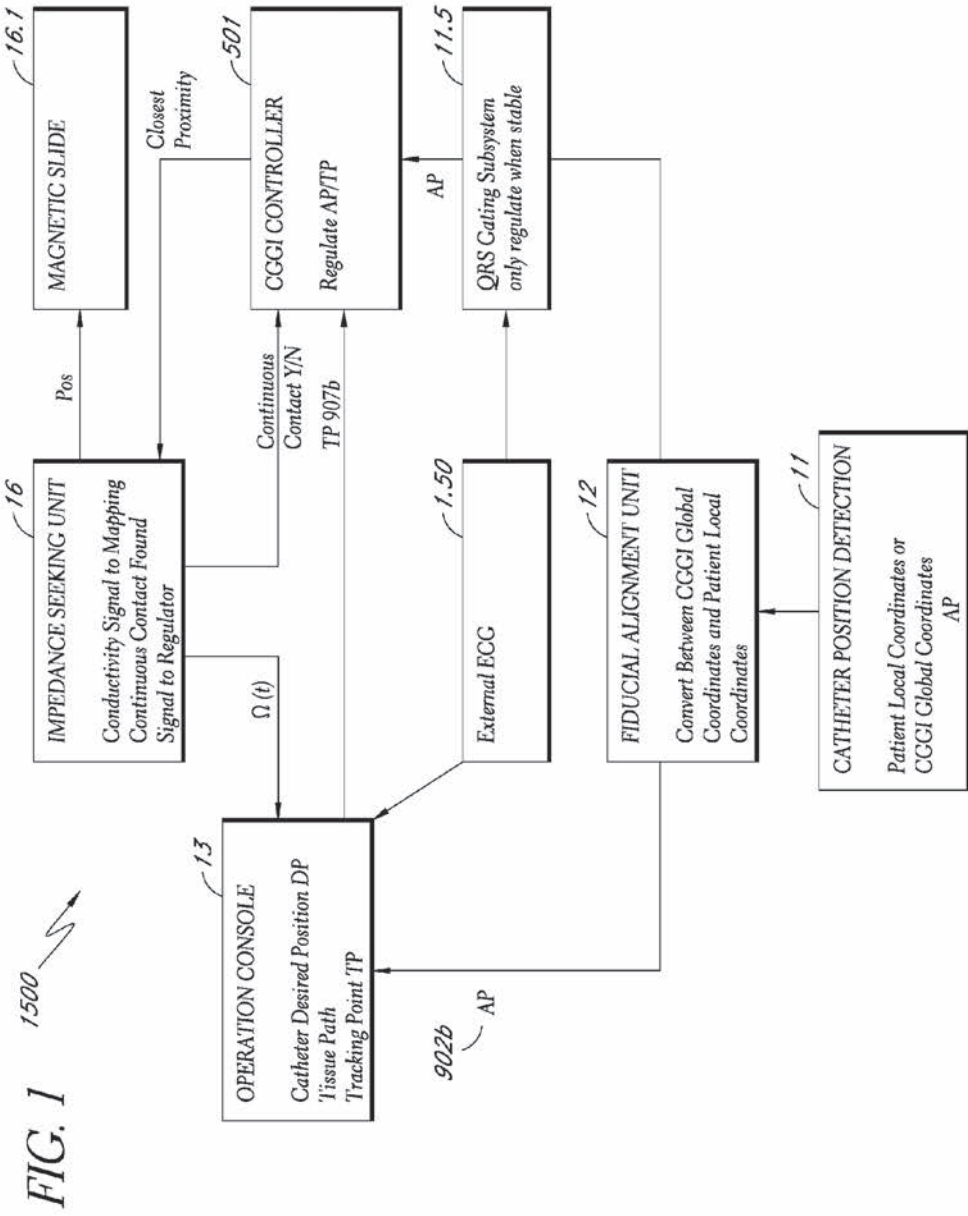
(21) **Appl. No.:** **12/113,804**

(22) **Filed:** **May 1, 2008**

A system method that tracks one or more points on the surface of a cardiac tissue throughout a cardiac cycle and collect various types of data points which are then subsequently used to generate a corresponding model of the tissue and display the model as a 3D color coded image is described. In one embodiment, the system determines the position and orientation of a distal tip of a catheter, manipulates the catheter tip so as to maintain constant contact between the tip and a region of cardiac tissue using the impedance method, acquires positional and electrical data of the tip-tissue configuration through an entire heartbeat cycle, repeats the measurements as many times as needed in different tissue regions, and forms a 3D color coded map displaying various mechanical and electrical properties of the heart using the acquired data.



03



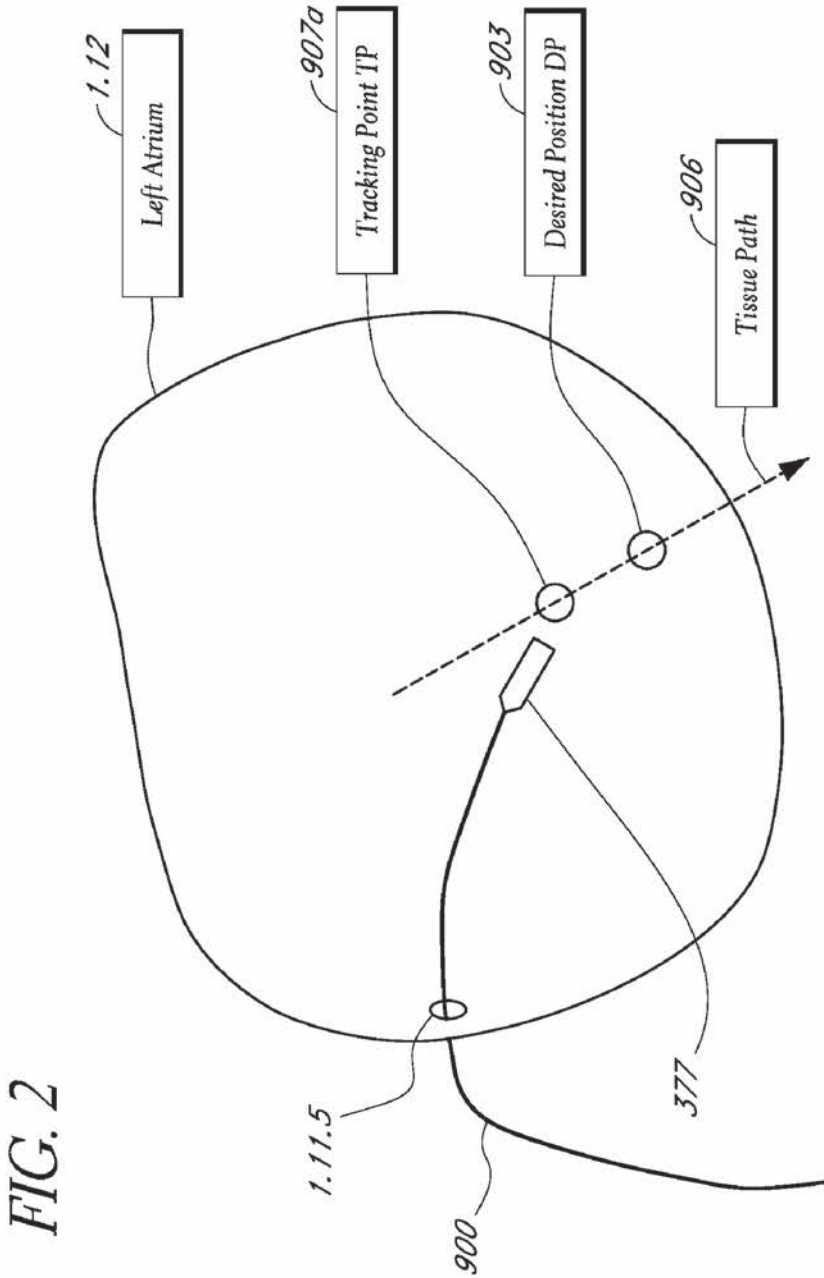


FIG. 2

03

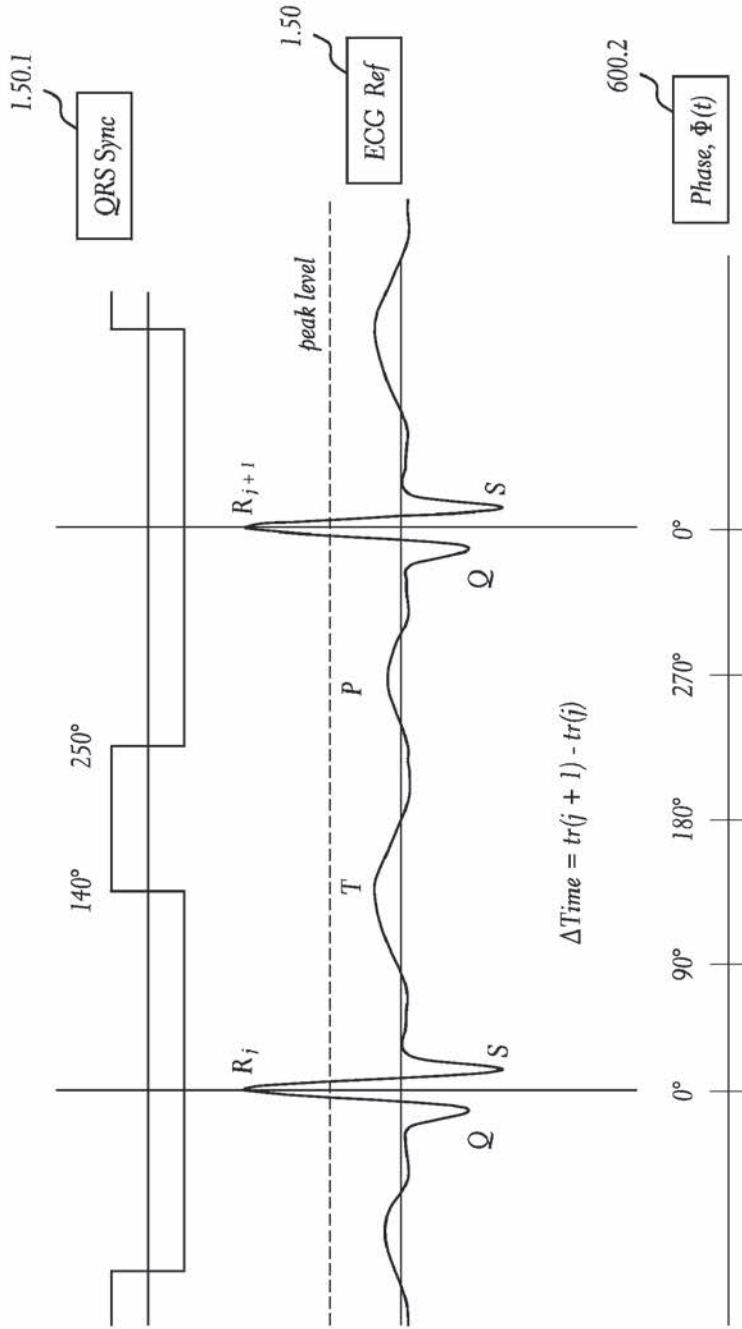


FIG. 3

03



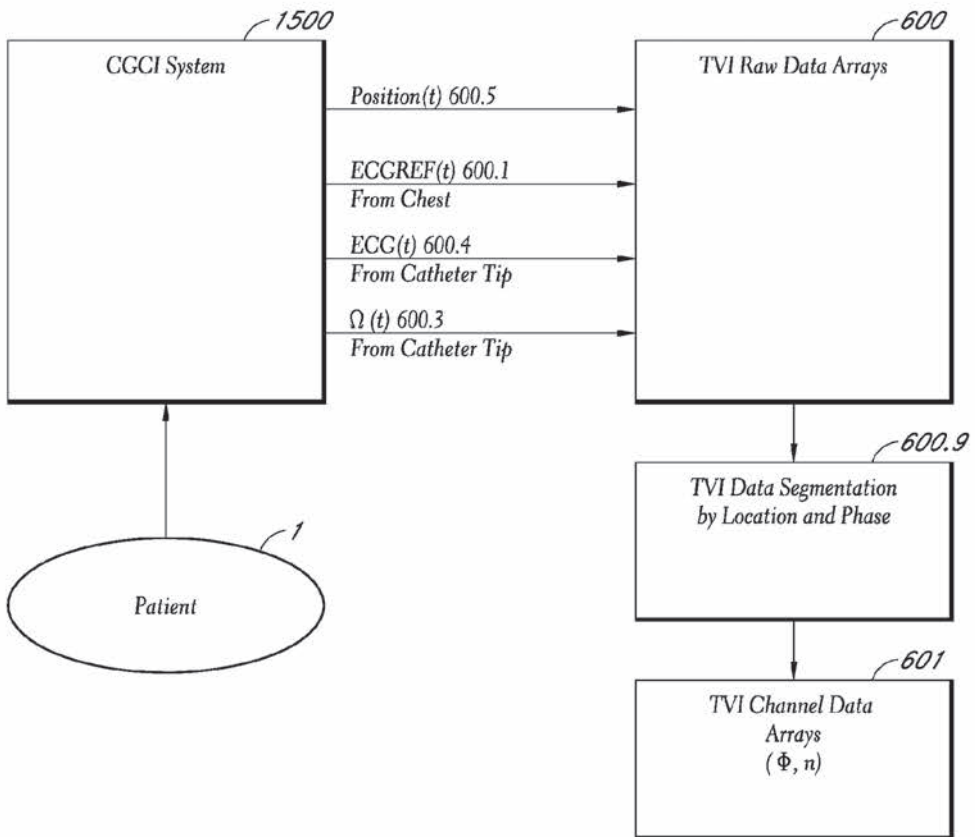


FIG. 4

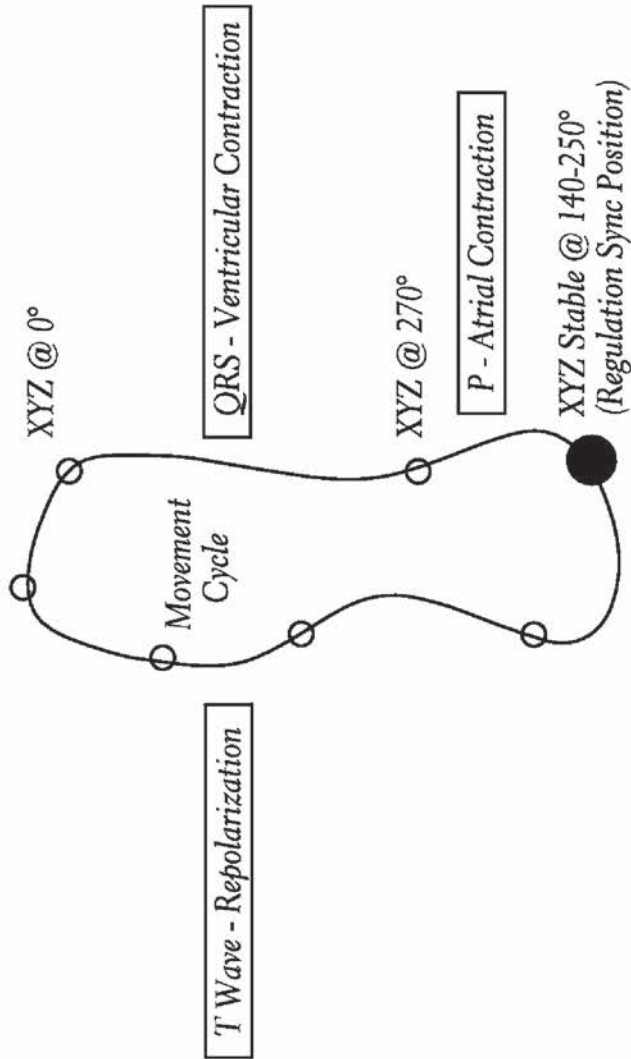


FIG. 5

03

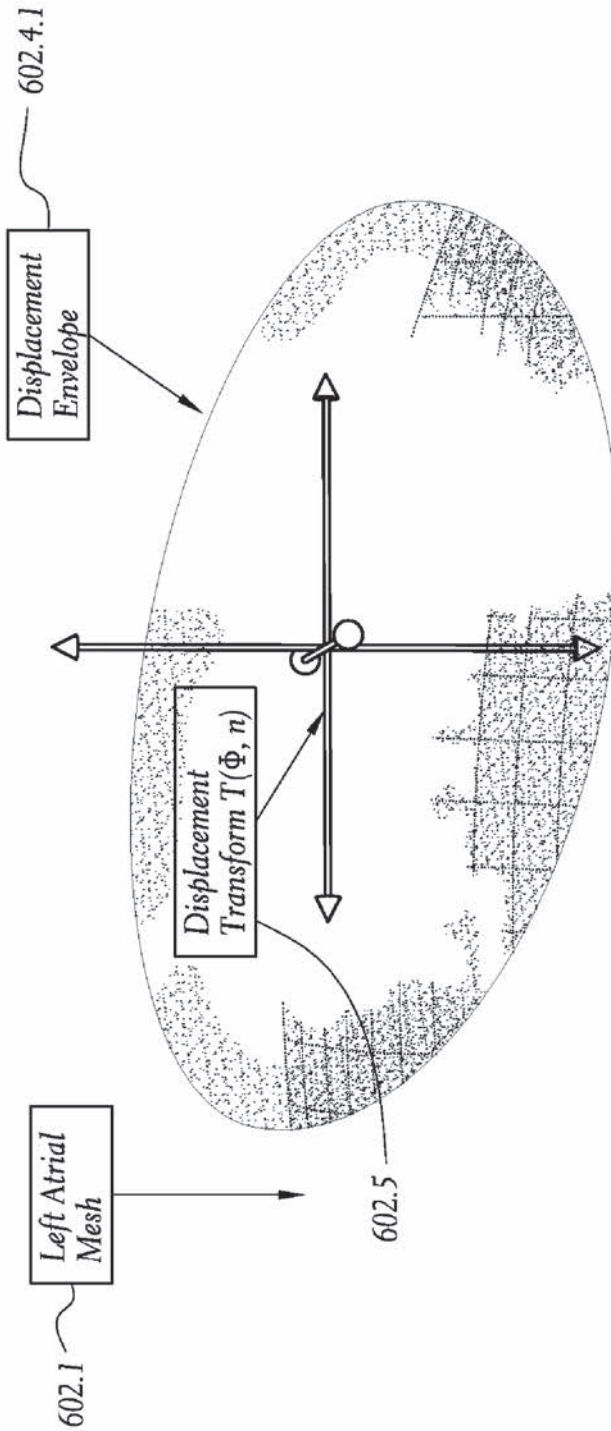


FIG. 6

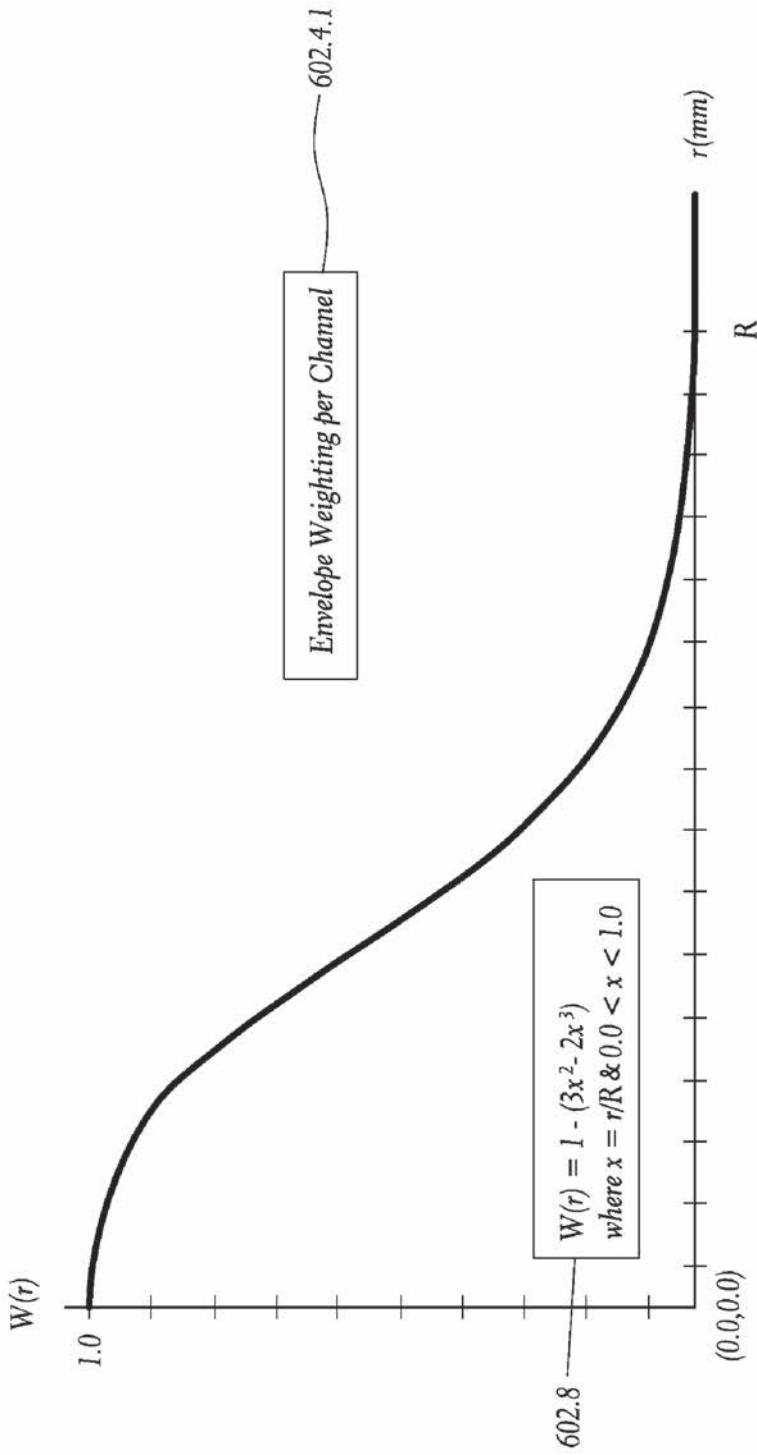
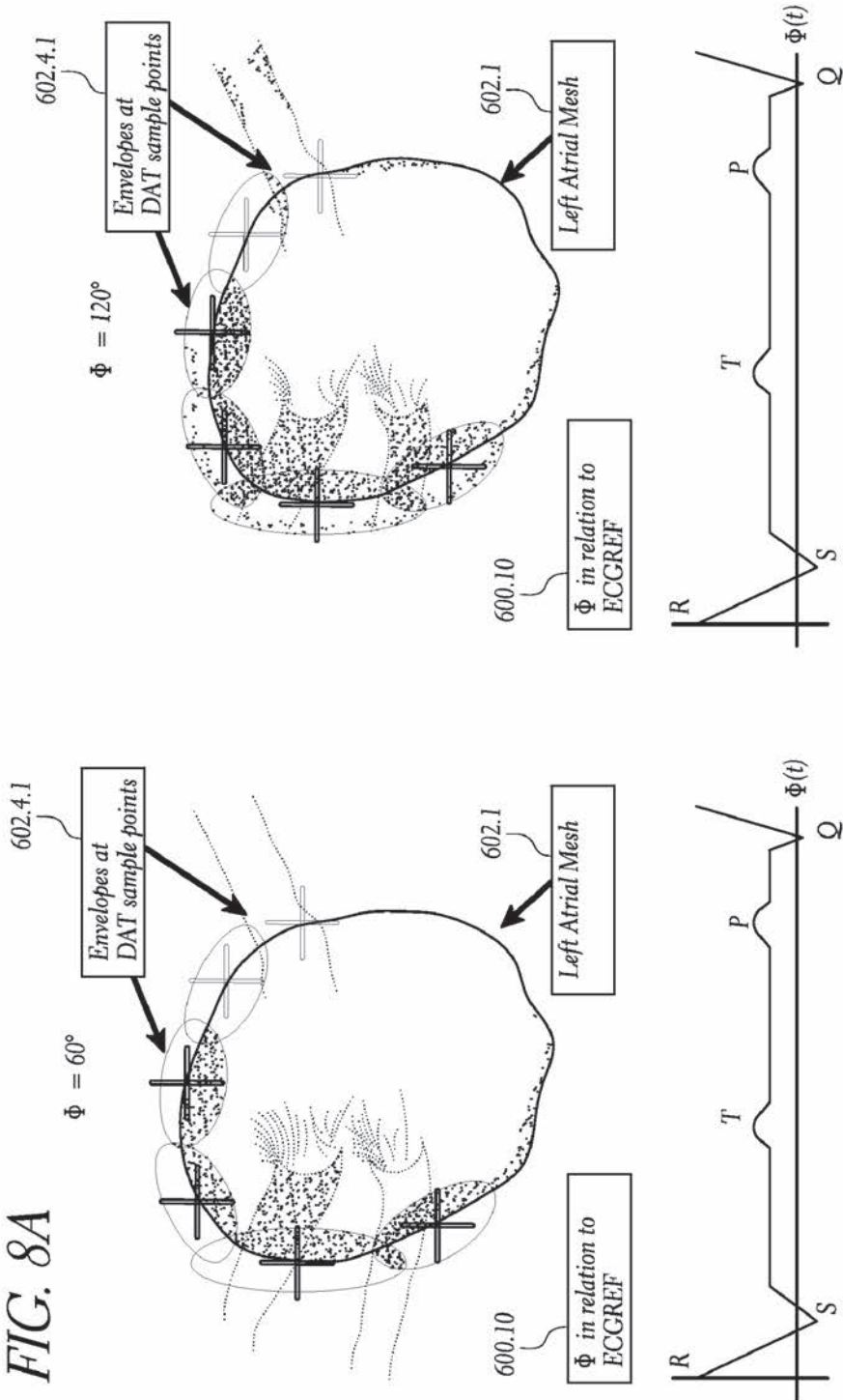


FIG. 7

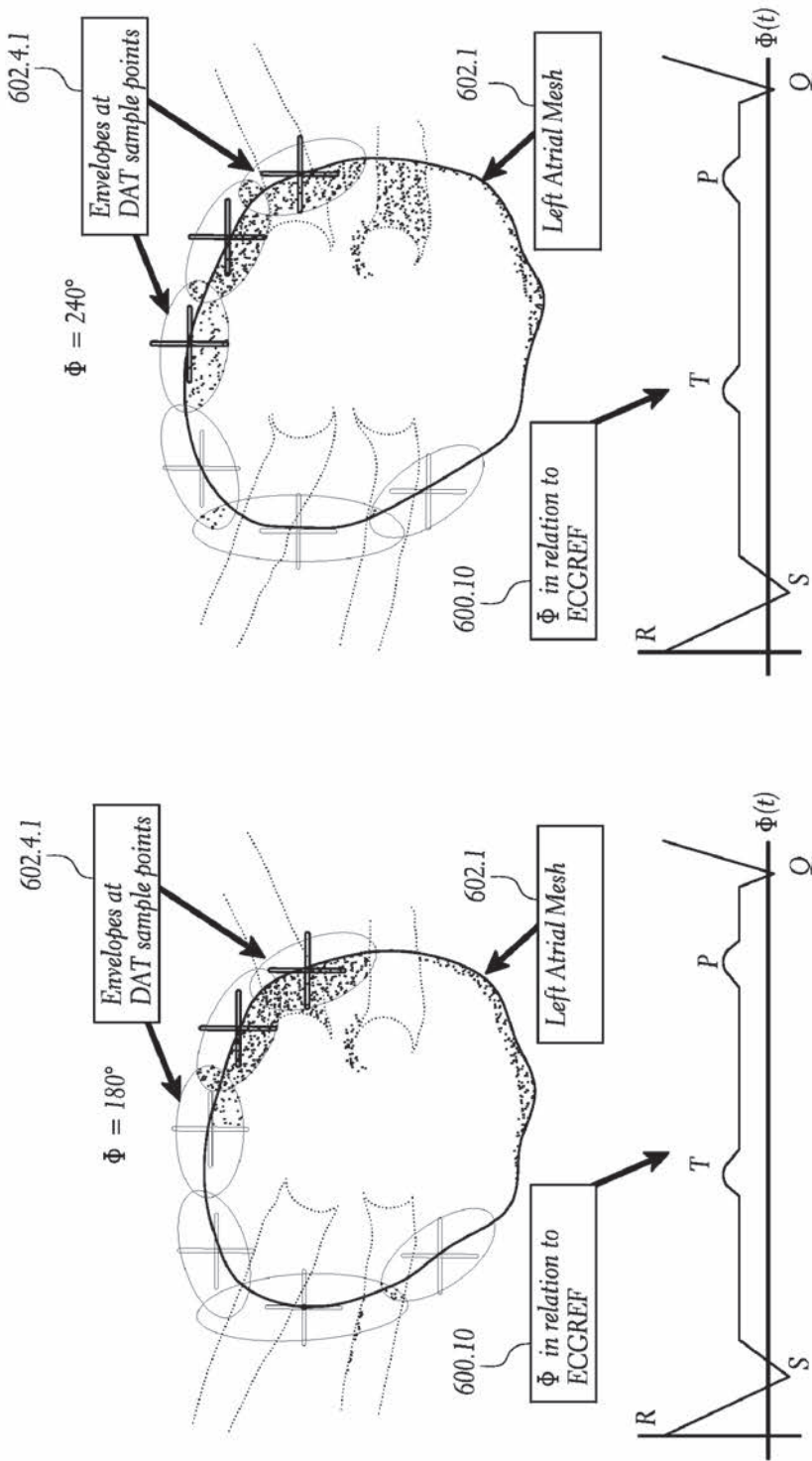
03



03

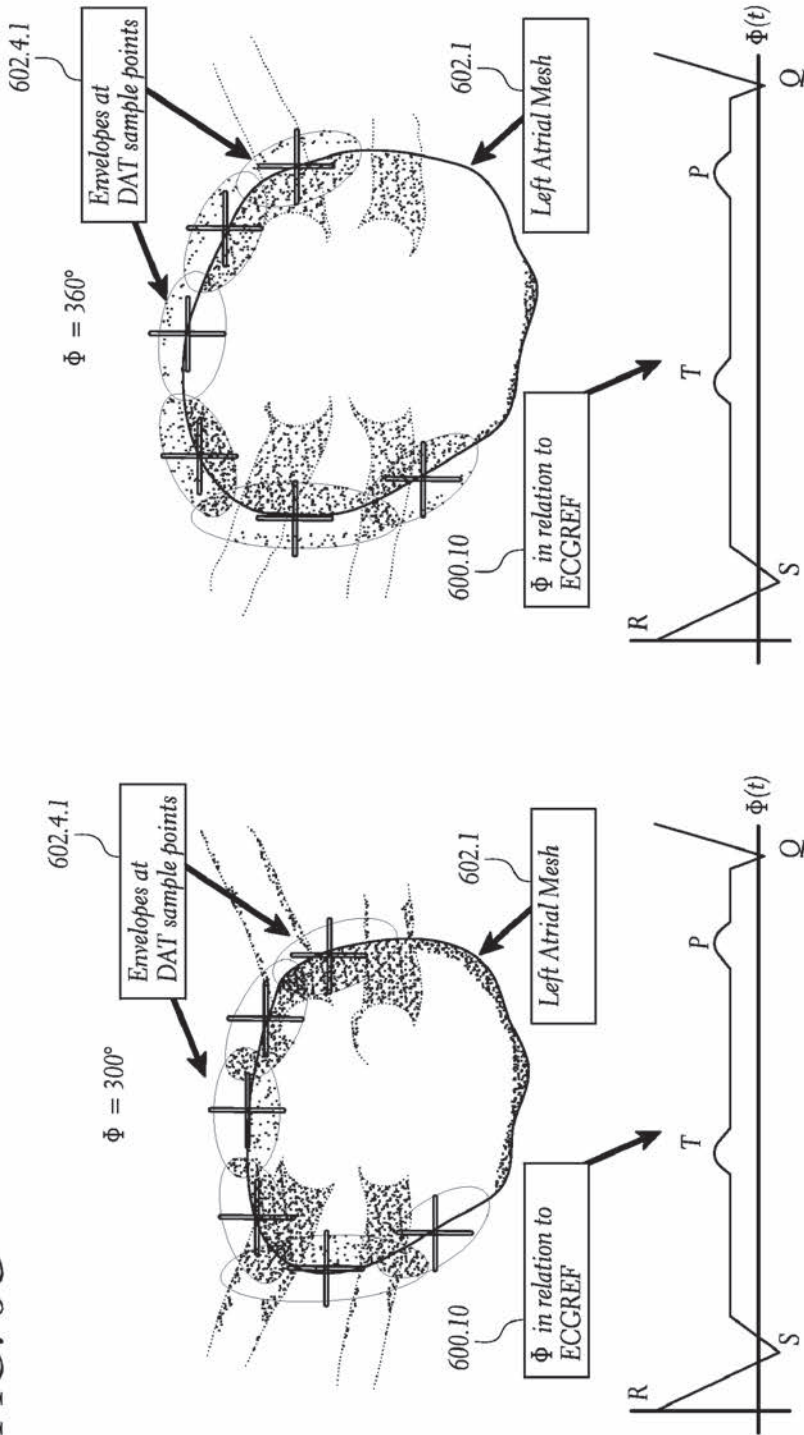


FIG. 8B



03

FIG. 8C



03

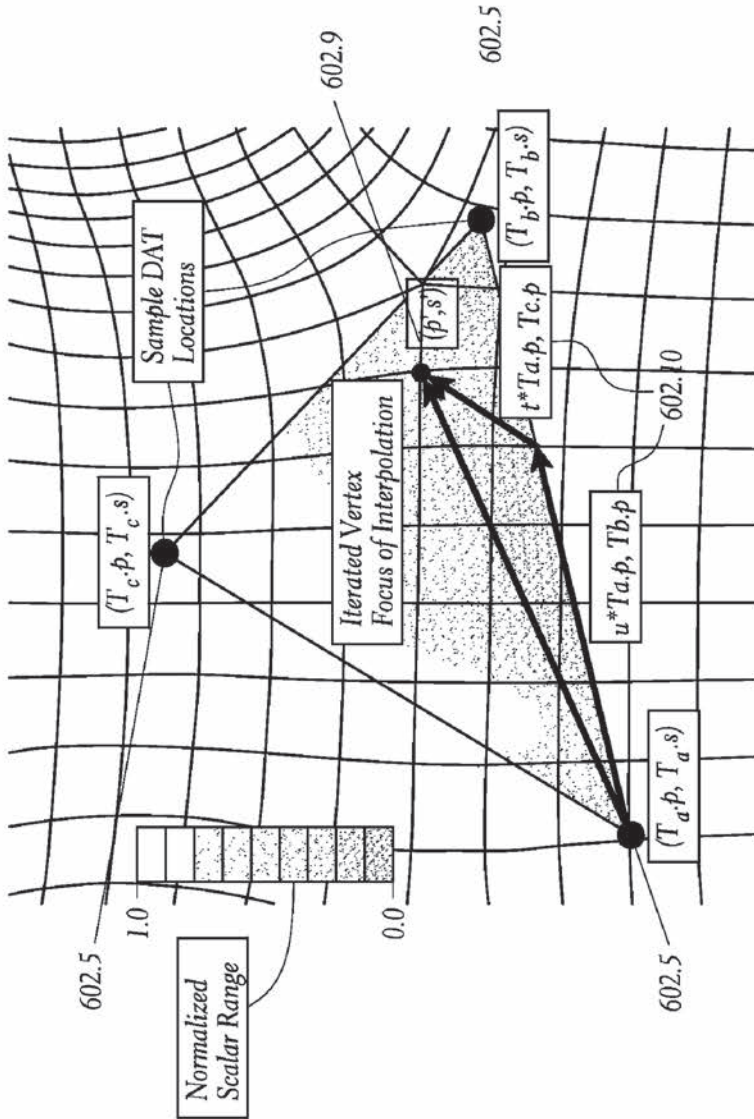


FIG. 9

03

03

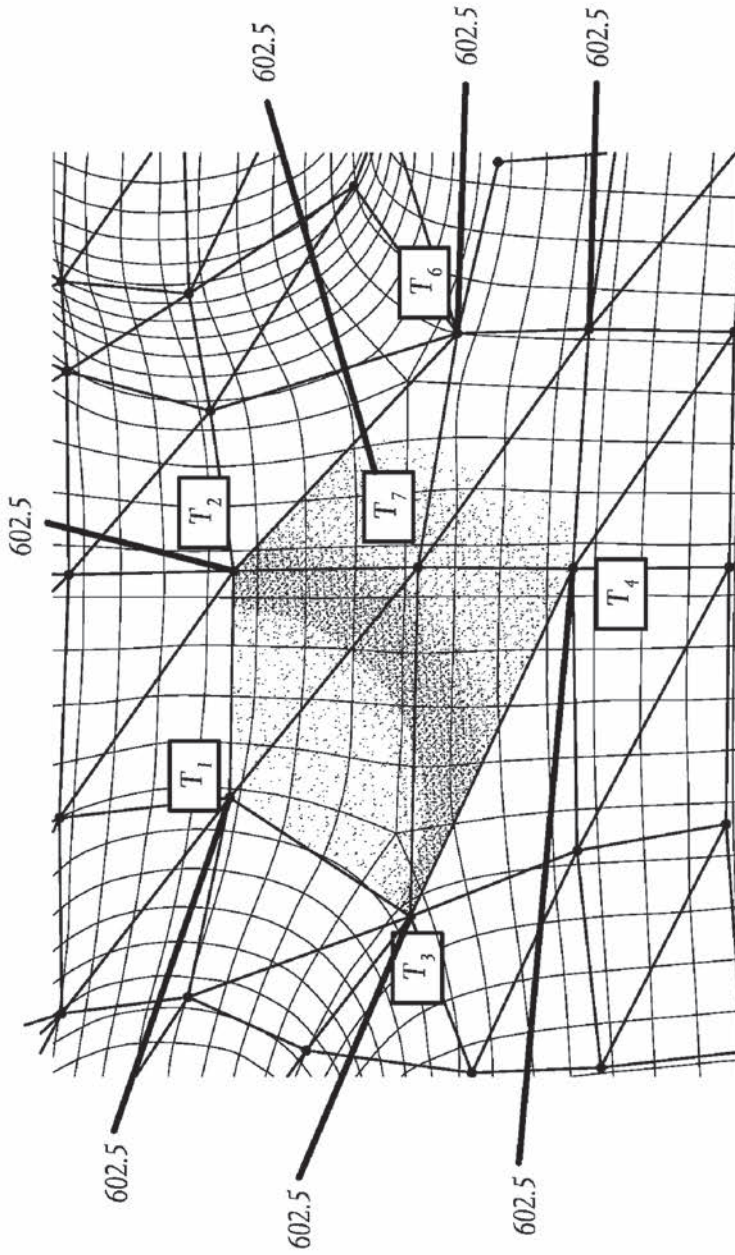


FIG. 10



## METHOD AND APPARATUS FOR CREATING A HIGH RESOLUTION MAP OF THE ELECTRICAL AND MECHANICAL PROPERTIES OF THE HEART

### BACKGROUND OF THE INVENTION

#### [0001] 1. Field of the Invention

[0002] The invention relates to the field of acquiring high-resolution clinical models of various properties of the heart using an invasive medical device and systems and methods for locating and tracking said invasive device.

#### [0003] 2. Description of the Related Art

[0004] Catheters and other invasive medical devices have long been used to perform electrical mapping of the heart. Typically, the catheter is inserted through a vein or other artery and is guided into the heart. Localization and mapping software operating from an outside system record the electrical and positional information of the distal tip of the catheter as it is guided about the volume of the heart chamber. The chamber walls are determined as the limit of acquired data, and the electrical properties associated with the presumed surface of the heart are mapped onto the generated single surface shell.

[0005] The prior art has primarily been concerned with acquiring a set of “data frames” of the tissue or organ that is to be modeled. These “data frames” are usually taken by an ultrasound or an MRI device and then the images obtained from them are used to interpolate or calculate various properties of the heart such as tissue velocity and strain rate for a specified region.

[0006] While prior methods are not without their successes, they are not without some serious disadvantages and limitations as well. For example, the prior art methods that employ a “data frame” acquisition procedure can not accurately track a point on the surface of a cardiac wall during a heartbeat.

[0007] Another disadvantage found in the prior art is the amount of error associated with such techniques and methods. For example, prior art that uses electrical localization distorts the positional information and limits the accuracy of the mechanical data. Additionally, prior art that applies geometric data to a previously sensed MRI and CT data inherently introduces approximations and errors that distort the mechanical data and average out specific irregularities that are extremely important when mapping biological tissue. Instead of tracking the position of a single point on the tissue surface, the prior art simply averages the point’s position as it travels through the cardiac cycle and displays it as a static location, thus decreasing its usefulness.

[0008] These and other problems are solved by a device and method that tracks one or more points on the surface of a cardiac tissue throughout a cardiac cycle and collect various types of data points which are then subsequently used to generate a corresponding model of the tissue and display the model as a 3D color coded image.

### SUMMARY OF THE INVENTION

[0009] In one embodiment the system determines the position and orientation of a distal tip of a catheter, manipulates the catheter tip so as to maintain constant contact between the tip and a region of cardiac tissue using the impedance method, acquires positional and electrical data of the tip-tissue con-  
tact through an entire heartbeat cycle, repeats the measurements as many times as needed in different tissue regions,

and forms a 3D color coded map displaying various mechanical and electrical properties of the heart using the acquired data.

[0010] In one embodiment, a magnetically-tipped catheter is inserted into a heart while under the QRS timing sequence (e.g., while undergoing the systole/diastole cycle). A catheter guidance and control imaging (CGCI) system guides the catheter around the heart by the generation of a shaped magnetic lobe.

[0011] The actual position, or AP, of the distal tip of the catheter is determined within the heart from either a third-party localization system, or from the CGCI’s own detection unit in small time increments to allow a relatively continuous view of the tip position which is traveling with the chamber wall. The position of the catheter tip is determined accurately without the need for data registration with known models. The CGCI catheter position detection unit determines the position and orientation of the magnetic tip by sensing the field about the tip using four hall-effect magnetic sensors. These sensors triangulate the position of the tip based on the strength of the magnetic field, and then determine the orientation of the tip by analyzing the magnetic field direction at each sensor with respect to the sensor-catheter tip direction.

[0012] Once the catheter tip has been detected, the CGCI controller adjusts the catheter tip from the actual position to the desired position in a closed loop control mode at a specific portion of the QRS cycle of the heartbeat. This maintains the reference position at one specific portion of the heartbeat cycle and allows it to travel freely with the tissue through the rest of the systole/diastole cycle.

[0013] The desired position, or DP, is a data acquisition point on or near the heart chamber wall. The CGCI impedance seeking unit specifies the DP on a tissue path trajectory to the tissue surface through the point of expected tissue contact. In other words, the catheter tip is guided in a straight line from the heart chamber center to the DP to locate the surface of the chamber by achieving tissue contact at a point closest to the DP.

[0014] Once the system has determined exactly where the tissue surface is located, the position of the catheter tip, as it moves along the chamber wall, is tracked while surface contact is continuously determined by impedance. The CGCI controller accomplishes this by following a tracking point, or TP, as the impedance seeking unit (ISU) moves the distal tip of the catheter down the tissue path until tissue contact is made and maintained continuously through the heartbeat cycle. The ISU also monitors the conductivity as a function of path stability and retracts the catheter tip when tissue contact is made off the path, or gives additional catheter length when the catheter is pointing at the path but cannot reach it. The degree of contact is determined by the amount of impedance seen at the tip.

[0015] Once tissue contact is made at the DP and is maintained, the position of the tip, the contact impedance, and the electrical ECG of the heart are all measured over several heartbeats to form a single tissue location’s characteristic data set. This process is repeated for several adjacent tissue locations and as each location is sampled, their data is assembled to represent the electrical and mechanical activity of the heart over the entire heartbeat cycle. Each catheter tip position is measured over many heartbeat cycles to assure that the position and associated electrical information is accurate.



**[0016]** The acquired data for position and electrical properties are then correlated with a system time and the current QRS phase of the heartbeat as a global reference for data processing.

**[0017]** Acquired data from the same location and heartbeat phase are filtered and then used to produce a time dependent geometric map of the heart throughout the heartbeat phases.

**[0018]** The acquired data is then manipulated and used to display several maps of various properties of the heart which then are placed over the recently created geometric map. These maps include the electrical potential, surface impedance, lateral surface velocity, internal tissue contraction, and the internal tissue contraction velocity.

#### BRIEF DESCRIPTION OF THE DRAWINGS

**[0019]** FIG. 1 is a system block diagram showing the imaging and synchronization subsystem, the impedance seeking subsystem, and its function in obtaining the actual position and specifying the desired position.

**[0020]** FIG. 2 is a schematic diagram relating the tracking point, tissue path, and desired position.

**[0021]** FIG. 3 is a schematic diagram of the data signals and data derived from the external ECG signal.

**[0022]** FIG. 4 is a block diagram of the impedance seeking subsystem and the associated data acquisition signals.

**[0023]** FIG. 5 is a schematic diagram of the test for cyclic motion of the catheter tip.

**[0024]** FIG. 6 is a detailed view of the initial conditions of a displacement envelope.

**[0025]** FIG. 7 is a graph of the weighting as a function of the distance of the vertex from the transform.

**[0026]** FIG. 8a is a series of illustrations depicting how the displacement envelopes affect the geometry of the constructed mesh images when the heart phase is at 60 and 120 degrees.

**[0027]** FIG. 8b is a series of illustrations depicting how the displacement envelopes affect the geometry of the constructed mesh images when the heart phase is at 180 and 240 degrees.

**[0028]** FIG. 8c is a series of illustrations depicting how the displacement envelopes affect the geometry of the constructed mesh images when the heart phase is at 300 and 360 degrees.

**[0029]** FIG. 9 is a schematic diagram of the geometric calculations used to interpolate a scalar field across the surface of the mesh.

**[0030]** FIG. 10 is a schematic diagram illustrating the construction of triangles from a plurality of sample point locations.

#### DETAILED DESCRIPTION OF THE PREFERRED EMBODIMENT

**[0031]** In one embodiment, the apparatus and method described herein acquires and displays the electrical and mechanical properties of the heart. The invention accomplishes this by first detecting the distal tip of a catheter that has been inserted into a heart, guiding the catheter tip around the chamber of the heart towards a desired position, detecting when the catheter has made tissue contact with the heart chamber wall, and finally measuring of the QRS signal of the heart throughout several heartbeats. This process can be repeated several times in order to accurately measure the tissue velocity, strain, and conduction velocity across the

surface of the heart. Once the appropriate amount of data has been collected, a set of data-rich meshes may be constructed for each phase of motion of the heart and then used to calculate and display the physical properties in a detailed clinical map.

**[0032]** Tissue velocity mapping requires linking multiple surface position and electrical readings to the current phase of the heart. This measurement and simultaneous analysis can be done in real-time if enough electrodes are available, or in non-real time by taking readings of position and electro-potential over two or more heartbeats and compiles them in a more detailed interactive clinical model.

**[0033]** Position detection, contact confirmation, electrode ECG and heartbeat phase are collected relatively contemporaneously. If there is delay in the signals due to filtering, the time-shift can be corrected in the final model. In a real-time display, compensation for time-shifts due to filtering can be done using predictive algorithms. Such predictive algorithms rely upon the previous beats. Irregularities between beats will result in electrical readings and mechanical displacements and velocities being somewhat out of sync with each other, and derived data between the two will be inaccurate on a scale corresponding to the irregularity.

**[0034]** To generate an analytical model, a single catheter can be used to accumulate points about the chamber over many heartbeats, or a basket or lasso may also be used to gather more points at once. A visual reference model can be displayed to indicate the progress of data collection, as well as any fiducial reference markers, catheters and 3D models.

**[0035]** For a real-time model, a sufficient number of electrodes are placed in contact with the surface, and the flexibility of the interstitial material or mesh should be sufficient that the electrode tracks the same point on the moving surface. Quantities computed based on surface point tracking such as tissue velocity and strain can be computed in real-time using such a catheter. If the electrodes do not track the same point on the surface, the color-coded map of the ECG will be available to map onto the surface mesh.

**[0036]** FIG. 1 is a system block diagram of the catheter guidance and control imaging (CGCI) system for position definition and guidance to locate and maintain tissue contact while acquiring data. The CGCI system for imaging and control of a catheter tip is described in U.S. patent application Ser. No. 11/697,690 "Method and Apparatus for Controlling Catheter Positioning and Orientation" and U.S. Pat. No. 7,280,863 "System and Method for Radar-Assisted Catheter Guidance and Control" and are hereby incorporated by reference.

**[0037]** Additionally, the current application is further supported and described in U.S. patent application Ser. No. 10/621,196 "Apparatus for Catheter, Guidance, Control, and Imaging," U.S. patent application Ser. No. 11/331,781 "System and Method for Controlling Movement of a Surgical Tool," U.S. patent application Ser. No. 11/331,994 "Apparatus and Method for Generating a Magnetic Field," U.S. patent application Ser. No. 11/331,485 "System and Method for Magnetic Catheter tip," U.S. patent application Ser. No. 11/140,475 "Apparatus and Method for Shaped Magnetic Field Control for Catheter, Guidance, Control and Imaging," U.S. patent application Ser. No. 11/362,542 "Apparatus for Magnetically Deployable Catheter with Mosfet Sensors : Method for Mapping and Ablation," and U.S. patent applica-

tion Ser. No. 11/869,668 "System and Method for Radar-Assisted Catheter Guidance and Control" are all hereby incorporated by reference.

**[0038]** An actual position (AP) **902** and orientation of the distal end of the catheter is defined by external or internal subsystems of the CGCI system. Position detection can be globally referenced, or with respect to a six degree of freedom fiducial catheter, such as a custom coronary sinus catheter. Where the AP is defined with respect to the CGCI global coordinate system a fiducial alignment unit **12** maintains alignment with the patient's local coordinate system and converts between local and CGCI global coordinates. An operation console **13** in FIG. **1** defines the desired position (DP) **903** of the catheter tip (shown in FIG. **2**) and a tissue path **906** (also shown in FIG. **2**) that passes through the desired position. A CGCI controller **501** in FIG. **1** is given an initial tracking point TP **907a** (shown in FIG. **2**) on the tissue path **906** and magnetically steers the catheter to point to a tracking point TP **907a**. The CGCI controller **501** sends the remaining positional error, the "closest proximity", between the AP **902** and the TP **907a** to an impedance seeking unit **16**.

**[0039]** Contact confirmation with the surface of the heart chamber wall can be done by several methods, including, but not limited to, measuring surface conductivity. The impedance seeking unit **16** generates a tissue contact signal **16.2** based on the degree of tissue contact, namely, a small DC direct current is injected at each location of tissue contact and the conduction is measured. If the tip of the catheter is in contact with the surface, the conduction will be higher than if it was within the blood stream. The level of conductivity is recorded in the data set for future use. A minimum value can be set to limit data collection to good surface contact.

**[0040]** The impedance seeking unit **16** advances the catheter using a magnetic slide **16.1** until continuous tissue contact is found by monitoring the tissue contact signal **16.2**, or until the point TP **907a** is reached, or in other words, when the AP **902** equals the TP **907a**. If the point TP **907a** is reached before continuous contact is made, the CGCI controller **501** advances the point TP **907a** in a positive direction along the tissue path **906** by a desired distance (e.g., 2 mm at a time), so as to maintain a predictable and repeatable approach to tissue contact. When full tissue contact is maintained, the impedance seeking unit **16** signals the CGCI controller **501** to stop all regulation and the catheter tip **377** is allowed to ride with the tissue surface under the current magnetic forces. If full tissue contact is made, but the location is too far from the tissue path (that is, the AP **902a** is greater than a specified distance (e.g., 5 mm) from the TP **907a**), the impedance seeking unit **16** retracts the catheter **900** a distance (e.g., 5 mm) to allow the CGCI controller **501** to redirect the catheter tip **377** towards the TP **907a** before the impedance seeking unit **16** advances the catheter again.

**[0041]** The magnetic slide **16.1** is used to regulate to the tracking point (TP) **907b**. If the tracking point TP **907b** is acquired by the magnetic slide **16.1** and the tissue contact signal **16.2** shows incomplete contact, the physical tracking point TP **907a** is moved down the tissue path **906** and the CGCI controller **501** regulates to the new tracking point, TP **907b**.

**[0042]** FIG. **2** is a schematic diagram of the left atrium **1.12** (facing the patient) and the tissue path **906** used by the CGCI system to guide the catheter to the moving tissue surface through the desired position DP **903** on the geometric static del. The CGCI system targets a unique position on the

tissue surface that, while the tissue is moving, passes through or near the selected position on the static geometric model. The desired position, DP **903**, is defined on or near the surface of the heart at a detected time on the QRS stable timing signal **1.50.1** (see FIG. **3**). The tissue path **906** can be selectively defined as the surface normal of the geometric heart model at the point DP **903**, a ray from the geometric center of the heart chamber through the DP **903**, or a ray of any direction of expected tissue travel drawn through the point DP **903**. The tracking point TP **907a** is the closed-loop regulator target point sent to the CGCI controller **501**. In FIG. **2**, a catheter **900** is inserted into the left atrium **1.12**, through the interatrial transseptum **1.11.5**. The magnetic tip **377** is guided to the tracking point **907a** by the CGCI controller **501**. Once the catheter tip **377** reaches the tracking point TP **907a**, the tracking point TP **907a** is advanced down the tissue path **906** until the impedance signal **16.2** shows continuous tissue contact.

**[0043]** FIG. **3** is a schematic diagram of the signals and data derived from the external ECG signal. An External ECG signal **1.50**, labeled ECG Ref, is used as a global reference signal to synchronize acquired data with a specific portion of the QRS heartbeat phase,  $\Phi(t)$  **600.2**.

**[0044]** The heartbeat phase,  $\Phi(t)$  **600.2**, is measured from R-peak to R-peak and is re-calculated after each heartbeat cycle to maintain the proper synchronization.

**[0045]** The QRS sync signal **1.50.1** provides a reference signal **10** to the CGCI controller **501** and CGCI operation console **13** when the heart is at its most stable point. This occurs between the end of the T-wave and the beginning of the P-wave, approximately 140-250° from the R-peak. In the QRS sync **1.50.1**, the CGCI catheter position detection unit **11** measures the stable reference position of the catheter tip **377** and the CGCI controller may make position adjustments to the catheter to maintain the desired position DP **903a** or tracking point, TP **907a**.

**[0046]** FIG. **4** is a schematic diagram of the tissue velocity imaging (TVI) data sets and processing routines. The CGCI system **1500** provides the external ECG reference signal ECGREF(t) **600.1**, the internal catheter tip ECG signal ECG(t) **600.4**, the catheter tip impedance signal  $\Omega(t)$  **600.3**, and the position of the catheter within the patient **1**, position(t) **600.5**.

**[0047]** Two data sets are created. The first data set contains records of each X, Y, Z position of the catheter tip **377**, the ECG, the contact conductivity, and the system time. The second data set records the external ECG with respect to system time. The second set serves as an electrical fiducial reference frame for the data and can be used to reconstruct the electromechanical behavior over many regular or irregular heartbeats. System time will be replaced with heartbeat phase as a time reference in analytical models.

**[0048]** The ECG map can be appended with the heartbeat phase ( $\Phi$ ) after the data is collected or while the data is being collected using a predictive algorithm. The phase is to be based on the period between the ECG's R intervals and the time since the last R peak.

**[0049]** The CGCI system **1500** measures the global external ECG reference signal from the patient's chest and produces the ECGREF(t) array **600.1**, where t is the CGCI system **1500** operation time in milliseconds. The Position(t) array is produced from the CGCI system's **1500** positioning

system and contains the xyz locations of the catheter tip 377. The tip electrocardial signal array, ECG(t) 600.4, and the tip impedance array,  $\Omega(t)$  600.3 are compiled from the sensed data at the catheter tip 377. These four arrays comprise the raw data arrays 600 which are used to create individual channel data arrays 601 for each location and phase.

[0050] The data segmentation routines 600.9 first calculates the heartbeat phase with respect to time,  $\Phi(t)$  600.2, then separates out each mapped location's data into the individual channel data arrays 601 which are indexed by location number and heartbeat phase. These channel data arrays 601 contain both the electrical and mechanical properties of each tissue location which are then later used to form the analytical model.

[0051] After the data has been collected, it is processed into the DirectX multi-platform mesh format that not only contains the location vertex points of the heart wall, but also the electrical ECG values of those locations, the conductivity readings, and any other desired data. The data is then manipulated to form a 3D color coded mesh structure that contains sub-meshes for each phase of motion which are registered to each other such that their vertices represent the same point on the heart wall in order to provide a consistent and accurate set of geometric calculation points.

[0052] The external reference ECG signal is recorded in an array with respect to system time, ECGREF(t) 600.1, where t is defined in milliseconds. This array is used to create the array of heartbeat phase with respect to system time,  $\Phi(t)$  600.2. This provides an index to relate all other system time referenced data acquisition signals to heartbeat phase.

$$\text{ECGREF}(t) \rightarrow \Phi(t)$$

[0053] Heartbeat phase is used to sequence the data without respect to heart rate. When these data are assembled, the mechanical contraction of the heart along with the associated color ECG map may be displayed in either real-time or non-real-time models. Other derived data, such as the tissue contraction velocity and acceleration, or the lateral wall velocity and acceleration depend at least in part on a registration between each phase-model of the heart. Registration involves the marking of key points on the heart wall in each phase to accurately track all surface points between phases. Some displays use this registered model. An algorithm for automatically registering models use the number of points and fine movement between the phases. After registration, the mesh for each phase can be regenerated such that each mesh vertex point represents the same heart surface point.

[0054] The QRS signal R peaks are detected whenever the ECGREF signal rises above the peak detection level, and their system times are recorded in the tr(j) array, where j indicates heartbeat number.

ECGREF(t) had R peaks at times tr(0), tr(1), tr(2), . . .  
tr(j).

[0055] The phase at time t, which lies between successive heartbeat peaks at times tr(j) and tr(j+1) is derived by equation 1.

$$\Phi(t) = 360 * (t - tr(j)) / (tr(j+1) - tr(j)) \tag{Eq. 1}$$

[0056] Phase is given the integer values of 0 to 359 degrees. Values that round to 360 are given the phase value of 0.

[0057] The raw data arrays are then defined in Table 1 below.

TABLE 1

Definitions of Raw Data Arrays		
FIG. 4 reference number	Data Array Description	Data Array Name
Not shown	CGCI System Operation Time, ms	T
600.1	External ECG Reference	ECGREF(t)
600.2	Phase at system time t	$\Phi(t)$
600.3	Impedance Signal, Ohms	$\Omega(t)$
600.4	Catheter Tip ECG, Volts	ECG(t)
600.5	Tip Position XYZ	Position(t)

[0058] FIG. 5 is a schematic diagram depicting a continuous motion cycle of the catheter tip 377. The Position(t) data array is analyzed for segments of continuous tissue contact from the data recorded in the impedance array,  $\Omega(t)$ , and where the catheter Position(t) returns within short distance (e.g., 1 mm) of the home position at a phase of  $\Phi(t)=200^\circ$ , indicating that the catheter tip travel conforms to a cyclic path. These continuous contact data segments are then mapped into the  $360^\circ$  phase-based arrays for that location, n. Where the array already contains data, the new data is averaged with the previous points. Where the array contains no data at the end of data compilation, the empty elements of the array are loaded with values that are interpolated from the nearest elements. This gives three arrays for each location, n, each containing  $360^\circ$  phase-mapped data values for the impedance, ECG and catheter tip 377 xyz position. These arrays and their respective symbols are displayed in Table 2 below.

TABLE 2

Mapped Arrays	
Data Array Description	Data Array Name
Heartbeat Phase, 0 to 359 degrees	$\Phi$
Impedance with respect to Phase $\Phi$ , Point n	$\Omega(\Phi, n)$
Local ECG as a function of Phase $\Phi$ , Point n	ECG( $\Phi, n$ )
Position of Catheter Tip for Phase $\Phi$ , Point n	Position( $\Phi, n$ )

[0059] The electrical and mechanical data for each sampled location in the heart can now be directly accessed by heartbeat phase. From this data, color-coded maps can be created based the values at each point. A registered data set is required for properties that are relative to two points, or to view the change in value at the same physical location on the surface.

[0060] The base mesh consists of an array of Mc vertices each with the following structure displayed in Table 3:

TABLE 3

```

struct Left_Atrial_Vertex
{
    VECTOR Pos; // Position
    float WEIGHT[Num_W]; // Displacement Weighting
    DWORD TR_Index[Num_W]; // Transform Index array
    float ECG; // Potential
    float Imp; // Impedance
    DWORD Color; // Vertex Color
};
    
```

[0061] The base mesh steady state initial condition is  $\Phi(t)_{ss}=140^\circ$ , and the transform/displacement channels are resented by  $T(n)=DAT(\Phi, n)$

**[0062]** FIG. 6 is a detailed view of the initial conditions of a displacement envelope created by the invention. This process is performed one time after the dataset has been assembled.

**[0063]** Displacement envelopes are regions that affect the movement of the vertices that constitute the mesh as a function of the movement of the base displacement transform. The radius of the envelope is the distance to the nearest neighbors sample point.

**[0064]** Each vertex in the mesh is assigned weights and is associated with transforms of influence through the TR\_Index array shown in Table 3 above. For each sample point  $T_n$ , the vertices of the mesh are processed. Weights are then calculated according to the following function including equation 2.

**[0065]** If  $(r>R)$ ,  $Weight(r)=0$ . Otherwise,  $x=r/R$  and  $Weight(r)=1-(3x^2-2x^3)$ , Eq. 2

where  $R=Radius$  of the left atrium 1.12 and  $r$  is a positive value.

**[0066]** FIG. 7 shows the weighting as a function of the distance of the vertex from the transform  $T_n$ . The time domain representation of the left atrium is accomplished by computing the position of each vertex as a function of  $\Phi$  according to equation 3.

$$\begin{aligned} \text{VertexPos} &= T_{1,P} W_{1+} \dots T_{n-1,P} W_{n-1+} T_n P (1.0 - \sum W_i) \\ \text{where } (i &= 1 \dots n) \end{aligned} \quad \text{Eq. 3}$$

**[0067]** FIGS. 8a-8c are a series of illustrations depicting how the displacement envelopes affect the geometry of the constructed mesh images and reflect the mechanical properties of the left atrium. The two scalars recorded in  $\Omega(\Phi, n)$  and  $ECG(\Phi, n)$  as shown in Table 3 above may be represented graphically on the left atrium 1.12 mesh using the following procedure. FIG. 9 illustrates the arrangement of the sample channels as points on a projection surface.

**[0068]** It is to be expressly understood that the procedure described below is conducted on each rendering frame for each triangle that constitutes the surface of the heart, not just for the six examples shown in FIGS. 8a-8c. Each vertex that makes up the left atrium mesh is considered. FIG. 10 depicts the calculation that occurs when a ray from the vertex of the triangle being processed intersects a ray along its normal surface. The point of intersection between these two rays is the focus of interpolation using equation 4 below.

$$s' = T_{a,s} + (T_{c,s} - T_{a,s}) + u(T_{b,s} - T_{a,s}), \quad \text{Eq. 4}$$

**[0069]** where  $t$  and  $u$  can be found using equations 5 and 6.

$$p'x = T_{a,p,x} + (T_{c,p,x} - T_{a,p,x}) + u(T_{b,p,x} - T_{a,p,x}) \quad \text{Eq. 5}$$

$$p'y = T_{a,p,y} + (T_{c,p,y} - T_{a,p,y}) + u(T_{b,p,y} - T_{a,p,y}) \quad \text{Eq. 6}$$

**[0070]** Once the appropriate amount of data has been collected and correctly weighted, the user of the apparatus then can use the data to determine a whole host of additional heart properties such as tissue displacement, contraction velocity, and contraction acceleration. These newly found properties can then be mapped on a position or phase basis using the electrical and mechanical differences between adjacent points. Data that is displayed is represented as change per degree of phase and may be linearly scaled to represent actual velocities in SI or English units for a given heart rate.

**[0071]** In cases where the real-time display of data is available, the 3D mesh formed by the electrode positions is displayed dynamically moving in space, or frozen and linked to

a single phase of the heartbeat to better display derived data on its surface. Color-coded values for tissue contraction velocity, acceleration, electrical potential and conduction velocity are displayed dynamically on the surface of the mesh, and other derived values for electromechanical interaction would be available as well. Any shift in the location of the catheter tip 377 with respect to the surface will shift the view of the data with respect to that surface, and shifts in position of individual electrodes with respect to each other will momentarily affect the accuracy of the derived data. Filtering based on the collected data from previous heartbeats can be used to stabilize the display and increase the accuracy of the measurements in patients with predictable and repeating heart rhythms. Where the catheter tip 377 loses contact with the surface, the mesh will be missing that location and both the geometric model and derived color-coding will be more coarse in that region. Real-time data is collected and may be used later to reconstruct a more detailed analytical model.

**[0072]** For non-real-time models, data is collected over a number of locations and a number of heartbeats and assembled into a heartbeat phase-linked data set. For unregistered models, several color-coded data sets are displayed on the surface of the geometry, including the electrical map and conductivity map. Color-coded data sets are displayed on the associated phase of the heart geometry, and with some electrical-geometric inaccuracy, the color-coded maps are animated on the surface of a single phase of the heart's geometry. The animations can be played in a loop, and/or a slide bar can be used to jog the animation back and forth over the desired portion of the cycle.

**[0073]** Where a registration map has been created, the color-coded animations are more accurately displayed on a static geometric model. In addition, other data sets may be created and displayed. The knowledge of how a single point, or pairs of points move through the phases gives us the tissue velocity in the contracting tissue between the points, the lateral velocity of the wall, the associated accelerations, and a more accurate view of how the conduction velocity is occurring at a particular location. Other derived quantities that link the electrical and mechanical properties of the heart may be accurately mapped and used as clinical indicators. Two points can be placed on the model and the quantities between these points may be tracked in detail. This also allows the electrical and mechanical properties to be measured parallel or perpendicular to the muscle fiber direction.

**[0074]** The tissue displacement,  $\sigma$ , between location numbers  $n=i$  and  $n=j$  at phase  $\Phi$  is defined by equation 7:

$$\sigma(i, j, \Phi) = (\Delta Pi - \Delta Pj) / (\text{Position}(\Phi, i) - \text{Position}(\Phi, j)), \quad \text{Eq. 7}$$

where

$$\Delta Pi = \text{Position}(\Phi, i) - \text{Position}(\Phi - 1, i) \quad \text{and} \quad \text{Eq. 8}$$

$$\Delta Pj = \text{Position}(\Phi, j) - \text{Position}(\Phi - 1, j). \quad \text{Eq. 9}$$

**[0075]** The relative contraction velocity between points on the surface,  $\sigma'$ , is defined by the first derivative of the strain  $\sigma$  with respect to the phase change in equation 10.

$$\sigma'(i, j, \Phi) = \sigma(i, j, \Phi) - \sigma(i, j, \Phi - 1) \quad \text{Eq. 10}$$

**[0076]** Relative contraction acceleration between points on the surface is defined by the second derivative of the strain  $\sigma$  with respect to the phase change in equation 11.

$$\sigma'' = \sigma'(i, j, \Phi) - \sigma'(i, j, \Phi - 1) \quad \text{Eq. 11}$$





**[0077]** It is important to note that all surface quantities are displayed in normalized units per unit length.

**[0078]** The first derivative of Local ECG with respect to heartbeat phase is defined by equation 12:

$$ECG(\Phi, i) = ECG(\Phi, i) - ECG(\Phi - 1, i) \quad \text{Eq. 12}$$

**[0079]** The global distance, velocity, and acceleration of location number *i* with respect to a fixed reference position, RefPos, are defined at a given phase by the equations 13, 14, and 15.

$$s(\Phi) = (\text{Position}(\Phi, i) - \text{RefPos}) \quad \text{Eq. 13}$$

$$v(\Phi) = s(\Phi) - s(\Phi - 1) \quad \text{Eq. 14}$$

$$a(\Phi) = v(\Phi) - v(\Phi - 1) \quad \text{Eq. 15}$$

**[0080]** The tissue contraction versus electrical gradient is defined by equation 16:

$$TCE(i, j, \Phi) = \alpha(i, j, \Phi) (ECG(\Phi, i) - ECG(\Phi, j)) \quad \text{Eq. 16}$$

**[0081]** Additional displays contemplated by the applicant but not shown include the tissue contraction direction vectors of the heart superimposed over the previously constructed geometric surface map of the heart.

**[0082]** Many alterations and modifications may be made by those having ordinary skill in the art without departing from the spirit and scope of the invention. Therefore, it must be understood that the illustrated embodiment has been set forth only for the purposes of example and that it should not be taken as limiting the invention as defined by the following invention and its various embodiments.

**[0083]** Therefore, it must be understood that the illustrated embodiment has been set forth only for the purposes of example and that it should not be taken as limiting the invention as defined by the following claims. For example, notwithstanding the fact that the elements of a claim are set forth below in a certain combination, it must be expressly understood that the invention includes other combinations of fewer, more or different elements, which are disclosed in above even when not initially claimed in such combinations. A teaching that two elements are combined in a claimed combination is further to be understood as also allowing for a claimed combination in which the two elements are not combined with each other, but may be used alone or combined in other combinations. The excision of any disclosed element of the invention is explicitly contemplated as within the scope of the invention.

**[0084]** The words used in this specification to describe the invention and its various embodiments are to be understood not only in the sense of their commonly defined meanings, but to include by special definition in this specification structure, material or acts beyond the scope of the commonly defined meanings. Thus if an element can be understood in the context of this specification as including more than one meaning, then its use in a claim must be understood as being generic to all possible meanings supported by the specification and by the word itself.

**[0085]** The definitions of the words or elements of the following claims are, therefore, defined in this specification to include not only the combination of elements which are literally set forth, but all equivalent structure, material or acts for performing substantially the same function in substantially the same way to obtain substantially the same result. In this sense it is therefore contemplated that an equivalent substitution of two or more elements may be made for any one of

the elements in the claims below or that a single element may be substituted for two or more elements in a claim. Although elements may be described above as acting in certain combinations and even initially claimed as such, it is to be expressly understood that one or more elements from a claimed combination can in some cases be excised from the combination and that the claimed combination may be directed to a subcombination or variation of a subcombination.

**[0086]** Insubstantial changes from the claimed subject matter as viewed by a person with ordinary skill in the art, now known or later devised, are expressly contemplated as being equivalently within the scope of the claims. Therefore, obvious substitutions now or later known to one with ordinary skill in the art are defined to be within the scope of the defined elements.

**[0087]** The claims are thus to be understood to include what is specifically illustrated and described above, what is conceptually equivalent, what can be obviously substituted and also what essentially incorporates the essential idea of the invention.

**[0088]** While the apparatus and method has or will be described for the sake of grammatical fluidity with functional explanations, it is to be expressly understood that the claims, unless expressly formulated under 35 USC 112, are not to be construed as necessarily limited in any way by the construction of “means” or “steps” limitations, but are to be accorded the full scope of the meaning and equivalents of the definition provided by the claims under the judicial doctrine of equivalents, and in the case where the claims are expressly formulated under 35 USC 112 are to be accorded full statutory equivalents under 35 USC 112. The invention can be better visualized by turning now to the following drawings wherein like elements are referenced by like numerals.

What is claimed is:

1. An apparatus for creating a high resolution map of the electrical and mechanical properties of the heart comprising:
  - a catheter;
  - a catheter guidance and control imaging system coupled to the catheter;
  - a data collection module for the catheter guidance and control imaging system to collect several different types of data from the catheter; and
  - a display for displaying the data collected by the catheter guidance and control imaging system in a three dimensional color-coded image format.
2. The apparatus of claim 1 wherein the catheter is magnetically tipped.
3. The apparatus of claim 2 wherein the catheter guidance and control imaging system further comprises a magnet system for generating a magnetic field in order to alter the course of the magnetically tipped catheter.
4. The apparatus of claim 3 wherein the catheter guidance and control imaging system alters the surrounding magnetic field for locating, orientating, and guiding the distal tip of the catheter to a desired position along an inner heart wall surface of a patient.
5. The apparatus of claim 4 wherein the catheter guidance and control imaging system maintains the distal tip of the catheter in a fixed position throughout a position of a cardiac cycle.
6. The apparatus of claim 5 further comprises a unit for measuring the impedance at the catheter tip and adjusting the distance from the catheter tip to the tissue surface so as to maintain a constant impedance reading.



7. The apparatus of claim 6 wherein the apparatus collects and records the system operation time, the ECG signal from the patient, the impedance signal from the catheter tip, the position of the tip, and the ECG signal from the catheter tip.

8. The apparatus of claim 7 wherein the data collected by the catheter guidance and control imaging system in a three dimensional color-coded image format further comprises correlating the obtained data with a measured heartbeat phase taken contemporaneously with the obtained data.

9. The apparatus of claim 8 wherein the format interpolates one or more data points that are found missing from the original data set.

10. The apparatus of claim 9 wherein the format calculates and displays tissue displacement between any two points located on the three dimensional image.

11. The apparatus of claim 9 wherein the means displays tissue contraction velocity between any two points located on the three dimensional image.

12. The apparatus of claim 9 wherein the apparatus displays tissue contraction acceleration between at least two points located on the three dimensional image.

13. The apparatus of claim 9 wherein the apparatus calculates and displays tissue displacement versus the electrical gradient between at least two points located on the three dimensional image.

14. A method of creating a high resolution map of the electrical and mechanical properties of the heart comprising: determining the position and orientation of a tip of a catheter within a patient's heart using a catheter guidance and imaging system operatively coupled to the catheter; changing the position of the catheter tip by altering the shape and polarity of a surrounding magnetic field; guiding the distal tip to a desired position along the inner surface of the heart wall; maintaining the catheter tip at the desired position along the inner surface of the heart wall for at least a portion of cardiac cycle; acquiring first data based on the patient and the distal tip during a cardiac cycle; calculating one or more electrical and mechanical properties of the heart from the first data; processing the first data into a three dimensional color-coded image according to the various electrical and mechanical properties; and displaying the three dimensional color-coded image on a display.

15. The method of claim 14 wherein maintaining the distal tip at the desired position along the inner surface of the heart wall for an entire cardiac cycle further comprises:

measuring the impedance value at the catheter tip; and adjusting the distance from the catheter tip to the tissue surface so as to maintain a constant impedance reading.

16. The method of claim 15 wherein acquiring a said first data comprises:

recording the system operation time;  
recording the ECG signal from the patient;  
recording the impedance signal for the distal tip;  
recording the position of the distal tip; and  
recording the ECG signal from the distal tip.

17. The method of claim 16 wherein calculating said one or more electrical and mechanical properties of the heart from the obtained data further comprises correlating the obtained data with a measured heartbeat phase taken contemporaneously with the first data.

18. The method of claim 17 wherein calculating said one or more electrical and mechanical properties of the heart from the obtained data further comprises interpolating data points that are found missing from the original data set.

19. The method of claim 18 wherein calculating said one or more electrical and mechanical properties of the heart from the obtained data further comprises calculating tissue displacement between two previously measured points located on the inner surface of the heart wall.

20. The method of claim 18 wherein calculating said one or more electrical and mechanical properties of the heart from the obtained data further comprises calculating tissue contraction velocity between two previously measured points located on the inner surface of the heart wall.

21. The method of claim 18 wherein calculating said one or more electrical and mechanical properties of the heart from the obtained data further comprises calculating tissue contraction acceleration between two previously measured points located on the inner surface of the heart wall.

22. The method of claim 18 wherein calculating said one or more electrical and mechanical properties of the heart from the obtained data further comprises calculating tissue displacement versus the electrical gradient between two previously measured points located on the inner surface of the heart wall.

23. An apparatus for creating a high resolution map of the electrical and mechanical properties of the heart comprising: a catheter;

a catheter guidance and control imaging system coupled to the catheter;

a means for the catheter guidance and control imaging system to collect several different types of data from the catheter; and

a means of displaying the data collected by the catheter guidance and control imaging system in a three dimensional color-coded image format.

24. The apparatus of claim 23 wherein the catheter is magnetically tipped.

25. The apparatus of claim 24 wherein the catheter guidance and control imaging system further comprises a means for generating a magnetic field in order to alter the course of the magnetically tipped catheter.

26. The apparatus of claim 25 wherein the catheter guidance and control imaging system further comprises a means for altering the surrounding magnetic field for locating, orientating, and guiding the distal tip of the catheter to a desired position along an inner heart wall surface of a patient.

27. The apparatus of claim 26 wherein the catheter guidance and control imaging system further comprises a means for maintaining the distal tip of the catheter in a fixed position throughout an entire cardiac cycle.

28. The apparatus of claim 27 wherein the means for maintaining the distal tip of the catheter in a fixed position throughout an entire cardiac cycle further comprises a means for measuring the impedance at the catheter tip and adjusting the distance from the catheter tip to the tissue surface so as to maintain a constant impedance reading.

29. The apparatus of claim 28 wherein the means for the catheter guidance and control imaging system to collect several different types of data from the catheter further comprises a means for collecting and recording the system operation time, the ECG signal from the patient, the impedance signal from the catheter tip, the position of the tip, and the ECG signal from the catheter tip.

30. The apparatus of claim 29 wherein the means of displaying data collected by the catheter guidance and control imaging system in a three dimensional color-coded image format further comprises a means of correlating the obtained data with a measured heartbeat phase taken contemporaneously with the obtained data.

31. The apparatus of claim 30 wherein the means of displaying data collected by the catheter guidance and control imaging system in a three dimensional color-coded image format further comprises a means for interpolating any data points that are found missing from the original data set.

32. The apparatus of claim 31 wherein the means of displaying data collected by the catheter guidance and control imaging system in a three dimensional color-coded image format further comprises a means for calculating and displaying tissue displacement between any two points located on the three dimensional image.

33. The apparatus of claim 31 wherein the means of displaying data collected by the catheter guidance and control

imaging system in a three dimensional color-coded image format further comprises a means for calculating and displaying tissue contraction velocity between any two points located on the three dimensional image.

34. The apparatus of claim 31 wherein the means of displaying data collected by the catheter guidance and control imaging system in a three dimensional color-coded image format further comprises a means for calculating and displaying tissue contraction acceleration between any two points located on the three dimensional image.

35. The apparatus of claim 31 wherein the means of displaying data collected by the catheter guidance and control imaging system in a three dimensional color-coded image format further comprises a means for calculating and displaying tissue displacement versus the electrical gradient between any two points located on the three dimensional image.

\* \* \* \* \*





US 20120310066A1

(19) **United States**

(12) **Patent Application Publication**  
**Shachar et al.**

(10) **Pub. No.: US 2012/0310066 A1**

(43) **Pub. Date: Dec. 6, 2012**

(54) **METHOD AND APPARATUS FOR CREATING  
A HIGH RESOLUTION MAP OF THE  
ELECTRICAL AND MECHANICAL  
PROPERTIES OF THE HEART**

**Publication Classification**

(51) **Int. Cl.**  
*A61B 5/042* (2006.01)  
*A61B 5/053* (2006.01)  
*A61B 5/0402* (2006.01)  
*A61M 25/095* (2006.01)  
(52) **U.S. Cl.** ..... **600/374**  
(57) **ABSTRACT**

(75) **Inventors:** **Yehoshua Shachar**, Santa Monica, CA (US); **Bruce Marx**, Ojai, CA (US); **Laszlo Farkas**, Ojai, CA (US); **David Johnson**, West Hollywood, CA (US); **Leslie Farkas**, Ojai, CA (US)

A system method that tracks one or more points on the surface of a cardiac tissue throughout a cardiac cycle and collect various types of data points which are then subsequently used to generate a corresponding model of the tissue and display the model as a 3D color coded image is described. In one embodiment, the system determines the position and orientation of a distal tip of a catheter, manipulates the catheter tip so as to maintain constant contact between the tip and a region of cardiac tissue using the impedance method, acquires positional and electrical data of the tip-tissue configuration through an entire heartbeat cycle, repeats the measurements as many times as needed in different tissue regions, and forms a 3D color coded map displaying various mechanical and electrical properties of the heart using the acquired data.

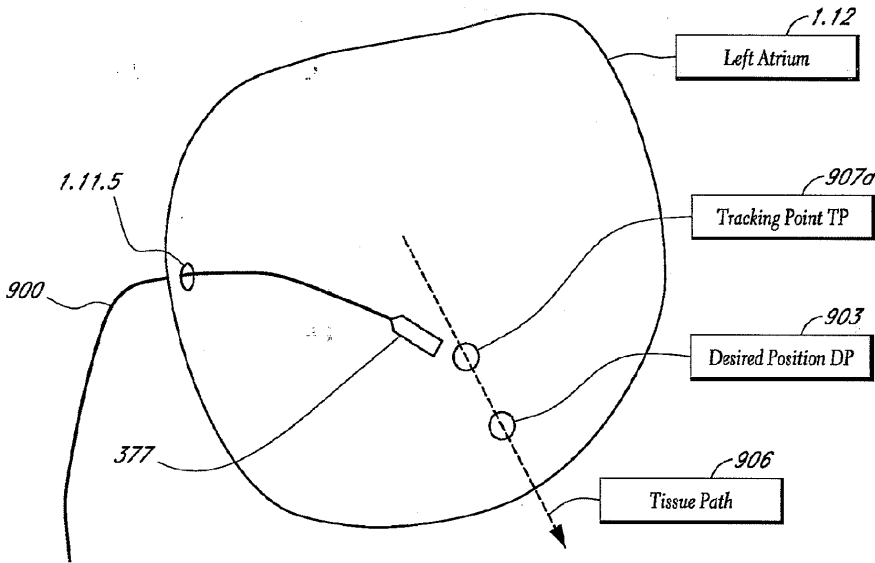
(73) **Assignee:** **MAGNETECS, INC.**, Inglewood, CA (US)

(21) **Appl. No.:** **13/491,300**

(22) **Filed:** **Jun. 7, 2012**

**Related U.S. Application Data**

(63) Continuation of application No. 12/113,804, filed on May 1, 2008.







INTERNATIONAL FILINGS FOR:  
*Method and Apparatus for Creating  
a High Resolution Map of the  
Electrical and Mechanical  
Properties of the Heart*

03

**INVENTOR: Yehoshua Shachar  
Bruce Marx  
Leslie Farkas  
David Johnson  
Lazlo Farkas  
Leslie Farkas**







(19)



Anmeldenummer:

Application Number: 9739407.6

Numéro de la demande :

Internationale Antrag an das  
Weltorganisation für geisties Eigentum unter der Nummer:  
**PCT/US2009/040242**

International application submitted to the World Intellectual  
Property Organization under number:  
**PCT/US2009/040242**

La demande internationale a présenté à l'Organisation  
mondiale de la propriété intellectuelle sous le numéro:  
**PCT/US2009/040242**

03



# (12) 发明专利申请

(10) 申请公布号 CN 102065746 A

(43) 申请公布日 2011.05.18

(21) 申请号 200980115528.0

(74) 专利代理机构 中科专利商标代理有限公司 11021

(22) 申请日 2009.04.10

代理人 杨静

(30) 优先权数据

12/113,804 2008.05.01 US

(51) Int. Cl.

A61B 5/00 (2006.01)

A61B 5/053 (2006.01)

A61B 5/11 (2006.01)

(85) PCT申请进入国家阶段日

2010.10.29

(86) PCT申请的申请数据

PCT/US2009/040242 2009.04.10

(87) PCT申请的公布数据

W02009/134605 EN 2009.11.05

(71) 申请人 麦格耐泰克斯公司

地址 美国加利福尼亚州

(72) 发明人 乔舒亚·沙哈尔 布鲁斯·马克斯

拉斯洛 法尔卡斯 戴维·约翰逊

莱斯烈·法尔卡斯

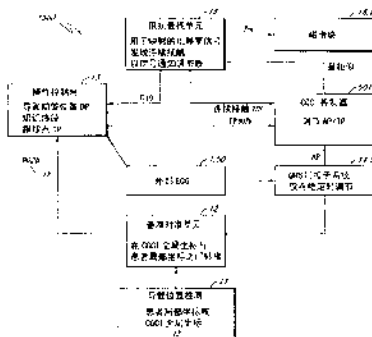
权利要求书 3 页 说明书 10 页 附图 11 页

## (54) 发明名称

创建心脏电特性和机械特性的高分辨率映射图的方法和设备

## (57) 摘要

描述了一种系统方法，该系统方法在整个心动周期内跟踪心脏组织表面上的一个或多个点，收集随后用于产生组织的对应模型的多类型的数据，并将模型显示为 3D 彩色编码图像。在一个实施例中，系统确定导管的远端尖端的位置和方向，使用阻抗方法处理导管尖端以便保持尖端与心脏组织的区域之间的恒定接触，获取整个心搏周期内尖端组织构型的位置数据和电数据，在不同组织区域中重复测量所需的次数，以及使用所获取的数据形成 3D 彩色编码映射图，所述 3D 彩色编码映射图显示了心脏的多种机械特性和电特性。





U.S. PATENT OFFICE FILINGS FOR:  
*System and Method for a Catheter  
Impedance Seeking Device*

***INVENTOR: Yehoshua Shachar  
Bruce Marx  
Leslie Farkas  
David Johnson  
Lazlo Farkas  
Dr. Eli Gang***

04



US 20100130854A1

(19) **United States**

(12) **Patent Application Publication**  
**Shachar et al.**

(10) **Pub. No.: US 2010/0130854 A1**

(43) **Pub. Date: May 27, 2010**

(54) **SYSTEM AND METHOD FOR A CATHETER IMPEDANCE SEEKING DEVICE**

(22) Filed: **Nov. 25, 2008**

**Publication Classification**

(75) Inventors: **Yehoshua Shachar**, Santa Monica, CA (US); **Bruce Marx**, Ojai, CA (US); **Leslie Farkas**, Ojai, CA (US); **Laszlo Farkas**, Ojai, CA (US); **David Johnson**, West Hollywood, CA (US); **Eli Gang**, Los Angeles, CA (US)

(51) **Int. Cl.**  
**A61B 5/055** (2006.01)  
(52) **U.S. Cl.** ..... **600/424**

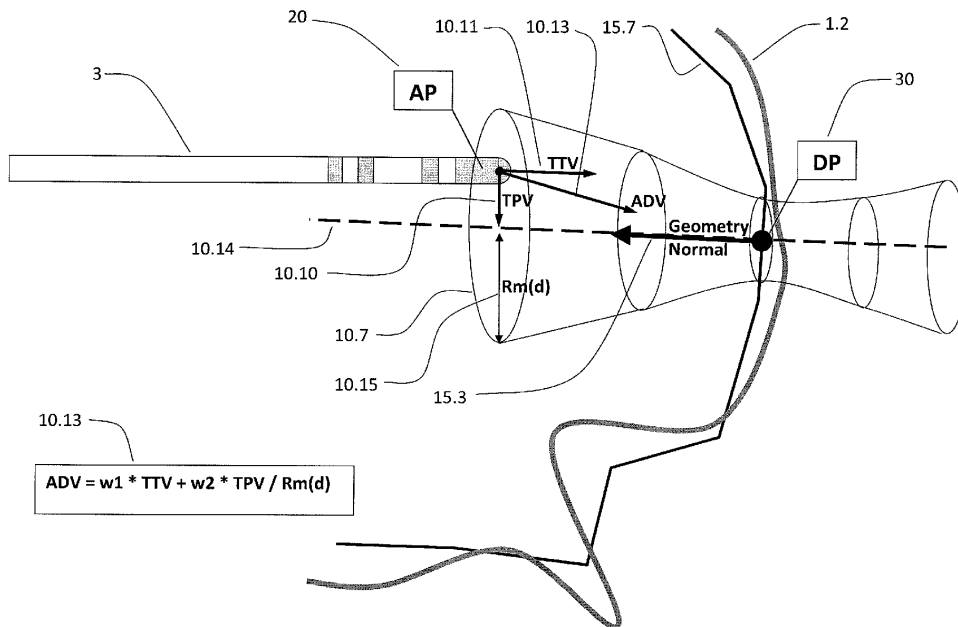
(57) **ABSTRACT**

A tissue-contact seeking method and apparatus is described that enhances catheter position detection and control systems in making and maintaining continuous tissue contact in a highly dynamic frame, such as under the rigors of cardiac motion. Tissue-seeking logical routines use a tissue contact sensing system to advance a catheter to relatively continuous tissue contact, or detect obstacles, in cooperation with the catheter position detection and control systems. Additional logical routines are capable of optimizing the contact direction of the catheter tip by controlling the rotation angle and chamber position of the introducer.

Correspondence Address:  
**KNOBBE MARTENS OLSON & BEAR LLP**  
**2040 MAIN STREET, FOURTEENTH FLOOR**  
**IRVINE, CA 92614 (US)**

(73) Assignee: **Magnetecs, Inc.**, Inglewood, CA (US)

(21) Appl. No.: **12/323,231**



04



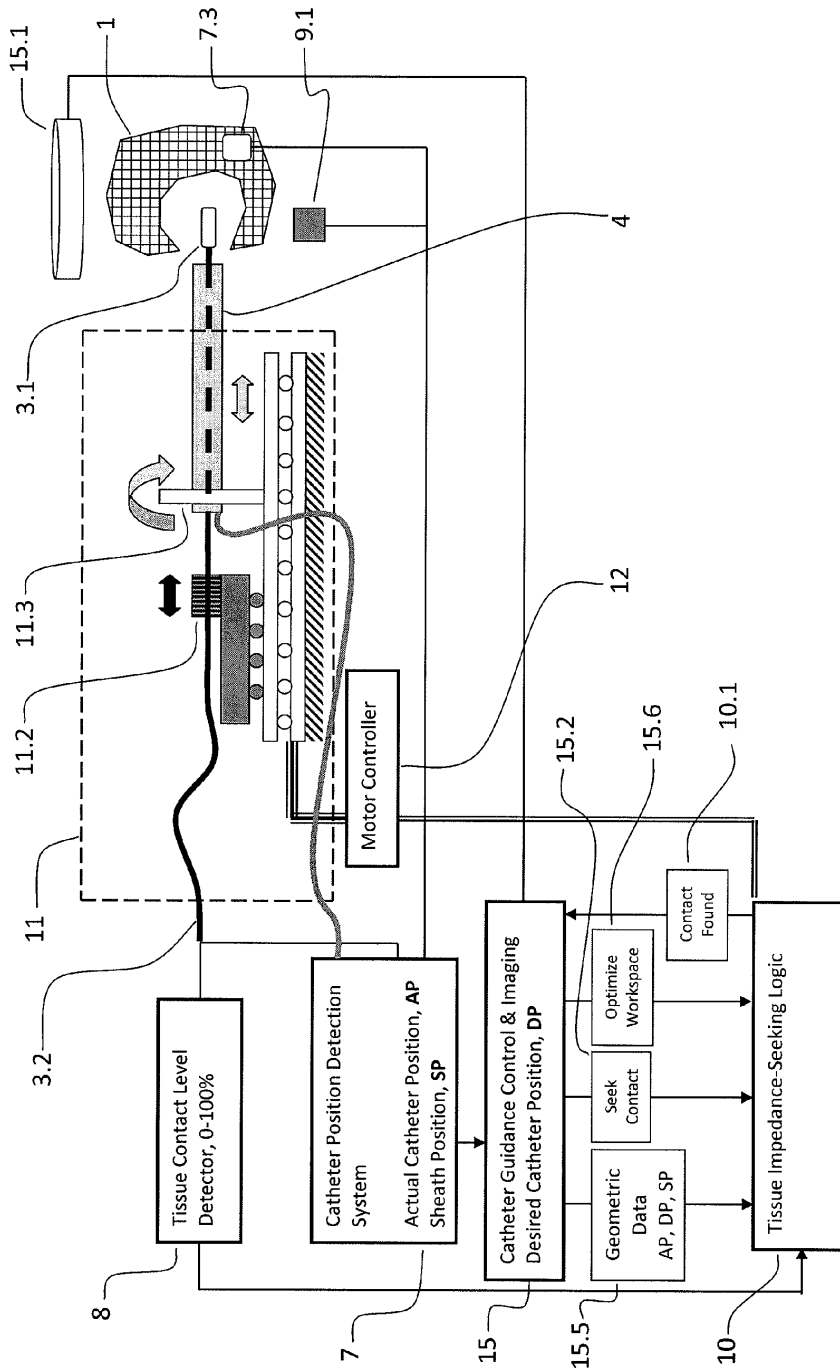


Figure 1



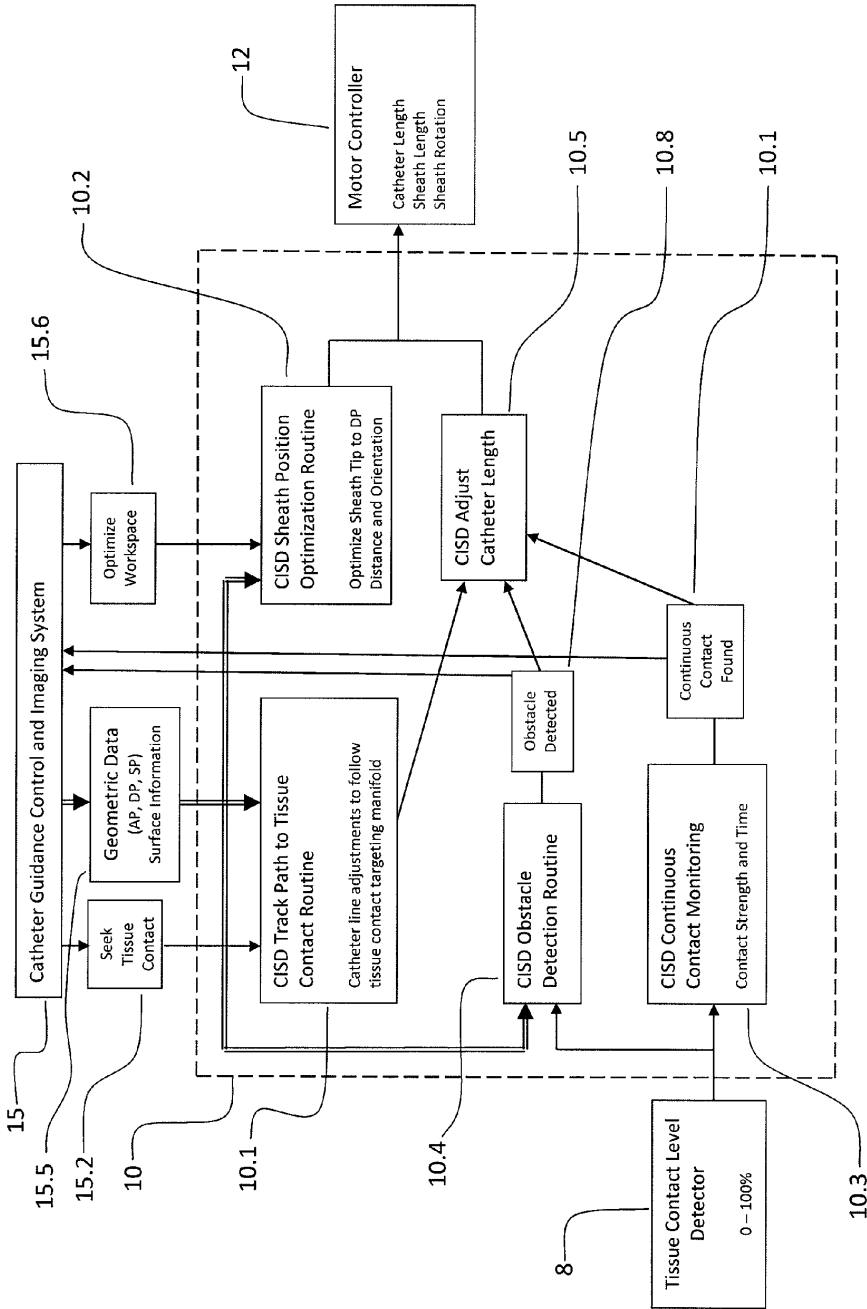


Figure 2

04



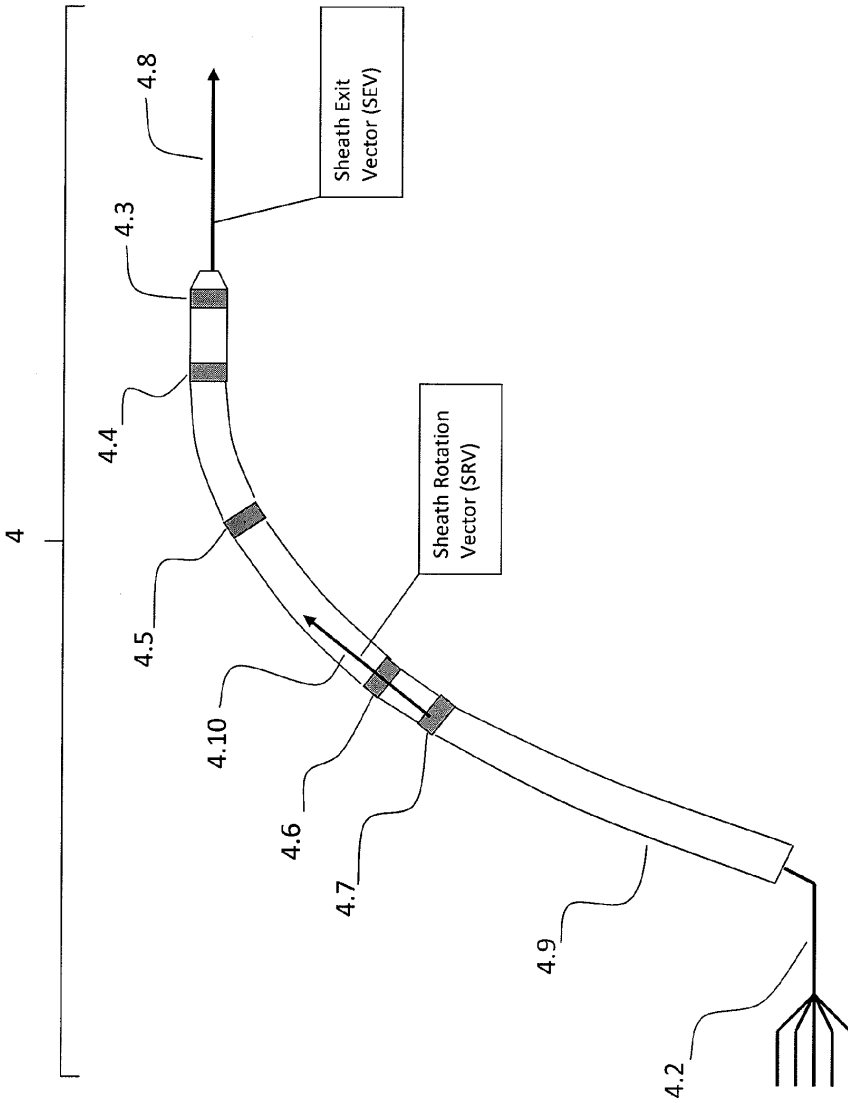


Figure 4A

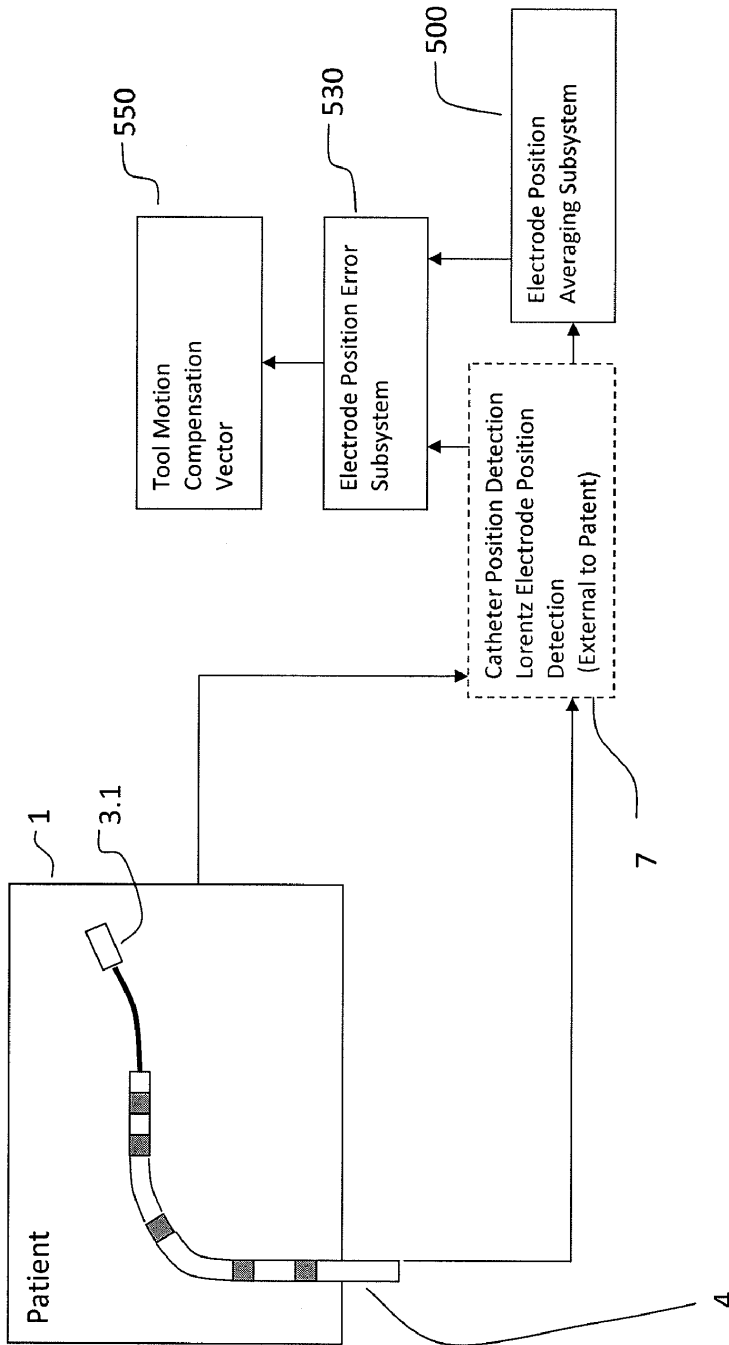


Figure 4B

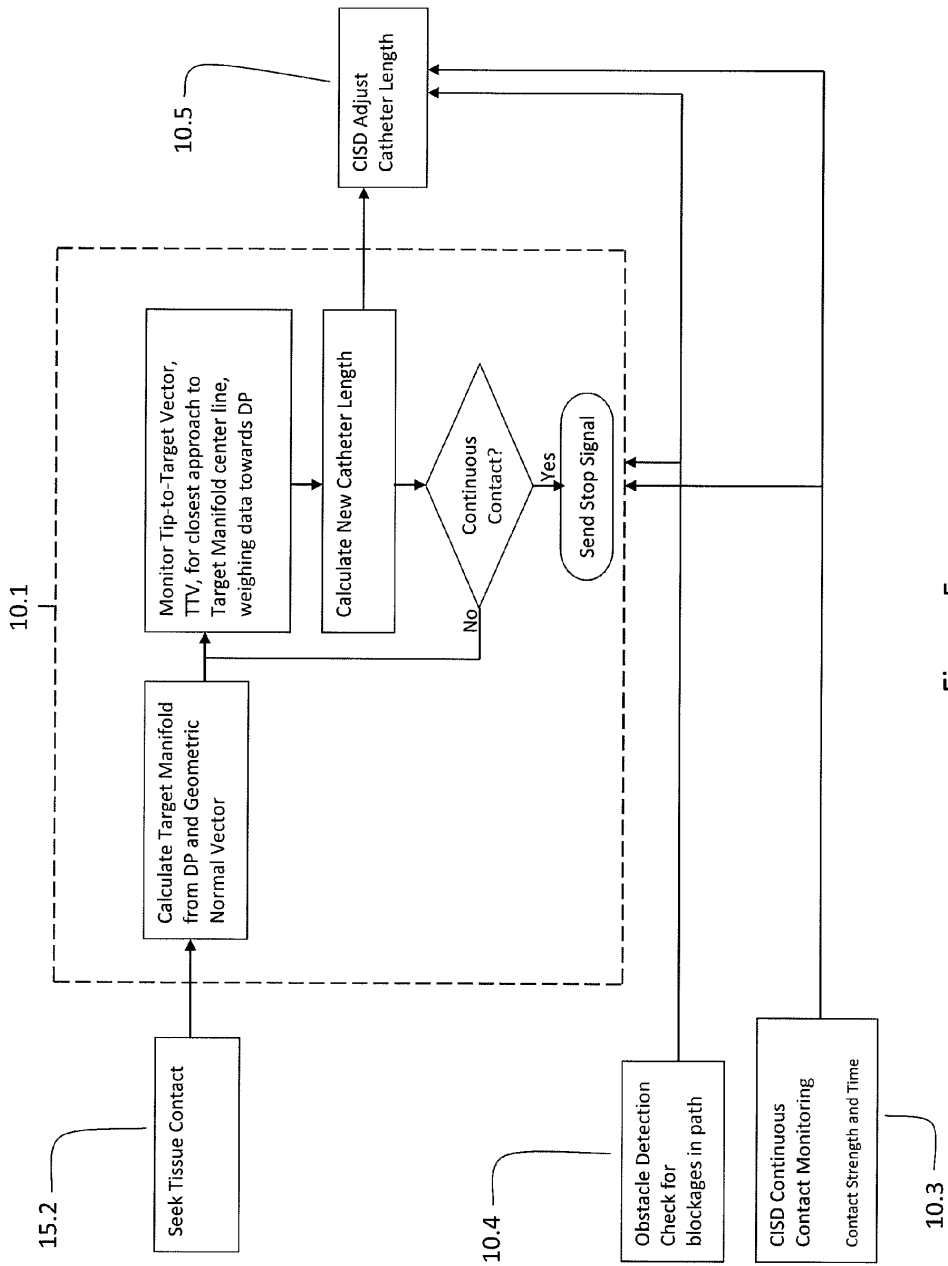


Figure 5

04



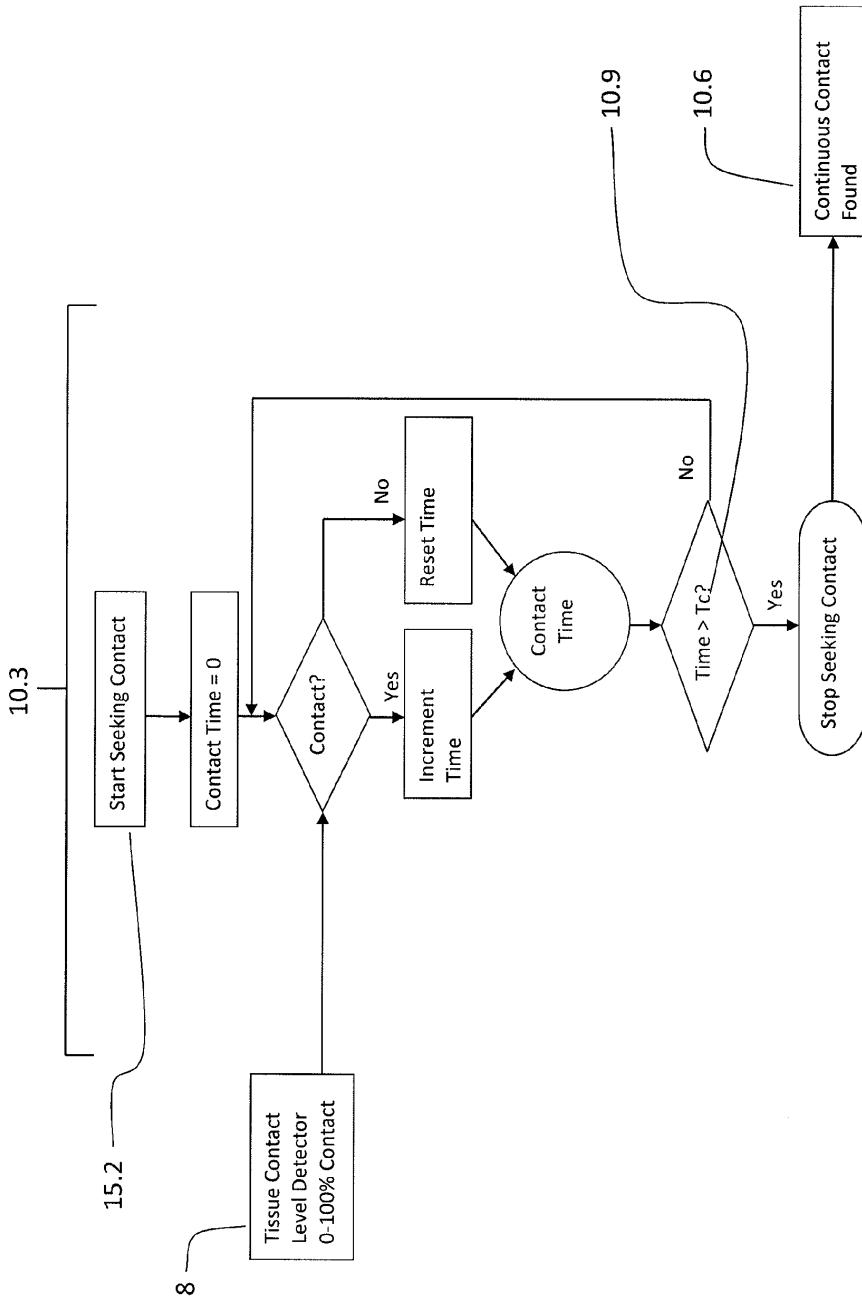


Figure 6



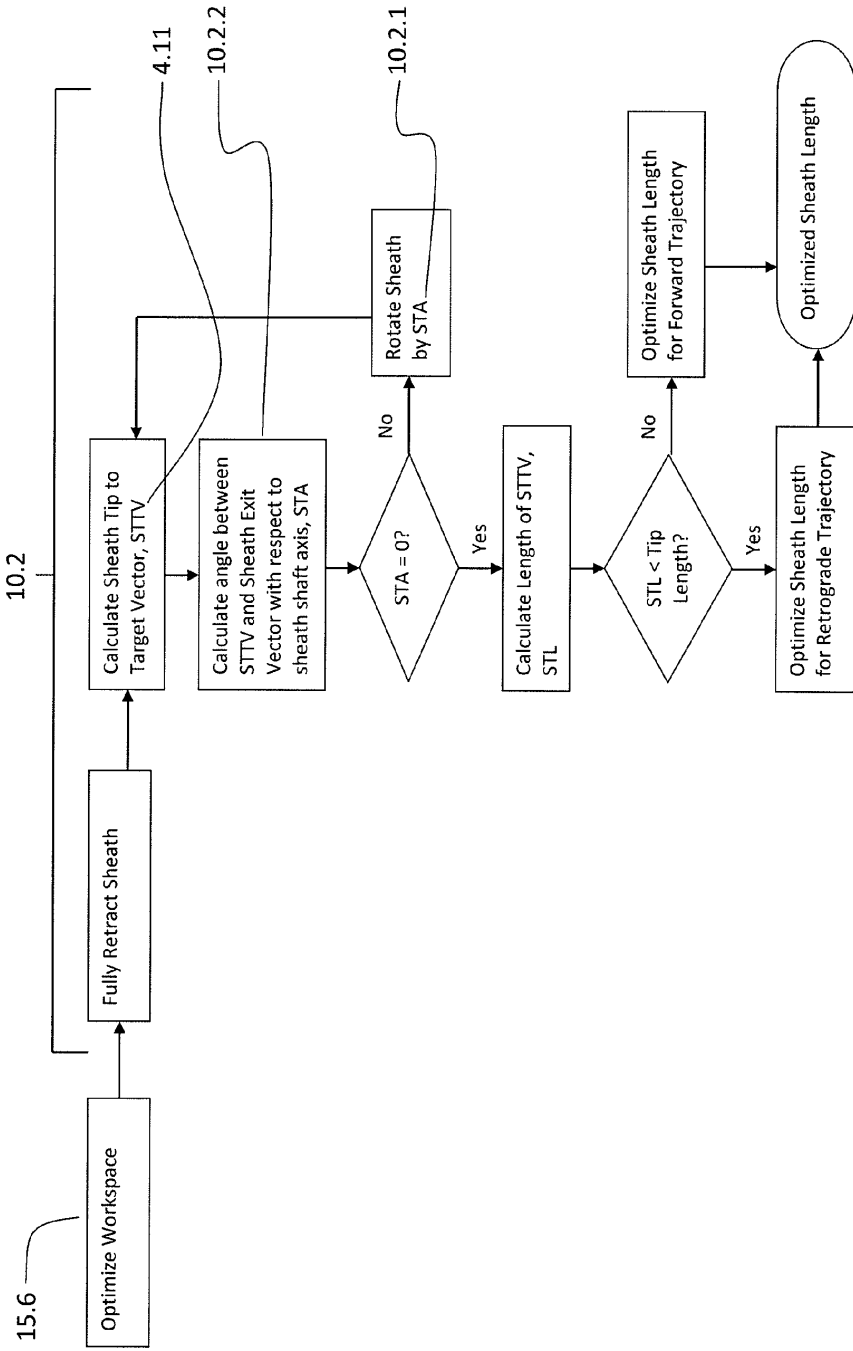


Figure 7

04

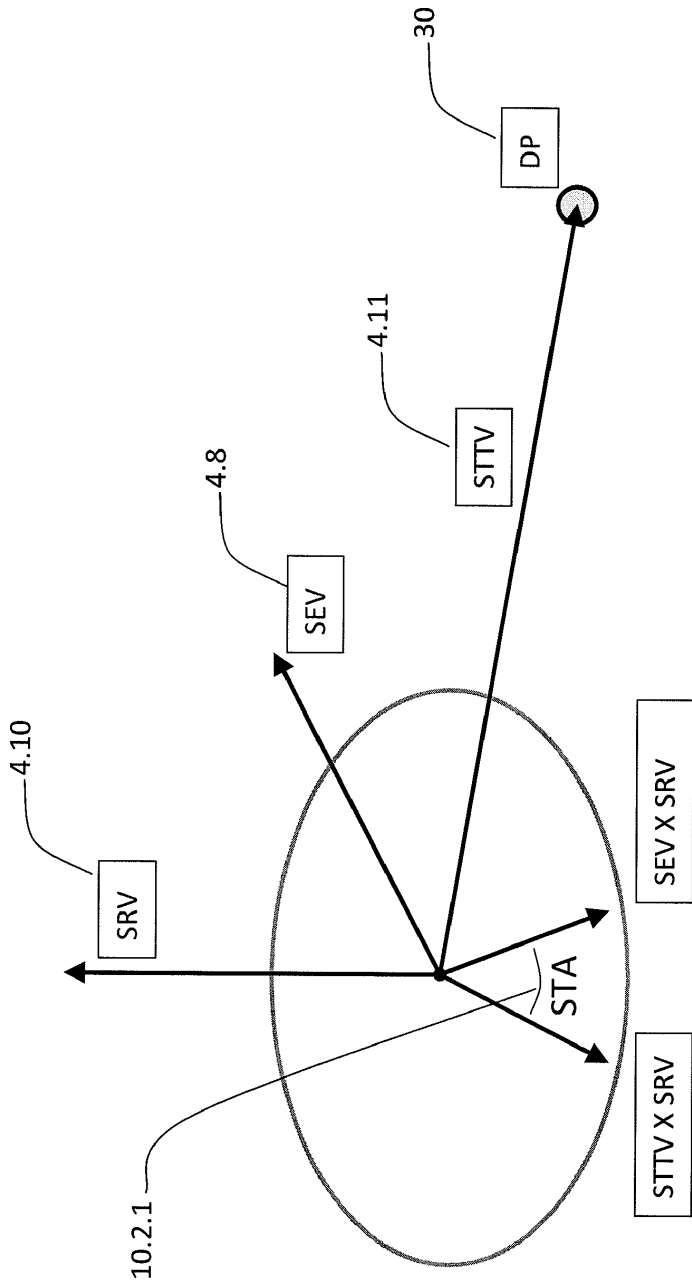


Figure 8

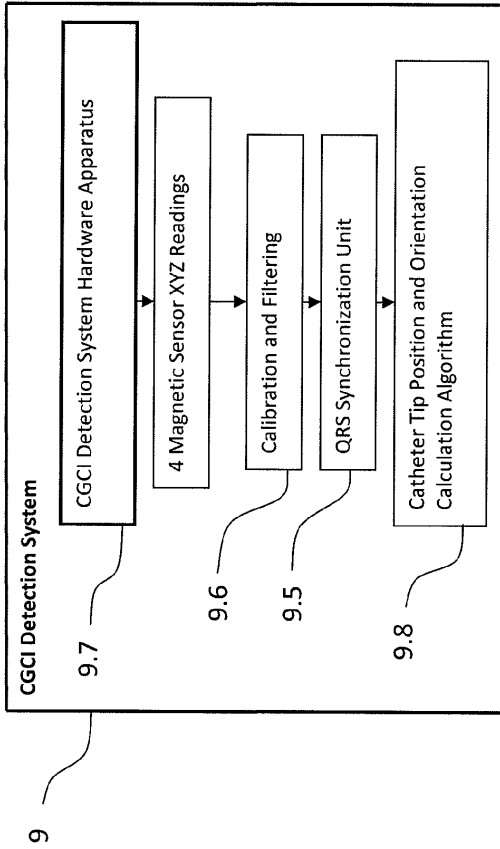


Figure 9A

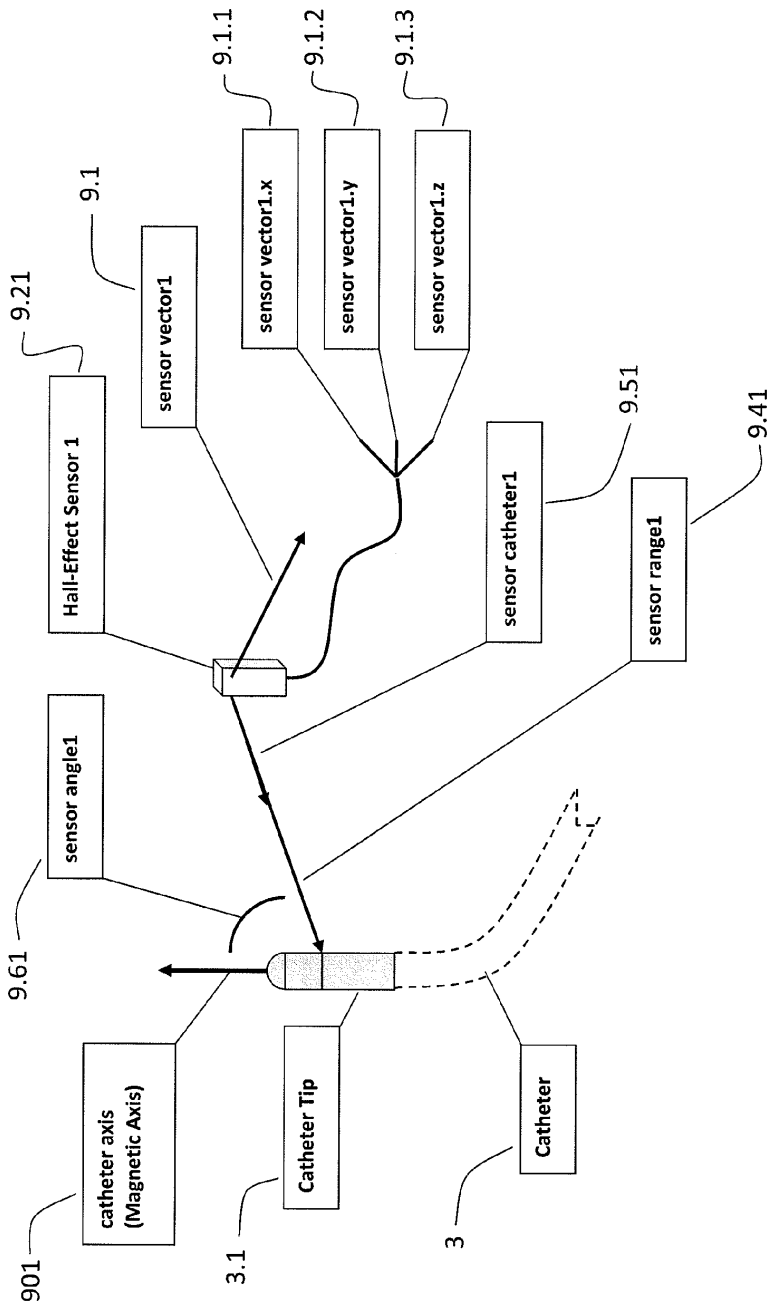


Figure 9B



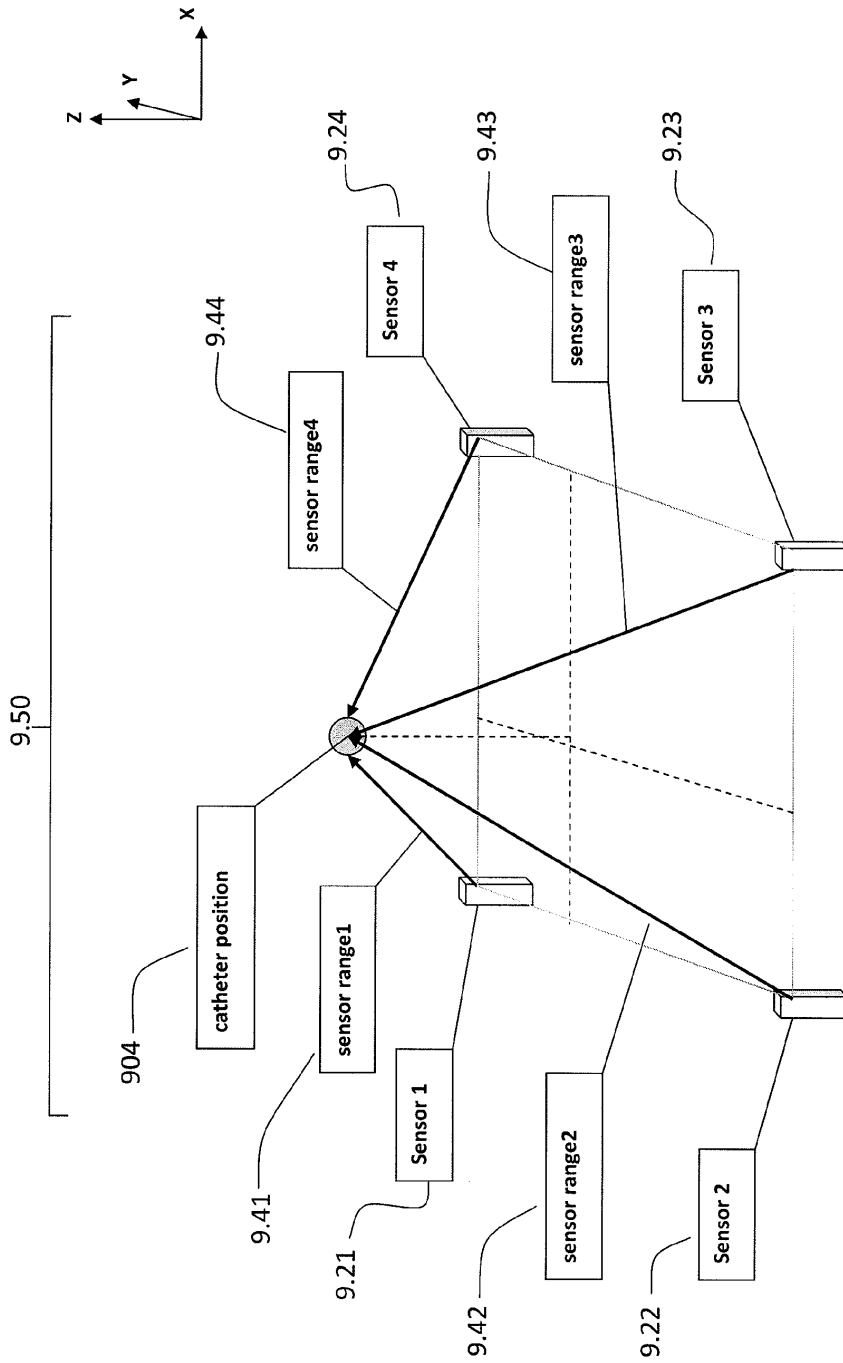


Figure 9C

04



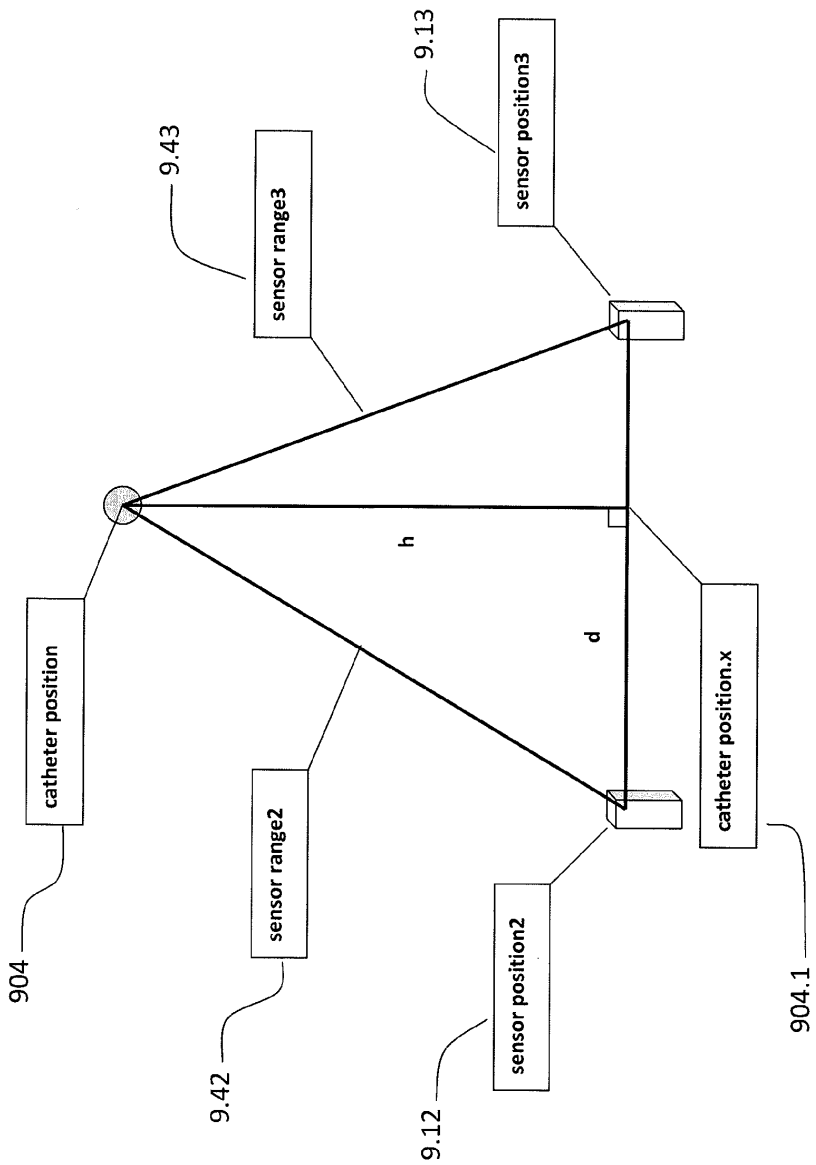


Figure 9D



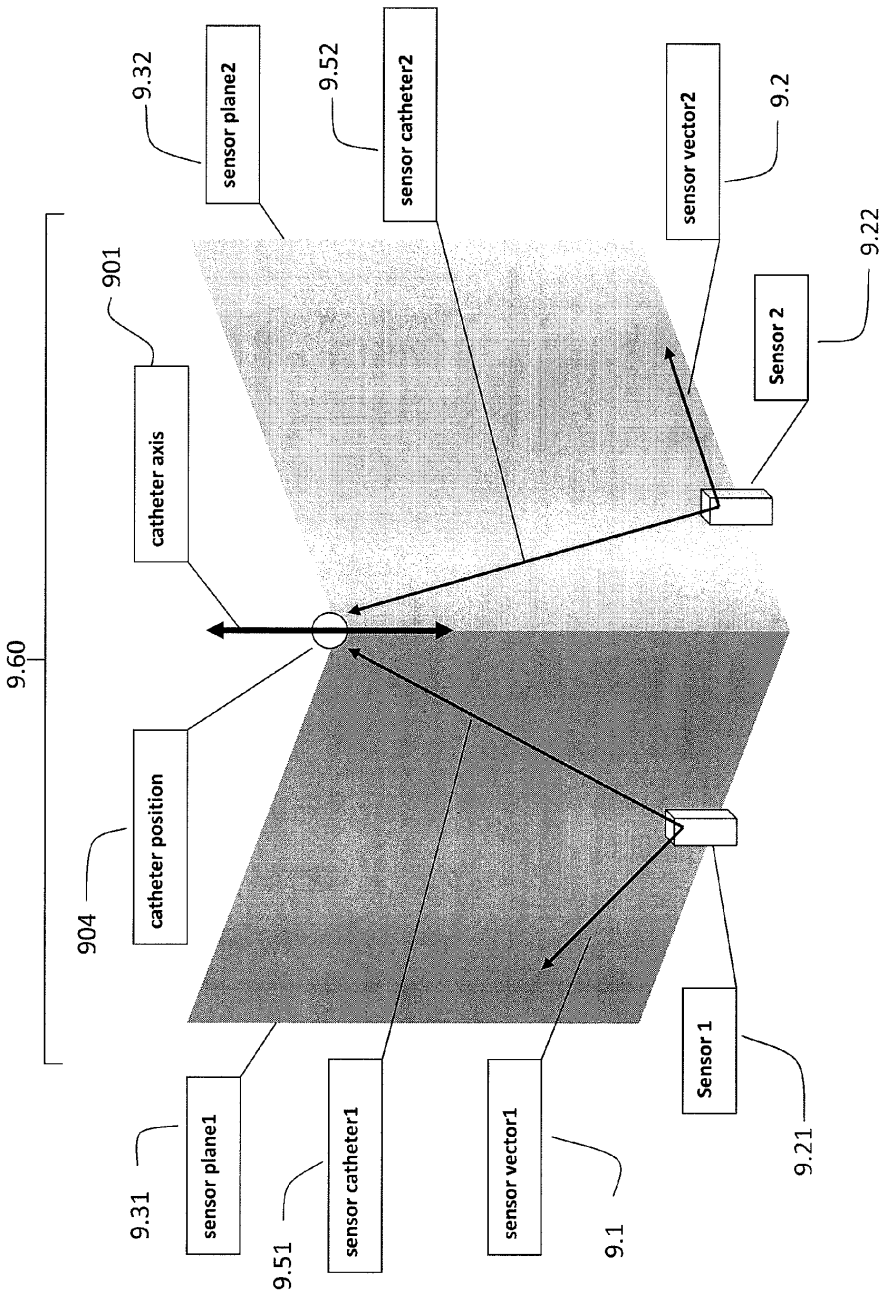


Figure 9E

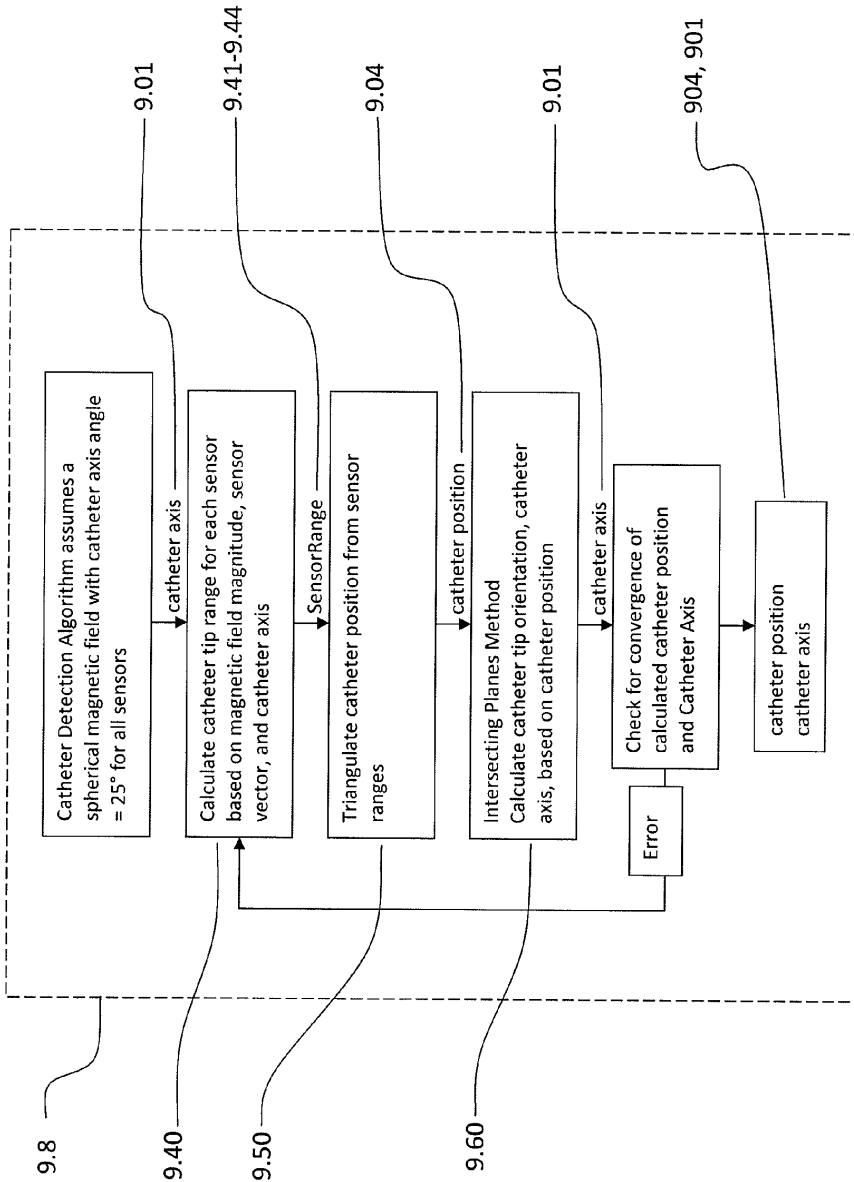


Figure 9F



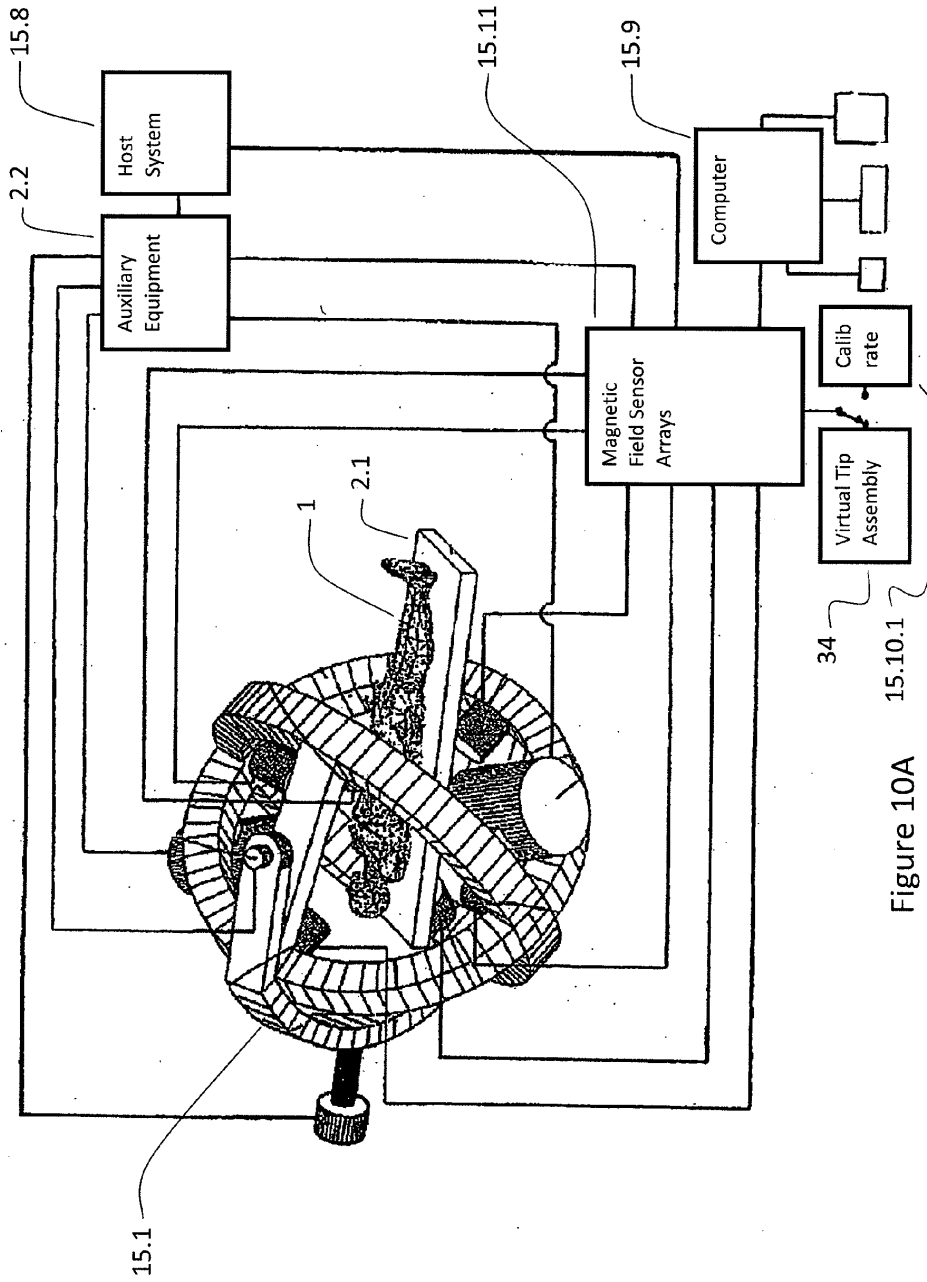


Figure 10A

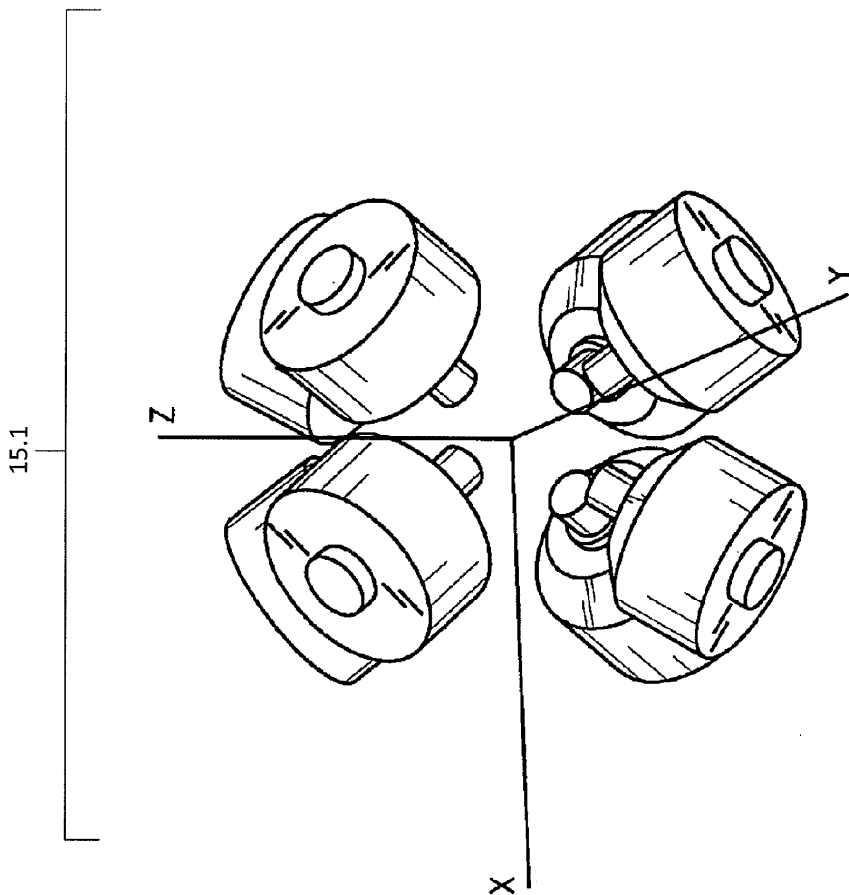


Figure 10B

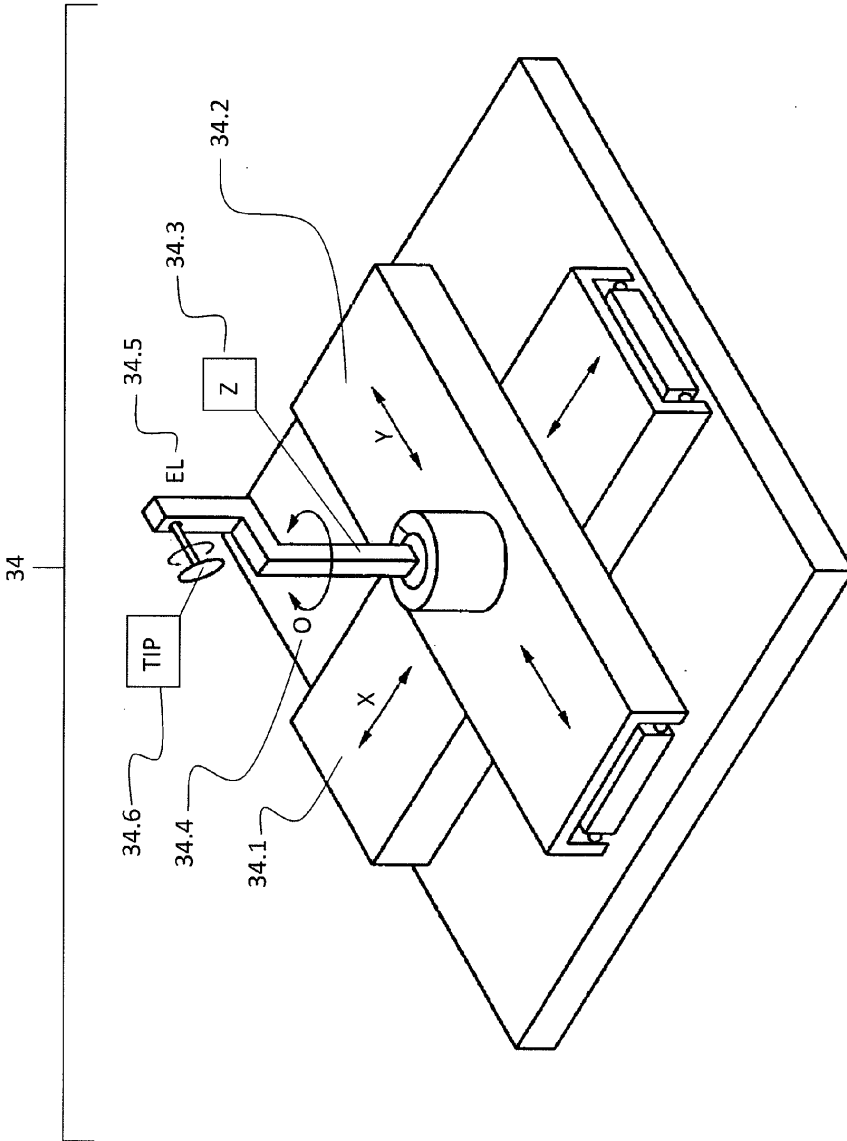


Figure 10C

04



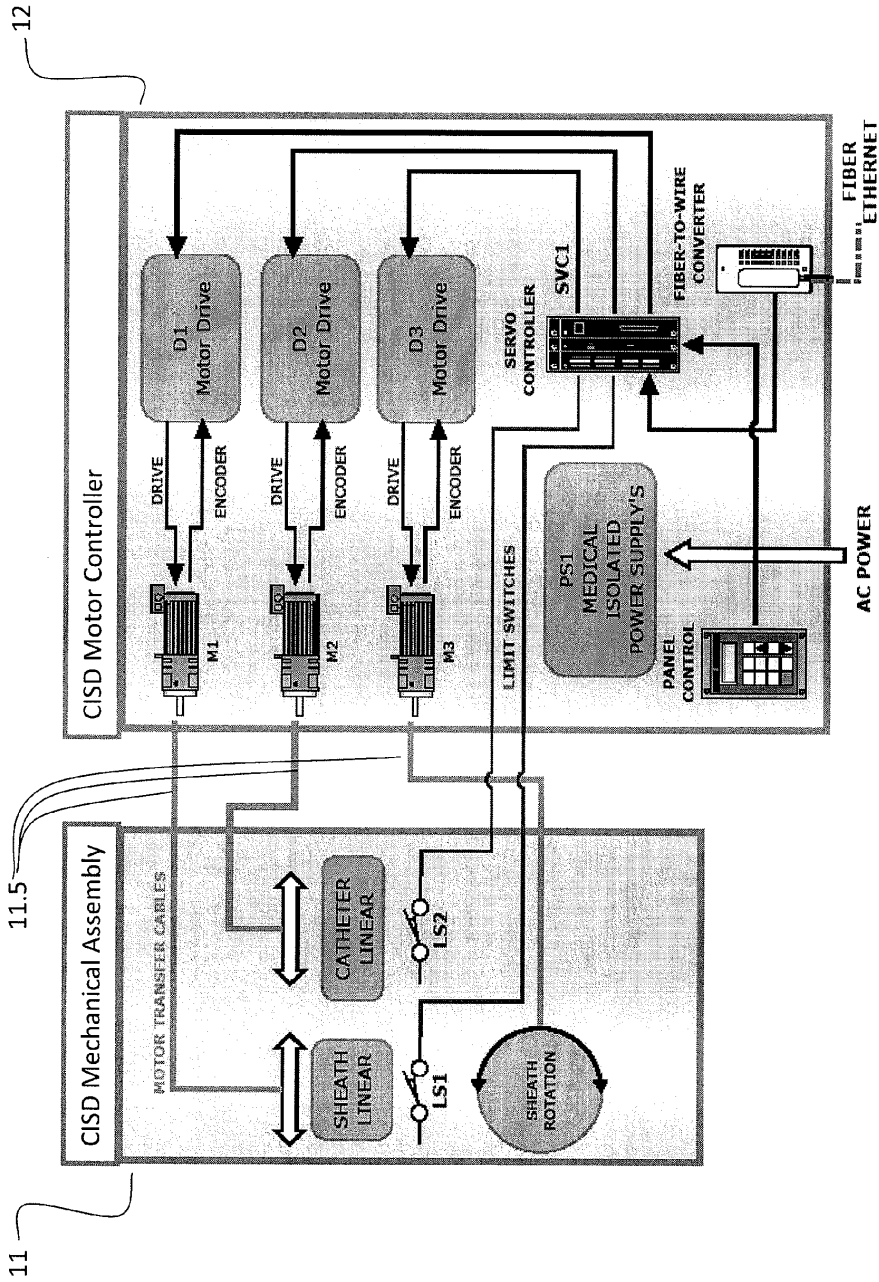


Figure 11A



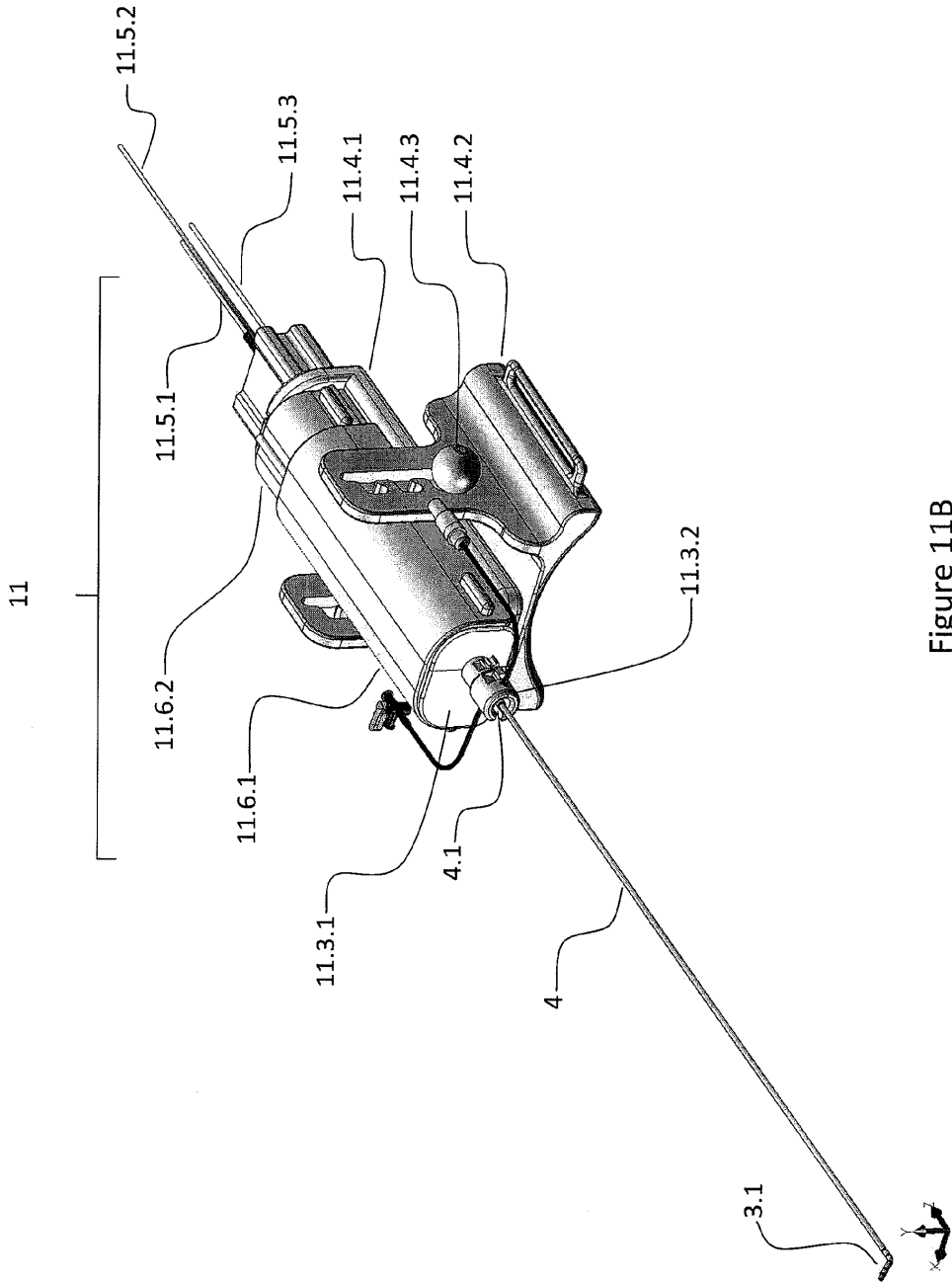


Figure 11B

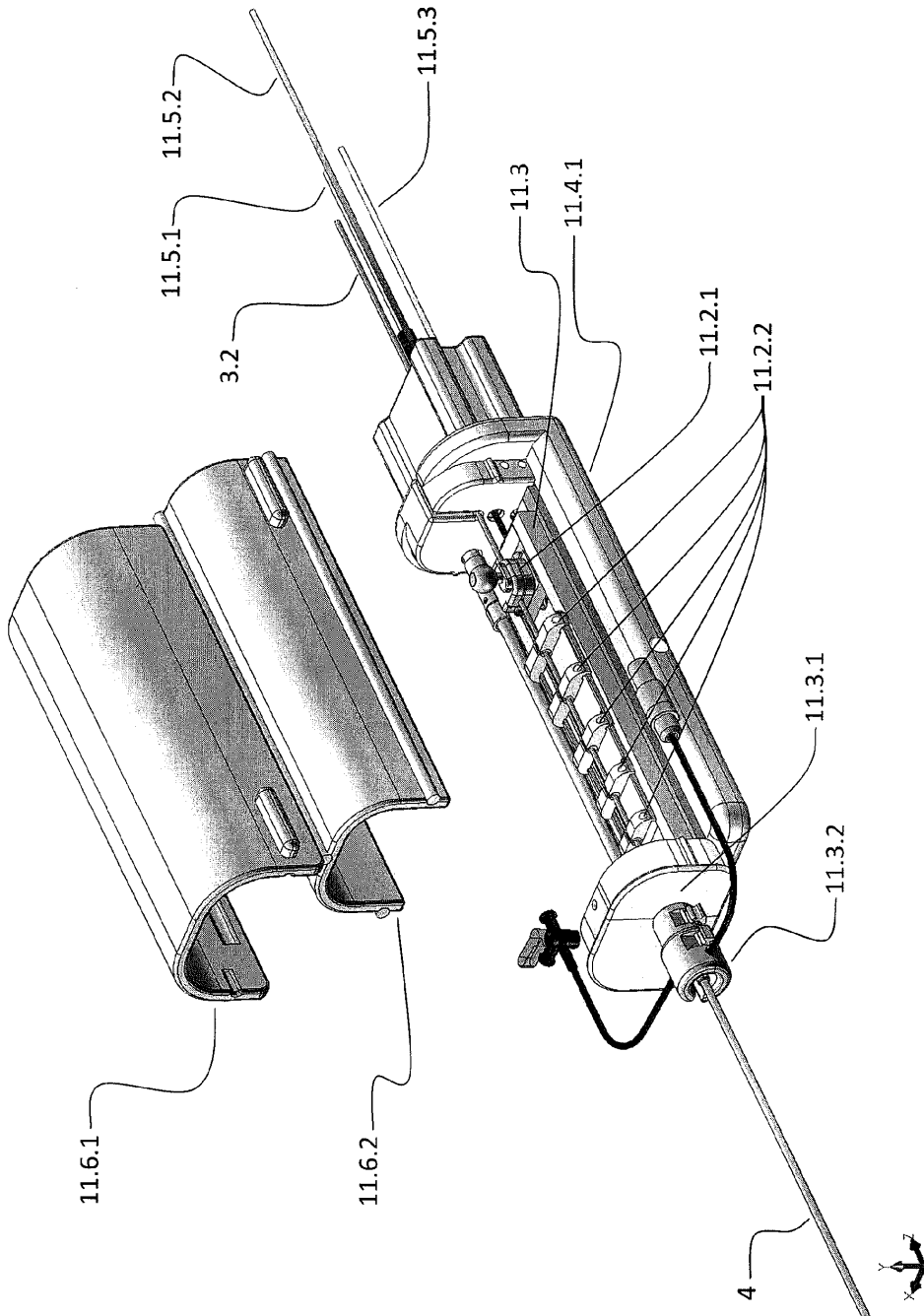


Figure 11C

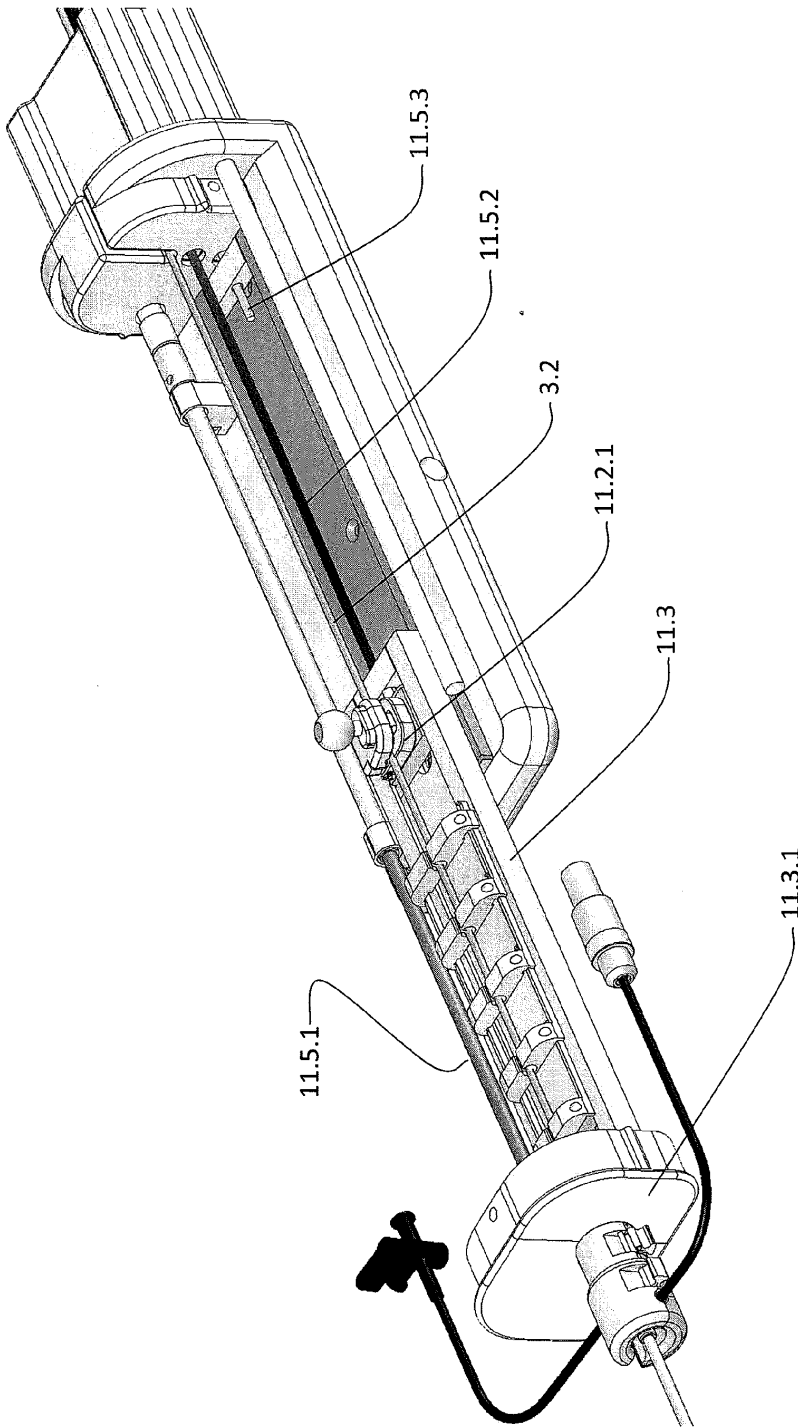


Figure 11D

04



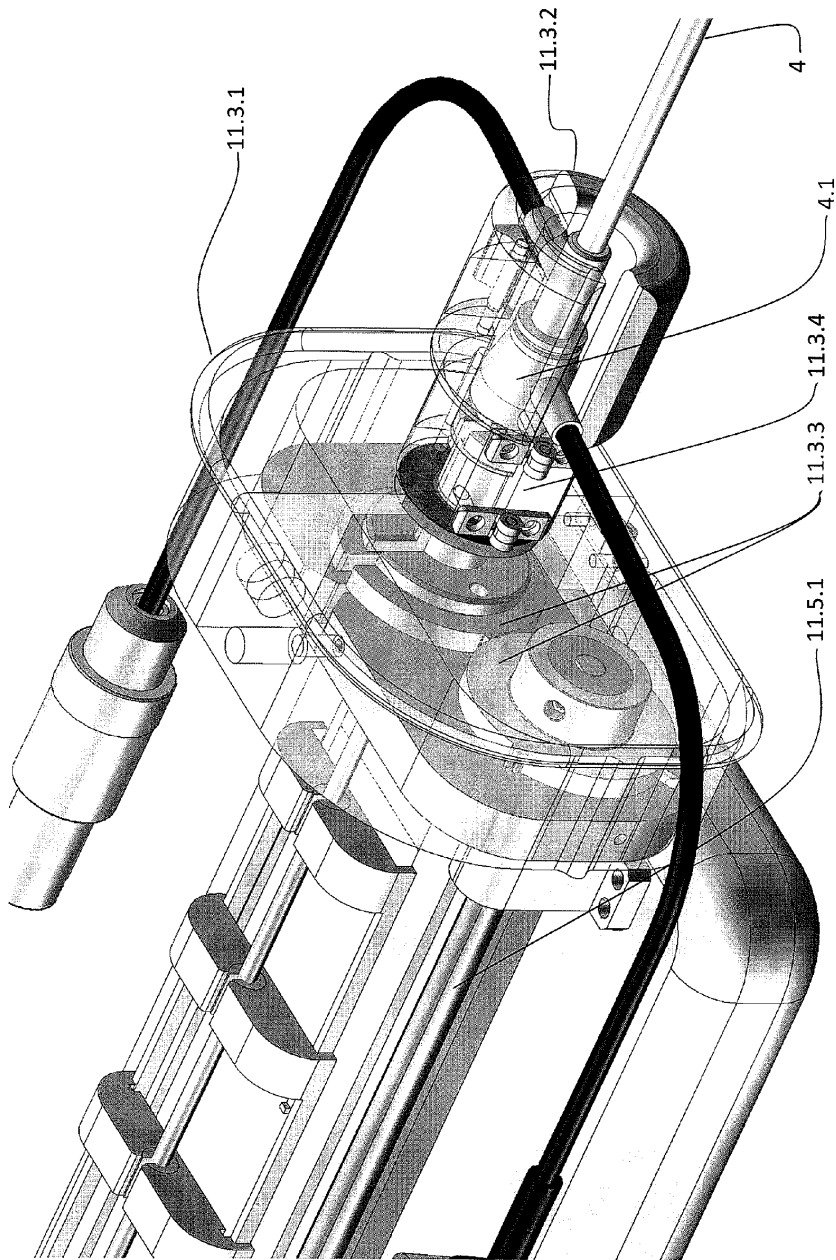


Figure 11E





## SYSTEM AND METHOD FOR A CATHETER IMPEDANCE SEEKING DEVICE

### BACKGROUND

**[0001]** 1. Field

**[0002]** The invention relates to the placement of catheters in contact with specific anatomical locations while optimizing the direction and orientation of tissue contact.

**[0003]** 2. Description of the Related Art

**[0004]** Cardiac rhythm disturbances are a major cause of morbidity and mortality in the adult population. A great deal of progress has been made in the past several decades in the diagnosis and treatment of many of the rhythm disorders of the heart. Intracardiac electrode catheters have been developed for defining the diagnosis of arrhythmias and for delivering ablative energy to specific intracardiac sites. Examples of arrhythmias that are susceptible to treatment with catheter ablation include: atrial fibrillation, atrial flutter, ablation of accessory atrio-ventricular pathways, AV nodal reciprocating tachycardia, ectopic atrial rhythms, ventricular tachycardia arising in either chamber or near the semilunar valves. Because atrial fibrillation is by far the most prevalent significant cardiac arrhythmia in the adult population, and because the ablation of this arrhythmia has become the most common ablation procedure performed in Electrophysiology Laboratories, we will focus our discussion on the putative mechanisms of this arrhythmia and on the various ablation strategies currently utilized for its treatment.

**[0005]** For clinical purposes atrial fibrillation (AF) can be 'paroxysmal', 'persistent' or 'chronic.' Haissaguerre is credited with having made the observation that paroxysmal AF is frequently triggered by a focal 'trigger', most frequently in one of the four pulmonary veins that insert into the left atrium. He further reported that ablation of such a trigger can eradicate paroxysmal AF. In patients with persistent or chronic AF, it appears that atrial 'remodeling' takes place which somehow augments the number of triggers or 'drivers' that initiate and perpetuate AF. In such patients, who, in fact, represent the vast majority of patients presenting with this arrhythmia, the AF 'drivers' are probably located further away from the ostia of the pulmonary veins. It is also thought that the autonomic nervous system plays a role in both paroxysmal and persistent AF, and that ablation at or near ganglionic plexi in the left atrium might be effective in the treatment of AF.

**[0006]** With the above observations in mind, empiric sets of RF lesions have been developed during the past several years. Since paroxysmal AF is thought to be trigger-dependent, circumferential lesions around the ostia of pulmonary veins are thought to be an integral part of the ablation procedure. Electrical isolation of the veins is thought to be critical for containment of the triggers within the veins. For patients with persistent of chronic AF, pulmonary vein isolation is usually also performed, but additional lesion sets are also often created so that the AF substrate is drastically modified, including linear sets of lesion across the 'roof' of the left atrium connecting the two superior pulmonary veins, as well as an 'isthmus' lesion line connecting the left inferior pulmonary vein and the mitral valve annulus. Some physicians also advocate searching for sites in the left atrium which manifest specific electrogram characteristics, such as continuous, low amplitude fragmented signals. Infrequently, the superior vena cava in the right atrium is also electrically isolated, when triggers can be demonstrated to originate from this structure. Finally, in patients who also manifest a typical form of atrial flutter, a

line of lesions is often created in the floor of the right atrium, connecting the tricuspid valve annulus to the inferior vena cava.

**[0007]** The foregoing discussion suggests that in order to achieve a therapeutic success with a catheter based ablation procedure, the proper energy source needs to be used, a thorough knowledge of the relevant anatomy needs to be obtained and used during the procedure, the lesions need to be deep enough and sufficiently contiguous in order to prevent electrical conduction at the relevant sites (achieve "isolation" of pulmonary vein ostia), and the catheters need to be able to reach the relevant sites and to remain stable at each site during the delivery of ablative energy.

**[0008]** As noted, in order to safely and effectively perform a left atrial ablation procedure, a detailed understanding of the relevant anatomy is essential. At present, 3D electroanatomic and impedance mapping systems are in use (CARTO, Biosense Webster, and EnSite NavX, St Jude Medical). These systems facilitate the creation of anatomic depictions of the left atrium. Recently, in an attempt to optimize catheter localization, these systems have also evolved to permit the integration of pre-acquired CT and MRI images with real-time 3D maps. One limitation associated with image integration is the potential for chamber wall deformation by catheter pressure on the endocardial surface of the heart; this can result in an inaccurate map and suboptimal image integration. Other limitations of current mapping systems include the occasional creation of anatomic "false spaces", i.e., computer depiction of regions that do not correspond to true anatomic structures.

**[0009]** The potential for serious complications during and after RF ablation in the heart has been well documented. Adverse outcomes can include tissue perforation with resultant pericardial tamponade and systemic shock, formation of thrombi at the site of ablation or on the tip of the catheter, inadvertent damage to important structures such as coronary arteries or the normal conduction system, late formation (1-2 weeks post-procedure) of an esophageal-left atrial fistula. It is likely that these complications are, at least in part, related to inadequate temperature and energy regulation available in current ablation systems.

**[0010]** As described above, it is common to steer the catheter to a specific position which has been referenced to an anatomical location via an acquired map. The static anatomical maps are used to specify either a median position or extreme limit of the moving tissue surface. Under the rigors of cardiac motion (e.g., the Systole/Diastole cycle), the catheter is guided to the specified surface location by synchronizing the average position of the catheter with the average position of the surface location, represented by a point on the anatomical map.

**[0011]** The prior art has been concerned with the placement of the distal portion of the catheter or medical device with respect to the current location and orientation, or with respect to a location on a static geometric map. The prior art has difficulty in acquiring and maintaining continuous tissue contact in the presence of a dynamic moving frame using static positional reference points. Such reference points, comprising the anatomical map, cannot account for the current location of the actual surface.

**[0012]** Where prior art advances a tool to a geometric location, it cannot specify an optimized tool orientation to acquire and maintain contact with a moving surface.

### SUMMARY

**[0013]** The system and methods described herein solve these and other problems by enhancing a Catheter Guidance



Control and Imaging (CGCI) system by employing relatively high-speed tissue contact information, a closed-loop regulator and a set of heuristic logic routines to aid in acquiring and maintaining tissue contact at or near the specified location on a static geometric map. The actual tissue surface is sought along a path relatively normal to the static geometric surface and passing through the desired geometric target location. In addition, the geometric map information is used to optimize the travel path of the distal portion of the catheter to the surface, as well as optimizing the orientation of the distal tip as to best maintain surface contact.

**[0014]** Moreover, the system and methods described herein correct problems arising from the prior art's inability to assess in a real-time fashion whether or not the catheter is actually in contact with endocardial tissue, the actual pressure exerted by the catheter tip, the actual stability of the catheter on any particular anatomic site, and the absence of a real-time assessment of the size of the lesion being formed during RF application. These systems and method improve over current techniques such as fluoroscopy by providing tactile feed-back to the clinician's hands (the "feel" of the catheter), and/or electrogram characteristics.

**[0015]** By employing relatively real-time tissue contact data in a closed-loop servo system, the map formed by the 3D mapping system (e.g., NavX) creates actual anatomic borders. Confirmation of true and stable electrode-tissue contact allows for employing the lowest amount of energy for safe lesion creation. The improved accuracy of the map allows for excellent stability of the catheter electrode tip-tissue contact, thereby reducing errors in the amount of energy applied to the cardiac surface. Relatively real-time impedance measurement allows for relatively real-time titration of energy delivery using the closed-loop feedback system. It also provides improved travel of the catheter within structures such as, for example, the left atrium, by regulating the rotation of the Lorentz sheath and advancing the catheter in the desired direction while seeking the appropriate tissue impedance data described herein. The system and methods herein improve the accuracy of the generated 3D map while decreasing the time that is required for creation of this map, increase the clinical success rate by assuring the contiguity of the RF lesions (at least in part by enhancing the ability of the catheter to reach all important anatomic sites, and by monitoring the size and depth of the lesions created by RF application), reduce or eliminating complications due to catheter delivery of RF energy by more accurately gauging the pressure exerted by the catheter against the chamber wall, and decreasing the length of time required for these procedures.

**[0016]** In one embodiment, an introducer is inserted into a patient via a vein or orifice, and the distal end guided to the area of interest. A Lorentz Active Sheath (LAS) introducer, as detailed below, is a modified introducer which has embedded electrodes and is thereby detectable by a Lorentz Catheter Position Detection System (CPDS). A catheter is inserted via the LAS sheath and the catheter's distal tip is extended into the area of interest. The proximal ends of the LAS and catheter shaft are attached to the catheter impedance-seeking device's (CISD) mechanical control fixtures. When an anatomical location is selected within the Catheter Guidance Control and Imaging system (CGCI), the invention first uses the geometric map and location information to optimize the workspace and direction of tissue contact by rotating, advancing or retracting the LAS sheath. As the CGCI guides the tool to the desired location, the higher speed tissue impedance-

seeking logic attempts to acquire and maintain tissue contact by advancing or retracting the catheter using tip location and contact information. The CGCI system activates the impedance-seeking system whenever it is attempting to reach continuous tissue contact. When contact is made and maintained, the impedance-seeking logic sends the CGCI a continuous-contact signal. When contact is made in the incorrect location on the tissue, the impedance-seeking logic may selectively retract the tip from tissue contact and try again, or it may stop and alert the CGCI as to the amount of error and allow the CGCI to decide what actions to perform next. When an unknown obstacle is encountered far from the expected tissue surface, the impedance-seeking logic will alert the CGCI system to plan a path around the obstacle.

**[0017]** The Lorentz-Active Sheath (LAS), serves as a conduit for other medical devices, such as catheters, balloons, biopsy needles, etc. The sheath is inserted into a vein or other body orifice and is guided into the area where the operation is to be performed. The position and orientation of the LAS is tracked via a position detection system which emits electrical signals that are sensed through several electrodes coupled to the LAS. The signals received from the LAS are used to calculate an accurate and reliable assessment of the actual position of the LAS within the patient.

**[0018]** The Catheter Position Detection System (CPDS) can be a conventional Lorentz positioning system, such as, for example, the EnSite system from St. Jude Medical Inc. Atrial Fibrillation Division, which sends electrical signals through patches placed upon the patient. These electrical signals are detected through electrodes on the surface of the catheters, giving the position of each electrode.

**[0019]** The Tissue Contact Detector is a Lorentz positioning system accessory device which differentiates between the impedance signals from tissue contact and blood-pool contact. The Tissue Contact Detector operates inside of the CPDS system, and is electrically connected to the distal electrode of the catheter.

**[0020]** The CGCI (Catheter Guidance Control and Imaging) uses the Catheter Position Detection System (CPDS) information and a magnetic chamber to push, pull, and steer a magnetically-tipped catheter. The operator uses a virtual tip controller to specify a desired catheter position and orientation, DP, in the CGCI. The CGCI directs the tip to DP using the actual position and orientation of the catheter, AP, which is received from the CPDS. In one embodiment, the CGCI system includes a system whereby a magnetic tip attached to a surgical tool is detected, displayed and influenced positionally so as to allow diagnostic and therapeutic procedures to be performed rapidly, accurately, simply, and intuitively. The tools that can be so equipped include catheters, guidewires, and secondary tools such as lasers and balloons, in addition biopsy needles, endoscopy probes, and similar devices. The magnetic tip allows the position and orientation of the tip to be determined by analyzing a magnetic field (with or without supplemental use of other systems, such as, for example, x-rays, ultrasonics, etc.). The magnetic tip further allows the tool tip to be pulled, pushed, turned, and forcefully held in the desired position by applying an appropriate magnetic field external to the patient's body. A Virtual Tip (a multi-axis joystick-like device providing up to six degrees of freedom or more) serves as an operator control. Movement of the operator control produces corresponding movement of the magnetic tip inside the patient's body. Additionally, the control provides tactile feedback to the operator's hand in the appro-

appropriate axis or axes if the magnetic tip encounters an obstacle. The output of the control combined with the magnetic tip position and orientation feedback allows a servo system to control the external magnetic field by pulse width modulating the positioning electromagnet. Data concerning the dynamic position of a moving body part, such as a beating heart, offsets the servo systems response in such a way that the magnetic tip, and hence the secondary tool is caused to move in unison with the moving body part. The tip position and orientation information and the dynamic body part position information are also utilized to provide a display that allows three dimensional viewing of the magnetic tip position and orientation relative to the body part. In one embodiment, an amount of tactile feedback is computed based at least in part on a difference between a desired position and an actual position of the catheter tip position. In one embodiment, tactile feedback is provided as a feedback vector computed based on a difference between a desired position vector (e.g., desired position and orientation) of the catheter tip and an actual position vector (e.g., actual position and orientation) of the catheter tip. Thus, when provided as a feedback vector, tactile feedback can be different as the virtual tip is moved in different directions (e.g., in connection with the different degrees of freedom). In one embodiment, tactile feedback is filtered to reduce noise. In one embodiment, tactile feedback is threshold filtered such that errors below a certain threshold do not produce tactile feedback.

**[0021]** In another embodiment, the Catheter Position Detection System (CPDS) is the CGCI Magnetic Catheter Position Detection System, including a method and apparatus for detecting position and orientation of catheter distal magnetic element while it moves in a patient's heart. In one embodiment, the apparatus includes four or more sensors for detecting the magnetic field generated by the catheter tip. The sensors transmit the field magnitude and direction to a detection unit, which filters the signals and removes other field sources, such as generated by CGCI coils and external medical hardware. The method allows the measurement of magnitude corresponding to the catheter tip distance from the sensor and the orientation of the field showing the magnetic tip orientation. Since the tip's magnetic field is not symmetric, the position and orientation computation technique are not independent of each other. Hence, an iterative calculation is used to converge to a solution. The method of determining tip position is calculated by triangulation from each sensor, and whereby the tip orientation is calculated by an intersecting-planes algorithm. The orientation is used to adjust the distances from each sensor, and the process is repeated until convergence for both position and orientation is achieved. The resultant value provides the actual catheter tip position and orientation (AP). The actual position is further filtered by synchronizing the AP measurements with the QRS signal of the heart, allowing the operator and CGCI controller to view the organ as a static object.

**[0022]** In one embodiment, a controllable magnetic field source produces a magnetic field to guide a tool (e.g., catheter, introducer, Lorenz sheath, guidewire, etc.) having a distal end responsive to the magnetic field. One or more sensors are configured to sense a current vector position of the distal end by measuring one or more impedances. A controller controls the magnetic field source to control a movement of the distal end according to a feedback calculation wherein the system controller is configured to compute a position error comprising a difference between a desired vector position of

the distal end and the current vector position of the distal end. An operator control is used to provide tactile feedback to an operator when the position error exceeds a predetermined amount, wherein the tactile feedback is computed by the controller at least in part according to the vector position error. In one embodiment, a correction input to the desired vector position is computed based on a position of a heart relative to a frame of reference, such that the system controller compensates for a dynamic position of a wall of a heart chamber such that the distal end maintains contact with the wall of the heart chamber at least in part by measuring at least one impedance between the distal end and the wall. In one embodiment, the tool includes a Lorenz sheath.

**[0023]** In one embodiment, one or more patches are provided to the patient, wherein the apparatus measures a position and orientation of a Lorenz sheath at least in part by measuring one or more impedances between the Lorenz sheath and the conductive patches.

**[0024]** In one embodiment, the controller is configured to control the magnetic field source to maintain the distal end in a desired vector orientation relative to the wall (e.g., an interior wall of a heart chamber, artery, vein, or other anatomical structure). In one embodiment, the controller is configured to control the magnetic field source to maintain the distal end substantially normal to the wall. In one embodiment, the controller is configured to differentiate between contact with the wall and contact with an obstruction by analyzing differences between a measured impedance and an expected impedance. In one embodiment, the controller is configured to compute a path around the obstruction. In one embodiment, the controller is configured to control the magnetic field source to maintain the distal end in a desired orientation relative to the wall. In one embodiment, the controller is configured to differentiate between contact with the wall and contact with other tissue by analyzing differences between a measured impedance and an expected impedance, the expected impedance corresponding to the wall. In one embodiment, the other tissue includes a blood pool.

**[0025]** In one embodiment, the controller is configured to seek contact with the wall by calculating a target manifold, monitoring a distal end-to-target vector with respect to the target manifold, calculating a new tool length, and adjusting a length of the tool according to the new tool length.

**[0026]** In one embodiment, the tool includes an introducer. In one embodiment, the controller controls a rotation and translation of the introducer.

**[0027]** In one embodiment, a method for positioning a surgical tool and maintaining relatively continuous contact between a distal end of the tool and a desired tissue location, includes controlling a position and orientation of a distal end of a surgical tool by adjusting currents in a plurality of electromagnets, measuring a plurality of impedance values between the distal end and a plurality of tissue locations, constructing an impedance map at least in part from the plurality of impedance values, determining a first impedance value corresponding to an impedance measured when the distal end touches the desired tissue location, and using a feedback controller to control the currents to maintain contact between the distal end and the desired tissue such that the distal end is oriented relatively normal to the desired tissue location in the presence of motion of the desired tissue location, wherein feedback information to the feedback controller includes periodic impedance measurements between the distal end and the desired tissue location.

**[0028]** In one embodiment, the method further includes, computing a position error comprising a difference between a desired vector position of the distal end and the current vector position of the distal end, and providing tactile feedback to an operator control when the position error exceeds a predetermined amount, wherein the tactile feedback is computed at least in part according to the position error.

**[0029]** In one embodiment, the method includes locating the distal end by measuring impedances between a plurality of patches provided to the patient and the surgical tool.

**[0030]** In one embodiment, the method includes differentiating between contact with the desired tissue location and contact with an obstruction by analyzing differences between a measured impedance and an expected impedance. In one embodiment, the method includes computing a path around the obstruction.

**[0031]** In one embodiment, the method includes distinguishing between contact with the desired tissue location and contact with other tissue by analyzing differences between a measured impedance and an expected impedance, the expected impedance corresponding to an impedance at the desired tissue location. In one embodiment, the other tissue includes a blood pool.

**[0032]** In one embodiment, the method includes seeking contact with the desired tissue location by calculating a target manifold, monitoring a distal end-to-target vector with respect to the target manifold, calculating a new tool length, and adjusting a length of the tool according to the new tool length. In one embodiment, the tool includes an introducer. In one embodiment, the method includes controlling a rotation and translation of the tool.

#### BRIEF DESCRIPTION OF THE DRAWINGS

**[0033]** FIG. 1 is a schematic diagram of the signals and systems used in tissue impedance seeking.

**[0034]** FIG. 2 is a block diagram of the Tissue Impedance-Seeking Logic.

**[0035]** FIG. 3 is a schematic diagram of a catheter in relationship to the virtual and real tissue surface with associated control vector information.

**[0036]** FIG. 4A is an isometric diagram of the Lorentz-Active Sheath (LAS) assembly and the associated vectors used in workspace optimization.

**[0037]** FIG. 4B is a block diagram of the signals and systems used to determine the position of the LAS Electrodes.

**[0038]** FIG. 5 is a logic flow diagram of the CISD Track Path to Tissue Contact routine.

**[0039]** FIG. 6 is a logic flow diagram of the CISD Continuous Contact Monitoring routine.

**[0040]** FIG. 7 is a logic flow diagram of the CISD Sheath Position Optimization routine.

**[0041]** FIG. 8 is a vector diagram of the sheath rotation angle calculation.

**[0042]** FIG. 9A is a block diagram of the CGCI Position Detection System.

**[0043]** FIG. 9B is a schematic diagram of a Hall-Effect sensor in relationship to the catheter tip, and its generated measurement data.

**[0044]** FIG. 9C is a schematic diagram of a catheter position triangulation using four Hall-Effect sensors and their respective range values.

**[0045]** FIG. 9D is a detailed schematic of the triangulation of the catheter position's X-coordinate using two sensors.

**[0046]** FIG. 9E is a diagram of the Intersecting Planes Method for determining the orientation of a magnetic catheter tip from its position and two sensor's magnetic field values.

**[0047]** FIG. 9F is a block diagram of the method for determining both position and orientation when they are not independent values.

**[0048]** FIG. 10A is a diagram of the signals and systems used in catheter position control.

**[0049]** FIG. 10B is an isometric diagram of another embodiment of the magnetic chamber used to control catheter position.

**[0050]** FIG. 10C is an isometric diagram of a virtual tip assembly.

**[0051]** FIG. 11A is a block diagram of the signals and systems of the CISD Mechanical Assembly and CISD Motor Controller.

**[0052]** FIG. 11B is an isometric drawing of an embodiment of the CISD Mechanical Assembly.

**[0053]** FIG. 11C is an isometric detail drawing of the internal assemblies within the CISD Mechanical Assembly.

**[0054]** FIG. 11D is an isometric drawing showing the sheath shuttle in a forward position.

**[0055]** FIG. 11E is an isometric detail drawing of the sheath rotator housing.

#### DETAILED DESCRIPTION

**[0056]** FIG. 1 is a schematic diagram of the signals and systems used in tissue impedance seeking. A catheter 3 is inserted through a sheath (LAS introducer) 4 and into a patient 1. A catheter tip 3.1 is advanced into the patient and a catheter shaft 3.2 is connected within a CISD Mechanical Assembly 11 to a Catheter Shuttle 11.2. The proximal portion of the LAS sheath 4 is provided to a Sheath Shuttle 11.3. The proximal end of the catheter shaft 3.1 is connected to both the Tissue Contact Level Detector 8 and a Catheter Position Detection System (CPDS) 7 by the catheter electrical connector. The sheath position and orientation, SP 40, is also detectable by the CPDS 7, so the sheath 4 is also provided to the CPDS 7 by an electrical connector. The Catheter Position Detection System 7 uses the signals from the catheter and from the Catheter Position Detection System Patches 7.3, placed on the patient 1, to determine catheter position and orientation, which is passed on to the Catheter Guidance Control and Imaging System (CGCI) 15. In this embodiment, the CGCI 15 uses electromagnets 15.1 to push, pull and steer the catheter tip 3.1 within the patient 1. The CGCI 15 operates in a closed-loop regulation mode with the Catheter Position Detection System 7 to synchronize the Desired Position and Orientation, DP 30, of the catheter tip 3.1 with the Actual Position and Orientation, AP 20, of the catheter tip 3.1. When the CGCI 15 is directed by the operator to seek a location on the tissue surface at or near DP 30, the CGCI 15 sends the Tissue Impedance-Seeking Logic routines 10 the Geometric Target Distance vector 15.1, the Geometric Normal Vector 15.3 (shown in FIG. 3) for tissue contact direction, and a command to Seek Tissue Contact 15.2. The Tissue Impedance Seeking Logic 10 uses the CISD Motor Controller 12 to extend or retract the sheath 4, rotate the sheath, or extend or retract the catheter 3 in cooperation with the CGCI's magnetic regulation. When continuous tissue contact is detected from the Tissue Contact Detector 8, and the contact is along the Geometric Normal Vector 15.3 which passes through the Geometric Target Position 15.4, the Tissue Impedance-Seeking Logic sends a Contact Found signal 10.1 to the CGCI 15. The

Tissue Impedance-Seeking Logic 10 contains routines that optimize the direction of tissue contact, detect obstructions and provide the CGCI 15 additional geometric information about the tissue surface. In an alternate embodiment, the Catheter Position Detection System (CPDS) is the CGCI Magnetic Catheter Position Detection System which uses a set of magnetic sensors 9.1 to determine catheter tip position and orientation, as described later in this document.

[0057] FIG. 2 is a block diagram of the Tissue Impedance-Seeking Logic 10. The Catheter Guidance Control and Imaging System 15 provides the Tissue Impedance-Seeking Logic 10 with the Geometry Normal Vector 15.3, Actual Catheter Position and Orientation, AP 20, Desired Catheter Position and Orientation, DP 30, Sheath Position and Orientation, SP 40, and commands to Seek Tissue Contact 15.5 and Optimize Workspace 15.6. The Tissue Impedance-Seeking Logic routines use the geometric information to calculate a Tissue Contact Manifold 10.7 (see FIG. 3), which is a volume of expected tissue contact extending through the Desired Catheter Position, DP 30, in the direction of the Geometry Normal Vector 15.3. The Tissue Impedance-Seeking Logic routines 10 provide the CGCI 15 with live tissue contact information 8.1, as well as a Continuous Contact Found signal 10.6, which indicates that the catheter has had continuous contact with the surface with the specified contact strength and for the desired length of time. When Continuous Contact Found 10.6 occurs outside of the Tissue Contact Manifold 10.7, the CISD Obstacle Detection Routine 10.4 signals the CGCI that a new path to tissue contact will be specified.

[0058] FIG. 3 is a schematic diagram of a catheter in relationship to the virtual and real tissue surface with associated control vector information. The Catheter 3 is guided by the Catheter Guidance Control and Imaging System 15 from its current Actual Position and Orientation, AP 20, through the Desired Position and Orientation, DP 30. DP 30 is on the surface of the CGCI's Geometric Map 15.7, and not on the actual Patient Tissue Surface 1.2, so the catheter is guided on a path to the surface, called the CISD Tissue Contact Targeting Manifold 10.7 until it makes continuous contact with the tissue surface, as indicated by the Tissue Contact Detector 8. The CPCS Normal Vector 15.3 at DP 30 gives the position and orientation of the CISD Tissue Contact Targeting Manifold 10.7. If the Continuous Contact Found 10.6 signal is located outside of the CISD Tissue Contact Targeting Manifold 10.7, the Catheter Impedance-Seeking Logic 15 will signal the CGCI system and a new path will be planned to the tissue surface. The CISD Tissue Contact Targeting Manifold 10.7 shape, size and orientation with respect to the CPCS Normal Vector 15.3 may all be adjusted for desired accuracy. The CISD Tissue Contact Targeting Manifold 10.7 is a set of radius values for the targeting manifold at each distance from the desired position, DP 30.  $Rm(d)$  10.15 may be defined as any function of distance,  $d$ , or by an array:

$$Rm(d)=d^2/10+2$$

$$\text{Or: } Rm(d)=2+d/4$$

$$\text{Or: } Rm(d)=\{ 2, 3, 4, 4, 5, 6, \dots \} \text{ for all integers } d, 0 \text{ to } n$$

$$\text{Or: } Rm(d)=4 \tag{10.15}$$

(etc.)

[0059] The tip-to-tissue vector, TTV 10.11, is the negative of the geometric normal vector 15.3 times the magnitude of the distance to DP 30.

$$TTV=-GNV*|DP-AP| \tag{10.11}$$

[0060] The tip to path vector, TPV 10.10, is the vector distance from the catheter tip to the tissue path 10.14 passing through DP 30.

$$TPV=GNV*|AP-DP|*[(AP-DP)/|AP-DP|+GNV]/(AP-DP) \tag{10.10}$$

[0061] |TPV| is limited to the values 0 to  $Rm(d)$ .

[0062] The advance vector, ADV 10.13, is the weighted sum of TPV and TTV using the weighting values  $w1$  10.16 and  $w2$  10.17, which may be adjusted for system performance and anatomical location.

$$ADV=w1*TTV+w2*TPV*(|TPV|/Rm(d))/|TPV| \tag{10.13}$$

$$\text{Which yields: } ADV=w1*TTV+w2*TPV/Rm(d)$$

[0063] The advance vector ADV 10.13 is then used in cooperation with the CGCI 15 to guide the catheter to tissue contact. The CGCI 15 regulates the magnetic field based on the component of ADV perpendicular to the catheter tip axis 901, and the CISD 11 advances the tip based on the component of ADV which is parallel to the catheter tip axis 901.

[0064] FIG. 4A is an isometric diagram of the Lorentz-Active Sheath (LAS) assembly 4 and the associated vector used in workspace optimization. The Lorentz detection system-sensitive electrodes 4.3-4.7 are integrated into the LAS shaft 4.9 and connected via embedded wires 4.2 to a coupling connector. The electrodes 4.3-4.7 are used to sense electrical signals generated by a Catheter Position Detection System 7. The two most distal electrodes 4.3 and 4.4 are used to determine tool exit position and tool exit direction, SEV 4.8. The two most proximal electrodes 4.5 and 4.6 are used to determine the LAS sheath rotation axis vector, SRV 4.10.

[0065] FIG. 4B is a block diagram of the signals and systems used to determine the position of the LAS Electrodes 4.3-4.7. In this embodiment, the LAS 4 is inserted in the patient 1 via a vein or orifice and electrically connected to the Catheter Position Detection System 7. The LAS-hosted tool 3 is inserted through the LAS and also connected to the Catheter Position Detection System 7. The position of each electrode 4.3-4.7 is provided by the Catheter Position Detection System via a conventional communications link. One of ordinary skill in the art can use these electrode positions to determine the tool exit position and tool exit direction, SEV 4.8 and sheath rotation axis, SRV 4.10. In this embodiment, the tool exit position and tool exit direction SEV 4.8 are averaged in the Electrode Position Averaging Subsystem 500 and subtracted from the current tool exit position and tool exit direction 4.8 in the Electrode Position Error Subsystem 530 to give a Tool Motion Compensation Vector 550, which is used to remove the LAS motion from the LAS-hosted tool's 3 position. The sheath rotation axis SRV 4.10 aids in determining the motion of the sheath's distal end and tool position while rotating the sheath.

[0066] FIG. 5 is a logic flow diagram of the CISD Track Path to Tissue Contact routine 10.1. The Seek Tissue Contact Signal 15.2 from the CGCI 7 begins the monitoring of the catheter tip position, AP 20, with respect to the Target Manifold 10.7. On a regular time interval, the catheter length is recalculated as to progress the catheter tip 3.1 down through the Target Manifold 10.7 until the Continuous Contact Moni-



toring routine 10.3 has determined that the tip is in continuous tissue contact. Signals from the Obstacle Detection routine 10.4 may also interrupt the CISD Track Path to Tissue Contact routine 10.1 when the CGCI 15 is used to steer around an unexpected surface contact.

[0067] FIG. 6 is a logic flow diagram of the CISD Continuous Contact Monitoring routine 10.3. When the Seek Tissue Contact command 15.2 is sent from the Catheter Guidance Control and Imaging system 15, the CISD Continuous Contact Monitoring routine 10.3 seeks a period of continuous contact which is greater than the time (Tc) 10.9. When this condition is met, the Continuous Contact Found signal 10.6 is sent to all monitoring systems.

[0068] FIG. 7 is a logic flow diagram of the CISD Sheath Position Optimization routine 10.2. The sheath 4 begins in a fully-retracted position. The sheath is first rotated, within certain geometric chamber limits, to optimize the alignment between the sheath exit vector, SEV 4.8 and the sheath-tip-to-target direction vector, STTV 4.11. The sheath insertion length is then adjusted depending upon whether the tissue contact may be reached directly, or is to be reached in retrograde fashion, steering the catheter tip 3.1 beyond 90 degrees from the sheath exit vector SEV 4.8. If the retracted sheath-tip-to-target vector length is shorter than the length of the catheter tip 3.1, or if the desired position, DP 30, requires a STTV beyond 90 degrees from the SEV 4.8, the target is considered retrograde.

[0069] FIG. 8 is a vector diagram of the sheath rotation angle calculation. The sheath targeting angle, STA 10.2.1 is on a plane orthogonal to the sheath rotation vector SRV 4.10. STA is defined by the following calculation, which the angle between the cross-products of the sheath rotation vector SRV 4.10 with the sheath exit vector SEV 4.8 and sheath-to-target vector STTV 4.11.

$$STA = \text{ACOS} \left[ \frac{((\text{STTV} \times \text{SRV}) / |\text{STTV}| |\text{SRV}|) \cdot (\text{STTV} \times \text{SRV}) / (|\text{SEV} \times \text{SRV}| / |\text{SEV}| |\text{SRV}|)}{|\text{SEV} \times \text{SRV}| / |\text{SEV}| |\text{SRV}|} \right] \quad (10.2.2)$$

[0070] This value is evaluated by heuristic logic routines to account for the orientation of the STTV 4.11.

[0071] FIG. 9A is a block diagram of the CGCI Position Detection System 9. The CGCI Detection System Hardware 9.7, including four 3-axis Hall-Effect magnetic sensors 9.21-9.24, amplifiers and associated data acquisition connections, sends four magnetic sensor readings 9.1-9.4 to the CGCI Calibration and Filtering software routines 9.6, where background magnetic fields are subtracted. The CGCI QRS Synchronization Unit 9.5 may then be used to synchronize the readings to the most stable portion of the heartbeat, using a sampling window offset from the heartbeat R-peak signal. The four filtered magnetic field vectors are then used by the Catheter Tip Position and Orientation Calculation Algorithm 9.8 to determine the position and orientation of the magnetic catheter tip 3.1.

[0072] FIG. 9B is a schematic diagram of a Hall-Effect sensor in relationship to the catheter tip, and its generated measurement data. The catheter 3 and its magnetic tip 3.1 are shown in proximity to Hall-Effect sensor number one 9.21, which is connected through the CGCI Position Detection System hardware (not shown) to provide the three magnetic sensor readings 9.1.1-9.1.3 representing the magnetic field components of magnetic sensor vector number one 9.1 in the X, Y, and Z Cartesian directions at the sensor's location. The other three magnetic sensors are defined as 9.22, 9.23, and 9.24 with sensor vectors 9.2, 9.3, and 9.4 respectively. The catheter tip axis is identical to the catheter tip magnetic axis

901, (which is the directional component of the six-degree of freedom Actual Position, AP 20) and the angle between the catheter tip axis and the direction vector from sensor 1-4 9.21-9.24 to the catheter tip 3.1 is defined as SensorAngle1-SensorAngle4 9.61-9.64. The distances from magnetic sensor 1-4 to the catheter tip are defined as SensorRange1-SensorRange4 9.41-9.44, which have unit direction vectors SensorCatheter1-SensorCatheter4 9.51-9.54.

[0073] FIG. 9C is a schematic diagram of a catheter position triangulation 9.50 using four Hall-Effect sensors and their respective range values. The magnitude of the magnetic field at each sensor 9.1-9.4 is converted to a range value SensorRange1-SensorRange4 9.41-9.44 by a magnetic field to distance calibration curve, the sensor ranging dataset 9.40 (not shown). The positions of magnetic sensor 1-4 9.11-9.14 are known and fixed values and form the baseline for triangulating the catheter position 904 (which is the positional component of the Actual Position, AP 20), which is always above the detection sensor array.

[0074] FIG. 9D is a detailed schematic of the triangulation of the catheter position's X-coordinate using two sensors, sensor #2 9.22 and sensor #3 9.23. Using standard Trigonometry, SensorRange2 9.42 and SensorRange3 9.43 are used with SensorPosition2 9.12 and SensorPosition3 9.13 to locate the x-coordinate of the catheter position 904, CatheterPositionX 904.1. In similar calculations, two solutions for CatheterPositionX 904.1 and CatheterPositionY 904.2 are calculated and averaged. CatheterPositionZ 904.3 is then determined as the average Trigonometric solution for each SensorRange value 9.41-9.44 and CatheterPositionX 904.1 and CatheterPositionY 904.2, giving the three Cartesian components to the catheter position 904.

[0075] FIG. 9E is a diagram of the Intersecting Planes Method 9.60 for determining the orientation of a magnetic catheter tip from its position and two sensor's magnetic field values. When the position of the catheter tip 904 is known, the orientation of the catheter tip's magnetic field axis 901 is calculated as being co-planar with each of the magnetic sensor vectors 9.1-9.4 and their corresponding sensor-to-catheter position vectors, SensorCatheter1-SensorCatheter4 9.51-9.54. The sensor-catheter planes, defined by the plane normal vectors 9.31-9.34, are calculated as the normalized cross-product of the normalized magnetic sensor vectors 9.1-9.4 and normalized sensor-to-catheter vectors 9.51-9.55. The intersection of any two sensor-catheter planes, calculated as the normalized cross-product of the plane normal vectors 9.31-9.34, gives a solution to the catheter magnetic axis 901. The direction of the magnetic axis along the intersection of the planes is determined by examining the direction of the plane normal vectors 9.31-9.34.

[0076] FIG. 9F is a block diagram of the method for determining both position and orientation when they are not independent values. The Catheter Tip Position and Orientation Calculation Algorithm 9.8 uses an iterative method to determine catheter position 904 and catheter orientation 901 since the catheter tip magnetic field is not spherical so therefore position and orientation are not independent variables. The data for magnetic tip field magnitude versus distance and orientation to the magnetic axis is known and stored internally to the algorithm as a calibrated dataset, the sensor ranging dataset 9.40. The magnetic sensor vectors 9.1-9.4 are first used to calculate the range from each sensor to the magnetic tip using the sensor ranging dataset 9.40, initially using the assumption that the field is spherical with the field magnitude



profile equal to a 25-degree declination from the catheter magnetic axis **901**. The catheter tip position **904** is then calculated by triangulation **9.50**. The catheter position **904** is then used to calculate the catheter's magnetic axis **901** using the Intersecting Planes Method **9.60**. The catheter magnetic axis **901** is used to recalculate the SensorRange values from the sensor range dataset **9.40**, and then to re-triangulate **9.50** the catheter position **904**. The catheter axis is then re-calculated as well by the Intersecting Planes Method **9.60**. The iterative method has been determined to be convergent, and when the successive values are within the desired error limits, the catheter position **904** and orientation **901** are known.

**[0077]** FIG. 10A is a diagram of the signals and systems used in catheter position control. The Catheter Guidance Control and Imaging System (CGCI) **15** uses the Catheter Position Detection System (CPDS) **7** information and a magnetic chamber **15.1** to push, pull, and steer a magnetically-tipped catheter **3** within the patient **1**. The operator uses the Virtual Tip **34** controller to specify a desired catheter position and orientation, DP **30**, in the CGCI, and the CGCI uses the actual position and orientation of the catheter, AP **20**, which is received from the CPDS to control the catheter in a closed-loop regulation mode. The CGCI "Host System" Controller computer **15.8** performs the real-time regulation of the CGCI using information from the CGCI Magnetic Field Sensor Arrays **15.11**, Virtual Tip **34**, and additional medical signals from the Auxiliary Equipment **2.2**. The Console computer **15.9** serves as the operator interface with a monitor, mouse and keyboard next to the Virtual Tip **34**. The Virtual Tip **34** is calibrated with an additional calibration fixture **15.10.1** before the operation begins.

**[0078]** FIG. 10B is an isometric diagram of another embodiment of the magnetic chamber used to control catheter position. In this embodiment, the magnetic chamber **15.1** is included of eight electromagnetic coils which is an optimized design to generate a magnetic guidance lobe while providing sufficient patient access.

**[0079]** FIG. 10C is an isometric diagram of the Virtual Tip assembly **34**. The control end of the Virtual Tip can be moved in six-degrees of freedom, including the X **34.1**, Y **34.2**, Z **34.3** Cartesian directions, Rotated **34.4**, Elevated **34.5**, and Twisted **34.6**.

**[0080]** FIG. 11A is a block diagram of the signals and systems of the CISD Mechanical Assembly and CISD Motor Controller. The CISD Motor Controller **12** (for the purposes of this patent is considered an external, off-the-shelf device) controls the position of the CISD Mechanical Assembly **11** (see FIGS. 11B-11E) components through the CISD Drive Cables **11.5**. The CISD Motor Controller **12** includes a set of three off-the-shelf packaged stepper motors, encoders, limit switches and stepper motor controllers. Each motor assembly actuates one of the three CISD Drive Cables **11.5**, two of which are linear drive cables, and one is a rotational drive cable. The motor controller assemblies accept a standard positional signal over the local Ethernet bus.

**[0081]** FIG. 11B is an isometric drawing of an embodiment of the CISD Mechanical Assembly **11**. In this embodiment, the CISD Motor Controller **11.1** (not shown) controls the device through the CISD Drive Cables (**11.5.1**, **11.5.2**, **11.5.3**). The CISD Mechanical Assembly **11** contains no motors or electronics, and may be sterilized so that it is compatible with

a surgical environment. The CISD Base Plate **11.4.1** is attached to the CISD Leg Mount **11.4.2** by the CISD Mount Pin **11.4.3** which allows the operator to elevate and rotate the CISD Mechanical Assembly **11**, as to align the device within the surgical environment. The drive elements are housed under protective telescoping covers. The CISD Outer Cover **11.6.1** is attached to the Sheath Rotator Housing **11.3.1** on the Sheath Shuttle **11.3** (see FIG. 4), and the CISD Inner Cover **11.6.2** is attached to the CISD Base Plate **11.4.1**. As the Sheath Shuttle **11.3** moves forward and backward along the CISD Base Plate **11.4.1**, the CISD Covers **11.6.1**, **11.6.2** telescope over each other. The Sheath Shuttle **11.3** pushes the sheath back and forth with respect to the patient's leg. The Sheath Rotator Housing **11.3.1** is mounted on the end of the Sheath Shuttle **11.3** and contains gears that rotate the Sheath Rotator Clip **11.3.2**. The proximal end of the Sheath **4** has the standard Hemostatic Seal **4.1** which is held within the Sheath Rotator Clip **11.3.2**. The Catheter Tip **3.1** is inserted through the rear of the CISD Mechanical Assembly **11** and through the attached Sheath **4**.

**[0082]** FIG. 11C is an isometric detail drawing of the internal assemblies within the CISD Mechanical Assembly. The CISD Covers **11.6.1**, **11.6.2** and CISD Leg Mount have been removed for clarity. The Sheath Shuttle **11.3** is moved over the CISD Base Plate **11.4.1** by the Sheath Shuttle Cable **11.5.3**. On the Sheath Shuttle **11.3**, the Catheter Shuttle Clamp **11.2.1** is attached to the Catheter Shuttle **11.2** and clamps to the Catheter Shaft **3.2**. The Catheter Shuttle **11.2** is moved by the Catheter Shuttle Cable **11.5.2** which moves the Catheter **3** with reference to the Sheath **4**. The spacing of the Catheter Alignment Supports **11.2.2** changes with the movement of the Catheter Shuttle **11.2** to keep the catheter line from kinking as it is pushed. The Sheath Rotator Cable **11.5.1** rotates the gears within the Sheath Rotator Housing **11.3.1** (see FIG. 6), which rotates the Sheath Rotator Clip **11.3.2** to which is fitted the Sheath Hemostatic Seal **4.1**, allowing for the rotation of the Sheath **4**.

**[0083]** FIG. 11D is an isometric drawing showing the Sheath Shuttle in a forward position. The Sheath Shuttle **11.3** is moved by the Sheath Shuttle Cable **11.5.3**. The Catheter Shuttle Cable **11.5.2** is attached to the Catheter Shuttle Clamp **11.2.1** to move the Catheter Line **3.2** with reference to the Sheath **4**. The end of the Sheath Rotator Cable **11.5.1** telescopes with the Sheath Shuttle **11.3**, and drives the gears within the Sheath Rotator Housing **11.3.1**.

**[0084]** FIG. 11E is an isometric detail drawing of the sheath rotator housing. Inside the Sheath Rotator Housing **11.3.1**, the Sheath Rotator Cable **11.5.1** turns the Sheath Rotator Drive Gears **11.3.3** to turn the Sheath Rotator Clip **11.3.2**. The Sheath's Hemostatic Seal **4.1** clips within the Sheath Rotator Clip **11.3.2**. The Sheath Rotator Torque Limiting Assembly **11.3.4** limits the amount of torque that may be applied to the sheath, as to keep the mechanical stress within safe limits.

**[0085]** It will be evident to those skilled in the art that the invention is not limited to the details of the foregoing illustrated embodiments and that the present invention may be embodied in other specific forms without departing from the spirit or essential attributed thereof; furthermore, various omissions, substitutions and changes may be made without departing from the spirit of the inventions. The foregoing description of the embodiments is therefore to be considered in all respects as illustrative and not restrictive, with the scope of the invention being delineated by the appended claims and their equivalents.



What is claimed is:

1. An apparatus for making and maintaining continuous tissue contact between a tool tip and moving tissue in a patient, comprising:

a controllable magnetic field source that produces a magnetic field;

a tool having a distal end responsive to said magnetic field; one or more sensors configured to sense a current vector position of said distal end by measuring one or more impedances;

a controller for controlling said magnetic field source to control a movement of said distal end according to a feedback calculation wherein said system controller is configured to compute a position error comprising a difference between a desired vector position of said distal end and said current vector position of said distal end; and

an operator control that provides tactile feedback to an operator when said position error exceeds a predetermined amount, wherein said tactile feedback is computed by said controller at least in part according to said vector position error, wherein a correction input to said desired vector position is computed based on a position of a heart relative to a frame of reference, such that said system controller compensates for a dynamic position of a wall of a heart chamber such that said distal end maintains contact with said wall of said heart chamber at least in part by measuring at least one impedance between said distal end and said wall.

2. The apparatus of claim 1, wherein said tool comprises a Lorenz sheath.

3. The apparatus of claim 1, further comprising one or more patches provided to said patient, wherein said apparatus measures a position and orientation of a Lorenz sheath at least in part by measuring one or more impedances between said Lorenz sheath and said conductive patches.

4. The apparatus of claim 1, wherein said controller is configured to control said magnetic field source to maintain said distal end in a desired vector orientation relative to said wall.

5. The apparatus of claim 1, wherein said controller is configured to control said magnetic field source to maintain said distal end substantially normal to said wall.

6. The apparatus of claim 1, wherein said controller is configured to differentiate between contact with said wall and contact with an obstruction by analyzing differences between a measured impedance and an expected impedance.

7. The apparatus of claim 6, wherein said controller is configured to compute a path around said obstruction.

8. The apparatus of claim 1, wherein said controller is configured to control said magnetic field source to maintain said distal end in a desired orientation relative to said wall.

9. The apparatus of claim 1, wherein said controller is configured to differentiate between contact with said wall and contact with other tissue by analyzing differences between a measured impedance and an expected impedance, said expected impedance corresponding to said wall.

10. The apparatus of claim 1, wherein said other tissue comprises a blood pool.

11. The apparatus of claim 1, wherein said controller is configured to seek contact with said wall by calculating a target manifold, monitoring a distal end-to-target vector with respect to said target manifold, calculating a new tool length, and adjusting a length of said tool according to said new tool length.

12. The apparatus of claim 1, wherein said tool comprises an introducer.

13. The apparatus of claim 12, wherein said controller controls a rotation and translation of said introducer.

14. A method for positioning a surgical tool and maintaining relatively continuous contact between a distal end of said tool and a desired tissue location, comprising:

controlling a position and orientation of a distal end of a surgical tool by adjusting currents in a plurality of electromagnets;

measuring a plurality of impedance values between said distal end and a plurality of tissue locations;

constructing an impedance map at least in part from said plurality of impedance values;

determining a first impedance value corresponding to an impedance measured when said distal end touches said desired tissue location; and

using a feedback controller to control said currents to maintain contact between said distal end and said desired tissue such that said distal end is oriented relatively normal to said desired tissue location in the presence of motion of said desired tissue location, wherein feedback information to said feedback controller comprises periodic impedance measurements between said distal end and said desired tissue location.

15. The method of claim 14, further comprising:

computing a position error comprising a difference between a desired vector position of said distal end and said current vector position of said distal end; and

providing tactile feedback to an operator control when said position error exceeds a predetermined amount, wherein said tactile feedback is computed at least in part according to said position error.

16. The method of claim 14, wherein said tool comprises a Lorenz sheath.

17. The method of claim 14, further comprising locating said distal end by measuring impedances between a plurality of patches provided to said patient and said surgical tool.

18. The method of claim 14, further comprising differentiating between contact with said desired tissue location and contact with an obstruction by analyzing differences between a measured impedance and an expected impedance.

19. The method of claim 15, further comprising computing a path around said obstruction.

20. The method of claim 14, further comprising distinguishing between contact with said desired tissue location and contact with other tissue by analyzing differences between a measured impedance and an expected impedance, said expected impedance corresponding to an impedance at said desired tissue location.

21. The method of claim 20, wherein said other tissue comprises a blood pool.

22. The method of claim 14, further comprising seeking contact with said desired tissue location by:

calculating a target manifold;

monitoring a distal end-to-target vector with respect to said target manifold;

calculating a new tool length; and

adjusting a length of said tool according to said new tool length.

23. The method of claim 14, wherein said tool comprises an introducer.

24. The method of claim 14, further comprising controlling a rotation and translation of said tool.

\* \* \* \* \*



US008457714B2

(12) **United States Patent**  
**Shachar et al.**

(10) **Patent No.:** **US 8,457,714 B2**  
(45) **Date of Patent:** **Jun. 4, 2013**

- (54) **SYSTEM AND METHOD FOR A CATHETER IMPEDANCE SEEKING DEVICE**
- (75) Inventors: **Yehoshua Shachar**, Santa Monica, CA (US); **Bruce Marx**, Ojai, CA (US); **Leslie Farkas**, Ojai, CA (US); **Laszlo Farkas**, Ojai, CA (US); **David Johnson**, West Hollywood, CA (US); **Eli Gang**, Los Angeles, CA (US)
- (73) Assignee: **Magnetecs, Inc.**, Inglewood, CA (US)

4,096,862	A	6/1978	DeLuca
4,162,679	A	7/1979	Reenstierna
4,173,228	A	11/1979	Van Steenwyk et al.
4,244,362	A	1/1981	Anderson
4,249,536	A	2/1981	Vega
4,270,252	A	6/1981	Harrison et al.
4,292,961	A	10/1981	Kawashima
4,354,501	A	10/1982	Colley et al.
4,392,634	A	7/1983	Kita
4,671,287	A	6/1987	Fiddian-Green
4,727,344	A	2/1988	Koga et al.
4,735,211	A	4/1988	Takasugi
4,809,713	A	3/1989	Grayzel

(\*) Notice: Subject to any disclaimer, the term of this patent is extended or adjusted under 35 U.S.C. 154(b) by 1060 days.

(Continued)  
**FOREIGN PATENT DOCUMENTS**

DE	102005045073	A1	3/2007
EP	0147082	A2	7/1985

(21) Appl. No.: **12/323,231**

(Continued)

(22) Filed: **Nov. 25, 2008**

**OTHER PUBLICATIONS**

(65) **Prior Publication Data**  
US 2010/0130854 A1 May 27, 2010

Office Action dated Aug. 25, 2009 from Related U.S. Appl. No. 10/621,196.

(Continued)

(51) **Int. Cl.**  
**A61B 5/05** (2006.01)  
**A61B 17/00** (2006.01)

*Primary Examiner* — John Lacy  
(74) *Attorney, Agent, or Firm* — Knobbe, Martens, Olson & Bear, LLP

(52) **U.S. Cl.**  
USPC ..... **600/424**

(58) **Field of Classification Search**  
USPC .... 600/433-435, 585, 424; 604/95.01-95.05, 604/528, 529; 606/108; 128/897-898  
See application file for complete search history.

(57) **ABSTRACT**

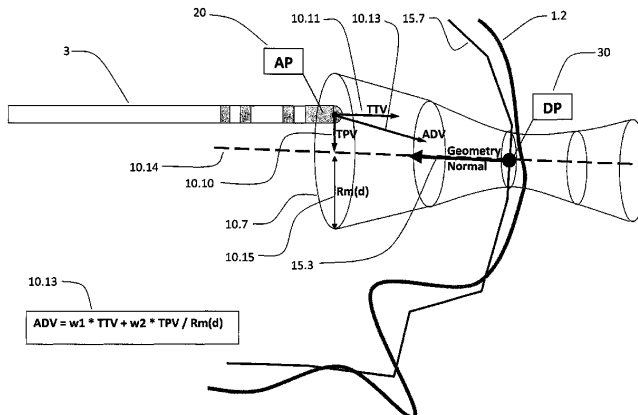
A tissue-contact seeking method and apparatus is described that enhances catheter position detection and control systems in making and maintaining continuous tissue contact in a highly dynamic frame, such as under the rigors of cardiac motion. Tissue-seeking logical routines use a tissue contact sensing system to advance a catheter to relatively continuous tissue contact, or detect obstacles, in cooperation with the catheter position detection and control systems. Additional logical routines are capable of optimizing the contact direction of the catheter tip by controlling the rotation angle and chamber position of the introducer.

(56) **References Cited**

**U.S. PATENT DOCUMENTS**

3,043,309	A	9/1959	McCarthy
3,358,676	A	12/1967	Frei et al.
3,622,869	A	11/1971	Golay
3,628,527	A	12/1971	West
3,746,937	A	7/1973	Koike
3,961,632	A	6/1976	Moossun
4,063,561	A	12/1977	McKenna

**24 Claims, 23 Drawing Sheets**



04

World Intellectual Property  
Organization  
International Bureau

WIPO  
OMPI



International Application Date  
14 October 2010 (14.10.2010)

PCT

International Application Number  
**PCT/US2010/052696**

**International Application Number:**

PCT/US2010/052696

**International Filing Date:**

14 October 2010 (14.10.2010)

**Filing Language:**

English

**Publication Language:**

English

**Priority Date:** 20 October 2009 (20.10.2009) US

**Applicant:** MAGNETECS, INC. [US/US]; 10524 S. La Cienega Blvd., Inglewood, CA 90304 (US).

**Inventors:** SHACHAR, Yehoshua; 2417 22nd St., Santa Monica CA 90405 (US). MARX, Bruce; 1233 Avila Drive, Ojai, CA 93023 (US).

JOHNSON, David; 8450 DeLongpre Avenue #6, West Hollywood, CA 90069 (US). FARKAS, Leslie; 254 N. Arnaz Street, Ojai, CA 93023 (US).

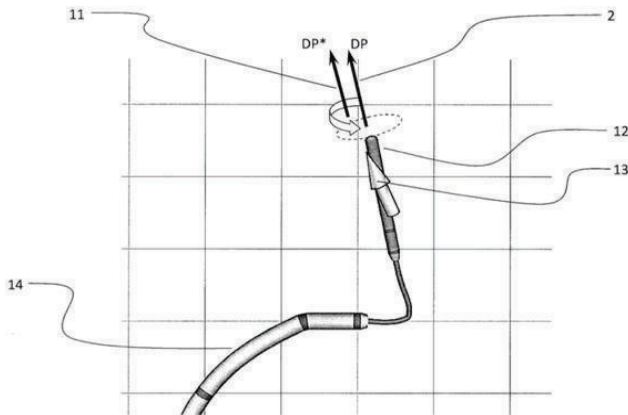
KIM, STEVEN; 10524 S. La Cienega Blvd. Inglewood, CA 90304 (US).

**Agent:** DELANEY, Karoline, A.; KNOBBE, MARTENS, OLSON & BEAR, LLP, 2040 Main Street, 14th Floor, Irvine, CA 92614 (US).

**Designated States** (unless otherwise indicated, for every kind of national protection available): AE, AG, AL, AM, AO, AT, AU, AZ, BA, BB, BG, BH, BR, BW, BY, BZ, CA, CH, CN, CO, CR, CU, CZ, DE, DK, DM, DO, DZ, EC, EE, EG, ES, FI, GB, GD, GE, GH, GM, GT, HN, HR, HU, ID, IL, IN, IS, JP, KE, KG, KM, KN, KP, KR, KZ, LA, LC, LK, LR, LS, LT, LU, LY, MA, MD, ME, MG, MK, MN, MW, MX, MY, MZ, NA, NG, NI, NO, NZ, OM, PG, PH, PL, PT, RO, RS, RU, SC, SD, SE, SG, SK, SL, SM, ST, SV, SY, TJ, TM, TN, TR, TT, TZ, UA, UG, US, UZ, VC, VN, ZA, ZM, ZW.

**Designated States** (unless otherwise indicated, for every kind of regional protection available): ARIPO (BW, GH, GM, KE, LS, MW, MZ, NA, SD, SL, SZ, TZ, UG, ZM, ZW), Eurasian (AM, AZ, BY, KG, KZ, MD, RU, TJ, TM), European (AT, BE, BG, CH, CY, CZ, DE, DK, EE, ES, FI, FR, GB, GR, HR, HU, IE, IS, IT, LT, LU, LV, MC, MK, MT, NL, NO, PL, PT, RO, SE, SI, SK, TR), OAPI (BF, BJ, CF, CG, CI, CM, GA, GN, GQ, GW, ML, MR, NE, SN, TD, TG).

**Title:** SYSTEM AND METHOD FOR A CATHETER IMPEDANCE SEEKING DEVICE



Abstract: The invention is a method of rotating a catheter while it is manually guided in order to increase the volume of space it passes through during a geometric mapping procedure as to provide a higher and more uniform location data point cloud density in a volumetric mapping system.

PCT/US2010/052696

04





INTERNATIONAL FILINGS FOR:  
*System and Method for a Catheter  
Impedance Seeking Device*

***INVENTOR: Yehoshua Shachar  
Bruce Marx  
Leslie Farkas  
David Johnson  
Lazlo Farkas  
Dr. Eli Gang***

04





PCT

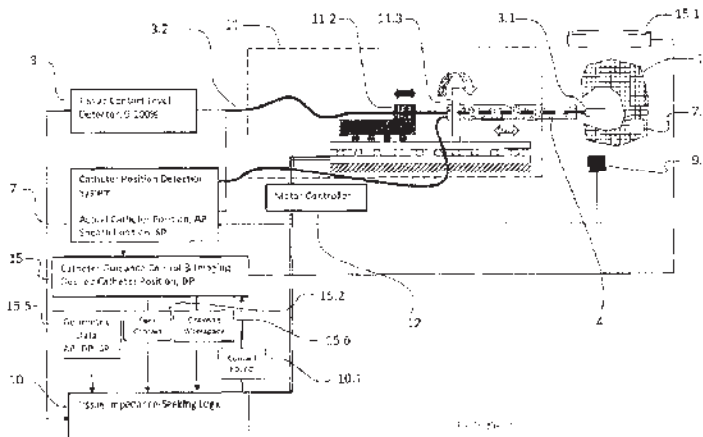
- (51) International Patent Classification:  
A61B 18/12 (2006.01) A61M 25/01 (2006.01)  
A61B 5/00 (2006.01)
- (21) International Application Number:  
PCT/US2009/064439
- (22) International Filing Date:  
13 November 2009 (13.11.2009)
- (25) Filing Language: English
- (26) Publication Language: English
- (30) Priority Data:  
12/323,231 25 November 2008 (25.11.2008) US
- (71) Applicant (for all designated States except US): MAG-  
NETECS, INC. [US/US]; 10524 S. La Cienega Blvd.,  
Inglewood, CA 90304 (US).
- (72) Inventors: SHACHAR, Yehoshua; 22nd Street, Santa  
Monica, CA 90405 (US). MARK, Bruce; 1233 Avila  
Drive, Ojai, California 93023 (US). FARKAS, Leslie;  
254 N. Amaz Street, Ojai, California 93023 (US).  
FARKAS, Laszlo; 29 Taormina Lane, Ojai, California  
93023 (US). JOHNSON, David; 8450 DeLongpre Av-  
enue #6, West Hollywood, California 90069 (US).  
GANG, Eli; 414 North Camden Drive, Beverly Hills,  
California 90210 (US).

- (74) Agent: ALTMAN, Daniel, E.; Knobbe, Martens, Olson  
& Bear, LLP, 2040 Main Street, 14th Floor, Irvine, CA  
92614 (US).
- (81) Designated States (unless otherwise indicated, for every  
kind of national protection available): AE, AG, AL, AM,  
AO, AT, AU, AZ, BA, BB, BG, BH, BR, BW, BY, BZ,  
CA, CL, CN, CO, CR, CU, CZ, DE, DK, DM, DO,  
DZ, EC, EE, EG, ES, FI, GB, GD, GE, GH, GM, GT,  
HN, HR, HU, ID, IL, IN, IS, JP, KE, KG, KM, KN, KP,  
KR, KZ, LA, LC, LK, LR, LS, LT, LU, LY, MA, MD,  
ME, MG, MK, MN, MW, MX, MY, MZ, NA, NG, NI,  
NO, NZ, OM, PE, PG, PH, PL, PT, RO, RS, RU, SC, SD,  
SE, SG, SK, SL, SM, ST, SV, SY, TJ, TM, TN, TR, TT,  
TZ, UA, UG, US, UZ, VC, VN, ZA, ZM, ZW.
- (84) Designated States (unless otherwise indicated, for every  
kind of regional protection available): ARIPO (BW, GH,  
GM, KE, LS, MW, MZ, NA, SD, SL, SZ, TZ, UG, ZM,  
ZW), Eurasian (AM, AZ, BY, KG, KZ, MD, RU, TJ,  
TM), European (AT, BE, BG, CH, CY, CZ, DE, DK, EE,  
ES, FI, FR, GB, GR, HR, HU, IE, IS, IT, LT, LU, LV,  
MC, MK, MT, NL, NO, PL, PT, RO, SE, SI, SK, SM,  
TR), OAPI (BF, BJ, CF, CG, CI, CM, GA, GN, GQ, GW,  
ML, MR, NI, SN, TD, TG).

Published:

— with international search report (Art. 21(3))

(54) Title: SYSTEM AND METHOD FOR A CATHETER IMPEDANCE SEEKING DEVICE



(57) Abstract: A tissue-contact seeking method and apparatus is described that enhances catheter position detection and control systems in making and maintaining continuous tissue contact in a highly dynamic frame, such as under the rigors of cardiac motion. Tissue-seeking logical routines use a tissue contact sensing system to advance a catheter to relatively continuous tissue contact, or detect obstacles, in cooperation with the catheter position detection and control systems. Additional logical routines are capable of optimizing the contact direction of the catheter tip by controlling the rotation angle and chamber position of the introducer.

WO 2010/065267 A1

04





U.S. PATENT OFFICE FILINGS FOR:

*Optically Coupled Catheter  
And Method Of Using The Same*

***INVENTOR: Yehoshua Shachar  
Marc Rocklinger  
Dr. Eli Gang***

05



US 20200375541A1

(19) **United States**

(12) **Patent Application Publication**  
**Shachar et al.**

(10) **Pub. No.: US 2020/0375541 A1**

(43) **Pub. Date: Dec. 3, 2020**

(54) **OPTICALLY COUPLED CATHETER AND METHOD OF USING THE SAME**

(71) Applicant: **Neurokinesis Corp.**, Los Angeles, CA (US)

(72) Inventors: **Josh Shachar**, Santa Monica, CA (US); **Marc Rocklinger**, Marina del Rey, CA (US); **Eli Gang**, Los Angeles, CA (US)

(73) Assignee: **Neurokinesis Corp.**, Los Angeles, CA (US)

(21) Appl. No.: **16/424,202**

(22) Filed: **May 28, 2019**

**Publication Classification**

(51) **Int. Cl.**  
**A61B 5/00** (2006.01)  
**A61B 5/04** (2006.01)

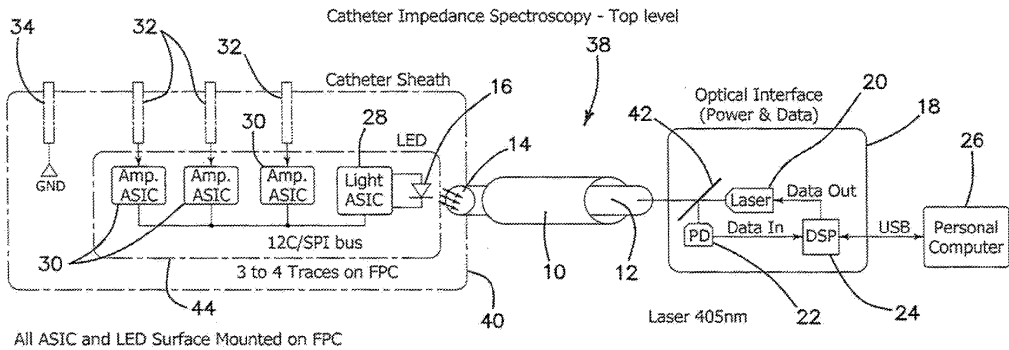
(52) **U.S. Cl.**

CPC ..... **A61B 5/6852** (2013.01); **A61B 5/04002** (2013.01); **A61M 2025/0166** (2013.01); **A61B 5/7435** (2013.01); **A61B 5/0084** (2013.01); **A61B 5/0017** (2013.01)

(57)

**ABSTRACT**

The embodiments include an apparatus used in combination with a computer for sensing biopotentials. The apparatus includes a catheter in which there is a plurality of sensing electrodes, a corresponding plurality of local amplifiers, each coupled to one of the plurality of sensing electrodes, a data, control and power circuit coupled to the plurality of local amplifiers, and a photonic device bidirectionally communicating an electrical signal with the data, control and power circuit. An optical fiber optically communicated with the photonic device. The photonic device bidirectionally communicates an optical signal with the optical fiber. An optical interface device provides optical power to the optical fiber and thence to the photonic device and receives optical signals through the optical fiber from the photonic device. The optical interface device bidirectionally communicates an electrical data, control and power signal to the computer.



05

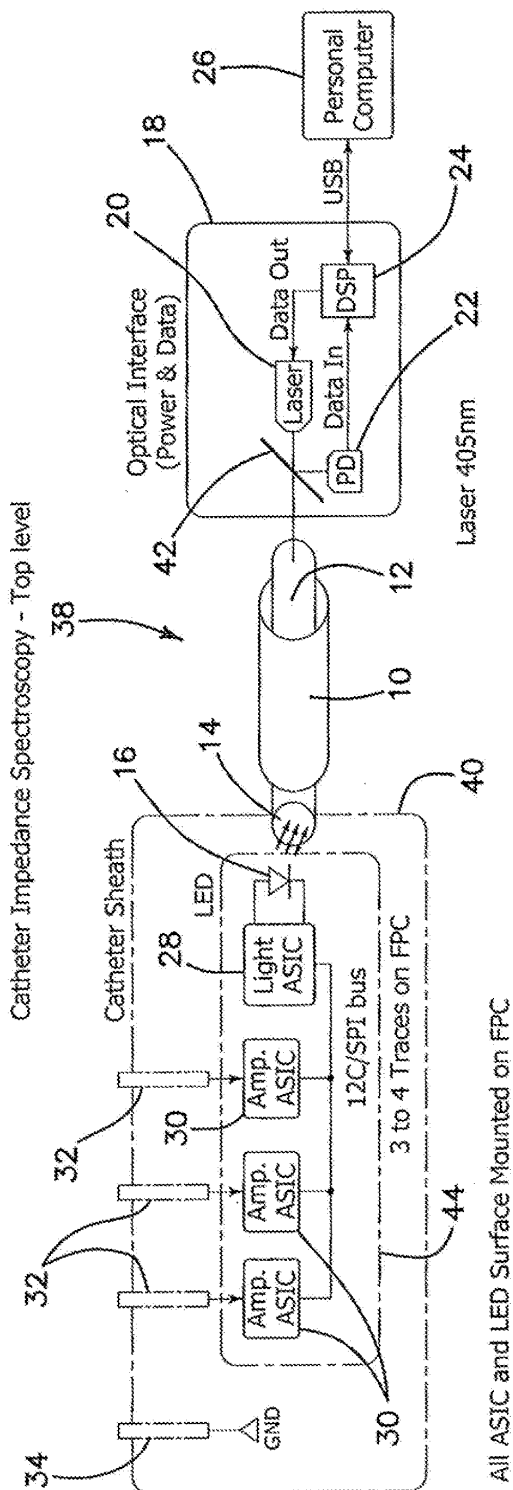


FIG. 1

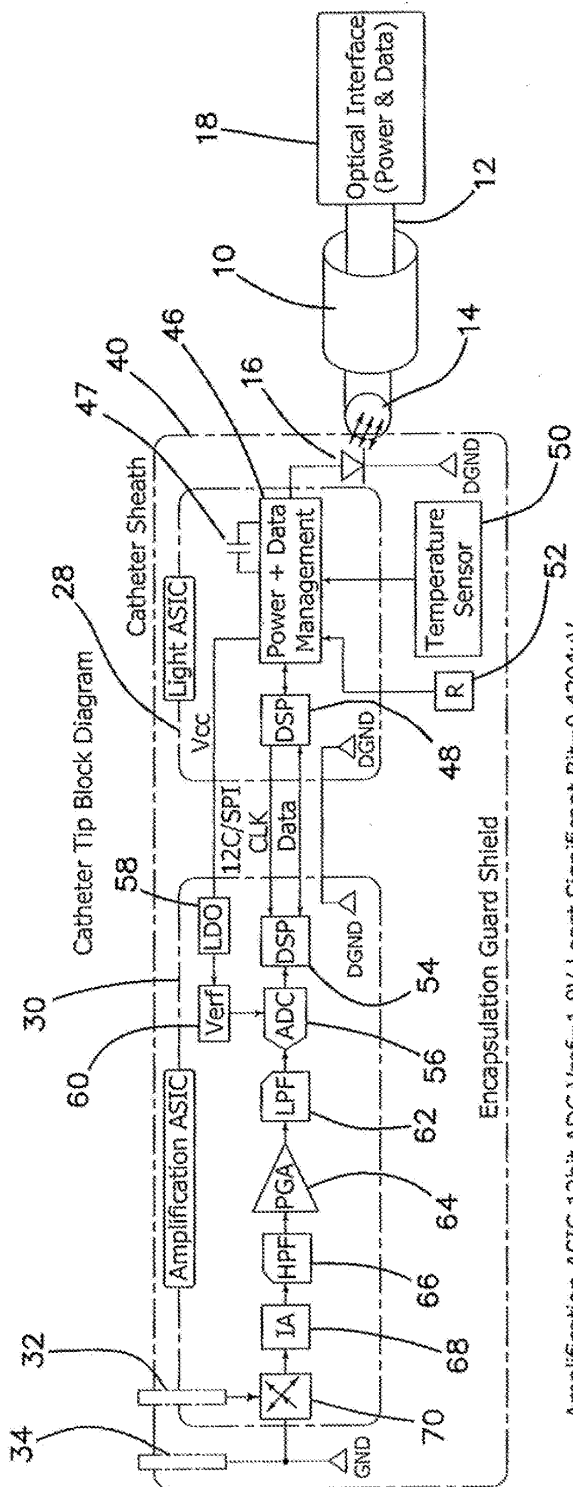


FIG. 2

Amplification ASIC 12bit ADC Vref=1.8V Least Significant Bit=0.4394uV

Input Range [uv]	Instrumental Amp. Fix Gain	Prog. Gain Amp. Management	ADC Input Voltage [mV]
1 - 500	50	10	5 to 250
1 - 10000	50	Scalable 1 to 50	0 to 1800
1000 - 100'000	50	Scalable 1 to 50	0 to 1800

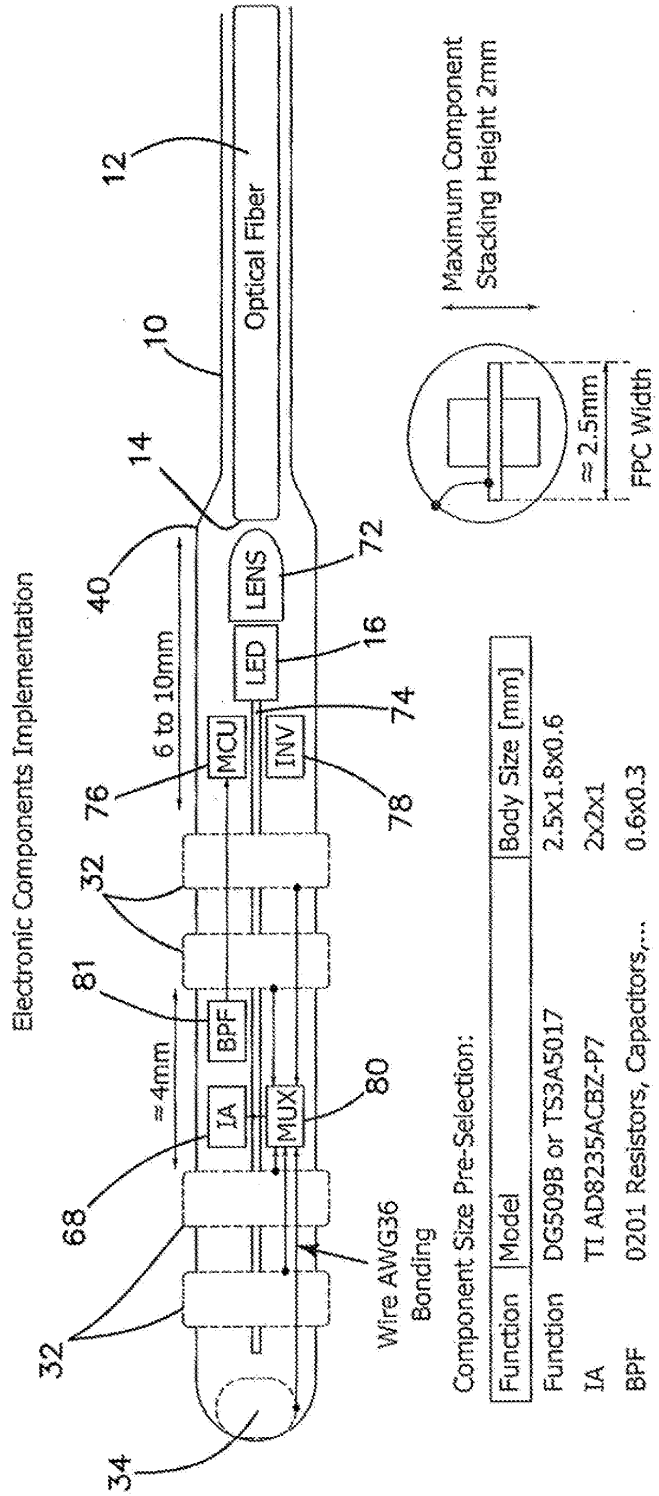


FIG. 3



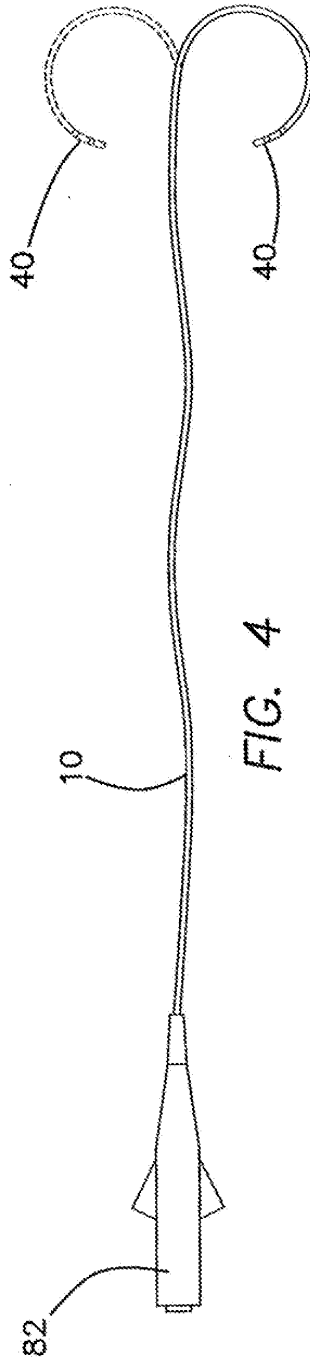


FIG. 4

05



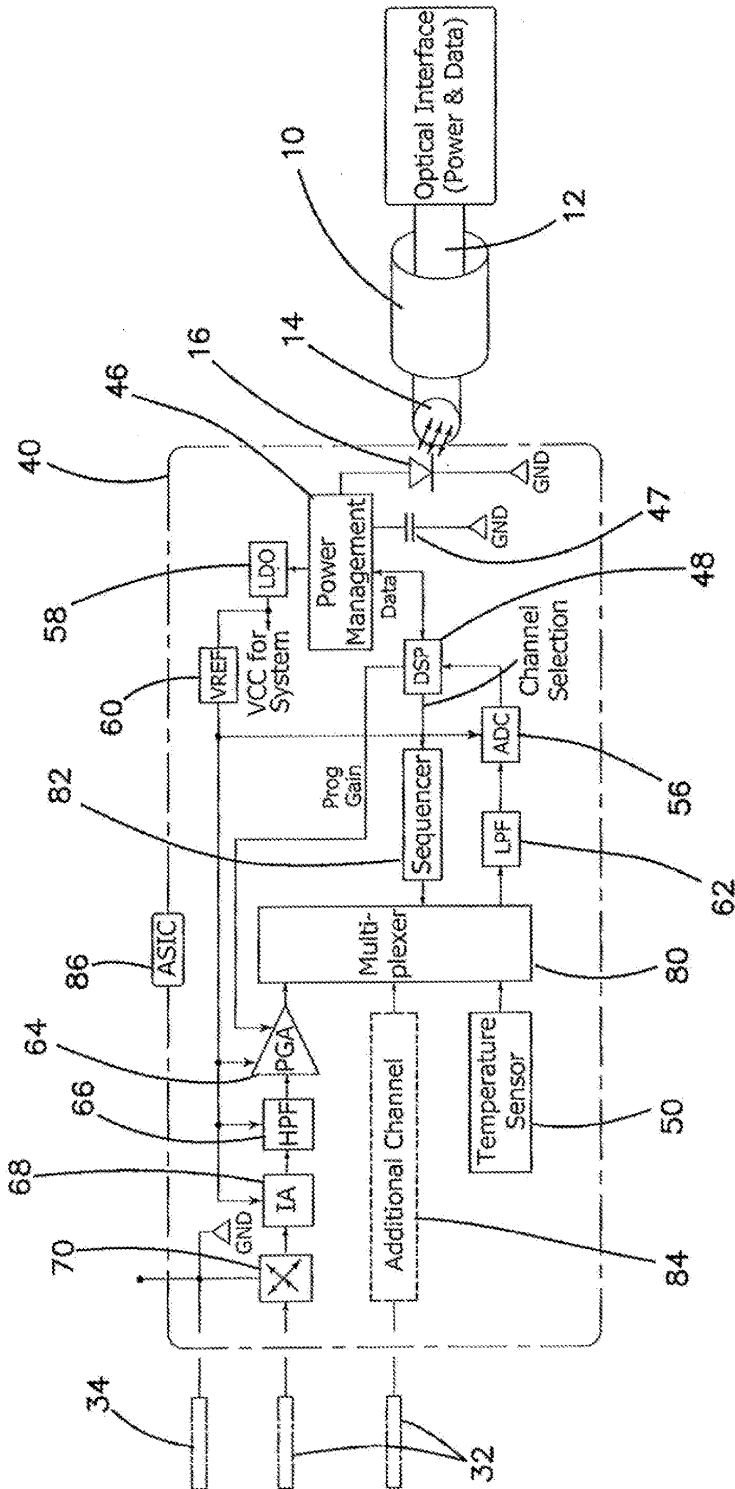


FIG. 5

05



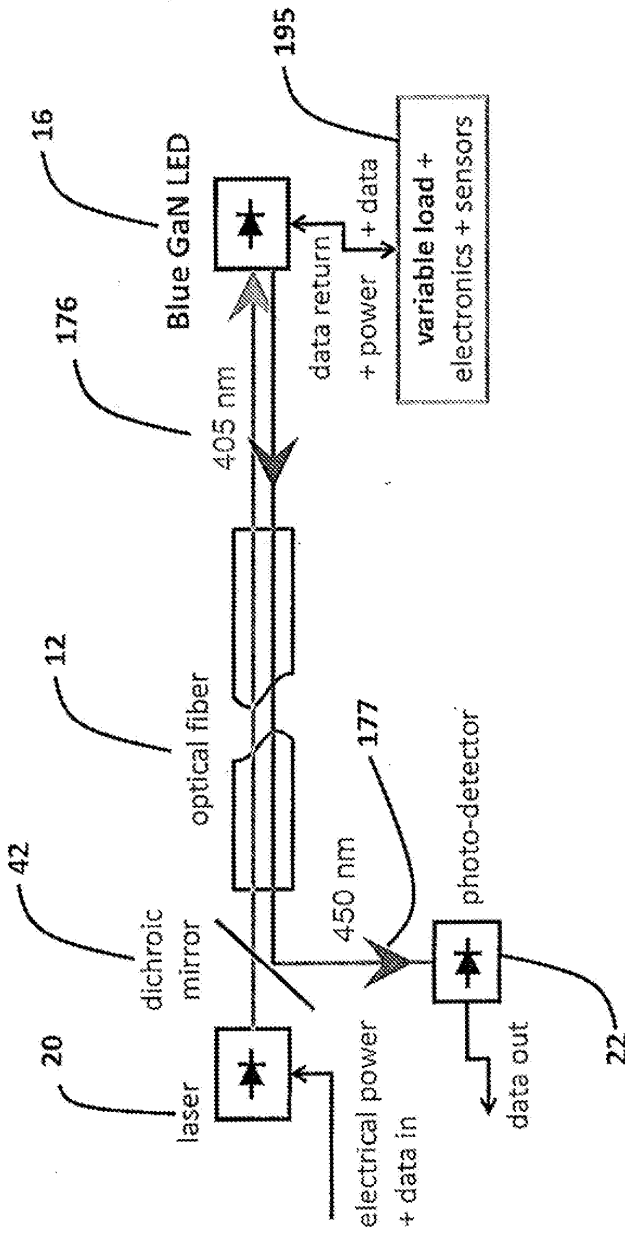


Fig. 6B



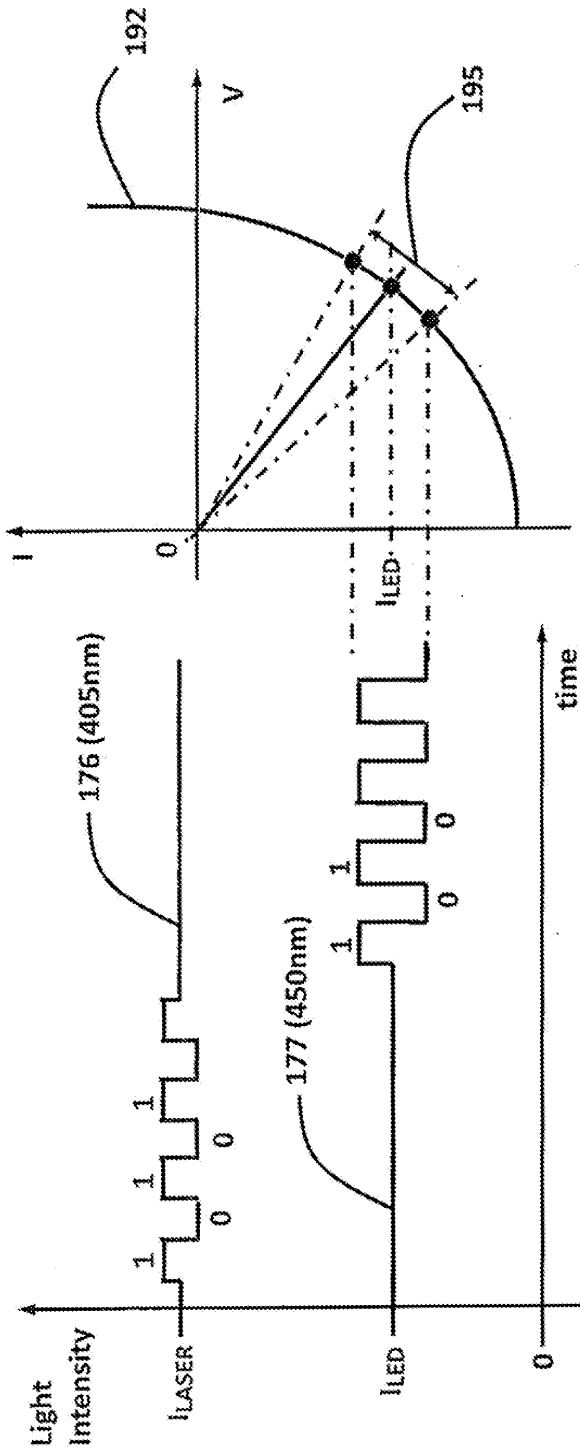


Fig. 6C

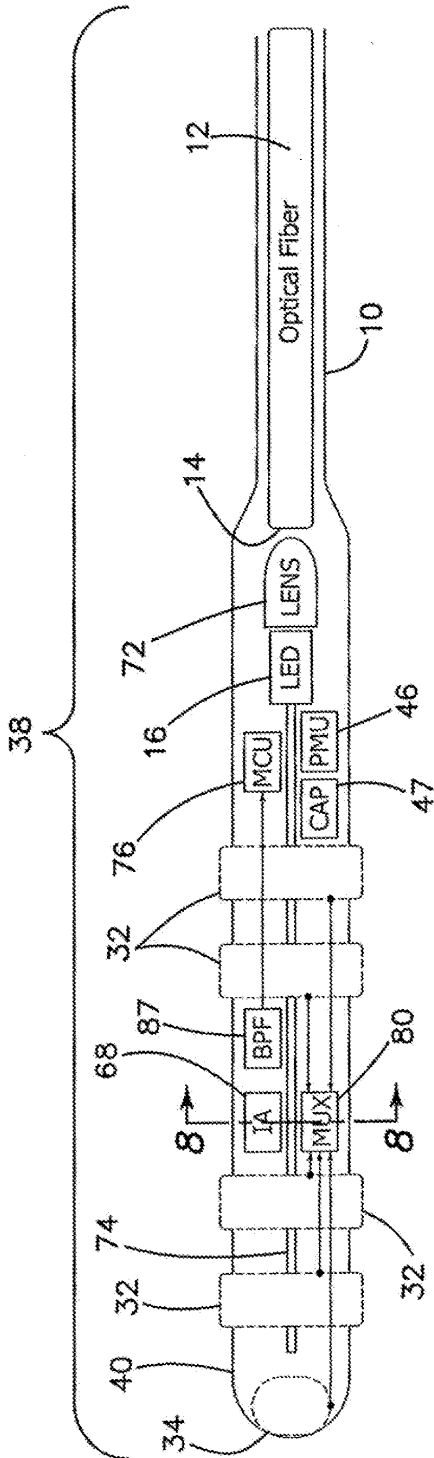


FIG. 7

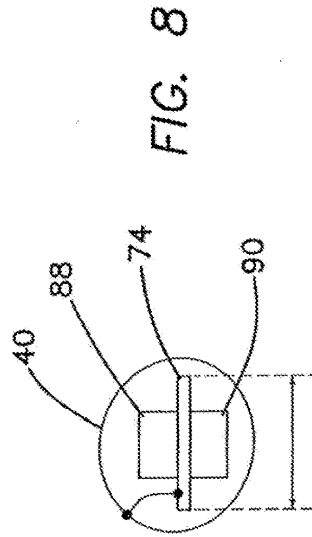


FIG. 8

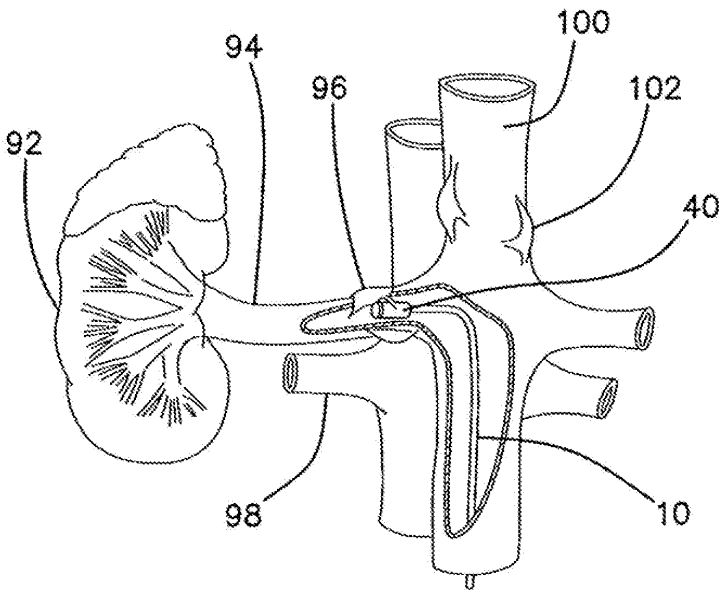


FIG. 9

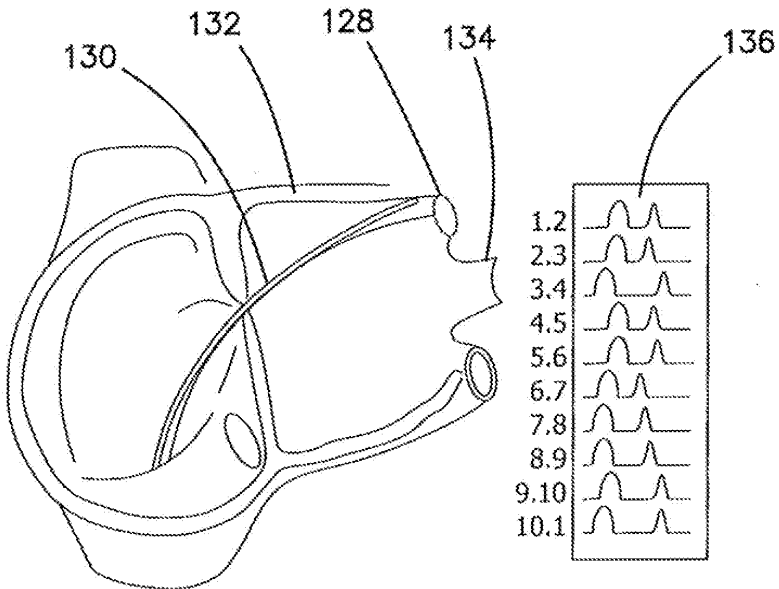


FIG. 11

05



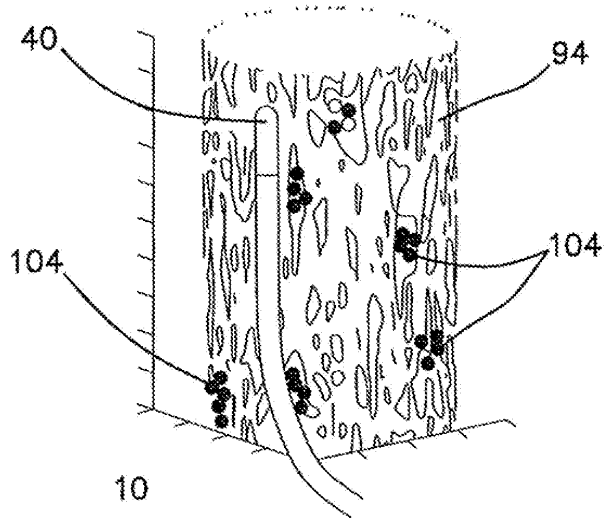


FIG. 10A

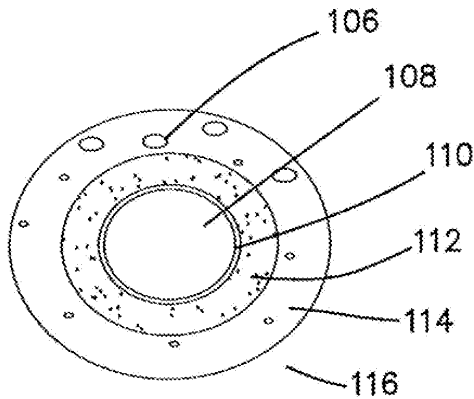


FIG. 10B

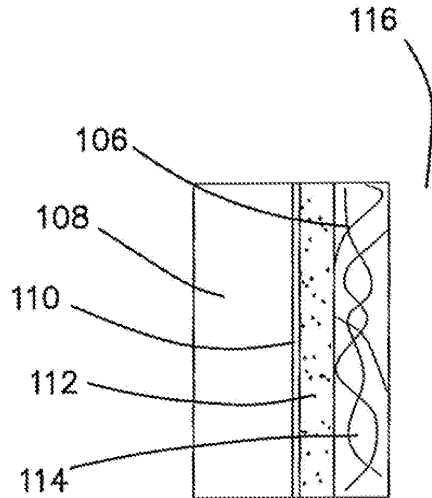


FIG. 10C

05

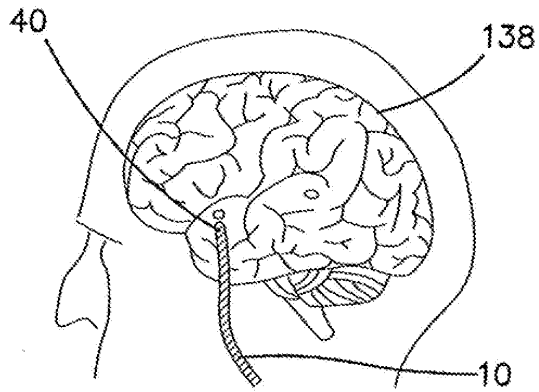


FIG. 12A

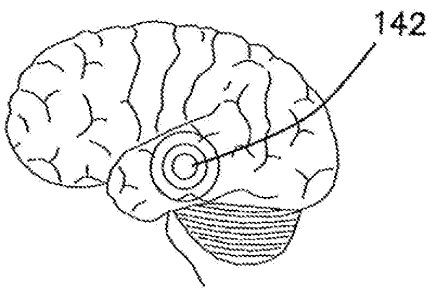
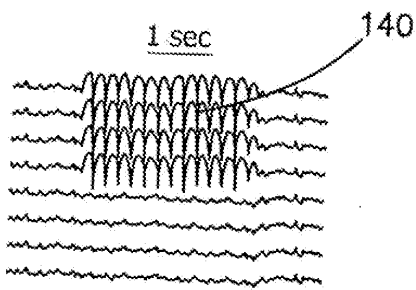


FIG. 12B

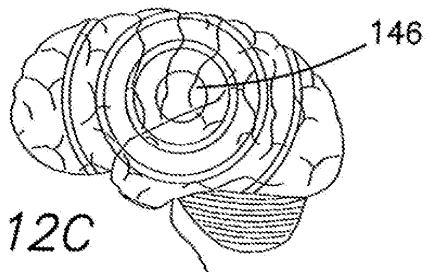
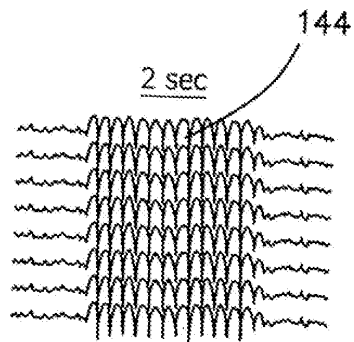


FIG. 12C

05

## OPTICALLY COUPLED CATHETER AND METHOD OF USING THE SAME

### BACKGROUND

#### Field of the Technology

**[0001]** The invention relates to the field of bioelectric catheters and in particular to catheters having MOSFET sensor arrays using a local amplifier, such as appear in CPC subclasses: GO1N 27/4145; GO1N 27/4146; GO1N 33/5438; HO1L 51/0049; and HO1L 51/0558.

#### Description of the Prior Art

**[0002]** In a conventional diagnostic catheter, the weak biopotential signals picked up by the right electrodes in the distal tip are amplified in external equipment that is separated from the electrodes by several meters of wiring. This wiring is vulnerable to noise pickup from 60 Hz power mains and higher frequency interference from operating room equipment. As a result, signals such as complex fractionated atrial electrograms with amplitudes in the 10's of  $\mu\text{Vpp}$  are often buried in the noise.

**[0003]** Existing intracardiac recording techniques, while they have served the clinician and basic scientists reasonably well over the past three to four decades, suffer from several inherent limitations. By the very nature of utilizing electrodes connected by long cables to a distant differential amplifier, these systems are subject to line "noise," ambient EMI, cable motion artifacts, and faulty connections.

**[0004]** Local signals are subject to recording of far-field signals, which at times render the interpretation of complex, rapid arrhythmias very difficult, if not impossible.

**[0005]** The conflation of far-field and signals of real interest, such as pulmonary vein fiber potentials, accessory pathway signals, and slow pathway potentials, can sometimes be the cause of failed ablations. The ability to record local electric activity with great precision and to the exclusion of far-field signals would be of paramount importance.

**[0006]** Current recording systems frequently cannot differentiate low-amplitude, high-frequency signals from background noise. Extremely low-amplitude signals, such as those generated during slow conduction within a myocardial scar, are frequently missed or lost in the background noise when amplifier gain is made sufficiently high to attempt to record such signals.

**[0007]** Continuous, low amplitude, fractionated high-frequency signals such as those frequently seen in the atria of patients with chronic atrial fibrillation, cannot be further characterized using existing recording technologies. These signals may contain important biologic and electrophysiologic information. For example, these signals may represent important areas of scarring that are responsible for formation of rotors. Alternatively, they may be manifesting discharges from contiguous epicardial parasympathetic ganglionated plexi.

**[0008]** In one application, such as in Renal Denervation, variabilities in human microanatomy of renal nerve distribution and density of nerve endings from patient to patient mean that we cannot take a "cookie cutter" approach to circumferential ablation sites. Variability in neuron function in type and size, from large to small means that we cannot only ablate the larger regular-discharging neuron sites but must also target the smaller irregular-discharging and non-

spontaneous neurons that are tonal and can drive signaling even when the large sites have been successfully ablated.

**[0009]** Mapping of the renal artery allows for a precise identification of renal nerve location and size. Location data can be used to identify precisely where to ablate, while size information can be used to discern neuron types (regular, irregular, and non-spontaneous). This can lead to greater efficacy and a reduced need for serial ablations if the first is ineffective.

**[0010]** Another such application is in electrophysiological studies for identifying different types of arrhythmia. Electrophysiology studies are performed by measuring small signals from electrodes placed in the patient's heart in a sometimes very noisy environment. As currently practiced, signal detection in the electrophysiological Lab is subject to external noise from pick-up during the travel of the signal from the catheter tip to the amplifier located several feet away. Signal processing at the multichannel recorder can subject small signals of interest to degradation when appropriately amplified, such that important microvolt-sized signals are lost when noise is filtered out.

**[0011]** Fractionation potentials recorded in scarred myocardial tissue, which serve as ablation targets, as well as pulmonary vein potentials and accessory pathway potentials, need to be accurately characterized.

**[0012]** Barbara Hubbard, in the text "The World According to Wavelets", expresses the fundamental problem of filtering as a method for smoothing the wave characteristics employing lowpass and high pass filtering, and the obvious problem of separating the noise component from the native signal, which is the inability of the system to identify which is which. If we know that a signal is smooth, i.e. changing slowly, and that the noise is fluctuating rapidly, we can filter out noise by averaging adjacent data to eliminate fluctuations while preserving the trend. Noise can also be reduced by filtering out high frequencies. For smooth signals, which change relatively slowly and therefore are mostly lower frequency, this will not blur the signal too much. Many interesting signals are not smooth; they contain high-frequency peaks. Eliminating all high frequencies mutilates the message, "cutting the daisies along with the weeds," in the words of Victor Wicker Hauser of Washington University in St. Louis, adequately expresses the main drawback of post-processing such signals.

#### BRIEF SUMMARY

**[0013]** The illustrated embodiments of the invention include an apparatus used in combination with a computer for sensing, biopotentials. The apparatus includes a catheter in which there is a plurality of sensing electrodes, a corresponding plurality of local amplifiers, each coupled to one of the plurality of sensing electrodes, a data, control and power circuit coupled to the plurality of local amplifiers, and a photonic device bidirectionally communicating an electrical signal with the data, control and power circuit. An optical fiber optically communicated with the photonic device. The photonic device bidirectionally communicates an optical signal with the optical fiber. An optical interface device provides optical power to the optical fiber and thence to the photonic device and receives optical signals through the optical fiber from the photonic device. The optical interface device bidirectionally communicates an electrical data, control and power signal to the computer.

**[0014]** The optical interface device includes a laser or provide optical power to the optical fiber.

**[0015]** The optical interface device includes a photodetector to receive optical signals through the optical fiber from the photonic device.

**[0016]** The optical interface device includes a digital signal processor to control and communicate with the laser and photodiode, and to communicate with the computer.

**[0017]** The apparatus further includes a catheter cable coupling the optical interface device and the catheter, where the optical fiber is included in the catheter cable, which is MRI compatible and EMI impervious. Only optical signals are communicated within the catheter cable.

**[0018]** The plurality of electrodes each comprise a MOS-FET electrode.

**[0019]** The apparatus further includes in one fabricated embodiment a flexible printed circuit board and where the local amplifiers and data, control and power circuit comprise application specific integrated circuits (ASICs) mounted on both sides of the flexible printed circuit board within the catheter having a size of 11 French or smaller.

**[0020]** In other words, the apparatus further includes a flexible printed circuit board and where the local amplifiers and data, control and power circuit comprise application specific integrated circuits (ASICs) mounted on both sides of the flexible printed circuit board having a width of 2.5 mm or less and a height including the ASICs of 2 mm or less.

**[0021]** The photonic device selectively operates as both a light emitting diode or a photodiode depending on bias control.

**[0022]** The data, control and power circuit include a multiplexer communicated to the plurality of electrodes.

**[0023]** The plurality of local amplifiers each have programmable gain.

**[0024]** The plurality of electrodes senses analog electrical biopotentials and the data control and power circuit include an analog to digital converter to process the electrical biopotentials in digital form and the photonic device communicates the electrical digital bipotential through the optical fiber to the optical interface as optical digital biopotential signals.

**[0025]** The catheter is configured as an electrophysiology catheter, renal denervation catheter, neuromodulation catheter, or an epileptic brain catheter.

**[0026]** The apparatus further includes a temperature sensor communicated to the data, control and power circuit.

**[0027]** The illustrated embodiments can also be characterized as a method for sensing biopotentials including the steps of: providing a catheter comprising a plurality of sensing electrodes, a corresponding plurality of local amplifiers, each coupled to one of the plurality of sensing electrodes, a data, control and power circuit coupled to the plurality of local amplifiers; and a photonic device; sensing the biopotentials with the plurality of sensing electrodes; bidirectionally communicating the biopotentials with the data, control and power circuit, providing an optical fiber in a catheter cable optically communicated with the photonic device; bidirectionally communicating an optical signal through the optical fiber; and catheter; providing optical power to the optical fiber and thence to the photonic device; receiving optical signals through the optical fiber from the photonic device; and bidirectionally communicating an electrical data, control and power signal to the computer, so that the catheter cable is MRI compatible and EMI impervious.

**[0028]** The step of sensing the biopotentials with the plurality of sensing electrodes includes the step of sensing the biopotentials with a plurality of locally amplified MOS-FET electrodes.

**[0029]** The step of providing a catheter comprising a plurality of sensing electrodes, a corresponding plurality of local amplifiers, each coupled to one of the plurality of sensing electrodes, a data, control and power circuit coupled to the plurality of local amplifiers and a photonic device includes the step of providing a flexible printed circuit board and mounting the local amplifiers and data, control and power circuit in the form of application specific integrated circuits (ASICs) mounted on both sides of the flexible printed circuit board within the catheter having a size of 11 French or smaller, or in the alternative mounted on both sides of the flexible printed circuit board having a width of 2.5 mm or less and a height including the ASICs of 2 mm or less.

**[0030]** The optically coupled catheter of the illustrated embodiments can be used in any field of medical diagnosis or therapy and in particular has specific application to electrophysiology, renal denervation, neuromodulation, nerve-ending measurements in the central nervous system (CNS), and for psychiatric therapy of patients with deep depression or manic depressive state where medicating agents are not effective. A special case is the use of such sensing modality in epileptic seizure, where the electrodes with such resolutions can augment the resolution of the focal point insertion of neuromodulating implantable electrodes where electrical potential at the site averts the epileptic event prior to its occurrence.

**[0031]** The illustrated embodiment is an optical catheter system which is scanner and magnetic resonance imaging (MRI) compatible. It is characterized by a highly flexible catheter without the use of an any shielded wires in the catheter cable. The catheter system is totally immune to any radio frequency (RF) or electromagnetic noise or interference.

**[0032]** While the apparatus and method has or will be described for the sake of grammatical fluidity with functional explanations, it is to be expressly understood that the claims, unless expressly formulated under 35 USC 112, are not to be construed as necessarily limited in any way by the construction of “means” or “steps” limitations, but are to be accorded the full scope of the meaning and equivalents of the definition provided by the claims under the judicial doctrine of equivalents, and in the case where the claims are expressly formulated under 35 USC 112 are to be accorded full statutory equivalents under 35 USC 112. The disclosure can be better visualized by turning now to the following drawings wherein like elements are referenced by like numerals.

#### BRIEF DESCRIPTION OF THE DRAWINGS

**[0033]** FIG. 1 is a block diagram of an apparatus used in catheter impedance spectroscopy according to the illustrated embodiments of the invention.

**[0034]** FIG. 2 is a block diagram of the components in the catheter tip of FIG. 1 according to the illustrated embodiments of the invention.

**[0035]** FIG. 3 is a schematic diagram of one embodiment of the fabrication of the components in the catheter tip

according to the illustrated embodiments of the invention in which the catheter system is included in a size 11 French catheter or smaller.

**[0036]** FIG. 4 is a side view of an assembled catheter system with a steerable tip.

**[0037]** FIG. 5 is a block diagram of another embodiment of the components in the catheter tip of FIG. 1.

**[0038]** FIG. 6A is a block diagram of the embodiments whereby photonic power and data transmitted optically employing an Indium Gallium Nitride (InGaN) bidirectional LED.

**[0039]** FIG. 6B is a schematic representation of the principle of operation of the photodiode and the laser forming the photonic scheme employed by the catheter for the detection of the biopotential.

**[0040]** FIG. 6C is a pair of graphs illustrating how an LED and a laser forming the photonic detection and power mechanism are employed in the detection and data transmission of biopotential measurement employing a catheter. The graph in the left portion of the figure is a graph of the laser and LED intensity as a function of time. The graph in the right portion of the figure is a graph of the LED intensity as a function of applied voltage.

**[0041]** FIG. 7 is a schematic of the fabrication of the circuitry of FIG. 6 into another embodiment of the flexible catheter.

**[0042]** FIG. 8 is a cross sectional view of the catheter of FIG. 7 as seen through section lines 8-8 of FIG. 7.

**[0043]** FIG. 9 is a diagram of the deployment of the catheter into the right renal tract for renal denervation using local amplification of biopotentials.

**[0044]** FIG. 10a is perspective diagram illustrating the renal detail of the renal artery of FIG. 9.

**[0045]** FIG. 10b is a perpendicular cross-sectional view of the renal artery of FIG. 10a.

**[0046]** FIG. 10c is a longitudinal cross-sectional view the renal artery of FIGS. 10a and 10b.

**[0047]** FIG. 11 is a diagram of a quadripolar and decapolar sensing catheter of the illustrated embodiments as disposed in the left ventricle of the heart.

**[0048]** FIG. 12a is a diagram illustrating the use of the catheter to identify a focal epileptic origin in the brain.

**[0049]** FIG. 12b is a diagram which in its upper portion illustrates the sensed biopotentials of a partial epileptic seizure and use of the catheter to identify a focal epileptic origin in the brain.

**[0050]** FIG. 12c is a diagram which in its upper portion illustrates the sensed biopotentials of a generalized epileptic seizure and use of the catheter to identify a focal epileptic origin in both sides of the brain.

**[0051]** The disclosure and its various embodiments can now be better understood by turning to the following detailed description of the preferred embodiments which are presented as illustrated examples of the embodiments defined in the claims. It is expressly understood that the embodiments as defined by the claims may be broader than the illustrated embodiments described below.

#### DETAILED DESCRIPTION OF THE PREFERRED EMBODIMENTS

**[0052]** FIG. 1 is a block diagram of illustrating an impedance catheter system 38 using local amplifiers 30 according to one of the illustrated embodiments of the invention. A catheter 40 is coupled via a catheter cable 10, which includes

an optical fiber 12 to an optical interface 18. Cable 12 and optical fiber 12, which may be several meters long, is coupled to optical interface 18, which in turn is coupled to a personal computer 26 or other data processor or control device or system through a conventional universal serial bus (USB). Optical interface 18 provides power to catheter 40 and serves to handle data flow to and from catheter 40. A laser 20 is included in optical interface 18 and is controlled by a digital signal processor (DSP) 24. For example, a 1 W 405 nm Titanium-Sapphire laser or laser diode with about 50 mW to 150 MW optical output may be used. Any electrical control signals from computer 26 are communicated through DSP 24 to laser 20, where they are output as optical or photonic signals, and are coupled into optical fiber 12. Similarly, photonic data on optical fiber 12 input into optical interface 18 is received by photodiode 22 and converted into an electrical data signal communicated to DSP 24 and hence to computer 26. Dichroic mirror 42 diverts a portion of the output of laser 20 to photodiode 22 for feedback control of the laser level.

**[0053]** The transmitted photonic signals from optical interface 18 a communicated through catheter cable 10 to emitting end 14 of optical fiber 12 and are directed into a GaN LED (Philips Lumileds Luxeon Z) or an InGaN/GaN light emitting diode (LED) and photodetector (PD) 16. According to the direction of bias applied to LED/PD 16, it operates either to receive a photonic signal and convert it into an electrical replica when biased as a photodiode or to generate a photonic signal in response to an electrical input when biased as an LED. A semiconductor such as InGaN/GaN with multiple quantum well structure commonly used for light emitting diodes can be employed for dual functions of optoelectronics devices exhibiting photodetector properties in under variable load conditions (bias). The principle of such device is noted by the fact that Optical emission resulting from 405 nm selective photoexcitation of carriers in the GaInN/GaN quantum well (QW) active region of a light-emitting diode, which reveals two recombination channels. The first recombination channel is the recombination of photoexcited carriers in the GaInN QWs. The second recombination channel is formed by carriers that leak out of the GaInN QW active region, which in turn self-bias the device in forward direction, and thereby induce a forward current, and subsequently recombine in the GaInN active region in a spatially distributed manner. The results indicate dynamic carrier transport involving active, confinement, and contact regions of the device. Thus, one can easily integrate photodetectors with LEDs using the same epi-structure to realize a GaN-based optoelectronic integrated circuit (OEIC). See Y. D. Zhou et. al., "Nitride-based light emitting diode and photodetector dual function devices with InGaN/GaN multiple quantum well structures", Solid State Electronics, Vol. 49, No. 8, August 2005, pp 1347-1351. And Martin F. Schubert et al. "Electroluminescence induced by photoluminescence excitation in GaInN/GaN light-emitting diodes" applied physics letter 95,191105, (2009).

**[0054]** LED/PD 16 is coupled to light application specific integrated circuit (ASIC) 28, which signal conditions and communicates a plurality of signals on serial peripheral interface (SPI) bus 44 to a plurality of amplifier ASIC's 30, each of which are coupled to an electrode 32. The plurality of MOSFET electrodes 32 together with tip ground electrode 34 are the sensing points of catheter 40, similar to the MOSFET electrodes described in greater detail in Shachar,



et. al., "Apparatus for magnetically deployable catheter with MOSFET sensor and method for mapping and ablation", U.S. Pat. No. 7,869,854 incorporated herein by reference as if set out in its entirety. Sensed biopotentials from MOSFET electrodes **32** are locally amplified by amplifier ASICs **30** and communicated via bus **44** into light ASIC **28** to be multiplexed out to LED/PD **16** and communicated as multiplexed photonic signals on optical fiber **12**.

**[0055]** FIG. 2 is a block diagram of the components in the catheter tip of FIG. 1 according to the illustrated embodiments of the invention. Light ASIC **28** includes a power and data module **46**, which converts the optical signal originating from laser **20** into both an electrical power signal for catheter **40** as well of control signals and output data signals. Module **46** converts electrical power from LED/PD **16** derived from pulsed light into continuous capacitive stored power stored on capacitor **47**, Module **46** is coupled to LED/PD **16** and controls the bias on to LED/PD **16** as well as bidirectionally communicating digital signals thereto and therefrom. Module **46** is coupled to the catheter ground via a coupling resistor **52** used to monitor any leakage current protection and to a temperature sensor **50** by which signal conditioning and compensation are provided for catheter **40**. PMU Module **46** is also bidirectionally coupled to DSP **48** by which a synchronizing clock signal is provided to amplifier ASICs **30** and through with data and control signals are bidirectionally communicated.

**[0056]** DSP **48** communicates with DSP **54** in amplifier ASIC **30**, which receives the data signal sensed by electrode **32** through an analog to digital converter (ADC) **56**. ADC **56** in turn is powered by module **46** through low dropout (LDO) voltage regulator **58** driving a reference voltage circuit **60** coupled to ADC **56**. ADC **56** receives the data signal from low pass filter (LPF) **62** driven by programmable gain amplifier (PGA) **64**. PGA **64** takes its input signal from high pass filter (HPF) **66** driven by a fixed gain instrumentation amplifier (IA) **68** (here a Texas Instrument or Analog Devices AD8235ACBZ-P7). Electrode **32** and tip ground electrode **34** are coupled to IA **68** through an electrostatic discharge protection circuit **70**. In the illustrated embodiment IA **68** has a fixed gain of 50 while PGA **64** is programmable from 1-50, thus making a 1-500  $\mu\text{V}$  sensed signal at electrode **32** can be programmable and appear as a 5-250 mV input signal to ADC **56**, if PGA **64** is given a gain of 10. Similarly, a 1-10,000  $\mu\text{V}$  sensed signal at electrode **32** can be scaled to appear as a 0-1800 mV input signal to ADC **56** by programming PGA **64** with a gain between 1 to 50; or a 1-100,000  $\mu\text{V}$  sensed signal at electrode **32** appears as a 0-1800 mV input signal to ADC **56** by programming PGA **64** with a gain between 1 to 50. In this manner different electrode input signal ranges are programmable and accommodated

**[0057]** FIG. 5 is a block diagram of another embodiment of the components in the catheter tip of FIG. 1, similar to the embodiment of FIG. 2. In the embodiment of FIG. 5 light ASIC **28** and amplifier ASIC **30** have been combined into an integrated ASIC **86**. In integrated ASIC **86** includes a multiplexer (MUX) **80** coupled to a plurality of electrode channels **84**, one of which is shown in detail in FIG. 5. Temperature sensor **50** is also provided as an input to MUX **80**. A sequencer circuit **82** is coupled between MUX **80** and DSP **48** bidirectionally coupled to module **46** to control the sequence of channels **84** sampled. A programmable gain control signal is generated by DSP **48** and coupled to PGA

**64**. Data is provided by PGA **64** for each electrode **32** through MUX **80** to a low pass filter **62** to analog-to-digital converter **56** for communication to DSP **56**.

**[0058]** FIG. 3 is a schematic diagram illustrating the fabrication of the components in the catheter tip according to the illustrated embodiments of the invention in which the catheter system is included in a size 11 French catheter or smaller. Optical fiber **12** in catheter cable **10** is coupled through end **14** to an aspherical lens **72** directing collimated light from optical fiber **12** into LED/DP **16**. LED/DP **16** is disposed adjacent to the proximate end of flexible printed circuit board (FPCB) **74** which extends through the body of catheter sheath **40**. In the embodiment of FIG. 3 a microcontroller (MCU) **76** with a built-in analog-to-digital converter is disposed on one side of FPCB **74** and an inverting amplifier circuit (INV) **78** is disposed on the opposing side of the FPCB **74**. INV **78** (here a Diodes 74AUP2G06) is a low-power dual inverter with open-drain output. It provides two inverting buffers with open-drain output. The output of the device is an open drain and can be connected to other open-drain outputs to implement active-LOW wired-OR or active-HIGH wired-AND functions. A Schmitt-trigger action at all inputs makes the circuit tolerant to slower input rise and fall times across the entire VCC range from 0.8 V to 3.6 V. INV **78** ensures a very low static and dynamic power consumption across the entire VCC range from 0.8 V to 3.6 V. It is fully specified for partial power-down applications using IOFF. The IOFF circuitry disables the output, preventing the damaging backflow current through the device when it is powered down. The stacked height of MCU **76**, INV **78** and FPCB **74** is about 2 mm and the width of FPCB **74** is about 2.5 mm, the width of MCU **76** and INV **78** being less. Also coupled to MCU **76** on FPCB **74** is a bandpass filter **81** and thence to IA **68**. Disposed on the opposing side of FPCB **74** from IA **68** is a multiplexer (MUX) **80**. MUX **80** is coupled to the plurality of MOSFET electrodes **32** on catheter **40** and to tip ground electrode **34**.

**[0059]** FIG. 6A is a block diagram of yet another embodiment of the components in the catheter tip of FIG. 1 in which MUX **80** is coupled to tip ground electrode **34** and through a plurality of ESD circuits **70** to a corresponding plurality of MOSFET electrodes **32**. IA **68** and bandpass filter **87** are then serially coupled between MUX **80** and the built-in ADC within MCU **76**. MCU **76** generates a control signal to MUX **80** which controls the sequencing of the multiplexed data input signals from MOSFET electrodes **32**. Temperature sensor **50** in turn is coupled to MCU **76** as is resistor **52**. The catheter system **38** of FIG. 6A is fabricated in one embodiment as shown in FIG. 7, similar to the embodiment of FIG. 3. In the embodiment as depicted in FIG. 7, IA **68**, BPF **87**, and MCU **76** are mounted on and coupled to the top surface of FPCB **74** as top components **88** with MUX **80**, capacitor **47** and module **46** are mounted on and coupled to the bottom surface of FPCB **74** as bottom components **90**. LED/PD **16** and lens **72** are adjacent to and midline with FPCB **74** with optical fiber **12**. As shown in the perpendicular cross sectional view of FIG. 8, as seen through section lines 8-8 of FIG. 7, top components **88** and bottom components **90** again present a stacking height with FPCB **74** of 2 mm or less with a width defined by the width of FPCB **74**, which can be selected as 2.5 mm or less. FPCB is electrically coupled by wiring to catheter **40** for grounding purposes, FIG. 6A is a block diagram of the embodiments whereby photonic power and data transmitted optically employing an Indium Gallium



Nitride (InGaN) bidirectional LED. FIG. 6A further shows the two sections of the catheter 40 whereby the catheter is schematically divided into a proximal section 175 represented by the handle 82 on FIG. 4 and a distal section of the catheter 185 containing the electrodes and the photonic machinery forming the bio sensing portion of the catheter.

[0060] FIG. 6B is a schematic representation of the principle of operation of the photodiode and the laser forming the photonic scheme employed by the catheter for the detection of the biopotential. The schematic forming the circuit of photonic power to the electronics where the laser 20 provides coherent light 176 (405 nm) through the dichroic mirror 42 and the optical fiber 12 to the LED/PD 16. The LED/PD 16 also selectively generates an optical signal 177 (450 nm) that returns through the optical fiber 12 to the dichroic mirror 42 where it is reflected to a photodiode 22. Further circuit 195 included in MCU 76 is a variable load which enables modulation of the signal formed by the blue InGaN LED/PD 16 to generate a data stream representing the biopotential detected by the electrodes 32. The operation of the laser 20 and the blue InGaN LED/PD 16 where DC power 176 (405 nm) is delivered to the catheter and where a return of a binary data stream to circuit 195 is further described by FIG. 6C.

[0061] FIG. 6C is a pair of graphs illustrating how an LED and a laser forming the photonic detection and power mechanism are employed in the detection and data transmission of biopotential measurement employing a catheter. The graph in the left portion of the figure is a representation of the laser and LED intensity as a function of time. The graph in the right portion of the figure is a representation of the LED current as a function of applied voltage.

[0062] FIG. 6C indicate two modes of operation in the photonic scheme which enables the bio-detection of potentials within biological tissue. Whereby Laser 20 shown in FIG. 6B generates a light beam transmitted through a dichroic mirror 42 and optical fiber 12 so that a continuous light source power signal 176 with a wave length of 405 nm is delivered the through LED/PD 16 to power the electronics of ASIC 86. When reverse biased LED/PD 16 is generated by the variable load condition 195 and set by microcontroller 76, the equivalent voltage potential measured at the biological species (Heart surface tissue or nerve ending) a data stream 177 with a wave length of 450 nm, is emitted by employing the modulation of circuit 195 (photonic equivalent emission of the potential measured at the biological site), whereby a variable load, changes the intensity of the light generated by LED/PD 16 to send a binary data stream. The use of bidirectional InGaN LED/PD 16 is possible by the employment of dichroic mirror 42 which splits the beam as well as the incorporation of a variable load which modulates the light intensity output by LED/PD 16. Clocked pulsed power is delivered at 405 nm and clocked binary data is returned at 450 nm as shown the left portion of FIG. 6C in a time-multiplexed fashion. The right portion of FIG. 6C graphically represents the relationship between the current/voltage curve 192 of LED/PD 16 and the variable load of circuit 195 to provide the binary states as represented in the left portion of FIG. 6C.

[0063] FIG. 4 is a side view of an assembled catheter system with a steerable tip, A catheter handle 82 includes optical interface 18. Catheter cable 10 extends from handle 82 to the site of operation and terminates in catheter 40. A conventional stylet is included in catheter cable 10 and is

controlled from handle 82 for steering and maneuvering the location of the catheter distal end, thereby enabling contact with the targeted site within the confinement of the biological species desired, e.g. heart surface tissue or nerve ending and, optionally catheter 40, to allow catheter 40 to be remotely steered from handle 82.

[0064] FIG. 9 illustrate a possible application of employing the invention within the current art of electrophysiological studies. The figure illustrates the deployment of the catheter 40 into the right renal arterial tract, adjacent to renal vein 98, for renal denervation (RDN), a minimally invasive procedure to treat resistant hypertension. The procedure uses radiofrequency ablation to burn the nerves in the renal arteries. This process causes a reduction in the nerve activity, which decreases blood pressure. The RDN protocol require a site-specific identification of renal artery 94, renal ganglion 96, and the electroanatomic location of arborized sympathetic renal nerve endings 104, the nerve 106 is then ablated by the use of radiofrequency modality through the adventitia 114, while correcting or modifying using local amplification of biopotentials sensed in the renal artery 94 of the left kidney 92. Catheter 40 is disposed through abdominal aorta 100 carrying aorto-corneal ganglion 102 into renal artery 94 in the proximity of renal ganglion 96. The use of the inventive device catheter 40 enable a proper definition of the location of the nerve ending and thereby will improve the diagnostic value of the current art of RDN.

[0065] FIG. 10a is perspective diagram illustrating the renal detail of the renal artery of FIG. 9 in relation to the tip of catheter 40 and the fact that the anatomical variability of the arborized sympathetic renal nerve endings 104 is human specific and cannot be assumed to be a generic map, most of RDN procedure fail. See Hitesh C Patel et al. "Renal denervation for the management of resistant hypertension", Integr Blood Press Control. 2015; 8: 57-69, published online 2015 Dec. 3, doi: 10.2147/IBPC.S65632. FIG. 10a is an illustration of a left kidney 92 where the nerves innervating the kidneys are either efferent or afferent nerves. The nerves innervating the kidneys are either efferent or afferent nerves 106 shown in FIG. 10c. The efferent nerves derive from the neuraxins, along the renal artery 94 and vein. The afferent renal nerves travel from the kidney toward the dorsal root ganglia 96 along the spinal cord. The efferent renal nerves are postganglionic, and the majority of these are adrenergic, i.e., they contain norepinephrine varicosities at their nerve terminals.

[0066] An important neurotransmitter role for norepinephrine is supported by the observations that decreasing renal sympathetic nerve activity to zero by chronic renal denervation reduced renal tissue norepinephrine concentration by >95%, conversely, increasing renal sympathetic nerve activity by renal sympathetic nerve stimulation increased norepinephrine concentration in renal venous blood. The signal characteristics of the efferent or the afferent nerves 106 is identified by the low noise high sampling rate ADC 56, DSP 48 and PMU 46 in FIG. 5 forming a digital "snap shot" associated by the employment of the electronic scheme 164 and nerve ending-signal signature representation.

[0067] The example of electro-anatomic cases, be it RDN in FIG. 9, electrophysiological study for arrhythmia indicated by schematic FIG. 11, or nerve ending variable anatomical placement of efferent or the afferent nerves shown in FIGS. 10A, 10B and 10C are further illustrations of the needs for accurate mapping of electro-anatomical features where a

proper diagnosis and spatial definition including a clear representation of the morphological characteristics of the signal(s) provides an important diagnostic information which in turn impact the therapeutic success of the medical interventional procedure i.e. RDN or EP study of arrhythmias. FIG. 10a further illustrates the incorporation of apparatus for facilitating guided delivery of a MOSFET mapping (and potentially), delivering RF energy for ablation via catheter 40 to innervated tissue and ganglia that contribute to renal sympathetic nerve activity in accordance with embodiments of the invention.

[0068] In another embodiment, the RF ablation catheter 40 is used cooperatively with an imaging system such as known in the art for example, an impedance mapping apparatus by such as the St. Jude Medical ENSITE or magnetic localization system, as exemplified as CARTO by J&J BioSense Webster, which enables a catheter to locate target within anatomical context and by provide geometric coordinates of specific anatomical destination e.g. renal nerves. This process of defining an anatomical site such as a renal plexus ganglion to effect a change of nerve signal or generally enhance a procedure, we generally classify as neuromodulation or a renal denervation. Specifically, where a surgical and/or electrical intervention deactivates the ability of the sympathetic nerve or its ganglia to influence the activity of the sympathetic autonomic nervous system to achieve a clinical outcome.

[0069] In another embodiment of the invention e improve the desired clinical outcome by employing the MOSFET sensor array of electrodes 32 within the catheter 40 in a stable position whereby the MOSFET sensor array of electrodes 32 registers a high bioelectrical potential and when an impedance sensor, which is software defined within the catheters digital circuitry, indicates a contact with a specific impedance value, the catheter 40 is than activated to deliver energy with a set value of e.g. 8-40 watts of RF energy. FIG. 10a describes a MOSFET sensor array of electrodes 32 and its irrigated RF ablation catheter 40 configured for maintaining the catheter in a stable position and orientation as detailed using the embodiments noted by the referenced patent noted above and by delivering the necessary energy to denervate the active site. The system and its methods provide the operator with the means to affect the modulation of nerve activity and achieve the desired goal of neuro-attenuation to achieve an optimal clinical goal.

[0070] The process described is governed by the use of the apparatus' ability to first provide an indication of position and orientation of the catheter 40 with constant impedance value indicating surface contact with the vessel lumen so as to be able to deliver he necessary RF energy through the adventitia and where the ablating energy is transmitted to the renal nerve and the ganglia in an optimal and safe mode.

[0071] According to one embodiment, the irrigated ablation catheter 40 with its integrated MOSFET sensor array of electrodes 32 is delivered to a location within a patient's renal artery 94. The MOSFET sensor array catheter 40 preferably includes a mapping device, (not shown) such as EnSite Navix of St. Jude Medical or other mapping device such as CARTO produced by J&J BioSense Webster.

[0072] FIG. 10b is a perpendicular cross sectional view of the renal artery of FIG. 10a and FIG. 10c is a longitudinal cross sectional view of the renal artery of FIGS. 10a and 10b, which illustrate the structure of renal artery 94, namely showing the nerves 106 in the renal wall, the renal lumen

108, the endothelium 110 providing the lining of renal artery 94, the media layer 112 backing the endothelium 110, the surrounding adventitia 114 and finally the encasing fat tissues 116. The above anatomical details are an illustration of the complexity and variability of the anatomical sits, where biopotential activities must be distinguished, identified and recorded with fidelity so as to enable a therapeutic optimal result. This is the mainstay of the utility of the inventive steps of employing a local amplification and digitizing such distinct signal with fidelity and ohmic value that the current art can't deliver, due to the inherent signal-to-noise ratio (SNR) in the current architecture of electrodes processed at a distance.

[0073] FIG. 11 is a diagrammatic longitudinal side cross section of the left atrium of the heart 150 and where an electrophysiological study employing an optical catheter 40 combined with a decapolar catheter 128 to identify electrical potential biosignals 136 within the left superior pulmonary vein 148. With the use of the novel optical catheter, the SNR and far-field/near-field averaging customarily used by the current art is reduced substantially by recording the biopotential on the sites without averaging the signal and the fact that the native signal is digitized within the distal end of the catheter 128, the measured output cannot be corrupted by any external noise and/or pickup by the long shaft of the catheter. FIG. 11 illustrates the sensing of an excitable cellular matrix typical for heart's muscle. The sensed biosignals 136 from the decapolar catheter 128 are depicted in graphic form to illustrate an electrophysiological study, where a physical placement of multiple catheters in the left atrium to sense and afterward ablate the desired site(s) in order to correct an arrhythmia, (e.g. such as Afib). The figure illustrates the case where multiple electrodes catheter 130 will display different biopotentials and unless we distinguish them and record them locally, the current art technology averages their values and can't distinguish between far and near field results.

[0074] Additionally, FIG. 11 is a graphical representation of a ganglionic waveform indicating the ability to distinguish characteristic waves. The use of the preferred embodiment in this application, with the ability to locally measure, amplify and record digitally the signal, is the mainstay of this application. The use of optical power and transmission of the digital data in a binary form further eliminates the needs to generate an averaging of the various electrodes, as the local signal may indicate a "non-standard" behavior which is the underlying representation of a disease. The conventional prior art employs electrodes, which inherently must average the signal over a timespan, and thereby reduce the resolution on a local level.

[0075] FIG. 11 is additionally an example of the embodiment of the invention where we use a graphic representation of ganglionic plexus signal and where the analogue complex wave is preserved by the machinery described above as it demonstrates the use of the catheter sensing capabilities and enables a consistent and measurable application of contact force as a function of impedance value to distinguish between the contact force over the tissue measured and the anatomical structure, and by further providing a safe and optimal contact force between the catheter distal end and the biological site or structure. This measure of force is essential for the fidelity of the measurement of the site, as nerve activity is subject to the physical inverse law. Hence the operator needs to know that the biopotential of the site in

question is a measure of a bioelectric potential of near field from the contacted tissue as opposed to far fields carried by the blood flow transfusing through the renal artery.

[0076] FIGS. 12a-12c are side cross sectional views of a patient's brain 138 and optical catheter 40 whereby an electroanatomic study of focal epilepsies and seizures that emanate from an epileptogenic focus within the brain. FIG. 12a is a diagram illustrating the use of the catheter 40 to identify a focal epileptic origin in the brain 138. FIG. 12b is a diagram which in its upper portion illustrates the sensed biopotentials 140 of a partial epileptic seizure and use of the catheter 40 to identify a focal partial seizure epileptic origin 142 in the brain 138. FIG. 12b indicates a clinical representation of a local seizure 142 identified by the corresponding electroencephalogram noted by the waveforms of the local seizure signals 144, which indicates the seizure epicenter. FIG. 12c is a diagram which in its upper portion illustrates the sensed biopotentials 144 of a generalized epileptic seizure and use of the catheter 40 to identify a generalized focal epileptic origin 146 in both sides of the brain. FIG. 12c further elaborates on the ability of a precise biopotential catheter of the type described by this invention which enables the distinction of such an apparatus to discriminate between localized seizures versus global seizures 146. The corresponding electroencephalogram 144 represents the various electrode of the existing arts of measuring brain output while the catheter 40 identifies the anatomical and topographical localization of the epicenter.

[0077] Many alterations and modifications may be made by those having ordinary skill in the art without departing from the spirit and scope of the embodiments. Therefore, it must be understood that the illustrated embodiment has been set forth only for the purposes of example and that it should not be taken as limiting the embodiments as defined by the following embodiments and its various embodiments.

[0078] Therefore, it must be understood that the illustrated embodiment has been set forth only for the purposes of example and that it should not be taken as limiting the embodiments as defined by the following claims. For example, notwithstanding the fact that the elements of a claim are set forth below in a certain combination, it must be expressly understood that the embodiments include other combinations of fewer, more or different elements, which are disclosed in above even when not initially claimed in such combinations. A teaching that two elements are combined in a claimed combination is further to be understood as also allowing for a claimed combination in which the two elements are not combined with each other but may be used alone or combined in other combinations. The excision of any disclosed element of the embodiments is explicitly contemplated as within the scope of the embodiments.

[0079] The words used in this specification to describe the various embodiments are to be understood not only in the sense of their commonly defined meanings, but to include by special definition in this specification structure, material or acts beyond the scope of the commonly defined meanings. Thus, if an element can be understood in the context of this specification as including more than one meaning, then its use in a claim must be understood as being generic to all possible meanings supported by the specification and by the word itself.

[0080] The definitions of the words or elements of the following claims are, therefore, defined in this specification to include not only the combination of elements which are

literally set forth, but all equivalent structure, material or acts for performing substantially the same function in substantially the same way to obtain substantially the same result. In this sense it is therefore contemplated that an equivalent substitution of two or more elements may be made for any one of the elements in the claims below or that a single element may be substituted for two or more elements in a claim. Although elements may be described above as acting in certain combinations and even initially claimed as such, it is to be expressly understood that one or more elements from a claimed combination can in some cases be excised from the combination and that the claimed combination may be directed to a sub combination or variation of a sub combination.

[0081] Insubstantial changes from the claimed subject matter as viewed by a person with ordinary skill in the art, now known or later devised, are expressly contemplated as being equivalently within the scope of the claims. Therefore, obvious substitutions now or later known to one with ordinary skill in the art are defined to be within the scope of the defined elements.

[0082] The claims are thus to be understood to include what is specifically illustrated and described above, what is conceptually equivalent, what can be obviously substituted and what essentially incorporates the essential idea of the embodiments.

We claim:

1. An apparatus used in combination with a computer for sensing biopotentials comprising:

a catheter comprising:

a plurality of sensing electrodes;

a corresponding plurality of local amplifiers, each coupled to one of the plurality of sensing electrodes;

a data, control and power circuit coupled to the plurality of local amplifiers; and

a photonic device bidirectionally communicating an electrical signal with the data, control and power circuit, an optical fiber optically communicated with the photonic device;

where the photonic device bidirectionally communicates an optical signal with the optical fiber; and

an optical interface device to provide optical power to the optical fiber and thence to the photonic device and to receive optical signals through the optical fiber from the photonic device,

where the optical interface device bidirectionally communicates an electrical data, control and power signal to the computer.

2. The apparatus of claim 1 where the optical interface device includes a laser to provide optical power to the optical fiber.

3. The apparatus of claim 1 where the optical interface device includes a photodetector to receive optical signals through the optical fiber from the photonic device.

4. The apparatus of claim 2 where the optical interface device includes a photodetector to receive optical signals through the optical fiber from the photonic device.

5. The apparatus of claim 4 where the optical interface device includes a digital signal processor to control and communicate with the laser and photodiode, and to communicate with the computer.

6. The apparatus of claim 1 further comprising a catheter cable coupling the optical interface device and the catheter,

where the optical fiber is included in the catheter cable, which is MRI compatible and EMI impervious.

7. The apparatus of claim 6 where only optical signals are communicated within the catheter cable,

8. The apparatus of claim 1 where the plurality of electrodes each comprise a MOSFET electrode.

9. The apparatus of claim 1 further comprising a flexible printed circuit board and where the local amplifiers and data, control and power circuit comprise application specific integrated circuits (ASICs) mounted on both sides of the flexible printed circuit board within the catheter having a size of 11 French or smaller.

10. The apparatus of claim 1 further comprising a flexible printed circuit board and where the local amplifiers and data, control and power circuit comprise application specific integrated circuits (ASICs) mounted on both sides of the flexible printed circuit board having a width of 2.5 mm or less and a height including the ASICs of 2 mm or less.

11. The apparatus of claim 1 where the photonic device selectively operates as both a light emitting diode or a photodiode depending on bias control.

12. The apparatus of claim 1 where the data, control and power circuit includes a multiplexer communicated to the plurality of electrodes.

13. The apparatus of claim 1 wherein the plurality of local amplifiers each have programmable gain.

14. The apparatus of claim 1 where the plurality of electrodes sense analog electrical biopotentials and where the data, control and power circuit includes an analog to digital converter to process the electrical biopotentials in digital form and where the photonic device communicates the electrical digital biopotential through the optical fiber to the optical interface as optical digital biopotential signals.

15. The apparatus of claim 1 where the catheter is configured as an electrophysiology catheter, renal denervation catheter, neuromodulation catheter, or an epileptic brain catheter.

16. The apparatus of claim 1 further comprising a temperature sensor communicated to the data, control and power circuit.

17. A method for sensing biopotentials comprising:  
providing a catheter comprising a plurality of sensing electrodes, a corresponding plurality of local amplifiers, each coupled to one of the pluralities of sensing

electrodes, a data, control and power circuit coupled to the plurality of local amplifiers; and a photonic device; sensing the biopotentials with the plurality of sensing electrodes;

bidirectionally communicating the biopotentials with the data, control and power circuit, providing an optical fiber in a catheter cable optically communicated with the photonic device;

bidirectionally communicating an optical signal through the optical fiber; and catheter;

providing optical power to the optical fiber and thence to the photonic device;

receiving optical signals through the optical fiber from the photonic device; and

bidirectionally communicating an electrical data, control and powersignal to the computer,

so that the catheter cable is MRI compatible and EMI impervious.

18. The method of claim 7 where sensing the biopotentials with the plurality of sensing electrodes comprises sensing the biopotentials with a plurality of locally amplified MOSFET electrodes.

19. The method of claim 17 where providing a catheter comprising a plurality of sensing electrodes, a corresponding plurality of local amplifiers, each coupled to one of the plurality of sensing electrodes, a data, control and power circuit coupled to the plurality of local amplifiers and a photonic device comprises providing a flexible printed circuit board and mounting the local amplifiers and data, control and power circuit in the form of application specific integrated circuits (ASICs) mounted on both sides of the flexible printed circuit board within the catheter having a size of 11 French or smaller.

20. The method of claim 17 where providing a catheter comprising a plurality of sensing electrodes, a corresponding plurality of local amplifiers, each coupled to one of the plurality of sensing electrodes, a data, control and power circuit coupled to the plurality of local amplifiers and a photonic device comprises providing a flexible printed circuit board and mounting the local amplifiers and data, control and power circuit in the form of application specific integrated circuits (ASICs) mounted on both sides of the flexible printed circuit board having a width of 2.5 mm or less and a height including the ASICs of 2 mm or less.

\* \* \* \* \*



INTERNATIONAL FILINGS FOR:  
*Optically Coupled Catheter  
And Method Of Using The Same*  
**INVENTOR: Yehoshua Shachar  
Marc Rocklinger  
Dr. Eli Gang**







- (51) **International Patent Classification:**  
*A61B 5/04* (2006.01) *A61B 5/0478* (2006.01)  
*A61B 5/042* (2006.01)
- (21) **International Application Number:**  
 PCT/US2020/032379
- (22) **International Filing Date:**  
 11 May 2020 (11.05.2020)
- (25) **Filing Language:** English
- (26) **Publication Language:** English
- (30) **Priority Data:**  
 16/424,202 28 May 2019 (28.05.2019) US
- (71) **Applicant:** NEUROKINESIS CORP. [US/US]; 10524 S. La Cienega Blvd, Inglewood, CA 90304 (US).
- (72) **Inventors:** SHACHAR, Josh; 2417 22nd St., Santa Monica, CA 90405 (US). ROCKLINGER, Marc; 13701 Marina Pointe Dr., #433, Marina Del Rey, CA 90202 (US). GANG, Eli; 2633 Zorada Dr., Los Angeles, CA 90046 (US).

- (74) **Agent:** DAWES, Daniel et al.; 5200 Warner Ave Ste 106, Huntington Beach, CA 92649 (US).
- (81) **Designated States** (unless otherwise indicated, for every kind of national protection available): AE, AG, AL, AM, AO, AT, AU, AZ, BA, BB, BG, BH, BN, BR, BW, BY, BZ, CA, CH, CL, CN, CO, CR, CU, CZ, DE, DJ, DK, DM, DO, DZ, EC, EE, EG, ES, FI, GB, GD, GE, GH, GM, GT, HN, HR, HU, ID, IL, IN, IR, IS, JP, KE, KG, KH, KN, KP, KR, KW, KZ, LA, LC, LK, LR, LS, LU, LY, MA, MD, ME, MG, MK, MN, MW, MX, MY, MZ, NA, NG, NI, NO, NZ, OM, PA, PE, PG, PH, PL, PT, QA, RO, RS, RU, RW, SA, SC, SD, SE, SG, SK, SL, ST, SV, SY, TH, TJ, TM, TN, TR, TT, TZ, UA, UG, US, UZ, VC, VN, WS, ZA, ZM, ZW.
- (84) **Designated States** (unless otherwise indicated, for every kind of regional protection available): ARIPO (BW, GH, GM, KE, LR, LS, MW, MZ, NA, RW, SD, SL, ST, SZ, TZ, UG, ZM, ZW), Eurasian (AM, AZ, BY, KG, KZ, RU, TJ, TM), European (AL, AT, BE, BG, CH, CY, CZ, DE, DK, EE, ES, FI, FR, GB, GR, HR, HU, IE, IS, IT, LT, LU, LV, MC, MK, MT, NL, NO, PL, PT, RO, RS, SE, SI, SK, SM,

(54) **Title:** AN OPTICALLY COUPLED CATHETER AND METHOD OF USING THE SAME

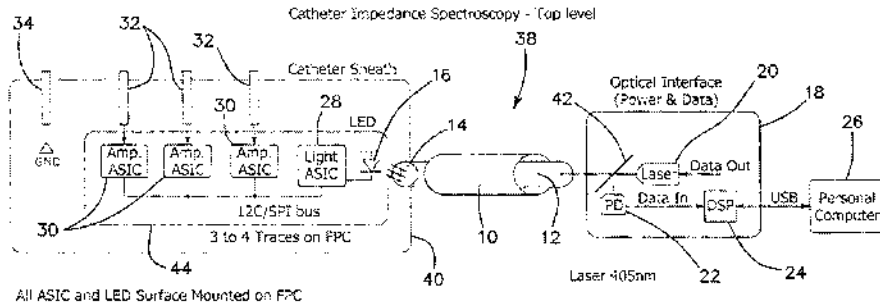


FIG. 1

(57) **Abstract:** The embodiments include an apparatus used in combination with a computer for sensing biopotentials. The apparatus includes a catheter in which there is a plurality of sensing electrodes, a corresponding plurality of local amplifiers, each coupled to one of the plurality of sensing electrodes, a data, control and power circuit coupled to the plurality of local amplifiers, and a photonic device bidirectionally communicating an electrical signal with the data, control and power circuit. An optical fiber optically communicated with the photonic device. The photonic device bidirectionally communicates an optical signal with the optical fiber. An optical interface device provides optical power to the optical fiber and thence to the photonic device and receives optical signals through the optical fiber from the photonic device. The optical interface device bidirectionally communicates an electrical data, control and power signal to the computer.



TR), OAPI (BF, BJ, CF, CG, CI, CM, GA, GN, GQ, GW,  
KM, ML, MR, NE, SN, TD, TG).

**Published:**

— with international search report (Art. 21(3))

## AN OPTICALLY COUPLED CATHETER AND

**[01]** *Background***[02]** *Field of the Technology*

**[03]** The invention relates to the field of bioelectric catheters and in particular to catheters having MOSFET sensor arrays using a local amplifier, such as appear in CPC subclasses: G01N 27/4143, G01N 27/4146; G01N 33/5438, HO1L 51/0049; and HO1L 51/0538.

[04]

**[05]** *Description of the Prior Art*

**[06]** In a conventional diagnostic catheter, the weak biopotential signals picked up by the right electrodes in the distal tip are amplified in external equipment that is separated from the electrodes by several meters of wiring. This wiring is vulnerable to noise pick up from 60 Hz power mains and higher frequency interference from operating room equipment. As a result, signals such as complex fractionated atrial electrograms with amplitudes in the 10's of  $\mu\text{V}$  are often buried in noise.

**[07]** Existing intracardiac recording techniques, while they have served the clinician and basic scientists reasonably well over the past three to four decades, suffer from several inherent limitations. By the very nature of utilizing electrodes connected by long cables to a distant differential amplifier, these systems are subject to line "noise," ambient EMI, cardiac motion artifacts, and faulty connections.

**[08]** Local signals are subject to recording of far-field signals, which at times render the interpretation of complex, rare arrhythmias very difficult, if not impossible. The conflation of far-field and signals of real interest, such as pulmonary vein fiber potentials, accessory pathway signals, and slow pathway potentials, can sometimes be the cause of failed ablation. The ability to record local electric activity with great precision and to the exclusion of far-field signals would be of paramount importance.

**[09]** Current recording systems frequently cannot differentiate low amplitude, high-frequency signals from background noise. Extremely low amplitude signals, such as those generated during slow conduction within a myocardial scar, are frequently missed or lost in the background noise when amplifier gain is made sufficiently high to attempt to record small signals.

**[10]** Continuous, low amplitude, fractionated high-frequency signals such as those frequently seen in the atria of patients with chronic atrial fibrillation, cannot be further characterized using existing recording technologies. These signals contain important biologic and electrophysiologic information. For example, these signals may represent important areas of scarring that are responsible for formation of rotors. Alternatively, they may be manifesting discharges from contiguous epicardial parasympathetic ganglionated plexi.

**[11]** In one application, such as in Renal Denervation, variabilities in human microanatomy of renal nerve distribution and density of nerve endings from patient to patient mean that we cannot take a "cookie cutter" approach to circumferential ablation sites. Variability in neuron function in type and size, from large to small means that we cannot only ablate the large

regular-discharging neuron sites but must also target the smaller irregular and can drive signaling even when the large sites have been successfully ablated.

[12] Mapping of the renal artery allows for a precise identification of renal nerve location and size. Location data can be used to identify precisely where to ablate, while size information can be used to discern neuron types (regular, irregular, and non-spontaneous). This can lead to greater efficacy and a reduced need for serial ablations if the first is ineffective.

[13] Another such application is in electrophysiological studies for identifying different types of arrhythmia. Electrophysiology studies are performed by measuring small signals from electrodes placed in the patient's heart in a sometimes very noisy environment. As currently practiced, signal detection in the electrophysiological Lab is subject to external noise from pick-up during the travel of the signal from the catheter tip to the amplifier located several feet away. Signal processing at the multichannel recorder can subject small signals of interest to degradation when appropriately amplified, such that important microvolt-sized signals are lost when noise is filtered out.

[14] Fractionation potentials recorded in scarred myocardial tissue, which serve as ablation targets, as well as pulmonary vein potentials and accessory pathway potentials, need to be accurately characterized. Barbara Hubbard, in the text "The World According to Wavelets", expresses the fundamental problem of filtering as a method for smoothing the wave characteristics employing low pass and high pass filtering, and the obvious problem of separating the noise component from the native signal, which is the inability of the system to identify which is which. If we know that a signal is smooth, i.e. changing slowly, and that the noise is fluctuating rapidly, we can filter out noise by averaging adjacent data to eliminate fluctuations while preserving the trend. Noise can also be reduced by filtering out high frequencies. For smooth signals, which change relatively slowly and therefore are mostly lower frequency, this will not blur the signal too much. Many interesting signals are not smooth, they contain high-frequency peaks. Eliminating all high frequencies mutilates the message. "cutting the daisies along with the weeds," in the words of Victor Wicker Hauser of Washington University in St Louis, adequately expresses the main drawback of postprocessing such signals.

[17]

#### [18] Brief Summary

[19] The illustrated embodiments of the invention include an apparatus used in combination with a computer for sensing biopotentials. The apparatus includes a catheter in which there is a plurality of sensing electrodes, a corresponding plurality of local amplifiers, each coupled to one of the plurality of sensing electrodes, a data, control and power circuit coupled to the plurality of local amplifiers, and a photonic device bidirectionally communicating an electrical signal with the data, control and power circuit. An optical fiber optically communicated with the photonic device. The photonic device bidirectionally communicates an optical signal with the optical fiber. An optical interface device provides optical power to the optical fiber and thence to the photonic device and receives optical signals through the optical fiber from the photonic device. The optical interface device bidirectionally communicates an electrical data, control and power signal to the computer.

[20] The optical interface device includes a laser to provide optical power to the optical fiber.

[21] The optical interface device includes a photodetector to receive optical signals through the optical fiber from the photonic device.

- [22] The optical interface device includes a digital signal processor, a photodiode, and to communicate with the computer.
- [23] The apparatus further includes a catheter cable coupling the optical interface device and the catheter, where the optical fiber is included in the catheter cable, which is MRI compatible and EMI impervious. Only optical signals are communicated within the catheter cable.
- [24] The plurality of electrodes each comprise a MOSFET electrode.
- [25] The apparatus further includes in one fabricated embodiment a flexible printed circuit board and where the local amplifiers and data, control and power circuit comprise application specific integrated circuits (ASICs) mounted on both sides of the flexible printed circuit board within the catheter having a size of 11 French or smaller.
- [26] In other words, the apparatus further includes a flexible printed circuit board and where the local amplifiers and data, control and power circuit comprise application specific integrated circuits (ASICs) mounted on both sides of the flexible printed circuit board having a width of 2.5mm or less and a height including the ASICs of 2mm or less.
- [27] The photonic device selectively operates as both a light emitting diode or a photodiode depending on bias control.
- [28] The data, control and power circuit include a multiplexer communicated to the plurality of electrodes.
- [29] The plurality of local amplifiers each have programmable gain.
- [30] The plurality of electrodes senses analog electrical biopotentials and the data, control and power circuit include an analog to digital converter to process the electrical biopotentials in digital form and the photonic device communicates the electrical digital biopotential through the optical fiber to the optical interface as optical digital biopotential signals.
- [31] The catheter is configured as an electrophysiology catheter, renal denervation catheter, neuromodulation catheter, or an epileptic brain catheter.
- [32] The apparatus further includes a temperature sensor communicated to the data, control and power circuit.
- [33] The illustrated embodiments can also be characterized as a method for sensing biopotentials including the steps of: providing a catheter comprising a plurality of sensing electrodes, a corresponding plurality of local amplifiers, each coupled to one of the plurality of sensing electrodes, a data, control and power circuit coupled to the plurality of local amplifiers; and a photonic device, sensing the biopotentials with the plurality of sensing electrodes, bidirectionally communicating the biopotentials with the data, control and power circuit, providing an optical fiber in a catheter cable optically communicated with the photonic device; bidirectionally communicating an optical signal through the optical fiber, and catheter; providing optical power to the optical fiber and thence to the photonic device; receiving optical signals through the optical fiber from the photonic device; and bidirectionally communicating an electrical data, control and power signal to the computer, so that the catheter cable is MRI compatible and EMI impervious.
- [34] The step of sensing the biopotentials with the plurality of sensing electrodes includes the step of sensing the biopotentials with a plurality of locally amplified MOSFET electrodes.
- [35] The step of providing a catheter comprising a plurality of sensing electrodes, a corresponding plurality of local amplifiers, each coupled to one of the plurality of sensing electrodes, a data, control and power circuit coupled to the plurality of local amplifiers and a photonic device includes the step of providing a flexible printed circuit board and

mounting the local amplifiers and data, control and power circuit

(ASICs) mounted on both sides of the flexible printed circuit board within the catheter having a size of 11 French or smaller, or in the alternative mounted on both sides of the flexible printed circuit board having a width of 2.5mm or less and a height including the ASICs of 2mm or less

[36] The optically coupled catheter of the illustrated embodiments can be used in any field of medical diagnosis or therapy and in particular has specific application to electrophysiology, renal denervation, neuromodulation, nerve ending measurements in the central nervous system (CNS), and for psychiatric therapy of patients with deep depression or manic depressive state where medicating agents are not effective. A special case is the use of such sensing modality in epileptic seizure, where the electrodes with such resolutions can augment the resolution of the focal point insertion of neuromodulating implantable electrodes where electrical potential at the site averts the epileptic event prior to its occurrence.

[37] The illustrated embodiment is an optical catheter system which is scanner and magnetic resonance imaging (MRI) compatible. It is characterized by a highly flexible catheter without the use of any shielded wires in the catheter cable. The catheter system is totally immune to any radio frequency (RF) or electromagnetic noise or interference.

[38] While the apparatus and method has or will be described for the sake of grammatical fluidity with functional explanations, it is to be expressly understood that the claims, unless expressly formulated under 35 USC 112, are not to be construed as necessarily limited in any way by the construction of "means" or "steps" limitations, but are to be accorded the full scope of the meaning and equivalents of the definition provided by the claims under the judicial doctrine of equivalents, and in the case where the claims are expressly formulated under 35 USC 112 are to be accorded full statutory equivalents under 35 USC 112. The disclosure can be better visualized by turning now to the following drawings wherein like elements are referenced by like numerals.

### [39] Brief Description of the Drawings

[40] Fig. 1 is a block diagram of an apparatus used in catheter impedance spectroscopy according to the illustrated embodiments of the invention.

[41] Fig. 2 is a block diagram of the components in the catheter tip of Fig. 1 according to the illustrated embodiments of the invention.

[42] Fig. 3 is a schematic diagram of one embodiment of the fabrication of the components in the catheter tip according to the illustrated embodiments of the invention in which the catheter system is included in a size 11 French catheter or smaller.

[43] Fig. 4 is a side view of an assembled catheter system with a steerable tip.

[44] Fig. 5 is a block diagram of another embodiment of the components in the catheter tip of Fig. 1.

[45] Fig. 6A is a block diagram of the embodiments whereby photonic power and data transmitted optically employing an Indium Gallium Nitride (InGaN) bidirectional LED.

[46] Fig. 6B is a schematic representation of the principle of operation of the photodiode and the laser forming the photonic scheme employed by the catheter for the detection of the biopotential.

- [47] Fig. 6C is a pair of graphs illustrating how an LED and a laser are employed in the detection and data transmission of biopotential measurement employing a catheter. The graph in the left portion of the figure is a graph of the laser and LED intensity as a function of time. The graph in the right portion of the figure is a graph of the LED intensity as a function of applied voltage.
- [48] Fig. 7 is a schematic of the fabrication of the circuitry of Fig. 6 into another embodiment of the flexible catheter.
- [49] Fig. 8 is a cross sectional view of the catheter of Fig. 7 as seen through section lines 8 – 8 of Fig. 7.
- [50] Fig. 9 is a diagram of the deployment of the catheter into the right renal tract for renal denervation using local amplification of biopotentials.
- [51] Fig. 10a is perspective diagram illustrating the renal detail of the renal artery of Fig. 9.
- [52] Fig. 10b is a perpendicular cross-sectional view of the renal artery of Fig. 10a.
- [53] Fig. 10c is a longitudinal cross-sectional view of the renal artery of Figs. 10a and 10b.
- [54] Fig. 11 is a diagram of a quadripolar and decapolar sensing catheter of the illustrated embodiments as disposed in the left ventricle of the heart.
- [55] Fig. 12a is a diagram illustrating the use of the catheter to identify a focal epileptic origin in the brain.
- [56] Fig. 12b is a diagram which in its upper portion illustrates the sensed biopotentials of a partial epileptic seizure and use of the catheter to identify a focal epileptic origin in the brain.
- [57] Fig. 12c is a diagram which in its upper portion illustrates the sensed biopotentials of a generalized epileptic seizure and use of the catheter to identify a focal epileptic origin in both sides of the brain.
- [58] The disclosure and its various embodiments can now be better understood by turning to the following detailed description of the preferred embodiments which are presented as illustrated examples of the embodiments defined in the claims. It is expressly understood that the embodiments as defined by the claims may be broader than the illustrated embodiments described below.

[59] **Detailed Description of the Preferred Embodiments**

- [60] Fig. 1 is a block diagram of illustrating an impedance catheter system 38 using local amplifiers 30 according to one of the illustrated embodiments of the invention. A catheter 40 is coupled via a catheter cable 10, which includes an optic fiber 12 to an optical interface 18. Cable 10 and optical fiber 12, which may be several meters long, is coupled to optical interface 18, which in turn is coupled to a personal computer 26 or other data processor or control device or system through a conventional universal serial bus (USB). Optical interface 18 provides power to catheter 40 and serves to handle data flow to and from catheter 40. A laser 20 is included in optical interface 18 and is controlled by a digital signal processor (DSP) 24. For example, a 1W 405nm Titanium-Sapphire laser or laser diode with about 50mW to 150mW optical output may be used. Any electrical control signals from computer 26 are communicated through DSP 24 to laser 20, where they are output as optical or photonic signals, and are coupled into optical fiber 12. Similarly, photonic data on optical fiber 12 input in optical interface 18 is received by photodiode 22 and converted into an electrical data signal communicated to DSP 24 and hence to computer 26. Dichroic mirror 42 diverts a portion of the output of laser 20 to photodiode 22 for feedback control of the laser level.



[61] The transmitted photonic signals from optical interface 18 a end 14 of optical fiber 12 and are directed into a GaN LED (Philips Lumileds Luxeon Z) or an InGaN/GaN light emitting diode (LED) and photodetector (PD) 16. According to the direction of bias applied to LED/PD 16, it operates either to receive a photonic signal and convert it into an electrical replica when biased as a photodiode or to generate a photonic signal in response to an electrical input when biased as an LED. A semiconductor such as InGaN/GaN with multiple quantum well structure commonly used for light emitting diodes can be employed for dual functions of optoelectronics devices exhibiting photodetector properties in under variable load conditions (bias). The principle of such device is noted by the fact that Optical emission resulting from 405 nm selective photoexcitation of carriers in the GaInN/GaN quantum well (QW) active region of a light-emitting diode, which reveals two recombination channels. The first recombination channel is the recombination of photoexcited carriers in the GaInN QWs. The second recombination channel is formed by carriers that leak out of the GaInN QW active region, which in turn self-bias the device in forward direction, and thereby induce a forward current, and subsequently recombine in the GaInN active region in a spatially distributed manner. The results indicate dynamic carrier transport involving active, confinement, and contact regions of the device. Thus, one can easily integrate photodetectors with LEDs using the same epi-structure to realize a GaN-based optoelectronic integrated circuit (OEIC). See Y.D. Zhou et al., "Nitride-based light emitting diode and photodetector dual function devices with InGaN/GaN multiple quantum well structures", *Solid State Electronics*, Vol. 49, No. 8, Aug. 2005, pp 1347 – 1351. And Martin F. Schubert et al. "Electroluminescence induced by photoluminescence excitation in GaInN/GaN light-emitting diodes" *applied physics letter* 95, 191105, (2009).

[62] LED/PD 16 is coupled to light application specific integrated circuit (ASIC) 28, which signal conditions and communicates a plurality of signals on serial peripheral interface (SPI) bus 44 to a plurality of amplifier ASIC's 30, each of which are coupled to an electrode 32. The plurality of MOSFET electrodes 32 together with tip ground electrode 34 are the sensing points of catheter 40, similar to the MOSFET electrodes described in greater detail in Shachar, et al., "Apparatus for magnetically deployable catheter with MOSFET sensor and method for mapping and ablation", US Patent 7,869,854 incorporated herein by reference as if set out in its entirety. Sensed biopotentials from MOSFET electrodes 32 are locally amplified by amplifier ASICs 30 and communicated via bus 44 into light ASIC 28 to be multiplexed out to LED/PD 16 and communicated as multiplexed photonic signals on optical fiber 12.

[63] Fig. 2 is a block diagram of the components in the catheter tip of Fig. 1 according to the illustrated embodiments of the invention. Light ASIC 28 includes a power and data module 46, which converts the optical signal originating from laser 20 into both an electrical power signal for catheter 40 as well of control signals and output data signals. Module 46 converts electrical power from LED/PD 16 derived from pulsed light into continuous capacitive stored power stored on capacitor 47. Module 46 is coupled to LED/PD 16 and controls the bias on to LED/PD 16 as well as bidirectionally communicating digital signals thereto and therefrom. Module 46 is coupled to the catheter ground via a coupling resistor 52 used to monitor any leakage current protection and to a temperature sensor 50 by which signal conditioning and compensation are provided for catheter 40. PMU Module 46 is also bidirectionally coupled to DSP 48 by which a synchronizing clock signal is provided to amplifier ASICs 30 and through with data and control signals are bidirectionally communicated.

[64] DSP 48 communicates with DSP 54 in amplifier ASIC 30, through an analog to digital converter (ADC) 56. ADC 56 in turn is powered by module 46 through low dropout (LDO) voltage regulator 58 driving a reference voltage circuit 60 coupled to ADC 56. ADC 56 receives the data signal from low pass filter (LPF) 62 driven by programmable gain amplifier (PGA) 64. PGA 64 takes its input signal from high pass filter (HPF) 66 driven by a fixed gain instrumentation amplifier (IA) 68 (here a Texas Instrument or Analog Device AD8235ACBZ-P7). Electrode 32 and tip ground electrode 34 are coupled to IA 68 through an electrostatic discharge protection circuit 70. In the illustrated embodiment IA 68 has a fixed gain of 50 while PGA 64 is programmable from 1 to 50, thus making a 1- 500  $\mu\text{V}$  sensed signal at electrode 32 can be programmable and appear as a 5 - 250 mV input signal to ADC 56, if PGA 64 is given a gain of 10. Similarly, a 1 - 10,000  $\mu\text{V}$  sensed signal at electrode 32 can be scaled to appear as a 0 - 1800 mV input signal to ADC 56 by programming PGA 64 with a gain between 1 to 50; or a 1 - 100,000  $\mu\text{V}$  sensed signal at electrode 32 appears as a 0 - 1800 mV input signal to ADC 56 by programming PGA 64 with a gain between 1 to 50. In this manner different electrode input signal ranges are programmable and accommodated.

[65] Fig. 5 is a block diagram of another embodiment of the components in the catheter tip of Fig. 1, similar to the embodiment of Fig. 2. In the embodiment of Fig. 5 light ASIC 28 and amplifier ASIC 30 have been combined into an integrated ASIC 86. Integrated ASIC 86 includes a multiplexer (MUX) 80 coupled to a plurality of electrode channels 84, one of which is shown in detail in Fig. 5. Temperature sensor 50 is also provided as an input to MUX 80. A sequence circuit 82 is coupled between MUX 80 and DSP 48 bidirectionally coupled to module 46 to control the sequence of channels 84 sampled. A programmable gain control signal is generated by DSP 48 and coupled to PGA 64. Data is provided by PGA 64 for each electrode 32 through MUX 80 to a low pass filter 62 to analog-to-digital converter 56 for communication with DSP 56.

[66] Fig. 3 is a schematic diagram illustrating the fabrication of the components in the catheter tip according to the illustrated embodiments of the invention in which the catheter system is included in a size 11 French catheter or smaller. Optical fiber 12 in catheter cable 10 is coupled through end 14 to an aspherical lens 72 directing collimated light from optical fiber 12 into LED/DP 16. LED/DP 16 is disposed adjacent to the proximate end of flexible printed circuit board (FPCB) 74 which extends through the body of catheter sheath 40. In the embodiment of Fig. 3 a microcontroller (MCU) 76 with a built-in analog-to-digital converter is disposed on one side of FPCB 74 and an inverting amplifier circuit (INV) 78 is disposed on the opposing side of the FPCB 74. INV 78 (here a Diodes 74AUP2G06) is a low-power dual inverter with open-drain output. It provides two inverting buffers with open-drain output. The output of the device is an open drain and can be connected to other open-drain outputs to implement active-LOW wired-OR or active-HIGH wired-AND function. A Schmitt-trigger action at all inputs makes the circuit tolerant to slower input rise and fall times across the entire VCC range from 0.8 V to 3.6 V. INV 78 ensures a very low static and dynamic power consumption across the entire VCC range from 0.8 V to 3.6 V. It is fully specified for partial power-down applications using IOFF. The IOFF circuitry disables the output, preventing the damaging backflow current through the device when it is powered down. The stacked height of MCU 76, INV 78 and FPCB 74 is about 2mm and the width of FPCB 74 is about 2.5mm. The width of MCU 76 and INV 78 is less. Also coupled to MCU 76 on FPCB 74 is a bandpass filter 81 and thence to IA 68. Disposed on the opposing side of FPCB

74 from IA 68 is a multiplexer (MUX) 80. MUX 80 is coupled to tip and to tip ground electrode 34.

[67] Fig. 6A is a block diagram of yet another embodiment of the components in the catheter tip of Fig. 1 in which MUX 80 is coupled to tip ground electrode 34 and through a plurality of ESD circuits 70 to a corresponding plurality of MOSFET electrodes 32. IA 68 and bandpass filter 87 are then serially coupled between MUX 80 and the built-in ADC within MCU 76. MCU 76 generates a control signal to MUX 80 which controls the sequencing of the multiplexed data input signals from MOSFET electrodes 32. Temperature sensor 50 in turn is coupled to MCU 76 as is resistor 52. The catheter system 38 of Fig. 6A is fabricated in one embodiment as shown in Fig. 7, similar to the embodiment of Fig. 3. In the embodiment as depicted in Fig. 7, IA 68, BPF 87, and MCU 76 are mounted on and coupled to the top surface of FPCB 74 as top components 88 with MUX 80, capacitor 47 and module 46 are mounted on and coupled to the bottom surface of FPCB 74 as bottom components 90. LED/PD 16 and lens 72 are adjacent to and midline with FPCB 74 with optical fiber 12. As shown in the perpendicular cross sectional view of Fig. 8, as seen through section lines 8 – 8 of Fig. 7, top components 88 and bottom components 90 again present a stacking height with FPCB 74 of 2mm or less with a width defined by the width of FPCB 74, which can be selected as 2.5mm or less. FPCB is electrically coupled by wiring to catheter 40 for grounding purposes. Fig. 6A is a block diagram of the embodiments whereby photonic power and data transmitted optically employing an Indium Gallium Nitride (InGaN) bidirectional LED. Fig. 6A further shows the two sections of the catheter 40 whereby the catheter is schematically divided into a proximal section 175 represented by the handle 82 on Fig. 4 and a distal section of the catheter 185 containing the electrodes and the photonic machinery forming the biosensing portion of the catheter.

[68] Fig. 6B is a schematic representation of the principle of operation of the photodiode and the laser forming the photonic scheme employed by the catheter for the detection of the biopotential. The schematic forming the circuit of photonic power to the electronics where the laser 20 provides coherent light 176 (405nm) through the dichroic mirror 42 and the optical fiber 12 to the LED/PD 16. The LED/PD 16 also selectively generates an optical signal 177 (450nm) that returns through the optical fiber 12 to the dichroic mirror 42 where it is reflected to a photodiode 22. Further circuit 195 included in MCU 76 is a variable load which enables modulation of the signal formed by the blue InGaN LED/PD 16 to generate a data stream representing the biopotential detected by the electrodes 32. The operation of the laser 20 and the blue InGaN LED/PD 16 where DC power 176 (405nm) is delivered to the catheter and where a return of a binary data stream to circuit 195 is further described by Fig. 6C.

[69] Fig. 6C is a pair of graphs illustrating how an LED and a laser forming the photonic detection and power mechanism are employed in the detection and data transmission of biopotential measurement employing a catheter. The graph in the left portion of the figure is a representation of the laser and LED intensity as a function of time. The graph in the right portion of the figure is a representation of the LED current as a function of applied voltage.

[70] Fig. 6C indicate two modes of operation in the photonic scheme which enables the bio-detection of potentials within biological tissue. Whereby Laser 20 shown in Fig. 6B generates a light beam transmitted through a dichroic mirror 42 and optical fiber 12 so that a continuous light source power signal 176 with a wave length of 405nm is delivered the through LED/PD 16 to power the electronics of ASIC 86. When reverse biased LED/PD 16 is generated by the variable load condition 195 and set by microcontroller 76, the equivalent voltage potential measured at the biological species

(Heart surface tissue or nerve ending) a data stream 177 with a wave modulation of circuit 195 (photonic equivalent emission of the potential measured at the biological site), whereby a variable load, changes the intensity of the light generated by LED/PD 16 to send a binary data stream. The use of bidirectional InGaN LED/PD 16 is possible by the employment of dichroic mirror 42 which splits the beam as well as the incorporation of a variable load which modulates the light intensity output by LED/PD 16. Clocked pulsed power is delivered at 405nm and clocked binary data is returned at 450nm as shown in the left portion of Fig. 6C in a time-multiplexed fashion. The right portion of Fig. 6C graphically represents the relationship between the current/voltage curve 192 of LED/PD 16 and the variable load of circuit 195 to provide the binary states as represented in the left portion of Fig. 6C.

[71] Fig. 4 is a side view of an assembled catheter system with a steerable tip. A catheter handle 82 includes optical interface 18. Catheter cable 10 extends from handle 82 to the site of operation and terminates in catheter 40. A conventional stylet is included in catheter cable 10 and is controlled from handle 82 for steering and maneuvering the location of the catheter distal end, thereby enabling contact with the targeted site within the confinement of the biological species desired, e.g. heart surface tissue or nerve ending and, optionally catheter 40, to allow catheter 40 to be remotely steered from handle 82.

[72] Fig. 9 illustrate a possible application of employing the invention within the current art of electrophysiologic studies. The figure illustrates the deployment of the catheter 40 into the right renal arterial tract, adjacent to renal vein 9 for renal denervation (RDN), a minimally invasive procedure to treat resistant hypertension. The procedure uses radiofrequency ablation to burn the nerves in the renal arteries. This process causes a reduction in the nerve activity, which decreases blood pressure. The RDN protocol requires a site-specific identification of renal artery 94, renal ganglion 96, and the electroanatomic location of arborized sympathetic renal nerve endings 104, the nerve 106 is then ablated by the use of radiofrequency modality through the adventitia 114, while correcting or modifying using local amplification of biopotential sensed in the renal artery 94 of the left kidney 92. Catheter 40 is disposed through abdominal aorta 100 carrying aortic ganglion 102 into renal artery 94 in the proximity of renal ganglion 96. The use of the inventive device catheter 40 enable a proper definition of the location of the nerve ending and thereby will improve the diagnostic value of the current art of RDN.

[73] Fig. 10a is perspective diagram illustrating the renal detail of the renal artery of Fig. 9 in relation to the tip of catheter 40 and the fact that the anatomical variability of the arborized sympathetic renal nerve endings 104 is human specific and cannot be assumed to be a generic map, most of RDN procedure fail. See Hitesh C. Patel et al. "Renal denervation for the management of resistant hypertension", *Integr Blood Press Control* 2015; 8: 57-69, published online 2015 Dec. 3, doi:10.2147/IBPC.S65632. Fig 10a is an illustration of a left kidney 92 where the nerves innervating the kidneys are either efferent or afferent nerves. The nerves innervating the kidneys are either efferent or afferent nerves 106 shown in Fig. 10. The efferent nerves derive from the neuraxis, along the renal artery 94 and vein. The afferent renal nerves travel from the kidney toward the dorsal root ganglia 96 along the spinal cord. The efferent renal nerves are postganglionic, and the majority of these are adrenergic, i.e., they contain norepinephrine varicosities at their nerve terminals.

[74] An important neurotransmitter role for norepinephrine is sympathetic nerve activity to zero by chronic renal denervation reduced renal tissue norepinephrine concentration by >90%, conversely, increasing renal sympathetic nerve activity by renal sympathetic nerve stimulation increased norepinephrine concentration in renal venous blood. The signal characteristics of the efferent or the afferent nerves 106 is identified by the low noise high sampling rate ADC 56, DSP 48 and PMU 46 in Fig. 5 forming a digital "snap shot" associated by the employment of the electronic scheme 164 and nerve ending-signal signature representation.

[75] The example of electro-anatomic cases, be it RDN in Fig.9, electrophysiological study for arrhythmia indicated by schematic Fig. 11, or nerve ending variable anatomical placement of efferent or the afferent nerves shown in Figs. 10A, 10B and 10C are further illustrations of the needs for accurate mapping of electro-anatomical features where a proper diagnosis and spatial definition including a clear representation of the morphological characteristics of the signal(s) provides an important diagnostic information which in turn impact the therapeutic success of the medical interventional procedure i.e. RDN or EP study of arrhythmias. FIG. 10a further illustrates the incorporation of apparatus for facilitating guided delivery of a MOSFET mapping (and potentially), delivering RF energy for ablation via catheter 40 to innervated tissue and ganglia that contribute to renal sympathetic nerve activity in accordance with embodiments of the invention.

[76] In another embodiment, the RF ablation catheter 40 is used cooperatively with an imaging system such as known the art for example, an impedance mapping apparatus by such as the St. Jude Medical ENSITE or magnetic localization system, as exemplified as CARTO by J&J BioSense Webster, which enables a catheter to locate target within anatomical context and by provide geometric coordinates of specific anatomical destination e.g. renal nerves. This process of defining an anatomical site such as a renal plexus ganglion to effect a change of nerve signal or generally enhance a procedure, we generally classify as neuromodulation or a renal denervation. Specifically, where a surgical and/or electrical intervention deactivates the ability of the sympathetic nerve or its ganglia to influence the activity of the sympathetic autonomic nervous system to achieve a clinical outcome.

[77] In another embodiment of the invention we improve the desired clinical outcome by employing the MOSFET sensor array of electrodes 32 within the catheter 40 in a stable position whereby the MOSFET sensor array of electrodes 32 registers a high bioelectrical potential and when an impedance sensor, which is software defined within the catheter's digital circuitry, indicates a contact with a specific impedance value, the catheter 40 is then activated to deliver energy with a set value of e.g. 8-40 watts of RF energy. FIG. 10a describes a MOSFET sensor array of electrodes 32 and its irrigated RF ablation catheter 40 configured for maintaining the catheter in a stable position and orientation as detailed using the embodiments noted by the referenced patent noted above and by delivering the necessary energy to denervate the active site. The system and its methods provide the operator with the means to affect the modulation of nerve activity and achieve the desired goal of neuro-attenuation to achieve an optimal clinical goal.

[78] The process described is governed by the use of the apparatus' ability to first provide an indication of position and orientation of the catheter 40 with constant impedance value indicating surface contact with the vessel lumen so as to be able to deliver the necessary RF energy through the adventitia and where the ablating energy is transmitted to the renal nerve and the ganglia in an optimal and safe mode.

[79] According to one embodiment, the irrigated ablation cath electrodes 32 is delivered to a location within a patient's renal artery 94. The MUSE:11 sensor array catheter 40 preferably includes a mapping device, (not shown) such as EnSite Navx of St. Jude Medical or other mapping device such as CART produced by J&J BioSense Webster.

[80] Fig. 10b is a perpendicular cross sectional view of the renal artery of Fig. 10a and Fig. 10c is a longitudinal cross sectional view of the renal artery of Figs. 10a and 10b, which illustrate the structure of renal artery 94, namely showing the nerves 106 in the renal wall, the renal lumen 108, the endothelium 110 providing the lining of renal artery 94, the medial layer 112 backing the endothelium 110, the surrounding adventitia 114 and finally the encasing fat tissues 116. The above anatomical details are an illustration of the complexity and variability of the anatomical sites, where biopotential activities must be distinguished, identified and recorded with fidelity so as to enable a therapeutic optimal result. This is the mainstay of the utility of the inventive steps of employing a local amplification and digitizing such distinct signal with fidelity, an ohmic value that the current art can't deliver, due to the inherent signal-to-noise ratio (SNR) in the current architecture of electrodes processed at a distance.

[81] Fig. 11 is a diagrammatic longitudinal side cross section of the left atrium of the heart 150 and where an electrophysiological study employing an optical catheter 40 combined with a decapolar catheter 128 to identify electric potential biosignals 136 within the left superior pulmonary vein 148. With the use of the novel optical catheter, the SN and far-field/near-field averaging customarily used by the current art is reduced substantially by recording the biopotential on the sites without averaging the signal and the fact that the native signal is digitized within the distal end of the catheter 128, the measured output cannot be corrupted by any external noise and/or pickup by the long shaft of the catheter. Fig. 11 illustrates the sensing of an excitable cellular matrix typical for heart's muscle. The sensed biosignals 136 from the decapolar catheter 128 are depicted in graphic form to illustrate an electrophysiological study, where a physical placement of multiple catheters in the left atrium to sense and afterward ablate the desired site(s) in order to correct an arrhythmia, (e.g. such as A-fib). The figure illustrates the case where multiple electrodes catheter 130 will display different biopotentials and unless we distinguish them and record them locally, the current art technology averages their values and can't distinguish between far and near field results.

[82] Additionally, Fig. 11 is a graphical representation of a ganglionic waveform indicating the ability to distinguish characteristic waves. The use of the preferred embodiment in this application, with the ability to locally measure, amplify and record digitally the signal, is the mainstay of this application. The use of optical power and transmission of the digital data in a binary form further eliminates the needs to generate an averaging of the various electrodes, as the local signal may indicate a "non-standard" behavior which is the underlying representation of a disease. The conventional prior art employ electrodes, which inherently must average the signal over a timespan, and thereby reduce the resolution on a local level.

[83] Fig. 11 is additionally an example of the embodiment of the invention where we use a graphic representation of a ganglionic plexus signal and where the analogue complex wave is preserved by the machinery described above as demonstrates the use of the catheter sensing capabilities and enables a consistent and measurable application of contact force as a function of impedance value to distinguish between the contact force over the tissue measured and the anatomic structure, and by further providing a safe and optimal contact force between the catheter distal end and the biological site.



or structure. This measure of force is essential for the fidelity of the the physical inverse law. Hence the operator needs to know that the topopotential of the site in question is a measure of a bioelectric potential of near field from the contacted tissue as opposed to far fields carried by the blood flow transfusing through the renal artery.

[84] Figs. 12a - 12c are side cross sectional views of a patient's brain 138 and optical catheter 40 whereby an electroanatomic study of focal epilepsies and seizures that emanate from an epileptogenic focus within the brain. Fig. 12a is a diagram illustrating the use of the catheter 40 to identify a focal epileptic origin in the brain 138. Fig. 12b is a diagram which in its upper portion illustrates the sensed biopotentials 140 of a partial epileptic seizure and use of the catheter 40 to identify a focal partial seizure epileptic origin 142 in the brain 138. Fig. 12b indicates a clinical representation of a local seizure 142 identified by the corresponding electroencephalogram noted by the waveforms of the local seizure signals 144, which indicates the seizure epicenter. Fig. 12c is a diagram which in its upper portion illustrates the sensed biopotentials 144 of a generalized epileptic seizure and use of the catheter 40 to identify a generalized focal epileptic origin 146 in both sides of the brain. Fig. 12c further elaborates on the ability of a precise biopotential catheter of the type described by this invention which enables the distinction of such an apparatus to discriminate between localized seizures verses global seizures 146. The corresponding electroencephalogram 144 represents the various electrode of the existing arts of measuring brain output while the catheter 40 identifies the anatomical and topographical localization of the epicenter.

[85] Many alterations and modifications may be made by those having ordinary skill in the art without departing from the spirit and scope of the embodiments. Therefore, it must be understood that the illustrated embodiment has been set forth only for the purposes of example and that it should not be taken as limiting the embodiments as defined by the following embodiments and its various embodiments.

[86] Therefore, it must be understood that the illustrated embodiment has been set forth only for the purposes of example and that it should not be taken as limiting the embodiments as defined by the following claims. For example, notwithstanding the fact that the elements of a claim are set forth below in a certain combination, it must be expressly understood that the embodiments include other combinations of fewer, more or different elements, which are disclosed in above even when not initially claimed in such combinations. A teaching that two elements are combined in a claimed combination is further to be understood as also allowing for a claimed combination in which the two elements are not combined with each other but may be used alone or combined in other combinations. The excision of any disclosed element of the embodiments is explicitly contemplated as within the scope of the embodiments.

[87] The words used in this specification to describe the various embodiments are to be understood not only in the sense of their commonly defined meanings, but to include by special definition in this specification structure, material or acts beyond the scope of the commonly defined meanings. Thus, if an element can be understood in the context of this specification as including more than one meaning, then its use in a claim must be understood as being generic to all possible meanings supported by the specification and by the word itself.

[88] The definitions of the words or elements of the following claims are, therefore, defined in this specification to include not only the combination of elements which are literally set forth, but all equivalent structure, material or acts for performing substantially the same function in substantially the same way to obtain substantially the same result. In this

sense it is therefore contemplated that an equivalent substitution of elements in the claims below or that a single element may be substituted for two or more elements in a claim. Although elements may be described above as acting in certain combinations and even initially claimed as such, it is to be expressly understood that one or more elements from a claimed combination can in some cases be excised from the combination and that the claimed combination may be directed to a sub combination or variation of a sub combination.

[89] Insubstantial changes from the claimed subject matter as viewed by a person with ordinary skill in the art, now known or later devised, are expressly contemplated as being equivalently within the scope of the claims. Therefore, obvious substitutions now or later known to one with ordinary skill in the art are defined to be within the scope of the defined elements.

[90] The claims are thus to be understood to include what is specifically illustrated and described above, what is conceptually equivalent, what can be obviously substituted and what essentially incorporates the essential idea of the embodiments.

We claim:

1. An apparatus used in combination with a computer for sensing biopotentials comprising: a catheter comprising:
  - a plurality of sensing electrodes; a corresponding plurality of local amplifiers, each coupled to one of the plurality of sensing electrodes; a data, control and power circuit coupled to the plurality of local amplifiers; and
  - a photonic device bidirectionally communicating an electrical signal with the data, control and power circuit, an optical fiber optically communicated with the photonic device;
    - where the photonic device bidirectionally communicates an optical signal with the optical fiber; and an optical interface device to provide optical power to the optical fiber and thence to the photonic device and to receive optical signals through the optical fiber from the photonic device, where the optical interface device bidirectionally communicates an electrical data, control and power signal to the computer.
2. The apparatus of claim 1 where the optical interface device includes a laser to provide optical power to the optical fiber.
3. The apparatus of claim 1 where the optical interface device includes a photodetector to receive optical signals through the optical fiber from the photonic device.
4. The apparatus of claim 2 where the optical interface device includes a photodetector to receive optical signals through the optical fiber from the photonic device.
5. The apparatus of claim 4 where the optical interface device includes a digital signal processor to control and communicate with the laser and photodiode, and to communicate with the computer.
6. The apparatus of claim 1 further comprising a catheter cable coupling the optical interface device and the catheter, where the optical fiber is included in the catheter cable, which is MRI compatible and EMI impervious.
7. The apparatus of claim 6 where only optical signals are communicated within the catheter cable.

8. The apparatus of claim 1 where the plurality of electrodes each comprise a MOSFET electrode.
9. The apparatus of claim 1 further comprising a flexible printed circuit board and where the local amplifiers and data, control and power circuit comprise application specific integrated circuits (ASICs) mounted on both sides of the flexible printed circuit board within the catheter having a size of 11 French or smaller
10. The apparatus of claim 1 further comprising a flexible printed circuit board and where the local amplifiers and data, control and power circuit comprise application specific integrated circuits (ASICs) mounted on both sides of the flexible printed circuit board having a width of 2.5mm or less and a height including the ASICs of 2mm or less.
11. The apparatus of claim 1 where the photonic device selectively operates as both a light emitting diode or a photodiode depending on bias control.
12. The apparatus of claim 1 where the data, control and power circuit includes a multiplexer communicated to the plurality of electrodes
13. The apparatus of claim 1 wherein the plurality of local amplifiers each have programmable gain
14. The apparatus of claim 1 where the plurality of electrodes sense analog electrical biopotentials and where the data, control and power circuit includes an analog to digital converter to process the electrical biopotentials in digital form and where the photonic device communicates the electrical digital biopotential through the optical fiber to the optical interface as optical digital biopotential signals
15. The apparatus of claim 1 where the catheter is configured as an electrophysiology catheter, renal denervation catheter, neuromodulation catheter, or an epileptic brain catheter.
16. The apparatus of claim 1 further comprising a temperature sensor communicated to the data, control and power circuit.

17. A method for sensing biopotentials comprising:  
providing a catheter comprising a plurality of sensing electrodes, a corresponding plurality of local amplifiers, each coupled to one of the pluralities of sensing electrodes, a data, control and power circuit coupled to the plurality of local amplifiers, and a photonic device;  
sensing the biopotentials with the plurality of sensing electrodes;  
bidirectionally communicating the biopotentials with the data, control and power circuit, providing an optical fiber in a catheter cable optically communicated with the photonic device;  
bidirectionally communicating an optical signal through the optical fiber and catheter;  
providing optical power to the optical fiber and thence to the photonic device;  
receiving optical signals through the optical fiber from the photonic device; and  
bidirectionally communicating an electrical data, control and power signal to the computer, so that the catheter cable is MRI compatible and EMI impervious.
18. The method of claim 17 where sensing the biopotentials with the plurality of sensing electrodes comprises sensing the biopotentials with a plurality of locally amplified MOSFET electrodes.
19. The method of claim 17 where providing a catheter comprising a plurality of sensing electrodes, a corresponding plurality of local amplifiers, each coupled to one of the plurality of sensing electrodes, a data, control and power circuit coupled to the plurality of local amplifiers and a photonic device comprises providing a flexible printed circuit board and mounting the local amplifiers and data, control and power circuit in the form of application specific integrated circuits (ASICs) mounted on both sides of the flexible printed circuit board within the catheter having a size of 11 French or smaller.
20. The method of claim 17 where providing a catheter comprising a plurality of sensing electrodes, a corresponding plurality of local amplifiers, each coupled to one of the plurality of sensing electrodes, a data, control and power circuit coupled to the plurality of local amplifiers and a photonic device comprises providing a flexible printed circuit board and mounting the local amplifiers and data, control and power circuit in the form of application specific integrated circuits (ASICs) mounted on both sides of the flexible printed circuit board having a width of 2.5mm or less and a height including the ASICs of 2mm or less.

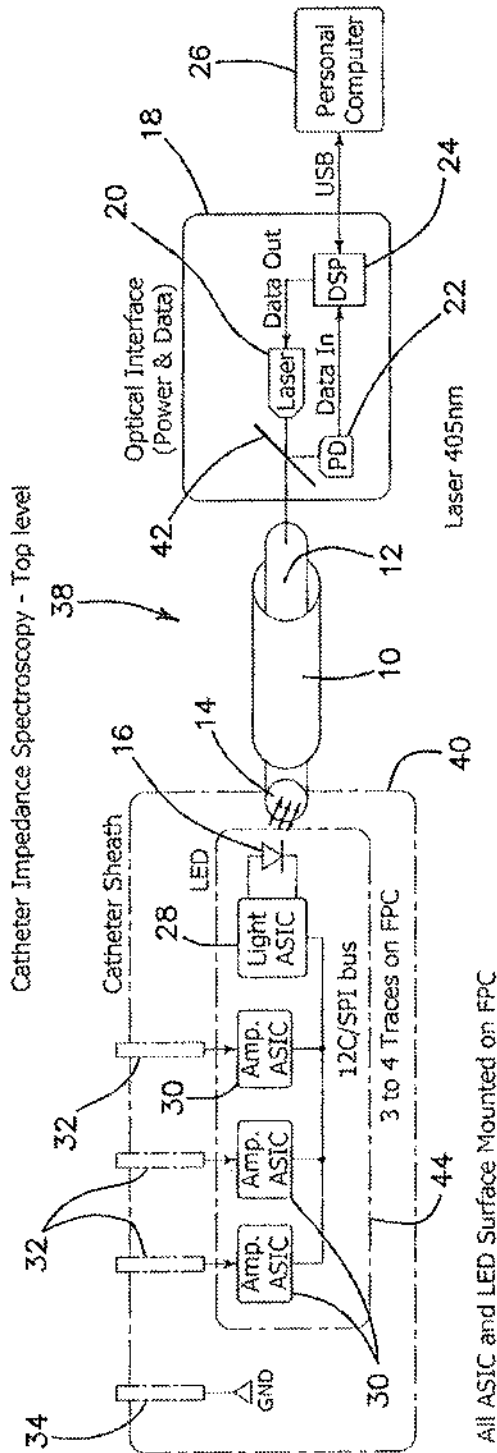


FIG. 1

05



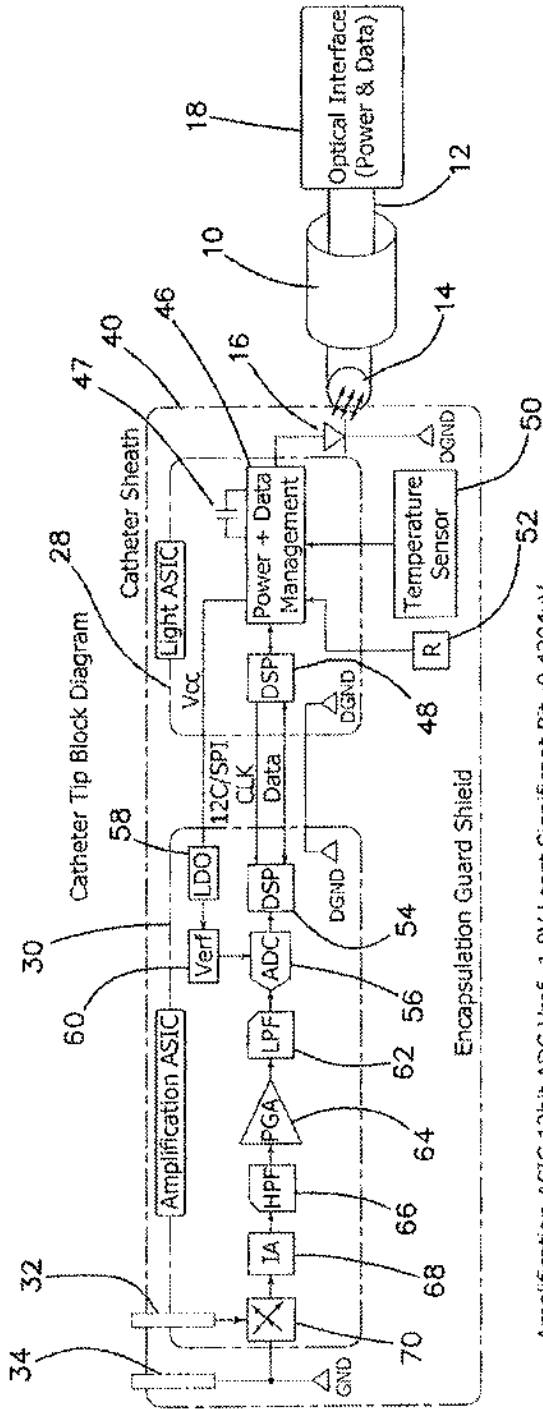


FIG. 2

Amplification ASIC 12bit ADC Vref=1.8V Least Significant Bit=0.4394uV

Input Range [uV]	Instrumental Amp. Fix Gain	Prog. Gain Amp. Management	ADC Input Voltage [mV]
1 - 500	50	10	5 to 250
1 - 10000	50	Scalable 1 to 50	0 to 1800
1000 - 100'000	50	Scalable 1 to 50	0 to 1800



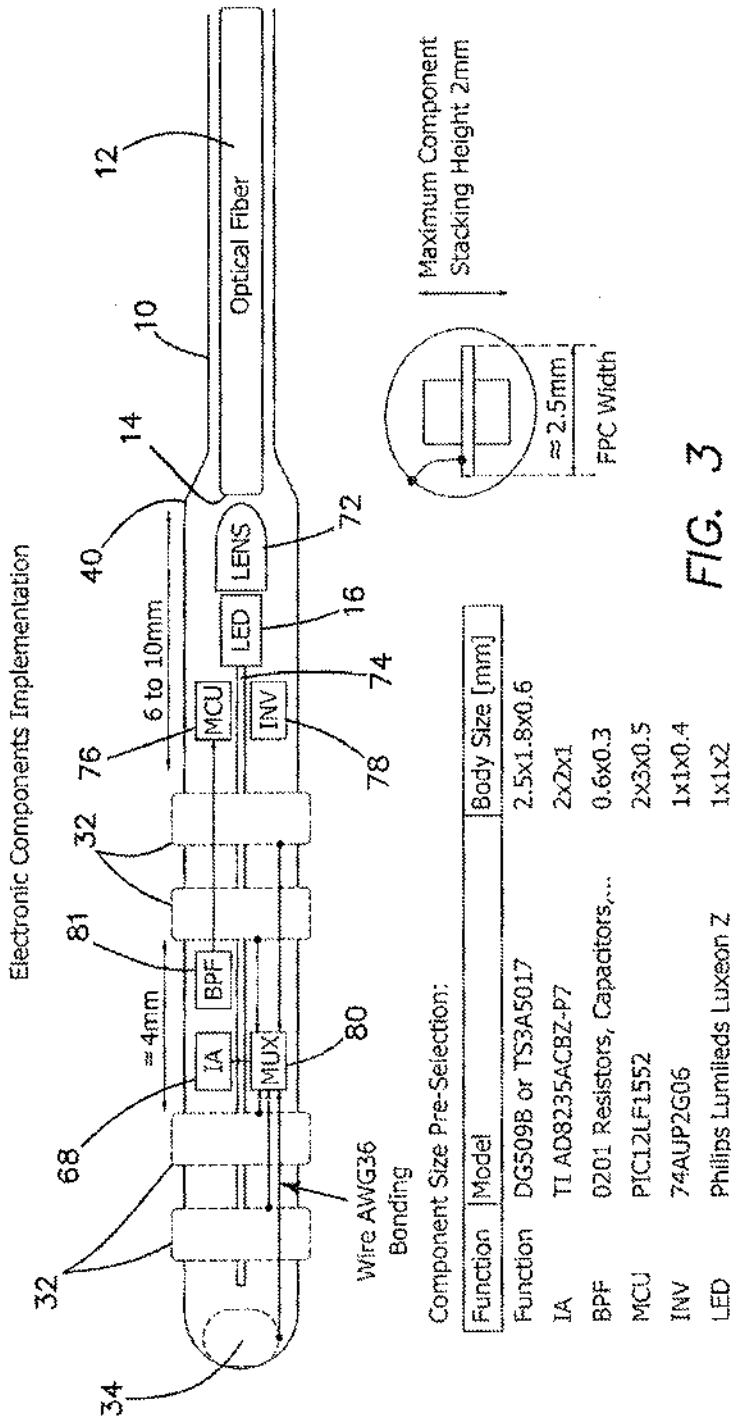


FIG. 3

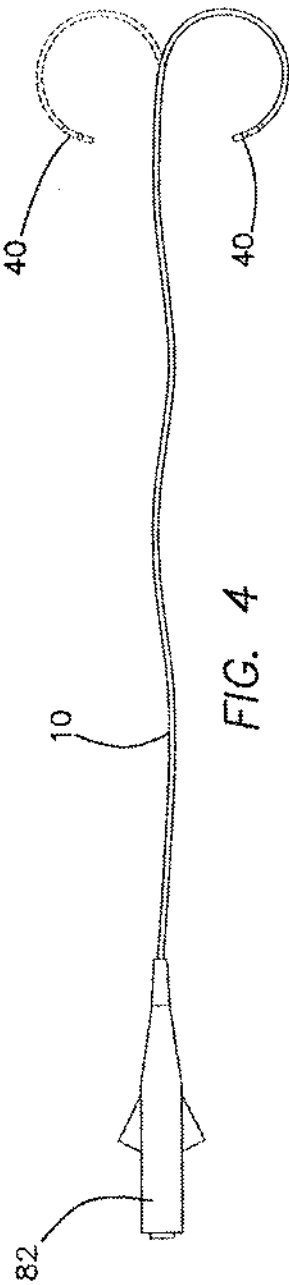


FIG. 4

05



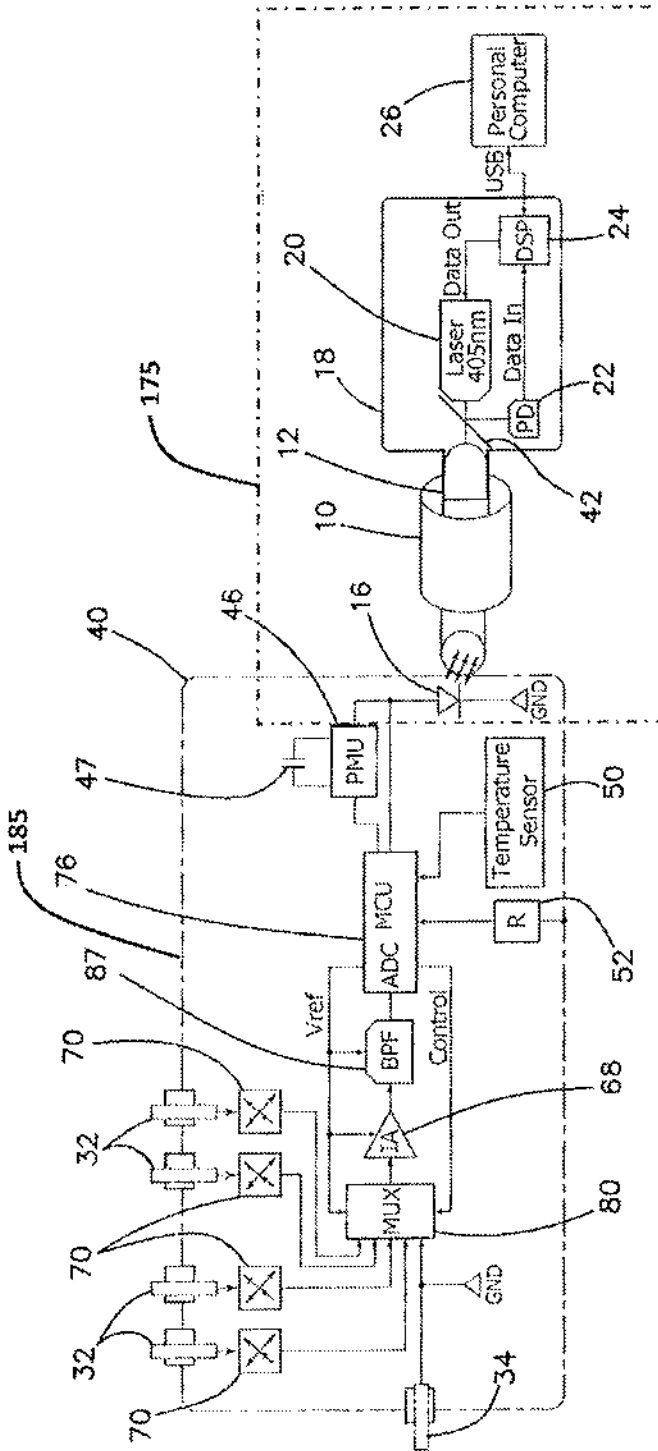


FIG. 6A

05

05

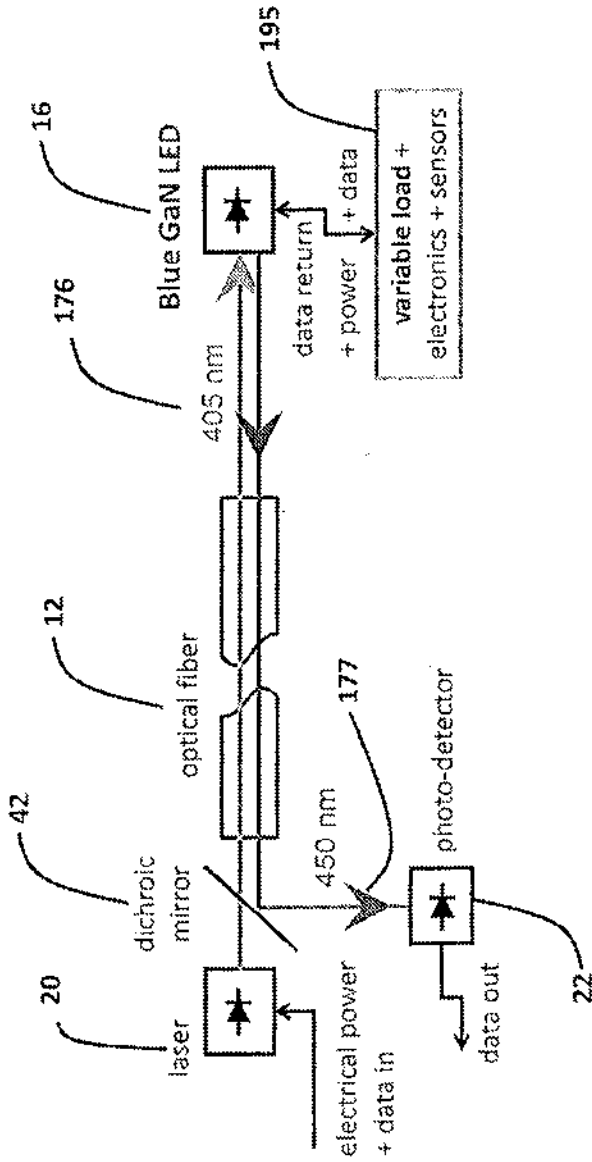


Fig. 6B



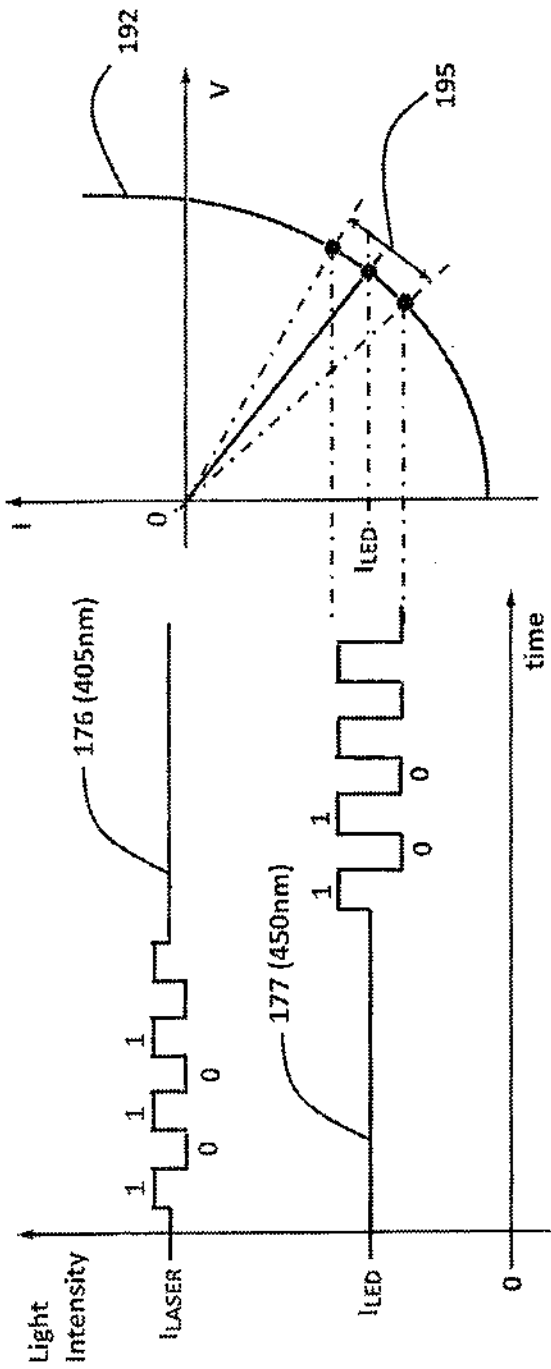


Fig. 6C



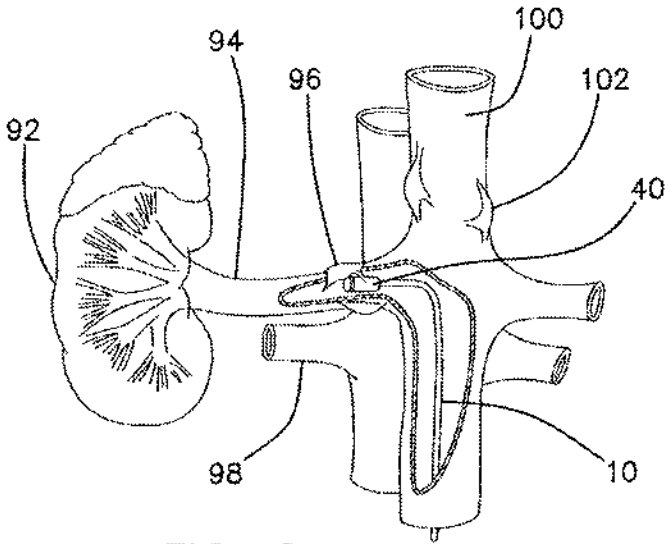


FIG. 9

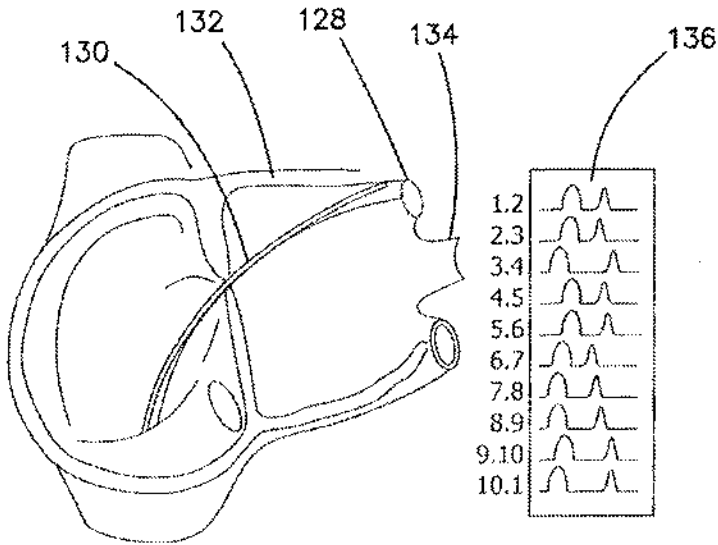


FIG. 11

05

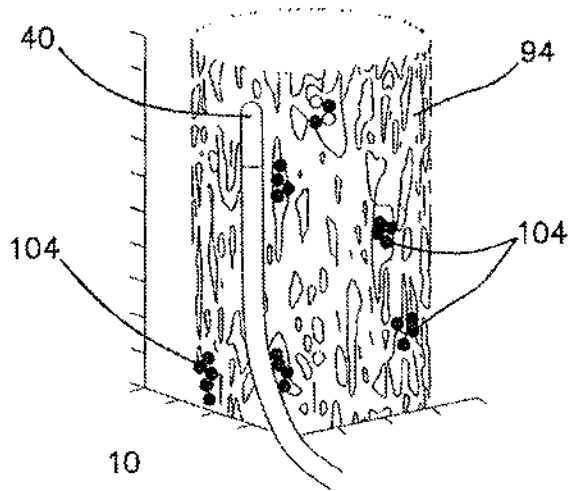


FIG. 10A

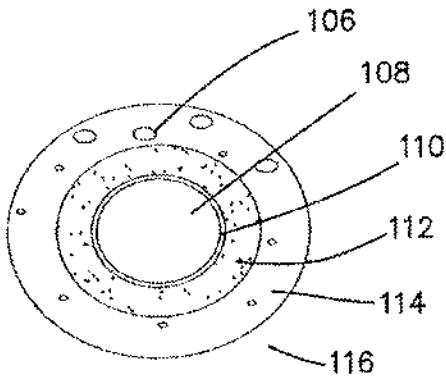


FIG. 10B

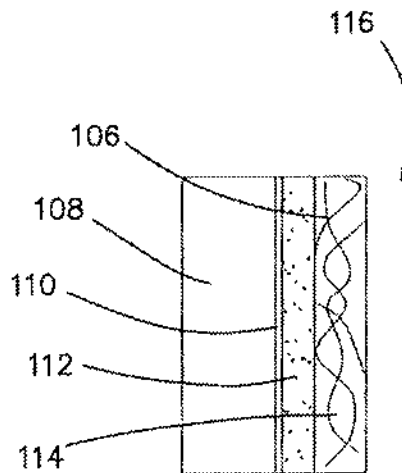


FIG. 10C

05

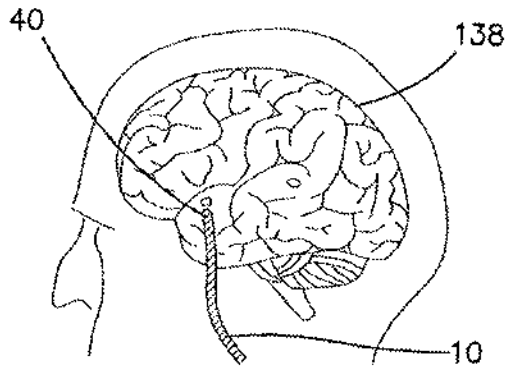


FIG. 12A

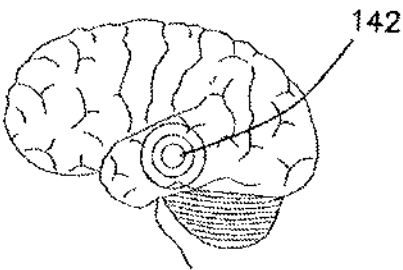
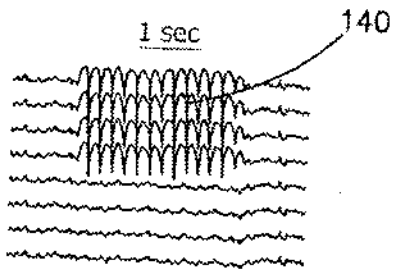


FIG. 12B

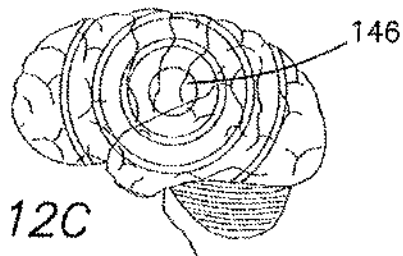
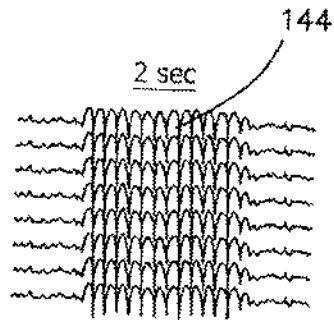


FIG. 12C

05

## INTERNATIONAL SEARCH REPORT

International application No.

PCT/US 2020/032379

A. CLASSIFICATION OF SUBJECT MATTER		
<p style="text-align: center;"><i>A61B 5/04 (2006.01)</i>  <i>A61B 5/042 (2006.01)</i>  <i>A61B 5/0478 (2006.01)</i></p> <p>According to International Patent Classification (IPC) or to both national classification and IPC</p>		
B. FIELDS SEARCHED		
Minimum documentation searched (classification system followed by classification symbols)		
A61B 18/18, 5/04, 5/0402-5/042, 5/0478		
Documentation searched other than minimum documentation to the extent that such documents are included in the fields searched		
Electronic data base consulted during the international search (name of data base and, where practicable, search terms used)		
PatSearch (RUPITO Internal), USPTO, PAJ, Espacenet, Information Retrieval System of IIPS		
C. DOCUMENTS CONSIDERED TO BE RELEVANT		
Category*	Citation of document, with indication, where appropriate, of the relevant passages	Relevant to claim No.
Y A	US 9381063 B2 (MAGNETICS INC.) 05.07.2016, col.11, lines 28-33, col. 15, lines 28-51, col. 21, lines 42-67, col. 22, lines 1-9, claim 1, fig. 1, la. 7, col. 27, lines 32-35, col. 24, lines 35-43, col. 31, lines 1-38, col. 15, lines 32-36, fig. 14, col. 35, lines 26-67, col. 36, lines 1-24	1-8, 11-18 9, 10, 19
Y	US 6898464 B2 (INNERSEA TECHNOLOGY) 24.05.2005, col. 4, lines 49-67, col. 4, lines 49-67, col. 5, lines 1-6	1-8, 11-18
Y	US 7992573 B2 (THE TRUSTEES OF THE UNIVERSITY OF PENNSYLVANIA) 09.08.2011, col. 12, lines 34-40, col. 20, lines 60-67, col. 21, lines 27-32	2, 5
Y	US 2016/0301188 A1 (HEWLETT PACKARD ENTERPRISE DEVELOPMENT LP) 13.10.2016, paragraph [0017]	11
<input type="checkbox"/> Further documents are listed in the continuation of Box C. <input type="checkbox"/> See patent family annex.		
* Special categories of cited documents:	"T" later document published after the international filing date or priority date and not in conflict with the application but cited to understand the principle or theory underlying the invention "A" document defining the general state of the art which is not considered to be of particular relevance "D" document cited by the applicant in the international application "E" earlier document but published on or after the international filing date "L" document which may throw doubts on priority claim(s) or which is cited to establish the publication date of another citation or other special reason (as specified) "O" document referring to an oral disclosure, use, exhibition or other means "P" document published prior to the international filing date but later than the priority date claimed "X" document of particular relevance: the claimed invention cannot be considered novel or cannot be considered to involve an inventive step when the document is taken alone "Y" document of particular relevance: the claimed invention cannot be considered to involve an inventive step when the document is combined with one or more other such documents, such combination being obvious to a person skilled in the art "Z" document member of the same patent family	
Date of the actual completion of the international search	Date of mailing of the international search report	
24 July 2020 (24.07.2020)	13 August 2020 (13.08.2020)	
Name and mailing address of the ISA/RU: Federal Institute of Industrial Property, Berezhkovskaya nab., 30-1, Moscow, G-59, GSP-3, Russia, 125993 Facsimile No: (8-495) 531-63-18, (8-499) 243-33-37	Authorized officer  A. Biche-ool  Telephone No. 8(495) 531-64-81	

Form PCT/ISA/210 (second sheet) (July 2019)





U.S. PATENT OFFICE FILINGS FOR:  
***Catheter for Cardiac and Renal Nerve  
Sensing and Mediation***

***INVENTOR: Yehoshua Shachar  
Marc Rocklinger  
Dr. Eli Gang  
Doyoung Kim***



(19) **United States**

(12) **Patent Application Publication**  
**Shachar et al.**

(10) **Pub. No.: US 2022/0047202 A1**

(43) **Pub. Date: Feb. 17, 2022**

(54) **CATHETER FOR CARDIAC AND RENAL NERVE SENSING AND MEDIATION**

*A61B 5/35* (2006.01)  
*A61B 5/20* (2006.01)

(71) Applicant: **Josh Shachar**, Santa Monica, CA (US)

(52) **U.S. Cl.**  
CPC ..... *A61B 5/367* (2021.01); *A61B 5/294* (2021.01); *A61B 5/388* (2021.01); *A61B 5/287* (2021.01); *A61B 5/686* (2013.01); *A61B 2562/0209* (2013.01); *A61B 5/35* (2021.01); *A61B 5/0017* (2013.01); *A61B 5/0006* (2013.01); *A61B 5/201* (2013.01); *A61B 5/7203* (2013.01); *A61B 5/4836* (2013.01)

(72) Inventors: **Josh Shachar**, Santa Monica, CA (US);  
**Marc Rocklinger**, Marina del Rey, CA (US);  
**Eli Gang**, Los Angeles, CA (US);  
**Doyoung Kim**, Montrose, CA (US)

(73) Assignee: **Neurokinesis Corp.**, Inglewood, CA (US)

(21) Appl. No.: **17/468,460**

(22) Filed: **Sep. 7, 2021**

**Related U.S. Application Data**

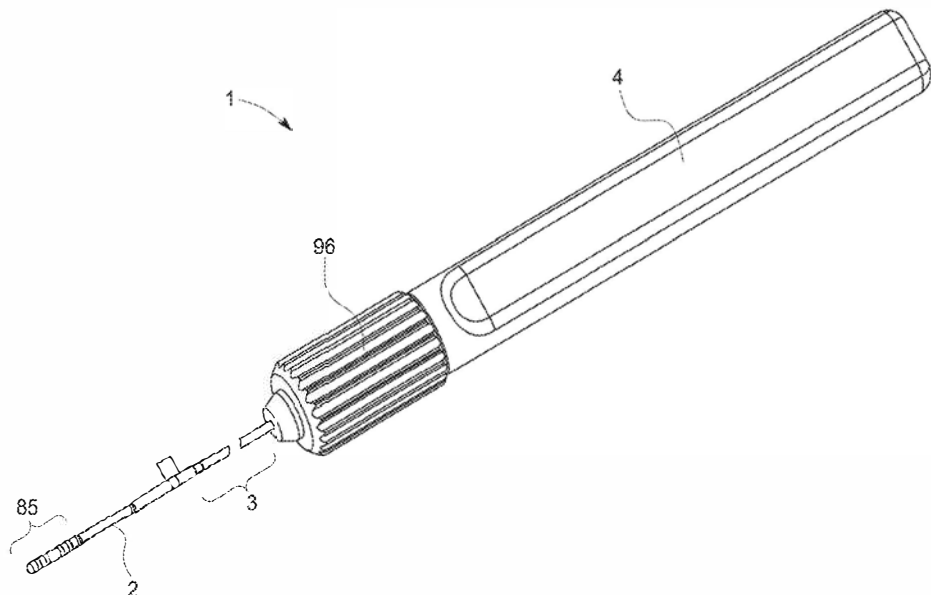
(63) Continuation-in-part of application No. 16/424,202, filed on May 28, 2019.

**Publication Classification**

(51) **Int. Cl.**  
*A61B 5/367* (2006.01)  
*A61B 5/294* (2006.01)  
*A61B 5/388* (2006.01)  
*A61B 5/287* (2006.01)  
*A61B 5/00* (2006.01)

(57) **ABSTRACT**

An electrophysiology catheter includes: a catheter with a movable catheter tip; electrodes provided on or in an electrode region in a most distal portion of the catheter tip; sensing and amplification circuitry communicated with the electrodes, the sensing and amplification circuitry communicated with digitizing circuitry disposed in a circuitry region in a least distal portion of the catheter tip for locally sensing tissue-based electrophysiological signals and for bidirectionally communicating digital data signals to and from the circuitry; a flexible bending region of the catheter tip between the most and least distal portions of the catheter tip; a flexible sheath communicated to the sensing and amplification circuitry and digitizing circuitry for transmission of signals thereon; and a handle communicated with the sheath for bidirectionally communicating signals through the sheath between the catheter tip and external mapping station, and for controlling movement of the catheter tip.



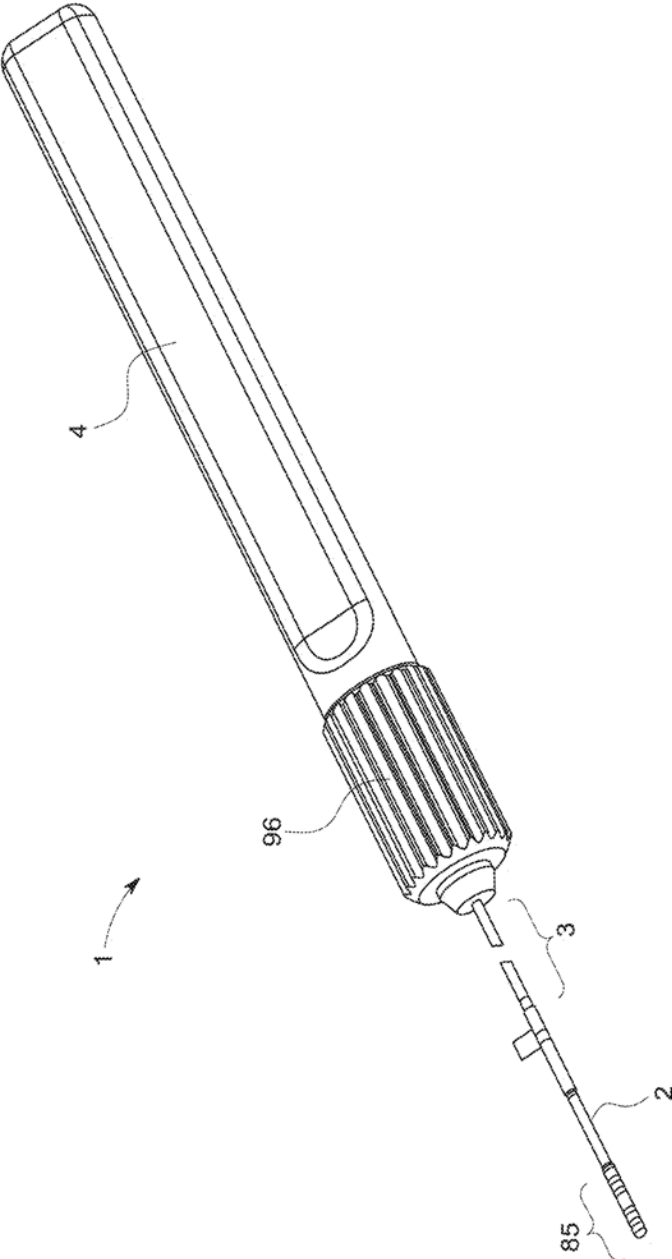


FIG. 1

06

06

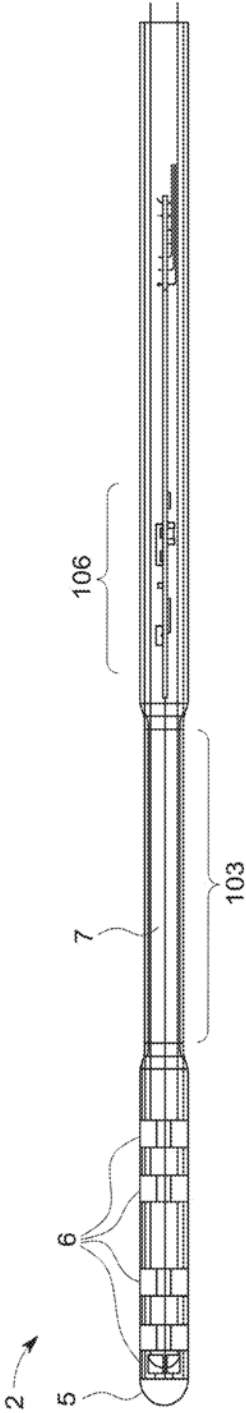


FIG. 2A



FIG. 2B

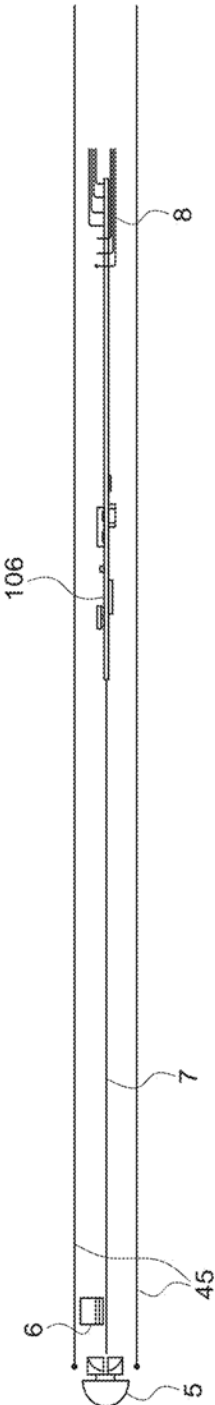


FIG. 2C

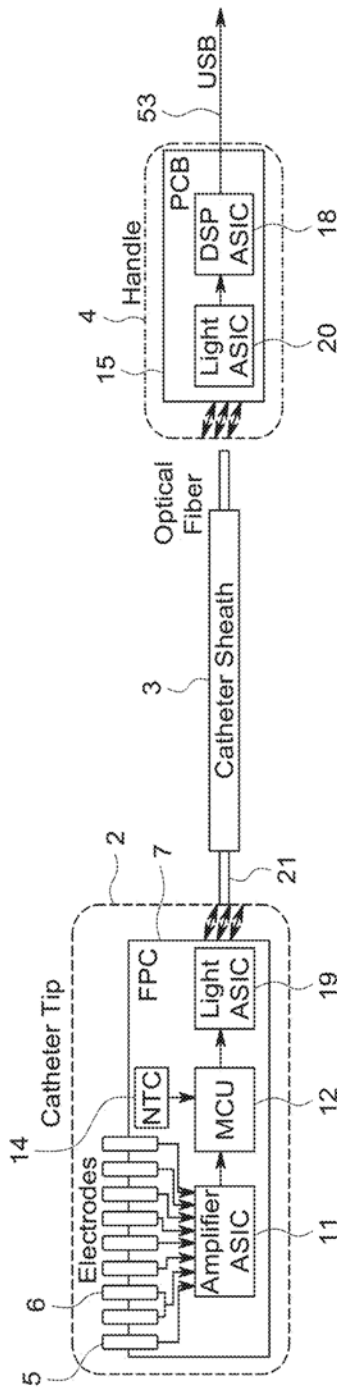


FIG. 3A

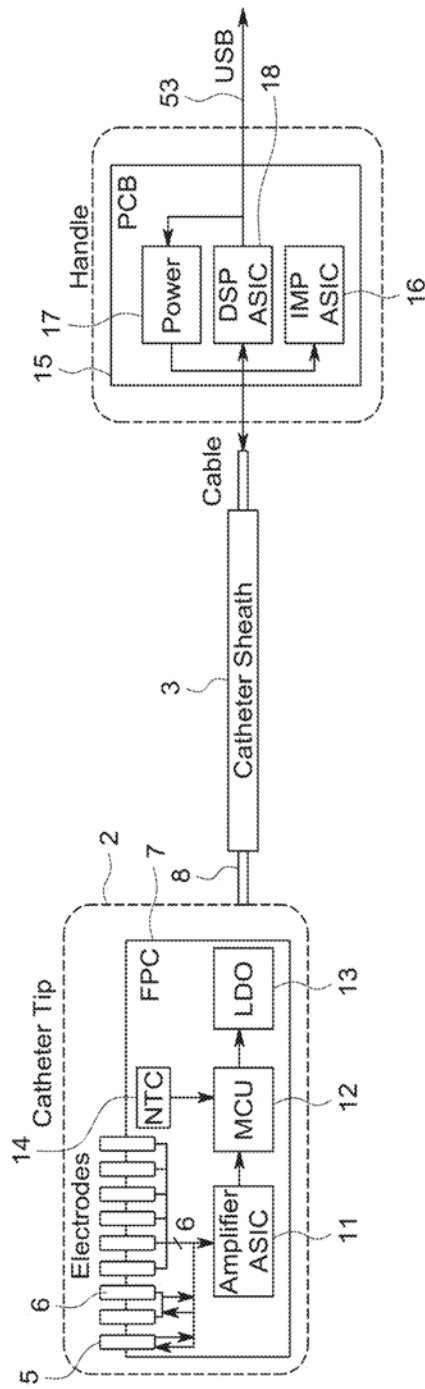


FIG. 3B



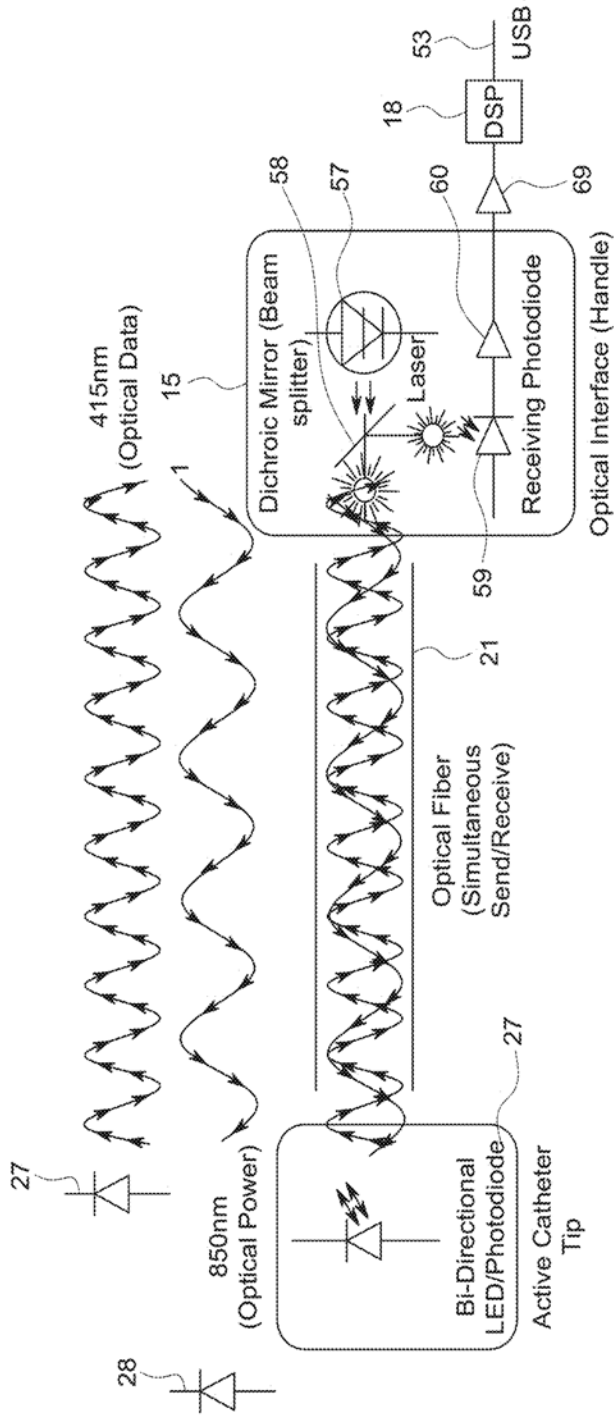


FIG. 3C



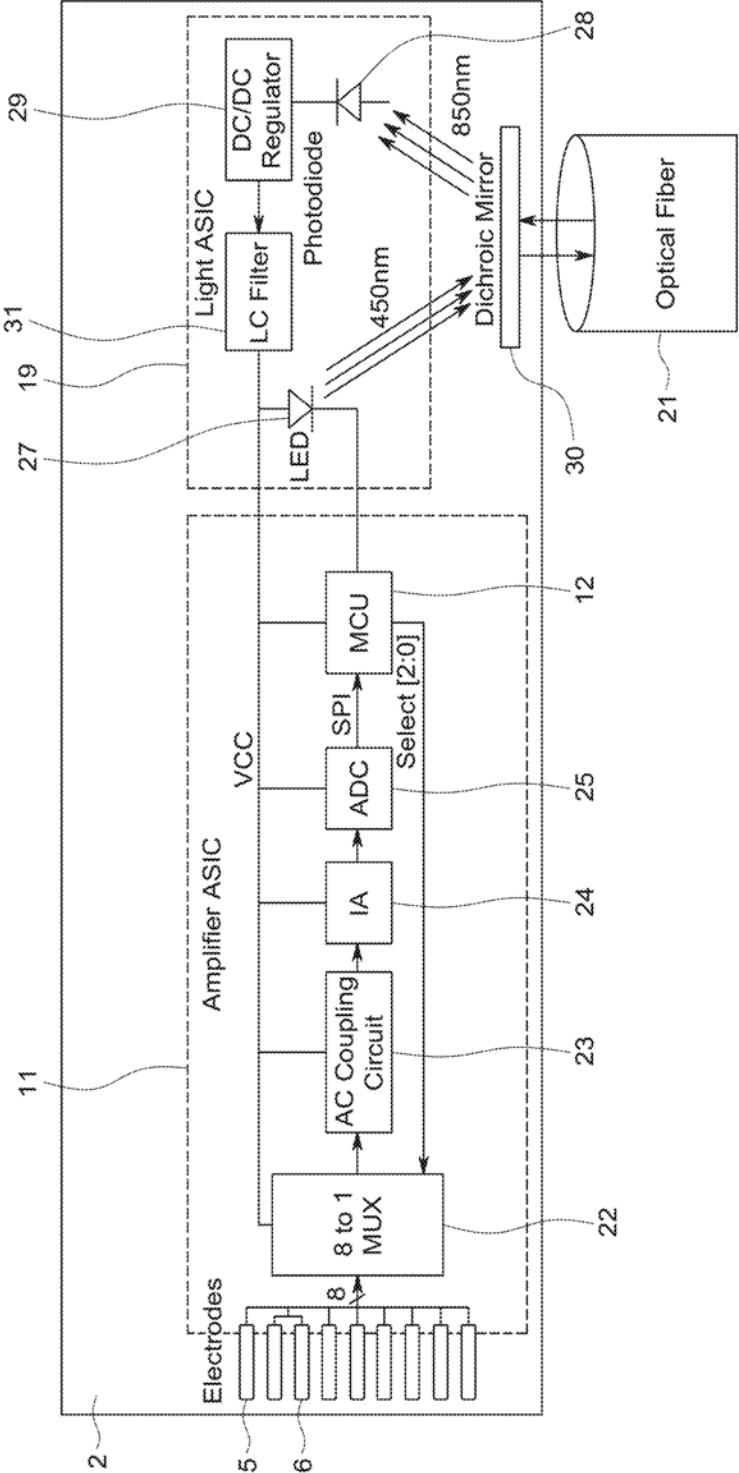


FIG. 4A



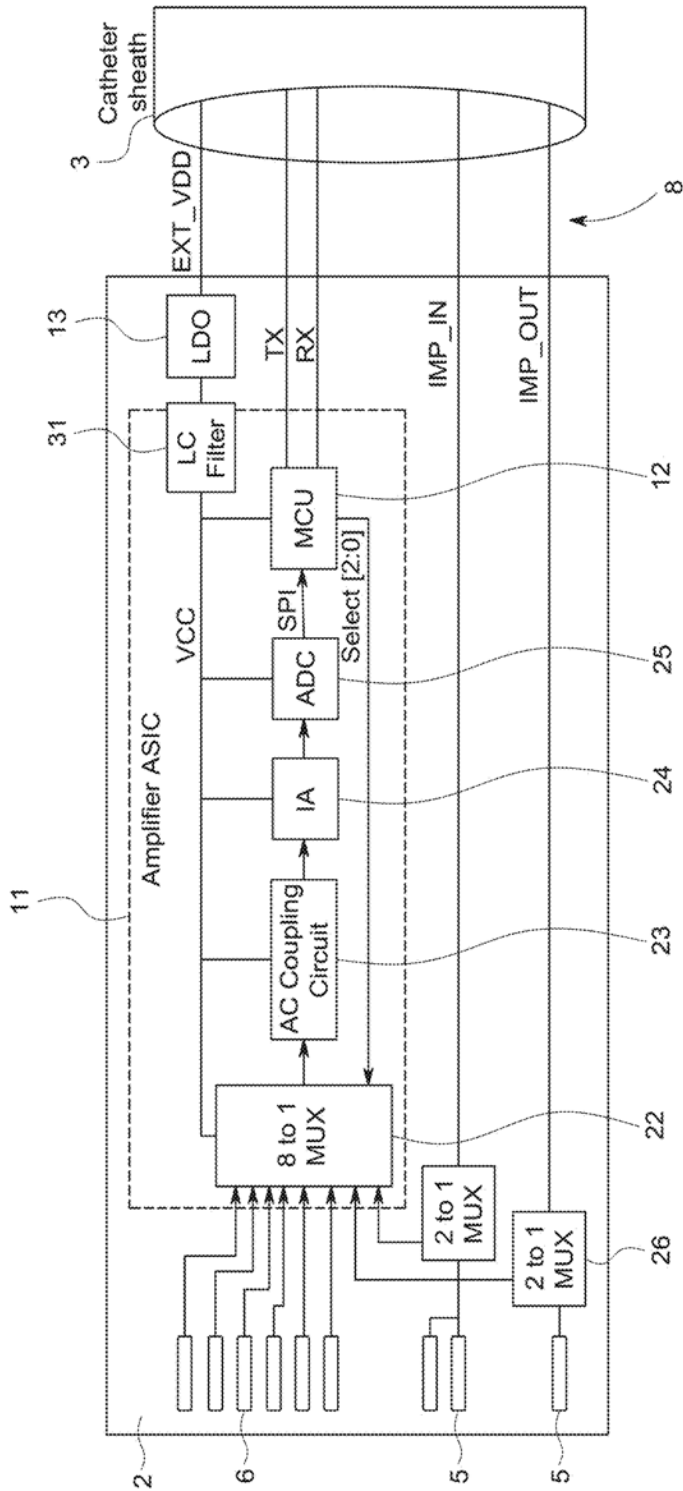


FIG. 4B

06

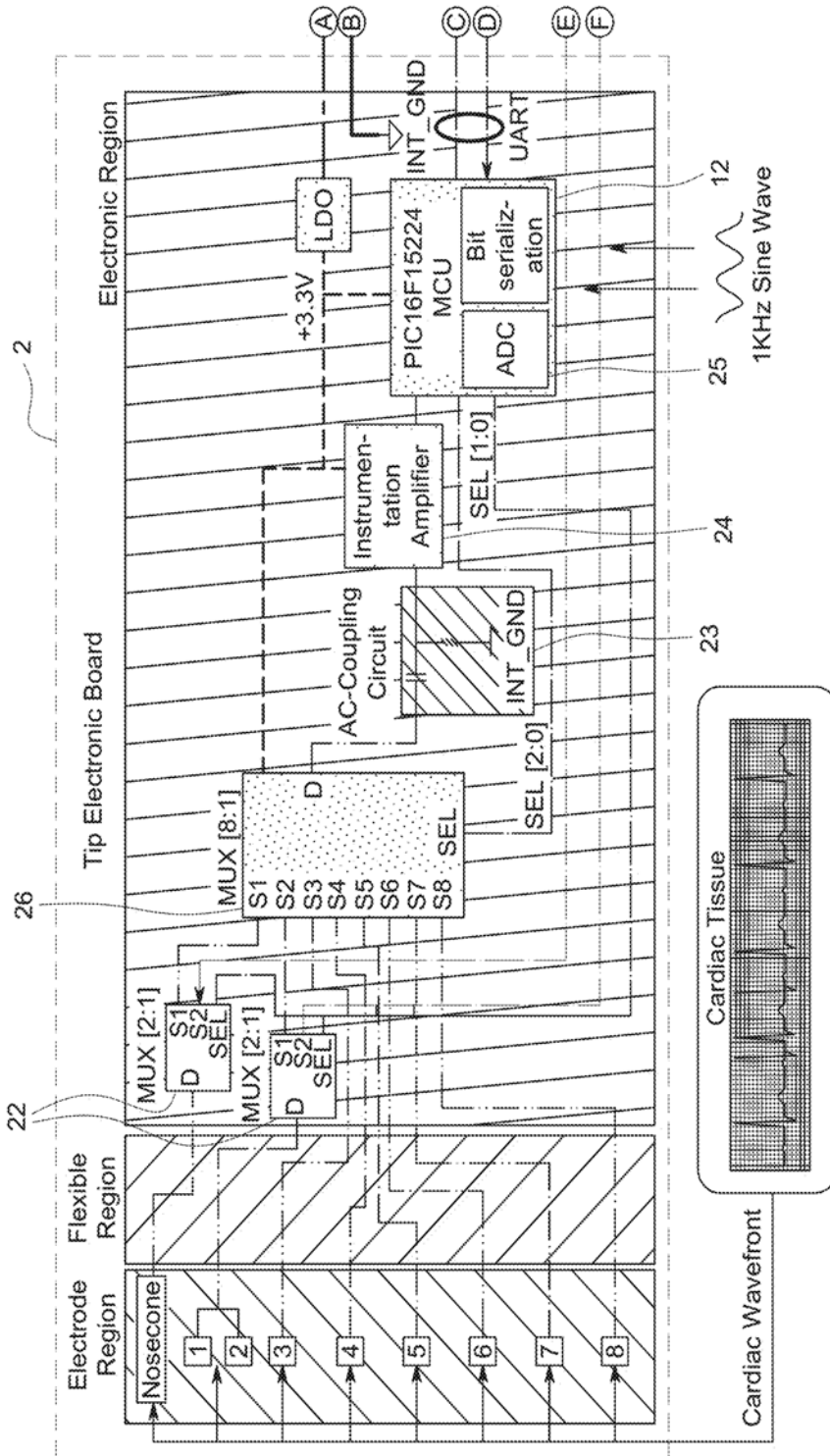


FIG. 5

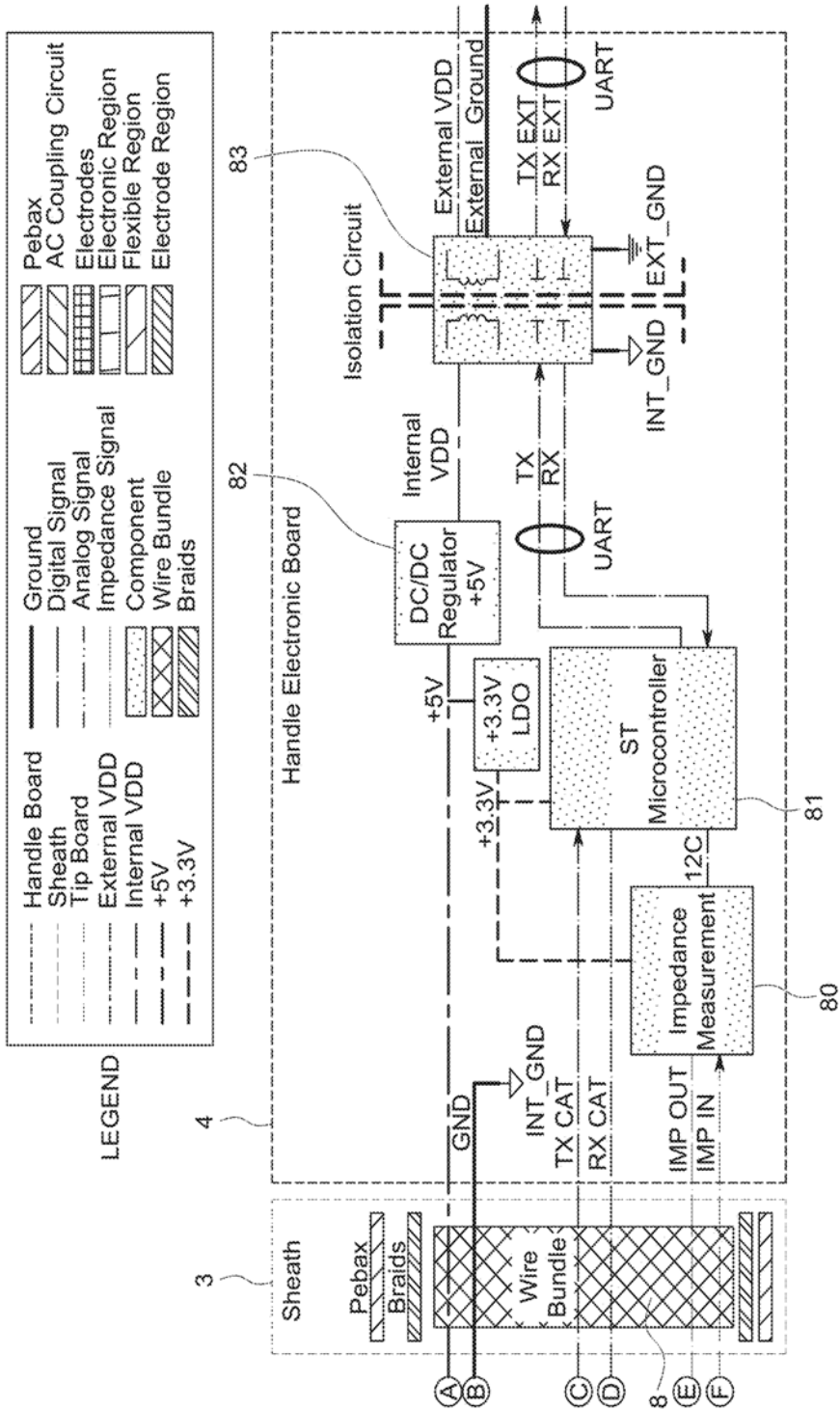


FIG. 5 (CONT.)

06

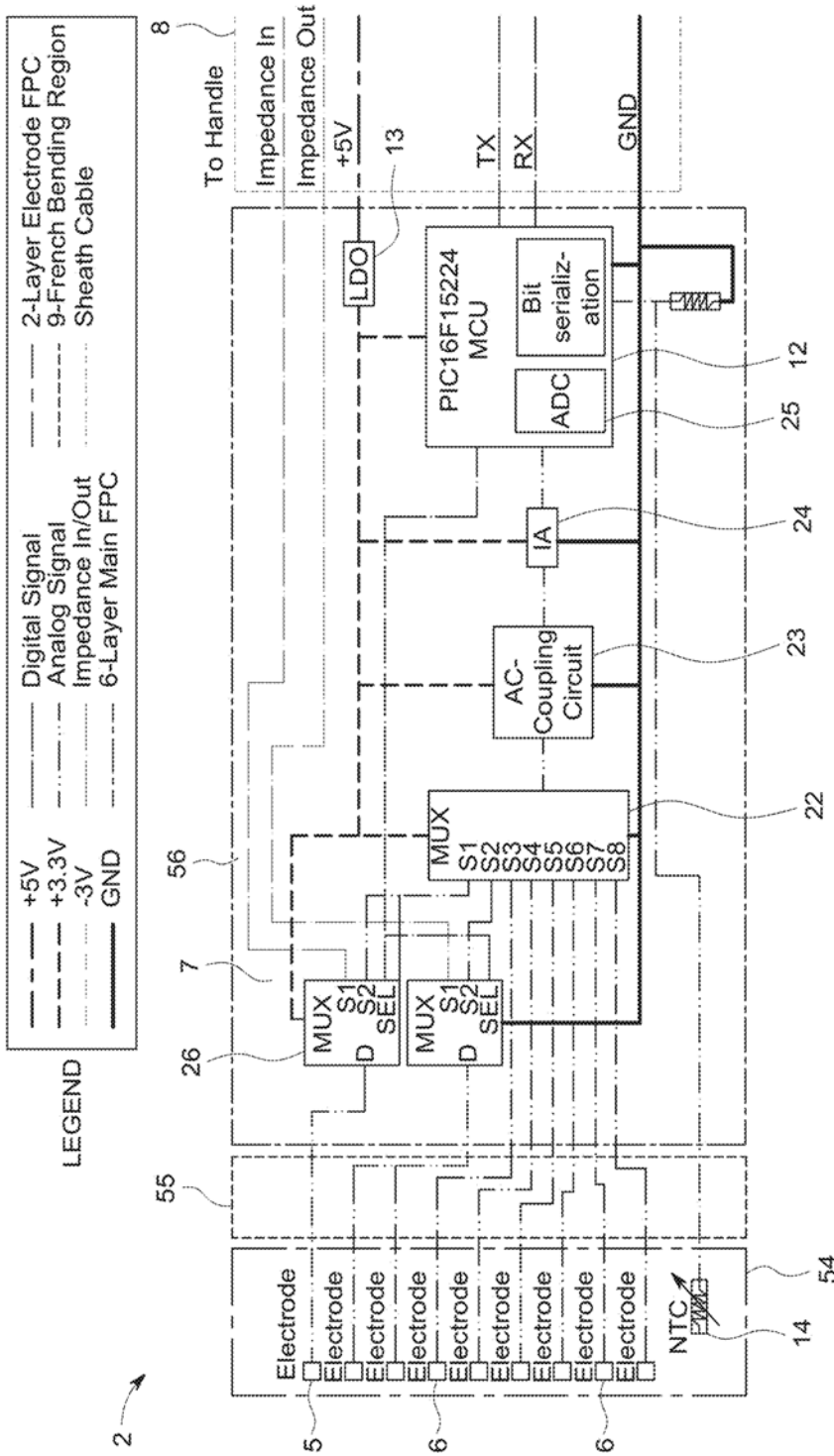
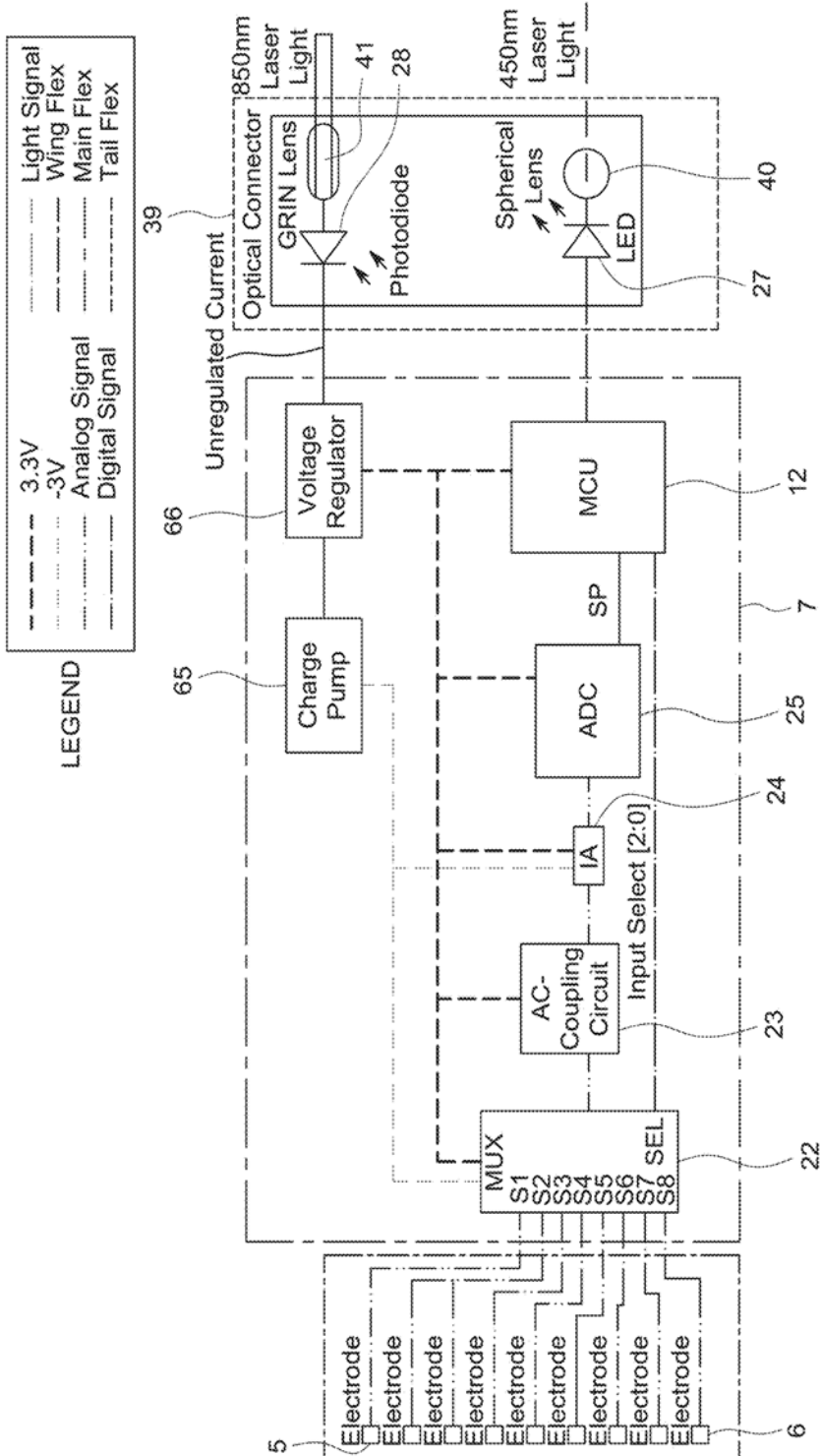


FIG. 6A





06



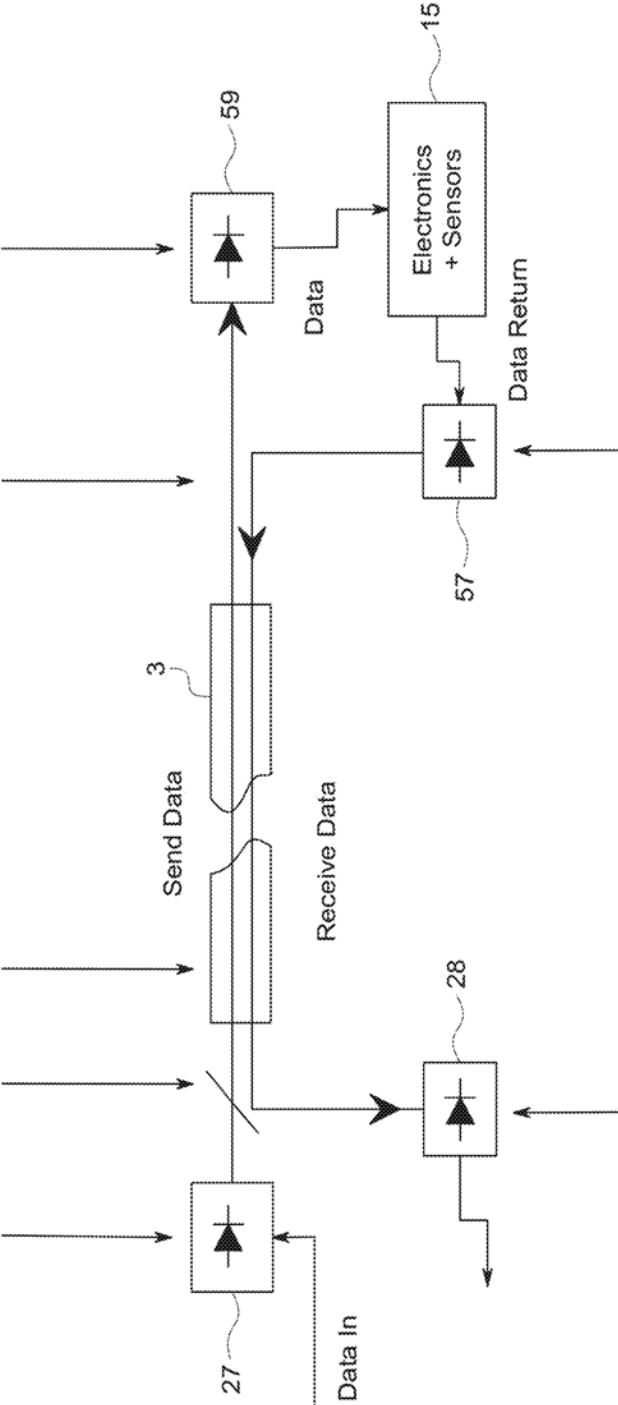


FIG. 7

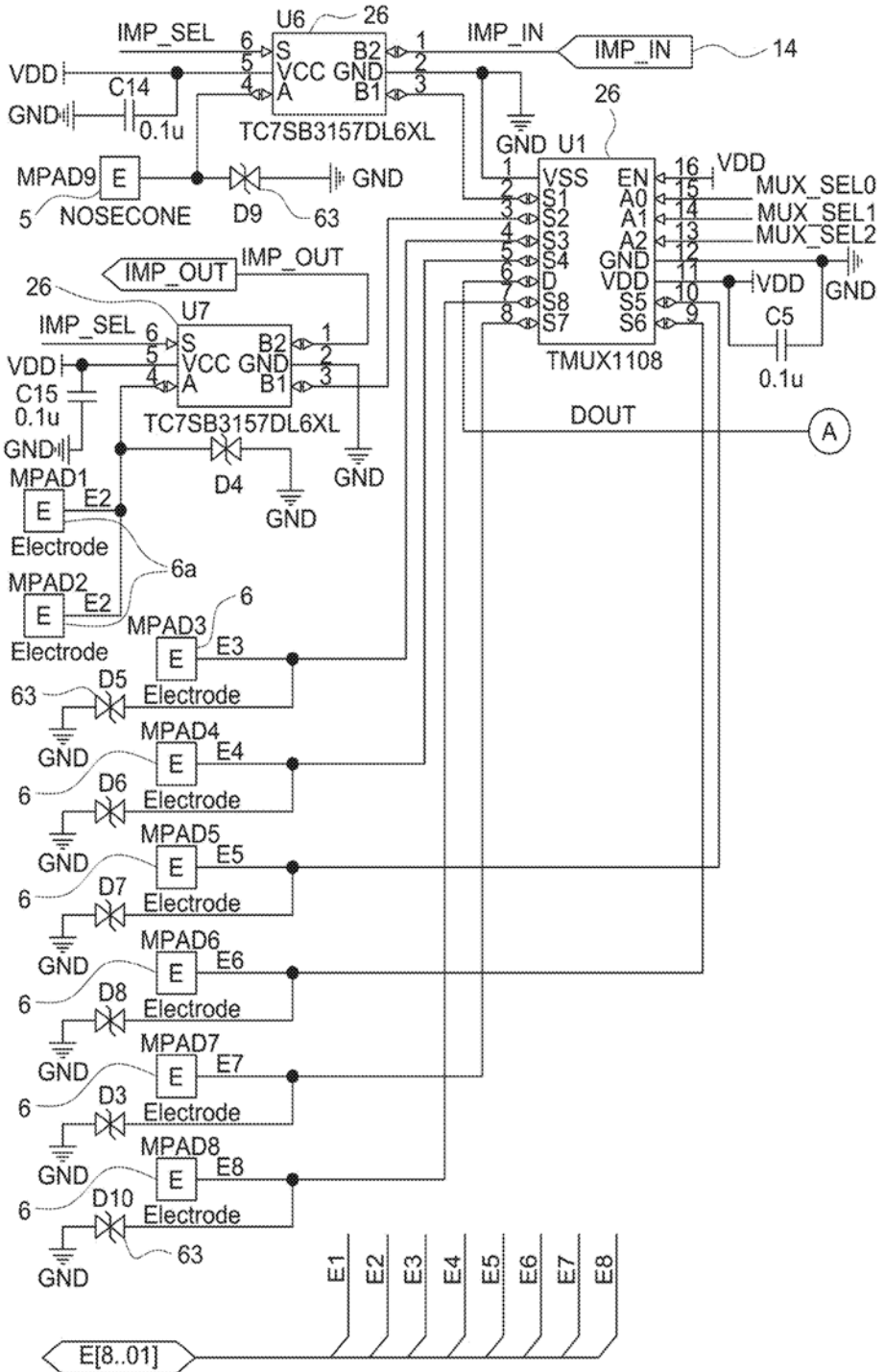


FIG. 8



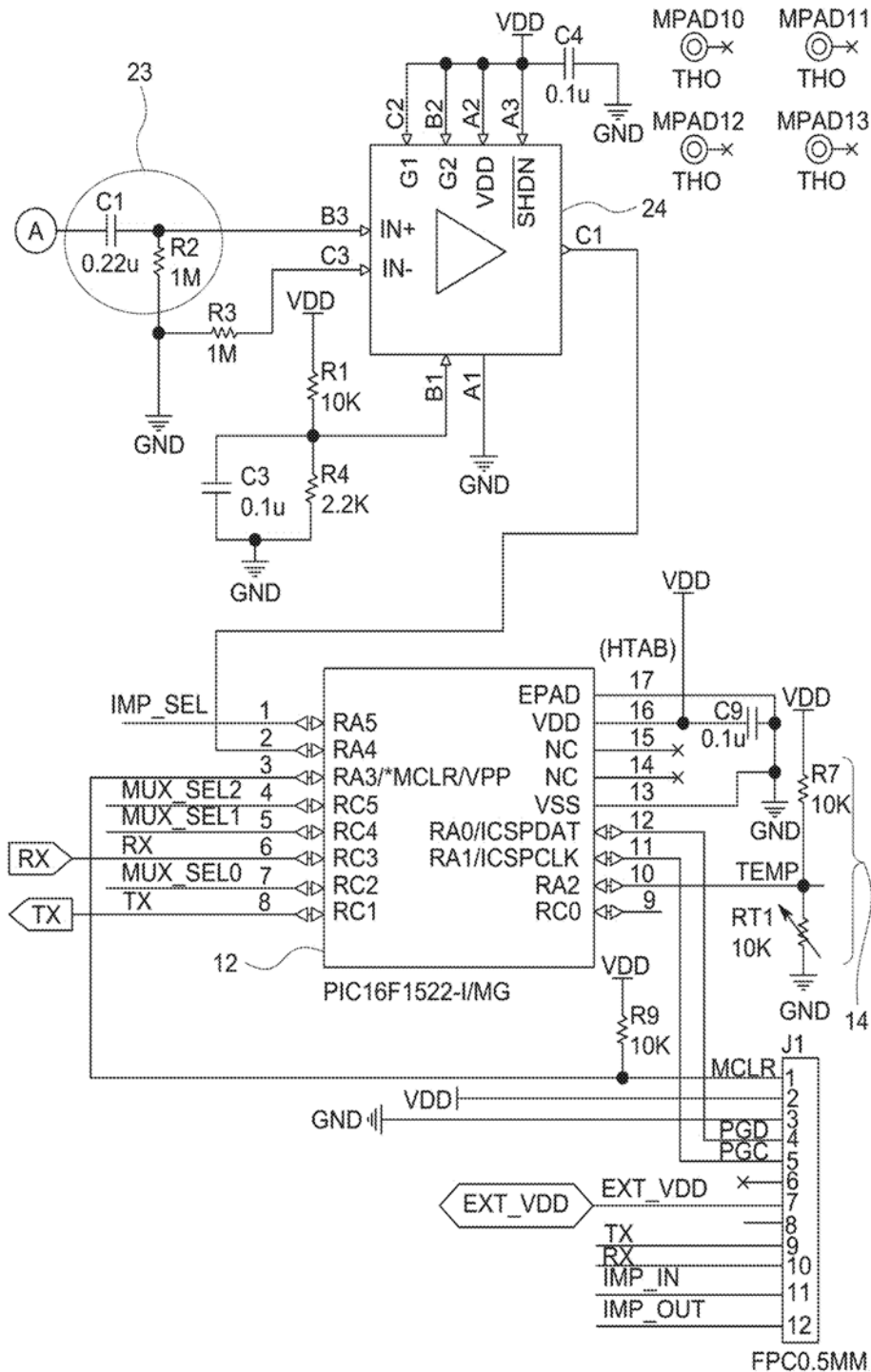


FIG. 8 (CONT.)



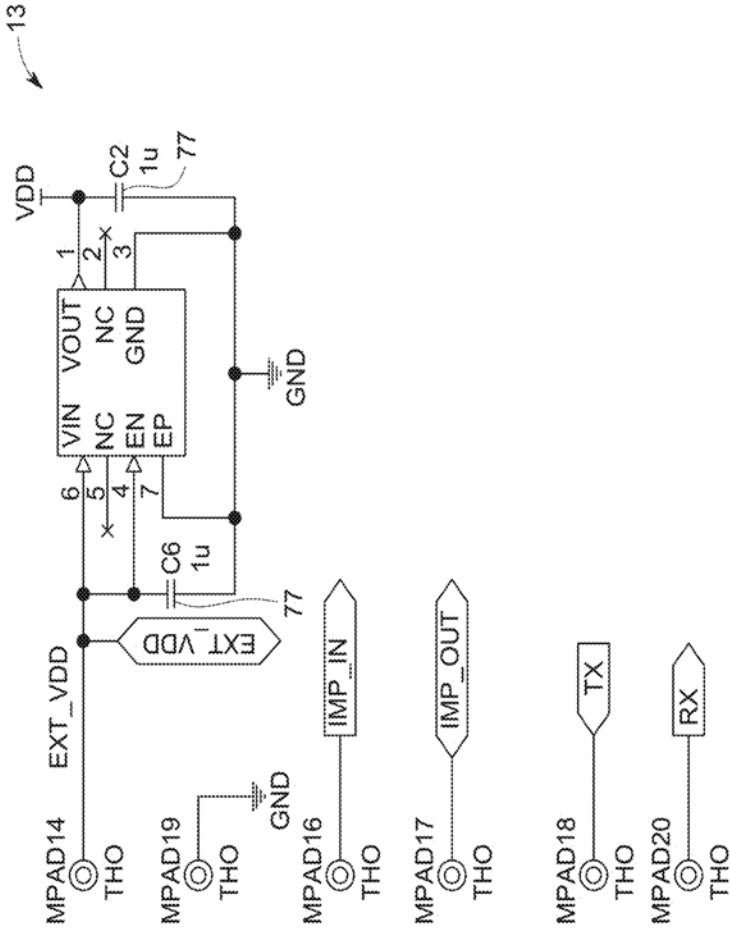


FIG. 9

06

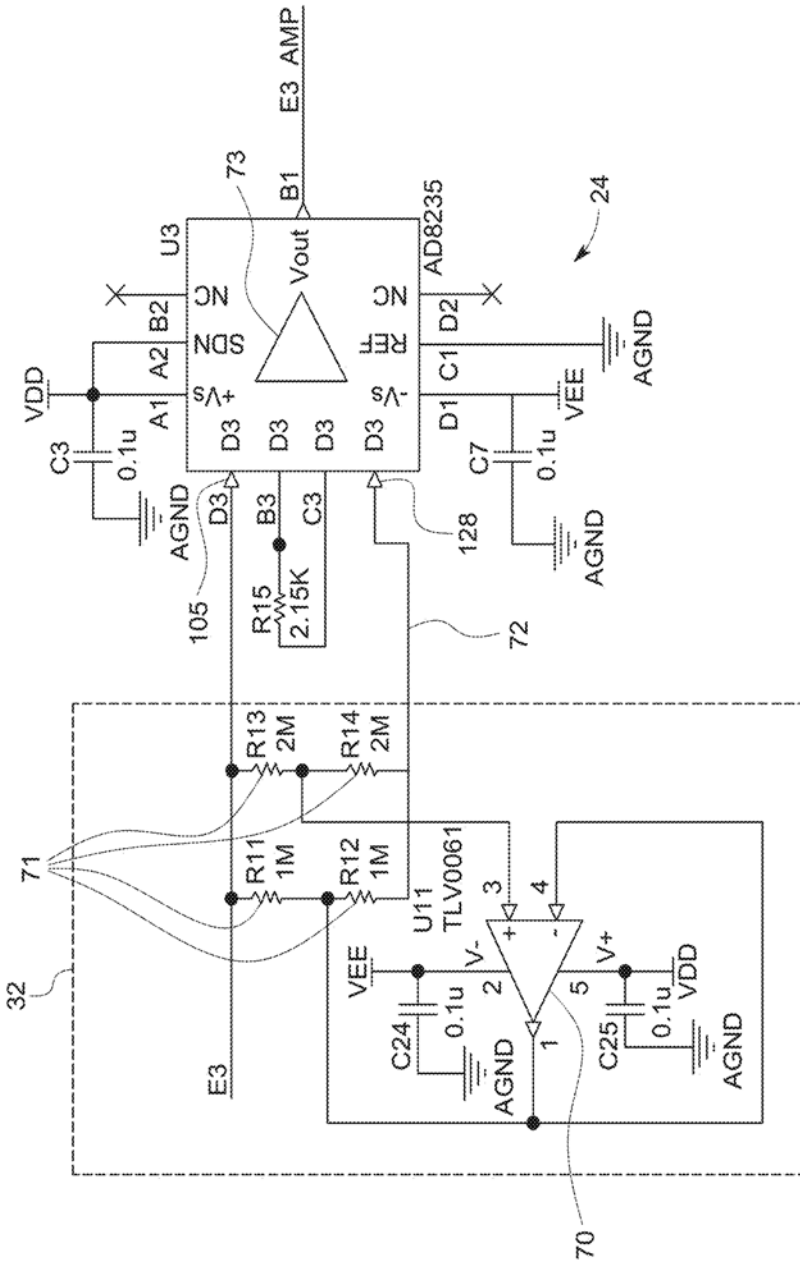


FIG. 10

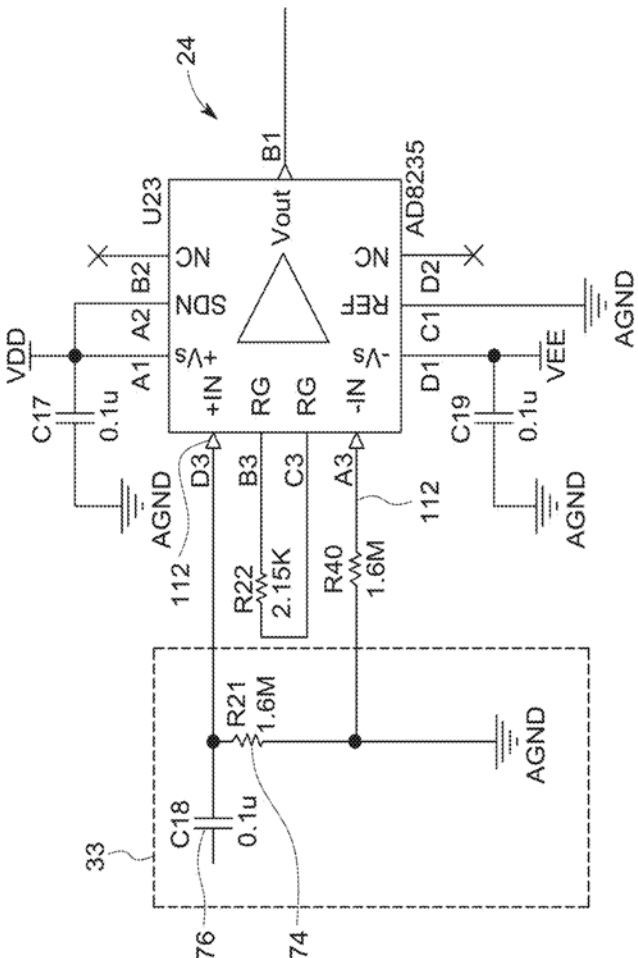


FIG. 11

06



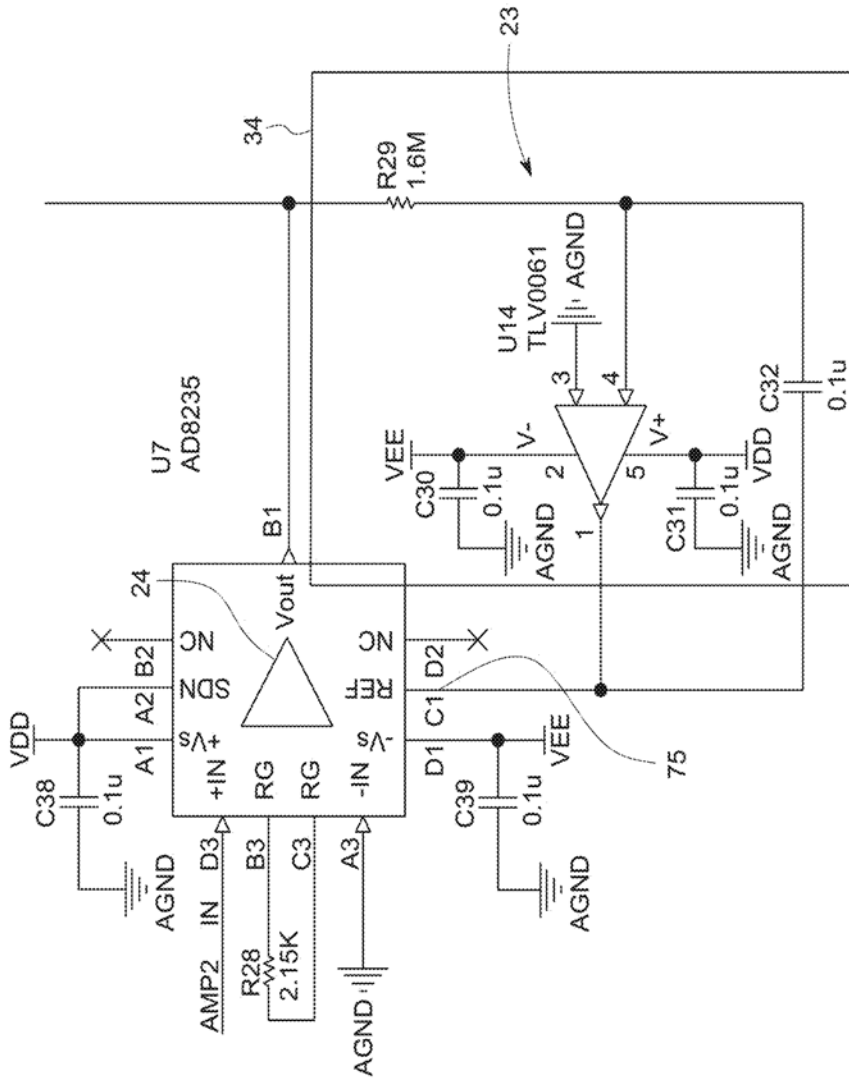


FIG. 12

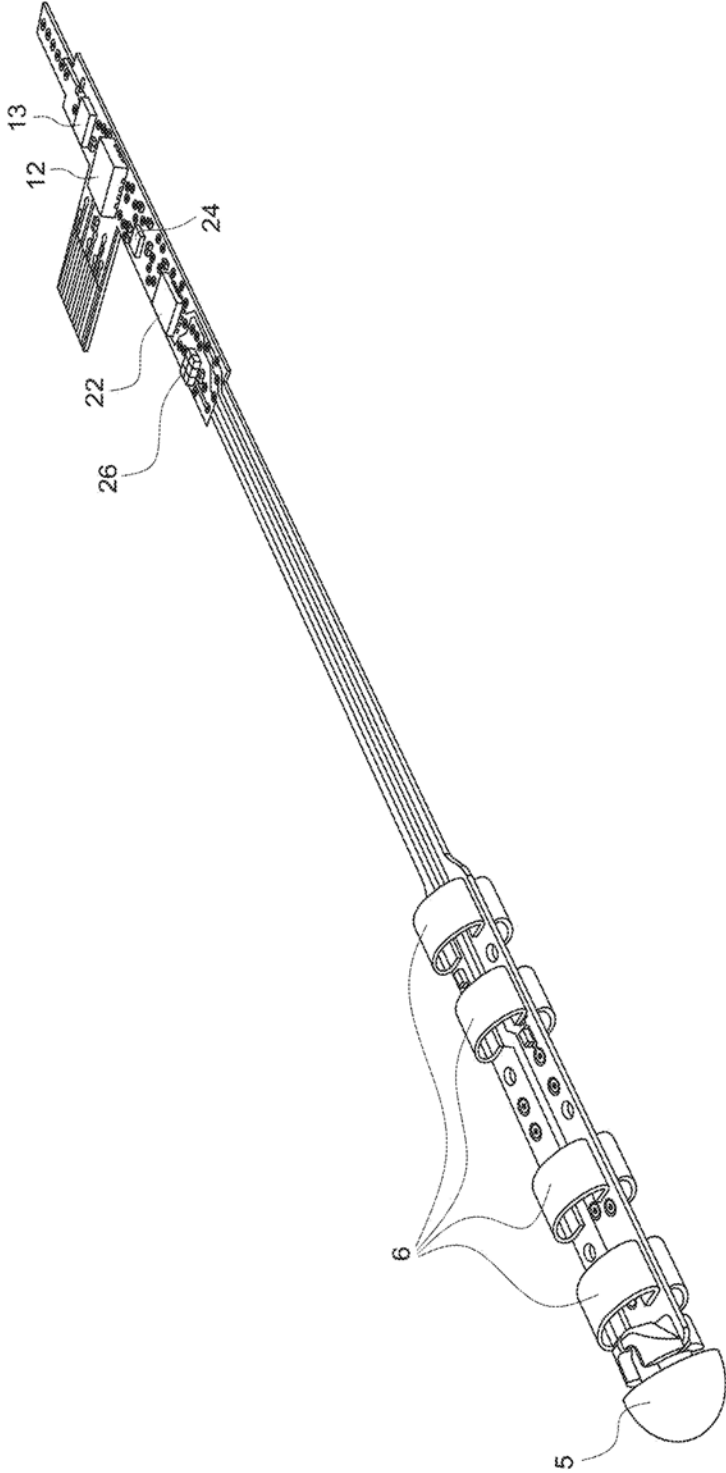


FIG. 13

06

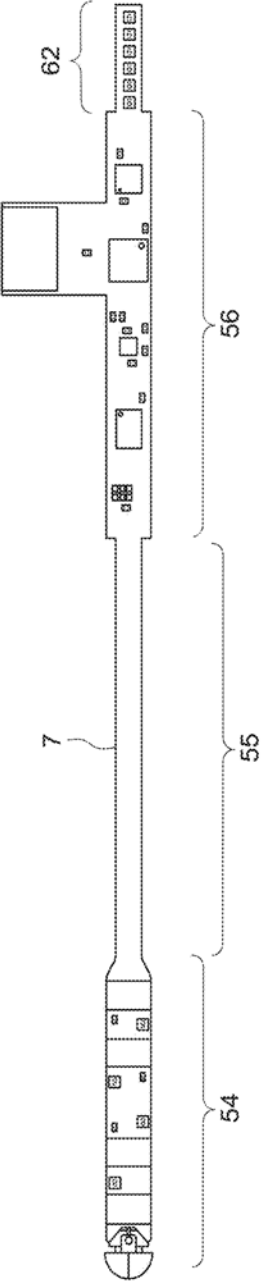
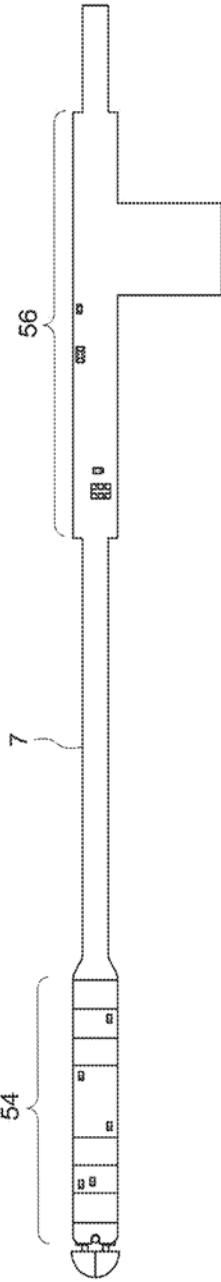
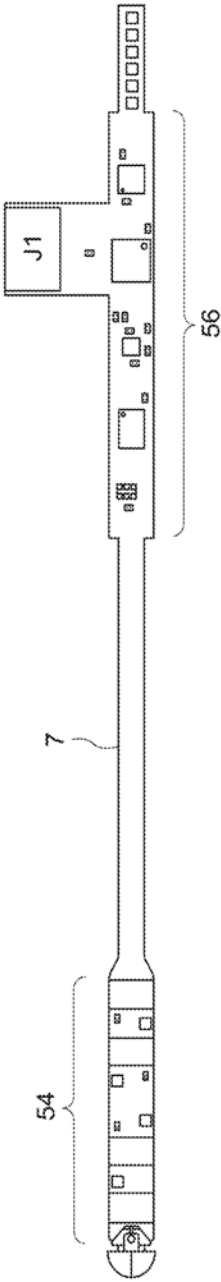


FIG. 14



06

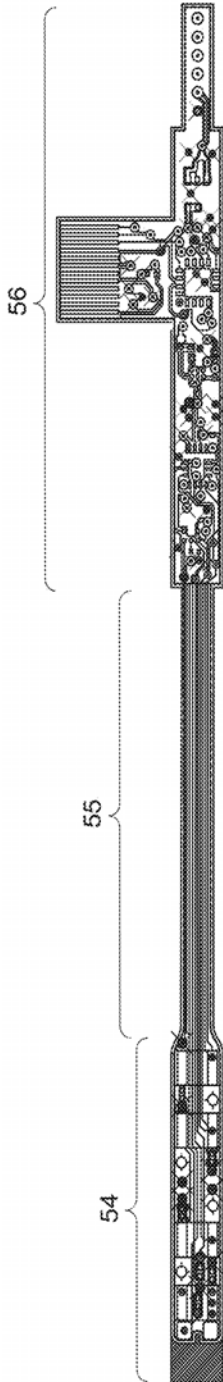


FIG. 16

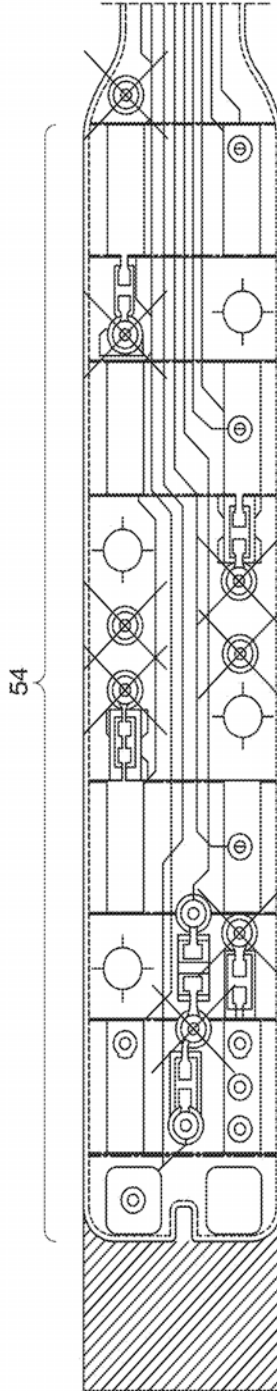


FIG. 17A

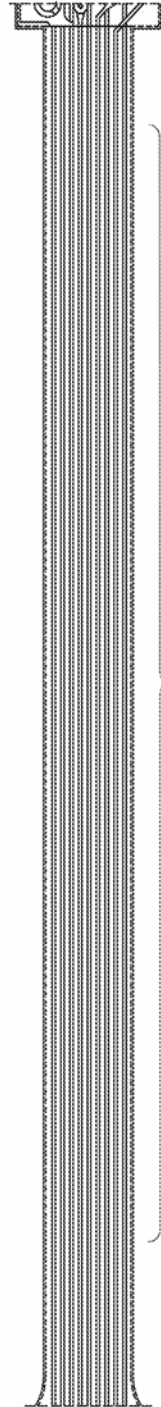
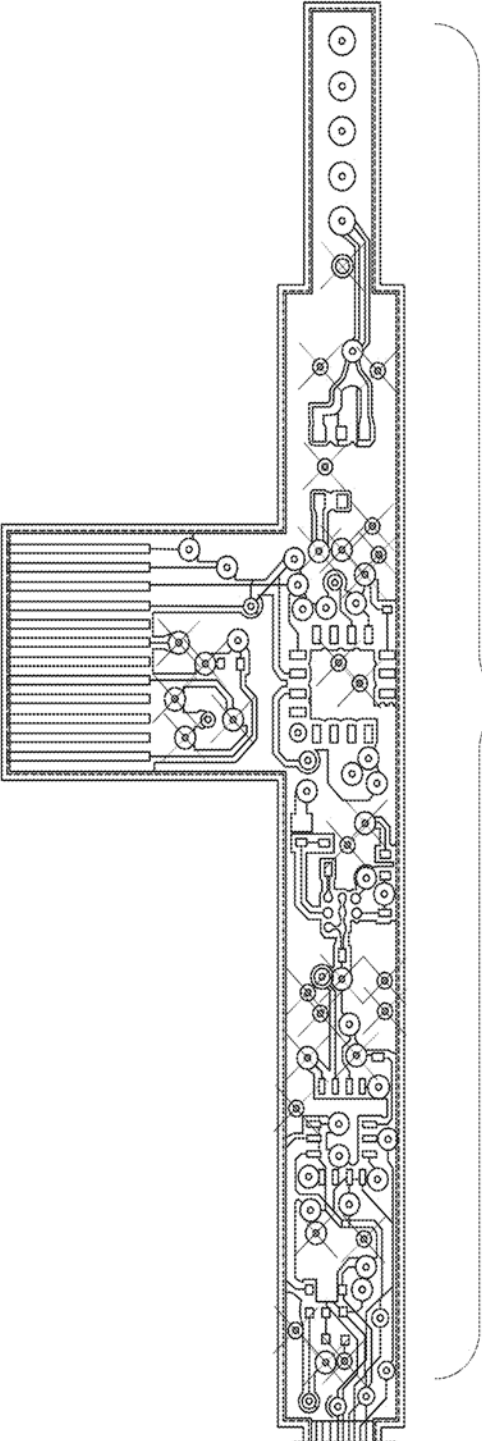


FIG. 17B



56  
FIG. 17C

06



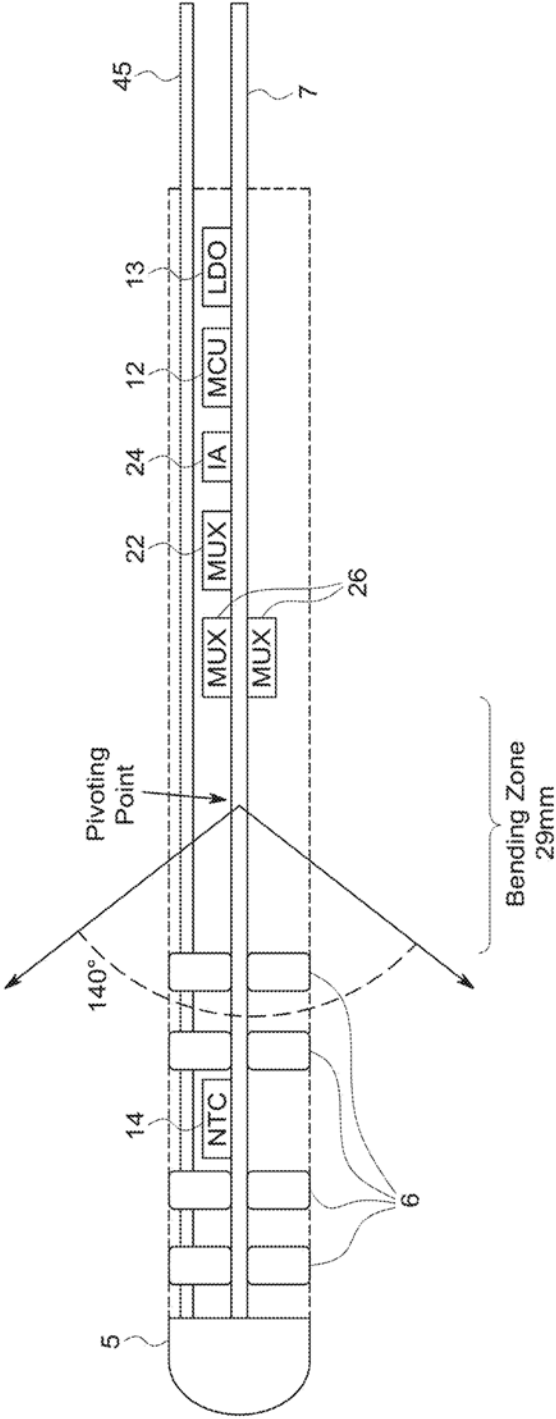


FIG. 18

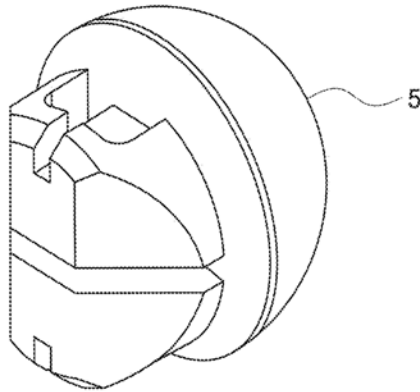


FIG. 19

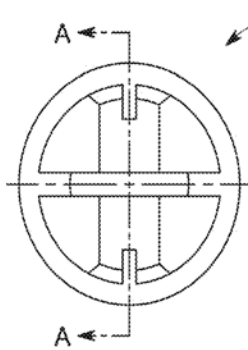


FIG. 20A

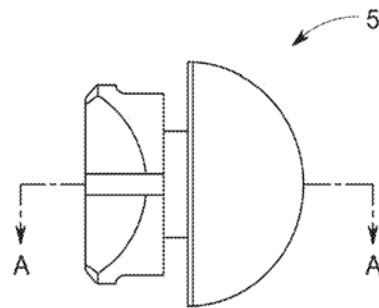


FIG. 20B

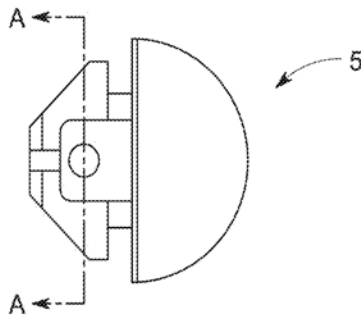


FIG. 20C

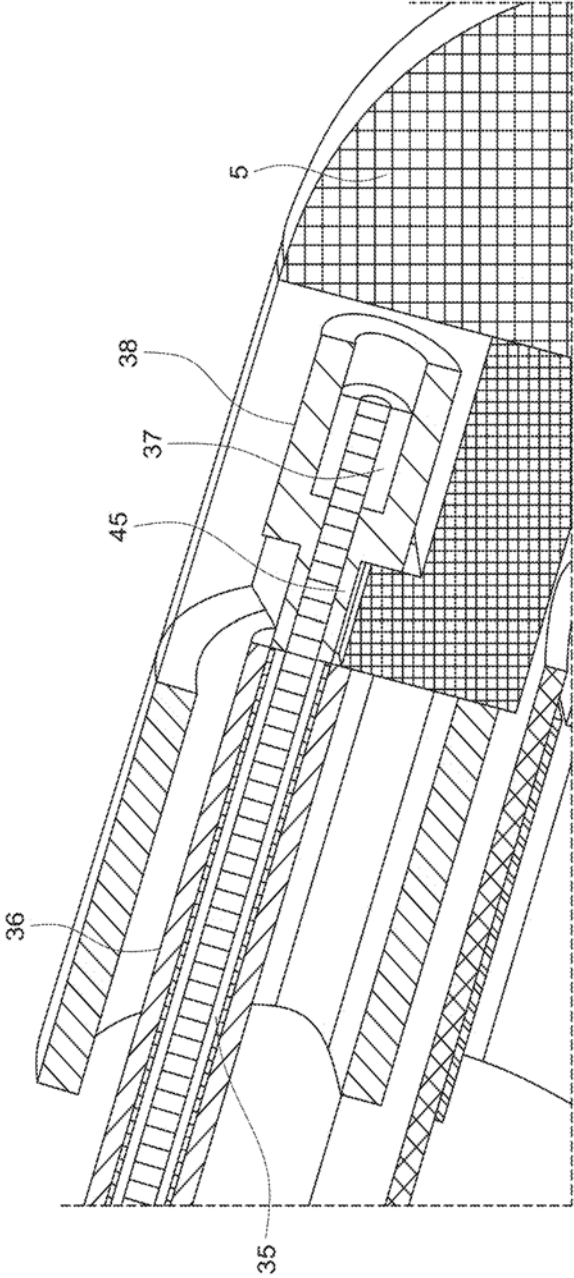


FIG. 21

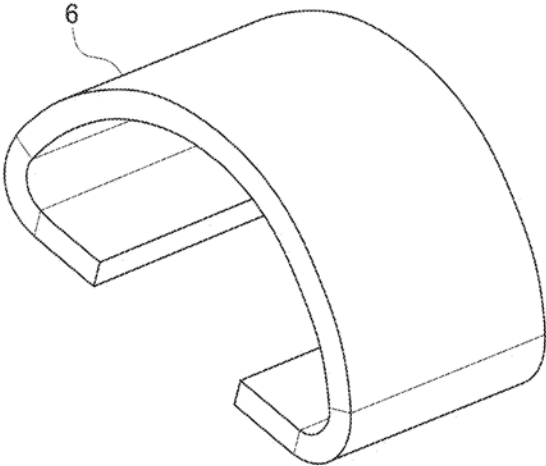


FIG. 22

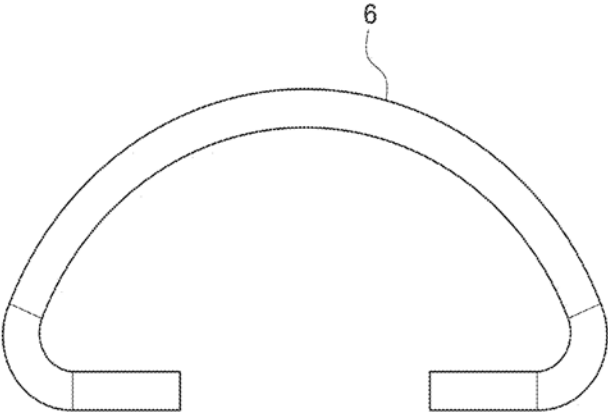


FIG. 23

06

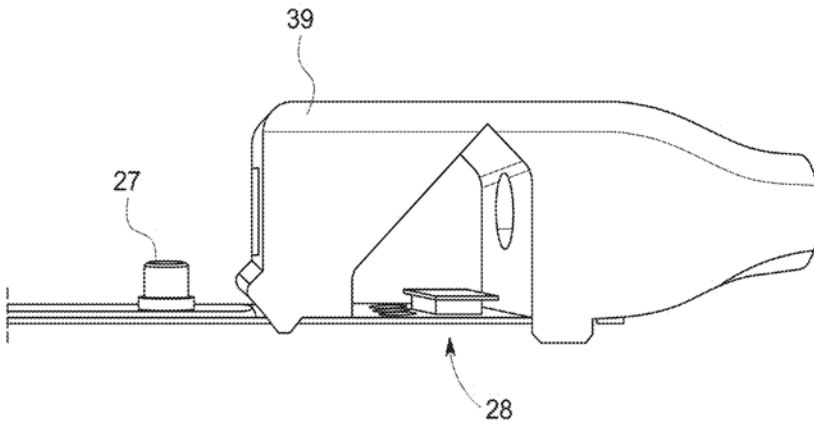


FIG. 24A

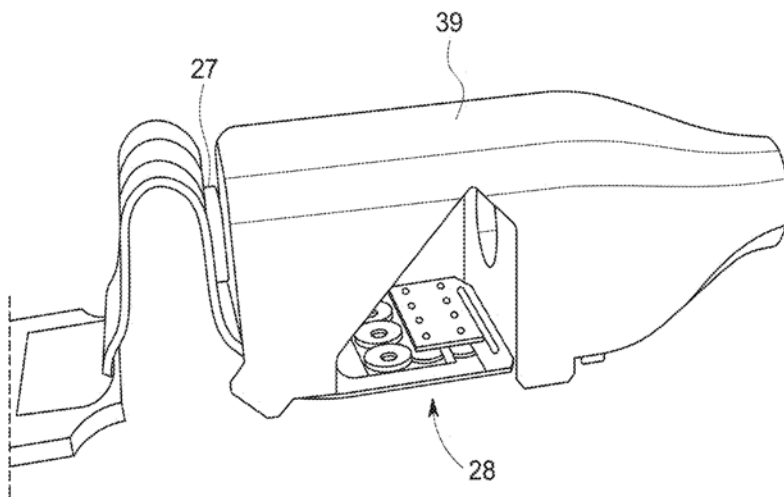


FIG. 24B

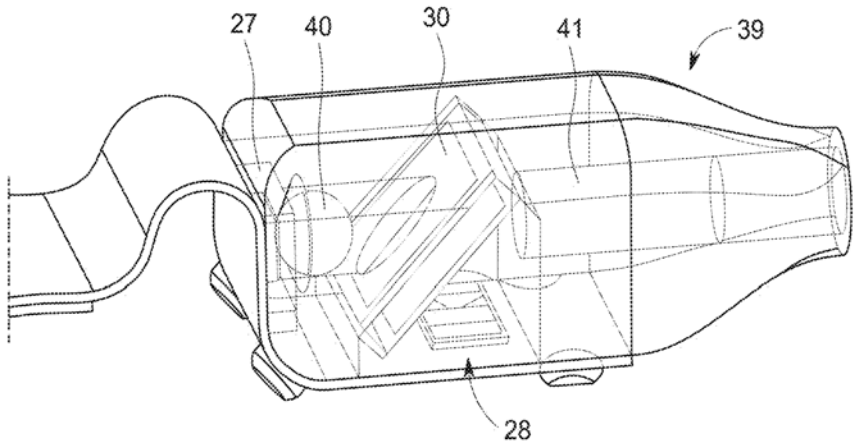


FIG. 25



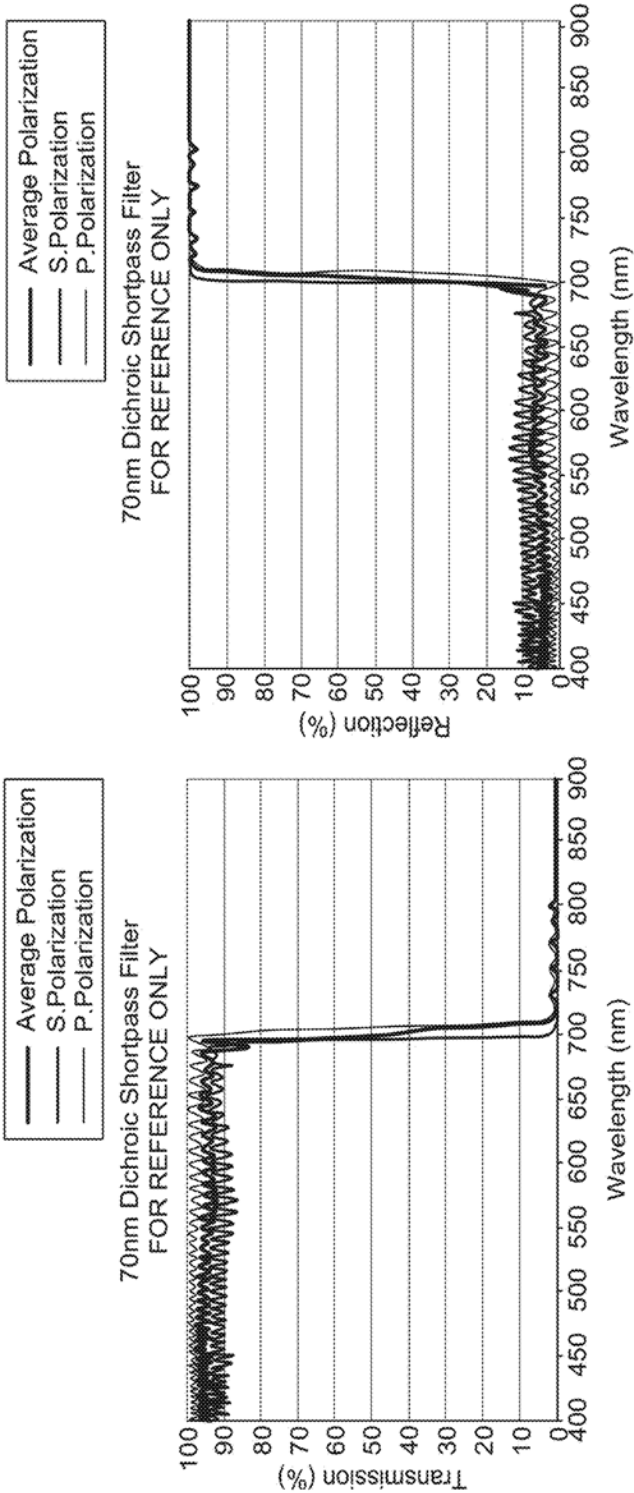


FIG. 26

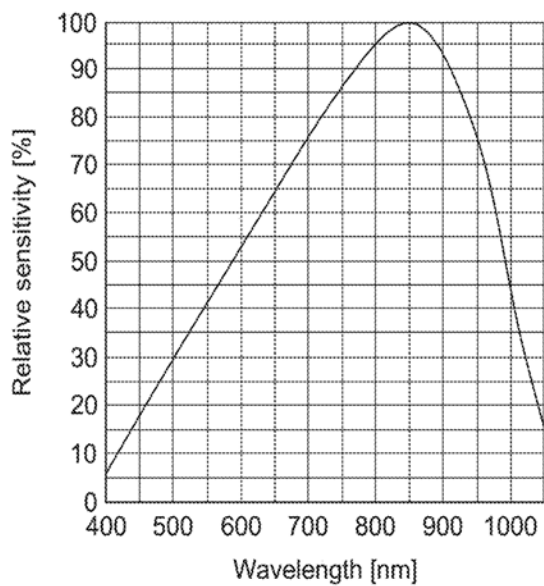


FIG. 27

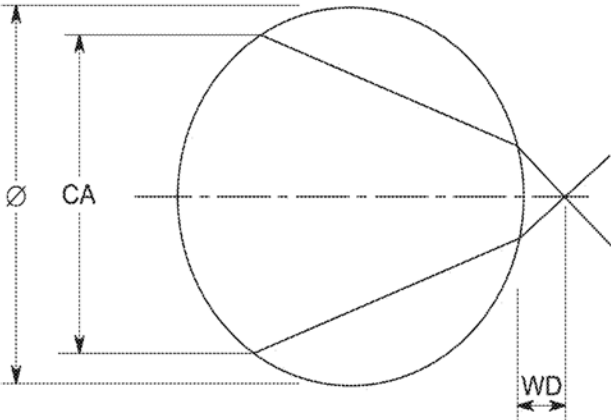


FIG. 28

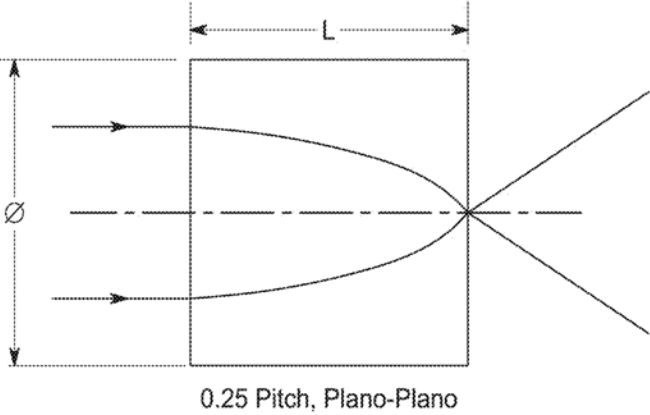


FIG. 29

06



FIG. 30

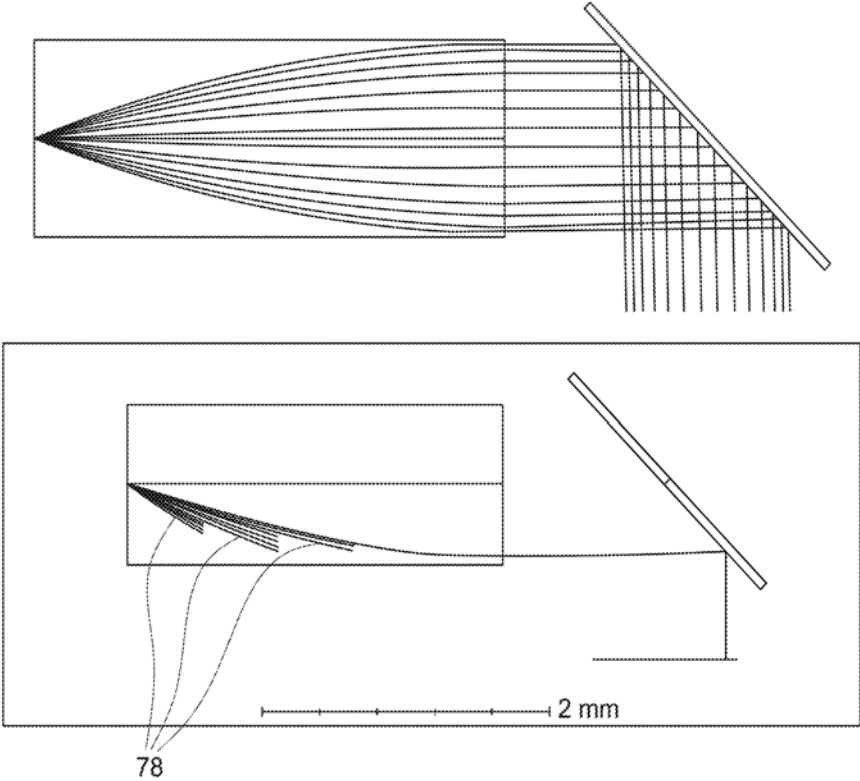


FIG. 31

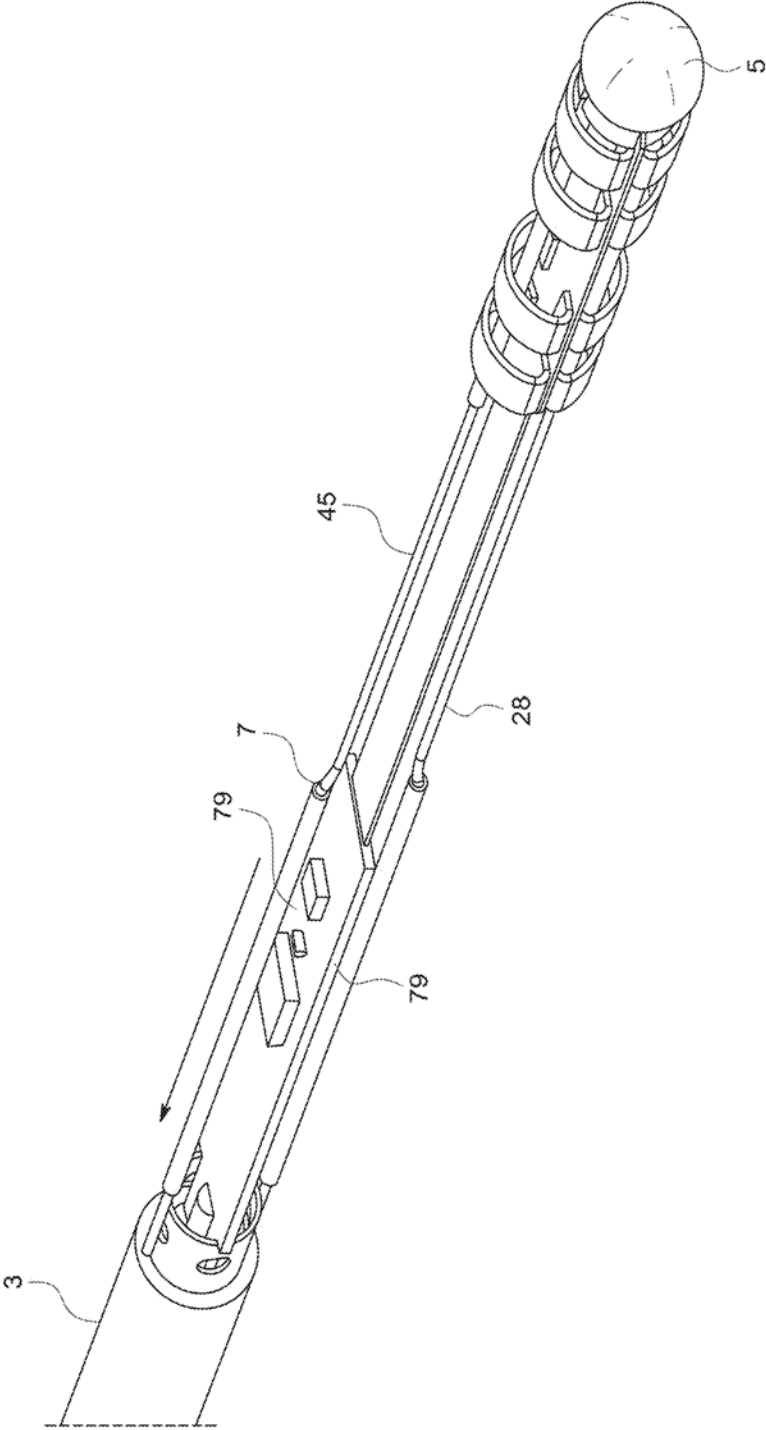


FIG. 32

06



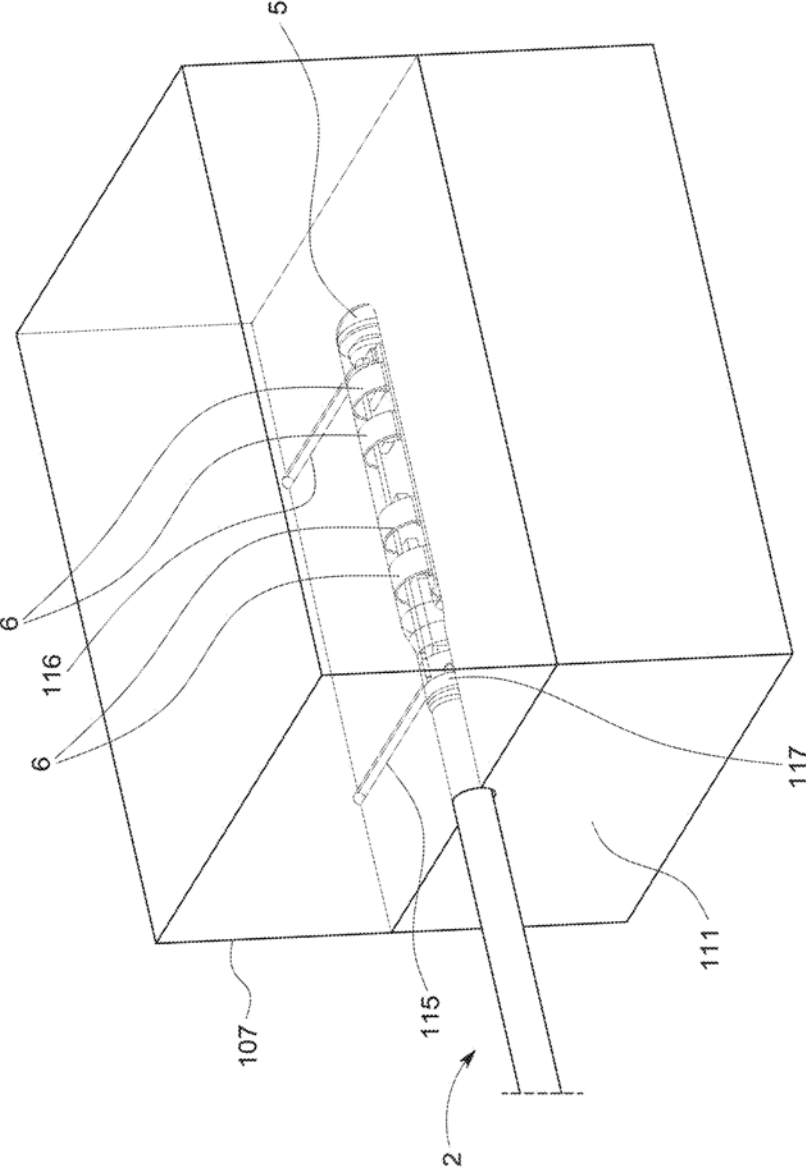


FIG. 33

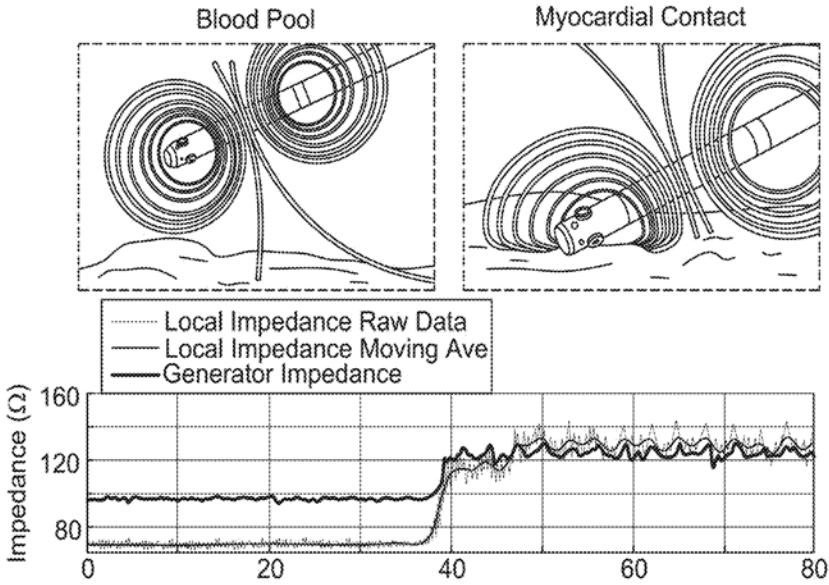


FIG. 34

06

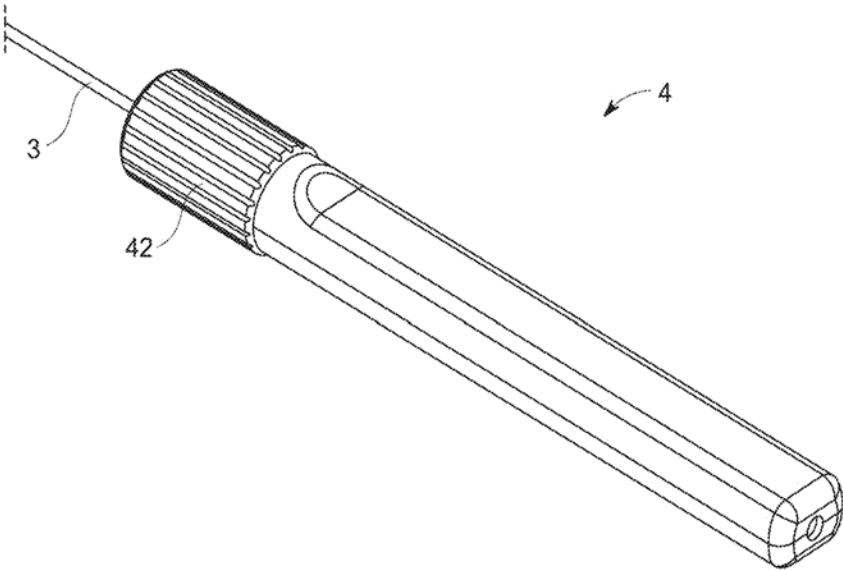


FIG. 35

06

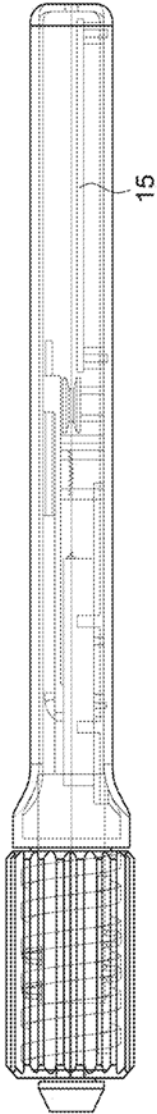


FIG. 36A

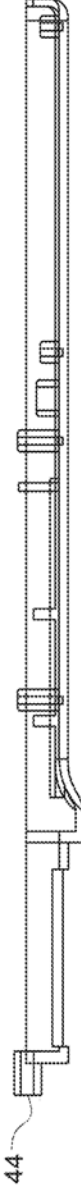
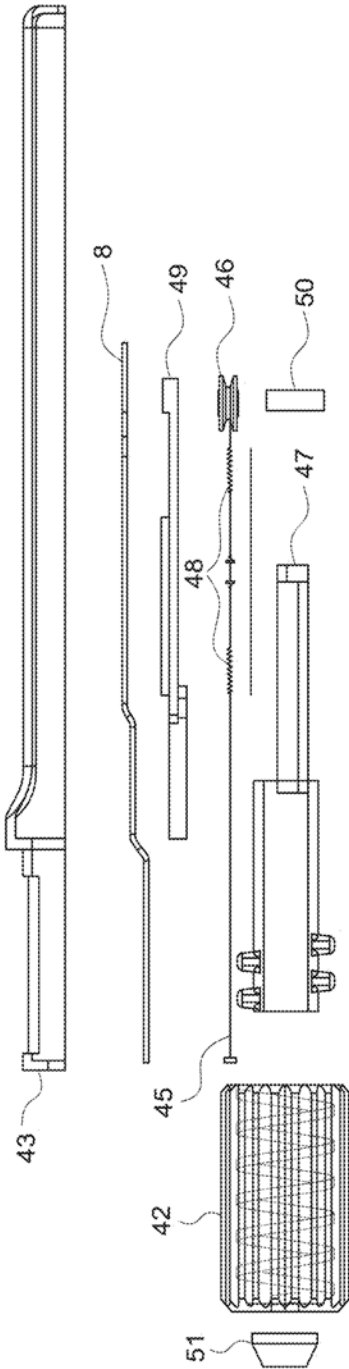


FIG. 36B

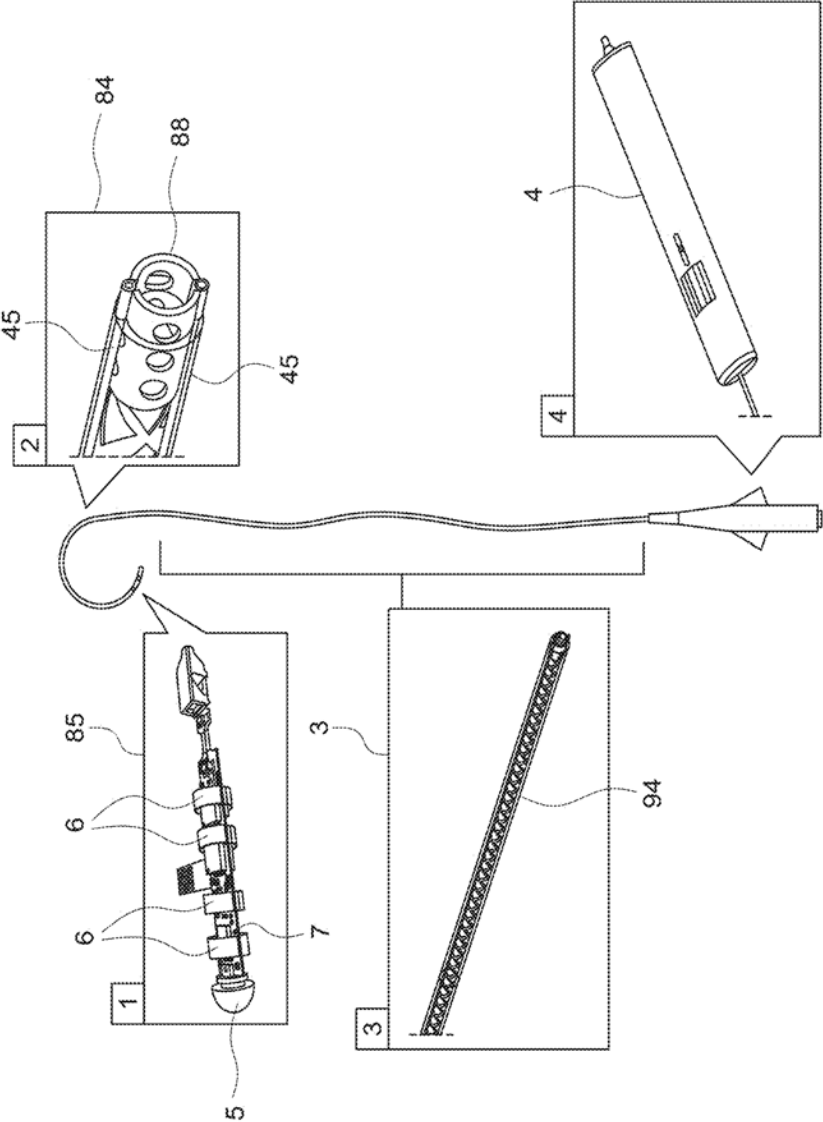


FIG. 37

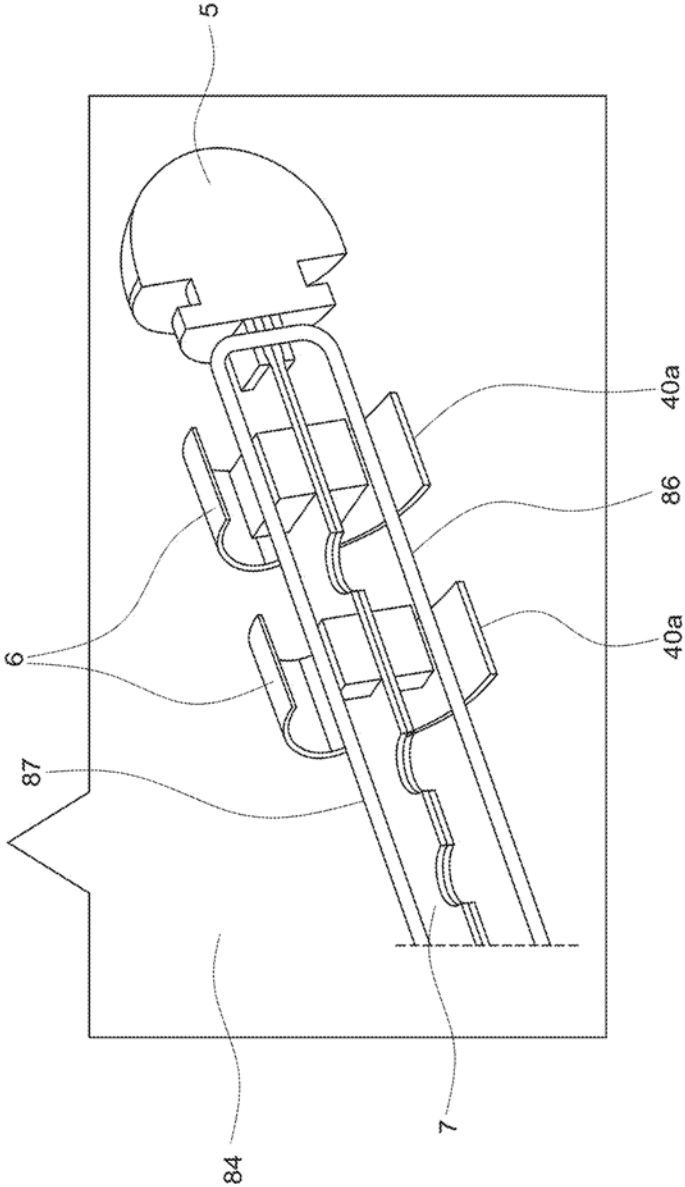


FIG. 37A

06



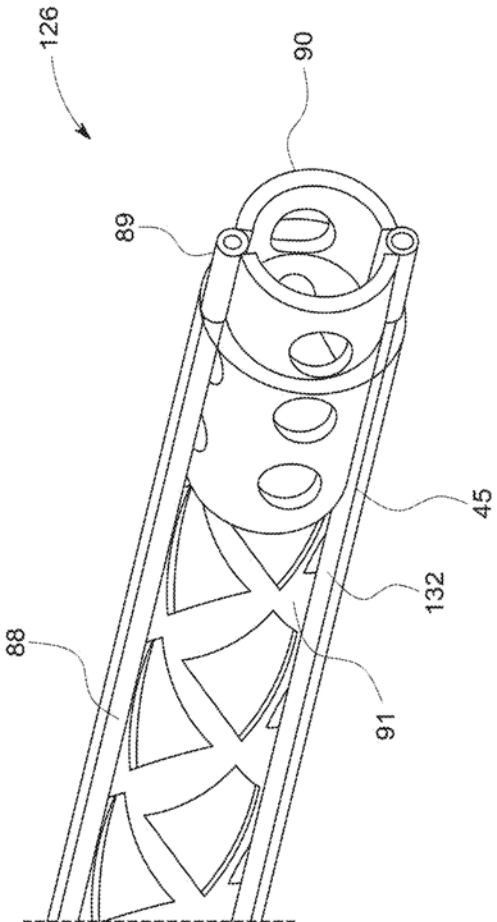


FIG. 37B

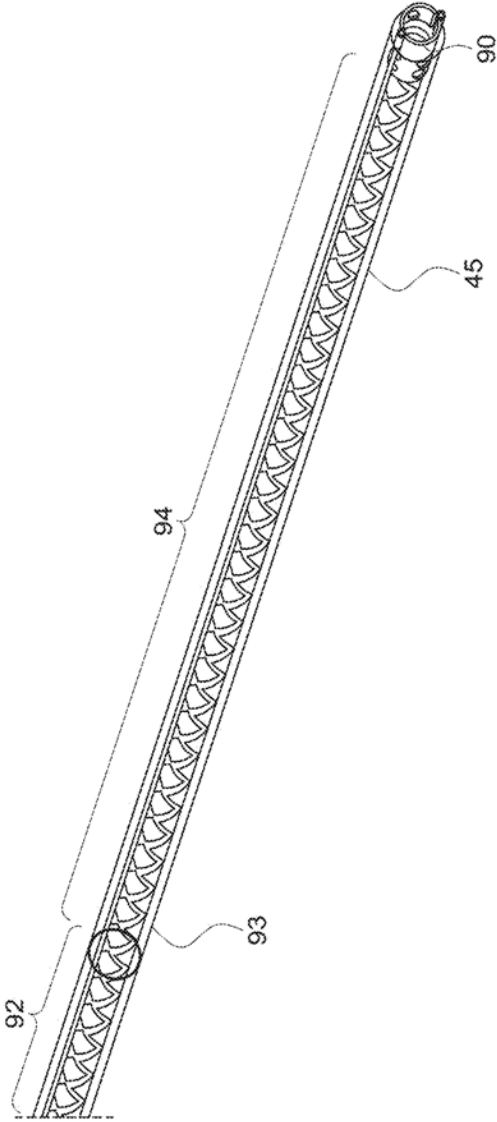


FIG. 37C

06

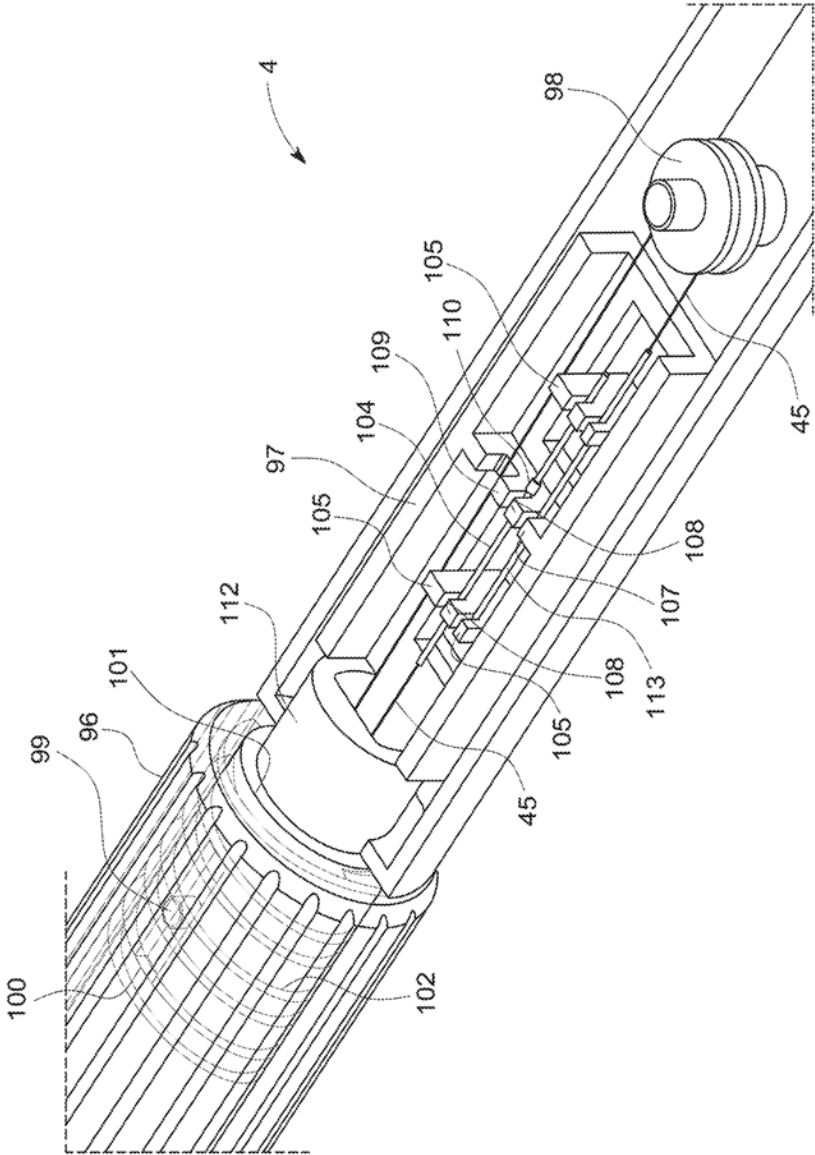


FIG. 38

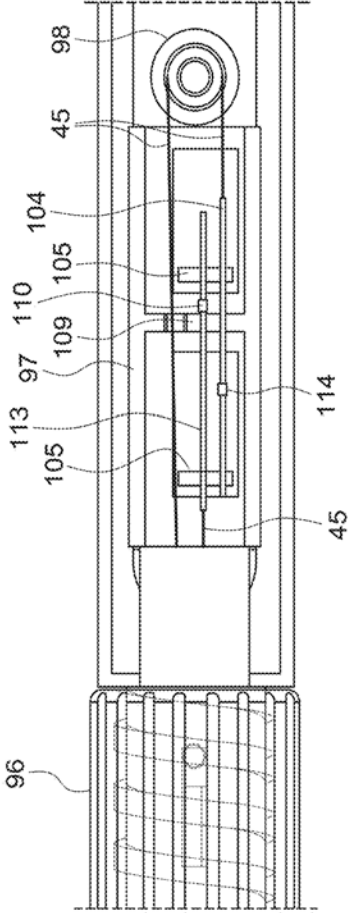


FIG. 39A

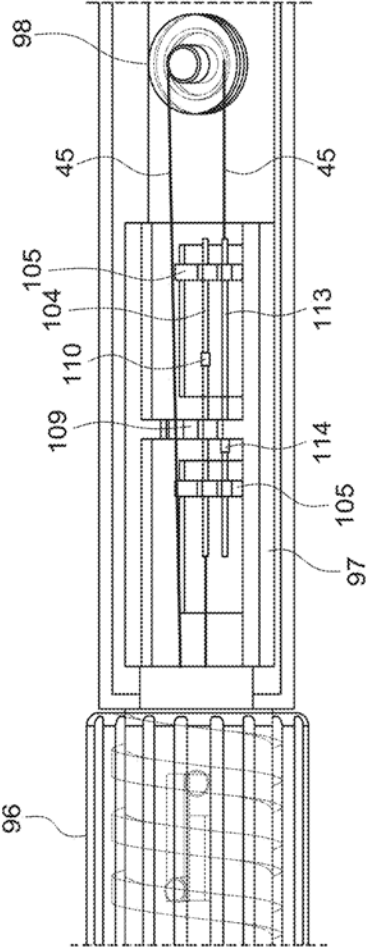


FIG. 39B

06

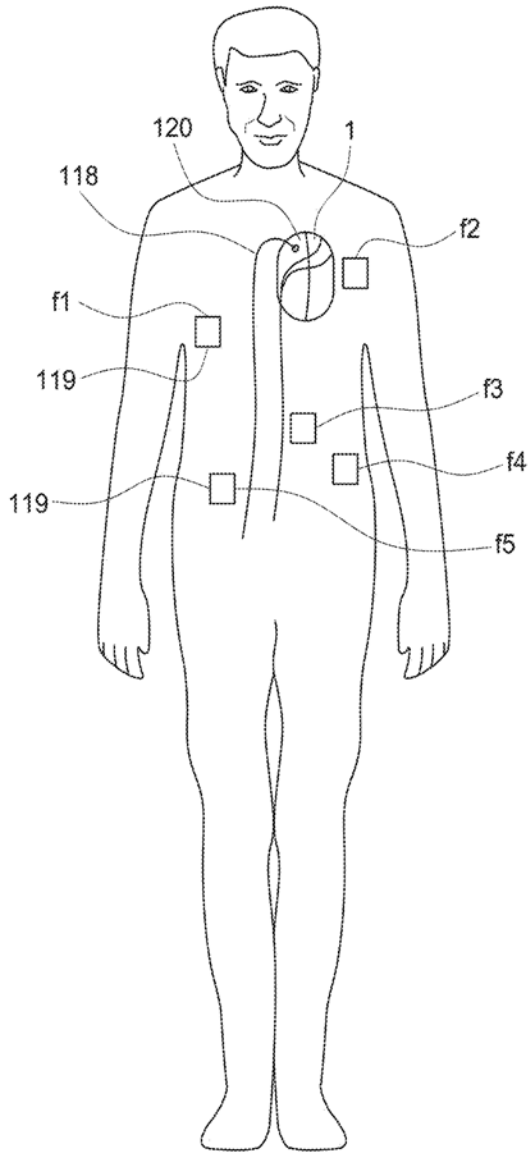


FIG. 40

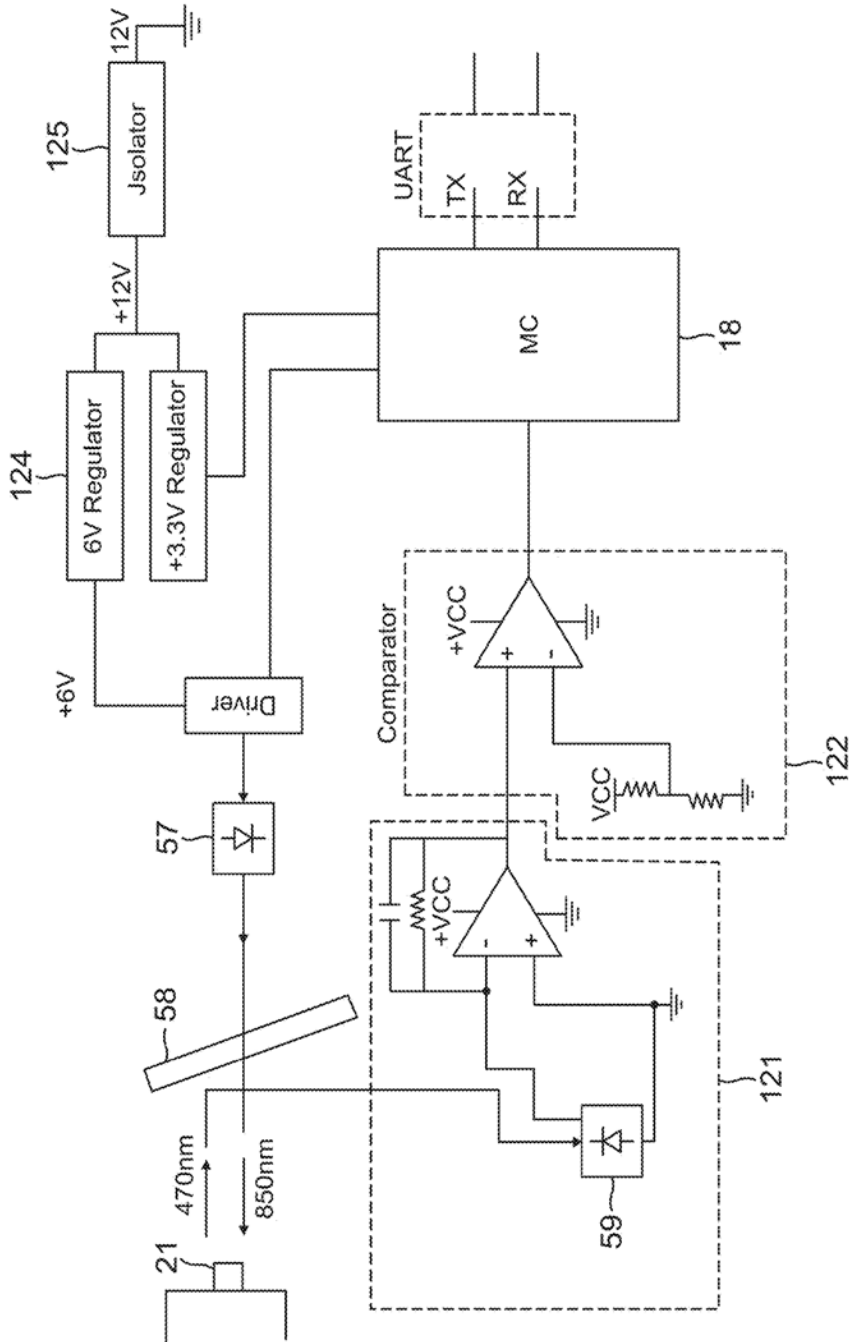


FIG. 41

06



## CATHETER FOR CARDIAC AND RENAL NERVE SENSING AND MEDIATION

**[0001]** This application claims priority to, and the benefit of the earlier filing date as a continuation in part of US patent application entitled, “Optically Coupled Catheter and Method of Using the Same, filed on May 28, 2019, Ser. No. 16/424,202 pursuant to 35 USC 120, the contents of which are incorporated herein by reference.

### BACKGROUND

#### Field of the Technology

**[0002]** The invention relates to the field of catheters as a diagnostic device with applications in electrophysiological studies, e.g.: mapping nerve pathways during ablative procedures such as renal denervation, in various cardiological procedures, and neurological mapping.

#### Description of the Prior Art

**[0003]** Clinical electrophysiologic mapping and ablation procedures are commonly performed in the Electrophysiology Laboratory (EP Lab). The successful ablation of cardiac arrhythmias is critically dependent on the acquisition and interpretation of multiple low amplitude signals (typically ranging in the 25  $\mu$ V to several mV size). As practiced today, both signal acquisition and interpretation suffer from shortcomings of existing recording equipment, as well as limitations of the physician’s ability to interpret the acquired intracardiac electrograms (EGM’s) owing to lack of signal clarity and knowledge about the nature of the propagated signal in complex three-dimensional cardiac tissue.

**[0004]** With respect to signal acquisition, the EGM’s are recorded in the presence of multiple sources of electric noise and interference. Displaying these signals with maximal signal-to-noise (S/N) ratio, in a clinically useful fashion, has been a major challenge over the years. From a noise standpoint, the EP Lab is a source of significant electromagnetic interference (EMI). The patient is connected to multiple pieces of electronic equipment, each of which generates a leakage current which needs to meet safety standards. The patient also acts as a grounded antenna, being both capacitively and inductively coupled to the main voltage wiring in the EP Lab as well as picking up noise from headsets, mobile phones from staff and other wireless monitors. As a result, significant voltages can be measured on the patient’s body (1-3 V RMS) in a wide range of frequency spectrum.

**[0005]** In addition, catheters used for signal acquisition from the patient’s heart, by their very nature, i.e., multiple electrodes connected by long cables to a distant differential amplifier, are subject to line “noise”, ambient EMI, cable motion artifacts, faulty connections, etc. Over the years, progress has been made in shielding and grounding of the EP Lab, as well as improvements in isolation of patient-connected instruments, and improvements of common-mode rejection ratios (CMRR) of differential amplifiers used to enhance the EGM’s of interest. Nonetheless, recording of small and complex signals in the EP Lab continues to be a critical problem and solutions need to be found so that cases are done more efficiently, and outcomes are improved.

**[0006]** Some of the technical and interpretive problems that continue to plague the clinical electrophysiologist in the clinical EP Lab include the following. High frequency signals such as pulmonary vein potentials and near-field

continuous fractionated signals (CAFÉ) may be inadvertently filtered out with a typical 50-60 Hz notch filter commonly used in standard EP systems. Common filters (analog or digital) limit our ability to distinguish between “near-field” signals (which have more high frequency content) from “far-field” signals (which typically have lower frequency energy).

**[0007]** Current analog-to-digital (A/D) sampling rates available in commercially available recording and mapping systems are inadequate to completely analyze the high frequency content of complex signals as well as in differentiating the small high frequency signals such as pulmonary vein potentials, accessory pathway potentials, and the complex details of scar-related conduction in diseased myocardium. High gain amplification is frequently used during mapping in an attempt to identify small signals (e.g., less than 100  $\mu$ V). Amplifiers introduce saturation artifacts (with relatively long offsets) which can conceal or envelop signals of interest that follow large signals such as those introduced during pacing in an EP study, e.g. entrainment mapping.

**[0008]** Conventional systems that use high gain settings also introduce “clipping” of the signals of interest; while software “clipping” of large signals can eliminate the saturation artifact mentioned above, one can be misled when looking at fused waveforms (i.e. pathway potentials during an accessory pathway ablation) if the selected clipping level by the software prevents visualization of two discrete, fused signals and instead represents them as a single, wide signal. Phantom signals or signals that appear real but are an artifact can also be seen because of the less-than-perfect CMRR of the input amplifiers, especially at higher frequencies.

**[0009]** Conventionally obtained unipolar and bipolar recordings have unique advantages and disadvantages. The disadvantage of conventionally band-passed filtered unipolar EGM recording is the inability to distinguish near-field from far-field signals when the near-filed is obtained from diseased myocardium verses far-field from healthy tissue. Using a higher high-pass cutoff frequency can minimize the far-field contribution, but then it may obscure the directional information which the unipolar EGM is meant to convey.

**[0010]** Another disadvantage of unipolar signals is the increased susceptibility to noise because of the differential coupling of interfering signals to the two widely spaced electrodes. Conventional bipolar EGM’s, which are the most commonly used electrode-electrode configuration in the EP Lab, also have certain drawbacks. For example, voltage maps of diseased myocardium are frequently obtained in the EP Lab as a means of estimating scar size and searching for conduction “channels”. However, given the difference in size between the tip electrode and the more proximal electrode of a bipolar pair, and the fact that, in most cases, the tip is in contact with the tissue with a perpendicular orientation, leaving the proximal electrode offset from the tissue by several millimeters, it is not clear if the voltage on the bipolar electrogram is truly representative of the “quality of tissue” beneath the catheter tip. Thus, differentiating a scar from viable tissue using bipolar voltage measurements can be grossly misleading.

**[0011]** Coupled noise interference during delivery of RF ablation energy is also a common problem during the performance of ablation of cardiac arrhythmias. During the delivery of 40-50 W into a 100-ohm load (i.e. cardiac tissue) requires about a 200 V peak-to-peak sine wave. The cardiac signal of interest is up to 200,000 smaller and is obscured

unless sophisticated filtering is used. However, the internal wiring of the mapping/ablation catheters is such that if pacing is performed during ablation, which is not infrequent, coupled interference in the form of high-frequency noise and large baseline drifts will be superimposed on the required electrograms, making observation of reduction and/or disappearance in electrogram amplitude during RF application difficult or even impossible.

**[0012]** With respect to interpretation of complex arrhythmias, especially when multiple colliding wavefronts are recorded, current signal acquisition technologies do not allow for differentiating signals coming from epicardial or mid-myocardial tissues, as opposed to the more readily recorded endocardial signal.

**[0013]** Another limitation of current mapping systems is the inability to measure the thickness of tissue being ablated. This is of paramount safety importance when delivering RF heat energy to potentially thin atrial tissue, and when trying to avoid collateral damage to nearby anatomic structures, such as the esophagus, which is uniquely adjacent to the posterior wall of the left atrium.

**[0014]** What is needed is a method and apparatus for an EP mapping catheter which overcomes each of these limitations and further realizes the advantages listed below.

#### BRIEF SUMMARY

**[0015]** Potential advantages of the disclosed “smart” Huygens catheter, not including the mechanical handle steering component improvement, include:

**[0016]** i. Elimination of the noise and electromagnetic (EM) interference inherent in the intracardiac electrogram (EGM) acquisition technology currently in use in electrophysiology (EP) Labs;

**[0017]** ii. Significant enhancement of the signal-to-noise (SN) ratio, thus enabling the detection of small (<25  $\mu\text{V}$ ) signals without the distortion inherent to current technologies when high-order filtering is employed;

**[0018]** iii. Detection of signals hitherto not available to conventional recording techniques, possibly signals <1-10  $\mu\text{V}$  in size, thereby further defining scar geometry and signal propagation in diseased tissue;

**[0019]** iv. Establishing new paradigms for in vivo description of circuits that involve mid-myocardial and epicardial conduction wavefronts.

**[0020]** v. Rendering the thickness of cardiac tissue, thereby enhancing the safety of ablation procedures.

**[0021]** vi. Further elucidation of the nature of fractionated and complex EGM's, by subtracting far-field signals and enhancing true local tissue potentials.

**[0022]** vii. Recording and localizing sympathetic nerve activity in renal arteries in patients with difficult to treat hypertension, thus making renal artery denervation a more precise procedure and improving the hitherto disappointing results obtained in large clinical trials done to date.

**[0023]** viii. Recording of nerve activity originating in nerve ganglia on the outer surface of the heart, the so-called epicardial ganglionated plexi. This might be crucial in the ablation of atrial fibrillation, the most common arrhythmia treated today in the EP Laboratory.

**[0024]** The catheter has higher resolution, 5-10 micro volts, at its distal end, because the electrodes are amplified locally-or adjacent to the electrode. The electrode signal is then selected by a multiplexer (MUX), converted to a digital

word via a local analog-to-digital converter (ADC). The power for the catheter electronics is generated and transmitted by an optical aperture that maintains a stable base direct current level (DC), at a wavelength of 850 nm, and a measured signal of the potential impedance measured at the electrode interface with the endocardial or renal tissue is transmitted back to the reader for display via an optical data signal with a wavelength of 450 nm. Such transmission of power to the electronics and its data signal return is transferred via an optical fiber from and to the proximal end of the catheter respectively, where an electronic driver circuit provides a stable photonic power to run the electronics at the distal end of the catheter. The control circuit at the tip is capable of receiving the information generated by the electrodes, namely the electro-anatomical data points containing the impedance of the measurement site, its position and its time step, as well as the correlation between contact impedance and contact force in grams. The sensors and circuits in the catheter tip is contained within a 7 Fr. (2.45 mm) catheter, while meeting the safety requirements defined by the standards of the FDA.

**[0025]** The illustrated embodiments of the invention include a method for using an electrophysiology catheter to map neuronal activity of tissue by employing sensing and amplification circuitry disposed in the distal portion of the catheter at the site of biopotential activity to detect and record a local native cardiac signal in cardiac tissue, which detection and recordation spatially and temporally localized with the generation of the native cardiac signal at the situs of its local generation without corruption from far field signals or external electromagnetic noise.

**[0026]** The step of employing sensing and amplification circuitry includes employing a local amplifier active sensor array with capabilities enabling an accurate “one-to-one” correlation while forming an electrophysiological map by measuring spatial position of the situs of local generation and vectorial direction of current movement of the local native signal in the cardiac tissue.

**[0027]** The step of employing the sensing and amplification circuitry includes using the circuitry to make a measurement of biopotential voltage and phase of the local native cardiac signal as a function of time correlated with impedance of the tissue and/or temperature at the local situs of measurement.

**[0028]** The step of employing the sensing and amplification circuitry includes employing the circuitry to detect and record impedance spectroscopy at the local situs of a measured biopotential signal.

**[0029]** The step of employing the sensing and amplification circuitry includes employing the circuitry to detect and record a native local bioelectrical signal in the form of ionic electrochemical avalanche dynamics at a measurement site in tissue by locating an active sensor element adjacent to the measurement site and measuring the native bioelectrical signal by relating its characteristics of time, magnitude and direction in the cardiac tissue without post-processing of the native bioelectrical signal.

**[0030]** The step of employing circuitry for using a native bioelectrical signal is characterized by using circuitry with an improved signal-to-noise ratio, improved spurious-free dynamic range (SFDR), improved signal fidelity, improved sampling rate, improved bandwidth, and improved differentiation of far-field from near-field components in the native signal.

**[0031]** The step of employing an electrophysiological mapping catheter establishes accurate diagnostic maps of axonal nerve endings as detected in renal denervation, measurement of ganglionic plexus activities and neuronal cellular matrices.

**[0032]** The step of employing the sensing and amplification circuitry includes employing an active sensor array in an implantable cardioverter defibrillator (ICD), in an implantable electrophysiological device, in a device for neuromodulation, and in pacemaker leads.

**[0033]** The step of employing the sensing and amplification circuitry comprises employing an active sensor array and where the optical fiber replaces all electrical wiring between the distal portion of the catheter and the handle, so that a signal detected by the active sensor array in the distal portion of the catheter is converted into an uncorruptible digital word and sent to the handle as digital optical data stream.

**[0034]** The step of employing sensing and amplification circuitry in an electrophysiology catheter includes arranging and configuring the catheter as a diagnostic device for use in electrophysiological studies, including mapping nerve pathways during ablative procedures, renal denervation, various cardiological procedures, and neurological mapping.

**[0035]** The method further comprising using an imaging system, including an impedance mapping apparatus in combination with the electrophysiology catheter, which imaging system locates a target within an anatomical context and provides geometric coordinates of specific anatomical destination including identifying different types of arrhythmia.

**[0036]** The step of employing the sensing and amplification circuitry includes accurately characterizing fractionation potentials recorded in scarred myocardial tissue, which serve as ablation targets, pulmonary vein potentials and accessory pathway potentials.

**[0037]** The method where further includes deploying one or more electrodes to comprise an array form with geometry configurations such as bipolar, quadripolar, decapolar, or any array with 64 or more electrodes thereby enabling a multiplicity of electrodes to simultaneously capture a complex electro-potential energetic event with an improved signal-to-noise ratio and improved sampling rate commensurate with an improved bandwidth and improved accuracy on a spatiotemporal domain.

**[0038]** The step of employing sensing and amplification circuitry in an electrophysiology catheter comprises providing a standard model for any assessment of the boundary conditions yielding consistent and repeatable data under similar conditions.

**[0039]** The step of providing the standard model includes unifying diagnostic observations under a measurement technique for defining an intracardiac electrogram (EGM) as energetic events, which provides a translation between the electrical map and its substrate so that the substrate is directly correlated to the pathophysiology.

**[0040]** The step of defining the intracardiac electrogram (EGM) includes generating a graphical representation of an energetic bioevent, based on the dielectric ( $\kappa$ ) and conductivity ( $\sigma$ ) measurements of underlying tissues.

**[0041]** The step of employing the sensing and amplification circuitry includes providing a local amplifier to sense and amplify a native local signal where the near-field as well as its far-field component can be distinguished without post-processing.

**[0042]** The illustrated embodiments also extend to a method for using a renal denervation catheter to map neuronal activity of renal tissue by employing pulsing, sensing and amplification circuitry disposed in the distal portion of the catheter at the site of biopotential activity to electrically stimulate, detect and record a local native renal signal in active renal tissue spatially and temporally localized with the generation of the active native renal signal at the situs of its local generation without corruption from far field signals or external electromagnetic noise.

**[0043]** The illustrated embodiments also include an electrophysiology catheter for combination with an external mapping station, which catheter includes: a catheter with a movable catheter tip; one or more electrodes provided on or in an electrode region in a most distal portion of the catheter tip; sensing and amplification circuitry communicated with the one or more electrodes, the sensing and amplification circuitry communicated with digitizing circuitry disposed in a circuitry region in a least distal portion of the catheter tip for locally sensing tissue-based electrophysiological signals and for bidirectionally communicating digital data signals to and from the sensing and amplification and digital circuitry; a flexible bending region of the catheter tip between the most and least distal portions of the catheter tip; a flexible sheath communicated to the sensing and amplification circuitry and digitizing circuitry for transmission of signals thereon; and a handle communicated with the sheath for bidirectionally communicating signals through the sheath between the catheter tip and external mapping station, and for controlling movement of the catheter tip.

**[0044]** In one embodiment the electrophysiology catheter provides transmission of data signals in the sheath is by optical digital signals.

**[0045]** In another embodiment the electrophysiology catheter transmission of data signals in the sheath is by electrical digital signals.

**[0046]** The electrophysiology catheter further includes: an electro-optical system coupled to the catheter tip for transducing digital electrical electrophysiological signals from the sensing and amplification circuitry and digitizing circuitry into digital optical electrophysiological signals; an optical fiber in the sheath for transmitting the digital optical electrophysiological signals to the proximal handle of the catheter; and an optical-electro system disposed in the proximal handle of the catheter for transducing digital optical electrophysiological signals into digital electrical electrophysiological signals.

**[0047]** The handle comprises a steering mechanism where movement of a distal tip of the catheter with respect to tissue contacted by the catheter tip is controlled.

**[0048]** The sensing and amplification circuitry comprises means for making a biopotential measurement to provide a representation of energy contents on a spatial domain and a time domain of a complex electrophysiological waveform, leading to a recursive relationship between a graphical representation of the complex electrophysiological waveform and an underlying biopotential substrate which causes the complex electrophysiological waveform.

**[0049]** The sensing and amplification circuitry includes means for employing a local amplifier active sensor array utilizing impedance spectroscopy at a bioevent site of a measured biopotential signal.

**[0050]** The sensing and amplification circuitry comprises means for using a native bioelectrical signal in the form of

ionic electrochemical avalanche dynamics at a measurement site in tissue by locating an active sensor element adjacent to the measurement site and measuring the native bioelectrical signal by relating its characteristics of time, magnitude and direction, without post-processing of the native bioelectrical signal.

**[0051]** The means for using a native bioelectrical signal is characterized by an improved signal-to-noise ratio, improved spurious-free dynamic range (SFDR), improved signal fidelity, improved sampling rate, improved bandwidth, and improved differentiation of far-field from near-field components in the native signal.

**[0052]** The catheter includes an electrophysiological mapping catheter adapted to establish accurate diagnostic maps of axonal nerve endings as detected in renal denervation, measurement of ganglionic plexus activities and neuronal cellular matrices.

**[0053]** The sensing and amplification circuitry comprises an active sensor array in an implantable cardioverter defibrillator (ICD), in an implantable electrophysiological device, in a device for neuromodulation, and in pacemaker leads.

**[0054]** The sensing and amplification circuitry comprises an active sensor array and where an optical fiber is employed instead of any electrical wiring between the catheter tip and the handle, so that a signal detected by the active sensor array in the catheter tip is converted into an uncorruptible digital word and sent to the handle in a digital optical data stream.

**[0055]** The catheter is arranged and configured as a diagnostic device for use in electrophysiological studies, including mapping nerve pathways during ablative procedures, renal denervation, various cardiological procedures, and neurological mapping.

**[0056]** The electrophysiology catheter further includes an imaging system in the external mapping station, including an impedance mapping apparatus, which imaging system enables location of a target within an anatomical context and provides geometric coordinates of specific anatomical destination including identifying different types of arrhythmia.

**[0057]** The sensing and amplification circuitry accurately characterizes fractionation potentials recorded in scarred myocardial tissue, which serve as ablation targets, pulmonary vein potentials and accessory pathway potentials.

**[0058]** The one or more electrodes comprise an array forming geometry configurations such as bipolar, quadripolar, decapolar, or any array with 64 or more electrodes to enable a multiplicity of electrodes to simultaneously capture a complex electro-potential energetic event with an improved signal-to-noise ratio and improved sampling rate commensurable with an improved bandwidth and improved accuracy on a spatiotemporal domain.

**[0059]** The electrophysiology catheter further includes means for providing a standard model for any assessment of boundary conditions yielding consistent and repeatable data under similar conditions.

**[0060]** The standard model unifies diagnostic observations under a measurement technique to define an intracardiac electrogram (EGM) as energetic events, which provides a translation between the electrical map and its tissue substrate so that the substrate is directly correlated to the pathophysiology.

**[0061]** The defined intracardiac electrogram (EGM) comprises a graphical representation of an energetic bioevent, based on the dielectric ( $\kappa$ ) and conductivity ( $\sigma$ ) measurements of underlying tissues.

**[0062]** The sensing and amplification circuitry comprises a local amplifier to sense and amplify a native local signal where the near-field as well as its far-field component can be distinguished without post-processing.

**[0063]** The electrophysiology catheter is in combination with an external computer where the optical-electro system disposed in the handle of the catheter for transducing digital optical electrophysiological signals into digital electrical electrophysiological signals comprises a digital signal processor, a laser controlled by the digital signal processor and coupled to the optical fiber, a dichroic mirror for feeding back a portion of light from the laser to a photodiode coupled to the digital signal processor to regulate the laser, where light carrying digital optical signals from the optical fiber are coupled to the photodiode and thence to the digital signal processor, the digital signal processor coupled to the external computer for data storage and processing.

**[0064]** The one or more electrodes comprise a plurality of electrodes and where the sensing and amplification circuitry includes: a light emitting diode/photodiode (LED/PD); a serial peripheral interface (SPI) bus; a plurality of amplifier application specific integrated circuits (amp ASIC) coupled to corresponding ones of the plurality of electrodes and to the serial peripheral interface (SPI) bus; and a light application specific integrated circuit (ASIC) coupled to the LED/PD, which light ASIC signal conditions and communicates a plurality of signals on the serial peripheral interface (SPI) bus to the plurality of amplifier ASIC's, each of which are coupled to one of the plurality of electrodes, used as sensing points of the catheter tip so that sensed biopotentials from electrodes are locally amplified by amplifier ASICs and communicated via the SPI bus into the light ASIC to be multiplexed out to LED/PD and communicated as multiplexed photonic signals on the optical fiber.

**[0065]** The sensing and amplification circuitry disposed in the distal portion of the catheter tip includes: an optical connector coupled to the optical fiber, the optical connector including a photodiode to convert an optical signal from the optical fiber into an electrical signal, and the optical connector including an LED to convert an electrical signal into an optical signal communicated to the optical fiber; a voltage regulator coupled to the photodiode and powered by a power optical signal received by the photodiode; a charge pump coupled to the voltage regulator; a microcontroller unit (MCU); an analog to digital converter (ADC) coupled to the MCU; an instrument amplifier (IA) coupled to the ADC; an AC-coupling circuit coupled to the IA; a multiplexer (MUX) coupled to the AC-coupling circuit and to the one or more electrodes; where the charge pump is coupled to the MUX and IA for the purpose of supplying power, where the voltage regulator powers and is coupled to the MCU, ADC, IA, AC-coupling circuit and MUX; where the MCU is coupled to the MUX and provides a selection command signals to the MUX to control selection of the one or more electrodes; and where sensed native signals from the one or more electrodes is communicated to the AC-coupling circuit, amplified by the IA, converted to a digital form by the ADC and communicated to the MCU for communication to the LED and transduction into a digital optical form into the optical fiber.



**[0066]** While the apparatus and method has or will be described for the sake of grammatical fluidity with functional explanations, it is to be expressly understood that the claims, unless expressly formulated under 35 USC 112, are not to be construed as necessarily limited in any way by the construction of “means” or “steps” limitations, but are to be accorded the full scope of the meaning and equivalents of the definition provided by the claims under the judicial doctrine of equivalents, and in the case where the claims are expressly formulated under 35 USC 112 are to be accorded full statutory equivalents under 35 USC 112. The disclosure can be better visualized by turning now to the following drawings wherein like elements are referenced by like numerals.

#### BRIEF DESCRIPTION OF THE DRAWINGS

**[0067]** The patent or application file contains at least one drawing executed in color. Copies of this patent or patent application publication with color drawing(s) will be provided by the Office upon request and payment of the necessary fee.

**[0068]** FIG. 1 is a perspective view of the Huygens catheter system, including the handle, sheath and catheter tip.

**[0069]** FIGS. 2A-2C are three side views of the catheter tip. FIG. 2A is a transparent side elevational view; FIG. 2B is a side elevational view of the exterior surface of the catheter tip of FIG. 2A not including exposed electrodes; and FIG. 2C is an exploded side view of certain components in the catheter tip shown in FIGS. 2A and 2B.

**[0070]** FIGS. 3A and 3B are the electrical block diagrams of the Huygens catheter in the optical embodiment and electrical cable embodiments respectively. FIG. 3C is a schematic diagram of the primary optical and electrical signals of the optical embodiment of FIG. 3A.

**[0071]** FIGS. 4A and 4B are block diagrams of an electrical and optical components of the catheter tip in the optical and electrical cable embodiments respectively.

**[0072]** FIG. 5 is a block diagram of the electrical circuits of the catheter tip, sheath and handle of the electrical cable embodiment of FIG. 4B of the Huygens catheter.

**[0073]** FIGS. 6A and 6B are electrical block diagrams of catheter tip of the electrical cable and optical embodiments respectively.

**[0074]** FIG. 7 is a diagram of the data flows in the optical embodiment of FIG. 6B between the catheter tip and the handle.

**[0075]** FIG. 8 is an electrical schematic of the multiplexer control of the catheter tip in the electrical cable embodiment of FIG. 6A.

**[0076]** FIG. 9 is a schematic of the connection from the six electrical wires from the sheath to the tip FPC in the electrical cable embodiment of FIG. 6B.

**[0077]** FIG. 10 is a schematic diagram of a first embodiment of the AC-coupling circuit and instrumentation amplifier.

**[0078]** FIG. 11 is a schematic diagram of a second embodiment of the AC-coupling circuit and instrumentation amplifier.

**[0079]** FIG. 12 is a schematic diagram of a third embodiment of the AC coupling circuit and instrumentation amplifier.

**[0080]** FIG. 13 is a perspective view of the tip FPC with the electronics assembled thereon.

**[0081]** FIG. 14 is a top elevational view of the tip flex printed circuit (FPC) of FIG. 13.

**[0082]** FIGS. 15A and 15B are top and bottom elevational views respectively of the assembly drawing of the tip flex printed circuit (FPC) of FIG. 14.

**[0083]** FIG. 16 is the top plan view of the entire catheter tip flex printed circuit board layout.

**[0084]** FIGS. 17A, 17B, and 17C are diagrams showing the layout of the three regions of tip FPC of FIG. 16, namely the electrode region, bending region, and electronic region respectively.

**[0085]** FIG. 18 is a transparent side view of the block diagram of the catheter tip and its mechanical flexure as well as its functional requirements.

**[0086]** FIG. 19 is a perspective view of the tip nosecone electrode.

**[0087]** FIGS. 20a, 20b and 20c are three views showing the mechanical dimension of the tip nosecone electrode. FIG. 20 is an end plan view showing where sections lines A-A are defined. FIG. 20b is a top plan view showing where sections lines A-A are defined. FIG. 20c is a cross sectional view as seen through section lines A-A.

**[0088]** FIG. 21 is a cutaway side cross sectional diagram showing how the safety wire is inserted into the nosecone electrode, while electrically isolated therefrom. FIG. 21 also shows the materials covering the safety wire.

**[0089]** FIG. 22 is a perspective view of a half-ring electrode.

**[0090]** FIG. 23 is a side cross sectional view showing the mechanical dimension of the half-ring electrode of FIG. 22.

**[0091]** FIG. 24A is a side perspective side view showing an optical connector couple to the tip FPC at its flat orientation, and FIG. 24B is a side perspective view showing when the FPC is fully bent.

**[0092]** FIG. 25 is a perspective phantom view of the optical connector of FIGS. 24A and 24B shown after the FPC is bent.

**[0093]** FIG. 26 is a graph of dichroic mirror's transmittance and reflectance response.

**[0094]** FIG. 27 shows a graph of photodiode's sensitivity across spectral wavelength range.

**[0095]** FIG. 28 is a diagram showing an optical tracing of the spherical micro lens.

**[0096]** FIG. 29 is a diagram showing an optical tracing of the cylindrical GRIN lens.

**[0097]** FIG. 30 is a diagram showing an optical ray tracing of the light collimation of the GRIN lens.

**[0098]** FIG. 31 is an optical ray tracing showing a light reflecting and bending simulation for the GRIN lens.

**[0099]** FIG. 32 is a perspective view showing the assembly procedure of the tip FPC to the catheter sheath.

**[0100]** FIG. 33 is a diagram showing the molding process of the catheter tip.

**[0101]** FIG. 34 is a graphic depiction of the electrical fields on the left side of the drawing of a local amplifier catheter tip in free fluid according to the illustrated embodiments of the invention and on the right side of the drawing of a local amplifier catheter tip in contact with tissue. The graph under the pictorial illustrations shows the corresponding impedance signals measured in each corresponding situation.

**[0102]** FIG. 35 is another perspective view of the catheter handle of FIG. 1.

[0103] FIG. 36A is a transparent side view of the assembled handle. FIG. 36B is an exploded side transparent view of the catheter handle of FIG. 36A and its mechanical components.

[0104] FIG. 37 is the schematic diagram of the catheter tip, sheath and handle printed circuit board (PCB). FIG. 37A is a cutaway side perspective view of the nosecone electrode and immediately adjacent portion of the catheter tip and safety wire. FIG. 37B is a side perspective view of the pull wire tip attachment region of the catheter tip. FIG. 37C is a side perspective view of the pull wires and sheath proximally located from the pull wire attachment region of FIG. 37B.

[0105] FIG. 38 is a top perspective opened internal view of the catheter handle showing the operation of the rotary knob.

[0106] FIGS. 39A and 39B are diagrams which show the operation of the pull wire to deflect the catheter tip in the full proximal position of the knob and pin, and in the full distal position of the knob and pin respectively.

[0107] FIG. 40 is a diagram of a patient with a plurality of body electrodes attached to provide a positional frame for a transeptal probing catheter and a reference catheter anchored in the coronary sinus.

[0108] FIG. 41 is a block diagram of one embodiment of the handle electronics.

[0109] The disclosure and its various embodiments can now be better understood by turning to the following detailed description of the preferred embodiments which are presented as illustrated examples of the embodiments defined in the claims. It is expressly understood that the embodiments as defined by the claims may be broader than the illustrated embodiments described below.

#### DETAILED DESCRIPTION OF THE PREFERRED EMBODIMENTS

##### System Overview

[0110] It is to be understood that the catheter 1 of the illustrated embodiments is used in a spatial reference frame established in a conventional manner using a plurality of RF emitting body patches 119 shown in FIG. 40, a reference catheter 118 anchored in the coronary sinus 120 to fix an anatomical origin in the heart, and the transeptal probing catheter 1. See for example, PCT/US2008/056277 “Method and apparatus for controlling catheter position and orientation”; PCT/US2009/039659 “Apparatus and method for Lorentz-active Sheath and control of surgical tool”; PCT/US2009/040242 “Method and Apparatus for creating a high resolution map of the electrical and mechanical properties of the heart”; PCT/US2009/064439 “System and Method for catheter Impedance seeking device”; PCT/US2010/052696 “Method for acquiring high density mapping data with a catheter guidance system”; and PCT/US2010/056069 “Method for targeting Catheter electrodes”, each and all of which are incorporated herein by reference. RF locational signals applied to and transmitted from the plurality of patches 119, each at a unique frequency assigned to each one of the patches 119, are detected by tip electrodes on catheter 1 and reference catheter 118 thereby returning a corresponding plurality of time stamped RF locational signals depending the time of flight of the locational signal to the reference catheter 118 and catheter 1. The distance from each patch 119 to the reference catheter 118 and catheter 1 is deter-

mined by the corresponding time stamp or time of flight of the RF locational signal. By triangulation the relative positions of the reference catheter 118 and catheter 1 are determined in a data processor in a connected conventional mapping station. The position of the reference catheter 118 anchored in the coronary sinus is assigned as the origin of the reference frame and the position of catheter 1 is determined in reference to it. The plurality of patches 118 are pulsed with the RF locational signal at a 50 Hz repetition rate. The periodic movement of the heart is at 1.5 Hz or less, so that relative positional changes of catheter 1 due to heart beat and breathing are easily tracked. The position of the tip of catheter 1 relative to an anatomical map of the heart as measured from the coronary sinus 120 is thus always determined at each instance of time.

[0111] The path of the dynamic, avalanche cardiac signals in the heart can be mapped in the cardiac tissue with catheter 1 by tracking the local pacing cardiac pulse, typically in the left atrium. In the case of a heart having scar tissue blocking the proper pathway, diverting the pacing path in usually a shortened path bypassing essential portions of the heart, and causing an arrhythmia, sinus rhythm of the heart can be restored if the shortened path is ablated by using an RF ablation catheter to create a small amount of scar tissue across the shortened path. The pacing current then seeks a different path through the heart tissue and hopefully it will be a pathway on or close to the normal pacing circuit. RF ablation continues until a sinus rhythm is achieved indicating the establishment of a normal or near normal pacing circuit. It can readily be appreciated that such ablation therapies are successful only if the local pacing signal, normal or abnormal, in the heart can be reliably and accurately mapped. If the physician is only guessing or estimating where the pacing signal goes, then the ablation sites will be chosen based on guesses, some bad. In order to accurately map native cardiac pulses, the clear and reliable spatial and temporal detection of the local native cardiac pulse must be achieved at each point in the cardiac tissue and recorded. The native cardiac pulse is typically from 25  $\mu$ V (scar related signals) to 5 mV (surface ECG) with a period of between 80 and 100 ms. When the duration is between 0.10 and 0.12 seconds, it is intermediate or slightly prolonged. A QRS duration of greater than 0.12 seconds is considered abnormal. Normal sinus rhythm and dysrhythmias that arise from above the ventricles will usually have normal QRS complexes. Abnormal QRS complexes are produced by abnormal depolarization of the ventricles. Duration of an abnormal QRS complex is greater than 0.12 seconds.

Complex fractionated atrial electrograms (CFAEs) are defined as electrograms with a cycle length  $\geq$ 20 ms or shorter, or that were fractionated or displayed continuous electric activity.

[0112] This biosignal is awash in larger cardiac signal of the order of mV and external electromagnetic signals from operation room and hospital equipment. In addition to this, the detected signal is transmitted on an EP catheter cable of the order of 1 m long to an external mapping station, possibly several more meters away, all of which is swamped in a sea of electromagnetic noise that endemic to the mapping station circuitry or is picked up on these long wires, leads and cables. Such wires and cables necessarily has some small self-capacitance and inductance to time varying signals with a frequency spectrum, which will distort the phase of the carried signal. Thus, if the native cardiac signal



is to be accurately detected and recorded, it must be locally detected at the situs in the heart of the native signal across the local temporal span of its generation, its amplitude and phase detected and recorded or frozen in time, and transmitted noise-free to the mapping station. The EP catheter system disclosed below achieves that goal. According to the disclosed embodiments, the local native pacing pulse in the heart tissue, which is detected and recorded, includes the spatial position of the tip of catheter 1  $\langle x, y, z \rangle$ , its angular direction to the next adjacent situs of the native pulse or direction of the native cardiac current  $\langle \theta, \varphi, \psi \rangle$ , time  $\langle t \rangle$ , amplitude and phase of the current  $\langle V, \Theta \rangle$ , impedance of the detection site  $\langle \Omega \rangle$  and temperature of the detection site  $\langle T \rangle$ , for a complete data string of  $\langle t, \{x, y, z\}, \{\theta, \varphi, \psi\}, V, \theta, \Omega, T \rangle$  digitized and transmitted at a 50 Hz repetition rate for each measured situs.

[0113] Signals in the EP lab range from 25  $\mu\text{V}$  (scar related signals) to 5 mV (surface ECG). Noise on clean EGM's is on the order of magnitude of less than 20  $\mu\text{V}$ , when everything is properly grounded and shielded. So achieving a SNR of 10, for example, with a biologic signal of 25  $\mu\text{V}$  and a noise of 2.5  $\mu\text{V}$ , is considered good. A signal seen at less than 50  $\mu\text{V}$  is viewed with skepticism. A mid-diastolic potential seen in an infarct scar, which is barely larger than background noise, needs to be seen repeatedly and in the same relationship to other larger signals, in order to be believed to originate from biologic tissue. The frequency content of noise picked up from the patient/antenna can range from 50 Hz to significant harmonics.

[0114] FIG. 1 is a perspective view of the Huygens catheter 1. The catheter 1 is divided into three regions, a catheter tip 2, a sheath 3, and a handle 4. Handle 4 includes an tension adjustment knob 96 described in greater detail in connection with FIG. 38. FIGS. 2A-2C are three side views of the catheter tip 2. FIG. 2A is a transparent side elevational view of tip 2 showing the end nosecone electrode 5, for sets of half cylindrical electrode pairs 6 proximally positioned in tip 2 behind nosecone electrode 5. The electrodes 5, 6 are coupled to FPC 7 and separated by a flexible section 55 of FPC 7. The circuit elements 106 in tip 2, described below, are then carried on FPC 7 proximally from flexible section 55. FIG. 2B is a side elevational view of the exterior surface of the catheter tip 2 which is molded over tip 2 of FIG. 2A as described in connection with FIG. 33.

[0115] FIG. 33 is a perspective view of a low pressure overmold used to encapsulate catheter tip 2. After catheter tip 2 is fully assembled, as described below, it is placed between upper mold half 107 and lower mold half 111. A medical grade polymer is injected with low pressure through gate 115 distally from sleeve seal 117 on tip 2 to fully pot the electrode array 6 of tip 2. The polymer is forced through electrodes 6 up to nosecone electrode 5 and then exits through vent 116.

[0116] FIG. 2C is an exploded side view of certain components in the catheter tip shown in FIGS. 2A and 2B, namely nosecone electrode 5, one of the half cylindrical electrodes 6 with the remaining electrodes 6 omitted for simplicity, FPC 7, pull wires 45, electronics 106 and sheath wires 8 in the electrical cable embodiment of FIG. 3B, all of which components are described below.

[0117] FIG. 3A is a block diagram of the Huygens catheter 1 illustrating an embodiment of the catheter system using local amplifiers 11 coupled to the tip electrodes 5, 6. Catheter tip 2 includes an electronic flexible printed circuit

(FPC) 7, which carries an amplifier application-specific integrated circuit (ASIC) 11 communicated with a microcontroller 12 (MCU), a negative thermal coefficient thermistor (NTC) 14 having its output coupled to MCU 12, and a tip light ASIC 19 having its input coupled to MCU 12. The light ASIC 19 is optically coupled to the catheter sheath 3 via which includes an optical fiber 21, described in greater detail below. Catheter sheath 3 and optical fiber 21, which may be several meters long, is optically coupled to handle light ASIC 20 which is in the handle printed circuit board (PCB) 15. The handle PCB 15 also carries a digital signal processor (DSP) ASIC 18 that processes the data received from the tip 2. DSP ASIC 18 is communicated with a personal computer 52 or other control system (such as EnSite cardiac mapping system by Abbott of Plymouth, Minn. or CARTO electro-anatomical mapping system by Biosense Webster of Irvine, Calif.) through a conventional universal serial bus 53 (USB). The USB 53 provides universal asynchronous receiver/transmitter (UART) formatted data communication as well as providing an external power source to the catheter handle 4.

[0118] FIG. 3B is a block diagram showing a functional block diagram of an electrical cable embodiment of the Huygens catheter 1, where the optical system is replaced by an electrical or wired communication scheme. At the handle electronics 15, the handle light ASIC 20 is replaced by a power supply 17. Since the tip 2 is connected through an electrical wire bundle 8 in sheath 3, an impedance measuring ASIC 16 is added into the handle PCB 15. The catheter sheath 3 is coupled with wire bundle 8, which comprises six electrical wires, carrying the signals and power lines: VDD, GND, impedance input (IMP IN), impedance output (IMP OUT), data transmission (Tx), and data reception (Rx). These wires are coupled to the tip FPC 7, where Tx and Rx connect to MCU 12, VDD and GND to low dropout regulator (LDO) 13, and impedance input and output to the electrodes 5, 6.

[0119] FIG. 4A is a more detailed block diagram of the electronics 106 in catheter tip 2. The electronic FPC 7 of the catheter tip 2 is divided into three sections, electrode section 6, amplifier ASIC 11, and tip light ASIC 19. The electrode section 6 includes eight half ring electrodes 6, and one nosecone electrode 5 at the distal end of the tip 2. Amplifier ASIC 11 includes an 8-to-1 multiplexer (MUX) 22 coupled to electrodes 6, AC coupling circuit 23 coupled to MUX 22, which comprises of a capacitor and a resistor, which in turn is coupled to an instrumentation amplifier 24, described in greater detail in the embodiments of FIGS. 10-12, which amplifier 24 is coupled in turn to an analog-to-digital converter 25, which in turn is coupled to microcontroller MCU 12. Light ASIC 19 includes a 470 nm LED 27 electrically controlled by MCU 12 and its optical output coupled to dichroic mirror 30.

[0120] Power is supplied optically in a 850 nm beam carried by fiber optic 21 from handle 4 as diagrammatically shown in FIG. 3C. The 850 nm light is reflected by dichroic mirror 30 into photodiode 28, which has its electrical output coupled to a DC/DC photovoltaic regulator 29, whose output in turn is coupled to an LC frequency band filter 31, whose output in turn is coupled to a voltage supply line VCC coupled to all the circuits components in tip 2. The mirror 30 effectively filters the laser light input into the photodiode 28 to prevent the LED light from entering photodiode 28 and creating a noisy power source. The photodiode 28 receives



850 nm laser light from the optical fiber 21 to provide more than 20 mW of power. This native power is processed through DC/DC regulator 29 that outputs 3.3V which becomes the main voltage source of the tip electronics. This main voltage is cleaned through LC choke filter 31 that truncates the unwanted ripple voltages. The 450 nm light from bidirectional LED/photodiode 27 bidirectionally communicates data signals through dichroic mirror 30 to optical fiber 21, which is then sent to the optical receiver 15 located at the handle 4.

[0121] FIG. 4B is a block diagram of another embodiment using an electrical cable comprised of wires 8 instead of an optical signal. The light ASIC 19 of FIG. 3A is removed and electrical wires 8 that include supply voltage VDD, ground, Tx, Rx, impedance input, and impedance output are physically wired to corresponding inputs and outputs on the tip FPC 7. The nosecone electrode 5 serves as both impedance input and biopotential reader, which is selected from 2-to-1 multiplexer 26. The two first ring electrodes also serve two functions as impedance output and biopotential reader, which are also controlled from another 2-to-1 multiplexer 26. Therefore, the 2-to-1 multiplexer's 26 input is connected to an electrode, and the two outputs are connected to the input of the 8-to-1 MUX 22 and the impedance measuring trace respectively. When biopotential reading is selected, the 2-to-1 MUX shorts electrodes to the impedance traces. A small signal is sent from the IMP\_IN trace, travels to the nosecone electrode 5, measures the impedance of the contacting element, then travels out to the first ring electrodes 5 and outputs to the IMP\_OUT trace as shown in FIG. 4B.

[0122] The cardiac biopotential signal is first picked up by electrodes 5, 6. These native signals enter the corresponding inputs of the 8-to-1 multiplexer 22. The multiplexer 22 outputs all eight inputs from electrodes 6 serially to the AC coupling circuit 23. Circuit 23 comprises of a capacitor and resistor in a low pass filter circuit topology, which truncates unwanted wandering baselines and DC offset voltages. The coupled signal is coupled to the instrumentation amplifier 24 with a gain of 200. The amplified signal is coupled to ADC 25 and digitizes the analog signal and then is processed by MCU 12 to convert the signal into a UART format communicated on wire TX 8.

[0123] FIG. 6a is a schematic block diagram of another embodiment of Huygens catheter 1 with six electrical wires 8 coupling tip 2 to handle 4. The block diagram of tip 2 is divided into four dashed regions, an electrode region 54, a flexible bending region 55, an electronics region 56, and sheath electrical wires 8. Electrode region 54 includes eight half-ring electrodes 6, one nosecone electrode 5, and a negative temperature coefficient (NTC) thermocouple 14 to measure the temperature of the catheter tip 2. The bending region 55 does not include any electronic components, but only includes PB traces from the electrodes 5, 6 and NTC 14 to the MUX 22, 26. The electronic region 56 includes the rest of the electronic components such as the two 2-to-1 MUX's 26, the one 8-to-1 MUX 22, the AC-coupling circuit 23, instrumentation amplifier 24, the LDO's 13, and the microcontroller 12. The sheath region 3 includes the six electrical wires 8 which are designated impedance IMP IN & OUT, +5V, or VDD, ground, Tx, and Rx.

[0124] In the optical embodiment of FIG. 3A, the handle electronics 15 requires an optical receiver that retranslates the optical signals communicated on optical fiber 21 generated from the sensed data signals from tip electrodes 5, 6

back into corresponding electrical signals. The handle electronics 15 shown in FIG. 41 also requires a handle laser diode 57, diagrammatically shown in FIG. 3C, with minimum of 200 mW power that can supply a minimum of 20 mW power to the tip electronic board 7 at 850 nm. The 850 nm power from laser diode 57 is transmitted through dichroic mirror 58 optical fiber 21 to GRIN lens 41 in optical connector 39 of FIG. 25 coupled to tip FPC 7 and focused on photodiode 28 of FIG. 3C and FIG. 4A. The output of photodiode 28 is coupled to a voltage regulator 66 and then to a charge pump 65 as shown in FIG. 6b and then coupled to MUX 22, and IA 14. Laser 57 is included in this handle 4 as shown diagrammatically in FIG. 3C and it is controlled by a DSP 18. Laser 57 is coupled to laser driver circuit 123, controlled by DSP 18, and powered by 6V regulator 124. Regulator 124 in turn is powered by isolator 125. The 3.3V regulator at the handle 4 is supplying the microcontroller and amplifiers. Through this laser power regulation, the tip electronics can receive more stable laser power.

[0125] As shown diagrammatically in FIG. 3C bidirectional LED/photodiode 27 transmits and receives 415 nm optical data on fiber 21, which as shown in FIG. 41 is reflected in handle 4 by dichroic mirror 58 into photodiode 59, which provides a digital input to a transimpedance amplifier 121. The output of transimpedance amplifier 121 is input into a comparator circuit 122, whose output is a clean digital version of its input. The digital output of comparator 122 is provided as a data input microcontroller or DSP 18 and thence under program control to RX and TX inputs and outputs. The 450 nm LED signal from the tip electronic FPC 7 is transmitted through the single mode optical fiber 21 to the handle receiver circuit 15. As diagrammatically shown in FIG. 3C, handle dichroic mirror 58 filters the signal from the output laser 57. The filtered optical input signal is reflected into the photodiode 59 in the photo conductive mode to generate an electrical current output proportional to the received optical input. The current is input into transimpedance amplifier 60 that outputs corresponding voltage and a clean electrical digital signal is formed through a comparator circuit 69. This signal is then processed and interpreted through the DSP 18.

[0126] FIG. 6B is a block diagram of the embodiment of the catheter tip electronics with an optical interface. Optical connector 39 is comprised of 850 nm photodiode 28, 450 nm LED 27, a dichroic mirror 30, and two lenses 40, 41 for collimation. The optical connector 39 receives 850 nm laser light from the optical fiber 21, collimates it through the GRIN lens 41, and transmits it to photodiode 28. The photodiode 28 outputs a proportional electrical current which is coupled to a photovoltaic voltage regulator 29 to generate a stable 3.3V voltage. The 3.3V output of the photovoltaic voltage regulator 29 becomes the main voltage source that powers MUX 22, instrumentation amplifier (IA) 24, ADC 25, and MCU 12. Data sensed by electrodes 5, 6 are selected by MUX 22, which is controlled by MCU 12. These data are multiplexed through MUX 22 to AC coupling circuit 23, which functions to eliminate DC offset from the native signal in order to avoid clipping from the amplifier. The data signal is amplified by IA 24, converted to a digital signal by ADC 25, and provided as data output to MCU 12 in a form of serial peripheral interface (SPI) protocol. The digital data signal drives 450 nm LED 27, whose output is collimated through the spherical lens 40 and directed into optical fiber 21.

[0127] Electrical System Requirements

[0128] The system input frequency range of the catheter determines the filter spectrum and its specification.

TABLE 1

System Input Frequency Requirement		
Requirement	Values or Configuration	Comments
EGM LF cutoff, $f_L$	30 Hz	30 Hz rejects undesirable baseline wander in bipolar EGMs due to far-field LF signals. Fixed $f_L$ 1 <sup>st</sup> order HPF likely sufficient at catheter front-end.
EGM HF cutoff, $f_H$	500 Hz max.	Assume digitization rate of 1 kS/s/channel unless oversampling used. Overall roll-off above $f_H$ should be 18 dB/octave (3 <sup>rd</sup> order filter)
EGM pass-band	Should be as flat as possible to preserve signal morphology	Butterworth filter characteristics
60/50 Hz power line interference rejection		60/50 Hz is within the EGM pass-band and mainly common-mode. System depends on good CMRR. DSP 60/50 notch filtering provision needed, but commonly distorts signals of interest.

[0129] The front-end amplifier ASIC 11 at the AC-coupling to the instrumentation amplifier IA 14 requires an electrical specification for safety and quality purposes.

TABLE 2

Amplifier Circuit Requirement		
Requirement	Values or Configuration	Comments
Inputs	Differential	
Electrode-amplifier coupling	AC coupling (TBD)	AC coupling likely required to reject DC electrode overpotentials, but requires close coupling capacitor matching to preserve CMRR. See section 6.2.
Stage input impedance	$\geq 20$ M $\Omega$ and well-matched	The higher the better. Hi-Z is required to minimize CMRR degradation due to electrode-tissue impedance difference. Must account for amplifier input bias current return path impedance. See section 6.1.
EGM low amplitude detection	$\leq 30$ $\mu$ Vpp required	The lower the better.
Amplifier Input-referenced noise	<5 $\mu$ V desirable	The lower the better.
EGM max. signal level	30 mVpp	
Differential AC max. signal level	Under investigation	Assume 50 to 100 mVpp at this time
Differential DC max. signal level	Up to $\pm 200$ mV	Due to platinum electrode polarization. Argues for input AC coupling.

[0130] Each intracardiac electrogram (EGM) channel is digitized to a resolution that does not limit channel sensitivity. Table 3 shows the minimum resolution required for ADC 25 to detect the lowest input signal. Assume the gain of instrumentation amplifier 24 is 200, the minimum resolution required is 4 mV. Table 4 shows the voltage resolution of the least significant bit (LSB) of the ADC 25 at different numbers of bits. Assume the 10-bit ADC is used with reference voltage of 3.3V, the resolution of this ADC 25 is around 3.2 mV. Since the resolution of ADC 25 is below the minimum input voltage specification, 10-bit ADC 25 is accurate enough to be used in catheter tip system.

TABLE 3

Minimum Input Voltage Calculation		
Minimum Input Voltage [in $\mu$ V]	Gain	Minimum Amplified Input Voltage [in mV]
20	1	20
	10	200
	50	1000
	100	2000
	150	3000
	200	4000
	250	5000

TABLE 4

ADC Voltage per Bit Calculation							
ADC Ref Voltage [in V]	10	12	14	16	18	20	ADC Bits
3.3	3222.656	805.6641	201.416	50.354	12.5885	3.147125	Bit Count
	Voltage per bits [ $\mu$ V/bit]						



**[0131]** Catheter Design Overview**[0132]** Huygens Catheter

**[0133]** The Huygens catheter 1 comprises the tip 2, the sheath 3, the handle 4, and the robotic arm 1 as shown in FIG. 1. The catheter tip 2 amplifies and translates biopotential signal into a precise digitalized electrical (or optical) signal. The sheath 3 contains all the mechanical integrity to provide durability and flexibility that is required during diagnostic procedure. The sheath 3 functions as the bridge that transmits the digitalized signal from the tip to the handle 4. Finally, the handle 4 processes the digitalized signals by undergoing digital signal processing and sends them to the mapping station and personal computer. The Huygens catheter handle 4 has capability to be coupled with the robotic arm.

**[0134]** Catheter Tip

**[0135]** The Huygens catheter tip 2 contains eight half-ring electrodes 6, one nosecone tip electrode 5, a flex printed circuit board (FPC) 7, and six holes 62 for electrical wire connector as shown in FIGS. 3A and 3B. If the catheter uses an optical system, then the tip additionally contains optical connector 39 . . . . Initially, the catheter tip diameter is 11 French (3.67 mm) or less and 82 mm long. The tip FPC 7 is a six-layer board with thickness of 0.34 mm and bend radius of 8.1 mm. Each of the nine electrodes 5 and 6 are connected to the assigned MUX 22 inputs that will be processed through the tip electronic circuits.

**[0136]** Tip flex printed circuit board (FPC) 7 is 82 mm long and 3.4 mm wide to fit in a 11 French system. The FPC 7 is divided into three sections, electrode region 54, bending region 55, and electronic region 56. As shown in FIG. 14, the electrode region 54 covers from the most distal tip and it is 23 mm long, followed by 29 mm of bending region 55. Finally, the last 30 mm of FPC is electronic region 56 with a small tail that contains six vias 62 for the electrical wire connection from the sheath 3.

**[0137]** Electrode region 54 as shown in FIG. 17A is the most distal region of FPC 7 that contains all nine electrodes (eight half-ring 6 and one nosecone 5). In the illustrated embodiment FPC 7 is a six layer printed circuit board, namely six layers of copper with intertying insulating layers. FIGS. 16, 17A-17C are top views in which all six layers are visible through the overlying layers. To provide more flexibility, the copper pour on top and bottom layers of FPC 7 are removed. Also, to protect copper traces from bending, all the electrode signal traces run on the inner layers. Next to each electrode, there is corresponding transient voltage suppression (TVS) diode 63 shown in FIG. 8 to protect the traces and electronic components from damage due to possible over voltage/over current from the patient body. The electrode region 54 also includes NTC thermistor 14 to measure the temperature of the patient body for safety purposes.

**[0138]** FIG. 17B shows the bend region 55, where most of the tip deflection occurs. Therefore, this region contains no copper pour as well as no electronic components. Bend region only contains nine traces from the electrodes on the inner layer. In order to provide most bending in this region 55, the width of this region is 2.0 mm compared to 3.4 mm width on the other two regions 54 and 56.

**[0139]** The electronic region 56, shown in FIG. 17C, includes all the electronic components required to perform amplification, digitization, and serialization, as well as electrical to optical conversion if the catheter contains optical

system as shown in FIG. 4A and FIG. 4B. These components include 8-to-1 MUX 22, 2-to-1 MUX 26, instrumentation amplifier 24, analog to digital converter 25, LDO 13, and microcontroller 12. To provide stable grounding, the top and bottom layer of the board is copper poured to ground. Due to the 11Fr limitation, the height of the components on this region must not exceed 1.5 mm (1.5 mm+0.34 mm+1.5 mm=3.34 mm).

**[0140]** As best seen in FIG. 13, Huygens catheter 1 is designed to be quadripolar (4 electrode rings), with two half-ring electrodes 6 per ring and a nosecone tip electrode 5, totaling nine electrodes reading biopotentials. Each ring 6 is divided into top and bottom portions respectively to precisely locate and isolate the tissue wall from the blood. Each electrode 5 and 6 can perform a unipolar reading, or it can combine with adjacent electrode to perform bipolar readings. The catheter 1 is limited to eight electrodes 6 due to the maximum input in a single multiplexer 22. Any additional electrode will require extra MUX capacity which is not recommended in the confined dimension.

**[0141]** Nosecone Tip Electrode

**[0142]** FIG. 19 is a perspective view of the tip electrode 5, which is the most essential element that the physician needs during diagnostic operation. This electrode 5 is coupled to the first input of the amplifier MUX 22 and connected to the impedance measuring MUX 26 in FIG. 4B. Therefore, nosecone tip 5 can function as the biopotential reader or an impedance measuring tool depending on the switch bits from the microcontroller 12.

**[0143]** Ring Electrode

**[0144]** FIG. 22 is a three dimensional view of a half-ring electrode 6. This electrode is mounted both top and bottom side of the electrode region 54 of tip FPC 7. Each half-ring band 6 is coupled to an independent MUX 22 input, except for the first ring band, where both top and bottom bands 6 are connected to the same second input of MUX 22. This is due to the nosecone electrode 5 being the 1<sup>st</sup> input, and since it requires a bipolar pair, both electrodes on the 1<sup>st</sup> ring band needed to be connected to the same MUX 22 input. The first ring band 6 is also connected to impedance MUX 26 where the electrode 6 can function both as a biopotential reader or as an impedance measuring tool. For bipolar measuring feature, there is a big gap between the second and third ring, and the rest of the rings are closely placed as shown in FIG. 14. The first and second ring can be a bipolar pair, as well as third and fourth ring.

**[0145]** Safety Wire

**[0146]** Safety wire 9 is a wire that is connected from the center lumen of the sheath 3 to the nosecone tip 5. It ensures that no components are left in the body when the catheter 1 is pulled out. This part requires high durability and very secure connection with the nosecone electrode 5 as shown in FIG. 21. It is electrically isolated to prevent from creating an antennae effect. In order to achieve electrical isolation, the tip of the pull wire 45 with a hypotube 37 is covered with a polyetheretherketone (PEEK) insulator 38.

**[0147]** Tip Electronics**[0148]** Multiplexer (MUX)

**[0149]** There are two types of multiplexers in the catheter tip system, an 8-to-1 MUX 22 and 2-to-1 MUX 26. The 8-to-1 multiplexer 22 in FIG. 4A is an eight-input, single-output, low-powered multiplexer. Each electrode 5, 6 is connected to a corresponding MUX input. In order to provide high resolution at the output stage of the catheter 1,

the MUX **22**, **26** is continuously switching at a rate of 10K samples per second. Multiplexers **22**, **26** have the smallest dimension that can fit inside a catheter, namely 2.6 mm×1.8 mm×0.5 mm.

The 2-to-1 MUX **26** is a two-input single output multiplexor that is connected to the nosecone electrode **5** and the first band of the half-ring electrodes **6**. This multiplexor **26** selects the function of the connected electrode either as a biopotential reader or impedance reader through the control of the microcontroller **12**.

**[0150]** Instrumentation Amplifier (IA)

**[0151]** The instrumentation amplifier (IA) **24** in FIG. **4A** and better shown the schematics of FIGS. **10-12** is a 65  $\mu$ A low-power instrumentation amplifier **24**. With high input impedance, it can achieve up to 130 dB of common mode rejection ratio (CMRR). The gain can be physically programmed by the two gain pins G1, G2, and by connecting both gain pins to VDD, the amplifier is set to have the gain factor of 200. The differential input of IA **24** includes a capacitor-resistor circuit that functions as an AC-coupling circuit **23**. This amplifier **24** is one of the smallest IA **24** in the market with dimension of 1.26 mm×1.23 mm×0.6 mm.

**[0152]** Instrumentation amplifier **24** must have an AC-coupling circuit **23** to remove the DC offset voltage. Three different AC-coupling techniques were presented as shown in FIGS. **10**, **11**, and **12**. FIG. **10** shows a capacitor-resistor circuit **32** that includes an active op amp **70**. This circuit **32** not only has AC-coupling effect, but also provides high common mode rejection ratio (CMRR) and electrode to electronics isolation. The CMRR value is directly proportional to the input impedance of the amplifier **70**. Since the resistors **71** are connected to the inputs **72** of another op-amp **73**, the input impedance of IA **24** is maintained, which preserved the high CMRR value.

**[0153]** The IA **24** of the embodiment of FIG. **11** uses a common high-pass filter with a simple capacitor-resistor circuit **33**. Since the input resistor **74** is in parallel with the IA **24** inputs, the equivalent input impedance will be reduced, which leads to lower CMRR.

**[0154]** Another embodiment shown in FIG. **12** has an AC-coupling circuit **23** option located at the output of an IA **24**. Output of the op-amp **24** is communicated to the reference pin **75** of the IA **24**, which regulates the voltage level.

**[0155]** From the theoretical assessment, the first IA embodiment **32** of FIG. **10** yields the best result by providing AC-coupling, high CMRR, and electronic isolation to electrodes. However, an extra Op-Amp, four resistors and two capacitors might cause a space issue in FPC **7**. The second embodiment **33** in FIG. **11** will be most promising in its simplicity, but the low CMRR must be carefully examined.

**[0156]** The resistance and capacitance of the AC coupling circuit **33** of FIG. **11** is determined by the following equation:

$$F_c=1/(2\pi RC)$$

**[0157]** Where  $F_c$  is the high-pass cutoff frequency, and R **74** and C **76** are the corresponding resistance and capacitance values. Solving for  $F_c=1$  Hz and R=1 M $\Omega$ , we get capacitance of

**[0158]**  $C=1/(2\pi RF_c)=1/(2\pi(1\times 10^6)(1))=159$  nF. Instead of 159 nF capacitance a more standard value of 220 nF is

chosen. Redoing the calculation with a 220 nF capacitance and 1 M $\Omega$  resistance, a cutoff frequency of 0.72 Hz is obtained.

**[0159]** Analog to Digital Converter (ADC)

**[0160]** The ADC **25** in FIG. **4A** is an 18-bit, pseudo-differential successive approximation register (SAR) ADC **25**. Input voltage of 3.3V is connected to the reference pin, which defines the resolution of this ADC **25** as

$$\frac{3.3V}{2^{bit}} = \frac{3.3}{262144} = 12.5 \times 10^{-6} = 12.5 \mu V \text{ per bit.}$$

② indicates text missing or illegible when filed

The digitized data is transmitted to the MCU **12** in a 3-wire serial peripheral interface (SPI). This device has a dimension of 3 mm×3 mm×0.75 mm.

**[0161]** Due to the spatial constraint, an internal ADC included in microcontroller **12** can be used. This internal ADC from MCU (PIC16F15224) has a 10-bit with reference voltage of 3.3V. This resolution can still meet a required specification of biopotential resolution.

**[0162]** Low Dropout Voltage Regulator (LDO)

**[0163]** FIG. **4B** shows low dropout voltage regulator **13** that feeds in the external voltage from the handle **4** and regulates it to a useable 3.3V supply for the entire tip electronics. FIG. **9** shows a schematic form of the LDO **13**. Each output and input are connected to a 1  $\mu$ F capacitor **77** for ripple reduction, and additional LC filter **31** is required for more stable voltage supply.

**[0164]** Microcontroller (MCU)

**[0165]** The microcontroller **12** in FIG. **4B** is a 16-bit, low-powered, PIC microcontroller **12** that has a dimension of 3 mm×3 mm×0.9 mm. This component controls the sampling rate of MUXs **22** and **26**. It also contains an internal ADC that can digitize the amplified biopotential signal. PIC16 microcontroller **12** processes the digitized biopotential data and NTC thermistor **14** output to a universal asynchronous receiver-transmitter (UART) format and outputs it to the handle **4**. If the catheter **1** contains optical system as shown in FIG. **3A**, the UART output is coupled to LED **27** to convert the digitized data to an optical data signal.

**[0166]** Step-Up DC/DC Voltage Regulator

**[0167]** LTC3105, a step-up DC/DC converter **29** shown in FIG. **4A** is used for light energy harvesting application. The parallel resistor network of 1 M $\Omega$  and 2.2 M $\Omega$  resistors regulate the output voltage to be 3.3V. This device contains a MPPC pin that maximizes power generation in I-V curve. The input pin is connected to the photodiode **28**, which generates an electrical current proportional to the photonic power received. This device has a dimension of 3 mm×3 mm×0.75 mm.

**[0168]** Optical System

**[0169]** Optical Connector

**[0170]** A mechanical optical connector **39** shown in two views in FIGS. **24A** and **24B** connects optical fiber **21** from the sheath **3** to the optical system at the catheter tip **2**. It is mounted at the distal end of main FPC **7**. The main purpose of the optical connector **39** is to precisely align GRIN lens **41**, dichroic mirror **30**, LED **27**, laser and photodiode **28** to minimize the photonic power loss. The four legs of the connector secure the FPC **7** bending angle to be consistent



as shown in FIG. 25. The back surface of the connector 39 has a pressure sensitive adhesive (PSA) and attaches to the tail FPC 7.

**[0171]** Photodiode

**[0172]** FIG. 25 shows four arrays of photodiodes 28 in parallel to detect the 850 nm laser light from the handle 4. The design input of photodiode array 28 requires a large active area to capture as much light energy as possible. Array 28 can achieve the design requirement with a component dimension of 2 mm×1 mm but total active area of 1.71 mm<sup>2</sup>. This data gives the percentage of active area on the surface of the photodiode 28:

$$\% \text{ of Active Area} = \frac{1.71\text{mm}^2}{2\text{mm} \times 1\text{mm}} \times 100 = 85.5\%$$

**[0173]** The purpose of photodiode array 28 is to provide electrical power to the tip electronics. Therefore, the photodiode array 28 needs to be in zero-biased configuration to operate in the photovoltaic mode.

**[0174]** 470 nm LED

**[0175]** LED 27 is 470 nm InGaN LED 27 that transmits the optical signal to the catheter handle 4. One of the design requirements for tip electronics is to minimize the power, so an LED 27 with low power consumption is selected. This LED 27 operates at a forward voltage of 2.65V and 2 mA current. The total power consumption is 2.65V×2 mA=5.3 mW. Another design requirement of the LED 27 is to provide maximum light intensity to the handle 4 in order to minimize the signal distortion. LED 27 can emit 45 millicandela of luminous intensity at a view angle of 100°. To transmit most of the light through the optical fiber 21, a spherical micro lens 40 in FIG. 25 is attached directly on top of the LED 27 to collimate the dispersing light.

**[0176]** Dichroic Mirror

**[0177]** A 700 nm shortpass dichroic mirror 30 filters the laser 64 light from the LED 27 light and vice versa. It is coupled with the optical connector 39, which transmits the 470 nm LED 27 light to the catheter sheath 4 and reflects 850 nm laser 64 light directly to the photodiode 28. FIG. 26 shows the transmission and reflection of the mirror 30 at different frequencies. The dichroic mirror 30 is diced by the wafer manufacturer in 2.5 mm×2.5 mm dimension and is 0.5 mm thick to fit inside the optical connector 39.

**[0178]** Spherical Micro Lens

**[0179]** The spherical ball micro lens 40 schematically shown in FIG. 28 is required in a catheter optical system to collimate the 470 nm LED 27 light to the optical fiber 21. It is an uncoated lens of size 1.0 mm in diameter with effective focal length (EFL) of 0.55 mm and clear aperture of 0.8 mm. With the given EFL and clear aperture (CA), the calculated f/CA is:

$$\frac{f}{CA} = \frac{\text{Effective Focal Length}}{\text{Clear Aperture}} = \frac{0.55\text{mm}}{0.8\text{mm}} = 0.69$$

**[0180]** The working distance of this component 40 is only 0.05 mm, so it must be placed very close to the source of LED 27.

**[0181]** Gradient Index (GRIN) Lens

**[0182]** The GRIN lens 41 in FIGS. 25, 29 is required in the optical system to collimate the laser 64 light from optical fiber 21 to the photodiode 28. It has 0.25-pitch with diameter of 1.0 mm. Since the length is 2.61 mm, this part will be cut to fit inside the optical connector 39. The working distance is 0.21, so it is placed very close to the fiber 21.

**[0183]** From the simulation, the GRIN lens 41 has different bending across the light spectrum. 470 nm of light concentrates more than the higher wavelength light (870 nm) as shown in FIG. 30.

**[0184]** The center focus of GRIN lens 41 needs to be very precise. According to the simulation shown in FIG. 31 the light rays 78 entering the GRIN lens 41 with more than 10 μm offset from the center would disperse and be lost.

**[0185]** Optical Fiber

**[0186]** Optical fiber 21 is a single mode fiber strand with 980 μm core diameter and 1.0 mm cladding diameter. It is a plastic fiber optic (POF) which provides resilience under tension and bending. It is also a better option than a glass optical fiber when transmitting light within a visible light spectrum. It has a numerical aperture of 0.5, so the dispersion angle will be arcsin(0.5)=30°. To prevent light dispersion from the optical fiber 21, a GRIN lens 41 is attached on the optical connector 39 to collimate the light to the photodiode 28.

**[0187]** Sheath

**[0188]** The catheter sheath 3 shown in the cutaway view of FIG. 32 shows braids and layers of Prebax material to achieve required durability and flexibility. It contains a bundle of six electrical wires 8 to transmit power from the handle 4 to the tip 2 and also transmit data from the tip 2 to the handle 4. There are two pull wires 45 from the handle 4 to the center ring, located at the proximal end of tip FPC 7. These pull wires 45 perform deflection of the catheter tip 2 at one axis, 140° bend on both directions from the centerline. From the center ring, these pull wires 45 change to a safety wire 9 made of PTFE liner as shown in FIG. 21. Since the region containing FPC 7 lacks durability and resilience, two stiffeners 79 are added to the safety wire 9 to provide rigidity. If the catheter 1 employs an optical data scheme, then the electrical wire bundle 8 is replaced with a single mode optical fiber 21.

**[0189]** Handle

**[0190]** Electrically, handle 4 includes a handle printed circuit board (PCB) that carries a microcontroller, a +5V DC/DC regulator, a +3.3V LDO, a power and signal isolator, an impedance measuring circuitry, and an USB connector to send the data to the mapping station as shown in FIG. 41. Mechanically, handle 4 includes a pull wire, a sled, a pulley, and a knob to perform a deflection at the tip when the knob is rotated as shown in FIG. 37.

**[0191]** Impedance Measuring Circuit

**[0192]** The impedance measuring circuit 80 controls the frequency of its output to indicate the impedance of the load at its input within a specified frequency range. The circuit 80 measures the sensed input impedance from 1 KΩ to 10 MΩ, but with additional circuitry, it can measure all the way down to 1000. The microcontroller 81 sets the sensing frequency to a stable 1 KHz. Circuit 80 sends a small 1 KHz current to the nosecone electrode 5 through the catheter sheath 3 and to the 2-to-1 MUX 22 as shown in FIG. 5. The current travels through the tissue load that is in contact with the nosecone electrode 5 and returns to the first ring electrode 6 and finally back to the impedance measuring circuit



**80** in handle **4**. Measured impedance is transmitted to handle microcontroller **81** through inter-integrated circuit, (I2C) protocol serial communication. Since the impedance of a blood pool is around 900 and cardiac tissue is around 1200, additional amplifier circuit is required in the return path of impedance sensing pins, IMP IN, IMP OUT.

**[0193]** 5V DC/DC Regulator

**[0194]** 5V DC/DC regulator receives a raw power from an external power source and steps down to a stable 5V, which supplies both 3.3V LDOs at the tip **2** and the handle **4**. Before supplying the output voltage to the catheter electronics, external power is coupled through an isolator **83** to provide an electrically isolated system.

**[0195]** Signal/Power Isolator

**[0196]** Electrical safety is a critical requirement in a minimally invasive medical device such as catheter **1**. In order to prevent the catheter **1** from delivering a fatal electrical current to the patients' body, all the power and electrical signals must be isolated from the outer environment. Texas Instrument's power and digital isolation provides up to 5000 VRMS isolation. It includes an isolation transformer for power and isolation capacitors for data inputs and outputs. The isolation circuit **83** is used in the Huygens catheter **1** is IEC 60601-1 compatible. IEC stands for International Electrotechnical Commission. IEC provides a standardized approach to testing and certification, IEC testing brings together the agreed upon set of rules, specifications, and terminology that allow manufacturers to have their devices tested for conformity.

**[0197]** Microcontroller

**[0198]** The microcontroller (MCU) **81** transmits and receives data from the tip **2** through UART communication. After receiving the digitized signal, the MCU **81** performs digital signal processing (DSP) to filter the noise and additional unwanted signals or baseline low frequency wanders. Also, it will restore the multiplexed digital signal into eight independent signals, each signal representing each electrode **6**. After running the digital signal processing, all the processed data are translated to a USB protocol communicated to the isolator circuit **83** and finally sent to an external mapping station in the operating room.

**[0199]** As shown in FIG. 13, by directionally limiting the contour of a single electrode **6** to a segment of the full catheter diameter (and thereby reducing its surface to a facing area), when placed in contact with myocardial tissue, the effective contact surface area of a single split electrode is maximized, while its paired opposite electrode may still be in full contact with the blood pool. The impedance data collected by the contact electrode therefore comprises a greater degree of direct signal from the tissue being studied, while any far-field signals being received by the complementing split electrode of the pair is exposed to the blood and can be discriminated from the tissue-based signal. The sampling from the exposed electrode **6** can be discerned apart from the fine-resolution transient myocardial signals of interest in the 10  $\mu$ V range, and further attenuated from the locally-amplified output by noise cancellation filtering capabilities of the digital signal processor **81** (DSP) if desired. FIG. 34 is a pair of illustrations aligned with a graph of impedance verses time, which depicts the impedance measurements made by an electrode **6** in the blood pool on the left half of the illustration and graph, and in myocardial contact on the right half of the illustration and graph. Illustrated on the left half in the bottom of FIG. 34 is a line

of the local impedance as a moving average and above that a line showing impedance both below 100 ohms. On the right half, the tip of the catheter **1** makes myocardial contact and both moving average and generator impedance jumps up to about 120 ohms with local impedance raw data shown as riding on top of the moving average.

**[0200]** Catheter Contact Force in Forming an Electroanatomical Map

**[0201]** The degree of force applied to myocardial tissues by the catheter tip **2** is an existing concern in various EP catheterization procedures, most commonly that of RF ablation where firm contact with the ablation site of interest is required to create a lesion with the depth needed for full isolation. From a patient safety standpoint, force control and measurement at the catheter tip **2** is also a desirable precautionary feature to regulate the application of mechanical pressure which can be potentially damaging to endocardial structures. Similarly, contact force (CF) has significance in EP mapping procedures, where there is a direct correlation of the degree of electrode-tissue contact with the quality of the bioelectrical signal detected.

**[0202]** While visualization methods are of primary importance during such procedures, intuitive navigation assistance methods which can improve physician accuracy and procedural efficacy remain a promising potential as an augmentation of standard practices. Ostensibly, the design of a "smart" catheter **1** should incorporate feedback from a number of digital sensory components with the goal of reducing the abstractions of the remotely-guided tool, and enhancing the ability of the physician to better perceive the tool as an extension of his or her own body to perform the most delicate of manual tasks. The scalpel, the needle and the saw are all tactile, intuitive implements compared to a catheter, a remote-controlled camera or a marionette. To bridge the gap between the virtual and the intuitive, the Huygens catheter **1** is designed with such intention.

**[0203]** While the actual force of contact could be measured, the measurement of local impedance (LI) provides greater insight into catheter-tissue coupling, and this information is already at our disposal directly. Because of the material difference between the impedance of myocardial tissue and that of the blood pool medium (appx. 130 $\Omega$  vs. 90 $\Omega$ ), any recorded signal can be evaluated by a corresponding resistance measurement; signals below a desired threshold can be selectively squelched, providing a complementary data masking channel for discriminate signal filtering between "hot" localized measurements and "cool" proximal measurements which are much more susceptible to the influence of far-field signals. This extra layer of surrogate information can be feasibly extrapolated for use in visual displays, audio enhancements, device feedback and control, including those of approximate force determination, haptic response, and conceivably extensible to pseudo-robotic automated functions.

**[0204]** In another embodiment, as the optical catheter gathers, digitizes and records all signals received in addition to parametric data about the state of the device itself, such as degree of deflection and orientation to a fiducial reference, this data is indexed to a lookup table, permitting various forms of detailed analysis including, but not limited to, a correlation of the extent of deflection from the control potentiometer in the handle **4** to the clarity and position of the measured impedance from the distal electrodes **5**, **6**. Real-time comparative operations on this matrix yields a



qualitative assessment of the electrode-tissue interface at the time of recording to provide further indication of optimal contact with the target structure.

[0205] FIG. 37 illustrates the various portions of catheter 1. The distal 20 mm is comprised of the electrode assembly 85, a puller wire terminus 84 proximally distanced from electrode assembly 85 by 82 mm, the catheter cable or sheath 3 approximately 85-90 cm long, and a proximal handle 4. As shown in FIG. 37 electrode assembly 85 includes semicylindrical ring electrodes 6 and nosecone electrode 5 mounted on PFCB 7. Running parallel to PFCB 7 is an insulated safety or retention wire 86 coupled to PFCB 7 through a block 87 to each electrode pair 6 and to tip electrode 5. The construction of puller wire terminus 84 is better shown in FIG. 37B wherein opposing metallic pull wires 45 on each side of catheter cable 3 are provided with polytetrafluoroethylene (PTFE or Teflon) liners 88 to lubricate the ease of movement of wires 45 under catheter sheath 3. Wires 45 are fixed or welded into sleeves 89, which in turn are fixed to pulling ring 90. Puller ring 90 is firmly attached or fixed both to catheter cable 3 and to electrode assembly 85 comprising the distal portion of catheter 1. Differential tension on pull wires 45 applied from handle 4 allows catheter 1 and its tip 2 to be steered. The catheter cable 3, which is ordinary very soft and flexible, is sheathed by a reinforcing open flat braid 91, which renders it torqueable. As shown in FIG. 37C the more proximal portion 92 of catheter 1 is comprised of inner and outer higher durometer Prebax tubing 93 (i.e. from handle 4) while the more distal portion 94 of catheter 1 is comprises of inner and outer lower durometer Prebax tubing 95 (i.e. 35 to 40 mm). Prebax is a block copolymer variation of PEBA (polyether block amide). It offers the great processing versatility across a range of flexural modulus and provides excellent mechanical, physical, chemical properties along with established biocompatibility in many commercial products. Prebax processing versatility allows it to be used in products that have a range of stiffness from soft distal segments of a catheter to stiff proximal segment for providing pushability along with smooth stiffness transitions to the distal segment for precise tip response and control. For these reasons Prebax is one of the most commonly specified polymer systems for catheter and medical tubing applications.

[0206] On the proximal end of catheter cable 3 is a manually operated embodiment of the handle 4 shown in cutaway view of FIG. 38, which includes a knob 96, sled 97 longitudinally movable in handle 4 and pulley 98. In FIG. 38 the distal end of handle 4 is to the left in the drawing and the proximal end of handle 4 is the right in the drawing. As seen in the transparent view of FIG. 38 a pin 99 is retained in a longitudinal slot 100 defined in a stationary cylindrical body 101 concentric with cylindrical knob 96. Pin 99 engages a helical track 102 defined into the interior hollow cylindrical surface of knob 96. As knob 96 is rotated, pin 99 is longitudinally advanced or retracted in slot 100. Pin 99 is connected to a longitudinally movable cylindrical body 112 concentrically disposed in cylindrical body 101 in which slot 100 is defined. Body 112 is connected to sled 97, so that as pin 99 is longitudinally displaced in slot 100 and body 112 longitudinally displaced, sled 97 with guide 109 is similarly longitudinally displaced relative to fixed guides 105 on both sides of guide 109. Guides 105 and 109 have aligned slots 108 defined in each of them into which longitudinally movable rods 104 and 113 are retained and guided. Rod 104

has a stop 110 disposed thereon between movable guide 109 and the proximal fixed guide 105 as seen in FIG. 38. As best seen in FIGS. 39A and 239B rod 113 has a stop 114 disposed thereon between movable guide 109 and the distal fixed guide 105. One end of pull wire 45, led from sheath 3 through handle 4, is connected to the distal end of rod 104 and the opposing end of pull wire 45 is connected to the proximal end of rod 113. The opposing end of pull wire 45 is connected to rod 113 and is bent around pulley 98 and led distally out of handle 4 to sheath 3.

[0207] Thus, as best seen in FIG. 39A when knob 96 is rotated to move pin 99 to its most proximal position, the end of pull wire 45 connected to rod 104 is fully tightened and sled 97 moved to its most proximal position in handle 4, moving rod 104 by means of stop 110 bearing against movable guide 109 and moving rod 104 to its most proximal position. This allows rod 113 to longitudinally move in the proximal direction thereby slackening the opposing end pull wire 45 connected to rod 113. The degree of slackening is determined by the mechanics in catheter tip 2 and is only limited by means of stop 114 on rod 113 bearing against movable guide 109, if at all. The net result is that catheter tip 2 will be bent in a first direction. The degree of bending of catheter tip 2 will depend on how much pull wires 45 are tensioned and slackened or by the degree of rotation of knob 96.

[0208] Similarly, as seen in FIG. 39B, when knob 96 is rotated to move pin 99 to its most distal position, the end of pull wire 45 connected to rod 113 is fully tightened and sled 97 moved to its most distal position in handle 4, moving rod 113 by means of stop 114 bearing against movable guide 109 and moving rod 113 to its most distal position. This allows rod 104 to longitudinally move in the distal direction thereby slackening the opposing end pull wire 45 connected to rod 104. The degree of slackening is determined by the mechanics in catheter tip 2 and is only limited by means of stop 110 on rod 104 bearing against movable guide 109, if at all. The net result is that catheter tip 2 will be bent in a second direction opposing the first direction.

[0209] Optical fiber 21 from catheter sheath 3 is lead back through handle 4 to PCB 15 on which is the circuitry of FIG. 3A. With the catheter handle control, the tip 2 of catheter 1 must be able to perform an axial movement of 180° in each of two defined directions. Also, the tip 2 needs to maintain its position when the pull wire 45 is at rest. The handle 4 provides many features such as motorized tip control and tip-pressure haptic feedback for ergonomics, as well as contact-force measurement that can accomplish far more accurate diagnostics.

[0210] The rapid growth in illness and death related to hypertension has put tremendous pressure on the medical field to develop better cures for those whose high-blood pressure cannot be remedied with medication and life-style changes. One of the potential cures that has been of great interest is in the area of renal denervation (RD). RD seeks to minimize or eliminate persistent hypertension through the ablation of the renal nerves in the kidney that regulate the release of renin, a protein produced by the kidneys that regulates the body's mean arterial blood pressure. The basic proposition and understanding of how RD can impact hypertension has been well researched and extrapolated, but effectively being able to perform the procedure with consistent degrees of success has fallen far short of expecta-

tions. The issue is twofold and lies in the inability for current EP mapping and detection tools to be able to overcome these challenges.

**[0211]** The first is that unlike the nerves in the heart, which are well known and fixed in their location that when ablated restore normal rhythms, the sympathetic renal nerves formation and location is individualized to each person. Much like a tree, the renal nerve plexus consists of a branching network of nerves that grow out from one another and attach to the renal artery in completely random locations. This makes locating them much harder to do.

**[0212]** The second issue is that the electrical signals that the nerves produce is not a consistent regular pattern as can be measured in the beating of the heart, even an irregular beating one. Instead, electrical impulses only occur when a biologic event occurs that triggers the nerve to signal the brain, which then signals back to the kidney to release renin. It is much like trying to find a road that can only be seen when the streetlight comes on with no way of knowing when that will happen. In addition, the signals that are produced are of a very high frequency and extremely short duration that makes capturing them for mapping purposes extremely difficult with the resolution of current EP mapping systems.

**[0213]** Including a programmable pulse generator, the disclosed EP catheter delivers a pacing pulse at a fixed rate and then senses a return response from the renal nerve ending like the sensed local native cardiac signal. In this way, the active renal nerves are mapped and an appropriate renal denervation or ablation plan is devised and executed.

**[0214]** Therefore, it must be understood that the illustrated embodiment has been set forth only for the purposes of example and that it should not be taken as limiting the embodiments as defined by the following claims. For example, notwithstanding the fact that the elements of a claim are set forth below in a certain combination, it must be expressly understood that the embodiments includes other combinations of fewer, more or different elements, which are disclosed in above even when not initially claimed in such combinations. A teaching that two elements are combined in a claimed combination is further to be understood as also allowing for a claimed combination in which the two elements are not combined with each other, but may be used alone or combined in other combinations. The excision of any disclosed element of the embodiments is explicitly contemplated as within the scope of the embodiments.

**[0215]** The words used in this specification to describe the various embodiments are to be understood not only in the sense of their commonly defined meanings, but to include by special definition in this specification structure, material or acts beyond the scope of the commonly defined meanings. Thus, if an element can be understood in the context of this specification as including more than one meaning, then its use in a claim must be understood as being generic to all possible meanings supported by the specification and by the word itself.

**[0216]** The definitions of the words or elements of the following claims are, therefore, defined in this specification to include not only the combination of elements which are literally set forth, but all equivalent structure, material or acts for performing substantially the same function in substantially the same way to obtain substantially the same result. In this sense it is therefore contemplated that an equivalent substitution of two or more elements may be made for any one of the elements in the claims below or that

a single element may be substituted for two or more elements in a claim. Although elements may be described above as acting in certain combinations and even initially claimed as such, it is to be expressly understood that one or more elements from a claimed combination can in some cases be excised from the combination and that the claimed combination may be directed to a subcombination or variation of a subcombination.

**[0217]** Insubstantial changes from the claimed subject matter as viewed by a person with ordinary skill in the art, now known or later devised, are expressly contemplated as being equivalently within the scope of the claims. Therefore, obvious substitutions now or later known to one with ordinary skill in the art are defined to be within the scope of the defined elements.

**[0218]** The claims are thus to be understood to include what is specifically illustrated and described above, what is conceptually equivalent, what can be obviously substituted and also what essentially incorporates the essential idea of the embodiments.

I claim:

1. An electrophysiology catheter for combination with an external mapping station comprising:

a catheter with a movable catheter tip;

one or more electrodes provided on or in an electrode region in a most distal portion of the catheter tip;

sensing and amplification circuitry communicated with the one or more electrodes, the sensing and amplification circuitry communicated with digitizing circuitry disposed in a circuitry region in a least distal portion of the catheter tip for locally sensing tissue-based electrophysiological signals and for bidirectionally communicating digital data signals to and from the sensing and amplification and digital circuitry; a flexible bending region of the catheter tip between the most and least distal portions of the catheter tip;

a flexible sheath communicated to the sensing and amplification circuitry and digitizing circuitry for transmission of signals thereon; and

a handle communicated with the sheath for bidirectionally communicating signals through the sheath between the catheter tip and external mapping station, and for controlling movement of the catheter tip.

2. The electrophysiology catheter of claim 1 where transmission of data signals in the sheath is by optical digital signals.

3. The electrophysiology catheter of claim 1 where transmission of data signals in the sheath is by electrical digital signals.

4. The electrophysiology catheter of claim 2 further comprising:

an electro-optical system coupled to the catheter tip for transducing digital electrical electrophysiological signals from the sensing and amplification circuitry and digitizing circuitry into digital optical electrophysiological signals;

an optical fiber in the sheath for transmitting the digital optical electrophysiological signals to the proximal handle of the catheter; and

an optical-electro system disposed in the proximal handle of the catheter for transducing digital optical electrophysiological signals into digital electrical electrophysiological signals.

5. The electrophysiology catheter of claim 1 where the handle comprises a steering mechanism where movement of a distal tip of the catheter with respect to tissue contacted by the catheter tip is controlled.

6. The electrophysiology catheter of claim 1 where the sensing and amplification circuitry comprises means for making a biopotential measurement to provide a representation of energy contents on a spatial domain and a time domain of a complex electrophysiological waveform, leading to a recursive relationship between a graphical representation of the complex electrophysiological waveform and an underlying biopotential substrate which causes the complex electrophysiological waveform.

7. The electrophysiology catheter of claim 1 where the sensing and amplification circuitry comprises means for employing a local amplifier active sensor array utilizing impedance spectroscopy at a bioevent site of a measured biopotential signal.

8. The electrophysiology catheter of claim 1 where the sensing and amplification circuitry comprises means for using a native bioelectrical signal in the form of ionic electrochemical avalanche dynamics at a measurement site in tissue by locating an active sensor element adjacent to the measurement site and measuring the native bioelectrical signal by relating its characteristics of time, magnitude and direction, without post-processing of the native bioelectrical signal.

9. The electrophysiology catheter of claim 8 where means for using a native bioelectrical signal is characterized by an improved signal-to-noise ratio, improved spurious-free dynamic range (SFDR), improved signal fidelity, improved sampling rate, improved bandwidth, and improved differentiation of far-field from near-field components in the native signal.

10. The electrophysiology catheter of claim 1 where the catheter comprises an electrophysiological mapping catheter adapted to establish accurate diagnostic maps of axonal nerve endings as detected in renal denervation, measurement of ganglionic plexus activities and neuronal cellular matrices.

11. The electrophysiology catheter of claim 1 where the sensing and amplification circuitry comprises an active sensor array in an implantable cardioverter defibrillator (ICD), in an implantable electrophysiological device, in a device for neuromodulation, and in pacemaker leads.

12. The electrophysiology catheter of claim 2 where the sensing and amplification circuitry comprises an active sensor array and where an optical fiber is employed instead of any electrical wiring between the catheter tip and the handle, so that a signal detected by the active sensor array in the catheter tip is converted into an uncorruptible digital word and sent to the handle in a digital optical data stream.

13. The electrophysiology catheter of claim 1 where the catheter is arranged and configured as a diagnostic device for use in electrophysiological studies, including mapping nerve pathways during ablative procedures, renal denervation, various cardiological procedures, and neurological mapping.

14. The electrophysiology catheter of claim 1 further comprising an imaging system in the external mapping station, including an impedance mapping apparatus, which imaging system enables location of a target within an

anatomical context and provides geometric coordinates of specific anatomical destination including identifying different types of arrhythmia.

15. The electrophysiology catheter of claim 1 where the sensing and amplification circuitry accurately characterizes fractionation potentials recorded in scarred myocardial tissue, which serve as ablation targets, pulmonary vein potentials and accessory pathway potentials.

16. The electrophysiology catheter of claim 1 where the one or more electrodes comprise an array forming geometry configurations such as bipolar, quadripolar, decapolar, or any array with 64 or more electrodes to enable a multiplicity of electrodes to simultaneously capture a complex electro-potential energetic event with an improved signal-to-noise ratio and improved sampling rate commensurable with an improved bandwidth and improved accuracy on a spatiotemporal domain.

17. The electrophysiology catheter of claim 1 further comprising means for providing a standard model for any assessment of boundary conditions yielding consistent and repeatable data under similar conditions.

18. The electrophysiology catheter of claim 17 where the standard model unifies diagnostic observations under a measurement technique to define an intracardiac electrogram (EGM) as energetic events, which provides a translation between the electrical map and its tissue substrate so that the substrate is directly correlated to the pathophysiology.

19. The electrophysiology catheter of claim 18 where the defined intracardiac electrogram (EGM) comprises a graphical representation of an energetic bioevent, based on the dielectric ( $\kappa$ ) and conductivity ( $\sigma$ ) measurements of underlying tissues.

20. The electrophysiology catheter of claim 1 where the sensing and amplification circuitry comprises a local amplifier to sense and amplify a native local signal where the near-field as well as its far-field component can be distinguished without post-processing.

21. The electrophysiology catheter of claim 4 in combination with an external computer where the optical-electro system disposed in the handle of the catheter for transducing digital optical electrophysiological signals into digital electrical electrophysiological signals comprises a digital signal processor, a laser controlled by the digital signal processor and coupled to the optical fiber, a dichroic mirror for feeding back a portion of light from the laser to a photodiode coupled to the digital signal processor to regulate the laser, where light carrying digital optical signals from the optical fiber are coupled to the photodiode and thence to the digital signal processor, the digital signal processor coupled to the external computer for data storage and processing.

22. The electrophysiology catheter of claim 1 where the one or more electrodes comprise a plurality of electrodes and where the sensing and amplification circuitry comprises:

- a light emitting diode/photodiode (LED/PD);
- a serial peripheral interface (SPI) bus;
- a plurality of amplifier application specific integrated circuits (amp ASIC) coupled to corresponding ones of the plurality of electrodes and to the serial peripheral interface (SPI) bus; and
- a light application specific integrated circuit (ASIC) coupled to the LED/PD, which light ASIC signal conditions and communicates a plurality of signals on the serial peripheral interface (SPI) bus to the plurality of



amplifier ASIC's, each of which are coupled to one of the plurality of electrodes, used as sensing points of the catheter tip so that sensed biopotentials from electrodes are locally amplified by amplifier ASICs and communicated via the SPI bus into the light ASIC to be multiplexed out to LED/PD and communicated as multiplexed photonic signals on the optical fiber.

**23.** The electrophysiology catheter of claim **1** where the sensing and amplification circuitry disposed in the distal portion of the catheter tip comprises:

an optical connector coupled to the optical fiber, the optical connector including a photodiode to convert an optical signal from the optical fiber into an electrical signal, and the optical connector including an LED to convert an electrical signal into an optical signal communicated to the optical fiber;

a voltage regulator coupled to the photodiode and powered by a power optical signal received by the photodiode;

a charge pump coupled to the voltage regulator;

a microcontroller unit (MCU);

an analog to digital converter (ADC) coupled to the MCU;

an instrument amplifier (IA) coupled to the ADC;

an AC-coupling circuit coupled to the IA;

a multiplexer (MUX) coupled to the AC-coupling circuit and to the one or more electrodes;

where the charge pump is coupled to the MUX and IA for the purpose of providing power;

where the voltage regulator powers and is coupled to the MCU, ADC, IA, AC-coupling circuit and MUX;

where the MCU is coupled to the MUX and provides a selection command signals to the MUX to control selection of the one or more electrodes; and

where sensed native signals from the one or more electrodes is communicated to the AC-coupling circuit, amplified by the IA, converted to a digital form by the ADC and communicated to the MCU for communication to the LED and transduction into a digital optical form into the optical fiber.

**24.** A method for using an electrophysiology catheter to map neuronal activity of tissue by employing sensing and amplification circuitry disposed in the distal portion of the catheter at the site of biopotential activity to detect and record a local native cardiac signal in cardiac tissue spatially and temporally localized with the generation of the native cardiac signal at the situs of its local generation without corruption from far field signals or external electromagnetic noise.

**25.** The method of claim **24** where employing sensing and amplification circuitry comprises employing a local amplifier active sensor array with capabilities enabling an accurate "one-to-one" correlation while forming an electrophysiological map by measuring spatial position of the situs of local generation and vectorial direction of current movement of the local native signal in the cardiac tissue.

**26.** The method of claim **24** where employing the sensing and amplification circuitry comprises using the circuitry to make a measurement of biopotential voltage and phase of the local native cardiac signal as a function of time correlated with impedance of the tissue and/or temperature at the local situs of measurement.

**27.** The method of claim **24** where employing the sensing and amplification circuitry comprises employing the cir-

cuitry to detect and record impedance spectroscopy at the local situs of a measured biopotential signal.

**28.** The method of claim **24** where employing the sensing and amplification circuitry comprises employing the circuitry to detect and record a native local bioelectrical signal in the form of ionic electrochemical avalanche dynamics at a measurement site in tissue by locating an active sensor element adjacent to the measurement site and measuring the native bioelectrical signal by relating its characteristics of time, magnitude and direction in the cardiac tissue without post-processing of the native bioelectrical signal.

**29.** The method of claim **28** where employing circuitry for using a native bioelectrical signal is characterized by using circuitry with an improved signal-to-noise ratio, improved spurious-free dynamic range (SFDR), improved signal fidelity, improved sampling rate, improved bandwidth, and improved differentiation of far-field from near-field components in the native signal.

**30.** The method of claim **24** where employing an electrophysiological mapping catheter establishes accurate diagnostic maps of axonal nerve endings as detected in renal denervation, measurement of ganglionic plexus activities and neuronal cellular matrices.

**31.** The method of claim **24** where employing the sensing and amplification circuitry comprises employing an active sensor array in an implantable cardioverter defibrillator (ICD), in an implantable electrophysiological device, in a device for neuromodulation, and in pacemaker leads.

**32.** The method of claim **24** where employing the sensing and amplification circuitry comprises employing an active sensor array and where the optical fiber replaces all electrical wiring between the distal portion of the catheter and the handle, so that a signal detected by the active sensor array in the distal portion of the catheter is converted into an uncorruptible digital word and sent to the handle as digital optical data stream.

**33.** The method of claim **24** where employing sensing and amplification circuitry in an electrophysiology catheter includes arranging and configuring the catheter as a diagnostic device for use in electrophysiological studies, including mapping nerve pathways during ablative procedures, renal denervation, various cardiological procedures, and neurological mapping.

**34.** The method of claim **24** further comprising using an imaging system, including an impedance mapping apparatus in combination with the electrophysiology catheter, which imaging system locates a target within an anatomical context and provides geometric coordinates of specific anatomical destination including identifying different types of arrhythmia.

**35.** The method of claim **24** where employing the sensing and amplification circuitry comprises accurately characterizing fractionation potentials recorded in scarred myocardial tissue, which serve as ablation targets, pulmonary vein potentials and accessory pathway potentials.

**36.** The method of claim **24** where further comprising deploying one or more electrodes to comprise an array form with geometry configurations such as bipolar, quadripolar, decapolar, or any array with 64 or more electrodes thereby enabling a multiplicity of electrodes to simultaneously capture a complex electro-potential energetic event with an improved signal-to-noise ratio and improved sampling rate commensurable with an improved bandwidth and improved accuracy on a spatiotemporal domain.

**37.** The method of claim **24** where employing sensing and amplification circuitry in an electrophysiology catheter comprises providing a standard model for any assessment of the boundary conditions yielding consistent and repeatable data under similar conditions.

**38.** The method of claim **37** where providing the standard model comprises unifying diagnostic observations under a measurement technique for defining an intracardiac electrogram (EGM) as energetic events, which provides a translation between the electrical map and its substrate so that the substrate is directly correlated to the pathophysiology.

**39.** The method of claim **38** where defining the intracardiac electrogram (EGM) comprises generating a graphical representation of an energetic bioevent, based on the dielectric ( $\kappa$ ) and conductivity ( $\sigma$ ) measurements of underlying tissues.

**40.** The method of claim **24** where employing the sensing and amplification circuitry comprises providing a local amplifier to sense and amplify a native local signal where the near-field as well as its far-field component can be distinguished without post-processing.

**41.** A method for using a renal denervation catheter to map neuronal activity of renal tissue by employing pulsing, sensing and amplification circuitry disposed in the distal portion of the catheter at the site of biopotential activity to electrically stimulate, detect and record a local native renal signal in active renal tissue spatially and temporally localized with the generation of the active native renal signal at the situs of its local generation without corruption from far field signals or external electromagnetic noise.

\* \* \* \* \*





U.S. PATENT OFFICE FILINGS FOR:  
*The Use of Local Amplifiers and  
Huygens Sensor Array in  
Measuring Bioelectric Signals  
and Clinical Applications Thereof*  
**INVENTOR: Yehoshua Shachar**

**PCT REQUEST**

(Original in Electronic Form)

<b>0</b>	<b>For receiving Office use only</b>	
<b>0-1</b>	International Application No.	
<b>0-2</b>	International Filing Date	
<b>0-3</b>	Name of receiving Office and "PCT International Application"	
<b>0-4</b>	<b>Form PCT/RO/101 PCT Request</b>	
0-4-1	Prepared Using	<b>ePCT-Filing for data package download Version 4.10.003 MT/FOP 20220711/1.1</b>
<b>0-5</b>	<b>Petition</b>	
	The undersigned requests that the present international application be processed according to the Patent Cooperation Treaty	
<b>0-6</b>	<b>Receiving Office (specified by the applicant)</b>	<b>United States Patent and Trademark Office (USPTO) (RO/US)</b>
<b>0-7</b>	<b>Applicant's or agent's file reference</b>	<b>PHA3PAU63PCT</b>
<b>I</b>	<b>Title of Invention</b>	<b>[The title is as provided on page 1 of the description]</b>
<b>II</b>	<b>Applicant</b>	
II-1	This person is	<b>Applicant only</b>
II-2	Applicant for	<b>All designated States</b>
II-4	Name	<b>NEUROKINESIS CORP.</b>
II-5	Address	<b>10604 S. LaCienega Blvd Inglewood, California 90304 United States of America</b>
II-6	State of nationality	<b>US</b>
II-7	State of residence	<b>US</b>
II-9	Facsimile No.	<b>13106412072</b>
II-10	e-mail	<b>info@neuro-kinesis.com</b>
II-10(a)	E-mail authorization The receiving Office, the International Searching Authority, the International Bureau and the International Preliminary Examining Authority are authorized to use this e-mail address, if the Office or Authority so wishes, to send notifications issued in respect of this international application:	<b>exclusively in electronic form (no paper notifications will be sent)</b>
<b>III-1</b>	<b>Applicant and/or inventor</b>	
III-1-1	This person is	<b>Inventor only</b>
III-1-3	Inventor for	<b>All designated States</b>
III-1-4	Name (LAST, First)	<b>SHACHAR, Josh</b>
III-1-5	Address	<b>2417 22nd St. Santa Monica, California 90405 United States of America</b>

**PCT REQUEST**

(Original in Electronic Form)

<b>IV-1</b>	<b>Agent or common representative; or address for correspondence</b> The person identified below is hereby/ has been appointed to act on behalf of the applicant(s) before the competent International Authorities as:	<b>Agent</b>
IV-1-1	Name (LAST, First)	<b>DAWES, Daniel</b>
IV-1-2	Address	<b>5200 Warner Ave Ste 106 Huntington Beach, California 92649 United States of America</b>
IV-1-3	Telephone No.	<b>7148400302</b>
IV-1-4	Facsimile No.	<b>7148405266</b>
IV-1-5	e-mail	<b>ddawes@dawespatents.com</b>
IV-1-5(a)	E-mail authorization The receiving Office, the International Searching Authority, the International Bureau and the International Preliminary Examining Authority are authorized to use this e-mail address, if the Office or Authority so wishes, to send notifications issued in respect of this international application:	<b>exclusively in electronic form (no paper notifications will be sent)</b>
IV-1-6	Agent's registration No.	<b>27123</b>
<b>V</b>	<b>DESIGNATIONS</b>	
<b>V-1</b>	<b>The filing of this request constitutes under Rule 4.9(a), the designation of all Contracting States bound by the PCT on the international filing date, for the grant of every kind of protection available and, where applicable, for the grant of both regional and national patents.</b>	
<b>VI-1</b>	<b>Priority claim of earlier national application</b>	
VI-1-1	Filing date	<b>07 September 2021 (07.09.2021)</b>
VI-1-2	Number	<b>17/468,460</b>
VI-1-3	Country or Member of WTO	<b>US</b>
<b>VI-2</b>	<b>Priority claim of earlier international application</b>	
VI-2-1	Filing date	<b>20 May 2022 (20.05.2022)</b>
VI-2-2	Number	<b>PCT/US2022/030399</b>
VI-2-3	PCT receiving Office	<b>US</b>
<b>VI-3</b>	<b>Priority document request</b> The receiving Office is requested to prepare and transmit to the International Bureau a certified copy of the earlier application(s) identified above as item(s):	<b>VI-1 VI-2</b>
<b>VI-4</b>	<b>Incorporation by reference :</b> where an element of the international application referred to in Article 11(1)(iii)(d) or (e) or a part of the description, claims or drawings referred to in Rule 20.5(a), or an element or part of the description, claims or drawings referred to in Rule 20.5bis(a) is not otherwise contained in this international application but is completely contained in an earlier application whose priority is claimed on the date on which one or more elements referred to in Article 11(1)(iii) were first received by the receiving Office, that element or part is, subject to confirmation under Rule 20.6, incorporated by reference in this international application for the purposes of Rule 20.6.	
<b>VII-1</b>	<b>International Searching Authority Chosen</b>	<b>United States Patent and Trademark Office (USPTO) (ISA/US)</b>

**PCT REQUEST**

(Original in Electronic Form)

<b>VIII Declarations</b>		Number of declarations	
VIII-1	Declaration as to the identity of the inventor	-	
VIII-2	Declaration as to the applicant's entitlement, as at the international filing date, to apply for and be granted a patent	-	
VIII-3	Declaration as to the applicant's entitlement, as at the international filing date, to claim the priority of the earlier application	-	
VIII-4	Declaration of inventorship (only for the purposes of the designation of the United States of America)	-	
VIII-5	Declaration as to non-prejudicial disclosures or exceptions to lack of novelty	-	
<b>IX Check list</b>		Number of sheets	Electronic file(s) attached
IX-1	Request (including declaration sheets)	<b>4</b>	✓
IX-2	Description	<b>30</b>	✓
IX-3	Claims	<b>3</b>	✓
IX-4	Abstract	<b>1</b>	✓
IX-5	Drawings	<b>11</b>	✓
IX-6a	Sequence listing part of the description (also to be used for the purposes of international search)	-	-
IX-7	TOTAL	<b>49</b>	
<b>Accompanying Items</b>		Paper document(s) attached	Electronic file(s) attached
IX-8	Fee calculation sheet	-	✓
<b>IX-20</b>	<b>Figure of the drawings which should accompany the abstract</b>	<b>8</b>	
<b>IX-21</b>	<b>Language of filing of the international application</b>	<b>English</b>	
<b>X-1</b>	<b>Signature of applicant, agent or common representative</b>	<b>/Daniel L. Dawes /, Reg. No. 27123/</b>	
<b>X-1-1</b>	Name (LAST, First)	<b>DAWES, Daniel</b>	
<b>X-1-3</b>	Capacity (if such capacity is not obvious from reading the request)	<b>Agent</b>	

**PCT REQUEST**

(Original in Electronic Form)

**FOR RECEIVING OFFICE USE ONLY**

10-1	Date of actual receipt of the purported international application	
10-2	<b>Drawings:</b>	
10-2-1	Received	
10-2-2	Not received	
10-3	<b>Corrected date of actual receipt due to later but timely received papers or drawings completing the purported international application</b>	
10-4	<b>Date of timely receipt of the required corrections under PCT Article 11(2)</b>	
10-5	<b>International Searching Authority</b>	<b>ISA/US</b>
10-6	<b>Transmittal of search copy delayed until search fee is paid</b>	

**FOR INTERNATIONAL BUREAU USE ONLY**

11-1	<b>Date of receipt of the record copy by the International Bureau</b>	
------	---	--

**THE USE OF LOCAL AMPLIFIERS AND A HUYGENS SENSOR ARRAY IN  
MEASURING BIOELECTRIC SIGNALS AND  
CLINICAL APPLICATIONS THEREOF**

**[01] Related Applications**

**[02]** This application is a continuation in part and claims priority to, and the benefit of the earlier filing date of ROBOTICALLY CONTROLLED ELECTROPHYSIOLOGY CATHETER WITH CLOSED LOOP CONTROL, PCT Pat. Appl. PCT/US22/30399, filed May 20, 2022, incorporated herein by reference and A CATHETER FOR CARDIAC AND RENAL NERVE SENSING AND MEDIATION, U.S. Pat. Appl. 17/468,460, filed Sept. 7, 2021, incorporated herein by reference pursuant to 35 USC 120.

**[03] Background**

**[04]** *Field of the Technology*

**[05]** The invention relates to the field of electrophysiological mapping methods using a catheter with capabilities of measuring impedance and local native biometric signals and employing such signals with a method that identify a “phase singularity” within the electroanatomical space and its dynamics.

**[06]** *Description of the Prior Art*

**[07]** Tissue electrode interface is common to all forms of biopotential recording (e.g., ECG, EMG, EEG) and functional electrical stimulation (e.g., pacemaker, cochlear implant, deep brain stimulation). The disclosed technology employs local amplification by means of a Huygens™ catheter (a trademark of Neurokinesis Corp., Inglewood, California) at the bioelectric site, which demonstrates substantial reduction in signal-to-noise ratio (SNR), while improving spurious-free dynamic range (SFDR). Details of the Huygens catheter as provided by U.S. Pat. Applications (PHA3.PAU.57A) ROBOTICALLY CONTROLLED ELECTROPHYSIOLOGY CATHETER WITH CLOSED LOOP CONTROL, PCT Pat. Appl. PCT/US22/30399, incorporated herein by reference and A CATHETER FOR CARDIAC AND RENAL NERVE SENSING AND MEDIATION, U.S. Pat. Appl. 17/468,460, filed Sept. 7, 2021, incorporated herein by reference.

**[08]** The problem to be solved is how to identify the arrhythmogenic cause of fibrillation, which the Huygens catheter is capable of doing by measuring the impedance value of the tissue, in order to create an actual measure of the anisotropic wave propagation.



**[09]** The current art of electrophysiology mapping techniques and its applications is detailed and described by a review paper by Li et al in *Physiol.*, 21 July 2020 “Standardizing Single-Frame Phase Singularity Identification Algorithms and Parameters in Phase Mapping During Human Atrial Fibrillation”, stating that “Recent investigations failed to reproduce the positive rotor-guided ablation outcomes shown by initial studies for treating persistent atrial fibrillation (*persAF*). Phase singularity (*PS*) is an important feature for *AF* driver detection, but algorithms for automated *PS* identification differ.”

**[10]** The authors conclude that “In the present study, we demonstrate that automated Phase Singularity detection – and consequently *persAF* ablation target identification – vary significantly for the same individual, depending on the method being used and parameters being applied. The present study represents a step toward a unified definition/algorithm of phase-derived *PS* detection with standardized gradient and spatial thresholds, which is essential to allow objective comparisons of outcomes of rotor ablation for *persAF* therapy among different research/clinical centers.”

**[11]** As noted by Li et al in a comprehensive monograph noted above, in which the authors’ process of obtaining the spatial coordinates of the *PS* is based on mathematical-statistical methods where a computational algorithm is capable of sorting the locus of the rotor generator focal position of the electrical activity by employing a “2048-channel virtual electrogram (*VEGM*) and electrocardiogram signals were collected for 30 s from 10 patients undergoing *persAF* ablation. *QRST*-subtraction was performed and virtual electrogram *EGMs* were processed using sinusoidal wavelet reconstruction. The phase was obtained using Hilbert transform. *PSs* were detected using four algorithms: (1) two dimensional image processing based and neighbor-indexing algorithm; (2) three dimensional neighbor-indexing algorithm; (3) two dimensional kernel convolutional algorithm estimating topological charge; and (4) topological charge estimation on a three dimensional mesh. *PS* annotations were compared using a structural similarity index (*SSIM*) and Pearson’s correlation coefficient (*CORR*). Optimized parameters to improve detection accuracy were found for all four algorithms using  $F_\beta$  score and 10-fold cross-validation compared with manual annotation. Local clustering with density-based spatial clustering of applications with noise was proposed to improve algorithms 3 and 4.”

**[12]** It is clear from the four methods proposed and its data acquisition modes by which the identification of the Phase Singularity is obtained are highly depended on the complex and subjective selections of parameters which in turn are subjected to the “ $F_\beta$  score” analysis, due to assignments of non-symmetric preferences of some of the parameters relative value in assessing the locus of the Phase Singularity.

**[13]** The differentiation between atrial flutter and atrial fibrillation in a location where such phenomenon occurs is another source of error which add to the identification of Phase Singularity.

**[14]** Our application teaches an apparatus and method for the identification of the locus associated with atrial fibrillation by the use of the Huygens catheter and its ability to measure with near real-time the impedance

as well as the tissue potential and thereby solving the variables in the algorithm we employ titled “Signal Anisotropy, Modeling Bipotential Activity with the Poynting Energy Vector (PEV)” described below. This technique is not available anywhere in the leading theories of the underlying mechanisms which defines the difference between a phenomenon called “atrial flutter” and one called “atrial fibrillation”. While flutter is marked by the gap associated with scar and fibrotic tissue, which inhibits the transport of the ionic charge of the wave propagation along the conduction path, fibrillation is a phenomenon physically correlated with a physical phenomenon described as “rotors”.

**[15]** In summary, the differentiation between flutter and fibrillation due to the anisotropic behavior of the wavefront dynamics, is the regeneration of the fibrillating foci, where the front of the wave and the tail of the wave are spiraling, while flutter is a simple fractionated electrogram, where the tail is just an end represented by a capacitance delay. In fibrillation the focus of the energy is a generator where its equivalent circuit representation is a variable resistor. The main difference between fibrillation and flutter is the gap or the nature of the encroachment of the front into the tail: the gap is fully excitable and quite large in flutter, whereas it is smaller and partially excitable in AF, because of the intermingled front and tail. A detailed study of the physics as well as the physiology of cardiac cell mechanism is articulated by Sandeep V. Pandit and José Jalife “Rotors and the Dynamics of Cardiac Fibrillation”

**[16]** The Huygens catheter is the only tool in existence today that can measure both the DC potential as well as the tissue contact impedance (conductivity) for the same tissue area. This enables us to employ the Maxwell second set of time-varying equations, by substituting the magnetic energy vector (MEV) with the Poynting Energy Vector (P) where we substitute the B terms with the impedance measured value Z. The impedance Z is measured nearly simultaneously with the measurement of the electric potential E of the heart wave using separately sensing electrodes on the Huygens catheter and sensing and signal processing circuitry. Since the E and B fields are in temporal quadrature, their strengths cannot be simultaneously measured, but they can be measured in near simultaneity since the sample rate of the Huygens catheter is of the order of 1 kHz compared to the 1Hz beat rate of the heart and the heart wave. Thus, an approximate value of the Poynting vector,  $E \times B$ , can be measured at any given time, substituting the measured impedance Z for a computed value for B. This is a derivation that was never described in the literature of the causal relationship between conduction path and fibrillation. The mechanism used to describe fibrillation is associated with the theory defined under the heading “phase singularity” whereby the computer on the back-end of the Huygens catheter performs a phase study separating normal tissue from fibrotic/scar tissue. The disclosed technique using the Huygens catheter with the algorithm provided using Maxwell’s equations distinguishes the invention from the existing art.

**[17]**

**[18] Brief Summary**

**[19]** The methodology of the illustrated embodiments of the apparatus of the invention is demonstrated by comparing the sensing a native QRS signal of the heart, generated and transmitted through a conventional decapolar catheter, where one pair of electrodes is configured to amplify the native heart signal with an analog-to-digital converter (ADC) and amplifier combination. An identical QRS signal is transmitted through a second pair of electrodes where the electrodes were modified to incorporate a Huygens™ sensor array in the form of amplifier circuit placed on the inner surface of the electrode(s).

**[20]** The measurement results of the conventional first electrode pair is compared with the results of a computer simulation, and compared with the electrode- Huygens™ sensor array output. The post-amplified cardiac path (using standard electrode technology) is measured to show that the reference signal is nearly imperceptible due to noise degradation. Spurious-free dynamic range (SFDR) is defined as the strength ratio of the fundamental signal to the strongest spurious signal in the output. The final result shows a spurious-free dynamic range (SFDR) of 9.3dB with a signal-to-noise ratio (SNR) of -50dB. In contrast, when the same signal is run through the pre-amplified Huygens™ cardiac path, it is shown to be well- formed and the cardiac properties are clear, and the final result shows a vastly improved SFDR of 24.9dB and SNR of only -13dB.

**[21]** The increase in signal quality of the Huygens™ sensor array as a local amplifier creates a new standard of quality in measuring bioelectric signals and well outperforms the current electrode technology.

**[22]** Electrograms are a manifestation of the underlying electrochemical activity of a biological substrate, and the attempt to functionalize and fashion a diagnostic value upon such graphical representation must first assume that the fidelity of the measured native signal is a true representation of an “energetic event,” as energy with its vectorial direction and magnitude is the appropriate parameters for a diagnostic measure. The question of focus becomes: “Can the electrogram path represent the underlying substrate composition?”

**[23]** What we demonstrate below is centered on the ability of a measuring apparatus employing a catheter fitted with an electrode technology (i.e. at the site of biopotential activity) to capture the signal in its native form. The current technology with its post-processing algorithms distorts and masks the true nature of the complex wavefronts and “washes out” substantial clinical details, resulting in a non-unique diagnosis as to the underlying nature of the disease mechanism.

**[24]** Conventional measuring apparatus employing electrode(s) with an amplifier at the distal end of the catheter shaft is compared below with use of a local amplifier in a Huygens™ sensor array, which array enables an accurate “one-to-one” correlation while forming an electrophysiological map. The biopotential measurement using a Huygens sensor array substantially improves the representation of the energy contents on the spatial and time domains of the complex cardiac waveform, leading to a recursive relationship between the graphical representation and the underlying biopotential substrate which causes such electrical activity.

**[25]** Conventional electrode technology utilizing post-processing algorithms has tried with limited success to resolve the diagnostic discrepancy between the bottom-up causal representation (i.e., substrate mapping) and the top-down causal description of the underlying mechanism generating the pathology observed. This limitation is cited in many clinical publications and is most clearly evident in the diagnosis and treatment of complex arrhythmias.

**[26]** As indicated by the current status of clinical results, there are presently at least two approaches to determining the underlying mechanism for modeling a disease: 1) the reductionist approach, which advocates “substrate mapping” correlations with ECG, ( See Volkmer et al. “Substrate Mapping vs. Tachycardia Mapping using CARTO in Patients with Coronary Artery Disease and Ventricular Tachycardia: Impact on Outcome of Catheter Ablation”, Oxford Journals Medicine EP Europace Volume 8, Issue 11Pp. 968-976) and 2) the anatomical approach, which supports “anatomical mapping.” (Deepak Bhakta et al., “Principles of Electroanatomic Mapping”, *Electrophysiol J.* 2008 Jan-Mar; 8(1): 32–50). In contrast, the discussion should be centered on the nature of the measuring apparatus’s fidelity and the establishment of a “standard model” in electrophysiology (EP) while employing an apparatus which will enable both methodologies to form a uniform mapping manifold. A standard model would provide for a common method of assessing the data and its “elementary building blocks,” which will improve not only the diagnostic and mapping procedures but also the therapeutic outcome.

**[27]** One of the foremost goals of the EP community is to develop a comprehensive mapping technique to characterize the global dynamics of wavefront activation. This must, first, be anchored in a bottom-up consensus where the elementary building blocks are accepted and agreed upon metrically, and whereby the cellular etiology and its electrical counterparts – e.g., dielectric ( $\kappa$ ) and conductivity ( $\sigma$ ) – are defined. The complexity and inter-relationships of the “avalanche” dynamics which are translated through the myocardial space, due to ionic potential on the spatial as well as time domains, can be resolved by the use of heuristic top-down causal theory, when employing the local amplifier Huygens™ sensor array.

**[28]** With respect to the methodology of using the Huygens sensing array, the illustrated embodiments of the invention include an improvement in a method of sensing biopotentials in tissue including the steps of: providing a Huygens sensor array; and sensing a native electrical biopotential signal using at least one electrode on a catheter with an amplifier circuit placed on the inner surface of the at least one electrode in the Huygens sensor array to generate a well- formed waveform of the biopotential showing clear electrical properties indicative of the tissue with a SFDR of at least 24.9dB and SNR of at least -13dB.

**[29]** In one embodiment the tissue is cardiac tissue and the biopotential signal sensed by the Huygens sensing array is a native cardiac waveform.

**[30]** In one embodiment the sensed biopotential signal is a manifestation of underlying electrochemical activity sensed by the Huygens sensing array of a biological substrate corresponding to the tissue.

**[31]** In one embodiment, the manifestation of underlying electrochemical activity of a biological substrate corresponding to the tissue is an energetic event characterized by vectorial direction and magnitude sensed by the Huygens sensing array.

**[32]** In one embodiment, the manifestation of underlying electrochemical activity of a biological substrate sensed by the Huygens sensing array corresponding to the tissue is a representation of the underlying substrate composition of the tissue.

**[33]** In one embodiment, the manifestation of underlying electrochemical activity of a biological substrate corresponding to the tissue is a biopotential measurement using the Huygens sensor array to generate a representation of the energy contents on the spatial and time domains of a complex cardiac waveform, leading to a recursive relationship between a graphical representation of the cardiac waveform and an underlying biopotential substrate which is a source of the cardiac waveform.

**[34]** In one embodiment, the manifestation of underlying electrochemical activity of a biological substrate corresponding to the tissue includes a mapping which characterizes global dynamics of cardiac wavefront activation based on cellular etiology and corresponding dielectric ( $\kappa$ ) and conductivity ( $\sigma$ ) characteristics of the tissue representing complex inter-relationships of avalanche dynamics translated through a measured myocardial space arising from spatial and temporal ionic potentials measured by a local amplifier Huygens sensor array.

**[35]** In one embodiment, sensing a native electrical biopotential signal using at least one electrode on a catheter with an amplifier circuit placed on the inner surface of the at least one electrode in the Huygens sensor array includes sensing by performing impedance spectroscopy.

**[36]** In one embodiment, sensing a native electrical biopotential signal using at least one electrode on a catheter with an amplifier circuit placed on the inner surface of the at least one electrode in the Huygens sensor array includes sensing an energetic event represented by the native electrical biopotential signal in the tissue by relating its inherent characteristics of time, magnitude and direction without post-processing of the native electrical biopotential signal.

**[37]** In one embodiment, sensing a native electrical biopotential signal using at least one electrode on a catheter with an amplifier circuit placed on the inner surface of the at least one electrode in the Huygens sensor array includes sensing the native electrical potential signal using a local amplifier which acts as variable resistor with an on-site electrical ground, which ground is not subject to noise pickup to improve signal-to-noise ratio (SNR), spurious-free dynamic range (SFDR), signal fidelity, sampling rate, bandwidth, and differentiation of far-field from near-field components of the sensed native electrical potential signal.

**[38]** In one embodiment, the method further includes the step of using the Huygens sensor array with mapping stations without alteration thereof.

**[39]** In one embodiment, the method further includes the step of detecting an energetic event in the tissue using the Huygens™ sensor array to generate an ensemble vector map to characterize spatiotemporal organization of cardiac fibrillation.

**[40]** In one embodiment, the method further includes the step of using the Huygens™ sensor array with a predetermined geometric configuration, including bipolar, quadripolar, decapolar, or any array with 64 or more electrodes, to enable a plurality of electrodes to simultaneously capture a complex electro-potential energetic event, with an improved SNR and sampling rate commensurable with a bandwidth and accuracy in a spatio-temporal domain.

**[41]** In one embodiment, the method further includes the step of capturing bioelectric potential data, which is anchored in a measurement that reveals the physical nature of a biological substrate's electrical properties of underlying tissue to allow for interpretation of the phenomenological expression of an electrogram (EGM) and its graphical representation in the context of an energetic event, based on the dielectric ( $\kappa$ ) and conductivity ( $\sigma$ ) measurements of underlying tissue.

**[42]** In one embodiment, the method further includes the step of connecting an electroanatomic map with an inherent physical relationship between an energy transfer function and its causal dependency on a substrate tissue as represented by an electrogram by using a Huygens™ sensor array for conducting an electrophysiological study.

**[43]** In one embodiment, the method further includes the step of connecting phenomenological data with clinical observation so that electrical properties of a conduction path within a cardiac substrate and its etiological constituents are correlated without the need to create a causal dependency.

**[44]** In one embodiment, the method further includes the step of synchronously capturing spatial and temporal complexity of an energetic cardiac event using the Huygens™ sensor array to mimic underlying cardiac dynamics by localizing and precisely identifying arrhythmogenic substrates removed from fluoroscopic landmarks and lacking characteristic electrogram patterns.

**[45]** In one embodiment, the method further includes the step of generating a cardiac map comprised of superimposed electric and energy wave maps by converging the electric heart vector with the magnetic heart vector by computing an impedance ( $Z$ ) value generated from the substrate.

**[46]** In one embodiment, the method further includes the step of simultaneously localizing and mapping (SLAM) magnetic fields during a cellular activation sequence to uncover a magnetic heart vector (MHV) by computing a vector derived from Maxwell's equations by deriving the Poynting energy vector PEV from a measured impedance vector ( $Z$ ) sensed using the Huygens™ sensor array with a computational algorithm.



**[47]** In one embodiment, the method further includes the step of measuring a phase difference,  $\beta$ , between PEV and EHV to infer features of anisotropy in a myocardium.

**[48]** While the apparatus and method has or will be described for the sake of grammatical fluidity with functional explanations, it is to be expressly understood that the claims, unless expressly formulated under 35 USC 112, are not to be construed as necessarily limited in any way by the construction of “means” or “steps” limitations, but are to be accorded the full scope of the meaning and equivalents of the definition provided by the claims under the judicial doctrine of equivalents, and in the case where the claims are expressly formulated under 35 USC 112 are to be accorded full statutory equivalents under 35 USC 112. The disclosure can be better visualized by turning now to the following drawings wherein like elements are referenced by like numerals.

### **[49] Brief Description of the Drawings**

**[50]** Fig. 1 is a wave trace of the voltage of a cardiac signal as a function of time in a post-amplified path which shows that the reference signal is nearly imperceptible at this level due to noise degradation.

**[51]** Fig. 2 is a wave trace of the voltage of the signal shown in Fig. 1 as a function of time after being run through the Huygens sensor array.

**[52]** Fig. 3 is a color electroanatomic map with high fidelity and accuracy depicting a local electrogram with its native dynamics, its geometrical as well as its time domain specificity and further providing for reconstruction of the anatomical and the extrapolated etiological characteristics of the cellular matrix by employing the Huygens™ sensor array.

**[53]** Fig. 4 illustrates the vulnerability to wave break and spiral wave formation due to diffuse fibrosis. Fig. 4 shows three snapshots in upper row A of the progression of two wavefronts initiated in a medium with 10% fibrosis and with a coupling interval of 321 ms between them; and three snapshots in lower row B of the progression of two wavefronts initiated in a medium with 30% fibrosis and with a coupling interval of 320 ms between them

**[54]** Fig. 5 on the left panel is a color electrogram showing precise lesion placement which is required for treatment of arrhythmias for which ablation shown in the right panel are most effective (e.g., accessory pathways, atrioventricular nodal re-entry tachycardia [AVNRT]) and which are largely anatomically based or directed substrates.

**[55]** Fig. 6 is a fluoroscopic image used with a prior art mapping catheter and sensory apparatus, which cannot accurately locate both the geometry and time domain of the wavefront’s activity generated by the “avalanche” of the cellular excitable matrix.

**[56]** Fig. 7 are three traces of the cardiac amplitude and corresponding power spectrographs of the cardiac signal.

**[57]** Fig. 8 is a set of color graphs of an energy and E vector display, ECG and conductivity map over a time graph of an EP signal showing how the location of a rotor or other endocardial blockage is determined.

**[58]** Fig. 9 is a circuit block diagram of the Huygens catheter circuitry showing the amplifiers deployed on the catheter electrodes and the impedance sensing electrodes from a figure in the Incorporated application A CATHETER FOR CARDIAC AND RENAL NERVE SENSING AND MEDIATION, U.S. Pat. Appl. 17/468,460.

**[59]** Fig. 10 is a circuit block diagram of the impedance measurement circuitry used in the Huygens catheter from a figure in the Incorporated application A CATHETER FOR CARDIAC AND RENAL NERVE SENSING AND MEDIATION, U.S. Pat. Appl. 17/468,460.

**[60]** Fig. 11 is a perspective view of a nonencapsulated Huygens catheter tip showing the tip electrodes, a flexible length of printed circuit board coupled to the electrodes and a proximal portion of the circuit board carrying all of the tip electronics for providing local amplification and digitization of the electrode signals for transmission to a remote data processing station.

**[61]** Fig. 12 is a diagram illustrated some basic concepts of rotors and spirals in heart waves.

**[62]** The disclosure and its various embodiments can now be better understood by turning to the following detailed description of the preferred embodiments which are presented as illustrated examples of the embodiments defined in the claims. It is expressly understood that the embodiments as defined by the claims may be broader than the illustrated embodiments described below.

**[63]**

#### **[64] Detailed Description of the Preferred Embodiments**

**[65]** Determining optimal treatment strategies for complex arrhythmogenesis in AF is conducted by the lack of consensus regarding the mechanisms causing AF. The studies report different mechanisms for AF, ranging from hierarchical drivers to multiple activation modes. Differences in assessment of AF mechanism are likely due to the different investigational tools employed, scaling and the population variabilities used in the studies. The Huygens catheter and the proposed algorithm employed enable a uniform derivation of the focal targeted locus for such application, where the ability of the system and method is to create a uniform data acquisition of the cardiac dynamics, simplicity in the operation of yielding such a target as a rotor initiator and ultimately the ability of the therapeutic application of ablation procedure to terminate the arrhythmogenic cause for persistent AF. In the leftmost side of Fig. 12 is a diagram which is a snapshot of a spiral cardiac wave: electrotonic effects of the core decrease conduction velocity (arrows), and action potential duration (representative examples shown from positions 1, 2, and 3), and wavelength (the distance from the wavefront [black line] to the wave tail [dashed line]). Conduction velocity (CV) decreases and wavefront curvature becomes more pronounced, near the rotor, which is a phase singularity at the point where the wavefront and the wave tail meet (shown in Fig. 12

by an asterisk\*). In the rightmost side of Fig. 12 is a depiction of a computer simulation of cardiac wave reentry. On the top position is a snapshot of the transmembrane voltage distribution during simulated reentry in chronic atrial fibrillation (AF) conditions in a two-dimensional sheet incorporating human atrial ionic math models. In the bottom position is a snapshot of inactivation variables of sodium current, “high” during reentry. Greater detail concerning spiral and reentry waveforms is given in Sandeep V. Pandit, José Jalife, “Rotors and the Dynamics of Cardiac Fibrillation”, *Circ Res.* 2013;112:849-862 (2012).

### **[66] The Huygens Solution**

**[67]** There is a relationship between the quality of the measuring apparatus and its ability to resolve the signal accuracy and its signal-to-noise ratio (SNR), as well as the fidelity and repeatability of the data generated. This disclosure will address the shortcoming of the current electrode technology and the improvement provided by the use of a local amplifier with its embodiments, as a solution to the limitations noted by the existing art.

**[68]** Current attempts to resolve the myriad of above-mentioned issues utilize the method of post-production processing which employs, subsequent to the native measurement, algorithmic tools such as a Fast Fourier Transform (FFT) technique or recursive methods. As a result, the EP community is currently faced with a state of affairs as described and exemplified in the published clinical journals cited below.

**[69]** The Huygens<sup>TM</sup> technology utilizes impedance spectroscopy at the event site of the biopotential signal. Just as microscopy provided for magnification which produced a novel view of matter at orders of magnitude which were previously imperceptible, impedance spectroscopy provides an additional tool for an electrophysiologist that can resolve the distortions caused by the noise characteristic of the current art to allow study of the inherent relationship between the substrate and its corresponding electrical activity.

**[70]** The use of a local amplifier in the Huygens<sup>TM</sup> sensor array is a solution to shortcomings of the prior art. That the native bioelectrical signal in the form of ionic electrochemical avalanche dynamics is addressed by locating the preamplifier (Huygens<sup>TM</sup>) element adjacent to the measurement site. That measurement is capable of “mining” the “energetic event” by relating its inherent characteristics of time, magnitude and direction without post-processing of the native signal, as in the prior art. These aims are achieved by employing a local pre-amplification with the characteristic signal fidelity as demonstrated below.

**[71]** The shortcoming of the prior electrode technology is emphasized by comparison with the improvements provided by the disclosure, which is defined by the term “Huygens<sup>TM</sup>.” Simply stated, a local amplifier acts as variable resistor. Its on-site electrical ground is not subject to noise pickup from the 5-

ft. antenna/conductor, which the catheter shaft forms, and which acts as a receiver/carrier for equipment located in the operating room with EMI frequencies ranging from 50-60 Hz to 5-10 kHz. Fig. 11 shows the tip of the Huygens catheter in which all amplification, signal sensing, and signal conditioning occurs in electronics provided at or on the catheter tip or at least proximate thereto. Fig. 11 is taken from Fig. 12 of incorporated patent application, U.S. Pat. Appl. 17/468,460, where additional detail and disclosure of the Huygens catheter tip is provided. Fig. 11 shows that all of the sensing, amplification and signal processing circuitry, including digitization, related to the sensed electrode signals occurs at or proximate to the electrodes at or near the catheter tip. The disclosed approach of local amplification employs pre-amplification technology which substantially improves signal-to-noise ratio (SNR), spurious-free dynamic range- SFDR- signal fidelity, sampling rate, bandwidth, and differentiation of far-field from near- field components.

**[72]** It can be appreciated that measuring small bioelectrical signals with the Huygens™ technology applies to a wide variety of medical applications. For example, electrophysiological maps can be created to establish accurate diagnostic maps which improve the subsequent therapeutic outcome. The electrical characteristics of Huygens™ can resolve many of the existing problems arising from the electrode technology interface, where the ratio of signal magnitude compared to the noise impairs the ability of the clinician to form an adequate and reliable diagnosis.

**[73]** Conventional electrode technology is limited in providing uniform diagnostic metrics, and thus the clinical observations provided are oftentimes merely anecdotal indications. The Huygens™ sensor array, as a model for local pre-amplification supplements the current electrode technology to provide benefits by complementing the existing technology when incorporated therein. The current architecture of mapping apparatus such as CARTO™ or EnSite®, as well as their tool sets (e.g., catheters), need not be modified with respect to their generic metrics (e.g., bipolar, quadripolar, decapolar, balloon, basket), and are not altered since the Huygens™ amplifier and its associated circuitry is adopted within the existing catheter shaft. The Huygens™ technology can be seamlessly incorporated into the existing hardware of mapping stations and operator skills. The change would be essentially invisible to the user.

**[74]**

**[75] The Huygens Pre-Amplification Compared to Post-Amplification Methods**

**[76]** Experimental application of the technology is discussed below to demonstrate a proof of concept and the superior performance of a Huygens™ sensor array in detecting bioelectric potentials in the circuit depicted in Fig. 1. A comparison of the local amplifier employing Huygens™ versus the remote amplifier was conducted.

**[77]** Simulated cardiac (QRS) signals are generated by a programmable generator (Agilent Trueform Wave Generator, 33500B Series) and measured along two different signal paths, one employing a post-amplified

(using current electrode technology) and the second channel containing a locally amplified Huygens™ sensor array. In the unamplified pathway, a conventional decapolar geometry catheter is post-amplified using ADC Pro computer software, simulating the current method of electrode technology. In the amplified pathway, the identical geometry and metric layout is employed using a common, single catheter shaft for both configurations, with the only difference being that the amplification now occurred at the site of the electrodes using the Huygens™ sensor array. Thus, the only variable measured was the fidelity of the simulated QRS, enabling a comparative evaluation of the resultant signals from each amplification method.

**[78]** The signal is first attenuated to under 50 $\mu$ V peak-to-peak by adding series attenuators to the input signal from conventional electrode technology with a total signal gain of 128. The post-amplified path is measured in Fig. 1 to show that the reference signal is nearly imperceptible at this level due to noise degradation. The final result shows a spurious-free dynamic range SFDR of 9.3dB with a signal-to-noise ratio (SNR) of -50dB.

**[79]** In contrast, when the same signal is run through the pre-amplified Huygens™ path as seen in Fig. 2, it is shown to be well-formed, and the cardiac properties are clear. Here, the total signal gain is only 100, with the location of the gain block having been moved from one end of the catheter to another and the final result shows a vastly improved SFDR of 24.9dB and SNR of only -13dB.

**[80]** When the QRS-simulated signal is captured by the local amplifier at the site of the electrodes, linked to a local Huygens™ sensor, the result is substantially identical to the “pure” standard. The cardiac signal, replicated using Trueform™ waveform generator technology (a trademark of Keysight, Colorado Springs, Colorado), is then repeated while the amplifier is located at the distal end of the catheter connector with post-amplification. The signal quality is due to the pre-amplified embodiment of locating the measurement at the site of the signal source. These and other features relating to the use of Huygens™ inherent local ground with its variable resistor, matching the characteristics of the biopotential at the measurement site, are material characteristics of Huygens.

### **[81] Clinical Observations Using the Huygens Sensor Array**

**[82]** The application of local pre-amplification to measure bioelectrical potential, with sufficient SNR reduction as well as bandwidth, transforms the art of measurement in electrophysiological studies from the current state of phenomenological correlations to a bottom-up discipline, where observations are anchored in a common mode application of the biological substrate and the measuring apparatus, and where matrices of such measurements are defined by what we term as a “standard model” employing addressable and measurable “elementary building blocks.” The “standard model” is the prior art method of defining “phase singularities” in a post-processing method using an analog signal with large noise content. The disclosed embodiment

eliminates noise content by measuring the DC potential locally, and which is thereafter locally amplified and digitized into a word that cannot be corrupted by noise-generating sources. The Huygens sensing array has a resolution of 5-25 $\mu$ V which the prior art standard model cannot resolve. The disclosed methodology simultaneously measures the impedance of tissue contact therefore providing two fundamental data points which are not interpolated mathematically, but are obtained through a direct measurement from the tissue in real time. The disclosed methodology incorporates an "elementary" data set for the measured vector which is the order tuple of position P, orientation O, impedance Z, DC voltage potential, time t:  $\langle P(xyz), O(xyz), Z, V, t \rangle$ . Fig. 9 is a circuit block diagram of the Huygens catheter circuitry showing the amplifiers deployed on the catheter electrodes and the impedance sensing electrodes from a Fig. 4B in the Incorporated application A CATHETER FOR CARDIAC AND RENAL NERVE SENSING AND MEDIATION, U.S. Pat. Appl. 17/468,460. Fig. 10 is a circuit block diagram of the impedance measurement circuitry used in the Huygens catheter from a Fig. 5 in the Incorporated application A CATHETER FOR CARDIAC AND RENAL NERVE SENSING AND MEDIATION, U.S. Pat. Appl. 17/468,460. The operation and details of the elements shown in Figs. 10 and 11 are further described in the incorporated application and illustrate the referenced local amplification and simultaneous impedance measurement discussed in this disclosure.

**[83]** Many studies have demonstrated that fibrillatory rhythms are not random phenomena, but rather have definable patterns (Kadish A, et al., "Characterization of fibrillatory rhythms by ensemble vector directional analysis." *Am J Physiol Heart Circ Physiol.* 2003 Oct; 285(4):H1705-19. Epub 2003 Jun 5). However, prior art mapping techniques have limitations in their ability to identify the organization of fibrillation. The purpose of the illustrated embodiments of the invention is to develop and apply a method for detecting the energetic event by the ability of local amplifier with its inherent variable resistor Huygens™ sensor module to generate, for example, an "ensemble vector mapping" to characterize the spatiotemporal organization of fibrillation.

**[84]** Catheter-based ablation has revolutionized arrhythmia management by offering the most definitive treatment for virtually all types of tachyarrhythmias. The reasons behind the success of ablation are many, but chief among them is the ability of the electrophysiologists to identify underlying mechanisms and to precisely localize and eliminate the tachycardia foci or circuits. Unfortunately, mapping of high-dominant-frequency areas has been shown not to be effective in chronic atrial fibrillation (AF) patients. On the other hand, mapping of complex fractionated atrial electrograms (CFAE) as target sites for AF ablation has shown great promise. During sustained AF, CFAEs often are recorded in specific areas of the atria and exhibit surprisingly remarkable temporal and spatial stability. CFAEs usually are low-voltage electrogram (0.05 to 0.25 mV) with highly fractionated potential or with a very short cycle length ( $\leq 120$ ms). See Koonlawee Nademane, "Trials and Travails of Electrogram-Guided Ablation of Chronic Atrial Fibrillation", *Circulation.* 2007; 115: 2592-2594



**[85]** This is an important observation that a complex arrhythmia cannot be assumed to be defined as well as treated unless the underlying mechanism and precise identification of the vectorial direction as well as its magnitude can be established. The notion that the native signal-measurement can somehow be improved through a smart algorithm or a sophisticated mathematical filtering, manipulated by recursive methods, and/or wavelet analysis, is a misleading one. The native signal cannot be improved beyond its energy domain in its time scale or its geometric spacing. The signal noise components (SNR) and their representations cannot be altered by a post-processing approach. In contrast we teach a technological departure from the electrode technology with its post-processing approach, which is the mainstay of the prior art of biopotential data acquisition.

**[86]** The operative departure is the incorporation of local amplification at the source using, for example, a Huygens™ sensor module in an array form with geometry configurations such as bipolar, quadripolar, decapolar, or any array with 64 or more electrodes, to enable a multitude of electrodes/pads to simultaneously capture the complex electro-potential energetic event, with the improved SNR and sampling rate commensurable with the bandwidth and accuracy on the spatio-temporal domain. A mature scientific theory is characterized by its power of prediction to uniquely project an outcome based on boundary conditions that can be reproduced, where the specificity of the well-formed question results in a well-defined answer. The art of EP is in need of a radical review of its methodologies with regard to the relationship between its diagnostic findings and its loosely correlated clinical observations.

**[87]** As an example of the prior art clinical literature describing the underlying mechanism of patients with supraventricular tachycardia and paroxysmal atrial fibrillation consider the following statement. “Each patient underwent a baseline electrophysiologic study with closely spaced electrode catheter. . . . Paroxysmal atrial fibrillation (PAF) frequently occurred in patients with paroxysmal supraventricular Tachycardia (PSVT). However, the mechanisms responsible for the occurrence of PAF were not fully understood. Although previous studies have suggested that atrioventricular (AV) accessory pathway or slow AV node pathway itself may play an important role in the genesis of PAF, disturbed atrial electrophysiology during PSVT may be the other mechanism of initiation of PAF. Klein et al. have shown increased atrial refractoriness during PSVT and considered mechano-electrical feedback a cause of PAF during.” Chen Y, et al. “Role of atrial electrophysiology and autonomic nervous system in patients with supraventricular tachycardia and paroxysmal atrial fibrillation”, J Am Coll Cardiol. 1998;32(3):732-738

**[88]** It is clear from this statement that while the underlying cause is nested within multiple potential explanations relating to the mechanism that might lead to such conditions, no unique underlying mechanism was cited. The literature as noted above provides the explanations that the variability of the identifications

provided by studies, yields different mechanisms for the causes and its underlying mechanism, as discussed by the in many of the clinical studies are fashioned along the general outline shown above by Li et al.

**[89]** The complexity is clarified in why such conditions manifest themselves in the specific class of PAF: a conventional model for any assessment of the boundary conditions must be first subject to the ability of the measurement and its methodology including its measuring apparatus to yield consistent and repeatable data under similar conditions. The ambiguity and non-unique distinction of the mechanism generating the condition is a typical narrative in many clinical discussions and intellectual chatter of the various conferences on the topic of the underlying mechanisms of arrhythmogenic causes. In order to improve the art of measuring apparatus we employ a platform comprising a local amplifier using Huygens™ sensor array located at the target site to enable the mining of bioelectrical potential with fidelity and repeatability not currently available in the discipline of EP studies.

**[90]** The aim to form a standard model for EP is centered on the fact that the etiological as well as morphological elements forming the substrate of a biostructure must obey unique boundary conditions so that their specificity can be studied and reconstructed as well as predicted. The fact that most of the EP studies are a collection of phenomenological observations supports the contention that EP as a scientific discipline must undergo a change which must first be organized under the tool set and the ability of the physicians' community to recognize a generally accepted standard of data capture as well as a data format. The fact that many researchers and their publications tend to exhibit colorful plates with interesting isochrones does not constitute a "standard model," as the collection methods vary and its solution has a low predictability and reproducibility value.

**[91]** Huygens™ technology improves the art of EP by creating such a standardized model, unifying the diagnostic observations under a measurement technique able to define the electrocardiogram (EGM) as energetic events, distinguishing such applications from the massive digital signal processing (DSP) manipulation customary in the prior art.

**[92]** An overall view of the field of EP reveals a landscape of phenomenological collections of data with little to no specificity associated with the fact that the cellular excitable matrix is the result of specific etiological characteristics of the underlying substrate. If these data points were anchored by a robust physical and biological model, it will enable a simple translation between the electrical map and its substrate. Hence, the substrate will be directly correlated to the pathophysiology.

**[93]** This state of affairs is dependent on the ability of the roaming catheter to collect the electrical potential and place such data on its anatomical target synchronously. Additionally, the signal must be distinguished from its noise components to separate the native signal effect of the far-field component and its near-field contributing element.

**[94]** The fundamental technique of local amplification provides the user with native local signal where the near-field as well as its far-field component can be distinguished without post-processing employing algorithmic “gimmicks” and other sophisticated DSP manipulations.

**[95]** The disclosure is directed to a technology for capturing bioelectric potential data, which is anchored in measurement techniques that reveal the physical nature of a biological substrate’s electrical properties. This technology allows for the interpretation of the phenomenological expression of the electrogram (EGM) and its graphical representation in the context of an energetic event, based on the dielectric ( $\kappa$ ) and conductivity ( $\sigma$ ) measurements of underlying tissues.

**[96]** Electrophysiology studies employ a variety of devices, specifically catheters with different electrical configurations of electrodes using magnetic as well as electrical impedance techniques to form an electro-anatomical map. The fact that electroanatomic mapping fails to connect the inherent physical relationship between an energy transfer function and its causal dependency on the substrate, as represented by the electrogram, is the foundation for the utility of the local amplification, exhibited herein via the use of a Huygens™ sensor array shown in Fig. 11 for conducting electrophysiological studies.

**[97]** The method and exemplary apparatus which is presented enables the creation of an electroanatomic map in Fig. 5 with high fidelity and accuracy while depicting a *local* electrogram with its native dynamics, its geometrical as well as its time domain specificity and further providing for reconstruction of the anatomical and the extrapolated etiological characteristics of the cellular matrix by employing the Huygens™ sensor array apparatus.

**[98]** The aim and utility of this *local amplifier* technology is to connect the phenomenological data with clinical observations. The electrical properties of the conduction path within the substrate and its etiological constituents (e.g., cellular matrix composition and its electrical counterparts) are correlated without the need to create a causal dependency after the fact. This allows for the formation of a robust and coherent standard model in forming the diagnostic basis for defining a disease model, as noted by Tusscher et al.’s study presented at Europace. The study notes, “During aging, after infarction, in cardiomyopathies and other cardiac diseases, the percentage of fibrotic (connective) tissue may increase from 6% up to 10–35%. The presence of increased amounts of connective tissue is strongly correlated with the occurrence of arrhythmias and sudden cardiac death.” Tusscher, Panfilov. “Influence of diffuse fibrosis on wave propagation in human ventricular tissue.” Europace (2007) 9(suppl 6): vi38-vi45 doi:10.1093/europace/eum206. Fig. 4 illustrates the vulnerability to wave break and spiral wave formation due to diffuse fibrosis. Fig. 4 shows three snapshots in upper row A of the progression of two wavefronts initiated in a medium with 10% fibrosis and with a coupling interval of 321 ms between them; and three snapshots in lower row B of the progression of two wavefronts initiated in a medium with 30% fibrosis and with a coupling interval of 320 ms between them.

**[99]** Because of its high success and low morbidity rates, radiofrequency (RF) catheter ablation has become first line of treatment for many arrhythmias. In this procedure, one or more electrode catheters are advanced percutaneously through the vasculature to contact cardiac tissues. A diagnostic study is performed to define the arrhythmia mechanism, and subsequently an ablation catheter is positioned adjacent to the arrhythmogenic substrate. Radiofrequency energy of up to 50W is delivered in the form of a continuous unmodulated sinusoidal waveform, typically for 60 seconds. The arrhythmia is eliminated via the destruction of arrhythmogenic tissues (e.g., accessory pathways) and its subsequent replacement with scars.

**[100]** Fig. 7 illustrates the vulnerability to wave break and spiral wave formation due to diffuse fibrosis. Fig. 7 shows three snapshots in upper row A of the progression of two wavefronts initiated in a medium with 10% fibrosis and with a coupling interval of 321 ms between them; and three snapshots in lower row B of the progression of two wavefronts initiated in a medium with 30% fibrosis and with a coupling interval of 320 ms between them.

**[101]** In the electrogram approach in Fig. 5, because precise lesion placement is required, arrhythmias for which ablation are most effective (e.g., accessory pathways, atrioventricular nodal re-entry tachycardia [AVNRT]) have largely anatomically based or directed substrates. An electrode catheter in the coronary sinus outlines the mitral annulus fluoroscopically, and is used to guide ablation catheter position. The relative amplitude of the atrial and ventricular components of the bipolar electrogram recorded by the ablation catheter further defines the tip position relative to the annulus. The earliest atrial or ventricular activation during pathway conduction identifies pathway location along the annulus. The target for catheter ablation of AVNRT occurs even more predictably in the posteroseptum. Ablation may be guided entirely by anatomic location relative to the HIS bundle and coronary sinus catheter positions, which serve as fluoroscopic landmarks, or by a combined anatomical and electrophysiological mapping, such as those generated by CARTO™ or EnSite®.

**[102]**

### **[103] Complex Arrhythmias and the Limitations of Prior Art**

**[104]** However, ablation of more complex arrhythmias, including some atrial tachycardia, many forms of intra-atrial re-entry, most ventricular tachycardia, and atrial fibrillation continue to pose a major challenge (PA Friedman, “Novel mapping techniques for cardiac electrophysiology”, *Heart*. 2002 June; 87(6): 575–582). The current art of mapping lacks sufficient resolution to capture the complexity of the substrate fibrotic tissue and the collection rate lacks a sufficient sampling rate to address the dynamic range of the wave form dynamics. Both problems are addressed by the Huygens catheter with its SNR improvements, its dynamic range of 1KHz. This challenge stems, in part, from the foregoing limitations of the conventional fluoroscopy used in Fig. 6 as well as in the construction of prior art mapping catheters and sensory apparatus, which cannot accurately locate both the geometry and time domain of the wavefront’s activity generated by the “avalanche” of the cellular excitable

matrix. Thus, the primary disadvantage of the existing and prior art of electrode technology is in its inability to account for the cellular biopotential transfer with the resolution necessary to capture the energetic event, and the insufficiency of the prior art electrode technology to account for ionic transfer time depicting the actual energetic event, measuring and representing the “avalanche” dynamics of this bioenergetic event.

**[105]** The aim of using transistorized electrodes (i.e., the Huygens<sup>TM</sup> local amplifier circuit) is to accurately identify the conduction path in the heart tissue. An ideal conductor might, in general, satisfy the accuracy representation employed by the prior art, but in disease modeling, most of our assumptions relating to linear behavior of the conduction path (the cable theory) cannot be reproduced by such modeling, due to the impact of secondary and significant noise generating phenomena, such as vectorial multiplicity of sources generating the EGM, magneto-electric anisotropy, and conduction in the cardiac strand where gap-junction-mediated mechanisms alternate. Conventional ‘cable theory’ does not satisfy the ionic conservation law, and the Navier-Stokes equations with its diffusion modeling might be a better approximation of the ionic heart conduction, and its energy vector with its magnitude and direction than is provided by the cable theory.

**[106]** An obvious problem in separating the noise component from the native signal is the inability of the system to identify which is noise and which is the native signal in Fig. 7. If we know that a signal is smooth or changing slowly and that the noise is fluctuating rapidly, we can filter out noise by averaging adjacent data to eliminate fluctuations while preserving the trend. Noise can also be reduced by filtering out high frequencies. For smooth signals, which change relatively slowly and therefore are mostly lower frequency, this will not blur the signal too much. Many interesting signals are not smooth; they contain high-frequency peaks. Eliminating all high frequencies mutilates the message, namely “cutting the daisies along with the weeds,” in the words of Victor Wickerhauser of Washington University in St. Louis, adequately expresses the main drawback of post-processing such signal wavefronts (B Hubbard, “The World According to Wavelets: The Story of a Mathematical Technique in the Making”, Natick, MA: A K Peters, 1998).

### **[107] Signal-to-Noise Ratios**

**[108]** High signal-to-noise ratios (SNR) thus requires the use of a very low-noise amplifier with a limited bandwidth. The current technologies provide a differential amplifier with voltage noise of less than 10nV  $\sqrt{1\text{Hz}}$  and current noise less than 1pA. However, both parameters are frequency-dependent and decrease approximately with the square root of frequency; the exact relationship depends on the technology of the amplifier input stage. Field-effect transistor (FET) preamplifiers exhibit about 5 times the voltage noise density compared to bipolar transistors and a current noise density that is about 100 times smaller.

**[109]** In summary, the problem of reconstruction of the electrophysiological activity in the prior art is two-fold: first, in the architectural design of the use of electrodes and their associated electrical circuit design, and

secondly, in the further handicap caused by modeling the biopotential activity as a physical phenomenon, whereby excitable cells are modeled by employing the cable theory with isotropic behavior. The use of electrodes and cable theory is a good approximation of idealized conditions of such energetic events, but suffers from the inability to associate accurately the intracardiac electrogram with a specific endocardial site which also limits the reliability with which the roving catheter tip can be placed at a site that was previously mapped. This results in limitations when the creation of long linear lesions is required to modify the substrate, and when multiple isthmuses or “channels” are present. Additionally, since in conventional endocardial mapping a single localization is made over several cardiac cycles, the influence of beat-to-beat variability on overall cardiac activation cannot be known.

**[110]** The sensory apparatus and methods we teach captures the complexity, as well the time domain, of such energetic events synchronously. The Huygens™ sensor array and its fidelity further mimics the underlying dynamics, and improves conventional catheter-based mapping techniques by localizing and identifying precisely the arrhythmogenic substrates that are removed from fluoroscopic landmarks and lack characteristic electrogram patterns.

### **[111] Modelling of Bioelectrical Activity and Diffusion**

**[112]** The need to improve modeling of cellular electrical activity is central to physiology and electrophysiological studies. Biopotential recording and mapping of such electrical activity enables the physician or researcher to form and fashion his or her understanding of the fundamental data gathering and analysis of such diverse biological activities as sensory perception, communication between neurons, initiation and coordination of skeletal-muscle contraction, synchronization of the heartbeat, and the secretion of hormones. Most mathematical models of cellular electrical activity are based on the cable model, which can be derived from a current continuity relation on a one-dimensional ohmic cable. As such, its derivation rests on several assumptions: ionic concentrations are assumed not to change appreciably over the time of interest, and a one-dimensional picture of cell geometry is assumed to be adequate for purposes of describing cellular electrical activity. These assumptions, however, may not hold in many systems of biological significance, especially in the central nervous system and within cardiac tissue, where micro-histological features may play an essential role in shaping physiological responses.

**[113]** The first and far most assumption of electrophysiological mapping is the notion of linearity as well as homogeneous conduction path, both are refuted in light of the clinical observation associated with ephaptic coupling effect on the conduction path well as magnetic heart vector anisotropy, both affect the ECG



representation and its informative content. The corruptive measure of the electrogram fidelity and its true nature as to the native signal is highlighted herein.

**[114] Signal Anisotropy – Ephaptic Coupling**

**[115]** There are many contributions to the resultant signal shown by the electrogram, we mention two of the organizing principles which if accounted for under the conventional method of capturing the electrogram clearly demonstrate the shortcomings of the prior art. The first principle of organizing the electrogram set is the ‘cable theory’ and the second principle of organizing the biopotential activity is the ability of the representation system to account for the complementary ‘magnetic vector’ impact on the ionic cellular matrix. In both of these principles and their accompanying observations, no filtering methods of any sort improve the native fidelity of the signal. It is further shown by observations and analytical methods that any attempts to reconstruct such activity artificially by post-programming activity are doomed to fail, as these inherent bioelectrical activities (ephaptic, electromagnetic) are fundamental elements of the native signal. Ephaptic coupling is a form of communication within the nervous system and is distinct from direct communication systems like electrical synapses and chemical synapses. It may refer to the coupling of adjacent (touching) nerve fibers caused by the exchange of ions between the cells, or it may refer to coupling of nerve fibers as a result of local electric fields. Simply stated, the cable theory representation is an ideal depiction of the conditions generating the biopotential cellular avalanche, and it properly accounts for and describes the isotropic influences, but lacks the ability to discern influences such as magnetic heart vector and ephaptic coupling.

**[116]** Ephaptic coupling can’t be ‘washed’ out by some filtering; its effects must be accounted for by measuring its influence on the conduction path. This major drawback of the prior art, whereby the dynamics of the ionic potential with the necessary fidelity mimicking the actual energetic event are not accounted for. An example of such influence is the contribution of the cardiac gap junctions which play a pivotal role for the velocity of impulse propagation in cardiac tissue. Under physiologic conditions, the specific sub-cellular distribution of gap junctions together with the tight packaging of the rod-shaped cardiomyocytes underlies anisotropic conduction, which is continuous at the macroscopic scale. However, when breaking down the three-dimensional network of cells into linear single cell chains, gap junctions can be shown to limit axial current flow and to induce saltatory conduction at unchanged overall conduction velocities. In two- and three-dimensional tissue, these discontinuities disappear due to lateral averaging of the depolarizing current flow at the activation wavefront (S Rohr, “Role of gap junctions in the propagation of the cardiac action potential”, *Cardiovasc Res* (2004) 62 (2): 309-322). In this theory, the cellular path is represented as a cable, and hence it is referred to as “cable theory” (Lin & Keener, “Modeling electrical activity of myocardial cells incorporating the effects of ephaptic coupling”, *PNAS*. December 7, 2010; 107(49): 20935-20940), or the mathematical

modeling of bioelectrical current along passive neuronal fibers. Existing hardware employing electrode technology, coupled with the general algorithmic representation of the biopotential dynamics under such theory (both hardware and cable theory) suffer from the above-mentioned limitations, which are eliminated by the use of a local amplifier, such as a Huygens™ sensor array, and its method of map reconstruction.

**[117]** As outlined above the effect of ephaptic coupling as an inherent source of anisotropic behavior, impacts the conduction path of the bioelectric signal and its influence, and is well expressed in cases such as described in Fig. 11 (Mori Y, et al., “Ephaptic conduction in a cardiac strand model with 3D Electrodiffusion”, Proc Natl Acad Sci U S A. 2008 Apr 29;105(17):6463-8). This and other examples in vitro, as well as in vivo animal studies, demonstrate that conduction velocity and gap junction parametrics play a significant role in the formation of the conduction path and its origin, and can be shown as the result of the etiology of the cellular matrix change due to fibrotic formation. The ephaptic coupling is only one argument out of many cited above in support of our advocacy of using the Huygens™ sensor array in acquiring the biopotential signal. The use of impedance spectroscopy in the form of a Huygens™ sensor array provides for accurate representation of the bioelectric signal; due to its inherent electrical characteristics.

#### **[118] Signal Anisotropy, Modeling Bipotential Activity with the Poynting Energy Vector (PEV)**

**[119]** According to the present disclosure the analytical relationship between conduction path and the vectorial representation of anisotropic influence of the magnetic dipole vector on the conduction path provides a better determination of cardiac function. The behavior of the Poynting energy vector (PEV) shows that a representation of the ECG signal with its post-processing modality is a very crude approximation of the native bioelectric signal. The argument relating to the ephaptic coupling influence on the conduction velocity is supplemented by the magnetic heart vector's (MHV) contribution to the conduction path geometry and its timing, including synchronicity. Analytical evidence for anisotropy is noted when we employ Maxwell's equation. The data analysis and extraction of additional diagnostic (and as a corollary, the pathological diagnostic) information of the substrate is revealed when we create a map as shown in Fig. 8, where we superimpose the electric and energy waves as shown in a SPICE simulation (Simulation Program with Integrated Circuit Emphasis) converging the electric with the magnetic heart vector influence by computing impedance (Z) value generated from the substrate. The rightmost panel in Fig. 8 is a map of the heart conductivity paths. A central green arrow path maps out the path of a healthy patient having no anisotropies in the heart conduction pathway. The ECG map shown in the center panel of Fig. 8 is a map of the electrical heart wave in the cardiac field as marked by the pathway of black arrows. These two traces are superimposed on each other in the leftmost panel in Fig. 8 where it can be seen that the energy or PEV wave marked by the orange arrows diverges at a point from the electrical wave given by the ECG map. The point of divergence of the two pathways indicates an anisotropy in between the direction of energy flow of the heart wave and the

electric wavefront flow of the heart wave. This is indicative of the phase shift from orthogonally between the electrical and magnetic wave components in the heart wave. The anisotropy may be a site of scar tissue or a rotor, which is the cause of AF and if ablated may result in eradication of AF. Ablation then only at the points of divergence indicated in the superimposition diagram of Fig. 8 results in a electrophysiological directed or optimal ablation procedure characterized by reduced procedure time and increase efficacy.

**[120]** The measure of impedance is derived from an injection of a small current via the AC circuit to obtain a measure of conductivity of the tissue. Measuring the potential in microvolt- millivolt range we can estimate the anisotropic verses the isotropic wave conduction path. Since the conductivity of the medium is a representation of the conduction path, and if no fibrotic tissue-insulator or scar tissue is on the conduction path, the wave form travel path will follow a zero-phase shift (beta-90 degree will equal =0). But the conduction path in Fig. 8 did not follow the conductivity measure, hence there will be a phase shift of Beta – 90 degrees > 0.

**[121]** The measure of impedance is a form of injecting a small current via an AC circuit to obtain a measure of conductivity of the measured tissue. Measuring the potential in microvolt- millivolt range, we can estimate the anisotropic verses the isotropic wave conduction path. Since the conductivity of the tissue medium is a representation of the conduction path, and if no fibrotic tissue-insulator or scar tissue is in the conduction path, the waveform travel path will follow a zero-phase shift (beta-90 degree will equal =0). But if the conduction path does not follow the measured conductivity, there will be a phase shift of beta – 90 degrees greater than 0.

**[122]** To overcome the measurement limitations and supplement the clear clinical findings of myocardial anisotropy, we observed that simultaneous localization and mapping (SLAM) magnetic fields during the cellular activation sequence uncovers the magnetic heart vector (MHV) by computing a vector derived from Maxwell's equations, a process of data collection available only if we derive the PEV from the impedance vector ( $Z$ ) using the Huygens™ sensor array supplemented with a computational algorithm. Clinical observations reported (J. Malmivuo, et al. “Bioelectromagnetism”, Oxford University Press 1995) that measuring the angle between vectors of an equivalent electric dipole (electric heart vector, EHV) and magnetic heart vector or dipole (MHV) provides significant corollary information about the myocardium conductivity. The overall anisotropic case of the myocardium conductivity is represented by a tensor (Gerardo I et al., “Knowledge-based tensor anisotropic diffusion of cardiac magnetic resonance images”, Medical Image Analysis (1999) volume 3, number 2, pp 1–25: Oxford University Press). The degree of anisotropic conductivity manifestation is characterized by the angle along the transverse and axial conductivity paths.

**[123]** The solution for measuring and deriving the relationship between the EHV and its respective MHV, which supplements the analytical mapping with information about the myocardium conductivity and anisotropy, is derived from Maxwell's equation as the PEV. The PEV is constructed from the potential and impedance vectors of the measurements. In one application of the Huygens™ sensor array, a mapping catheter

is used for biopotential sensing. The phase difference  $\beta$  between the PEV and EHV is measured and is used to infer the features of anisotropy in the myocardium. The anisotropy of conductivity is uniform; that is to say, the change of activation energy generated and consumed by the ionic diffusion process is within the activation region of the measurement. The assumption is a healthy heart where there is no anisotropy in conduction path because the dielectric media formed by the excitable cells is uniform. Once scar tissue or fibrotic tissue is in the path, the permeability ( $\mu$ ) is changed, and the wave is shifted due to changed dielectric value. Hence there is a capacitive load which delays and/or prevents electrical charge transfer. Anisotropic shift is represented by the angle data of  $90 \text{ deg} - \beta$ .

**[124]** Thus, the volumes of integration are accurate with a margin of error reduction based on independent statistical samplings of the measured site over multiple heartbeats. “Accurate” means that the statistical measure is the averaging of the waveform relative to the QRS clock registered by the electrogram.

**[125]** The PEV derivation is based on the law of energy conservation when used for the time period over two QRS cycles to acquire the initial baseline data foundation to form the map. The validity of the PEV derivation is corroborated by the fact that the activation spread obeys a mathematical identity, namely the phase angle relationship between B (magnetic) and E (electrical) fields are at 90 degrees perpendicularity as defined by the formalism of Maxwell’s equations. The PEV directly exhibits the E and B fields’ phase angle relationship. The integral form of Maxwell’s equations leads to the PEV, and to the substitution of E and Z derivations of PEV. The following set of derivations from Maxwell’s time dependent equations provides a formal basis for the clinical observations of a Huygens™ sensor array to derive the Z impedance vector, hence demonstrating that the conduction path is measurable. The inverse method, namely substituting the B (magnetic flux density) and the Z (impedance value) formally in the 2<sup>nd</sup> varying Maxwell equation, and with the resultant PEV (Poynting Energy Vector) further supports the argument that the nature of the resultant electrogram supplemented by the use of the Huygens™ sensor array enables a clinical derivation of PEV from Maxwell’s equations. The availability of Z impedance vector is further evidence that the complex fractionated wavefront cannot be resolved by post-processing methodology as currently practiced by the use of conventional electrode technology.

**[126]** The argument is shown below using Maxwell’s equations.

**[127]** By multiplying B and E respectively and subtracting Equation (2) from (1) and using vector identities yields (3) and (4).

**[128]** (1)  $\nabla \times \mathbf{E} = -d\mathbf{B}/dt$

**[129]** (2)  $\nabla \times \mathbf{B} = \zeta\mu d\mathbf{E}/dt + \mu\mathbf{j}$

**[130]** (3)  $\mathbf{B} \cdot (\nabla \times \mathbf{E}) = -\mathbf{B} \cdot d\mathbf{B}/dt$

[131] (4)  $\mathbf{E} \cdot (\nabla \times \mathbf{B}) = \zeta \mu (\mathbf{E} \cdot d\mathbf{E}/dt) + \mu (\mathbf{E} \cdot \mathbf{J})$

where  $\zeta$  is conductivity derived from the impedance measurement. Subtracting, rearranging and using vector identities yields Eq. (5) which simplifies as Eq. (6)

[132] (5)  $\nabla \cdot (\mathbf{E} \times \mathbf{B}) = \mathbf{B} \cdot (\nabla \times \mathbf{E}) - \mathbf{E} \cdot (\nabla \times \mathbf{B})$

[133] (6)  $\nabla \cdot (\mathbf{E} \times \mathbf{B}) = -d/dx (1/2 \mathbf{B} \cdot \mathbf{B}) - d/dx (\zeta \mu \mathbf{E} \cdot \mathbf{E}) - \mu \mathbf{J} \cdot \mathbf{E}$

[134] Integrating both sides of Eq. (7) over the volume V and within the boundary Y gives (8), which is a representation of the energy equation in which the first term is the energy flux out of Y boundary of V.

[135] (7)  $\nabla \cdot [(1/\mu) \mathbf{E} \times \mathbf{B}] + d/dx [\zeta/2 \mathbf{E}^2 + 1/2 \mu \mathbf{B}^2] + \mathbf{J} \cdot \mathbf{E} = 0$

(8)  $\int_y \frac{1}{\mu} (\mathbf{E} \times \mathbf{B}) \cdot d\mathbf{S} + \frac{d}{dx} \int_v \left( \frac{\zeta}{2} \mathbf{E}^2 + \frac{1}{2\mu} \mathbf{B}^2 \right) d\tau + \int_v (\mathbf{J} \cdot \mathbf{E}) d\tau = 0$

[136] The second term in Eq. (8) is the rate of change of the sum of the electric and magnetic fields; the third term is the rate of work within V done by the fields on the ionic charges. This third term in Eq. (8) assumes the inclusion of the energy of the multiple sources of cellular ionic charge exchanges, thus (9) leads to the PEV, as shown in (11) where s below is the measurement of impedance value Z and a subsequent measurement of the position and orientation of the distal end of the Huygens catheter. Such measurement yields the input data point (in a mapping system such as EnSite NavX of St. Jude as described in electroanatomical mapping by L. Gepstein and S. J.Evans:PMID “Electroanatomical Mapping of the Heart: Basic Concepts and Implications for The Treatment of Cardiac Arrhythmias” where the position, orientation is performed by trilateration and the impedance by injection of ~2 millivolts of current to the endocardial tissue. The value of DC potential, Impedance and position/orientation of the catheter distal end indicate whether the site of such measurement computed by equation (8), yields the value of displacement (measured by angular displacement) leading to the results as shown in equation (12).

[137] (9)  $\mathbf{E} = 1/\mu (\mathbf{E} \times \mathbf{B}) + \mathbf{s}$  where  $\nabla \cdot \mathbf{s} = 0$

[138] (10)  $(\nabla \cdot \sigma) \nabla V_m = 0$  and  $\mathbf{E} = -\nabla \cdot V_m$

[139] (11)  $\mathbf{E} = 1/\mu ((\mathbf{E} \cdot \mathbf{E}) 1/Z) + \mathbf{c}$

[140] The parameter of interest is the angle  $\beta$  between the electric field and energy field; Eq. (12).

[141] (12)  $90^\circ - \alpha = \beta$

[142] The vector E is obtained from energy vector field measurements by calculating the Z impedance vector; Eq. (11). By using the measured potentials  $V_m$  and by employing Poisson equation, the E electric field is

obtained, Eq. (10). Then, the PEV can be written as Eq. (11). The E vector and impedance Z can be calculated from the measured data points. The value obtained by the use of this mathematical procedure,

$90^\circ - \alpha = \beta$ , indicates the maximal displacement between the magnetic heart vector (MHV) and the electric field. Such data is used to compute MHV- (which otherwise couldn't be measured directly), but by the use of the Poynting Energy Vector (PEV) technique, it is derived, thereby enabling the computation of the displacement of the MEV from its E electric field- using equation 10, the Poisson equation).

**[143]** It should be noted that such derivation is possible only by the use of the impedance value Z measured by the Huygens sensor array, and its preferred embodiment where position and orientation of the catheter distal end is captured in a tuple including time, DC potential, impedance, and the vector position/orientation of the catheter, thereby performing the mathematical operation noted above by identifying the maximal displacement of the MHV and its location, thereafter enabling a therapeutic procedure to correct the possible arrhythmogenic cause for a pacing disturbance.

**[144]** This is where the use of the Huygens™ sensor array plays the role of uncovering the substrate using the calculated impedance value Z which is used to plot the conduction path generated by the secondary effects associated with ephaptic coupling and the magnetic heart vector (MHV), both of which are inherent characteristics of the underlying substrate and cannot be manipulated by employment of post-processing filtering techniques. One can further calculate the angle  $\beta$  between the E field and E energy vector, where the difference is such that a display of the PEV energy vector is useful for cardiac disorder identification. The measurements of PEV energy data and Z conductivity data are collected from the electrocardiographic mapping and ablation catheter for further processing and display of the resultant anisotropic data, enhancing the current method. The PEV indicates that there is a flux of energy where E and B are simultaneously present. The spread of the energy flux in the case of Maxwell's derivation is further defined by the wave equation (13).

**[145]** (13)  $\nabla \times E = -dB/dt$

**[146]** Taking the curl of each side, Eq. (14), yields Eq. (15), which is the wave equation (16).

**[147]** (14)  $\nabla \times \nabla \times E = -d/dx (\nabla \times B)$

**[148]** (15)  $\nabla(\nabla \cdot E) - \nabla^2 E = -d/dx (\zeta\mu dE/dt)$

**[149]** (16)  $\nabla^2 E - \zeta\mu (\partial^2 E)/(\partial t^2) = 0$

**[150]** Utilizing the above-described technique, the electrophysiological map can be accurately tailored using post-processing methodologies, such as diffusion tensor and geometric representation (e.g., Ricci flow geometry). (I Bakas, "The algebraic structure of geometric flows in two dimensions", 2005; V Ivancevic,



“Ricci Flow and Nonlinear Reaction–Diffusion Systems in Biology”, Chemistry and Physics. 2011.) The data generated by the Huygens™ sensory array, in contrast, can serve to enhance the existing formation of electrophysiological maps and provide substantial improvement in the art of biopotential measurement and analysis.

**[151]** The resulting angular displacement of the MHV is then graphically indicated in the mapping created within the EnSite NavX and it is schematically illustrated by Fig. 8, where the measured Z impedance value is mapped using SPICE simulation against the electric potential and the magnetic heart vector. The resulting data collection shown in Fig. 8 is then graphically superimposed over the electroanatomical map generated by the use of EnSite NavX® system (Endocardial Solutions, St. Jude Medical, Inc., St. Paul, MN, USA). The geometrical site(s) indicating the position of a divergence between the electric field (E) and the magnetic field (B) are then graphically displayed as focal points and indicated by the graphic as “energy and E vector display” and marked as “a problem” in Fig 8. This schematic representation enables a diagnostic site for the operator to evaluate the treatment modality necessary such as it is customarily employed, namely a therapeutic application of ablation is employed to eliminate the focal sites of the pacing disturbance.

**[152]** The use of the Huygens™ sensor array for mapping of electrophysiological attributes is centered on the formation of a junction by bipolar electrodes/pads between the cellular matrix and the contact surface of the bioelectrical signals generated by nerves and muscles, recorded as potentials, voltages, and electrical field strengths. The measurements involve voltages at very low levels, typically in the vast range from 1μV–100mV, with high source impedances and superimposed high level interference signals and noise. Furthermore, the signals are amplified for compatibility with devices such as displays, recorders, or A/D converters for computerized equipment. To adequately measure these signals, an amplifier must satisfy very specific requirements: (1) to provide selective amplification to the physiological signal, and (2) to reject superimposed noise and interference signals.

**[153]**

**[154] Local Amplifier Huygens Biopotential Measurements**

**[155]** The basic requirements that a biopotential amplifier such as the Huygens™ sensor array and its catheter structure must satisfy are: (1) The physiological process to be monitored should not be influenced in any way by the amplifier. No galvanic contact exists between the cellular surface and the conducting part of the sensor, thus preventing the occurrence of any Faradic current. (2) The measured signal should not be distorted. Ephaptic coupling as well as PEV must be accounted for by synchronously measuring such effects with suitable quality by the Huygens™ sensor array. (3) The amplifier should provide the best possible separation of signal and interferences. Near-field versus far-field phenomenon must be separated by mining the inherent differentiating elements without averaging such contributions. (4) The amplifier must offer protection to the patient from any hazard of electrical shock, such as using isolated FET and circuit architecture. (5) The amplifier itself has to be protected against damage that might result from high input voltages as they occur during the application of defibrillators or electrosurgical instrumentation and application of RF energy during ablation.

**[156]** A fundamental aspect of clinical EP, the discipline of diagnosing and treating cardiac arrhythmias, is the interpretation of intracardiac electrical signal electrograms. All EGMs represent a voltage difference between two electrodes, whether the electrodes are in close proximity (e.g., bipolar EGMs) or at a relatively great or theoretically infinite distance (e.g., unipolar EGMs). A major disadvantage of unipolar recordings is that they contain a significant amount of “far-field” signal, i.e.: signals generated by depolarization of tissue remote from the recording electrode. The near-field signal exhibits a decay to zero potential along the X-axis, while the far-field indicates that the signal does not decay to zero potential, and is asymptotically parallel to the X-axis. Hence the use of the Huygens™ local amplifier with its variable resistor and ground at the site of measurement enables a clean separation between the far-field and near-field contribution to prevent the averaging of the resultant signal from the native measured potential. This advantage has an enormous contribution to the diagnostic value of the electrogram and can clearly improve the behavior of the ICD leads’ optimal performance when detecting such a composite signal.

**[157]** For example, EGMs from pulmonary vein ostia frequently manifest large far-field atrial signals recorded from regions that are at the border between the atrium and the pulmonary vein. Separating the signal of interest, in this case the pulmonary vein fiber potential (high-frequency signal) from the far-field atrial signal, which is a lower-frequency, and usually much larger signal, can sometimes be difficult, and requires pacing maneuvers and empirical RF energy application. In addition, differences in electrode sizes, for example a large ablation distal electrode compared to a smaller proximal electrode, might exaggerate the potential differences between the two electrodes and distort the resultant EGM signal amplitude, which is important for recording

scar voltage. In addition, the direction of wavefront propagation influences the amplitude of the bipolar EGM, but not that of the unipolar EGM. Theoretically, a wavefront that propagates in a direction that is exactly perpendicular to the axis of the recording dipole would produce no potential difference, hence no EGM signal. The clinical significance of this scenario in mapping scarred tissue is unknown, as these maps are dependent on displaying areas of low voltage as areas of scarred myocardium.

**[158]** Prior art intracardiac recording techniques, while they have served the clinician and basic scientists reasonably well over the past three to four decades, suffer from several inherent limitations, which this patent collection seeks to address, such as: (1) By the very nature of utilizing electrodes connected by long cables to a distant differential amplifier, these systems are subject to line “noise,” ambient EMI, cable motion artifacts, and faulty connections. (2) Local signals are subject to recording of far-field signals, which at times render the interpretation of complex, rapid arrhythmias very difficult, if not impossible. (3) The conflation of far-field and signals of real interest, such as pulmonary vein fiber potentials, accessory pathway signals, and slow pathway potentials, can sometimes be the cause of failed ablations. The ability to record local electric activity with great precision and to the exclusion of far-field signals would be of paramount importance. (4) Current recording systems frequently cannot differentiate low-amplitude, high-frequency signals from background noise. Extremely low-amplitude signals, such as those generated during slow conduction within a myocardial scar, are frequently missed or lost in the background noise when amplifier gain is made sufficiently high to attempt to record such signals. (5) Continuous, low amplitude, fractionated high-frequency signals such as those frequently seen in the atria of patients with chronic atrial fibrillation, cannot be further characterized using existing recording technologies. These signals may contain important biologic and electrophysiologic information. For example, these signals may represent important areas of scarring that are responsible for formation of rotors. Alternatively, they may be manifesting discharges from contiguous epicardial parasympathetic ganglionated plexi.

**[159]** In a near-field waveform the potential decreases monotonously with distance from the source, whereas an overlying far field source is constant and non-vanishing, representing the difference in potential between far-field and near-field (Cracco RQ, et al. “Somatosensory Evoked in Man: Far-field Potentials.” *Electroenceph Clin Neurophysiol* 1976; 41:460-46). This difference between the waveform relative to the distance does not decrease over time, and can be subtracted by using a fast-acting local bipolar measurement available through the use of the Huygens™ sensor array.

**[160]** In conclusion, the limitations in the prior art of electrode technology indicate the need to supplement the existing technology with a local amplifier technology, such as exhibited in the use of the Huygens™ sensor array. The Huygens sensor array may be geometrically configured as unipolar, bipolar, quadripolar, decapolar, and other linear arrays, and optionally as, for example, an 8x8 sensor matrix placed on a basket- or balloon-like structure, as well as incorporated into other related devices in various arrayed and matricular configurations.

**[161]** These applications of the Huygens™ sensor technology offer great potential in the furthering of electrophysiological studies, including the understanding of the mechanisms of complex arrhythmias.

**[162]** Many alterations and modifications may be made by those having ordinary skill in the art without departing from the spirit and scope of the embodiments. Therefore, it must be understood that the illustrated embodiment has been set forth only for the purposes of example and that it should not be taken as limiting the embodiments as defined by the following embodiments and its various embodiments.

**[163]** Therefore, it must be understood that the illustrated embodiment has been set forth only for the purposes of example and that it should not be taken as limiting the embodiments as defined by the following claims. For example, notwithstanding the fact that the elements of a claim are set forth below in a certain combination, it must be expressly understood that the embodiments include other combinations of fewer, more or different elements, which are disclosed in above even when not initially claimed in such combinations. A teaching that two elements are combined in a claimed combination is further to be understood as also allowing for a claimed combination in which the two elements are not combined with each other, but may be used alone or combined in other combinations. The excision of any disclosed element of the embodiments is explicitly contemplated as within the scope of the embodiments.

**[164]** The words used in this specification to describe the various embodiments are to be understood not only in the sense of their commonly defined meanings, but to include by special definition in this specification structure, material or acts beyond the scope of the commonly defined meanings. Thus, if an element can be understood in the context of this specification as including more than one meaning, then its use in a claim must be understood as being generic to all possible meanings supported by the specification and by the word itself.

**[165]** The definitions of the words or elements of the following claims are, therefore, defined in this specification to include not only the combination of elements which are literally set forth, but all equivalent structure, material or acts for performing substantially the same function in substantially the same way to obtain substantially the same result. In this sense it is therefore contemplated that an equivalent substitution of two or more elements may be made for any one of the elements in the claims below or that a single element may be substituted for two or more elements in a claim. Although elements may be described above as acting in certain combinations and even initially claimed as such, it is to be expressly understood that one or more elements from a claimed combination can in some cases be excised from the combination and that the claimed combination may be directed to a subcombination or variation of a subcombination.

**[166]** Insubstantial changes from the claimed subject matter as viewed by a person with ordinary skill in the art, now known or later devised, are expressly contemplated as being equivalently within the scope of the claims. Therefore, obvious substitutions now or later known to one with ordinary skill in the art are defined to be within the scope of the defined elements.

**[167]** The claims are thus to be understood to include what is specifically illustrated and described above, what is conceptionally equivalent, what can be obviously substituted and also what essentially incorporates the essential idea of the embodiments.

---

What is claimed is:

1. An improvement in a method of sensing biopotentials in tissue comprising:  
providing a Huygens sensor array characterized by native biopotential signal sensing with local amplification and signal processing at or proximate to electrode signal pickup; and  
sensing the native electrical biopotential signal using at least one electrode on the Huygens catheter to generate a well-formed waveform of the biopotential showing electrical properties indicative of the tissue with a SFDR of at least 24.9dB and SNR of at least -13dB.
2. The method of claim 1 where the tissue comprises cardiac tissue and where the biopotential signal comprises a native cardiac waveform.
3. The method of claim 1 where the biopotential signal comprises a manifestation of underlying electrochemical activity of a biological substrate corresponding to the tissue.
4. The method of claim 3 where the manifestation of underlying electrochemical activity of a biological substrate corresponding to the tissue comprises an energetic event characterized by vectorial direction and magnitude.
5. The method of claim 3 where the manifestation of underlying electrochemical activity of a biological substrate corresponding to the tissue comprises a representation of underlying substrate composition of the tissue.
6. The method of claim 3 where the manifestation of underlying electrochemical activity of a biological substrate corresponding to the tissue comprises a biopotential measurement using the Huygens sensor array to generate a representation of the energy contents on the spatial and time domains of a complex cardiac waveform, leading to a recursive relationship between a graphical representation of the cardiac waveform and an underlying biopotential substrate which is a source of the cardiac waveform.
7. The method of claim 3 where the manifestation of underlying electrochemical activity of a biological substrate corresponding to the tissue comprises a mapping technique which characterizes global dynamics of cardiac wavefront activation based on cellular etiology and corresponding dielectric ( $\kappa$ ) and conductivity ( $\sigma$ )



characteristics of the tissue representing complex inter-relationships of avalanche dynamics translated through a measured myocardial space arising from spatial and temporal ionic potentials measured by a local amplifier Huygens sensor array.

8. The method of claim 1 where sensing a native electrical biopotential signal using at least one electrode on a catheter with an amplifier circuit placed on the inner surface of the at least one electrode in the Huygens sensor array comprises sensing by performing impedance spectroscopy.

9. The method of claim 1 where sensing a native electrical biopotential signal using at least one electrode on a catheter with an amplifier circuit placed on the inner surface of the at least one electrode in the Huygens sensor array comprises sensing an energetic event represented by the native electrical biopotential signal in the tissue by relating its inherent characteristics of time, magnitude and direction without post-processing of the native electrical biopotential signal.

10. The method of claim 1 where sensing a native electrical biopotential signal using at least one electrode on a catheter with an amplifier circuit placed on the inner surface of the at least one electrode in the Huygens sensor array comprises sensing the native electrical potential signal using a local amplifier which acts as variable resistor with an on-site electrical ground, which ground is not subject to noise pickup to improve signal-to-noise ratio (SNR), spurious-free dynamic range(SFDR), signal fidelity, sampling rate, bandwidth, and differentiation of far-field from near- field components of the sensed native electrical potential signal.

11. The method of claim 1 further comprising using the Huygens sensor array with a conventional mapping station without alteration of the mapping station.

12. The method of claim 1 further comprising detecting an energetic event in the tissue using the Huygens™ sensor array to generate an ensemble vector map to characterize spatiotemporal organization of cardiac fibrillation.

13. The method of claim 1 further comprising using the Huygens™ sensor array with a predetermined geometric configurations, including bipolar, quadripolar, decapolar, or any array with 64 or more electrodes, to enable a plurality of electrodes to simultaneously capture a complex electro-potential energetic event, with an improved SNR and sampling rate commensurable with a bandwidth and accuracy in a spatio-temporal domain.

14. The method of claim 1 further comprising capturing bioelectric potential data, which is anchored in a measurement that reveals the physical nature of a biological substrate's electrical properties of underlying tissue to allow for interpretation of the phenomenological expression of an electrogram (EGM) and its graphical representation in the context of an energetic event, based on the dielectric ( $\kappa$ ) and conductivity ( $\sigma$ ) measurements of underlying tissue.
15. The method of claim 1 further comprising connecting an electroanatomical map with an inherent physical relationship between an energy transfer function and its causal dependency on a substrate tissue as represented by an electrogram by using a Huygens<sup>TM</sup> sensor array for conducting an electrophysiological study.
16. The method of claim 1 further comprising connecting phenomenological data with clinical observation so that electrical properties of a conduction path within a cardiac substrate and its etiological constituents are correlated without the need to create a causal dependency.
17. The method of claim 1 further comprising synchronously capturing spatial and temporal complexity of an energetic cardiac event using the Huygens<sup>TM</sup> sensor array to mimic underlying cardiac dynamics by localizing and precisely identifying arrhythmogenic substrates removed from fluoroscopic landmarks and lacking characteristic electrogram patterns.
18. The method of claim 1 further comprising generating a cardiac map comprised of superimposed electric and energy (Poynting) wave maps by converging electric heart vector with the magnetic heart vector by computing an impedance ( $Z$ ) value generated from the substrate.
19. The method of claim 1 further comprising simultaneously localizing and mapping (SLAM) magnetic fields during a cardiac activation sequence to uncover a magnetic heart vector (MHV) by computing a Poynting energy vector (PEV) from a measured impedance vector ( $Z$ ) sensed using the Huygens<sup>TM</sup> sensor array with a computational algorithm.
20. The method of claim 1 further comprising measuring a phase difference,  $\beta$ , between PEV and EHV to infer features of anisotropy in a myocardium.
21. The method of claim 1 further comprising differentiating far-field from near-field signal sources in a pacemaker lead by using a Huygens<sup>TM</sup> sensor array to effectively prevent false positive events.



**[168] Abstract of the Disclosure**

**[169]** With respect to the methodology of using the Huygens sensing array, the invention includes an improvement in a method of sensing biopotentials in tissue including the steps of: providing a Huygens sensor array; and sensing a native electrical biopotential signal using at least one electrode on a catheter with an amplifier circuit placed on the inner surface of the at least one electrode in the Huygens sensor array to generate a well- formed waveform of the biopotential showing clear electrical properties indicative of the tissue with a SFDR of at least 24.9dB and SNR of at least -13dB. In one embodiment the tissue is cardiac tissue and the biopotential signal sensed by the Huygens sensing array is a native cardiac waveform. In one embodiment the sensed biopotential signal is a manifestation of underlying electrochemical activity sensed by the Huygens sensing array of a biological substrate corresponding to the tissue.

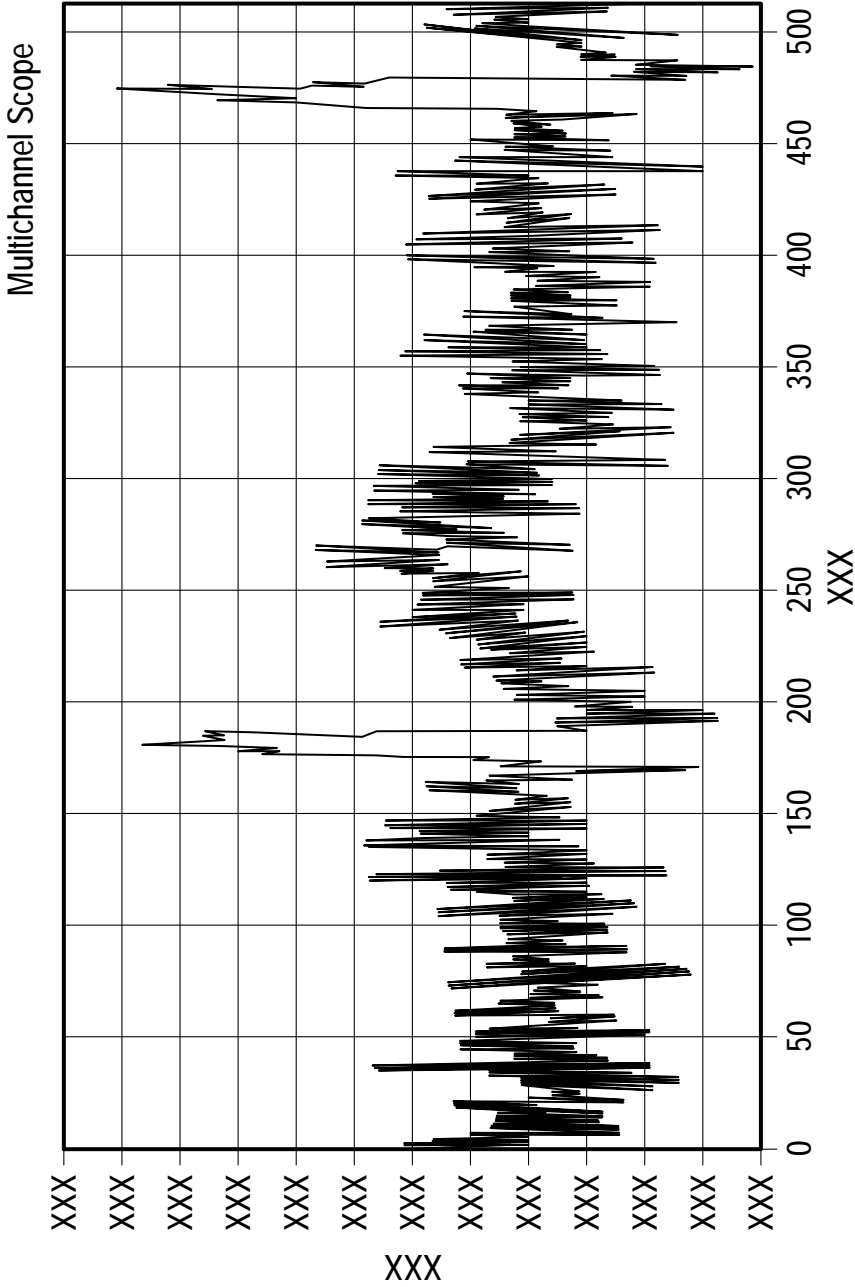


FIG. 1

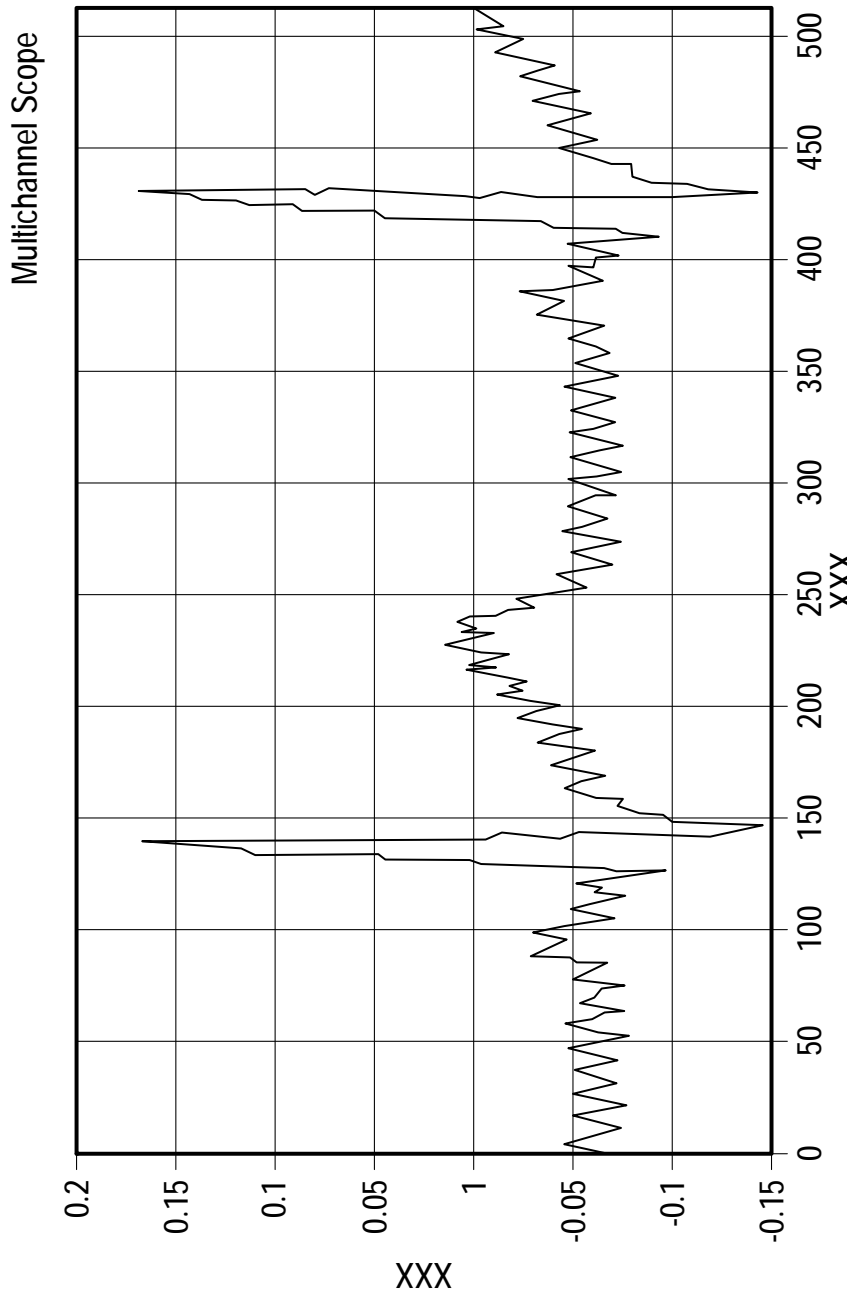


FIG. 2



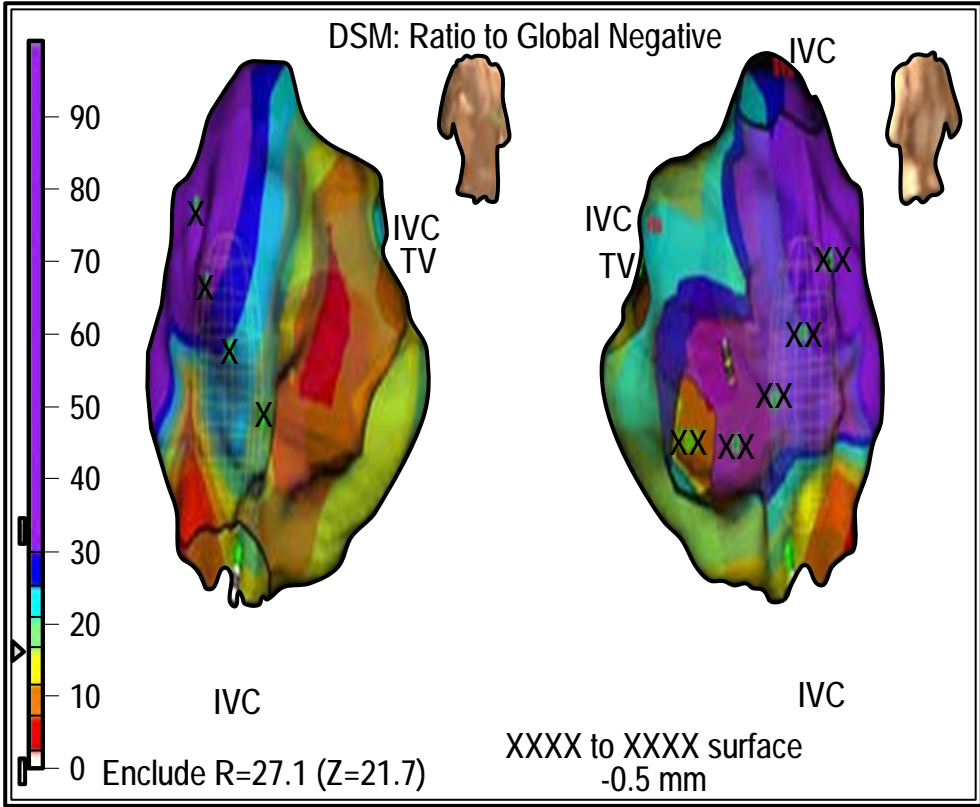


FIG. 3

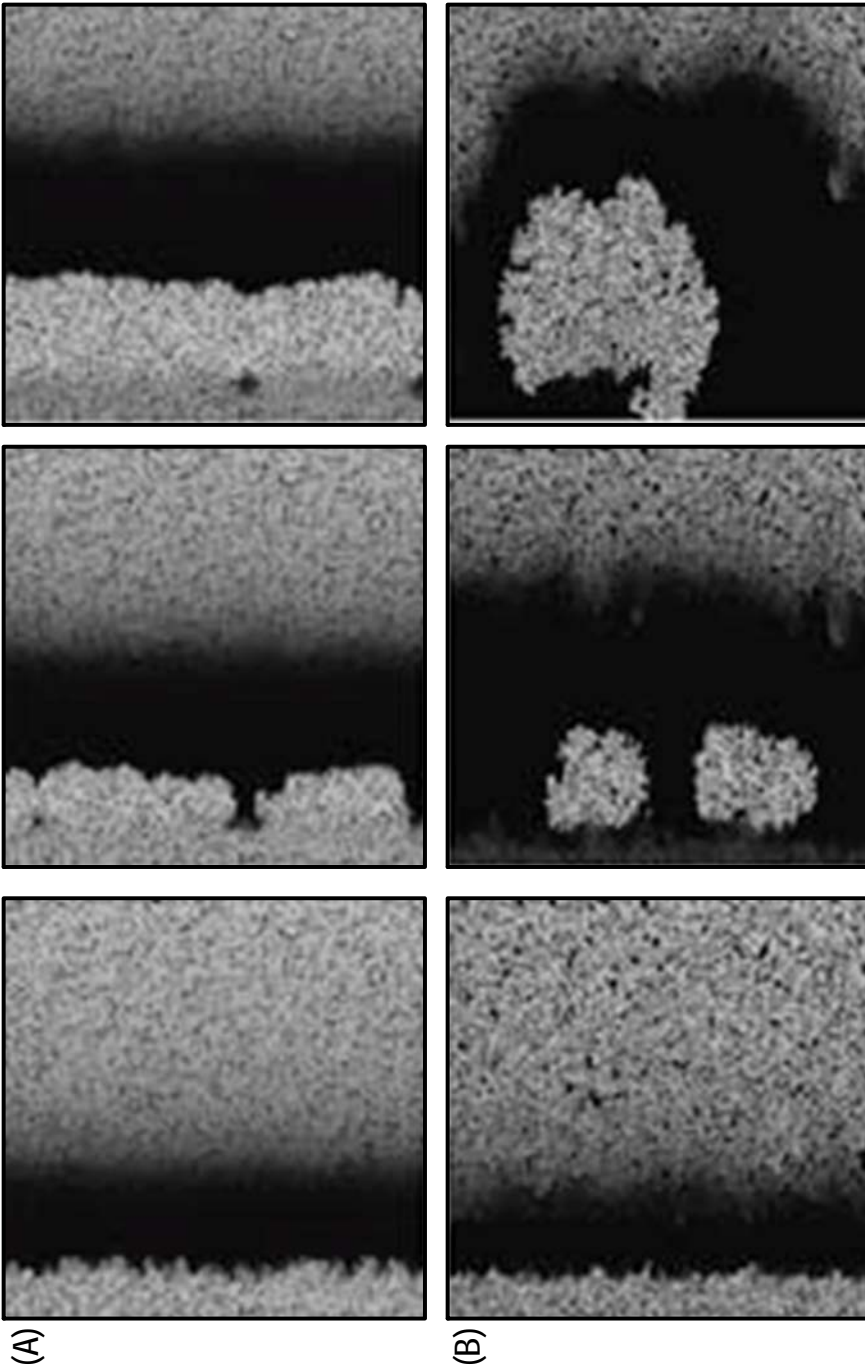


FIG. 4

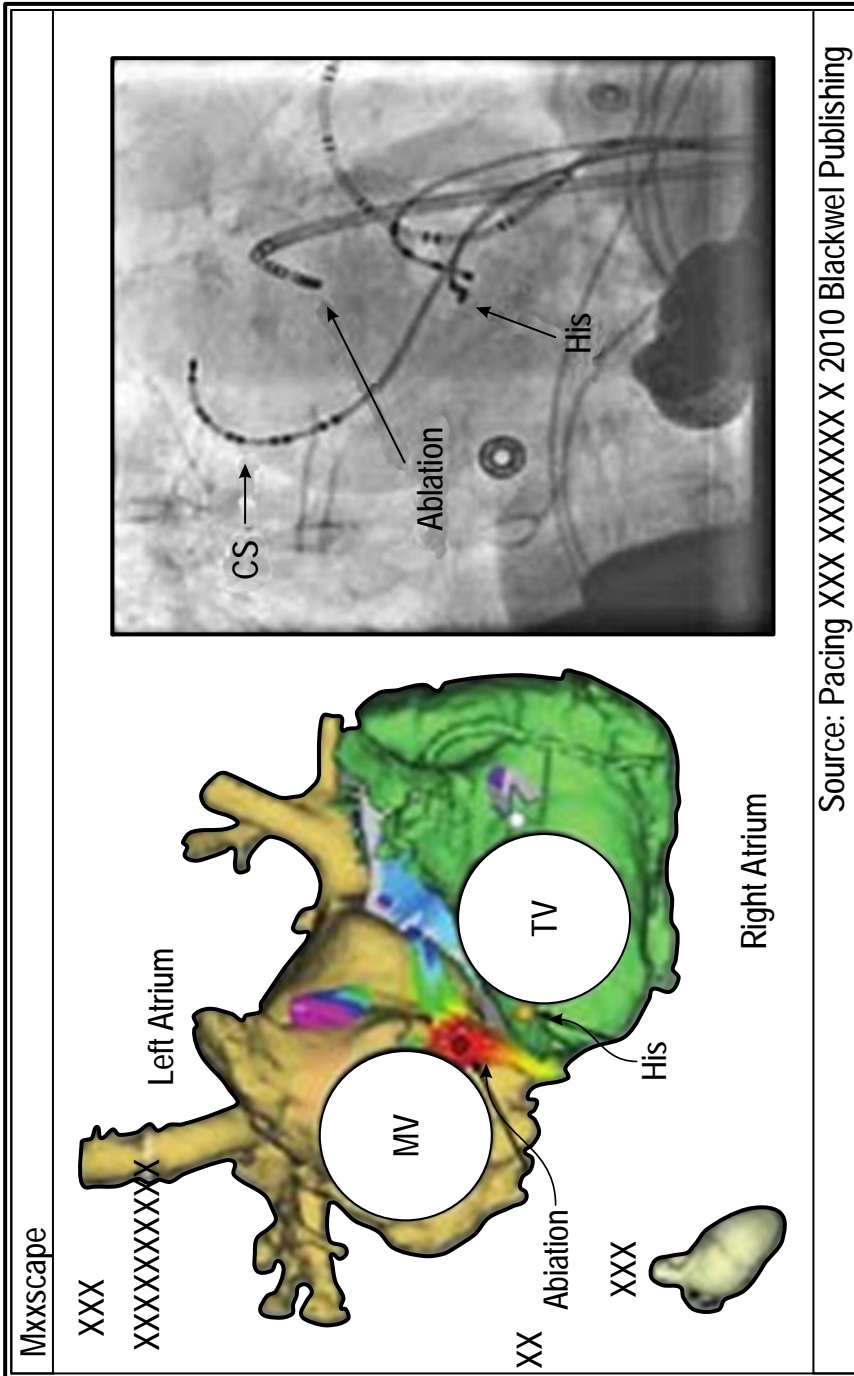


FIG. 5

6/11

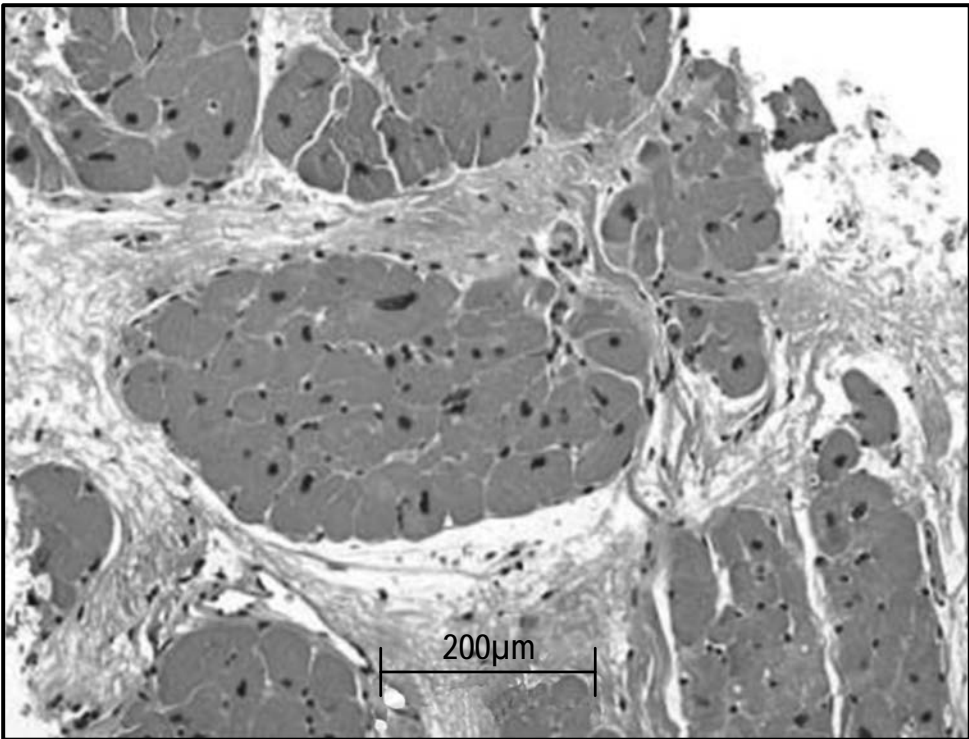


FIG. 6

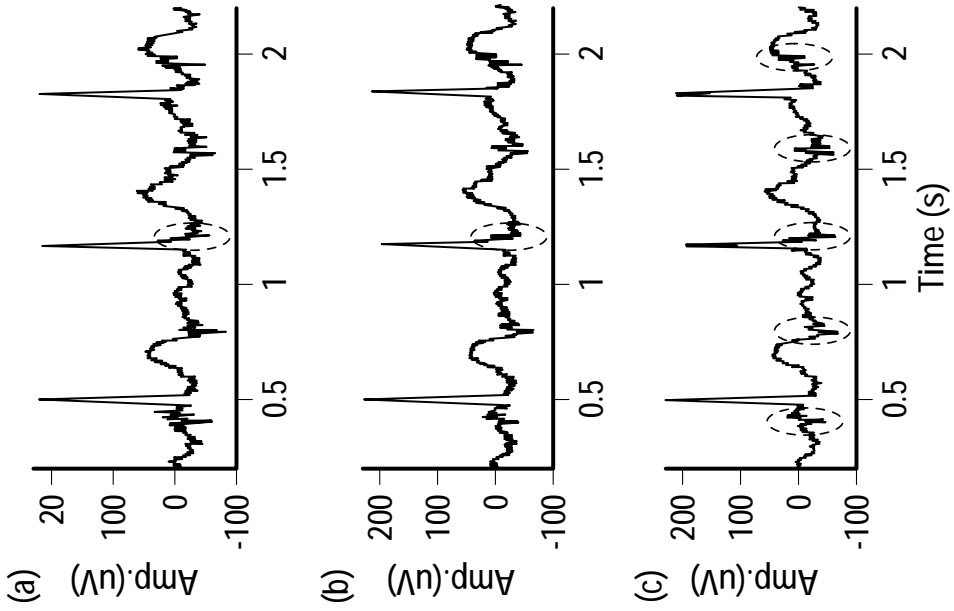
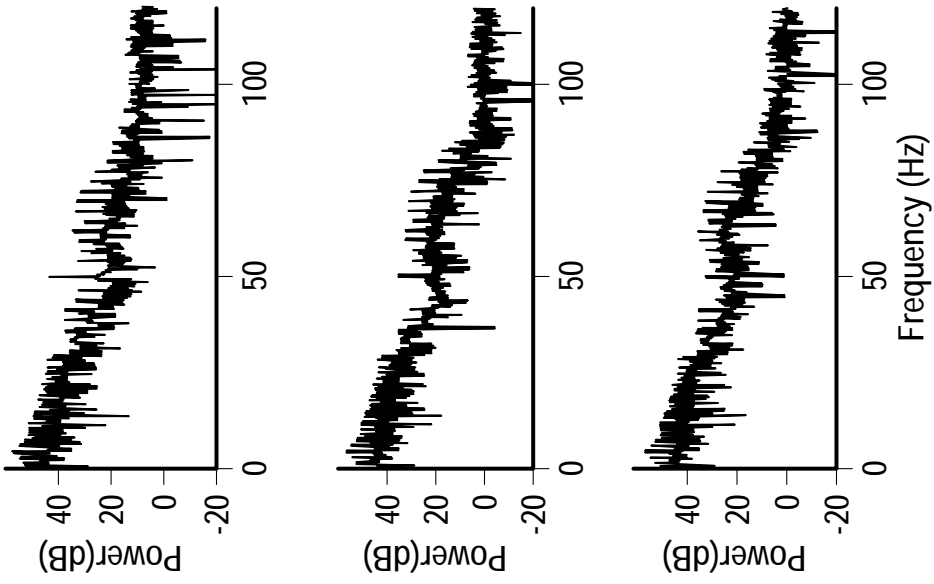


FIG. 7



7/11

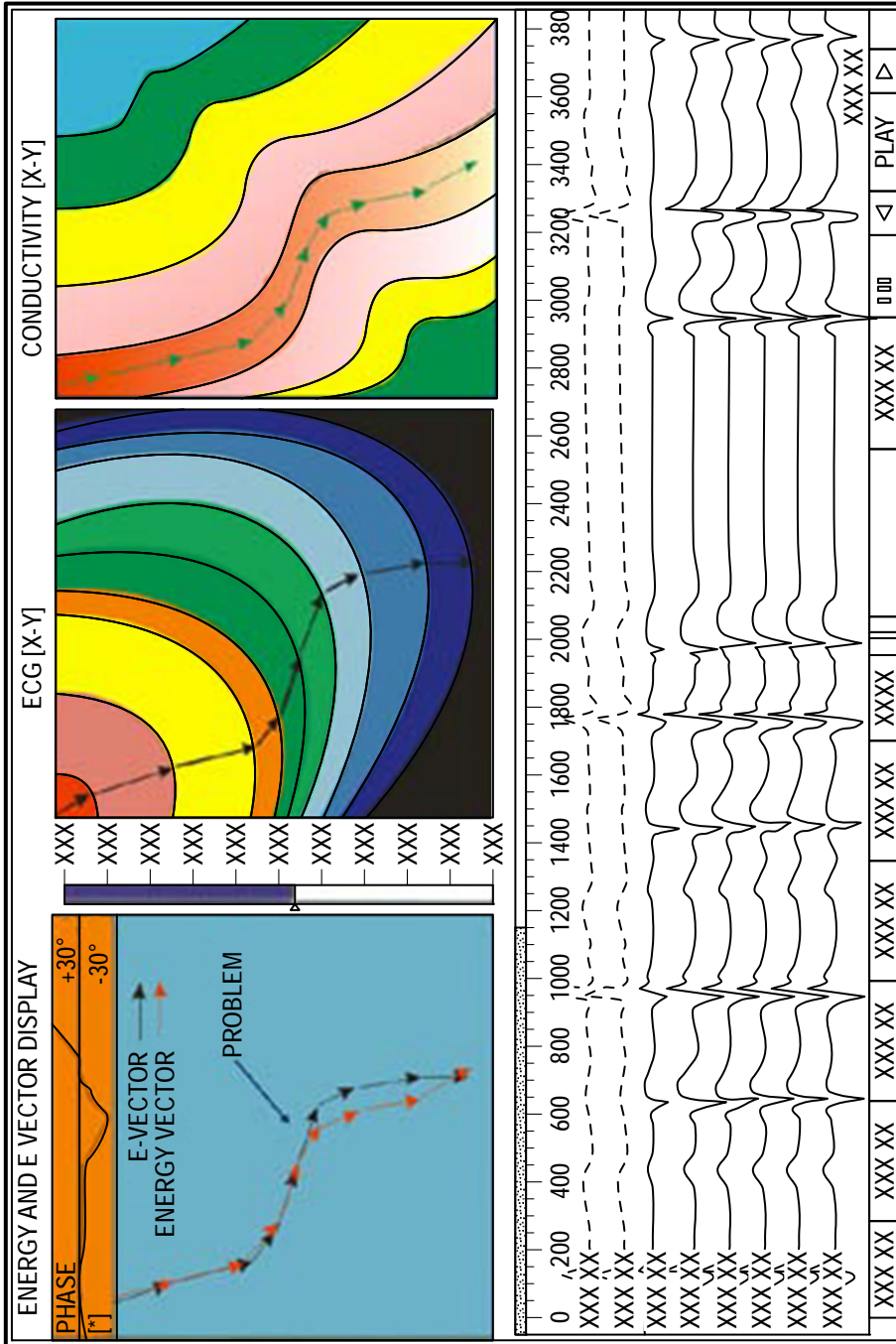


FIG. 8

9/11

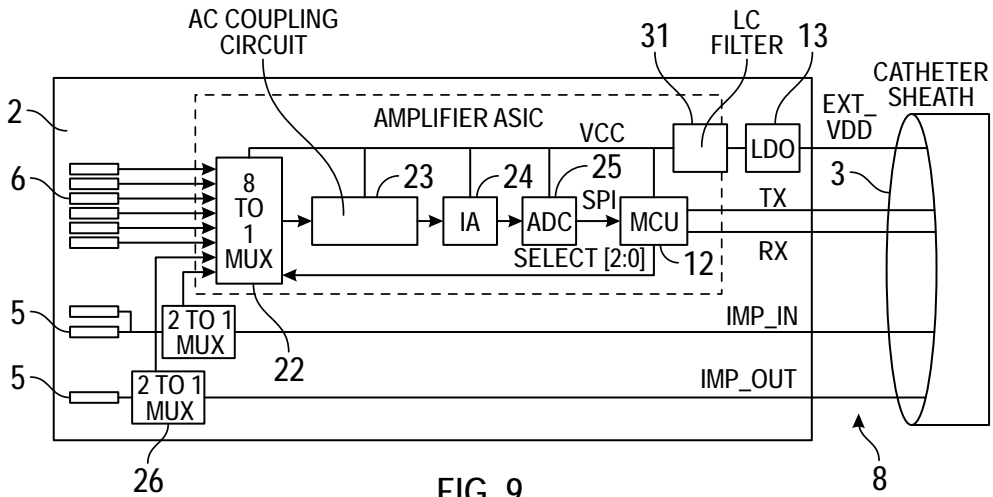


FIG. 9

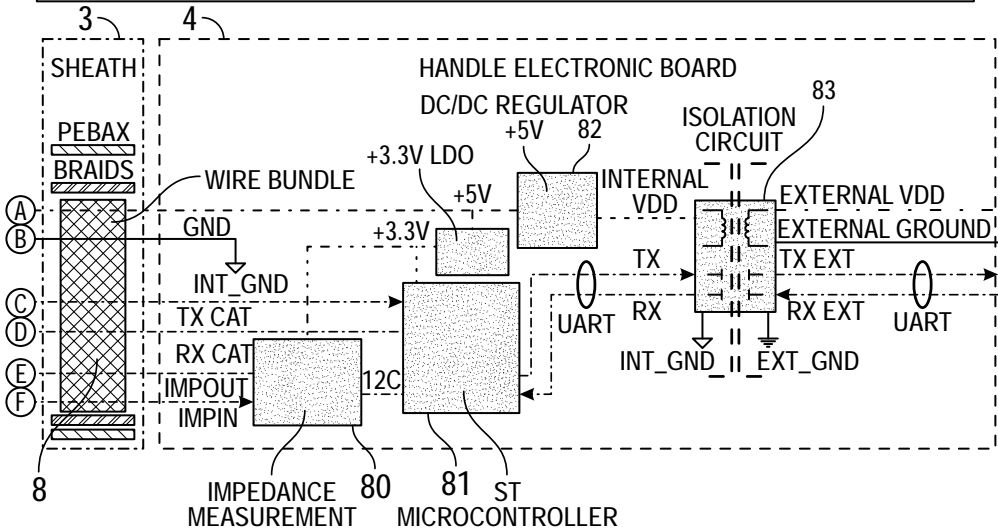
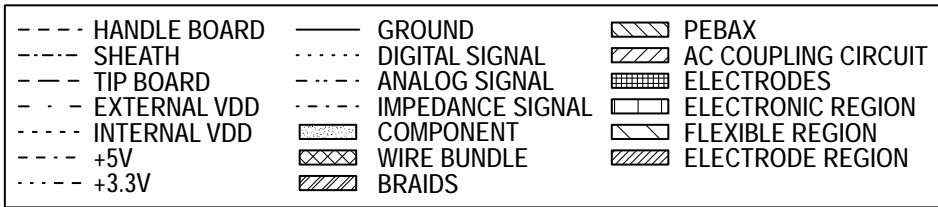


FIG. 10



10/11

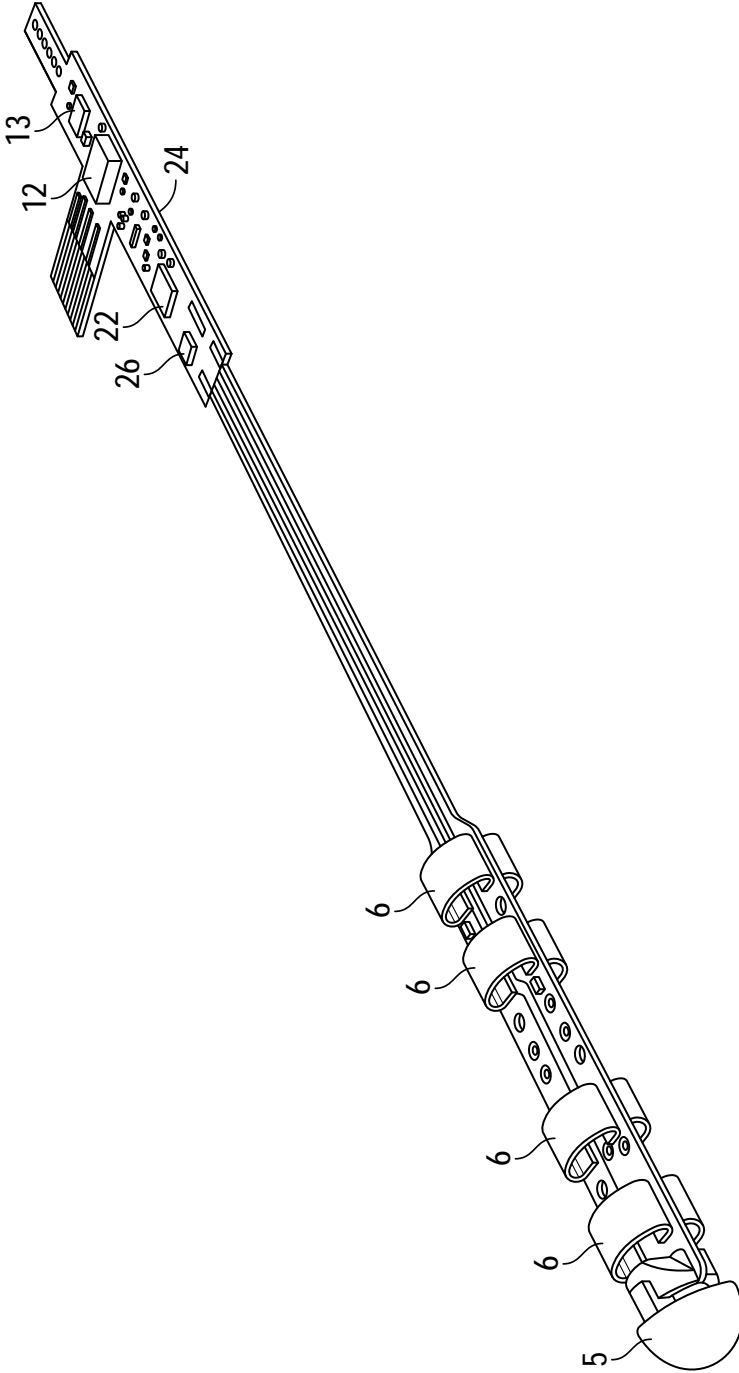


FIG. 11

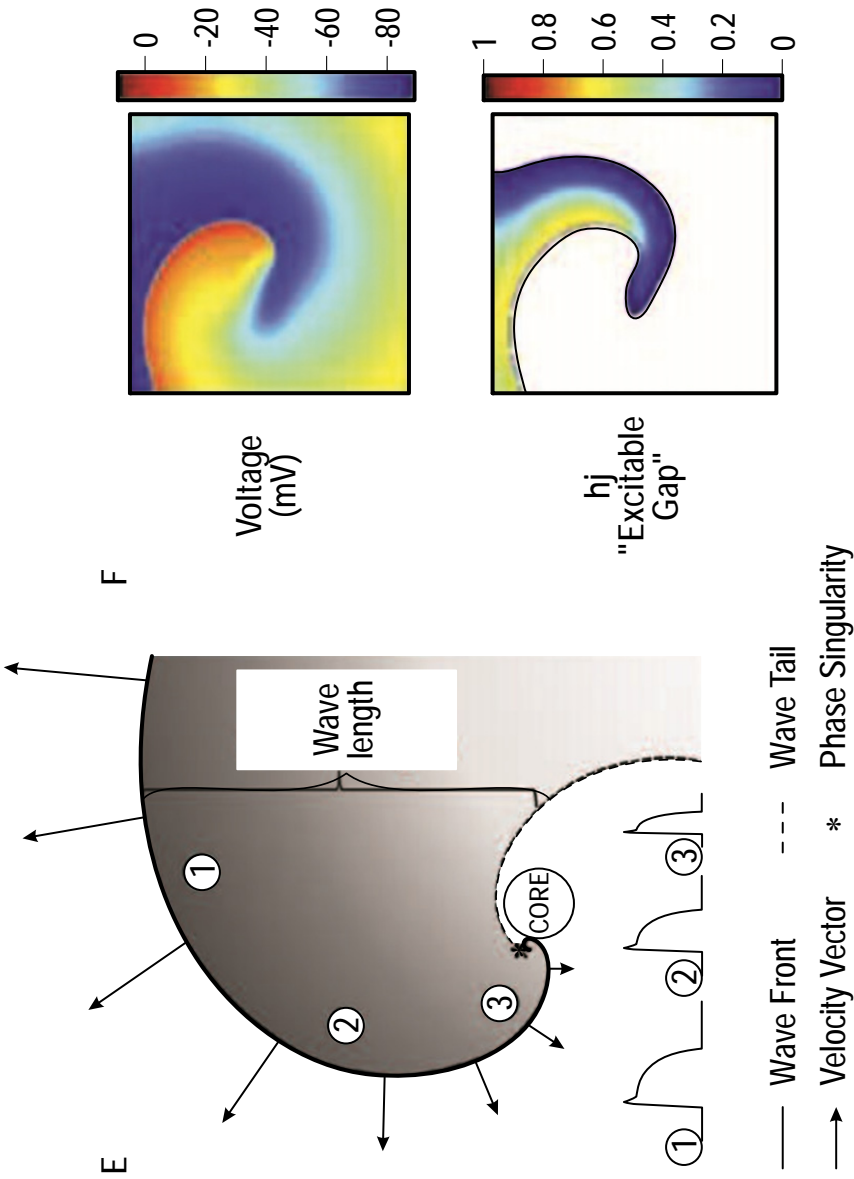


FIG. 12

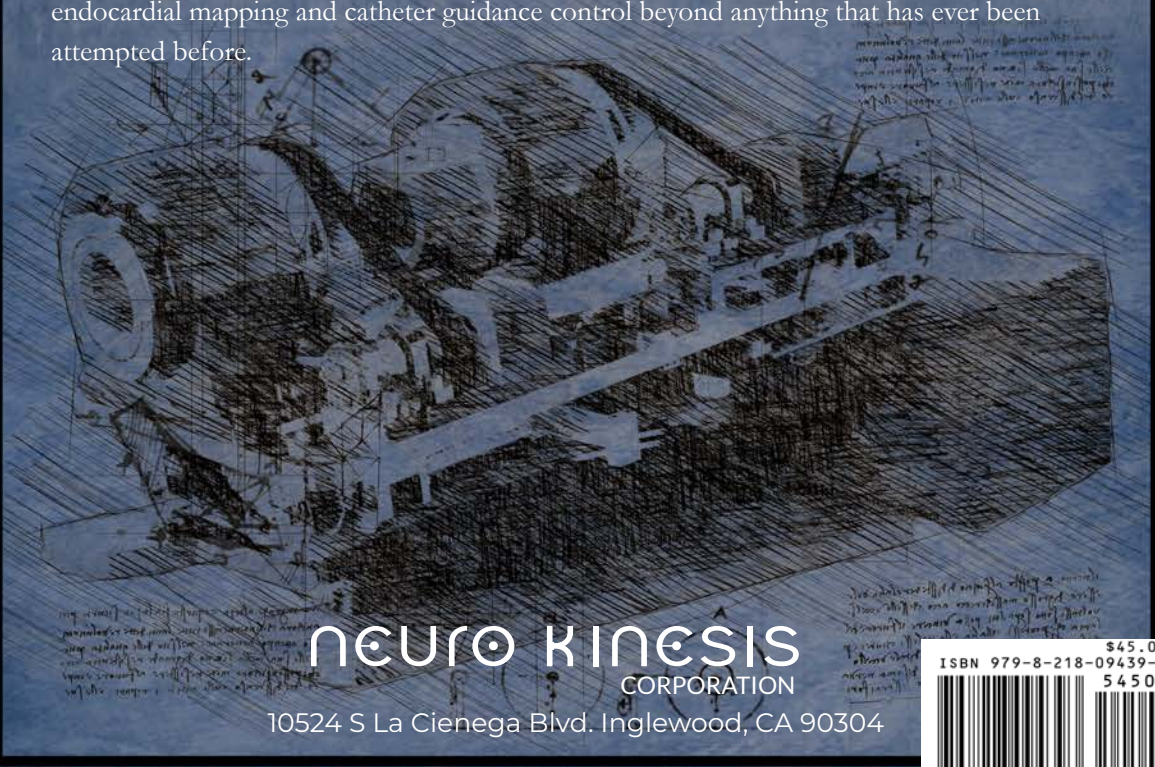




“Through all my work runs the mantra, ‘Do it better, do it smarter to create a better outcome for everyone.’ In creating the vision for Neuro-Kinesis, our focus was to take the discoveries we had made in robotic-assisted catheter guidance over the last two decades and re-imagine it not only for the modern electrophysiology needs, but for the future needs that are rapidly coming with the increasing innovation in robotics, Artificial Intelligence, and cloud-networked devices. This book contains the results of the effort and gives a glimpse ahead to what will come next.”

— *Josh Yeboshua Shachar*

Neuro-Kinesis Corp. (NKC) was founded in 2015 to further the innovative work of Josh Shachar and his engineering team in developing a new array of intelligent SMART surgical tools that combined advanced biosensor technologies with AI, robotic-control, and cutting-edge micro-miniaturization processes that could push the envelope of possibilities for cure in the surgical arenas they were created for. This book focuses on the work done in creating NKC’s groundbreaking Huygens™ Mapping Catheter and the Proteus™ Robotic Arms which are the key components of NKC’s vision for its Huygens™ – Proteus™ Robotic Surgical Platform. With Huygens™ and Proteus™, Josh and his team have taken the groundbreaking work achieved with their 9-ton CGCI system and have reduced it down to a 9kg portable plug-and-play system that can deliver endocardial mapping and catheter guidance control beyond anything that has ever been attempted before.



neuro KINESIS  
CORPORATION

10524 S La Cienega Blvd. Inglewood, CA 90304

ISBN 979-8-218-09439-3  
\$45.00  
54500>  
9 798218 094393